Transition metal complexes as G-quadruplex DNA binders

by

Katherine Jane Castor

Department of Chemistry, McGill University

Montreal, QC, Canada

February 2014

A thesis submitted to McGill University in partial fulfillment of the requirements of the degree of Doctor of Philosophy

I dedicate this thesis to my family: my father Kim Castor, my mother Carolyn Castor and my brother Michael Castor, for your constant support and encouragement and for always believing in me. And to Rosie – may the grass be as green on your side of the fence (but within reason, of course).

Table of Contents

Copyright Statement

Some of the material presented in this thesis is adapted from published papers and is therefore subject to copyright:

Material in Chapter 2 is reproduced in part from Castor, K. J.; Mancini, J.; Fakhoury, J.; Weill, N.; Kieltyka, R.; Englebienne, P.; Avakyan, N.; Mittermaier, A.; Autexier, C.; Moitessier, N. and Sleiman, H. F.; "Platinum(II) phenanthroimidazoles for targeting telomeric G-quadruplexes"; *ChemMedChem*, **7**, 85-94, 2012. © 2014 Wiley Interscience; Used by permission.

Material in Chapter 3 is reproduced in part from Castor, K. J.; Liu, Z.; Fakhoury, J.; Hancock, M. A.; Mittermaier, A.; Moitessier N. and Sleiman, H. F.; "A platinum(II) phenylphenanthroimidazole with an extended side-chain exhibits slow dissociation from a c-kit G-quadruplex motif"; *Chemistry – A European Journal*, **19**, 17836-17845, 2013. © 2014 Wiley Interscience; Used by permission.

Contribution of Authors

All scientific contributions presented in this dissertation were conducted under the guidance and supervision of the research director, **Prof. Hanadi F. Sleiman**, who is also a co-author of the work.

Chapter 2

This chapter represents a highly collaborative effort among the Sleiman (Department of Chemistry), Moitessier (Department of Chemistry), and Autexier (Departments of Anatomy & Cell Biology and Experimental Medicine) laboratories at McGill University, with data interpretation assistance from **Prof. Anthony Mittermaier** (Department of Chemistry). The synthesis of the complexes and biophysical studies were performed by **Katherine Castor** (who was also responsible for project design) and aided by **Dr. Roxanne Kieltyka**, with assistance from a summer undergraduate, **Nicole Avakyan**. The computer-aided studies were performed by **Dr. Pablo Englebienne** and **Dr. Nathanael Weill** under the supervision of **Prof. Nicolas Moitessier**. The TRAP-Lig assays were performed by **Dr. Johans Fakhoury** (Sleiman and Autexier laboratories) and **Johanna Mancini** (Autexier). Lastly, **Johanna Mancini** also conducted the celluar assays under the supervision of **Prof. Chantal Autexier**. The findings in this chapter were published in a manuscript accepted by ChemMedChem in 2012 entitled "Platinum(II) phenanthroimidazoles for targeting telomeric G-quadruplexes".

Chapter 3

This chapter represents a collaborative effort among the Sleiman and Moitessier laboratories at McGill University, with data interpretation assistance from **Prof. Anthony Mittermaier**. **Katherine Castor** was responsible for the design, synthesis, and characterization of the complexes, as well as project design and biophysical assays (HT-FID, CD, and HPLC). **Dr. Mark A. Hancock** (McGill SPR Facility) conducted the SPR assays and **Dr. Guillaume Lesage** (CIAN, Department of Biology) ran the robot for the HT-FID assays. The

computer-aided studies were performed by **Zhaomin Liu** under the supervision of **Prof. Nicolas Moitessier**. The biological assays (MTS, mRNA analysis, and western blot) were performed by **Dr. Johans Fakhoury**. The findings in this chapter were published in a manuscript accepted by Chemistry − A European Journal in 2013 entitled "A platinum(II) phenylphenanthroimidazole with an extended side-chain exhibits slow dissociation from a *c-Kit* G-quadruplex motif".

Chapter 4

This chapter represents a collaborative effort between the Sleiman and Mauzeroll laboratories. **Katherine Castor** was responsible for the design, synthesis, and characterization of the complexes as well as project design and biophysical assays (UV/Vis and luminescence assays). The X-ray crystallography was conducted by **Dr. Christopher Serpell**. The CV and ECL experiments were conducted by **Dr. Kimberly Metera** and **Dr. Ushula Tefashe**. The high-throughput flourescence assay was designed by myself conducted by **Dr. Guillaume Lesage** (CIAN, McGill University). The findings in this chapter are to be published in a manuscript submitted to the Journal of the American Chemical Society in 2014.

Chapter 5

Katherine Castor was responsible for the synthesis and characterization of the complexes, as well as project design and biophysical assays. Operation of the robot for the HT-FID assay was done by **Dr. Guillaume Lesage** of the Cell Imagining and Analysis Network (CIAN) (McGill University Department of Biology) **Dr. Mark Hancock** performed the SPR assays at the McGill SPR Facility.

Abstract

Guanine quadruplexes are non-canonical secondary structures that can form in guanine-rich DNA and are stabilized by monovalent cations present in physiological conditions. Bioinformatics studies have identified putative G-quadruplex forming sequences throughout the human genome, in the telomeres and promoter regions of oncogenes. Small molecules that promote the folding of these G-rich sequences into a G-quadruplex structure can result in biologically relevant phenomena that have profound effects on cancer cell proliferation, generally through telomerase inhibition and suppression of oncogene expression, thereby accomplishing one of the main goals of chemotherapy: to halt tumor growth.

G-quadruplex forming sequences vary in their nucleobase composition, which allows for topologically distinct monomeric structures. These varying topologies present a means of targeting one polymorph rather than all, which permits site-specific therapies for small molecules that can discriminate between the structures. To date, both organic and inorganic compounds with varying degrees of efficacy in their targeting of this DNA structure have been reported. From this wealth of empirical data, it has been shown that small molecules can bind to G-quadruplexes most often through end π-stacking, although interaction with the loops and groove environments can be permitted with extended side-chains from a highly aromatic core.

Herein, we present efforts made towards the creation of transition metal-based G-quadruplex binders consisting of phenanthroimidazole ligands coordinated to platinum(II) and iridium(III) centers. These complexes are ideally suited for recognition of G-quadruplex motifs due to their electron-poor heteroaromatic nature and inherent positively-charged metal center for optimal π-stacking with the G-tetrad surface. Through the use of molecular modeling, biophysical (circular dichroism, fluorescence intercalator displacement assays, surface plasmon resonance, continuous variation analysis, fluorescence binding assays), biological (telomerase inhibition assays, cell cytotoxicity assays, mRNA levels analysis, western blotting), and electrochemical (cyclic voltammetry,

electrogenerated chemiluminescence) techniques, we study the properties of these complexes and their interaction with biologically relevant G-quadruplexes.

In Chapter 2, we structurally evolve our library of phenanthroimidazole ligands towards optimal G-quadruplex binding to the human telomeric G-quadruplex motif. This occurs, specifically, through examining the effect of increasing π-surface area of the ligands. Chapter 3 describes the addition of protonable side-chains to our phenanthroimidazole core that allows for a multivalent binding mode to G-quadruplex DNA. In Chapter 4, we exchange our platinum(II) metal with iridium(III). This substitution allows us to harness the luminescent "quadruplex light-switch" effect and evaluate the series of complexes as G-quadruplex probes. Chapter 5 describes our attempts towards expanding our library of platinum(II) complexes to include electron-withdrawing and electron-donating substituted phenylphenanthroimidazole ligands and their abilities to discriminate between G-quadruplex polymorphs. In all, this work provides a basis for the development of our scaffolds as small molecule probes for the advancement of G-quadruplex-based therapeutics.

Résumé

Les quadruplexes de guanine sont des structures secondaires non-canoniques pouvant être trouvées dans des séquences d'ADN riches en guanine. Ces derniers sont stabilisés par des cations monovalents présents dans les conditions physiologiques. Des études bioinformatiques ont permis d'identifier des séquences au sein du génome humain pouvant former des G-quadruplexes, notamment dans les télomères et les régions promotrices de certains oncogènes. Les petites molécules qui promeuvent l'agencement de ces séquences riches en guanine en G-quadruplexes peuvent donner lieu à des phénomènes bouleversant l'équilibre de prolifération cellulaire de par une inhibition de l'enzyme télomérase et une tendance à réduire l'expression d'oncogènes. Ainsi, il serait possible d'atteindre un des principaux objectifs de la chimiothérapie : stopper la croissance d'une tumeur.

Les séquences formant des G-quadruplexes diffèrent en terme de composition nucléotidique ce qui leur permet de s'associer en structures monomériques aux topologies variées. Ces différences topologiques représentent un moyen d'agir sur un polymorphe plutôt qu'un autre, ce qui permet la mise en place de thérapies ciblées grâce à l'utilisation de petites molécules capables de discriminer entre les structures. Jusqu'à maintenant, des composés organiques et inorganiques aux degrés de spécificité divers et variés ont été recensés. A partir de cette abondance de données empiriques, il a été démontré que, le plus souvent, les petites molécules se lient en surface des G-quadruplexes via des interactions aromatiques-aromatiques («π-stacking »), bien que les interactions directes avec les boucles ou les brins de la structure soient possibles dans le cas de molécules possédant de longues chaînes annexes à un cœur hautement aromatique.

Nous présentons ici les travaux réalisés visant à la création de composés comportant un métal de transition se liant aux G-quadruplexes. Ceux-ci consistent en des complexes de platine (II) ou d'iridium (III) coordinés à des molécules de phénantroimidazoles. En raison de leur nature hétéroaromatique pauvre en électrons et de leur centre métallique chargé positivement, ils sont conçus pour interagir de façon optimale avec les G-quartets en surface des G-quadruplexes. Grâce à l'utilisation d'outils variés comme la modélisation moléculaire, des

techniques biophysiques (dichroisme circulaire, tests par déplacement d'agents intercalants fluorescents, résonance plasmon de surface, analyse de variations continues, tests par reconnaissance spécifique d'agents fluorescents), biologiques (tests d'inhibition de télomérase, tests de cytotoxicité cellulaire, quantification d'ARN messagers, immunobuvardage de type western), et électrochimiques (voltampérométrie cyclique, électrochimiluminescence), nous étudions les propriétés de ces complexes et leurs interactions avec des G-quadruplexes biologiquement pertinents.

Dans le chapitre deux, nous faisons évoluer notre panel de ligands de type phénantroimidazole d'un point de vue structural dans le but d'optimiser la spécificité des complexes pour les motifs des G-quadruplexes télomériques humains. Plus précisément, nous examinons les effets de l'augmentation de la surface des orbitales π des ligands. Nous décrivons dans le chapitre trois l'impact de l'ajout de chaînes annexes acceptrices de protons au ligand phénantroimidazole qui permettent un mode de liaison multivalent aux G-quadruplexes. Dans le chapitre quatre, nous échangeons l'atome de platine (II) par de l'iridium (III). Cette substitution permet l'exploitation du l'effet interrupteur (« light-switch ») des quadruplexes et l'évaluation de la capacité de nos composés à reconnaître spécifiquement les G-quadruplexes. Enfin, nous décrivons dans le chapitre cinq nos tentatives pour agrandir notre panel de complexes au platine(II) et y inclure des ligands phénylphénantroimidazoles substitués donneurs ou accepteurs d'électrons pouvant distinguer différents polymorphes des G-quadruplexes. Globalement, les squelettes moléculaires développés dans cette étude représentent une base solide pour l'élaboration de petites molécules ciblant les G-quadruplexes dans un contexte thérapeutique.

Translation provided by Donatien de Rochambeau and Katherine Bujold

Acknowledgements

Firsty, I would like to thank my supervisor, Dr. Hanadi Sleiman, for the opportunity to work together, and to gain valuable knowledge from her.

I would like to thank all of my group members, past and present, for sharing their knowledge in chemistry and cultures. Specifically, I thank Roxanne Kieltyka for pioneering the G-Quadruplex project- without you, I would not have had such a wonderful research project with which to spend the past 5-ish years in a love/hate relationship.

In addition, I would like to thank our collaborators on this thesis work: Chantal Autexier, Johanna Mancini, Johans Fakhoury, Nicolas Moitessier, Zhaomin Liu, Nathaniel Weill, Anthony Mittermaier, Guillaume Lesage, Kimberly Metera, Ushula Tefashe, Janine Mauzeroll, and Mark Hancock. Your assistance in all aspects of this project was greatly appreciated and this thesis could not have happened without your participation.

Beyond collaborators, I would like to thank others at McGill who helped in acquiring and interpreting some of the results obtained in this thesis- as well as teaching me how to use certain instruments in the department: Petr Fiurasek for help with all CSACS instrumentation, Rodrigo Mendoza-Sanchez for HPLC and reverse-phase Combiflash training (in addition to belting out Disney songs or impromptu salsa dancing at all times of the day and night), Matthew Hassler for DNA HPLC training and Combiflash troubleshooting (in addition to the occassional shoulder rub), and Katerina Krumova for painstakingly describing in detail exactly how to acquire quantum yield measurements, for combing my chapters with a **very** fine-toothed comb (and Joris!!! Whew. I owe you.), and all those late-night conversations on street corners and elsewhere. I thank Daniel Rivalti for always smelling so nice. And for the hugs. And the “I hate my life” procrastination conversations. And for saving me from Mitch’s stench in the Tally-Ho mobile. It’s always about how nice you smell, isn’t it? To the dirty dangles, Kunal Tiwari and Kevin Conley, I’d close out McConnell Arena with you guys any night. I can still hear you coughing. Better Tom and JCon: when I make some $$, I’ll invest in your microbreweries. Josh Pottel: I said I’d

acknowledge you. So here's your acknowledgement. Supposedly it's thought to be for your charming good looks, but the jury is still out on that one. And I should also include Alex G-H here because you actually read my thesis and gave comments, and said that if Josh goes in and you don't, you're going to do something unspeakable (maybe I made up that last part, but I can't imagine what you're capable of, so I think this covers my bases). To everyone that attended my Mock Defense, you guys are the absolute best- shout-outs to Ricky, Tim, Tom, Better Tom, Michelle, Mitch, Lana, and Andrew for asking questions, and to Nude Bob, Kunal, Lesser Graeme, Andrea, and Josh (in addition to KK) for being a pretty sweet Faux Committee.

I would also like to thank the amazing friends I made over the years – without you in my life, I certainly would not have made it through my PhD:

1) Laurie Lim for being my first grad school lady friend. I'm glad we both ended up TAing intro organic lab together because that lead to some pretty fantastic times... Sports Station teamers, "God, women", that time you blew up the air mattress with a hair dryer post-birthday, and of course, Momma Lim's spring rolls. You can bring those to my defense party.
2) Adrienns Langillw for brunches, boozing, climbing wet trees (only once), American Thanksgiving Turkey Adventures, Malibu...?, tearful late-night conversations, and every honest opinion and thought we ever shared. I couldn't imagine life without you. Well played, Bob.
3) Chris 'Piggy McBoom' McLaughlin for training in most things Sleiman-lab related, for being my angry partner-in-crime, for dealing with Grumpy Gnomey and always being up for "more dudes!". Thanks so much for including me as part of your family – trips to Tamworth kept the longing for home at bay as part of my home-away-from-home. Marg can continue to send me Food & Drink where ever I may end up. I'll be in touch.
4) Danielle 'Sweet D' Vlaho for all of the things! I don't even know where to start. You are my rock, you are my other half, you are exactly

what I needed at the exact right time in my life. Pole dancing, shenanigans in the park by Place des Arts (fountain wading?!), Pimms, more pole dancing, softball, wine, wine, more wine, gin, your amazing cooking ability, French 75s, the IRT…, games nights, geesh, I could go on for hours- days, even. Dammit Moon Moon, shut up before you make everyone cry!

5) Mitchie Huot for being my sports partner-in-crime. You make a great assistant coach/stats keeper/general manager. Without you, Nice Snatch would have been Mediocre Snatch at best. Also, I'll never forget that horrible pour or how scared you are of skunks.
6) Blanda Greene- super glad I got to know you. You're a fantastic skiing partner and the perfect person to talk horses with for hours. Keep working on those hockey skills, you'll get it eventually. Maybe Kenny can help you work on your form... don't tell him about your love of KD or he will make your life miserable. ;)
7) And lastly, Graham 'Gammy' Hamblin. You are my bestest friend- and have been from day one. You kept me (reasonably) sane these past 5-ish years. I've learned as much from you as I have from everyone else combined. I greatly appreciate your help in all things computer-related. Who am I kidding, thanks for help in all things life-related. I can always count on you to finish my meal, split a few teamers, get into shenanigans, watch some TV, make a good meal, be down for whatever I'm down for, doubles squash, and the Dong Seminar. And thanks for being a shoulder to cry on and to hold onto when I find myself otherwise incapable to do it alone. I hrtae you, too.

List of Symbols and Abbreviations

2-CLIP	2-chlorophenylimidazo[4,5-*f*]1,10-phenanthroline
2,6-diCLIP	2,6-dichlorophenylimidazo[4,5-*f*]1,10-phenanthroline
3-CLIP	3-chlorophenylimidazo[4,5-*f*]1,10-phenanthroline
3,4-diCLIP	3,4-dichlorophenylimidazo[4,5-*f*]1,10-phenanthroline
3,5-diCLIP	3,5-dichlorophenylimidazo[4,5-*f*]1,10-phenanthroline
3,5-diFLIP	3,5-difluorophenylimidazo[4,5-*f*]1,10-phenanthroline
A172	human brain glioblastoma
A549	human adenocarcimona
A	adenine
ABAM	antibiotics and antimycotics
ACN	acetonitrile
ACX	reverse primer used in the teolmeric repeat amplification protocol assay
ADP	adenosine diphosphate
ALT	alternative lengthening of telomeres
AMBER	assisted model building with energy refinement
AML	acute myeloid leukemia
ATP	adenosine triphosphate
B	base
B-DNA	right-handed DNA
Bcl-2	B-cell lymphoma 2
BODIPY	boron dipyrromethene
BSA	bovine serum albumin
C	cytosine
CF_3PIP	4-trifluoromethylphenylimidazo[4,5-*f*]1,10-phenanthroline
c-KIT	cytokine tyrosine kinase
CLIP	4-chlorophenylimidazo[4,5-*f*]1,10-phenanthroline
c-MYC	myelocytomatosis viral oncogene homolog
CD	circular dichroism
CuAAC	copper-assisted alkyne azide coupling

CV	cyclic voltammetry
DC_{50}	concentration required to reduce the fluorescence by 50%
DCM	dichloromethane
ddH_2O	doubly distilled water
DDR	DNA damage response
DFT	density functional theory
dGTP	2'-deoxyguanosine 5`-triphosphate
DMSO	dimethyl sulfoxide
DNA	2'-deoxyribonucleic acid
dNTP	deoxynucleotide triphosphate
ds	double-stranded
$E_{1/2}$	half-wave potential
ECL	electrogenerated chemiluminescence
EDC	1-ethyl-3-(3-dimethylaminopropyl)carbodiimide
EDTA	ethylenediamine tetraacetic acid
en	ethylenediamine
EGTA	ethyleneglycol tetraacetic acid
ESI-MS	electrospray ionization mass spectrometry
EtOH	ethanol
FAM	carboxyfluorescein
FBS	fetal bovine serum
FID	fluorescence intercalator displacement
FITTED	flexibility induced through targeted evolutionary description
FLIP	4-fluorophenylimidazo[4,5-*f*]1,10-phenanthroline
FRET	Förster resonance energy transfer
G	guanine
G4	guanine quadruplex
GIST	gastrointestinal human stromal tumor
h-telo	G-quadruplex sequence from human telomere
HeLa	immortal cancer cell line named after Henrietta Lacks

HIV-RT	human immunodificiency virus reverse transcriptase
HOAt	1-hydroxy-7-azabenzotriazole
HOMO	highest occupied molecular orbital
HP	hairpin DNA
HPLC	high-performance liquid chromatography
HR-MS	high resolution mass spactrometry
HT	high throughput
hTERT	human telomerase reverse transcriptase
hTR	human telomerase RNA template
IC	internal control
IC_{50}	ligand concentration that inhibits fifty percent of the total enzyme activity
ICD	induced circular dichroism
K	binding constant
KRAS	Kirsten rat sarcoma viral oncogene
LUMO	lowest unocupied molecular orbital
MCF-7	human breast cancer
MD	molecular dynamics
MeOH	methanol
MLCT	metal-to-ligand charge transfer band
MQ-H_2O	Milli-Q water
MRC-5	human normal lung tissue
mRNA	messenger RNA
MTS	3-(4,5-dimethylthiazol-2-yl)-5-(3-carboxymethoxyphenyl)-2-(4-sulfophenyl)-2H-tetrazolium)
NIP	2-hydroxy-1-naphthylimidazo[4,5-*f*]1,10-phenanthroline
nitroPIP	4-nitrophenylimidazo[4,5-*f*]1,10-phenanthroline
NMR	nuclear magnetic resonance
NT	internal control primer
PCR	polymerase chain reaction
PD	percentage displacement

PDB	protein data bank
PDGF-A	platlet-derived growth factor alpha
phen	phenanthroline
PII	indolylimidazo[4,5-f]1,10-phenanthroline
PIN	naphthylimidazo[4,5-f]1,10-phenanthroline
PIP	phenylimidazo[4,5-f]1,10-phenanthroline
PIQ	quinolinylimidazo[4,5-f]1,10-phenanthroline
pOH(PIP)	*p*-hydroxyphenylimidazo[4,5-*f*]1,10-phenanthroline
ppy	phenylpyridine
PQS	putative quadruplex sequence
ProCESS	protein conformational ensemble system set up
r	ratio of complex to G-quadruplex
RMSD	root mean square distance
RNA	ribonucleic acid
rRNA	ribosomal RNA
SIP	2-salicylimidazo[4,5-f]1,10-phenanthroline
SMART	small molecule atom type and rotatable torsion assignment
SPR	surface plasmon resonance
T	thymine
TAMRA	carboxytetramethylrhodamine
THF	tetrahydrofuran
TO	thiazole orange
TRAP	telomerase repeat amplification protocol
TRAP-Lig	TRAP assay, with ligand purification step
Tris	trishydroxyaminomethane
TS	telomeric substrate primer
UV/Vis	ultraviolet-visible
VEGF	vascular endothelial growth factor
$\Delta T_{1/2}/\Delta T_m$	(change in) thermal denaturation temperature
ε	molar extinction coefficient

List of Figures and Tables

Figures:

Tables:

“I hear the jury’s still out on science.”
-George Oscar Bluth II

“Never memorize something that you can look up.”
-Albert Einstein

1 G-Quadruplex DNA: Biological Implications

1.1 B-DNA: A brief structural discussion

Deoxyribonucleic acid (DNA) contains the genetic code of which all organisms are composed. Along with ribonucleic acids (RNA) and proteins, these three macromolecules are essential for all living entities. Since its discovery in 1869 by Friedrich Miescher[1] and subsequent flurry of structural determinations in 1953 by Rosalind Franklin,[2,3] Maurice Wilkins,[4] James Watson and Francis Crick,[5] research into all aspects of DNA − from biology to materials science − has fascinated many scientists and become the focus of numerous research groups.

The canonical structure of double-stranded DNA consists of the purine (adenine and guanine) and pyrimidine (thymine and cytosine) nucleobases hybridized to each other in a very predictable code (adenine with thymine, cytosine with guanine) termed Watson-Crick base-pairing. Individual strands are composed of nucleobases connected to a deoxyribose sugar *via* the 1' carbon, which is connected to phosphate groups *via* a phosphodiester bond at both the 3' and 5' hydroxyl groups. The base, sugar, and phosphate group are collectively called a nucleotide. The hybridization of two complementary strands results in a thermodynamically stable structure due to the selective hydrogen bonding and the π-stacking of the aromatic nucleobases.[5] The two strands run in opposite directions (anti-parallel) around a central axis to create a double helix in the right-handed direction with well-defined dimensions, described as B-form DNA (Figure 1.1). Because of the structure of the double helix, the anti-parallel strands have non-identical grooves − the major and the minor groove − that can be distinguished from each other by their widths, 2.2 nm and 1.2 nm, respectively.

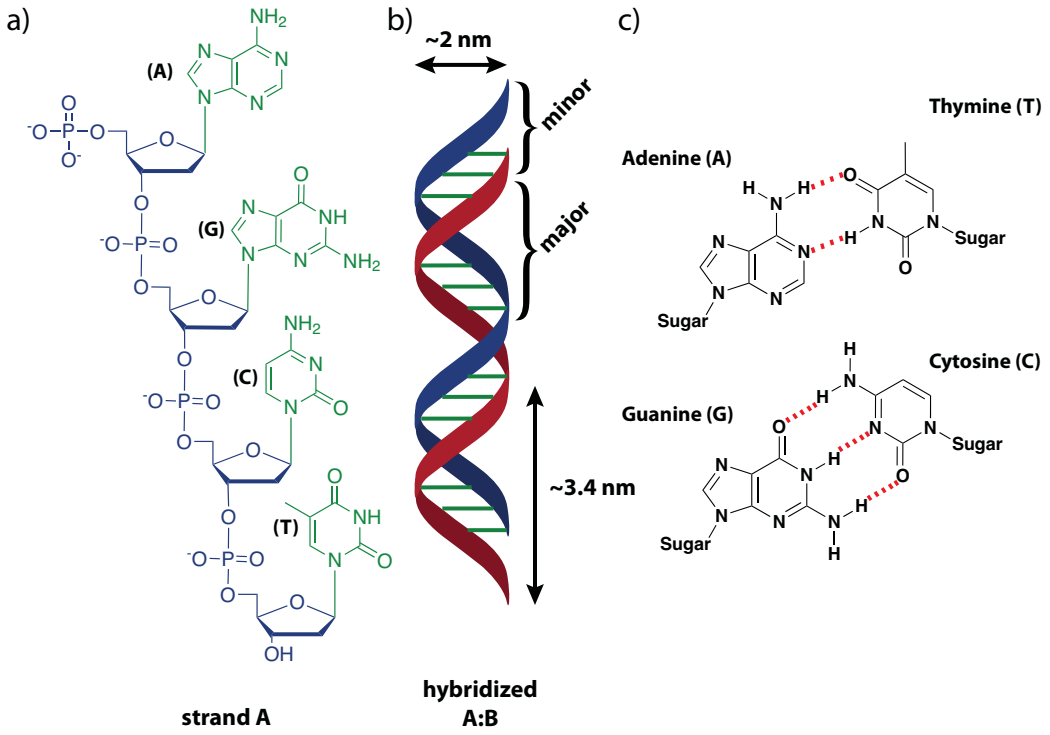

Figure 1.1 Structural properties of DNA: a) Chemical make-up of a strand with the sugar-phosphate backbone shown in blue and the nucleobases shown in green. b) Two complementary strands (A: blue and B:red) hybridize *via* hydrogen bonding between the nucleobases (green) to form a double helix with major and minor grooves, as illustrated. The double helix has a diameter of ~ 2 nm and one helical turn has a length of ~ 3.4 nm. Each base is spaced ~ 0.34 nm from the next, meaning it requires 10.5 bases to complete a full turn. c) Examination of Watson-Crick base-pairing motifs: A:T with 2 hydrogen bonds, G:C with 3 hydrogen bonds, represented by red dashes.

While B-DNA is the most well-known structure of DNA, it is certainly not the only one. Other forms including A-,[6,7] and Z-,[8,9] also exist, and are relevant in some biological contexts. These structures vary from B-DNA based on the spatial arrangement of the base-pairs, the ring-pucker of the sugar, and other structural differences resulting from hydration, salt concentration, under- or over-winding, and protein binding, among others (Figure 1.2).[10] However, these forms all consist of Watson-Crick base-pairs. What if Watson-Crick base-pairing was not the only method by which DNA can assemble?

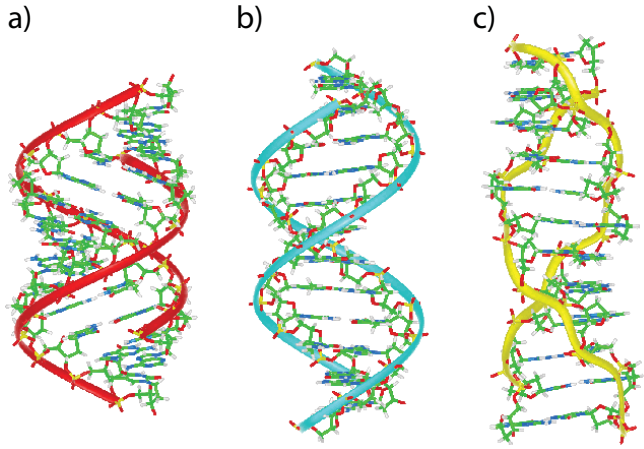

Figure 1.2 Structural isomers of DNA: a) A-form, b) B-form, and c) Z-form. The phosphate backbones are represented in red (A-form), cyan (B-form), and yellow (Z-form) to illustrate the differences between the isomers. Image used under terms from the GNU Free Documentation License.

1.2 G-Quadruplex DNA

1.2.1 Discovery

Forty years before the structure of the DNA double helix was determined,[2-5] Bang reported in 1910 that high concentrations of guanylic acid (GMP) formed a gel.[11] As was common with most findings in the biological world pre-modern era, the structure of this gel was not determined until much later, when in 1962, Gellert and coworkers proposed a structure based on the examination of the optical properties of the GMP gel and subsequent x-ray diffraction (Figure 1.3a).[12] In the report, they proposed a helical structure with four units per turn of the helix. These units (the guanylic acid) could be oriented in such a way that two hydrogen bonds per unit are bonded to the next to form a square planar arrangement (Figure 1.3b). The existence of these structures in solution could aggregate in a linear fashion to form the fibers that make up the gels due to the strong van der Waals and π-stacking attractions (Figure 1.3c). They also hypothesized that if the GMP units were linked by a phosphodiester backbone such as that found in DNA, a regular helical twist would be observed (Figure 1.3d) which would explain diffraction patterns with similar characteristics to B-DNA.

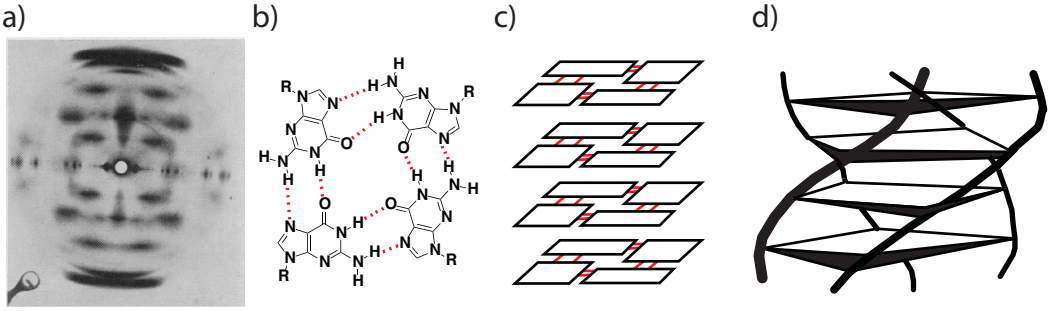

Figure 1.3 Proposed structure of the basic unit of the GMP gels by Gellert:[12] a) X-ray diffraction pattern of the 3'-GMP structure where the fiber axis is approximately vertical, b) proposed arrangement of the bases in GMP gels, c) aggregation of the planar tetrads results in π-stacking, and d) proposed linking of the GMPs *via* a phosphodiester bond resulting in a helical twist of the tetrads. Hydrogen bonds are represented as red lines. Figure adapted from references 12 and 13 with permission, © National Academy of Sciences.

Gellert was able to make the assumption that non-Watson-Crick base-pairing could occur based on a publication by Donohue in 1956.[14] In his report, he cites Watson and Crick's work, stating that the structure of DNA must contain equimolar amounts of A and T, and G and C, due to the base-pairing code. However, Donohue points out that:

"Since it is by no means certain that all nucleic acids ... will conform to this composition, it becomes of interest to inquire into the possibility of other structures which satisfy the chemical evidence concerning the bonding in a single nucleotide chain and which also conform to our knowledge of molecular structures."

It is with this mindset that he predicted four types of guanine-guanine base pairs (pairings 9-12) which would result in a purine-purine two-chain structure.[14] It was not until 1962 when Karst Hoogsteen refined the structure of the hydrogen-bonded 1:1 complex of 1-methylthymine and 9-methyladenine that the delineation between the Watson-Crick and Hoogsteen faces of nucleobases was decided.[15] As further evidence, a report by Ralph, Connors, and Khorana demonstrated aggregation and high thermal stability of tri-, tetra-, and pentanucleotide repeats of deoxyguanine, which suggested that other secondary structures of DNA could in fact, exist.[16] After 1962, the field of guanine tetraplexes lay dormant until renewed interest in the late 1980s, when future Nobel Prize winner Dr. Elizabeth

Blackburn discovered that telomeric DNA could form non-Watson-Crick, guanine-guanine base-paired, intramolecular structures and these structures could be important for telomere function, thus setting the precedent for the guanine tetraplex's biological relevance.[17] The area of biologically relevant G-quadruplexes thus exploded in the late 1980s with a report by Dipankar Sen and Gilbert in 1988,[18] who hypothesized that self-recognition of guanine-rich motifs in the telomeres could serve to bring together four homologous chromatids during meiosis. There has yet to be direct evidence of this hypothesis, however, support has arisen through the finding that the Hop1 protein of *S. cerevisiae* promotes quadruplex formation i*n vitro* and plays a key role in meiosis.[19,20] A report by James Williamson in 1989 demonstrated that telomeric DNA based on the repeats found in *Oxytricha* and *Tetrahymena* genomes could form G-quadruplexes in conditions containing monovalent cations, (sodium, potassium, and cesium) and these secondary structures must be dealt with by the enzyme components involved in replication of the telomeres.[21] Thus the field of G-quadruplexes was born, with research areas in molecular biology, drug design, and materials science. In fact, a Scopus search reveals many instances of the search term "quadruplex" or "tetraplex" (in relation to "nucleic acid") in areas including chemistry, medicine, pharmacology, chemical engineering, immunology, agricultural sciences, computer science, and neuroscience, among others. The rise in the number of publications from the late 1980s to present day is shown in Figure 1.4.

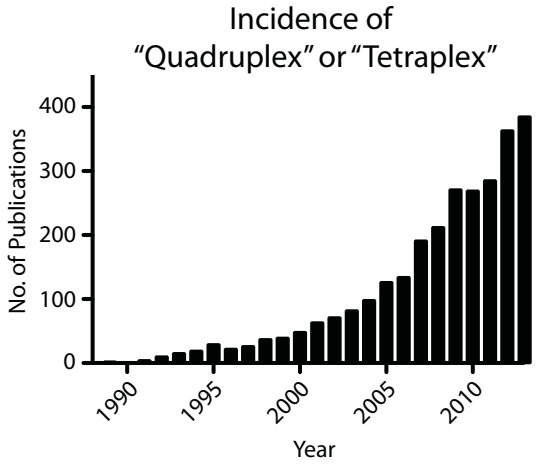

Figure 1.4 Incidence of "quadruplex" or "tetraplex" in the literature from a Scopus search in relation to "nucleic acid" from 1988-2013.

1.2.2 Structure of the quadruplex motif

Since the development of the field in the 1980s, G-quadruplexes have been demonstrated to form in physiological conditions *in vitro*[22,23] and the first example of quadruplex formation *in cellulo* was established in ciliates[24,25] and in human cells.[26] Bioinformatics studies have identified potential G-quadruplex forming sequences throughout the human genome,[27,28] and several characteristics determining the structure of these motifs have been elucidated. The basic structure of a G-quadruplex can be described with such descriptors as the helical parameters of twist and rise, the backbone strand polarity (parallel or antiparallel), the number of strands involved (unimolecular, bimolecular, tetramolecular), the connecting loop length and type (lateral, diagonal, or propeller), groove widths (wide, medium, narrow), and the nature of the ion channel; these parameters are visualized in Figure 1.5.

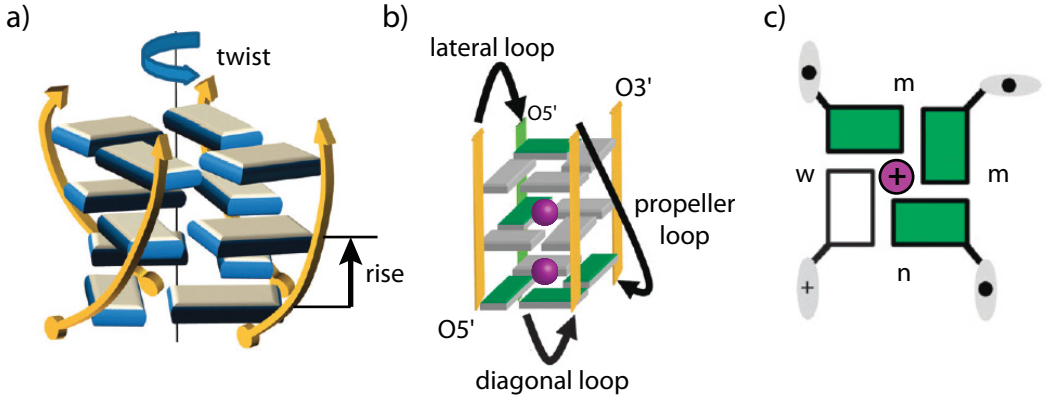

Figure 1.5 Basic G-quadruplex descriptors: a) helical parameters twist and rise, b) linking loop motifs (black arrows) and backbone strand polarity, O5' and O3' are defined, where parallel strands are orange and anti-parallel strands are green. Glycosidic torsion angles are shown with the *anti*-corformation in gray and the *syn*-fonformation in dark green, and c) groove dimensions, where w = wide, m = medium, and n = narrow. *Anti*-conformation bases are in white and *syn*-conformation bases are dark green. In the 5'-3' directionality, the (•) represents strand polarity away, while the (+) denotes strand polarity towards. The magenta spheres in b) and c) represent the locations of the ions in the ion channel. Figure adapted from reference 29 with permission from The Royal Society of Chemistry.

Due to the number of parameters involved, a large variety of structural diversity exists in the G-quadruplex motif, and each contributes to the significant thermodynamic and kinetic stability.[30] In fact, Williamson states that the "schizophrenia" of the G-quadruplex motif arises from the desire to create the

ideal core for ion coordination by the O6 oxygens. The polymorphic nature of the quadruplex motif can best be described on a per-sequence basis and is illustrated in Figure 1.6.

1.2.3 Biologically relevant intramolecular G-quadruplexes

In intramolecular (unimolecular) G-quadruplexes, the G-runs are linked by loops containing nucleotides in such a way that a general pattern can be shown by GnLmGnLmGnLmGn where n = 3−5, m = 1−7, G = guanine, and L = base in the loop.[29] Huppert and Balasubramanian[27] developed a "folding rule" based on the above pattern to allow them to discover putative quadruplex sequences (PQS) within the human genome by using an algorithm they named *quadparser*. From this algorithm, they identified an astounding 188,836 G-patterns and 187,610 C-patterns (indicating a G-pattern in the complementary strand) for a total of 376,446 PQS within the whole human genome. This number has been corroborated through a study by Todd and Neidle whereby they used a different bioinformatic approach to identify ca. 375,000 PQS.[28] Amazingly, many of these PQS are found in specific areas of the genome (both eukarotic and prokaryotic genomes), including telomeric DNA, promoter regions of oncogenes,[31] immunoglobulin class switch regions,[32] ribosomal DNA,[33,34] and untranslated regions of RNA,[35-37] rather than distributed randomly. Given this clustered distribution, a biological importance is very likely. In the following sections, the telomeres and promoter regions will be described in detail as they are particularly relevant to this thesis work.

1.2.3.1 Telomeres and telomerase

In eukaryotes, telomeres are the protein-DNA complexes located at the ends of the linear chromosomes – they protect the coding DNA from being damaged or recognized as double-stranded breaks. From their discovery in ciliated protozoans *Tetrahymena*[38] and *Oxytricha*,[39,40] it is well known that the

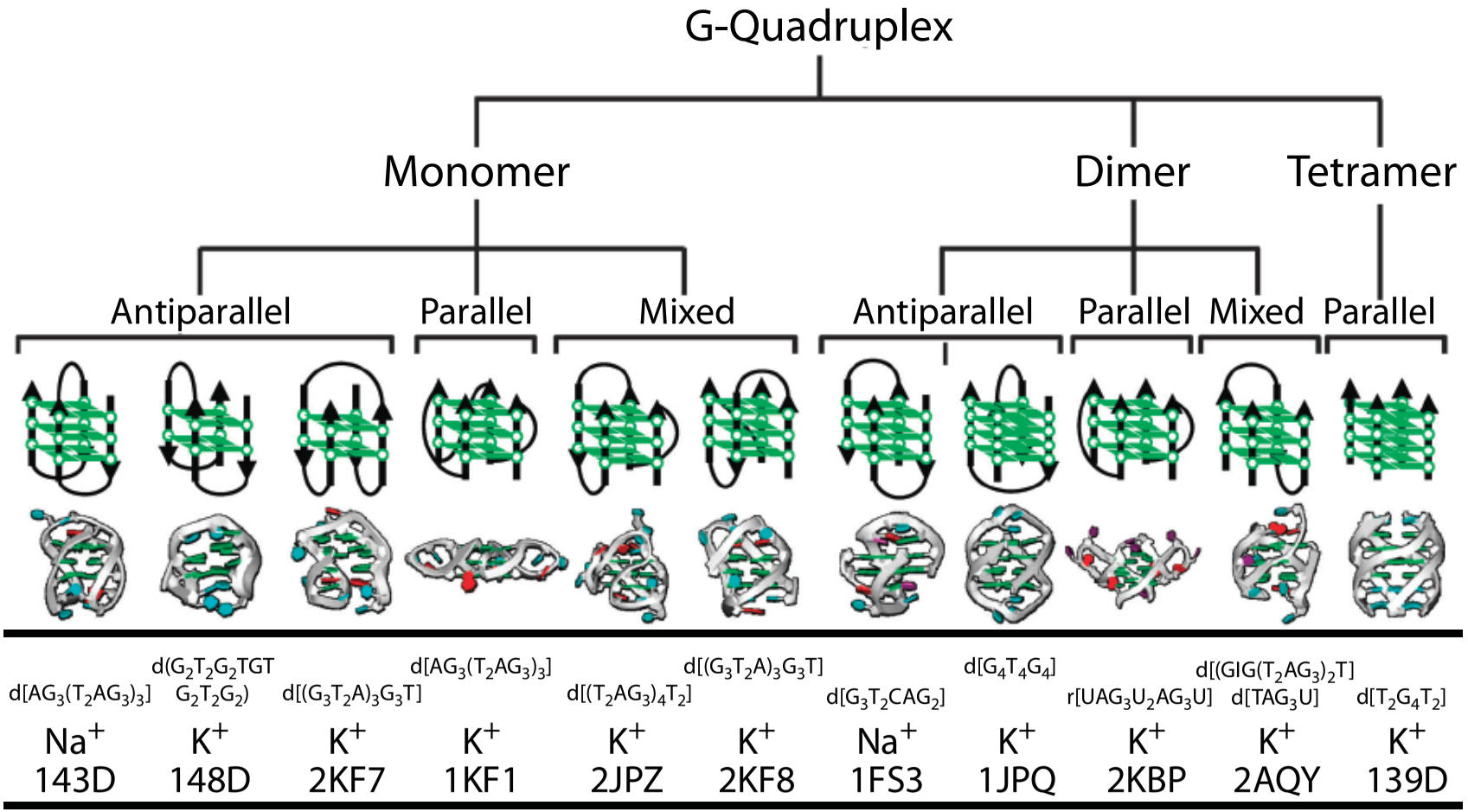

Figure 1.6 Polymorphic G-quadruplexes derived from telomeric sequences. The sequence, metal ion involved, and the PDB ID code are shown below each structure. Figure reproduced from reference 41 with permission from The Royal Society of Chemistry.

telomeres are highly conserved across species from single-celled organisms to higher plants and animals, and consist of repetitive guanine-rich DNA sequences that are 10−15kb in length and are mostly double-stranded. At the extreme 3'-terminus of the human telomere is a single DNA strand composed of $(TTAGGG)_n$ repeats.[42,43] The telomere is normally encapsulated by the shelterin complex,[44-46] which is a group of six proteins (TRF1, TRF2, TIN1, TPP1, POT1, and RAP1) that folds the single-stranded end into a t-loop (Figure 1.7a).

In normal cells, prior to each cellular division, the chromosomes are replicated during S phase of the cell cycle. Due to the inefficiency of the DNA replication machinery for the lagging strand, the telomeres lose 25−200 bases in the process, known as the "end-replication problem".[47-50] After several cycles of replication, the telomeres reach a critical length when tumor supressing proteins p53 and Rb are activated, which forces the cells into replicative senescence. The normal cells can continue to survive, but replication is halted. Replicative senescence was first discovered by Leonard Hayflick and Paul Moorhead who, in 1961, realized that the number of replications by cultured normal human cells is regulated by a biological clock, rather than the initial belief that cells explanted into culture were immortal.[51] Today, the biological clock that causes replicative senescence is known to be due to critically short telomeres.[52] However, in 85−90% of cancer cells, the processive reverse transcriptase enzyme telomerase is responsible for elongation of the telomeres.[53] Prior to cellular division, the t-loop is lost and the 3'-end becomes available for telomerase extension (Figure 1.7b,c). Processive telomere elongation by telomerase (Figure 1.7d,e) allows the cancer cells to evade activation of p53 and Rb, thus becoming immortal. Almost all human cancers exhibit the biomarker of maintaining telomere length, which suggests that preservation of telomere length is required for immortality.[54-61] In fact, one of the hallmarks of cancer as defined by Hanahan and Weinberg,[62,63] is unlimited proliferation, and the existence of telomerase establishes a link between immortality and cancer.

The telomerase enzyme was first discovered in 1985 by Carol Greider under the supervision of Elizabeth Blackburn.[64] Her experiment, based on a

previous observation by Blackburn in 1984 that *Tetrahymena* telomeric sequences introduced in yeast could be extended by a yet unknown mechanism,[65] involved the incubation of single-stranded $(TTGGGG)_4$ substrates in a cell-free extract isolated from *Tetrahymena* with yeast telomeric sequences. The result of this experiment was that the TTGGGG repeats were added to the yeast sequence and that this activity must be the act of an enzyme, thus suitably named telomere terminal transferase. Later, the enzyme was renamed telomerase and found to contain an RNA substrate (hTR, or telomeric RNA) complementary to the telomeric sequence (in a species-specific manner), with a reverse-transciption mechanism of nucleotide addition.[66-69] Due to the inclusion of the hTR into the telomerase enzyme, and its subsequent reverse-transcription from the RNA template to the telomere DNA, it was determined that the substrate of the telomerase enzyme would be the G-rich single-stranded 3'-end of the telomere rather than the C-rich strand or Watson-Crick base-paired duplexes.[64,70]

1.2.3.1.1 Inhibition of telomerase

The inhibition of telomerase is an attractive way to selectively target cancer cells over normal cells as a chemotherapy. This is because 85−90% of cancer cells express telomerase,[53] while adjacent healthy cells do not.[54,71] This can be done *via* several approaches, including the interference with the expression of telomerase or hTR through antisense or small interfering RNA therapies,[72-75] or through the inhibition (direct or indirect) of the catalytic activity of the enzyme.

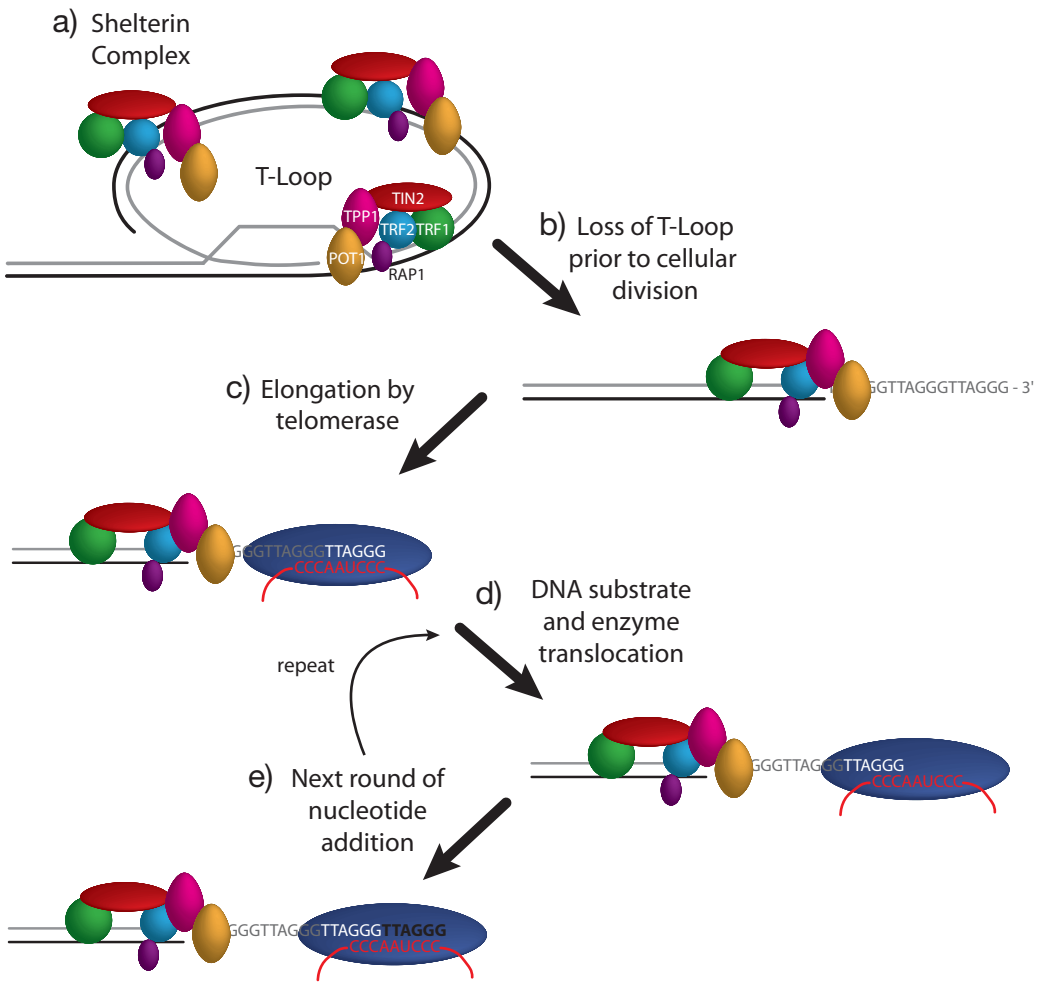

Figure 1.7 Mechanism of action of telomerase: a) Diagram of the proposed t-Loop structure of human telomeres. b) Loss of the t-Loop prior to cellular division results in an exposed single-stranded telomeric end. The processive nature of the enzyme is shown in c), d), and e), where c) the single-stranded telomeric end is available for extension by telomerase; d) the translocation of telomerase repositions the 3'-end of the DNA to allow for e) another round of addition. Steps d) and e) repeat to allow for further extension.

Since telomerase is a reverse transcriptase, nucleotidic reverse transcriptase chain-terminators like those used for HIV-RT inhibition, have been successful for application to telomerase (Figure 1.8a).[76,77] Additionally, small molecules that modulate phosphorylation patterns involved in telomerase regulation, like some protein kinase C inhibitors, can also inhibit telomerase activity (Figure 1.8b-c).[78] A small molecule that has shown promise in preclinical trials on some model systems is BIBR1532 (Figure 1.8e), a non-competitive inhibitor that interferes with telomerase processivity. This molecule leads to the reduction in number of TTAGGG repeats by either affecting translocation of the

enzyme-DNA substrate complex or by promoting dissociation of the complex after completion of hTR copying.[79,80] A modified oligonucleotide clinical candidate that inhibits telomerase by antagonistic binding to hTR is GRN163L (Imetelstat), by Geron Corporation (Figure 1.8d). Imetelstat is a 13mer thiophosphoramidate oligonucleotide of the sequence 5'-TAGGGTTAGACAA-3', with a lipophilic palmitoyl tail that allows for increased cellular uptake.[75,81] This drug candidate is currently in four Phase II and ten Phase I clinical trials.[82]

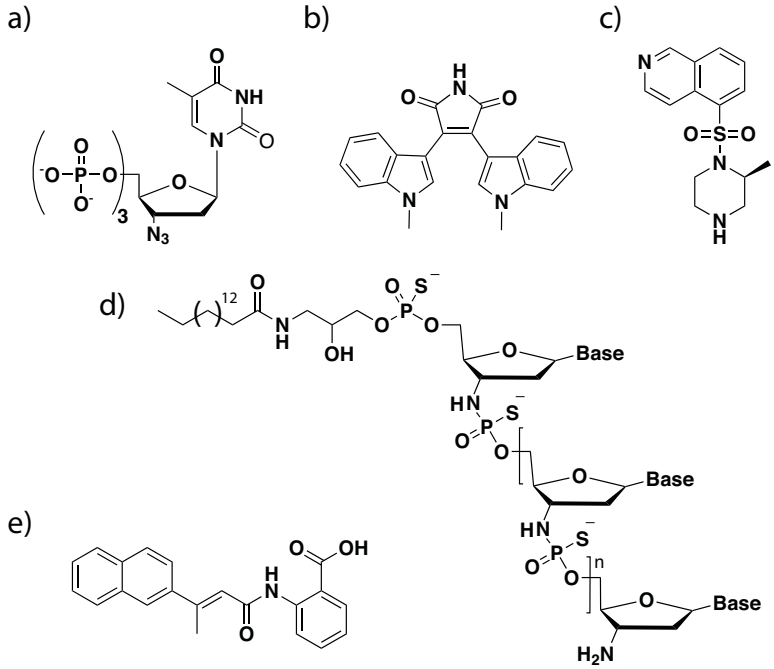

Figure 1.8 Known inhibitors of catalytic activity of telomerase: a) AZT-TP,[76,77] b) bismaleimide,[78] c) H7,[78] d) GRN163L (Imetelstat) where the nucleotide sequence is 5'-TAGGGTTAGACAA-3',[75,81] and e) BIBR1532.[79,80]

Although these drug candidates have shown promise for telomerase inhibition, a major drawback is their dependence on extensive telomere shortening which results in significant phenotypic lag – that is, the delay between telomere shortening due to inhibition of telomerase and cell growth arrest owing to a dysfunctional telomere.[83] This lag has been shown to be ~ 100 days for cultured cells treated with BIBR1532,[84] however, the lag time may vary depending on initial telomere length. Although this lag time is an issue, some of these candiates, namely BIBR1532 and Imetelstat, have been shown to sensitize telomerase-

positive cells towards other chemotherapeutic treatments.[85,86] Due to the phenotypic lag and the potential need for combination therapies, other methods to target telomerase and cause more rapid cell growth arrest and/or death should be investigated.

1.2.3.1.2 G-Quadruplex binding molecules as telomerase inhibitors

Rather than direct inhibition of telomerase and the resulting slow cell growth arrest (*vide supra*), a more rapid means of achieving growth arrest exists through indirect inhibition of telomerase. Small molecules have been shown to bind to G-quadruplexes and promote the formation of this motif *in vitro*.[87-91] The G-rich single-stranded end of the telomere can fold into a G-quadruplex structure, consequently sequestering the single-stranded substrate for telomerase, which has been shown to cause indirect inhibition of the enzyme.[17,92-95] This process is demonstrated in Figure 1.9 and is of key importance in the motivation for this thesis work. Besides telomerase inhibition, other biologically relevant phenomena are reported to occur upon the folding of this sequence into a G-quadruplex structure by small molecules, including the loss of telomere integrity through disruption of the shelterin complex (uncapping of the chromosomal termini).[96] This results in the activation of DNA damage response (DDR) mechanisms that follow recognition of double-strand breaks,[97,98] such as the activation of poly-(ADP-ribose) polymerase,[99] and ataxia telangiectasia mutated gene product signaling.[100,101] Due to the inherent genetic instability in cancer cells,[102] the inhibition of any of the DDR pathways may result in cellular senescence and/or apoptosis.[103,104] Hence, the stabilization of G-quadruplexes is predicted to have profound effects on cancer cell proliferation,[105] thereby accomplishing one of the main goals of chemotherapy: *to halt tumor growth*. Indeed, this uncapping phenomenom resulting in immediate growth arrest, apoptosis, and telomere dysfunction has been shown with the small molecule telomestatin (Figure 1.18c, described later).[45,101,106] Additionally, G-quadruplex forming sequences have been identified throughout the human genome and have been implicated in oncogene expression and cancer cell maintenance (Section 1.2.3.2, described later). In fact, the interaction of small molecules with genome-wide quadruplex motifs has been

shown in down-regulate oncogene expression in cancer cells.[107,108] Thus, the use of small molecule binders to stabilize the G-quadruplex DNA motif has become a promising approach to not only inhibit telomerase, but to aid in the *eradication of cancer cells*.[53,105,109-111]

1.2.3.1.2.1 The human telomeric G-quadruplex motif

After the initial discovery that G-quadruplex structures could exist in the telomeres of non-human organisms under physiological conditions, and that the repetitive G-tracts were conserved across species,[17] the first NMR solution structure of a G-quadruplex formed in human telomere 5'-$TTAGGG_n$ repeats was published in 1993 by Wang and Patel.[114] In their report, they investigated the structure formed by the sequence 5'-$AG_3(TTAG_3)_3$ in a Na^+-containing aqueous solution. They found that this 22mer sequence forms a single intramolecular polymorph, now called the "basket" structure, that has two medium, one narrow, and one wide groove. The strand direction of the medium grooves run parallel, while the strands that make up the narrow and wide grooves run antiparallel to each other. From the 5'-end, the three TTA loops are characterized as lateral, diagonal, and lateral, respectively (Figure 1.10a).

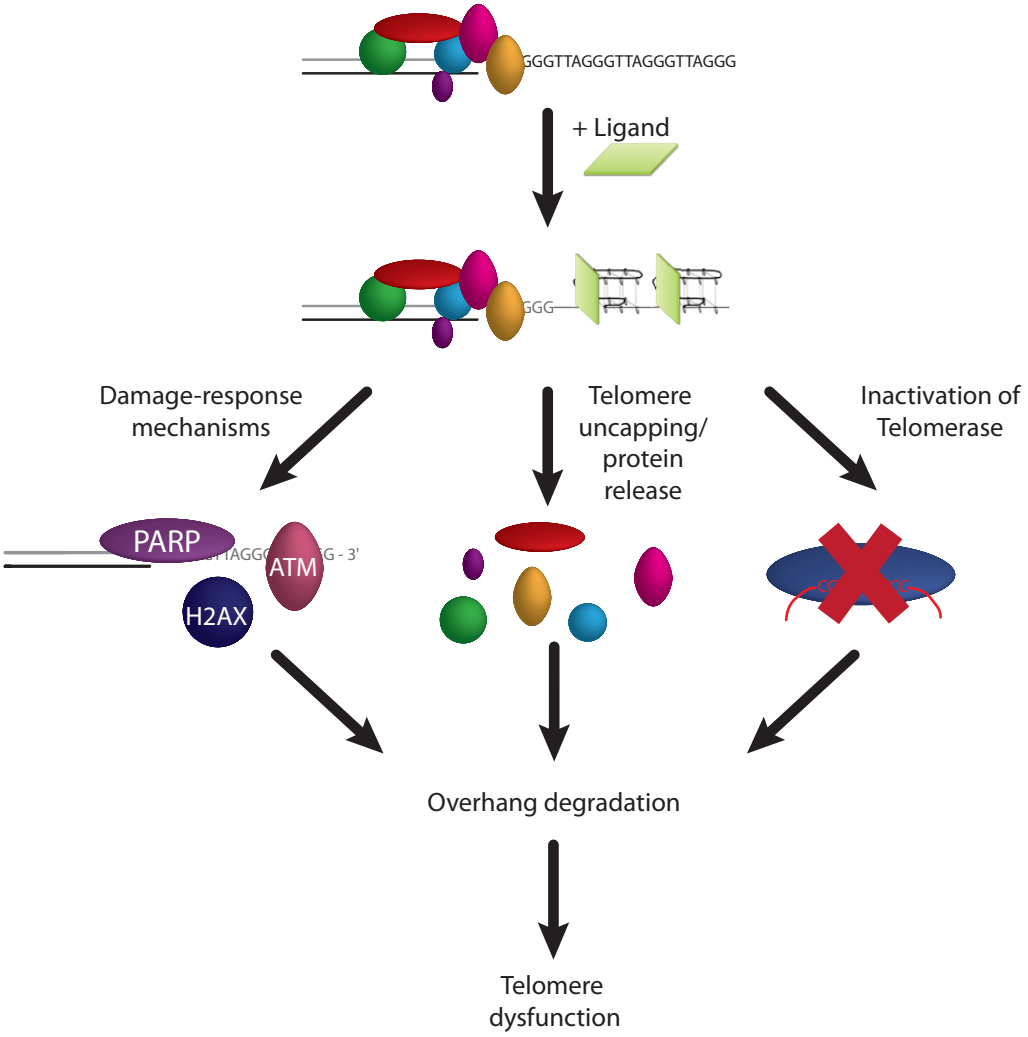

Figure 1.9 The folding of the G-rich telomere can bring about several phenomena, including the inactivation of telomerase, telomere uncapping and protein release, and the activation of DNA damage-response mechanisms. Any of these phenomena can result in overhang degradation and ultimate telomere dysfunction. Figure adapted from references 112 and 113, with permission.

Since then, much effort has gone into the determination of the structure of the "most biologically relevant" polymorph of the telomeric G-quadruplex, as the cellular environment is dominated by high K^+-levels. Through crystallographic[115] and NMR solution methods,[22,116,117] several foldings have been proposed. While there has only been one folding discovered for Na^+-containing solutions, several foldings have appeared for K^+-containing solutions. Interestingly, the K^+-crystal polymorph differs quite a lot from those found in solution (Figure 1.10b-e). A single-molecule spectroscopy study by Lee[118] demonstrates this conformational diversity and has proposed that six states exist ranging from long lived, to short

lived, to partially folded, and fully unfolded depending on the temperature and K^+ concentration. These diverse conformations are thought to have implcations *in vivo* for proteins and drugs that bind to specific polymorphs. Li and Chaires[119] postulate that the different forms respond to environmental conditions and that this responsiveness could trigger a switching mechanism to allow the participation of different polymorphs in different stages of the cell cycle. Two aspects became clear following these studies: i) the G-quadruplexes formed in human telomeric DNA are remarkably stable and ii) are very diverse, which leads to probable *in vivo* existence in humans and a potential selective targeting capability. Indeed, Oganesian said it best,[96] regarding the existence of quadruplexes *in vivo*:

"There is a growing list of proteins that bind to, cleave, resolve, or promote the formation of telomeric G-quadruplexes from a number of species in vitro*. Since it is unlikely that all of these interactions in multiple species are artefactual, this array of G-quadruplex interacting molecules lends support to the view of the quadruplex as a biologically significant entity."*

A 2009 review by Lipps and Rhodes presents studies aimed at uncovering the *in vivo* presence and function of G-quadruplexes.[120] The breakthrough that finally gave direct evidence of quadruplex formation in telomeres (albeit in ciliates) came through the development of antibodies with 0.1−1.0 nM binding affinities for antiparallel quadruplexes.[13] Lipps and Rhodes suggest that G-quadruplex specific ligands with 1.0−5.0 nM binding affinities could be used as *in vivo* probes for G-quadruplex formation. While this has not yet been demonstrated *in vivo*, promising *in cellulo* studies with quadruplex-targeting fluorogenic probes like carbazoles[121] and guanidinium-modified zinc-phthalocyanines,[122] could help reach the *in vivo* goal.

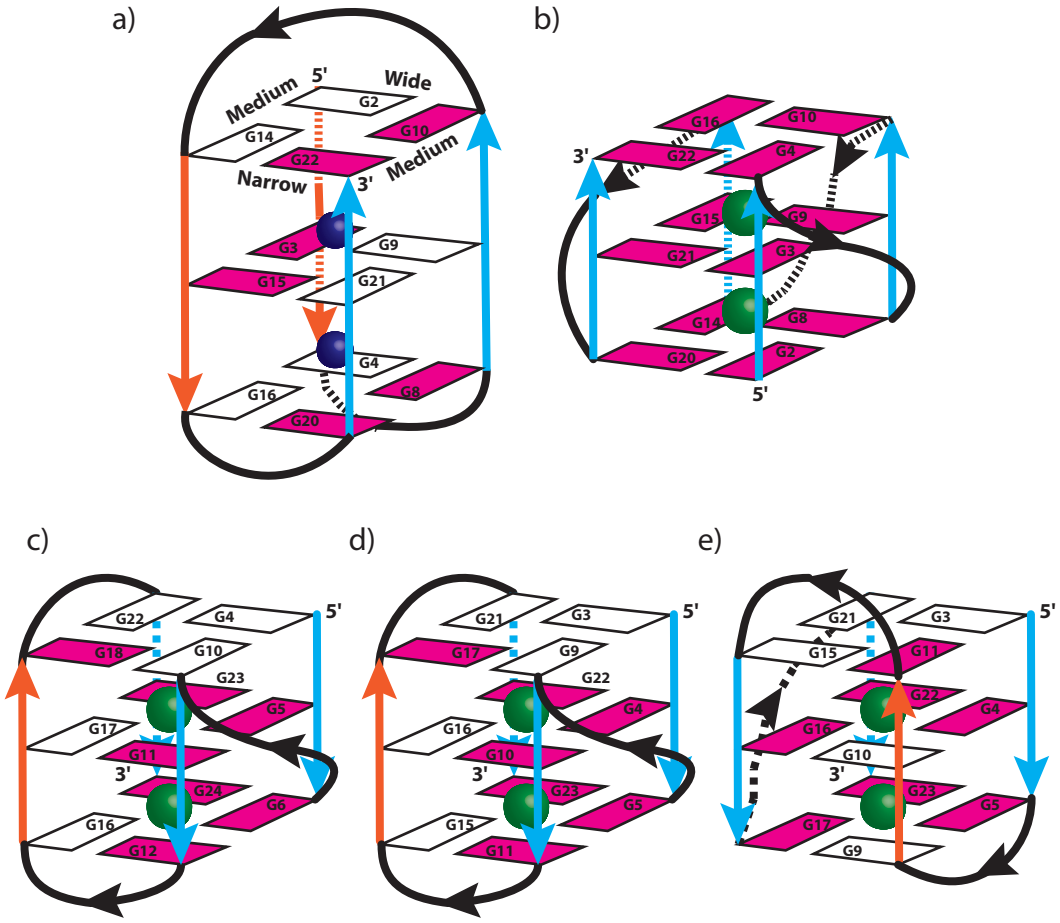

a) and b) 22mer sequence: 5'- A GGG TTA GGG TTA GGG TTA GGG

c) 26mer sequence: 5'- TTA GGG TTA GGG TTA GGG TTA GGG TT

d) 24mer equence: 5'- TT GGG TTA GGG TTA GGG TTA GGG A

e) 25mer sequence: 5'- TA GGG TTA GGG TTA GGG TTA GGG TT

Figure 1.10 Schematics depicting the structures of the human telomeric G-quadruplex motif in a) Na^+-containing solution by NMR, b) K^+-containing crystal by x-ray diffraction, and c-e) K^+-containing solution by NMR. The bases are represented by parallelograms where magenta and white depict the *anti-* and *syn-* bases, respectively. The Na^+ and K^+ ions are represented by the dark blue and green spheres, respectively. The strands containing the G-tracts that are running in the same direction are depicted in the same color, either light blue or orange to demonstrate strand orientation with respect to neighboring strands. The TTA loops are shown in black. Images adapted from references 114 and 115, with permission.

1.2.3.2 Oncogene promoters

Besides telomeric DNA, the bioinformatics studies on the locations of putative quadruplex sequences (PQS) genome-wide revealed their existence in promoter regions of oncogenes − that is, the region immediately upstream from

the transcription start site in genes that have potential to cause cancer.[123] Remarkably, these genes tend to be important in cell signaling, some of which are included in Hanahan and Weinberg's six hallmarks of cancer (Figure 1.11).[62,63] Included in the list of genes that contain PQS in the promoter region are MYC,[124-127] KIT,[128,129] B cell lymphoma 2 (BCL-2),[130,131] vascular endothelial growth factor (VEGF),[132,133] platelet-derived growth factor α polypeptide (PDGFA),[134,135] KRAS,[136,137] and human telomerase reverse transcriptase (hTERT),[138] among others.[28,98,139]

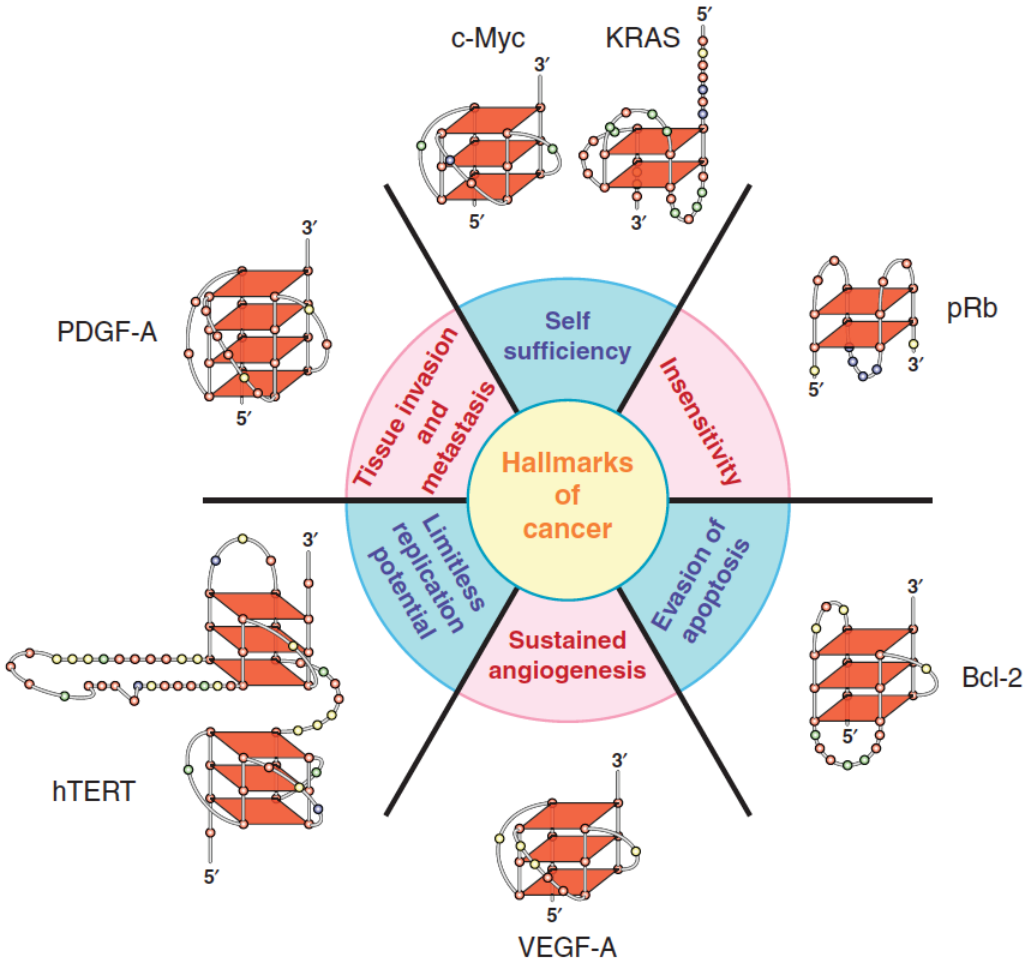

Figure 1.11 The six hallmarks of cancer shown with the associated G-quadruplexes found in the promoter regions of these genes. Figure reproduced from reference 139 with permission.

PQS can form in the promoter regions of some oncogenes, raising questions of their biological relevance. It is now a widely accepted hypothesis that the existence of PQS in gene promoters can be linked to the transcriptional

activity of the proximal gene. This hypothesis has led to the implication that small molecules that can selectively interact with such motifs may exert functional changes by specifically regulating the expression of the gene(s) modulated by these promoter sequences.[98,111,140] A simple representation of this concept is illustrated in Figure 1.12. In fact, the first example of this ability came from a study in the laboratory of Laurence Hurley in 2002, where they demonstrated that the small molecule porphyrin TMPyP4 (5, 10, 15, 20-tetra-(*N*-methyl-4-pyridyl)porphine, described later: Figure 1.18a) could down-regulate c-MYC and hTERT expression *in vitro*.[125,141]

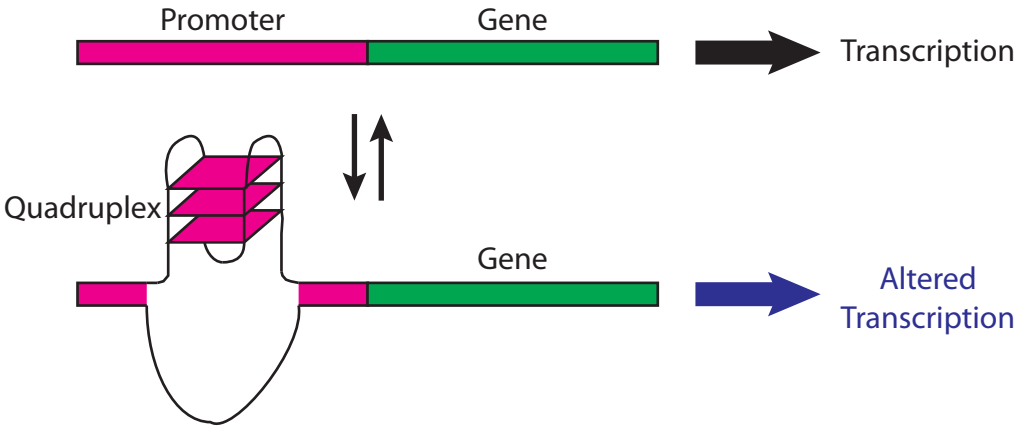

Figure 1.12 Schematic of the promoter G-quadruplex hypothesis. G-quadruplex-forming sequence motifs in the upstream (promoter) region (magenta) of genes (green) may fold into a G-quadruplex structure, resulting in altered transcription. Figure adapted from reference 111 with permission.

1.2.4 Targeting G-quadruplexes with small molecules

1.2.4.1 Binding modes

Duplex DNA has several features that present many avenues through which proteins and small molecules can interact with this motif. As previously mentioned, the biologically relevant B-form DNA consists of a double helix made up of two complementary strands that run antiparallel to each other, and are associated by hydrogen-bonding between A-T and C-G base-pairs. The single strands connect the bases *via* a deoxyribose-phosphate backbone which has an overall negative charge due to the phosphodiester linkage. The grooves (major and minor, *vide supra*) are also distinct and allow for recognition by binding

entities. Due to these features, small molecules typically bind to B-DNA *via* intercalation between the base-pairs, groove-binding, and electrostatic interaction with the backbone.[142] In a similar manner, small molecules can also bind to G-quadruplex DNA. One of the main goals in the design of G-quadruplex binders is to optimize selectivity and potency to this target while minimizing interactions with the far more abundant duplex DNA. G-quadruplexes are geometrically different from B-DNA with a surface area approximately twice as large as the double helix (Figure 1.13). Thus, almost all G-quadruplex binders reported to date have extended planar chromophores that are ideally suited to π-stack on or between G-tetrad(s) as they are too large to allow for intercalation between base-pairs of B-DNA (techniques for the characterization of these interactions are discussed later for both duplex and quadruplex DNA, Section 1.3).[143-145]

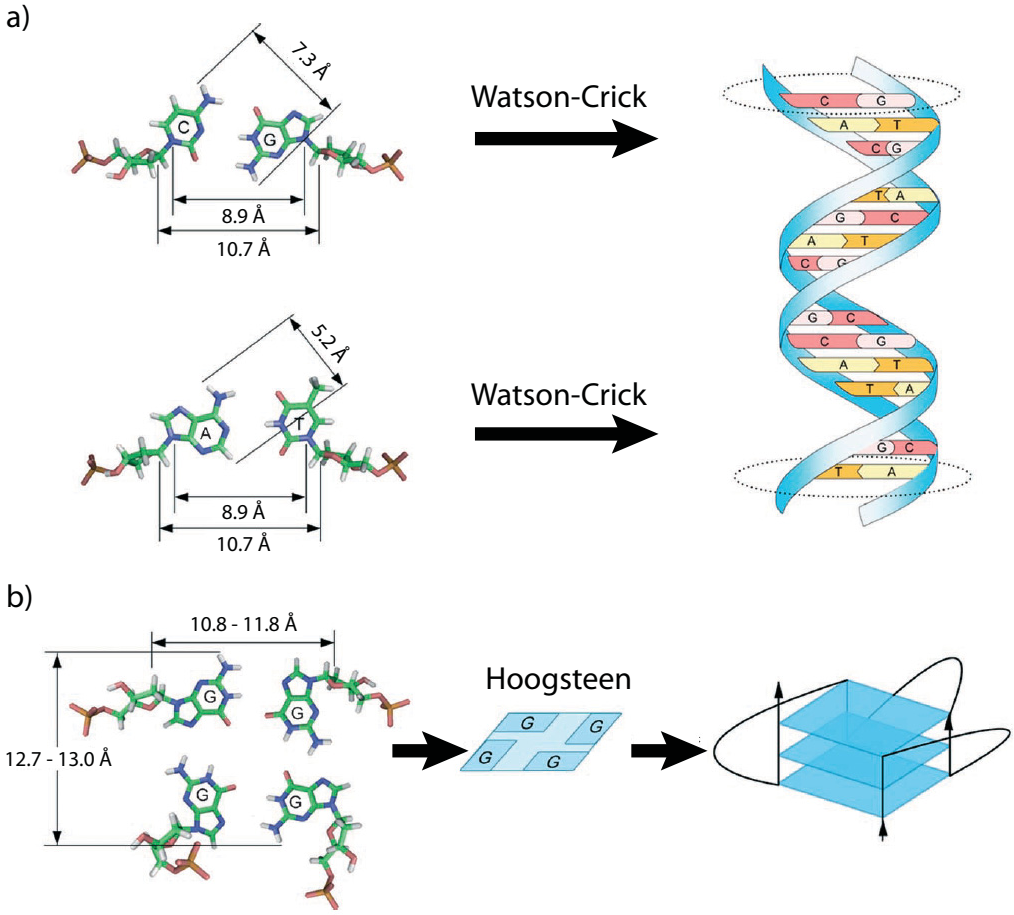

Figure 1.13 Comparison of the dimensions of duplex and G-quadruplex DNA structures; a) the double helix and base pair surface, and b) the quadruplex structure and G-tetrad surface. Reproduced from reference 146 with permission, John Wiley & Sons, 2014.

G-quadruplexes may also have several different groove environments defined by negatively-charged phosphate backbones, which allows for optimized design of cationic appendages for insertion into these grooves. The cation channel through the center of the tetrad stack also presents a targetable region. Finally, the different loop arrangements create various pockets into which features of the binders can insert, much like the binding pockets of proteins.[146,147] These different binding modes are illustrated in Figure 1.14. It is thought that small molecules that can achieve any combination of these binding modes would have higher affinity to G-quadruplex DNA than to B-DNA. The "true" intercalation shown in Figure 1.14b is thought to be an energetically costly binding mode requiring the unfolding or distortion of a tetrad layer. No molecules to date have been shown to exhibit this binding mode, preferring instead those modes shown in Figure 1.14a, and c-d.[67,135]

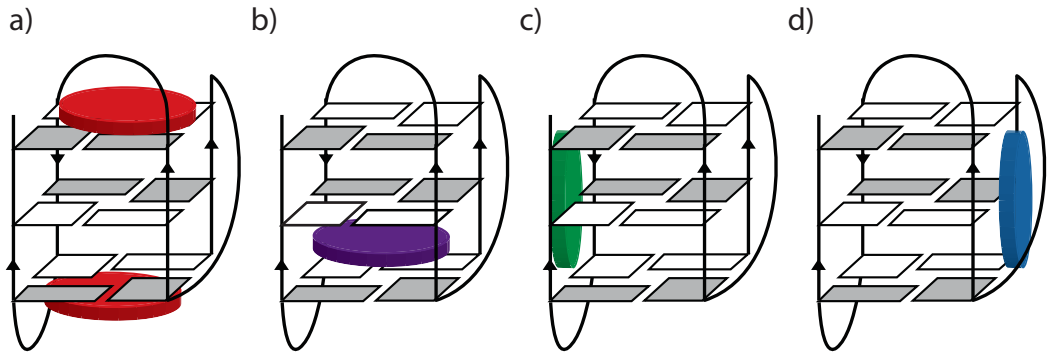

Figure 1.14 Representation of ligand-quadruplex binding modes with a) external stacking (red), b) intercalation (purple), c) groove binding (green), and d) loop interaction (blue). In general, intercalation (b) is thought to be difficult to achieve due to i) occupation therein by cations and ii) an energetically costly distortion of the structure to allow for insertion of a large molecule.[72,146]

The past decade was ripe with the development of a large variety of ligands that were designed with the characteristics of an ideal G-quadruplex binder in mind. These ligands have since been extensively reviewed and categorized mainly by elemental components – for example, organic or metal-based.[148-151] Within the organic realm, binders have been organized into categories by which a positive charge is introduced into the scaffold (e.g., *N*-methylation, *in situ* protonation, etc.) or by ring structure (e.g., fused, macrocyclic, etc.). Within the metal-based category, they are sorted by geometry and type of metal present,

as well as how many metal centers are included. Herein, the binders have been split into the two main types: organic and metal-based. The organic category is then split into species based on core ring structure (fused aromatics, macrocycles, other), while the metal-based category is split into species based on metal geometry (octahedral, square-planar, other).

1.2.4.2 Organic G-quadruplex binders

1.2.4.2.1 Fused aromatic systems

The first published report of a G-quadruplex interactive ligand appeared in 1997 from the Neidle laboratory on the interaction of a 2,6-diamidoanthraquinone with telomeric DNA and subsequent telomerase inhibition *in vitro* (Figure 1.15a).[152] This compound demonstrated a 23 μM IC_{50} for telomerase inhibition from a standard primer extension assay. Subsequent additions of alkyl-amino side-arms to the anthraquinone scaffold lead to compounds with IC_{50} values less than 5 μM. However, these compounds displayed inescapable binding to duplex DNA leading to poor selectivity for the quadruplex motif.[153,154] This series of compounds was a good starting point for quadruplex-ligand design and led to the observations that a larger π-surface area for more optimal overlap with the tetrad surface, and the inclusion of several side-arms with *in situ* protonable side-arms could increase affinity for quadruplex DNA while decreasing affinity for B-DNA. From a structure-activity relationship between side-arm length and telomerase inhibition, the Neidle laboratory demonstrated that the ideal appendage was a pyrrolidinylpropanamide from the 3- and 6- positions.[155] Further substitution at the 9- position lead to the development of BRACO-19 (Figure 1.15b), a compound that was shown to have a higher binding affinity to G-quadruplex DNA compared to B-DNA (10–70x larger), using surface plasmon resonance (SPR) assays.[156] Since then, a flurry of investigations into alternate trisubstitution patterns (2,6,9- and 2,7,9- versus 3,6,9-),[157] and longer groups at the 3-, 6-, and 9- [158,159] positions, did not significantly improve upon BRACO-19 binding. This compound has been studied both *in vitro* and *in vivo* and has been shown to induce growth arrest in mice with human tumor models in addition to exhibiting a

low nanomolar IC_{50} for telomerase.[160,161] Despite all its favorable characteristics, lack of membrane permeability and a small therapeutic window size are drawbacks of BRACO-19 as a candidate for clinical trials.[162] However, patents issued by Cancer Research Technology Limited, UK, could prove interesting for the development of BRACO-19 as a clinical candidate.[163]

Similarly to the trisubstituted acridines, the design of trisubstituted isoalloxazines presents an avenue for selective binder design (Figure 1.15c). The most remarkable in this series is a binder that showed a 14-fold selectivity for a *c-Kit* quadruplex motif over the telomeric motif through SPR assays.[164] This finding allowed the suggestion that binders could be selective between quadruplex motifs rather than just between quadruplex and duplex DNA.

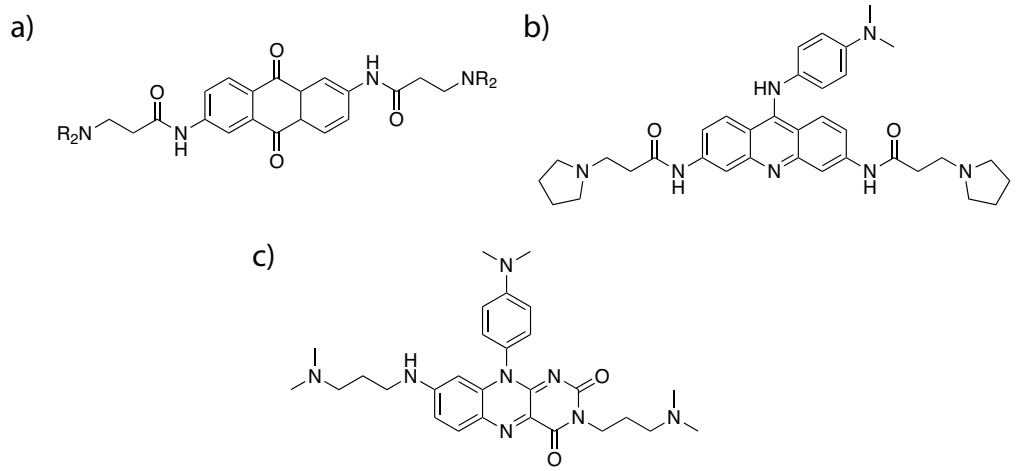

Figure 1.15 G-quadruplex binders based on a) anthroquinone, b) acridine (BRACO-19), and c) isoalloxazine scaffolds.

Extending the 3-ring system of the anthroquinone, acridine, and isoallozazine scaffolds to a 4-ring system brings us to the quindoline scaffold. In general, there are two types of these crescent shaped molecules, the disubstituted,[165,166] and the 11-substituted[167,168] derivatives. Initially, this scaffold showed modest selectivity to quadruplexes over B-DNA, but further investigations have led to the development of SYUIQ-5 (Figure 1.16a), a compound that could induce senescence and telomere shortening in cells.[169] It was later discovered that SYUIQ-5 achieved this outcome through the down-regulation of *c-Myc* transcription and expression which in turn, inhibited hTERT expression, thus inhibiting telomere elongation.[170] However, this conclusion has

been disputed recently. Studies from the Hurley laboratory on SYUIQ-5 and its analogs have shown that these quindoline compounds are primarily non-selective for particular quadruplex motifs and any anticancer activity should be attributed to interaction with multiple quadruplex elements. This disagreement encourages caution when assigning effects of *in vitro* G-quadruplex-interactive compounds to those effects arising *in cellulo*.[171]

Further extension of the ring scaffold to 5-ring systems leads to pentacyclic quinacridine (or dibenzophenanthroline) and acridinium salts. This ring-extension results in a larger π-surface area of the compound, translating into more optimal overlap with the surface of the quadruplex. A representative of these quinacridines is shown in Figure 1.16b. Through a fluorescence-based melting assay (See Section 1.3.1.2.1 for details on this assay), this compound, MMQ_3, demonstrated high thermal stabilization of a telomeric quadruplex motif ($\Delta T_{1/2}$ = 19.7°C, where $\Delta T_{1/2}$ refers to the change in melting temperature resulting from stabilization of the quadruplex by the compound compared to quadruplex without added compound) and considerable telomerase inhibition (IC_{50} = 0.028 μM).[172] However, derivatives of this compound with more or longer alkyl-amino side-arms containing several protonable sites did not show higher selectivity for G-quadruplex DNA over B-DNA, as was the case with the acridine series.[173,174] It was assumed that the increased positive charge allowed for groove-binding to B-DNA. Efforts to link two MMQ compounds to create a macrocycle (BOQ_1, Figure 1.16c) resulted in a compound that is more selective for quadruplex over B-DNA, due to its inability to insert into the double helix and preference for end-stacking.[175] While this compound did exhibit higher thermal stabilization of the telomeric quadruplex motif ($\Delta T_{1/2}$ = 28°C), it was not able to achieve the same telomerase inhibition as MMQ_3 (IC_{50} = 0.13 μM).

The acridinium salts, on the other hand, have exhibited notable telomerase inhibition even without the inclusion of side-arms. Interestingly, RHPS4 (Figure 1.16d) binds selectively to triplex and quadruplex structures over B-DNA by differential dialysis and shows an IC_{50} value less than 0.50 μM for telomerase, in addition to exhibiting favorable pharmaceutical properties including significant

uptake into the nucleoli of MCF-7 breast cancer and A459 adenocarcinoma cell lines.[176,177] RHPS4 was also shown to cause apoptosis in melanoma lines *via* its ability to cause telomere-capping alterations.[178] In fact, these desirable characteristics led to success as a single agent with high therapeutic efficacy in melanoma mouse models,[179] and as a combination therapy with taxol in uterus carcinoma xenografts,[180] which validates RHPS4 as a candidate for clinical development.

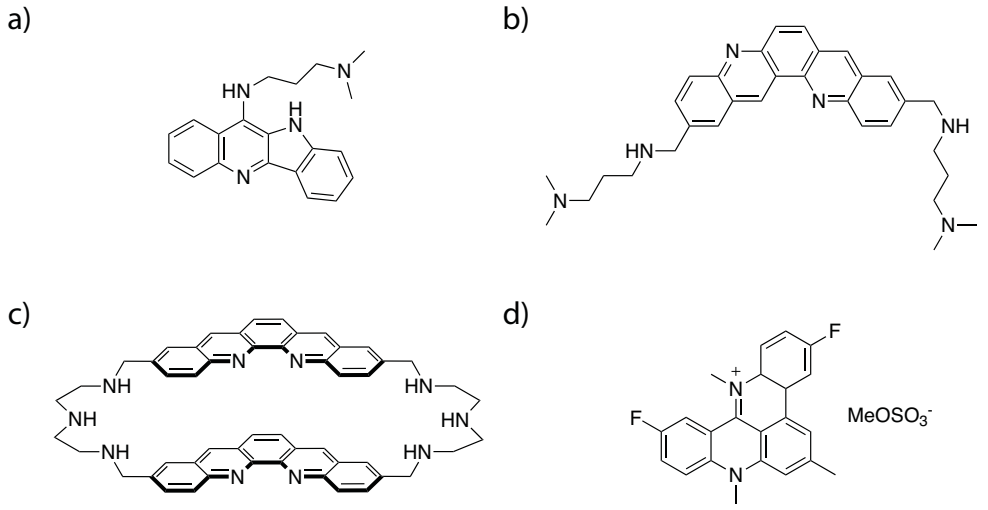

Figure 1.16 Four- and five- ring G-quadruplex binders a) SYUIQ-5, b) MMQ_3, c) BOQ_1, and d) RHPS4.

Fluoroquinolone scaffolds represent one of the most successful G-quadruplex binders in clinical trials to date. Quarfloxin (Figure 1.17a), by Cylene Pharmaceuticals, has two chiral amino side-arms that may allow for it to recognize groove and loop regions of specific polymorphs. In fact, it has been shown to disrupt the interaction between the protein nucleolin and a quadruplex motif that forms in ribosomal DNA.[34,181] The interaction between nucleolin and ribosomal DNA is critical for rRNA biogenesis in cancer cells.[182]

The last scaffold to mention here is the highly π-extended perylene derivatives, namely PIPER (Figure 1.17b). Interestingly, PIPER exhibits a higher IC_{50} value than the previously discussed binders ($IC_{50} > 20$ μM),[183] but was shown to bind selectively to G-quadruplex DNA at pH 8.5 *via* an aggregation binding mode. The aggregation of this complex at pH 8.5 is not surprising as the alkyl-amino side-arms are presumed to be neutral and the highly π-extended surface is

far from water-soluble, thus the hydrophobic aggregation on the surface of the G-tetrads is expected.[184] Due to the insolubilities, the Bianco group has investigated water-soluble perylene derivatives prepared through the incorporation of alkyl-amino side-chains on the bay-area of the core.[185] The compounds show much less self-aggregation spectroscopically and exhibit IC_{50} values around 5 μM for telomerase, compared to 20 μM for the first generation.[186] The best in the series was shown to induce selective telomere damage in transformed human fibroblast cells through the dissociation of telomeric protein POT1 and subsequent growth arrest.[187] These studies, and others,[188,189] have validated the use of water-soluble perylene derivatives as G-quadruplex interactive agents and the next challenge is to find success in a clinical setting.

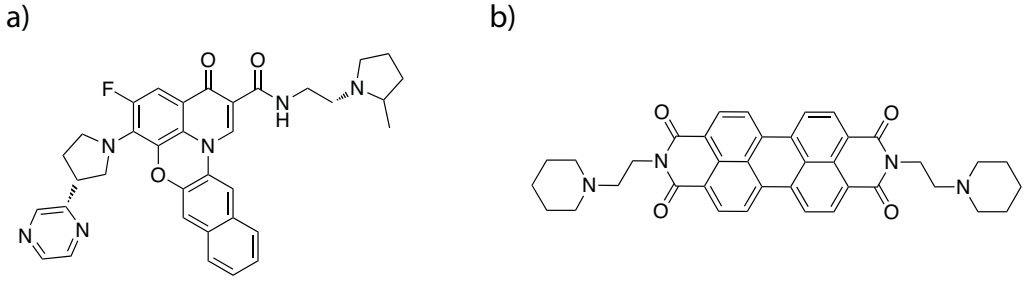

Figure 1.17 G-quadruplex binders a) quarfloxin and b) PIPER.

1.2.4.2.2 Macrocyclic systems

Beyond the binders of the fused aromatic ring variety, including macrocyclic rings composed of fused aromatics like BOQ_1 (Figure 1.16c), another category exists that contains two classes of the most commonly studied compounds: porphyrins and the natural product telomestatin (and derivations thereof). The cationic porphyrin TMPyP4 (Figure 1.18a) has been the subject of many studies since Photofrin® (a mixture of dihematoporphyrins) was shown to be successful for photodynamic therapy on superficial cancers.[190,191] TMPyP4 has a 4+ charge due to the N-methylated pyridines at the vertices of the porphyrin core. While this 4+ charge does allow for water solubility, it also contributes to its promiscuous nature and low selectivity between quadruplex and B-DNA.[192] This promiscuity also holds true between quadruplex polymorphs, and there are a large number of *in vitro* studies of TMPyP4 targeting a variety of said

polymorphs.[125,133,134,136,141,193-195] Derivations of the porphyrin scaffold have shown varied success for selective targeting[196] with the most successful being a pentacationic manganese(III) version with four extended side-arms that exhibits 10,000-fold selectivity for telomeric sequences over B-DNA from an SPR assay (*vide infra*, Figure 1.24b).[88] Besides adding bulky side-arms, the expansion of the porphyrin core to a diselenosapphryn moiety (Se2SAP, Figure 1.18b) has increased selectivity 40-fold between the c-myc sequence and B-DNA by SPR.[197]

The "gold-standard" G-quadruplex binder telomestatin is a member of the polycyclic oxazole macrocycle family. Telomestatin is a natural product that can be isolated from *Streptomyses anulatus*. It consists of seven oxazole and one thiazoline ring and is ideally suited as a G-quadruplex binder based on size match to the G-tetrad surface (Figure 1.18c).[198] Indeed, this size match allows telomestatin to induce the formation of intramolecular quadruplex structures from duplex DNA containing the human telomeric sequence. Additionally, telomestatin was found to be a potent telomere maintenance-disabling drug candidate in cervical carcinomas, multiple myeloma, leukemia, and breast cancer by inducing apoptosis in cancer cells without harming normal cells.[45,101,106,199,200] While telomestatin is considered the "gold-standard", its synthesis is lengthy and not suited for the pharmaceutical setting.[201,202]

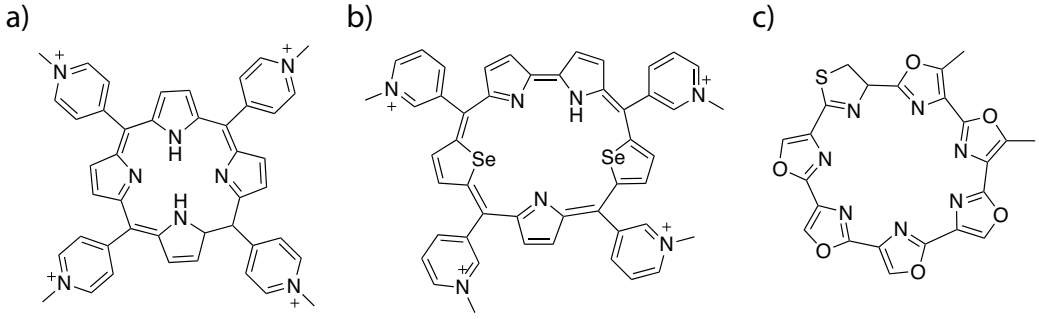

Figure 1.18 Macrocyclic G-quadruplex binders a) TMPyP4, b) Se2SAP and c) telomestatin.

The macrocyclic nature of telomestatin is a favorable molecular model for quadruplex binders and has inspired the development of oxazole-based peptides,[203,204] cyclo[n]pyrroles,[205] and macrocyclic hexa- and heptaoxazoles,[206-209] among others.[89] Of note are the oxazole-based peptides of the

Balasubramanian group that contain three amino side-arms that are protonated at physiological pH. Biophysical studies suggest that appropriate side-arms are critical for designing binders that can select between polymorphs, as the ring-system π-stacking with the G-tetrad surface is common among all polymorphs. An example of this improved selecticity comes from Figure 1.19a, a compound whose side-arms affect 3-fold selectivity for the ckit quadruplex motif over human telomeric sequences.[203,204] Interestingly, a heptaoxazole has found success as a fluorescent probe for visualizing G-quadruplexes in human adenocarcinoma and cervical cancer cells. When 7OTD (Figure 1.19b) is conjugated to a BODIPY dye and then incubated with the cancer cells, it is shown to colocalize with DAPI-labelled nuclei.[208,209] This study demonstrates that G-quadruplex binding agents can be utilized as probes for G-quadruplex formation *in cellulo* in addition to cell growth arrest and apoptosis-inducing agents.

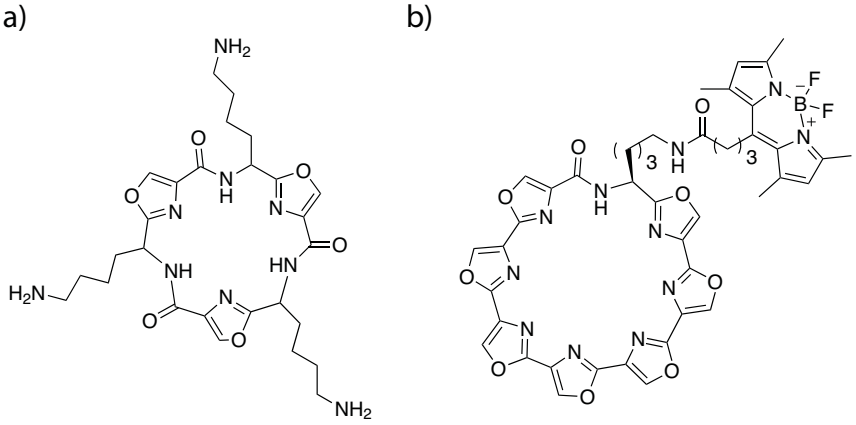

Figure 1.19 Macrocyclic G-quadruplex binders; a) oxazole-based peptide, and b) 7OTD conjugated to a BODIPY dye.

1.2.4.2.3 Other systems

The final category of organic binders contains a mixture of systems whose cores are not *fully* fused aromatic rings nor macrocyclic in nature. The butterfly-shaped bisquinolinium compounds like those in Figure 1.20a (360A is shown) utilize internal hydrogen bonds to hold the core of the compound in a planar conformation rather than relying on fused aromatics to do the same. These internal hydrogen bonds result in high affinity for G-quadruplex DNA ($\Delta T_{1/2}$ = 21°C, > 50-100 fold selectivity for G-quadruplex over B-DNA).[210] Analogs

containing inverted amide connectivities, and thus, inability to internally hydrogen bond, exhibited loss of affinity.[211] Further expansion of aromaticity from pyridine to bipyridine to phenanthroline was shown to significantly enhance its interaction with G-quadruplex DNA (Figure 1.20b).[212] Fluorescent probes have also been developed from this scaffold, similarly to the heptaoxazole-BODIPY conjugates previously described, where the dye thiazole orange is incorporated (Figure 1.20c).[213] Although thiazole orange is a promiscuous dye,[214] inclusion into the G-quadruplex binding scaffold appears to increase fidelity to the G-quadruplex motif.[213]

Other butterfly-shaped compounds have been reported that include the biocompatible 1,4-substituted 1,2,3-triazole (e.g., Figure 1.20d).[215] This synthetic building block has been shown to help discriminate between G-quadruplex grooves as well as increase binding strength.[216-220] Interestingly, the compound in Figure 1.20d was shown to exhibit extensive groove-binding to G-quadruplex structures in molecular models, potentially explaining its ability to cause a structural rearrangement of the *c-Kit* polymorph by circular dichroism analysis. Interaction of the alkyl-amino arms with the grooves are thought to cause a decrease in the stacking of the tetrads which is consistent with unfolding.[220]

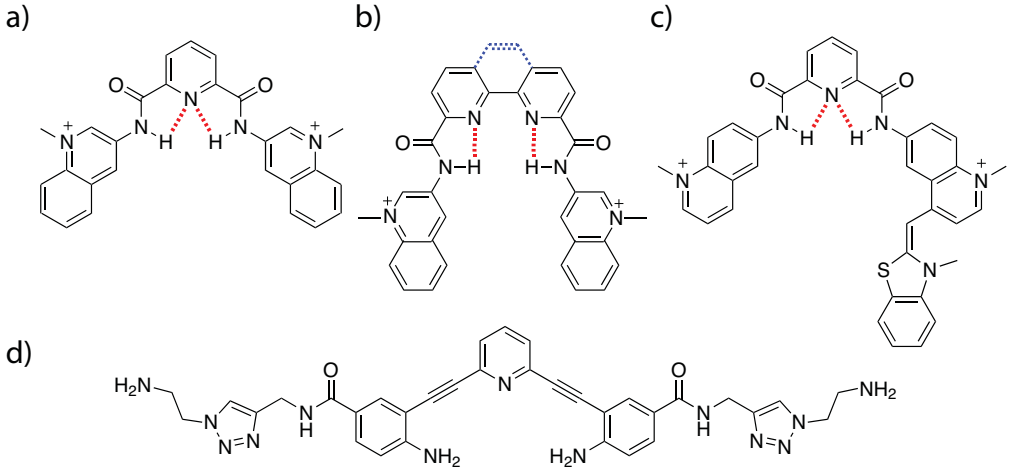

Figure 1.20 Butterfly-shaped G-quadruplex binders: a) 360A with a 2,6-pyridine-carboxamide core, b) bipyridine and phenanthroline derivatives, c) thiazole orange-conjugate, and d) triazole-containing groove binder. Internal hydrogen bonds are represented by red dashed lines.

From the examples presented above, several characteristics for optimal G-quadruplex binders are evident. These include optimal size and shape overlap of

the π-surfaces of the binder and the G-tetrad, and the inclusion of alkyl-amino side-arm(s) to interact with the grooves while aiding in solubility in aqueous solutions.

1.2.4.3 Metal-based G-quadruplex binders

Metal-based complexes represent a growing field of G-quadruplex binders.[151] Metal complexes exhibit structural geometries that are unattainable for carbon-based molecules, in addition to electronic properties that can be successfully exploited for quadruplex recognition. Besides obtaining tight binding to quadruplex motifs, metal complexes can be harnessed for their catalytic, luminescent, and electrochemical properties. Furthermore, metal complexes can cause cleavage of DNA strands, resulting in promising cancer therapy alternatives.[221,222]

1.2.4.3.1 Octahedral complexes

Originally, octahedral complexes of zinc, cobalt, and ruthenium tris(phenanthroline) were discovered to be efficient B-DNA binders by intercalation, and the ruthenium complex exhibited a convenient "light-switch" effect upon binding.[223-230] Since then, the "light-switch" effect has been best described through [$Ru(phen)_2dppz$], (where dppz = dipyridophenazine, Figure 1.21a) and refers to the increased luminescence intensity of the complex in the bound state as compared to the free state, characterized by the group of Jacqueline Barton.[231,233] After extensive studies into the mechanism by which this occurs,[229,232,234] they determined that upon intercalation, the DNA base pairs protect the intercalated ligand from water, thereby resulting in enhanced luminescence. While this process is complex, in simple terms, protic solvents allow for partial proton donation to the nitrogens in the dppz ligand which in turn causes a new metal-to-ligand charge-transfer (MLCT) transition that results in radiationless decay rather than the intersystem crossing that results in MLCT emission in aprotic solvents.[233] Expansion of the ligand scaffold from small intercalating ligands like phenanthroline, bipyridine, and dipyridophenazine can create octahedral complexes with π-extended aromatic ligands that are ideal G-

quadruplex DNA binders. This is because they can bind electrostatically to the DNA backbone and hydrophobically to the G-tetrad surface.[235] The larger the π-surface of the ligands, the less likely the complex is to intercalate between the base pairs of duplex DNA. One of the first examples of an octahedral complex as a G-quadruplex binder is that of dinuclear $[Ru_2(phen)_4(tppz)]^{4+}$ (Figure 1.21a, where phen = 1,10-phenanthroline and tppz = tetrapyrido[3,2-*a*:2',3'-*c*:3",2"-*h*:2",3"-*j*]phenazine).[236] In the report, $[Ru_2(phen)_4(tppz)]^{4+}$ did show binding affinity towards duplex DNA, however, there was a more pronounced blue-shifted "light-switch" effect when bound to human telomeric quadruplex sequences, indicating a greater overlap between the aromatic surfaces of the ligands and the tetrads (and therefore more solvent exclusion) when bound to quadruplex as opposed to duplex DNA. While this complex does exhibit similar binding affinity between duplex and quadruplex DNA, the "quadruplex light-switch" effect could enable similar complexes as useful *in vivo* quadruplex probes. Another ruthenium complex that exhibits the "quadruplex light-switch" effect is dinuclear $Ru_2(obip)L_4$ (Figure 1.21b, where obip = 2-(2-pyridyl)imidazo[4,5-*f*][1,10]-phenanthroline and L = 2,2'-bipyridine) that behaves similarly to $[Ru_2(phen)_4(tppz)]^{4+}$ although selectivity between duplex and quadruplex was not reported.[237] In Figure 1.21, the difference between a duplex binder (Figure 1.21a) and quadruplex binders (Figure 1.21b-c) is shown through a comparison of the intercalation-capable $[Ru(dppz)(phen)_2]^{2+}$ complex with the larger π-extended tppz and obip dinuclear complexes.

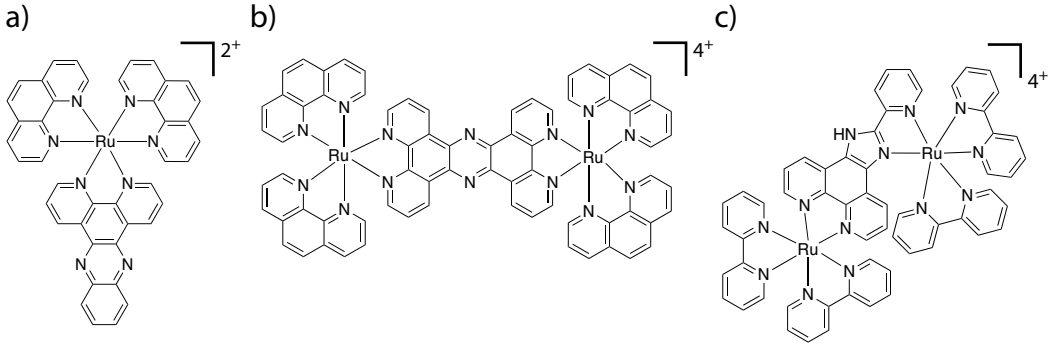

Figure 1.21 Octahedral ruthenium G-quadruplex binders: a) $[Ru(phen)_2(dppz)]^{2+}$, b) $[Ru_2(phen)_4(tppz)]^{4+}$, and c) $[Ru_2(obip)L_4]^{4+}$.

More recently, a few reports have emerged from Dik-Lung Ma's group on the interaction of iridium(III) complexes with G-quadruplex motifs. These complexes are mainly luminescent detectors of various activities involving the formation of G-quadruplexes, including the sensing of endonuclease IV activity, [238] adenosine triphosphate (ATP),[239] gene deletion,[240] and sub-nanomolar concentrations of lead(II) ions.[241] Worth mentioning here are the two cyclometallated complexes shown in Figure 1.22. The first, $[Ir(phq)_2(biq)][PF_6]$ (Figure 1.22a, where phq = phenylquinoline and biq = 2,2'-biquinoline) is a c-myc G-quadruplex stabilizer ($K = 8.26 \times 10^5\ M^{-1}$) that was shown to down-regulate c-myc oncogene expression in HepG2 cells transfected with a c-myc P1 promoter *via* a luciferase reporter assay. In this assay, when $[Ir(phq)_2(biq)][PF_6]$ stabilizes the transfected c-myc quadruplex *via* binding, the downstream luciferase gene expression is suppressed, resulting in reduction in luciferase activity compared to cells that have not been incubated with $[Ir(phq)_2(biq)][PF_6]$. Additionally, this complex was shown to be cytotoxic to HeLa cells ($IC_{50} \sim 0.2\ \mu M$), but was not tested for selectivity against normal cells.[242] The second complex, $[Ir(ppy)_2(bcp)][PF_6]$ (Figure 1.22b, where ppy = 2-phenylpyridine and bcp = 2,9-dimethyl-4,7-diphenyl-1,10-phenanthroline), was used in an elegant assay to detect endonuclease IV activity after cleavage of an abasic site of an engineered DNA sequence that releases a G-quadruplex motif. When the quadruplex is released, the complex binds, giving off an enhanced luminescence response.[238]

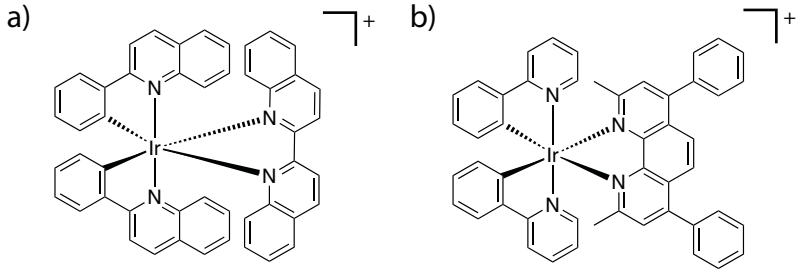

Figure 1.22 Examples of octahedral iridium G-quadruplex binders: a) $[Ir(phq)_2(biq)][PF_6]$ and b) $[Ir(ppy)_2(bcp)][PF_6]$.

The octahedral complexes presented demonstrate how much more these complexes can do besides behaving as simple G-quadruplex binders and telomerase inhibitors that elicit an anticancer effect. While they can still do all of

the above, the interesting luminescent properties allow for the development of various detection assays (see Chapter 4 for more information) and the complexes can be easily tuned for optimal *in vivo*/*in vitro* probing abilities through incorporation of different ligands.

1.2.4.3.2 Square-planar complexes

Since the discovery by Stephen Lippard and William Bauer in 1976 that ligand planarity is a stereochemical requirement for intercalation of platinum complexes into DNA,[243] square-planar metal complexes have become an especially interesting class of metal-based G-quadruplex binders These complexes are geometrically ideal in that the core of the molecule is enforced planar through ligand coordination, which results in optimal π-stacking with the surface of the tetrads. The most common binders of this variety are platinum(II)-based. In general, the core-ligand is either π-extended bipyridine, phenanthroline, or terpyridine-based that may or may not include alkyl-amino side-arms. We have reported several generations of platinum(II) phenanthroimidazole complexes that show preferential binding to quadruplex DNA over B-DNA,[244] in addition to selective killing of cancer cells compared to normal cells (see Chapters 2 and 3).[245] Interestingly, one of our side-arm containing complexes (Figure 1.23a) has shown high affinity to a *c-Kit* quadruplex motif with unprecedented slow unbinding kinetics from SPR assays (see Chapter 3).[246] The incorporation of the platinum metal presents an inherent positive charge and can, in principle, be positioned at the center of the G-tetrad binding surface. This is demonstrated through molecular modeling of a platinum(II) phenanthroline complex by Neidle and Vilar (Figure 1.23b).[247] Besides bidentate ligands, platinum(II) can also coordinate to the tridentate terpyridine.[248-250] Platinum(II) terpyridine complexes with alkyl-amino side-arms have seen moderate success in selectivity for quadruplex over duplex DNA with the complex in Figure 1.23c demonstrating a 13-fold preference for a *c-Myc* motif over duplex *via* fluorescent intercalator displacement (FID) assays with a binding affinity of $K = 1.2 \times 10^6\ M^{-1}$ from SPR.[249] Interestingly, the exchange of platinum(II) for palladium(II) in selected terpyridine complexes has demonstrated an increase in thermal stabilization of

quadruplex motifs compared to the platinated analogs by FRET melting assays ($\Delta T_{1/2}$ ~ 35°C versus ~ 9°C for the telomeric motif).[251] This is thought to be due to the faster activation of the reactive aqua-complex of palladium through the labile chloride ligand compared to platinum, and corresponding covalent binding to the N7 of guanine bases rather than the traditional non-covalent electrostatic binding (*vide infra*).[252-254]

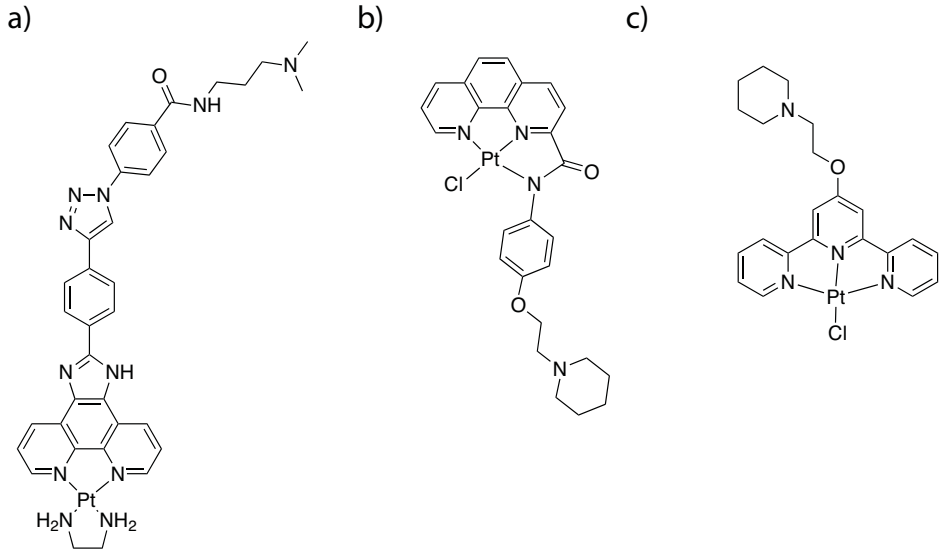

Figure 1.23 Square planar G-quadruplex binders: a) platinum(II) phenyl-phenanthroimidazole with triazole-linked side-arm, b) platinum(II) phenanthroline complex, and c) platinum(II) terpyridine complex with alkyl-amino side-arm.

Another interesting class of planar metal-based complexes arises from those whose ligands are not intrinsically planar. In this case, the metal itself induces the planar conformation. An example of this category is that of the nickel(II) salphen complexes by Neidle and Vilar.[87,255,256] The most notable complex (Figure 1.24a) demonstrated $\Delta T_{1/2}$ ~ 30°C from FRET melting assays for telomeric quadruplex DNA and ca. 1400-fold selectivity for quadruplex versus B-DNA *via* UV/Vis titrations ($K = 1.27 \times 10^7$ versus 8.96×10^3 M^{-1}).[256] In addition to nickel(II), salphen and salen complexes of copper(II), zinc(II), vanadium(IV), and manganese(II) have also been explored as G-quadruplex binders with varying success.[151,257]

The final class of planar complexes contains the metalloporphyrins. Since the unmetallated cationic porphyrins demonstrated great potential as quadruplex

binders (*vide supra*), the introduction of a metal center was thought to be an interesting avenue to increase binding strength and selectivity of this class of molecule. Additionally, metalloporphyrins introduce luminescent properties that can be utilized for studying interactions with the nucleic acid structures.[258,259] One of the first examples, in 2004, was the copper(II)-containing TMPyP4 binding to an intermolecular quadruplex motif with $K \sim 10^5\ M^{-1}$, however, binding affinity compared to TMPyP4 (unmetallated) was not significantly increased.[260] Since then, manganese(III), nickel(II), and zinc(II) derivatives have been reported with varying success.[261,262] One of the most successful metalloporphyrins in achieving selectivity between quadruplex and duplex DNA is the pentacationinc manganese(III) derivative (Figure 1.24b) with four extended side-arms that exhibits 10,000-fold selectivity for telomeric sequences over B-DNA from an SPR assay.[88] Iron(III)-heme porphyrins are an interesting topic as hemin-quadruplex complexes have been shown to be catalytically active, especially in oxidation reactions (see Appendix B).[263-267]

Porphyrin-analog scaffolds like phthalocyanines and corroles containing metal centers have also been reported.[41,268-270] Of note is the octa-cationic quaternary ammonium phthalocyanine by Ren *et al.*, (Figure 1.24c).[269] This complex was shown to have selectivity over an order of magnitude between telomeric quadruplexes and duplex DNA by SPR assays ($K \sim 8.3 \times 10^6\ M^{-1}$ versus $2.2 \times 10^5\ M^{-1}$). Besides telomeric G-quadruplexes, phthalocyanines can bind to promoter G-quadruplexes and regulate gene expression, demonstrating promise as transcription-interactive agents.[41] A manganese corrole (Figure 1.24d), on the other hand, was shown to selectively bind to telomeric G-quadruplexes with binding affinities ca. two orders of magnitude greater than duplex DNA by SPR assays ($K \sim 2 \times 10^6\ M^{-1}$ versus $3 \times 10^4\ M^{-1}$).[270]

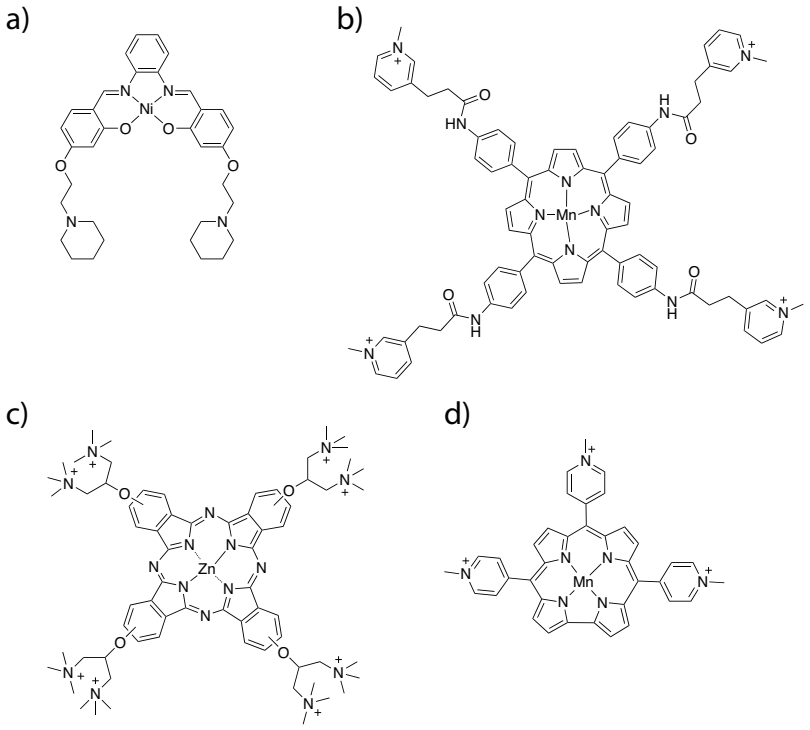

Figure 1.24 a) Nickel salphen complex, and porphyrin-analog scaffolds: b) pentacationic manganese(III) side-arm derivative, c) quaternary ammonium zinc phthalocyanine, and d) manganese corrole.

1.2.4.3.3 Other metal binders

While binders with other metal geometries (including square pyramidal and trigonal bipyramidal) have been reported,[248,271] these complexes tend to be poor binders, as the non-planar geometry interferes with favorable π-overlap of the binding surfaces. The greatest successes in this category have come from the supramolecular assemblies of metals linked by rigid organic bridges. We (*vide infra*), and others, have studied the use of the platinum(II)-square scaffolds of Fujita[272] and Stang[273] as G-quadruplex binders (Figure 1.25a-b).[274,275] Supramolecular self-assembly is an appealing strategy for synthesizing a large variety of complexes in a more expeditious way than traditional chemistry methods, as the spontaneous association of small building blocks into large, ordered systems can occur in a single, high yielding step.[276,277] In addition, the synthesis of these square scaffolds can be performed *via* mechanochemistry (see Appendix A).[278] The chiral helicate structure by Yu *et al.*,[279] (Figure 1.25c), was shown to bind to telomeric quadruplexes in its enantiomerically pure P-form and

greatly prefers this motif over duplex DNA by circular dichroism, gel electrophoresis, and fluorescence measurements.

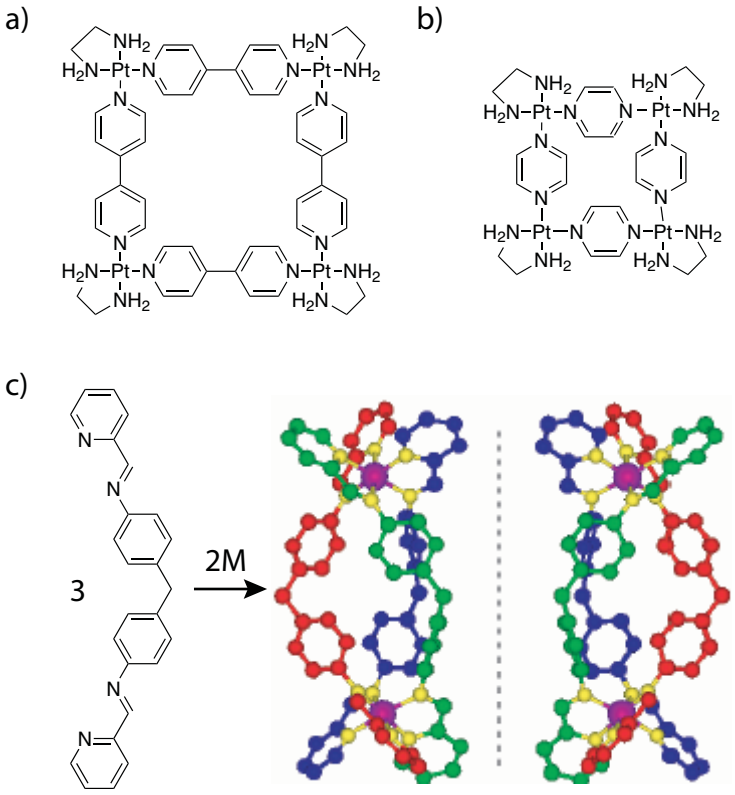

Figure 1.25 Supramolecular G-quadruplex binders: a) $[Pt(en)(4,4'\text{-bpy})]_4^{4+}$, b) $[Pt(en)(pyz)]_4^{4+}$, and c) helicate $[M_2L_3]$ where en = ethylenediamine, bpy = bipyridine, pyz = pyrazine, M = Ni or Fe. In a) and b) the en can be replaced with $-NH_3$ groups. Figure reproduced in part from reference 279 with permission.

While this is certainly not an exhaustive list of metal-containing G-quadruplex binders in the literature, the majority of the classes are represented. As previously indicated, metal complexes introduce electronic, geometric, catalytic, optical, electrochemical, and magnetic properties that are unobtainable with purely organic heteroaromatics. It was with these characteristics in mind that the development of metal-based G-quadruplex binders was first explored in the Sleiman laboratory.

1.2.4.4 Previous work from the Sleiman laboratory

Since the discovery of the structure of duplex DNA in 1953,[5] much interest has been in developing drug candidates that bind DNA, both covalently and non-covalently, due to their ability to destroy rapidly dividing cells.[280] One of

the most widely used class of metal covalent-DNA binders today is exemplified by *cis*-diamminedichloroplatinum(II) (cisplatin), a square planar platinum(II) complex with labile ligands (and its analogs). These compounds bind directly to two adjacent DNA bases upon loss of their chloride ligands (Figure 1.26).[281-283] By covalently binding to DNA in the genome causing both inter- and intrastrand crosslinks, cisplatin causes substantial damage to the DNA and its main biochemical effect is the inhibition of cellular replication (Figure 1.26b-c).[281,284] While this makes it a particularly valuable chemotherapy, a very important drawback is its lack of selectivity. Cisplatin indiscriminately affects all cells within the body, cancer or not, causing toxic side-effects. This non-selective targeting is a result of the lability of the chloride ligands under physiological conditions, thus allowing for the "activation" of the therapeutic aqua-form of the complex.

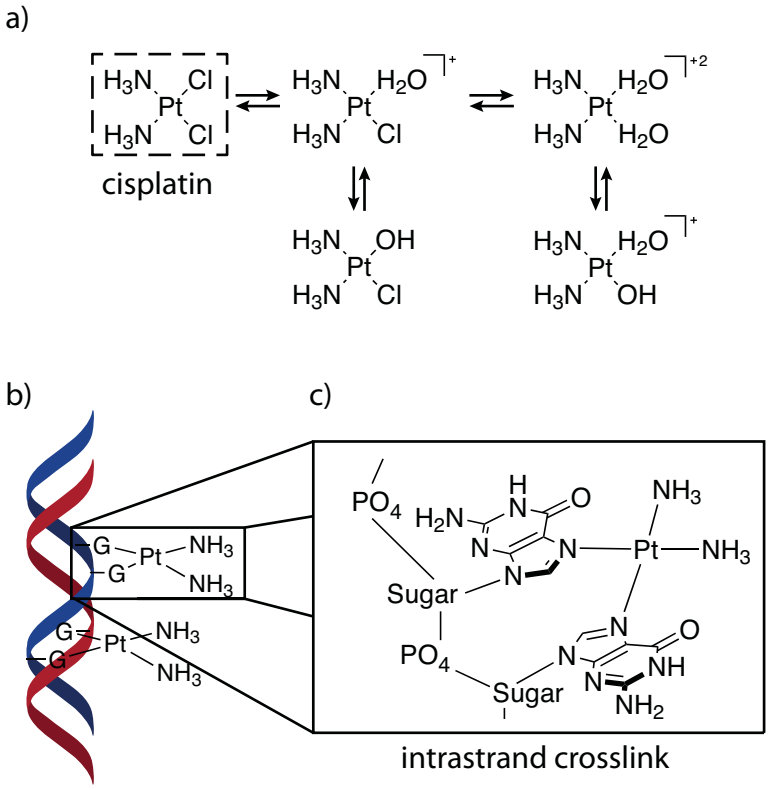

Figure 1.26 Method of action of cisplatin. a) Hydrolysis of cisplatin; as cisplatin loses the labile chloride ligands, several aqua-species may exist. b) These aqua-species are able to undergo inter- and intrastrand crosslinks with DNA (through the N7 of guanine bases), and c) zoom in of the mechanism of intrastrand-crosslink formation between adjacent guanine bases. Figure adapted from reference 281 with permission.

Although much success has been found with B-DNA targeting drugs, they are often very cytotoxic and cause unnecessary side-effects. Due to the target being rapidly-dividing cells, these chemotherapies can kill stem and germ cells, as well as bone marrow and hair follicles. Because of these off-target effects, more specific methods of DNA targeting are in need of development.

To this end, Roxanne Kieltyka, a previous student in the laboratory of Dr. Hanadi Sleiman, developed the use of platinum(II) ethylenediamine and phenanthroline complexes as G-quadruplex targeting agents. These complexes behave differently in aqueous media than do cisplatin-like species. Here, the ethylenediamine ligand is a stronger σ-donor than is ammonia, resulting in a larger ligand-field splitting, and therefore, a more stable complex. Additionally, the phenanthroline ligand is a π-acceptor, rather than a π-donor like chloride, which results in π back-bonding and further increases the ligand-field splitting. Together, this allows these complexes to possess more stable ligand shells than cisplatin and, as a result, they can display more selective antitumor profiles, (e.g. unable to covalently bond indiscriminately to DNA).

Using a combination of molecular modeling (in collaboration with Prof. Nicolas Moitessier's group) and biophysical studies, Roxanne was able to show that two platinum(II) phenanthroimidazoles with extended π-surfaces afford greater binding affinity to the tetrameric, intermolecular G-quadruplex than to duplex DNA. Her studies suggested that coupling the square-planar geometry of platinum(II) with phenanthroimidazole ligands of the π-extended variety could result in a simple and modular method to create effective G-quadruplex selective binders (Figure 1.27).[244]

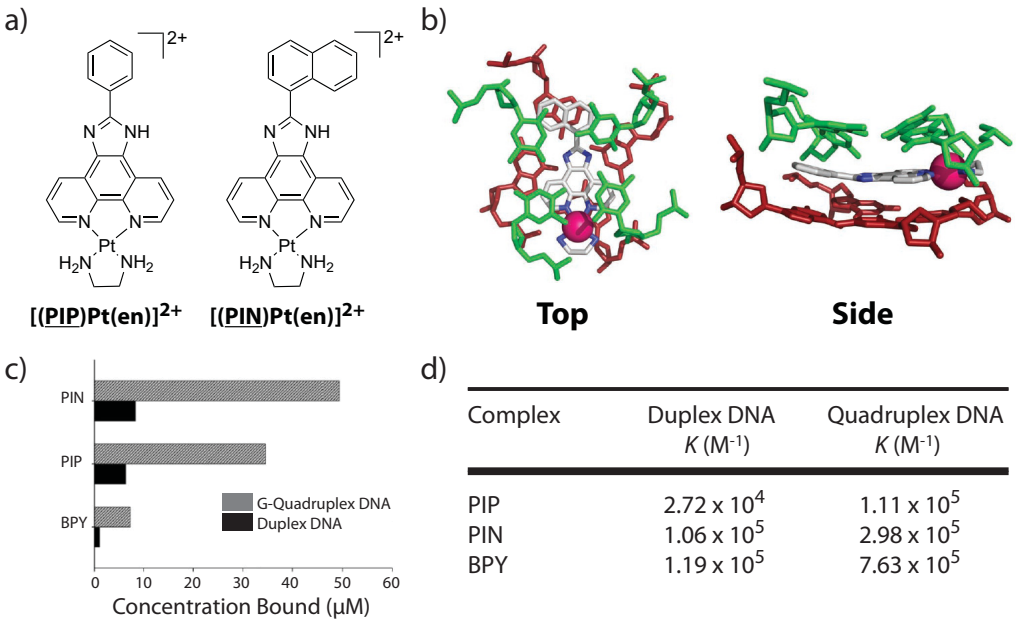

Complex	Duplex DNA K (M^{-1})	Quadruplex DNA K (M^{-1})
PIP	2.72×10^4	1.11×10^5
PIN	1.06×10^5	2.98×10^5
BPY	1.19×10^5	7.63×10^5

Figure 1.27 Previous work from our laboratory: a) platinum(II) phenanthroimidazole complexes **[(PIP)Pten]$^{2+}$** and **[(PIN)Pten]$^{2+}$**; b) predicted interaction of **[(PIN)Pten]$^{2+}$** and the intermolecular G-quadruplex; c) competitive dialysis results showing preference for binding to G-quadruplex over B-DNA for the complexes compared to a negative control **[(BPY)Pten]$^{2+}$**; d) binding affinities towards calf-thymus and G-quadruplex DNA determined *via* equilibrium dialysis experiments. Figure reproduced from reference 244 with permission, John Wiley & Sons, 2014.

In addition to phenanthroimidazole complexes, Roxanne also showed that the supramolecular platinum(II) square complex developed by Fujita[272] and Stang[273] was an effective G-quadruplex binder and telomerase inhibitor. In this study, she used molecular modelling, FRET-melting (Section 1.3.1.2.1) and telomerase inhibition assays to demonstrate that the platinum square complex displays high binding affinity to human telomeric G-quadruplexes and inhibition of telomerase activity, thus showing the potential of supramolecular self-assembly for the development of scaffolds that can effectively target these biological structures.[274]

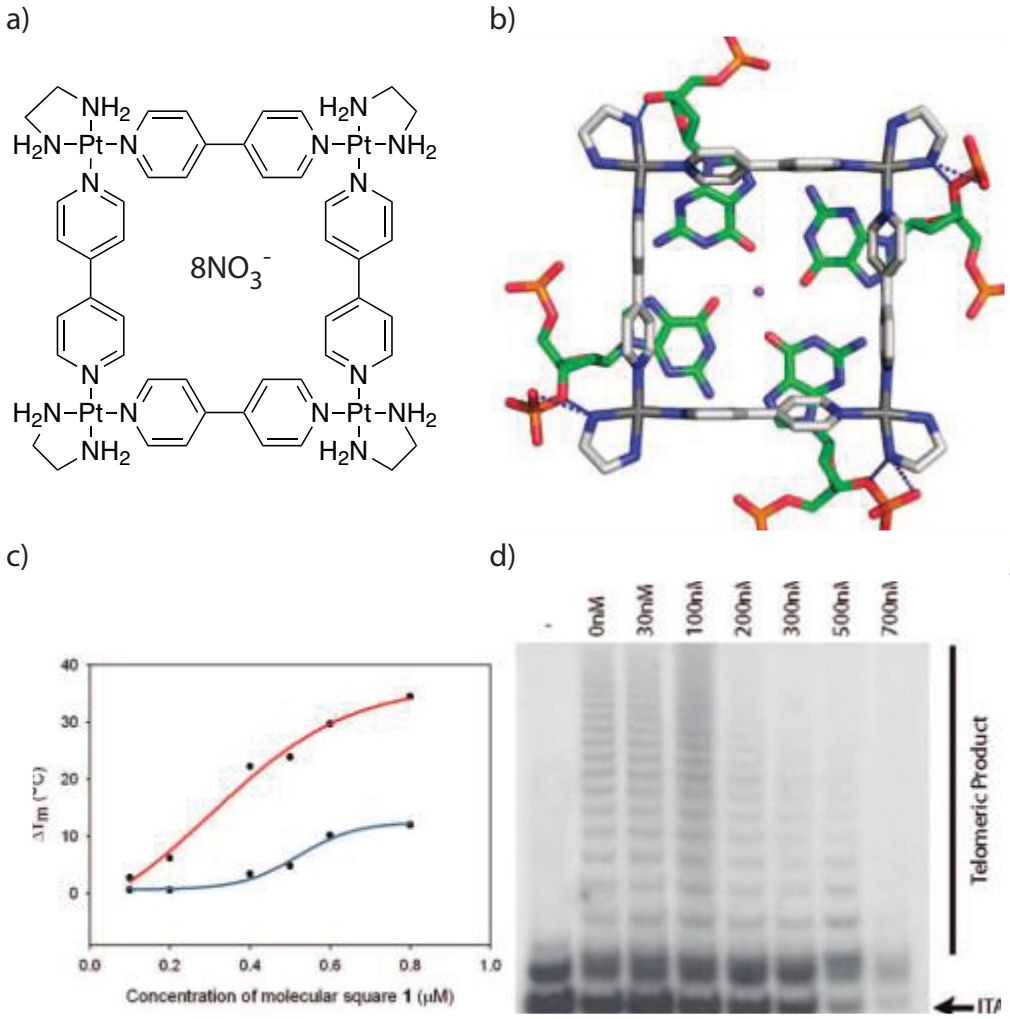

Figure 1.28 Previous work from our laboratory: a) structure of the platinum molecular square; b) average structure of the complex between the square and the h-telo G-quadruplex; c) FRET stabilization curve of the square with quadruplex (red) and B-DNA (blue) as a function of concentration of square; d) TRAP assay results showing ladders generated by the action of telomerase on a telomeric substrate primer. Figure reproduced from reference 274 with permission, Americal Chemical Society, 2014.

Taken together, Roxanne's thesis work demonstrated that platinum(II) phenanthroimidazoles and supramolecular platinum(II) assemblies represent synthetically accessible motifs that are ideally suited for G-quadruplex recognition. Additionally, with the help of molecular modelling, these motifs can be expanded into libraries of complexes that are readily tunable for optimal quadruplex discrimination.

1.3 Biophysical and techniques for characterization of G-quadruplex structure and binding

The most common experiments in chemical biology involve assays that determine to what extent molecules interact with each other. In the context of this thesis, we are interested in the interactions between small molecule drug candidates and DNA motifs (both G-quadruplex and B-DNA). To this end, we have conducted several biophysical assays utilizing absorbance, fluorescence, and surface-mediated techniques to evaluate the thermodynamic and/or kinetic aspects of DNA binding by small molecules. The techniques listed below include circular dichroism (CD) and UV/Vis spectroscopies, Förster resonance energy transfer (FRET) melting studies, fluorescence intercalator displacement (FID) assays, and surface plasmon resonance (SPR) assays. However, there are instances in the literature of other techniques including, but not limited to, nuclear magnetic resonance (NMR),[107,173,183,285-291] electrospray ionization mass spectrometry (ESI-MS),[251,292-298] isothermal titration calorimetry (ITC),[236,275,289,299-301] and gel electrophoresis.[175,242,302-304]

1.3.1 Spectroscopic techniques

1.3.1.1 Absorbance-based techniques

1.3.1.1.1 Circular dichroism

CD templation studies are carried out in **Chapter 2**, **Chapter 3**, and **Chapter 5**. CD titrations with quadruplex and duplex motifs are performed in **Chapter 5**.

Circular dichroism is a spectroscopic technique that has been used to investigate the structure of B-DNA, G-quadruplex DNA and ligand binding modes to different motifs, as characteristic spectral signatures correspond to specific features thereof.[305-307] This method relies on irradiation of either a chiral complex or an achiral complex in a chiral environment with circularly polarized light. As the light passes through the sample, there is differential absorption of right- and left-handed circularly polarized light, which results in a CD absorption spectrum or signature.[306] As the G-quadruplex structure is chiral, we can observe specific peaks that are characteristic of certain polymorphs. For example,

antiparallel G-quadruplexes typically exhibit a strong negative peak around 260 nm and a strong positive peak around 295 nm. On the other hand, wholly parallel G-quadruplexes show a weak negative peak around 240 nm and a strong positive peak at 260 nm. Additionally, as many polymorphs share both antiparallel and parallel strands, their signatures may comprise a mixture of the above.[307] The spectra of the antiparallel and mixed parallel/antiparallel G-quadruplexes from the human telomeric DNA are shown in Figure 1.29, for example.

Besides determining structural information of the G-quadruplexes themselves, one can also obtain information regarding ligand orientation when binding to G-quadruplexes. When a non-chiral molecule interacts with a chiral molecule in such a way that the non-chiral molecule adopts the chirality of its binding partner, induced CD (ICD) peaks may be present. They are so called, because the binding event "induces chirality" upon the non-chiral molecule. One can determine from the ICD whether the molecule is a groove-binder (large positive ICD) or an intercalator of DNA (small negative or small positive ICD). Even if no ICD is present, we can still obtain valuable information on how a ligand binds by the changes to the spectra of the G-quadruplex. If the peaks of the G-quadruplex are enhanced or unchanged, one can conclude that the ligand may stabilize the structure. If the peaks undergo dramatic differences (either partial/complete disappearance of peaks and/or development of new peaks altogether), one can conclude that the ligand either destablilizes the structure or converts it into a new polymorph.

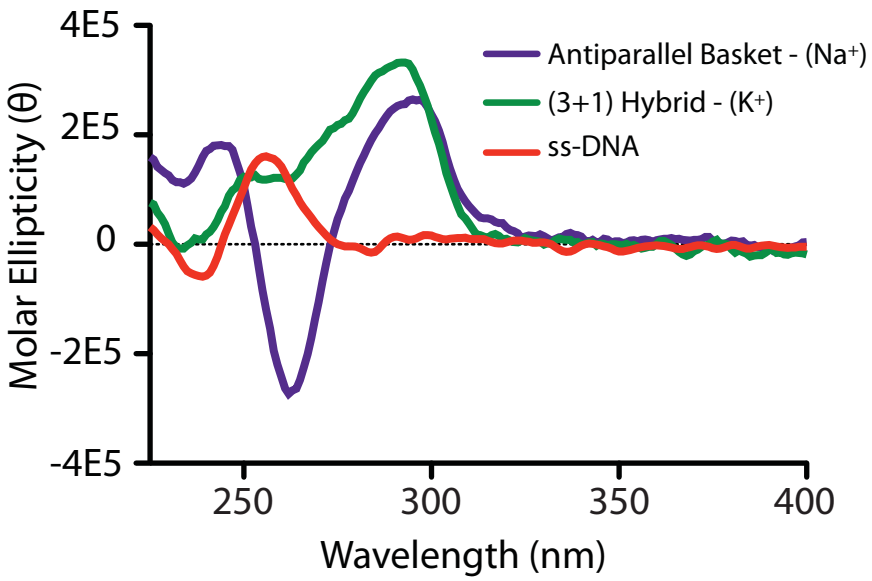

Figure 1.29 The CD spectra of the antiparallel (purple) and mixed parallel/antiparallel (green) G-quadruplexes based on the human telomeric DNA sequence (5'-A($G_3T_2A)_3G_3$-3'), and (red) single-stranded DNA of the same sequence.

CD templation experiments can be conducted to determine whether a G-quadruplex binder templates or enhances the folding of an unstructured putative quadruplex sequence (PQS) into a specific G-quadruplex polymorph. This is carried out by titration of the single-stranded or unstructured sequence with a small molecule binder. In order to ensure that the PQS is unstructured, it is best to dialyze the sequence against deionized water for 1−3 days before aliquoting into a tris(hydroxymethyl)aminomethane-based buffer since the presence of potassium and sodium cations induces quadruplex formation. Lithium-containing cacodylate buffers or added lithium salts (e.g. LiCl), could be used as lithium does not induce the formation of G-quadruplexes.[308,309] In this assay, if templation occurs, a decrease in the circular dichroic peaks associated with the single-stranded oligonucleotide (slight negative peak at 238 nm and strong positive peak at 257 nm) and the concomitant appearance of peaks associated with G-quadruplex structures are expected.

1.3.1.1.2 UV/Vis spectroscopy

Molecules can undergo electronic excitation from the ground to excited state by absorbing UV/Visible light. Specifically, these electronic transitions are evident from 200−900 nm for molecules like biopolymers, conjugated organic

compounds and transition metal complexes, as the energy difference between the highest occupied molecular orbital (HOMO) and lowest unoccupied molecular orbital (LUMO) decreases.[310] The greater the electronic conjugation (or unsaturation) of the molecule, the smaller the π-π* energy gap becomes, meaning lower energy light can enable the transition.[311] When studying interactions between DNA and small molecule binders, the changes to their respective transitions through monitoring their UV/Vis spectra reflect the intensity and specificity of the interactions (e.g. binding constants).[312] As DNA is a conjugated biopolymer, the absorbance of the whole is a sum of the spectra of the component parts that arise from transitions of the purine and pyrimidine bases, as such the absorbance maximum is located at 260 nm. For the small platinum molecules studied herein, the heterocyclic nature of the phenanthroimidazole ligands results in strong absorbance between 250−320 nm (assigned to ligand-centered π-π* transitions), which overlaps significantly with the absorbance of the DNA. Weaker platinum(II) dπ-π* metal-to-ligand charge-transfer (MLCT) bands around 400 nm are not intense enough at the desired concentrations (1−10 μM) for determination of binding affinity by UV titrations. As such, the significant overlap in absorbance at 260 nm has caused difficulty in the measurement of binding affinity.

Generally, binding constants can be determined for ligands binding to DNA *via* spectroscopic binding titrations.[313] In this assay, a solution of ligand at a known concentration is titrated with increasing amounts of DNA with the UV/Vis spectrum measured between titration points. If binding occurs, a decrease in absorbance maximum and concomitant red-shift of the peaks for the ligand will be evident. This is due to the alignment of electric transition dipole moments of the DNA-ligand complex and π-stacking, respectively. Typically, the absorbance maximum of the small molecule should be significantly different from that of the DNA (> 300 nm) such that the signals do not overlap.[313]

In **Chapter 2**, we attempted to measure the binding affinity of complexes **2.1**-**2.7** to G-quadruplex and B-DNA by monitoring the changes in the UV/Vis spectrum of the complexes after titrating solutions of DNA. As previously

mentioned, the absorbance maximum of the ligand should be greater than 300 nm, however in our case, due to the weak metal-to-ligand charge-transfer (MLCT) around 400 nm, the shoulders of the ligand-centered π-π* transitions around 300−320 nm were used. This made it necessary to subtract the absorbance of the DNA from each titration point so that only the changes in the platinum(II) chromophores would be observed. For these extended aromatic complexes, the experiment was complicated by the aggregation of the platinum complexes in solution at the start of the experiment and the consequent difficulty in obtaining the initial absorbance for the free, unstacked complex (Figure 1.30). This is a common problem for this technique,[314] since most G-quadruplex binders possess extended aromatic rings. In light of this observation, other methods were investigated, namely the fluorescence intercalator displacement assay (*vide infra*).

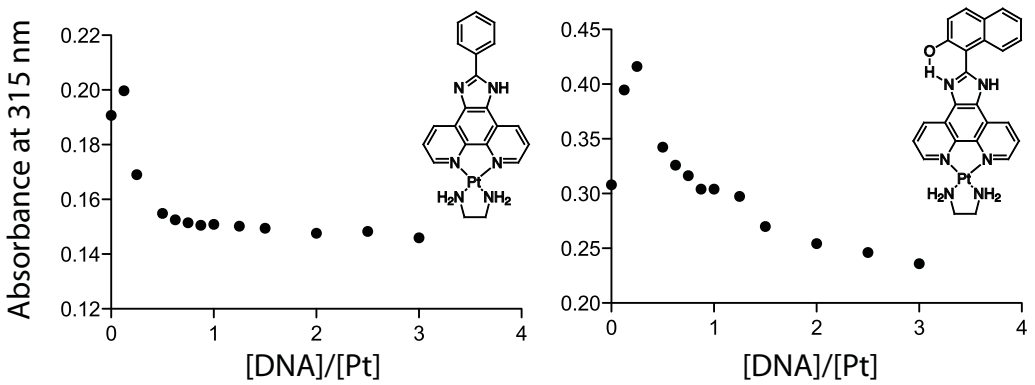

Figure 1.30 Example of data obtained for UV/Vis titrations with complex **2.1** (left) and **2.6** (right). For complex **2.1**, the absorbance at the zero point is lower than the point corresponding to the first aliquot of quadruplex, representing aggregation of the complex at the start of the experiment. For complex **2.6**, the zero point and the point corresponding to the first aliquot of quadruplex are lower than the second aliquot. This demonstrates that the greater the aggregation of the complex in solution, the more pronounced this effect becomes.

In **Appendix B**, we use the biologically relevant Fe(III)-hemin molecule as the ligand for binding to the G-quadruplex motifs. In this case, the absorbance maximum is 389 nm and is far removed from the DNA absorbance signal. Thus, UV/Vis binding titrations were used to determine binding constants with human-telomeric G-quadruplexes in a 96-well microplate format.

1.3.1.2 Luminescence-based techniques

1.3.1.2.1 FRET melting

The Förster resonance energy transfer (FRET) melting experiment gains insight into stability imparted by the small molecules on G-quadruplex motifs at elevated temperatures. This is a well-established technique[315] that relies on heating a dually-labelled nucleic acid structure (either quadruplex or duplex hairpin-forming sequences) with carboxyfluorescein (FAM, Figure 1.31a) and carboxytetramethylrhodamine (TAMRA, Figure 1.31b) at the ends of the sequence, in the presence of DNA binders while monitoring DNA denaturation from the onset of fluorescence. FRET is a spectroscopic technique that can provide information on the distance between the dyes with increasing temperature. When the DNA is folded, the dyes are in close proximity, allowing an energy transfer to occur from the excited donor (FAM) through a weak dipole-dipole interaction in a nonradiative process to the unexcited acceptor (TAMRA) if the dyes are within 10–80 Å of each other.[316] Other dyes can be used as long as there is spectral overlap between the emission wavelength of the donor and the absorption band of the acceptor.[317,318] Upon denaturation, the dyes separate, disallowing energy transfer, thus resulting in observable fluorescence by the donor. Therefore the $T_{1/2}$ is the temperature at which onset of fluorescence is detected and this is taken to be the structure's melting temperature. In this assay, compounds that cause the elevation of the $T_{1/2}$ of the DNA motifs compared to DNA without the presence of the compound are said to thermally stabilize the motif, and hence exhibit a higher binding affinity.[319] This process is illustrated in Figure 1.31c).

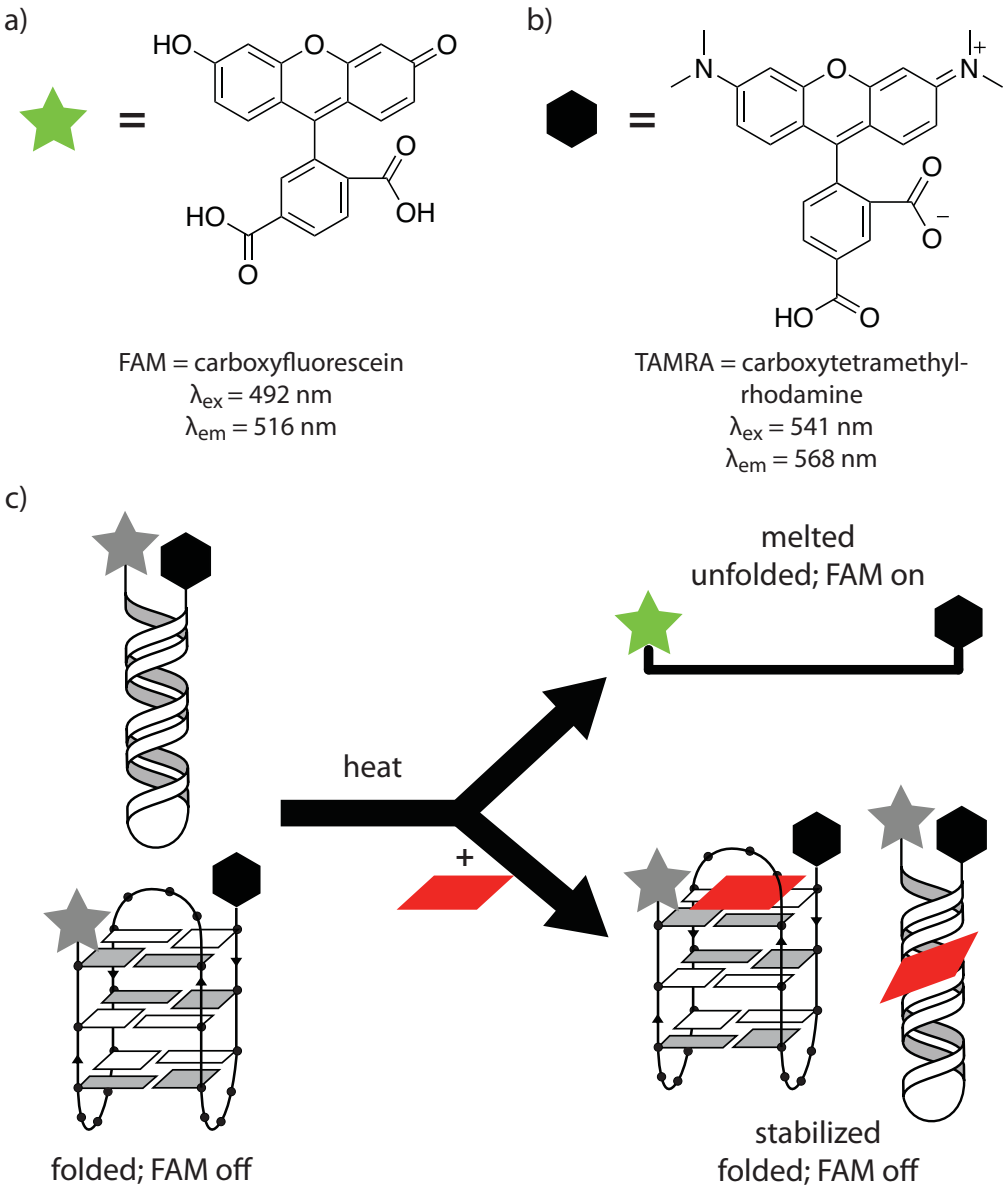

Figure 1.31 Structures of a) FAM, and b) TAMRA, with c) the schematic of the FRET melting assay. As the temperature increases, without added binder (c, top) fluorescence onset occurs at a lower melting temperature, whereas a binder (c, bottom) retards the melting, delaying the onset of fluorescence.

In **Chapter 2**, we used a human telomeric sequence (5'-FAM-$G_3(T_2AG_3)_3$-TAMRA-3') and a duplex hairpin (5'-FAM-TATAGCTATA-HEG-TATAGCTATA-TAMRA-3', where HEG = hexaethylene gylcol) for comparison. While there were significant melting temperature differences with and without our platinum complexes ($\Delta T_{1/2} \sim 20°C$), the concentration of complexes required to effect these changes was higher than for other potent G-quadruplex binders (5

μM versus 1 μM). The control experiment in Figure 1.32 using the monolabelled sequence 5'-FAM-$G_3(T_2AG_3)_3$-3', showed that platinum complex **2.4** can quench the fluorescence of the FAM dye attached to the DNA strand, thus interfering with the fluorescence measurement. Therefore, we discontinued the use of the FRET melting experiments as the interpretation of our results were complicated by changes in the dye fluorescence by the extended aromatic G-quadruplex binders.[320] As previously mentioned, a wide variety of other biophysical assays exist that are used to determine binding affinity of binders to DNA.

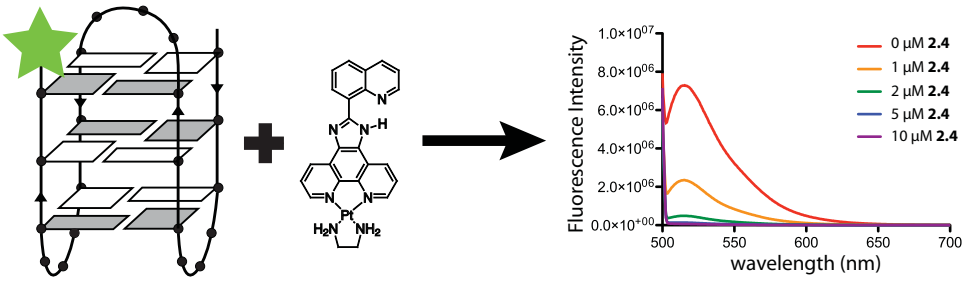

Figure 1.32 Schematic representing a control experiment for quenching of FAM by complex **2.4**. First, the mono-FAM labelled G-quadruplex (200 nM) is excited at 494 nm and the fluorescence is measured (red line on graph). Then, aliquots of complex **2.4** are added and the fluorescence of the FAM is measured after each aliquot. After 1 μM of added complex **2.4**, more than half of the fluorescence of FAM is quenched.

1.3.1.2.2 FID and HT-FID assay

FID assays were performed in **Chapter 2**. HT-FID assays were performed in **Chapter 3** and **Chapter 5**.

The fluorescence intercalator displacement (FID) assay is a binding assay based on work by Teulade-Fichou and coworkers.[214] It relies on competitive displacement of the dye thiazole orange (TO, Figure 1.31a) from the DNA target using small molecule binders, with concomitant decrease in the fluorescence intensity of the dye. Thiazole orange is highly fluorescent when bound to the G-quadruplex (or B-DNA) motif and exhibits binding affinities between $1.0x10^{6.0}$ and $1.0x10^{6.7}$ M^{-1} depending on the sequence to which it is bound,[321] and generally binds *via* intercalation (B-DNA)[322] and end-stacking (quadruplex DNA).[323] Conversely, the fluorescence of TO is negligible when unbound, that is, in aqueous solution. Thus, displacement of the dye by a stronger binder results in a reduction of the fluorescence of the dye. Binding affinity is evaluated from the

concentration of platinum complex that is required to give a 50% decrease in the dye fluorescence (DC_{50}). This process is illustrated in Figure 1.33b.

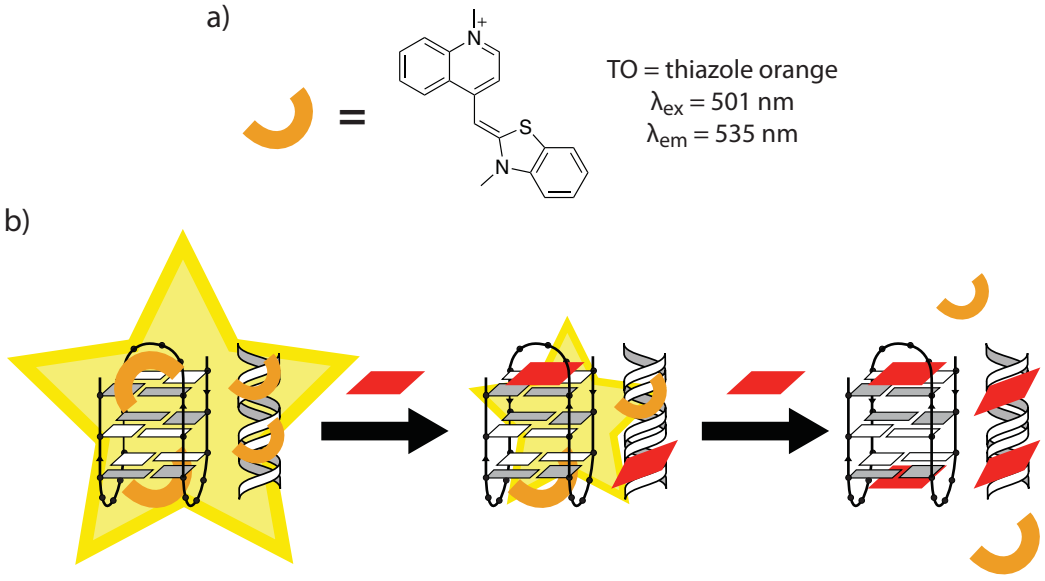

Figure 1.33 Structure of a) thiazole orange and b) schematic of the FID assay. Thiazole orange dye (orange crescent) fluoresces when bound to DNA. Additions of binder (red parallelogram) causes the displacement of the dye, and hence, decreased fluorescence.

Herein, two methods of the FID assay were conducted. In **Chapter 2,** the manual titration method was used. In this method, a solution of DNA and TO is measured, allowing TO to bind DNA (λ_{ex} = 501 nm). After this, a solution of ligand is titrated into the cuvette, with a 5−10 minute incubation before reading the fluorescence spectrum of the dye. In the end, a data set is obtained from 0−10 equivalents of added ligand (equivalents based on concentration of DNA). Percentage displacement (PD) is calculated by PD = 100 − [(F/F_0) × 100], in which F_0 is fluorescence intensity (F) without addition of platinum complexes, and F is the fluorescence intensity obtained from each titration point. The concentration of added complex is then plotted against the PD, and a DC_{50} value is determined by the concentration of platinum complex needed to achieve a 50% displacement of thiazole orange.

The second method involves the adaptation of the high-throughput FID (HT-FID) method of Teulade-Fichou and coworkers[321] so that it could be performed by a Biomek FX liquid handler and a SAGIAN core robot, carried out in a 96-well microplate. Briefly, buffer and complexes were aspirated from

dedicated reservoirs in a two-step procedure for a total volume of 100 μL into black 96-well plates. The complexes are tested in quadruplicate (that is two complexes per plate) where the buffer is first dispensed in decreasing volumes across the rows (100 to 0 μL), followed by each complex dispensed in increasing volumes across the rows (0 to 100 μL). Then, such that the final volume is 200 μL, 100 μL of a solution of the desired sequence plus TO is transferred to every well using the 96-multichannel pipetting head. After the incubation period, the fluorescence is read on a plate reader equipped with 485 ± 20 nm and 535 ± 35 nm filters for excitation and emission of thiazole orange, respectively. In the end, a data set is obtained from 1−10 equivalents of added ligand, and the DC_{50} is determined in an identical manner to the manual method. We found that this method was much more streamlined and allowed for lower standard deviations obtained between titrations. The HT-FID assay was conducted in **Chapter 3** and **Chapter 5**. For this assay, we used black polypropylene microplates rather than the suggested black quartz microplates.[321,324] Teulade-Fichou and coworkers noticed non-specific binding of their ligands to the surface of polypropylene plates which resulted in artificially high DC_{50} values.[321] We saw a similar phenomenon when we compared the results between the manual and the HT-methods for complex **2.7**. Due to this effect, we believe our values in **Chapter 5** may be overestimated and the manual method may be warranted for absolute determination of DC_{50} values.

1.3.1.2.3 Direct HT-luminescence assay

High-throughput luminescence assays were performed in **Chapter 4**.

In Chapter 5, in order to assess the binding affinity between the iridium complexes and G-quadruplex DNA, we harnessed their "G-quadruplex light-switch" ability – that is, the enhanced luminescence of the iridium complexes when bound to quadruplex DNA compared to aqueous solution. This assay is conducted in a similar manner to the HT-FID, except there was no need to use thiazole orange, and the assay was carried out in a 384-well microplate. Briefly, buffer and complexes were aspirated from dedicated reservoirs in a two-step procedure for a total of 40 μL in black polypropylene 384-well microplates. The

complexes are tested in quadruplicate (that is four complexes per plate) where the buffer is first dispensed in decreasing volumes across the rows (40 to 0 μL), followed by each complexes dispensed in increasing volumes across the rows (0 to 40 μL). Then, such that the final volume is 80 μL, 40 μL of a solution of the desired sequence is transferred to every well using the 96-multichannel pipetting head. After an incubation period of ~ 20 minutes, the luminescence is read on a plate reader equipped with 260 ± 10 nm and 595 ± 35 nm filters for excitation and emission of the iridium complexes, respectively. Due to the background luminescence of unbound complex, a blank run containing the complexes at the same concentrations in buffer (no added DNA) was used for subtraction. In the end, a data set is obtained from 1−10 equivalents of added ligand. The concentration of complex is graphed versus luminescence intensity and K_D values are obtained from fitting of the curves to a one-site binding model in GraphPad Prism 5.

1.3.2 Surface plasmon resonance assay (SPR)

SPR assays were performed in **Chapter 3** and **Chapter 5**.

Surface plasmon resonance (SPR) is a powerful technique to examine the binding specificity and kinetics of ligands for duplex versus G-quadruplex DNA.[194,249,261,291,325] Simply put, the technique involves the immobilization of one binding partner (here, DNA) on a the surface of a sensor chip, followed by the introduction of the other binding partner (here, the small molecule ligands) *via* flowing the solution over the immobilized surface. The binding between the DNA and the ligand can be monitored in real-time by SPR, which is a surface-sensitive detection technique. In a typical experiment, each sensor chip has four channels for analysis where one channel does not contain immobilized DNA, so that any non-specific interactions of the ligands with the surface of the sensor can be monitored. In our experiments, we use a gold-layered glass sensor chip coated with streptavidin that is attached to the surface *via* carboxymethyl dextran (CM-dextran). CM-dextran is a commonly-used coating composed of a linear polymer of 1,6-linked glucose units terminated with a carboxymethyl group (Figure 1.34).

It then attaches to streptavidin *via* an amide-linkage after activation through NHS-ester formation.[326] It also serves as a coating of the gold surface to minimize non-specific interactions with the surface itself.[327] The streptavidin coating allows for the capture of biotinylated-DNA sequences for DNA-ligand binding analysis (Figure 1.34). Fortunately, BIACore offers CM-dextran and streptavidin-coated chips that are ready for use, thus streamlining the entire process.

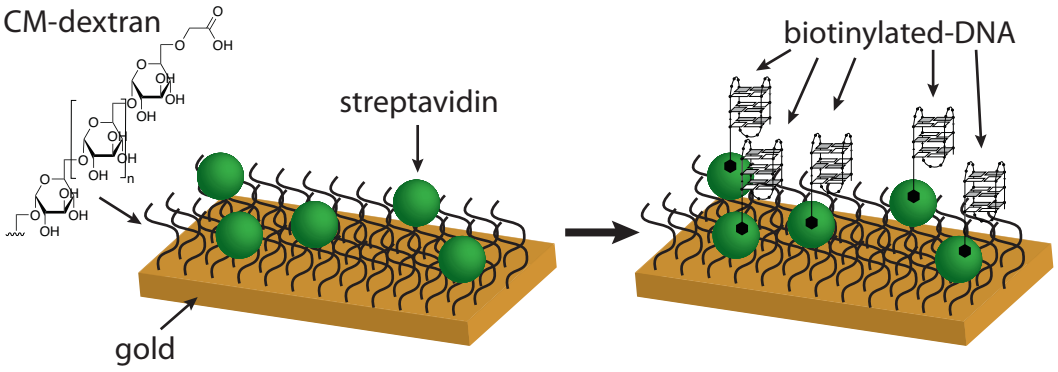

Figure 1.34 Simple schematic of an SPR sensor chip. A thin layer of gold is coated with CM-dextran to which streptavidin can bind. Biotinylated DNA is then immobilized on the surface through the streptavidin-biotin interaction.

After the immobilization of the biotinylated-DNA on the streptavidin-coated sufaces (Figure 1.35a), solutions of ligands are flowed over the entire chip at a controlled rate and allowed to interact with the DNA on the surface (Figure 1.35b).[328] SPR is a phenomenom that occurs from the light reflectivity of thin metal films and is sensitive to optical changes on the opposite surface.[329] The angle of reflection changes when the refractive index of the environment on the surface changes. Simply put, when a binding event occurs on the opposite side of the gold surface on which a light at a specific angle is shown, the reflected angle changes due to a change in refractive index.[329,330] A sensogram is obtained from the result of the detection of change in refractive index. If equilibrium is reached a constant signal will be seen (Figure 1.35b). Then, replacing the sample with buffer causes the bound molecules to dissociate, and the sensogram response decreases (Figure 1.35c). From the sensogram, one can acquire the binding affinity, specificity, and kinetics of the interaction.

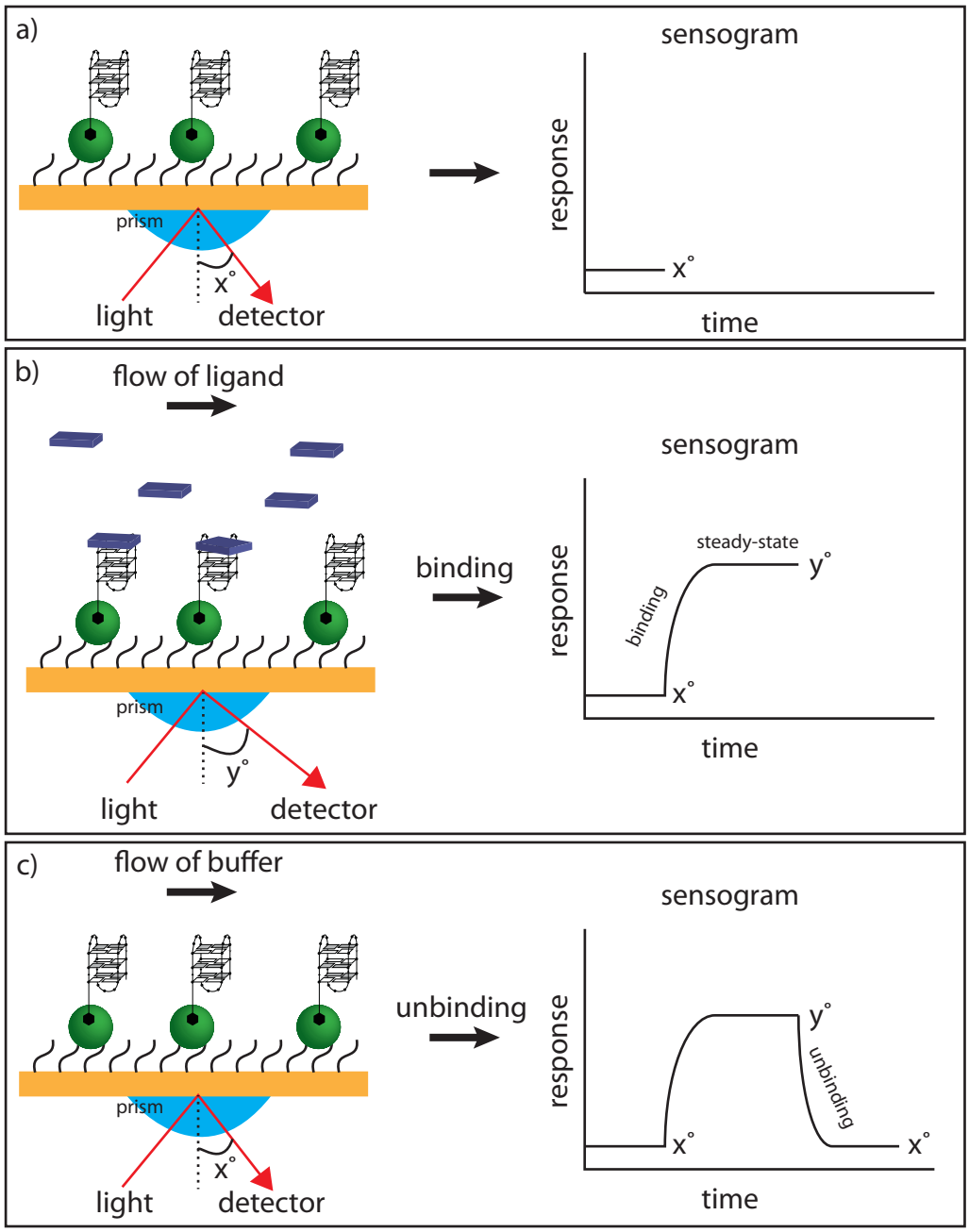

Figure 1.35 SPR assay schematic: a) in the first stage of the assay the angle of the reflected light from the unbound DNA-surface is measured as **x**. In step b), ligand is flowed over the surface at a controlled flow rate allowing for the interaction of the ligand with the immobilized DNA. Binding results in the change of refractive index to **y**, as shown on the sensogram. If equilibrium is reached, then no further change in refractive index is measured. In the last step c) the ligand is replaced by a flow of buffer to facilitate unbinding, which results in reestablishment of the initial refractive index **x**.

1.4 Thesis objectives

1.4.1 Phenanthroimidazole platinum(II) G-quadruplex complexes with extended π-surfaces as binders of human telomeric motifs

It has previously been shown in the Sleiman laboratory that platinum(II) phenanthroimidazoles display selective binding to intermolecular G-quadruplex motifs compared to B-DNA.[244] However, the more biologically relevant target in the human genome involves the intramolecular G-quadruplex based on the $TTAGGG_n$ repeats found in human telomeres. Additionally, the incorporation of intramolecular hydrogen bonds in the organic 2,6-pyridine, 2,9-bipyrine, and phenanthroline-dicarboxamide complexes (Figure 1.20a-c) was shown to enforce planarity of the binders and increase binding strength and selectivity for G-quadruplex motifs. With these goals in mind, in Chapter 2 we structurally evolve our library of phenanthroimidazole ligands towards optimal G-quadruplex binding. This occurs, specifically, through examining the effect of increasing π-surface area of the ligands through aromatic ring extension, through the introduction of different hydrogen bonding interactions and an electron-withdrawing substituent within the ligands. We investigate the complexes' interactions with telomeric G-quadruplexes through CD and FID assays, and we evaluate their abilities to inhibit telomerase through a modified telomerase repeat amplification protocol (TRAP-Lig). Lastly, we demonstrate selective cytotoxicity to HeLa cells, thus further validating our scaffold as potential therapeutics. This work was published in ChemMedChem under the title "Platinum(II) phenanthroimidazoles for targeting telomeric G-quadruplexes," **Castor, K.J.**; Mancini, J.; Fakhoury, J.; Weill, N.; Kieltyka, R.; Englebienne, P.; Avakyan, N.; Mittermaier, A.; Autexier, C.; Moitessier, N.; and Sleiman, H.F., ChemMedChem, **2012**, *7(1)*, 85-94.

1.4.2 Development of a platinum(II) phenylphenanthroimidazole with and extended side-arm for specific targeting of the *c-Kit* G-quadruplex

In Chapter 3, we utilize copper(II)-assisted azide-alkyne coupling (CuAAC) to create 1,4-substituted-1,2,3-triazole containing alkyl-amino side-arms. With the aid of molecular modelling, we hypothesized that the addition of the side-arm would allow for a multivalent binding mode of our platinum(II) complexes to G-quadruplex DNA (Figure 1.23a). Through the use of CD, HT-FID, and SPR, we discover that the presence of the side-arm allows for unprecedented slow dissociation kinetics from a quadruplex motif formed in the *c-Kit* oncogene promoter. Biological assays including an mRNA levels analysis of *c-Kit* mRNA and a western blot for cKIT protein exhibit an increase in cKIT production rather than the intended decrease that is expected from a promoter quadruplex-interacting agent. The findings in Chapter 3 warrant further mechanistic investigation into what happens *in cellulo* when oncogene-G-quadruplex interactive agents are utilized. This work was published in Chemistry – A European Journal under the title "A platinum(II) phenylphenanthroimidazole with an extended side-chain exhibits slow dissociation from a *c-Kit* G-quadruplex motif," **Castor, K.J.**; Liu, Z.; Fakhoury, J.; Hancock, M.A.; Mittermaier, A.; Moitessier, N.; and Sleiman, H.F., Chem. Eur. J, **2013**, *19(52)*, 17836-17845.

1.4.3 Incorporation of a cyclometallated iridium(III) metal into the phenylphenanthroimidazole scaffold and investigations of interactions with G-quadruplex DNA

In Chapter 4, we exchange our platinum(II) metal with iridium(III). This switch allows us to harness the luminescent "quadruplex light-switch" effect and evaluate the series of complexes as G-quadruplex probes. We characterize the complexes spectrophotometrically *via* UV/Vis and luminescence and utilize direct luminescence assays to measure the binding affinity and "light-switching" of the iridium(III) complexes with biologically relevant quadruplex sequences including telomeric, *c-Kit*, *c-Myc*, KRAS, BCL-2, VEGF, and PDGF-A. Additionally, the

iridium(III) complexes were shown to be electrochemically active, so cyclic voltammetry (CV) and electrochemiluminescence (ECL) studies were conducted. The ability of these complexes to bind to G-quadruplex DNA and their subsequent luminescence and electrochemiluminescence properties render them very amenable to development as G-quadruplex probes.

1.4.4 Expansion of the library of phenylphenanthroimidazole platinum(II) binders and subsequent interactions with biologically relevant G-quadruplex sequences

In Chapter 5, we further build upon our findings from Chapter 2 by expanding our library of complexes to include electron-withdrawing and electron-donating substituted phenylphenanthroimidazole ligands. In addition, we broaden our sequence library to include biologically relevant sequences from the *c-Kit* and *c-Myc* oncogene promoters. Through CD, FID assays, and SPR, we examine this expanded library's ability to select between quadruplex polymorphs.

1.5 References

1. Dahm, R., Discovering DNA: Friedrich Miescher and the early years of nucleic acid research. *Hum Genet* **2008,** *122* (6), 565-581.
2. Franklin, R. E.; Gosling, R. G., Molecular Configuration in Sodium Thymonucleate. *Nature* **1953,** *171* (4356), 740-741.
3. Franklin, R. E.; Gosling, R. G., Evidence for 2-Chain Helix in Crystalline Structure of Sodium Deoxyribonucleate. *Nature* **1953,** *172* (4369), 156-157.
4. Wilkins, M. H. F.; Stokes, A. R.; Wilson, H. R., Molecular Structure of Nucleic Acids: Molecular Structure of Deoxypentose Nucleic Acids. *Nature* **1953,** *171* (4356), 738-740.
5. Watson, J. D.; Crick, F. H. C., Molecular Structure of Nucleic Acids: A Structure for Deoxyribose Nucleic Acid. *Nature* **1953,** *171* (4356), 737-738.
6. McCall, M.; Brown, T.; Kennard, O., The crystal structure of d(G-G-G-G-C-C-C-C) a model for poly(dG) · poly(dC). *J Mol Biol* **1985,** *183* (3), 385-396.
7. Lu, X. J.; Shakked, Z.; Olson, W. K., A-form conformational motifs in ligand-bound DNA structures. *J Mol Biol* **2000,** *300* (4), 819-840.
8. Wang, A. H. J.; Quigley, G. J.; Kolpak, F. J.; Crawford, J. L.; van Boom, J. H.; van der Marel, G.; Rich, A., Molecular structure of a left-handed double helical DNA fragment at atomic resolution. *Nature* **1979,** *282* (5740), 680-686.

9. Rich, A.; Zhang, S., Timeline: Z-DNA: the long road to biological function. *Nat Rev Genet* **2003,** *4* (7), 566-572.
10. Leslie, A. G. W.; Arnott, S.; Chandrasekaran, R.; Ratliff, R. L., Polymorphism of DNA double helices. *J Mol Biol* **1980,** *143* (1), 49-72.
11. Bang, I., Untersuchungen uber die Guanylsaure. *Biochemische Zeitschrift* **1910,** *26*, 293-311.
12. Gellert, M.; Lipsett, M. N.; Davies, D. R., Helix formation by guanylic acid. *Proc Natl Acad Sci USA* **1962,** *48* (12), 2013-2018.
13. Schaffitzel, C.; Berger, I.; Postberg, J.; Hanes, J.; Lipps, H. J.; Pluckthun, A., In vitro generated antibodies specific for telomeric guanine-quadruplex DNA react with Stylonychia lemnae macronuclei. *Proc Natl Acad Sci USA* **2001,** *98* (15), 8572-8577.
14. Donohue, J., Hydrogen-bonded helical configurations of polynucleotides. *Proc Natl Acad Sci USA* **1956,** *42* (2), 60-65.
15. Hoogsteen, K., The crystal and molecular structure of a hydrogen-bonded complex between 1-methylthymine and 9-methyladenine. *Acta Crystallographica* **1963,** *16* (9), 907-916.
16. Ralph, R. K.; Khorana, H. G.; Connors, W. J., Secondary Structure and Aggregation in Deoxyguanosine Oligonucleotides. *J Am Chem Soc* **1962,** *84* (11), 2265-2266.
17. Henderson, E.; Hardin, C. C.; Walk, S. K.; Tinoco Jr, I.; Blackburn, E. H., Telomeric DNA oligonucleotides form novel intramolecular structures containing guanine·guanine base pairs. *Cell* **1987,** *51* (6), 899-908.
18. Sen, D.; Gilbert, W., Formation of parallel four-stranded complexes by guanine-rich motifs in DNA and its implications for meiosis. *Nature* **1988,** *334* (6180), 364-366.
19. Muniyappa, K.; Anuradha, S.; Byers, B., Yeast Meiosis-Specific Protein Hop1 Binds to G4 DNA and Promotes Its Formation. *Mol Cell Biol* **2000,** *20* (4), 1361-1369.
20. Anuradha, S.; Muniyappa, K., Meiosis-specific yeast Hop1 protein promotes synapsis of double-stranded DNA helices via the formation of guanine quartets. *Nucleic Acids Res* **2004,** *32* (8), 2378-2385.
21. Williamson, J. R.; Raghuraman, M. K.; Cech, T. R., Monovalent cation-induced structure of telomeric DNA: The G-quartet model. *Cell* **1989,** *59* (5), 871-880.
22. Luu, K. N.; Phan, A. T.; Kuryavyi, V.; Lacroix, L.; Patel, D. J., Structure of the human telomere in K^+ solution: an intramolecular (3+1) G-quadruplex scaffold. *J Am Chem Soc* **2006,** *128* (30), 9963-9970.
23. Chang, C. C.; Kuo, I. C.; Ling, I. F.; Chen, C. T.; Chen, H. C.; Lou, P. J.; Lin, J. J.; Chang, T. C., Detection of quadruplex DNA structures in human telomeres by a fluorescent carbazole derivative. *Anal Chem* **2004,** *76* (15), 4490-4494.
24. Schaffitzel, C.; Berger, I.; Postberg, J.; Hanes, J.; Lipps, H. J.; Pluckthun, A., In vitro generated antibodies specific for telomeric guanine-quadruplex DNA react with Stylonychia lemnae macronuclei. *Proc Natl Acad Sci USA* **2001,** *98* (15), 8572-8577.

25. Paeschke, K.; Simonsson, T.; Postberg, J.; Rhodes, D.; Lipps, H. J., Telomere end-binding proteins control the formation of G-quadruplex DNA structures in vivo. *Nat Struct Mol Biol* **2005,** *12* (10), 847-854.
26. Granotier, C.; Pennarun, G.; Riou, L.; Hoffschir, F.; Gauthier, L. R.; De Cian, A.; Gomez, D.; Mandine, E.; Riou, J. F.; Mergny, J. L.; Mailliet, P.; Dutrillaux, B.; Boussin, F. D., Preferential binding of a G-quadruplex ligand to human chromosome ends. *Nucleic Acids Res* **2005,** *33* (13), 4182-4190.
27. Huppert, J. L.; Balasubramanian, S., Prevalence of quadruplexes in the human genome. *Nucleic Acids Res* **2005,** *33* (9), 2908-2916.
28. Todd, A. K.; Johnston, M.; Neidle, S., Highly prevalent putative quadruplex sequence motifs in human DNA. *Nucleic Acids Res* **2005,** *33* (9), 2901-2907.
29. Collie, G. W.; Parkinson, G. N., The application of DNA and RNA G-quadruplexes to therapeutic medicines. *Chem Soc Rev* **2011,** *40* (12), 5867-5892.
30. Williamson, J. R., Guanine Quartets. *Curr Opin Struct Biol* **1993,** *3* (3), 357-362.
31. Huppert, J. L.; Balasubramanian, S., G-quadruplexes in promoters throughout the human genome. *Nucleic Acids Res* **2007,** *35* (2), 406-413.
32. Maizels, N., Dynamic roles for G4 DNA in the biology of eukaryotic cells. *Nat Struct Mol Biol* **2006,** *13* (12), 1055-1059.
33. Duquette, M. L.; Handa, P.; Vincent, J. A.; Taylor, A. F.; Maizels, N., Intracellular transcription of G-rich DNAs induces formation of G-loops, novel structures containing G4 DNA. *Genes Dev* **2004,** *18* (13), 1618-1629.
34. Drygin, D.; Siddiqui-Jain, A.; O'Brien, S.; Schwaebe, M.; Lin, A.; Bliesath, J.; Ho, C. B.; Proffitt, C.; Trent, K.; Whitten, J. P.; Lim, J. K.; Von Hoff, D.; Anderes, K.; Rice, W. G., Anticancer activity of CX-3543: a direct inhibitor of rRNA biogenesis. *Cancer Res* **2009,** *69* (19), 7653-7661.
35. Kostadinov, R.; Malhotra, N.; Viotti, M.; Shine, R.; D'Antonio, L.; Bagga, P., GRSDB: a database of quadruplex forming G-rich sequences in alternatively processed mammalian pre-mRNA sequences. *Nucleic Acids Res* **2006,** *34* (Database issue), D119-24.
36. Wieland, M.; Hartig, J. S., RNA quadruplex-based modulation of gene expression. *Chem Biol* **2007,** *14* (7), 757-763.
37. Kumari, S.; Bugaut, A.; Huppert, J. L.; Balasubramanian, S., An RNA G-quadruplex in the 5' UTR of the NRAS proto-oncogene modulates translation. *Nat Chem Biol* **2007,** *3* (4), 218-221.
38. Blackburn, E. H.; Gall, J. G., A tandemly repeated sequence at the termini of the extrachromosomal ribosomal RNA genes in Tetrahymena. *J Mol Biol* **1978,** *120* (1), 33-53.
39. Yoshio, O.; Susumu, S.; Sumiko, N.; Yasuyoshi, N.; Shunzo, O., Inverted terminal repeat sequence in the macronuclear DNA of Stylonychia pustulata. *Gene* **1980,** *10* (4), 301-306.

40. Klobutcher, L. A.; Swanton, M. T.; Donini, P.; Prescott, D. M., All gene-sized DNA molecules in four species of hypotrichs have the same terminal sequence and an unusual 3' terminus. *Proc Natl Acad Sci USA* **1981,** *78* (5), 3015-3019.
41. Yaku, H.; Fujimoto, T.; Murashima, T.; Miyoshi, D.; Sugimoto, N., Phthalocyanines: A new class of G-quadruplex-ligands with many potential applications. *Chem Commun* **2012,** *48* (50), 6203-6216.
42. Moyzis, R. K.; Buckingham, J. M.; Cram, L. S.; Dani, M.; Deaven, L. L.; Jones, M. D.; Meyne, J.; Ratliff, R. L.; Wu, J. R., A highly conserved repetitive DNA sequence, $(TTAGGG)_n$, present at the telomeres of human chromosomes. *Proc Natl Acad Sci USA* **1988,** *85* (18), 6622-6626.
43. Morin, G. B., The human telomere terminal transferase enzyme is a ribonucleoprotein that synthesizes TTAGGG repeats. *Cell* **1989,** *59* (3), 521-529.
44. Palm, W.; de Lange, T., How shelterin protects mammalian telomeres. *Annu Rev Genet* **2008,** *42*, 301-334.
45. Tahara, H.; Shin-Ya, K.; Seimiya, H.; Yamada, H.; Tsuruo, T.; Ide, T., G-Quadruplex stabilization by telomestatin induces TRF2 protein dissociation from telomeres and anaphase bridge formation accompanied by loss of the 3' telomeric overhang in cancer cells. *Oncogene* **2006,** *25* (13), 1955-1966.
46. Rodriguez, R.; Muller, S.; Yeoman, J. A.; Trentesaux, C.; Riou, J. F.; Balasubramanian, S., A novel small molecule that alters shelterin integrity and triggers a DNA-damage response at telomeres. *J Am Chem Soc* **2008,** *130* (47), 15758-15759.
47. Watson, J. D., Origin of Concatemeric T7DNA. *Nat New Biol* **1972,** *239* (94), 197-201.
48. Harley, C. B.; Futcher, A. B.; Greider, C. W., Telomeres shorten during ageing of human fibroblasts. *Nature* **1990,** *345* (6274), 458-460.
49. Blackburn, E. H., Switching and signaling at the telomere. *Cell* **2001,** *106* (6), 661-673.
50. Ohki, R.; Tsurimoto, T.; Ishikawa, F., In Vitro Reconstitution of the End Replication Problem. *Mol Cell Biol* **2001,** *21* (17), 5753-5766.
51. Hayflick, L.; Moorhead, P. S., The serial cultivation of human diploid cell strains. *Exp Cell Res* **1961,** *25* (3), 585-621.
52. Bodnar, A. G., Extension of Life-Span by Introduction of Telomerase into Normal Human Cells. *Science* **1998,** *279* (5349), 349-352.
53. Mergny, J. L.; Riou, J. F.; Mailliet, P.; Teulade-Fichou, M. P.; Gilson, E., Natural and pharmacological regulation of telomerase. *Nucleic Acids Res* **2002,** *30* (4), 839-865.
54. Kim, N. W.; Piatyszek, M. A.; Prowse, K. R.; Harley, C. B.; West, M. D.; Ho, P. L.; Coviello, G. M.; Wright, W. E.; Weinrich, S. L.; Shay, J. W., Specific association of human telomerase activity with immortal cells and cancer. *Science* **1994,** *266* (5193), 2011-2015.

55. Counter, C. M.; Avilion, A. A.; Lefeuvre, C. E.; Stewart, N. G.; Greider, C. W.; Harley, C. B.; Bacchetti, S., Telomere Shortening Associated with Chromosome Instability Is Arrested in Immortal Cells Which Express Telomerase Activity. *EMBO J.* **1992,** *11* (5), 1921-1929.
56. de Lange, T., Activation of telomerase in a human tumor. *Proc Natl Acad Sci USA* **1994,** *91* (8), 2882-2885.
57. Counter, C. M.; Hirte, H. W.; Bacchetti, S.; Harley, C. B., Telomerase activity in human ovarian carcinoma. *Proc Natl Acad Sci USA* **1994,** *91* (8), 2900-2904.
58. Counter, C. M.; Botelho, F. M.; Wang, P.; Harley, C. B.; Bacchetti, S., Stabilization of short telomeres and telomerase activity accompany immortalization of Epstein-Barr virus-transformed human B lymphocytes. *J Virol* **1994,** *68* (5), 3410-3414.
59. Shay, J. W.; Wright, W. E., Role of telomeres and telomerase in cancer. *Semin Cancer Biol* **2011,** *21* (6), 349-353.
60. Mocellin, S.; Pooley, K. A.; Nitti, D., Telomerase and the search for the end of cancer. *Trends Mol Med* **2013,** *19* (2), 125-133.
61. Xu, L.; Li, S.; Stohr, B. A., The role of telomere biology in cancer. *Annu Rev Pathol* **2013,** *8*, 49-78.
62. Hanahan, D.; Weinberg, R. A., The hallmarks of cancer. *Cell* **2000,** *100* (1), 57-70.
63. Hanahan, D.; Weinberg, R. A., Hallmarks of cancer: the next generation. *Cell* **2011,** *144* (5), 646-674.
64. Greider, C. W.; Blackburn, E. H., Identification of a specific telomere terminal transferase activity in tetrahymena extracts. *Cell* **1985,** *43* (2), 405-413.
65. Shampay, J.; Szostak, J. W.; Blackburn, E. H., DNA sequences of telomeres maintained in yeast. *Nature* **1984,** *310* (5973), 154-157.
66. Greider, C. W., *Identification and Characterization of Telomere Terminal Transferase*. University of California, Berkeley: 1987.
67. Greider, C. W.; Blackburn, E. H., A telomeric sequence in the RNA of Tetrahymena telomerase required for telomere repeat synthesis. *Nature* **1989,** *337* (6205), 331-337.
68. Shippen-Lentz, D.; Blackburn, E. H., Telomere terminal transferase activity from Euplotes crassus adds large numbers of TTTTGGGG repeats onto telomeric primers. *Mol Cell Biol* **1989,** *9* (6), 2761-2764.
69. Yu, G. L.; Bradley, J. D.; Attardi, L. D.; Blackburn, E. H., In vivo alteration of telomere sequences and senescence caused by mutated Tetrahymena telomerase RNAs. *Nature* **1990,** *344* (6262), 126-132.
70. Greider, C. W.; Blackburn, E. H., The telomere terminal transferase of tetrahymena is a ribonucleoprotein enzyme with two kinds of primer specificity. *Cell* **1987,** *51* (6), 887-898.
71. Shay, J. W.; Bacchetti, S., A survey of telomerase activity in human cancer. *Eur J Cancer* **1997,** *33* (5), 787-791.

72. Mergny, J. L.; Mailliet, P.; Lavelle, F.; Riou, J. F.; Laoui, A.; Helene, C., The development of telomerase inhibitors: the G-quartet approach. *Anticancer Drug Des* **1999,** *14* (4), 327-339.
73. Asai, A.; Oshima, Y.; Yamamoto, Y.; Uochi, T.; Kusaka, H.; Akinaga, S.; Yamashita, Y.; Pongracz, K.; Pruzan, R.; Wunder, E.; Piatyszek, M.; Li, S. H.; Chin, A. C.; Harley, C. B.; Gryaznov, S., A novel telomerase template antagonist (GRN163) as a potential anticancer agent. *Cancer Res* **2003,** *63* (14), 3931-3939.
74. Folini, M.; Brambilla, C.; Villa, R.; Gandellini, P.; Vignati, S.; Paduano, F.; Daidone, M. G.; Zaffaroni, N., Antisense oligonucleotide-mediated inhibition of hTERT, but not hTERC, induces rapid cell growth decline and apoptosis in the absence of telomere shortening in human prostate cancer cells. *Eur J Cancer* **2005,** *41* (4), 624-634.
75. Jackson, S. R.; Zhu, C.-H.; Paulson, V.; Watkins, L.; Dikmen, Z. G.; Gryaznov, S. M.; Wright, W. E.; Shay, J. W., Antiadhesive Effects of GRN163L − An Oligonucleotide N3→P5 Thio-Phosphoramidate Targeting Telomerase. *Cancer Res* **2007,** *67* (3), 1121-1129.
76. Pai, R. B.; Pai, S. B.; Kukhanova, M.; Dutschman, G. E.; Guo, X.; Cheng, Y.-C., Telomerase from Human Leukemia Cells: Properties and Its Interaction with Deoxynucleoside Analogues. *Cancer Res* **1998,** *58* (9), 1909-1913.
77. Gomez, D. E.; Tejera, A. M.; Olivero, O. A., Irreversible Telomere Shortening by 3-Azido-2',3'-Dideoxythymidine (AZT) Treatment. *Biochem Biophys Res Commun* **1998,** *246* (1), 107-110.
78. Ku, W.-C.; Cheng, A.-J.; Wang, T.-C. V., Inhibition of Telomerase Activity by PKC Inhibitors in Human Nasopharyngeal Cancer Cells in Culture. *Biochem Biophys Res Commun* **1997,** *241* (3), 730-736.
79. Pascolo, E.; Wenz, C.; Lingner, J.; Hauel, N.; Priepke, H.; Kauffmann, I.; Garin-Chesa, P.; Rettig, W. J.; Damm, K.; Schnapp, A., Mechanism of human telomerase inhibition by BIBR1532, a synthetic, non-nucleosidic drug candidate. *J Biol Chem* **2002,** *277* (18), 15566-15572.
80. El-Daly, H.; Kull, M.; Zimmermann, S.; Pantic, M.; Waller, C. F.; Martens, U. M., Selective cytotoxicity and telomere damage in leukemia cells using the telomerase inhibitor BIBR1532. *Blood* **2005,** *105* (4), 1742-1749.
81. Herbert, B. S.; Gellert, G. C.; Hochreiter, A.; Pongracz, K.; Wright, W. E.; Zielinska, D.; Chin, A. C.; Harley, C. B.; Shay, J. W.; Gryaznov, S. M., Lipid modification of GRN163, an N3'→P5' thio-phosphoramidate oligonucleotide, enhances the potency of telomerase inhibition. *Oncogene* **2005,** *24* (33), 5262-5268.
82. Jennifer Girard, N. P., Novel Therapeutics Targeting Telomerase and Telomeres. *J Cancer Sci Ther* **2013,** *05* (10).
83. Harley, C. B., Telomerase and cancer therapeutics. *Nature Rev Cancer* **2008,** *8* (3), 167-179.

84. Damm, K.; Hemmann, U.; Garin-Chesa, P.; Hauel, N.; Kauffmann, I.; Priepke, H.; Niestroj, C.; Daiber, C.; Enenkel, B.; Guilliard, B.; Lauritsch, I.; Muller, E.; Pascolo, E.; Sauter, G.; Pantic, M.; Martens, U. M.; Wenz, C.; Lingner, J.; Kraut, N.; Rettig, W. J.; Schnapp, A., A highly selective telomerase inhibitor limiting human cancer cell proliferation. *EMBO J* **2001,** *20* (24), 6958-6968.

85. Ward, R. J.; Autexier, C., Pharmacological telomerase inhibition can sensitize drug-resistant and drug-sensitive cells to chemotherapeutic treatment. *Mol Pharmacol* **2005,** *68* (3), 779-786.

86. Uziel, O.; Beery, E.; Dronichev, V.; Samocha, K.; Gryaznov, S.; Weiss, L.; Slavin, S.; Kushnir, M.; Nordenberg, Y.; Rabinowitz, C.; Rinkevich, B.; Zehavi, T.; Lahav, M., Telomere shortening sensitizes cancer cells to selected cytotoxic agents: in vitro and in vivo studies and putative mechanisms. *PLoS ONE* **2010,** *5* (2), e9132.

87. Reed, J. E.; Arnal, A. A.; Neidle, S.; Vilar, R., Stabilization of G-quadruplex DNA and inhibition of telomerase activity by square-planar nickel(II) complexes. *J Am Chem Soc* **2006,** *128* (18), 5992-5993.

88. Dixon, I. M.; Lopez, F.; Tejera, A. M.; Esteve, J. P.; Blasco, M. A.; Pratviel, G.; Meunier, B., A G-quadruplex ligand with 10000-fold selectivity over duplex DNA. *J Am Chem Soc* **2007,** *129* (6), 1502-1503.

89. Shirude, P. S.; Gillies, E. R.; Ladame, S.; Godde, F.; Shin-Ya, K.; Huc, I.; Balasubramanian, S., Macrocyclic and helical oligoamides as a new class of G-quadruplex ligands. *J Am Chem Soc* **2007,** *129* (39), 11890-11891.

90. Waller, Z. A.; Shirude, P. S.; Rodriguez, R.; Balasubramanian, S., Triarylpyridines: a versatile small molecule scaffold for G-quadruplex recognition. *Chem Commun* **2008,** (12), 1467-1469.

91. Wang, L.; Wen, Y.; Liu, J.; Zhou, J.; Li, C.; Wei, C., Promoting the formation and stabilization of human telomeric G-quadruplex DNA, inhibition of telomerase and cytotoxicity by phenanthroline derivatives. *Org Biomol Chem* **2011,** *9* (8), 2648-2653.

92. Zahler, A. M.; Williamson, J. R.; Cech, T. R.; Prescott, D. M., Inhibition of telomerase by G-quartet DNA structures. *Nature* **1991,** *350* (6320), 718-720.

93. Fletcher, T. M.; Sun, D.; Salazar, M.; Hurley, L. H., Effect of DNA secondary structure on human telomerase activity. *Biochem* **1998,** *37* (16), 5536-5541.

94. Zaug, A. J.; Podell, E. R.; Cech, T. R., Human POT1 disrupts telomeric G-quadruplexes allowing telomerase extension in vitro. *Proc Natl Acad Sci USA* **2005,** *102* (31), 10864-10869.

95. Oganesian, L.; Moon, I. K.; Bryan, T. M.; Jarstfer, M. B., Extension of G-quadruplex DNA by ciliate telomerase. *EMBO J* **2006,** *25* (5), 1148-1159.

96. Oganesian, L.; Bryan, T. M., Physiological relevance of telomeric G-quadruplex formation: a potential drug target. *BioEssays* **2007,** *29*, 155-165.

97. Neidle, S., Human telomeric G-quadruplex: the current status of telomeric G-quadruplexes as therapeutic targets in human cancer. *FEBS Journal* **2010,** *277* (5), 1118-1125.
98. Balasubramanian, S.; Hurley, L. H.; Neidle, S., Targeting G-quadruplexes in gene promoters: a novel anticancer strategy? *Nature Rev Drug Disc* **2011,** *10* (4), 261-275.
99. Isabelle, M.; Moreel, X.; Gagne, J. P.; Rouleau, M.; Ethier, C.; Gagne, P.; Hendzel, M. J.; Poirier, G. G., Investigation of PARP-1, PARP-2, and PARG interactomes by affinity-purification mass spectrometry. *Proteome Sci* **2010,** *8*, 22.
100. Khalil, H.; Tummala, H.; Chakarov, S.; Zhelev, N.; Lane, D., Targeting ATM pathway for therapeutic intervention in cancer. *Biodisc* **2012**.
101. Tauchi, T.; Shin-ya, K.; Sashida, G.; Sumi, M.; Okabe, S.; Ohyashiki, J. H.; Ohyashiki, K., Telomerase inhibition with a novel G-quadruplex-interactive agent, telomestatin: in vitro and in vivo studies in acute leukemia. *Oncogene* **2006,** *25* (42), 5719-5725.
102. Stratton, M. R.; Campbell, P. J.; Futreal, P. A., The cancer genome. *Nature* **2009,** *458* (7239), 719-724.
103. Jackson, S. P.; Bartek, J., The DNA-damage response in human biology and disease. *Nature* **2009,** *461* (7267), 1071-1078.
104. Ciccia, A.; Elledge, S. J., The DNA damage response: making it safe to play with knives. *Mol Cell* **2010,** *40* (2), 179-204.
105. Riou, J. F., G-quadruplex interacting agents targetting the telomeric G-overhang are more than simple telomerase inhibitors. *Curr Med Chem - Anti-Cancer Agents* **2004,** *4* (5), 439-443.
106. Shammas, M. A.; Shmookler Reis, R. J.; Li, C.; Koley, H.; Hurley, L. H.; Anderson, K. C.; Munshi, N. C., Telomerase inhibition and cell growth arrest after telomestatin treatment in multiple myeloma. *Clin Cancer Res* **2004,** *10* (2), 770-776.
107. Wu, P.; Ma, D. L.; Leung, C. H.; Yan, S. C.; Zhu, N.; Abagyan, R.; Che, C. M., Stabilization of G-quadruplex DNA with platinum(II) Schiff base complexes: Luminescent probe and down-regulation of c-myc oncogene expression. *Chem Eur J* **2009,** *15* (47), 13008-13021.
108. McLuckie, K. I.; Waller, Z. A.; Sanders, D. A.; Alves, D.; Rodriguez, R.; Dash, J.; McKenzie, G. J.; Venkitaraman, A. R.; Balasubramanian, S., G-quadruplex-binding benzo[a]phenoxazines down-regulate c-KIT expression in human gastric carcinoma cells. *J Am Chem Soc* **2011,** *133* (8), 2658-2663.
109. Rezler, E. M.; Bearss, D. J.; Hurley, L. H., Telomere inhibition and telomere disruption as processes for drug targeting. *Annu Rev Pharmacol Toxicol* **2003,** *43*, 359-379.
110. De Cian, A.; Lacroix, L.; Douarre, C.; Temime-Smaali, N.; Trentesaux, C.; Riou, J. F.; Mergny, J. L., Targeting telomeres and telomerase. *Biochimie* **2008,** *90* (1), 131-155.
111. Balasubramanian, S.; Neidle, S., G-quadruplex nucleic acids as therapeutic targets. *Curr Opin Chem Biol* **2009,** *13* (3), 345-353.

112. Haince, J. F.; Kozlov, S.; Dawson, V. L.; Dawson, T. M.; Hendzel, M. J.; Lavin, M. F.; Poirier, G. G., Ataxia telangiectasia mutated (ATM) signaling network is modulated by a novel poly(ADP-ribose)-dependent pathway in the early response to DNA-damaging agents. *J Biol Chem* **2007,** *282* (22), 16441-16453.
113. Chen, Y.; Qu, K.; Zhao, C.; Wu, L.; Ren, J.; Wang, J.; Qu, X., Insights into the biomedical effects of carboxylated single-wall carbon nanotubes on telomerase and telomeres. *Nat Commun* **2012,** *3*, 1074.
114. Wang, Y.; Patel, D. J., Solution structure of the human telomeric repeat d[$AG_3(T_2AG_3)_3$] G-tetraplex. *Structure* **1993,** *1* (4), 263-282.
115. Parkinson, G. N.; Lee, M. P.; Neidle, S., Crystal structure of parallel quadruplexes from human telomeric DNA. *Nature* **2002,** *417* (6891), 876-880.
116. Ambrus, A.; Chen, D.; Dai, J.; Bialis, T.; Jones, R. A.; Yang, D., Human telomeric sequence forms a hybrid-type intramolecular G-quadruplex structure with mixed parallel/antiparallel strands in potassium solution. *Nucleic Acids Res* **2006,** *34* (9), 2723-35.
117. Phan, A. T.; Luu, K. N.; Patel, D. J., Different loop arrangements of intramolecular human telomeric (3+1) G-quadruplexes in K^+ solution. *Nucleic Acids Res* **2006,** *34* (19), 5715-5719.
118. Lee, J. Y.; Okumus, B.; Kim, D. S.; Ha, T., Extreme conformational diversity in human telomeric DNA. *Proc Natl Acad Sci USA* **2005,** *102* (52), 18938-18943.
119. Li, J.; Correia, J. J.; Wang, L.; Trent, J. O.; Chaires, J. B., Not so crystal clear: the structure of the human telomere G-quadruplex in solution differs from that present in a crystal. *Nucleic Acids Res* **2005,** *33* (14), 4649-4659.
120. Lipps, H. J.; Rhodes, D., G-quadruplex structures: in vivo evidence and function. *Trends Cell Biol* **2009,** *19* (8), 414-422.
121. Tseng, T. Y.; Chien, C. H.; Chu, J. F.; Huang, W. C.; Lin, M. Y.; Chang, C. C.; Chang, T. C., Fluorescent probe for visualizing guanine-quadruplex DNA by fluorescence lifetime imaging microscopy. *J Biomed Opt* **2013,** *18* (10), 101309.
122. Alzeer, J.; Vummidi, B. R.; Roth, P. J.; Luedtke, N. W., Guanidinium-modified phthalocyanines as high-affinity G-quadruplex fluorescent probes and transcriptional regulators. *Angew Chem Int Ed* **2009,** *48* (49), 9362-9365.
123. Hardin, J.; Bertoni. G.; Kleinsmith, L. J.; Becker, W. M., *Becker's world of the cell*. Benjamin Cummings: Boston, 2012.
124. Simonsson, T.; Pecinka, P.; Kubista, M., DNA tetraplex formation in the control region of c-myc. *Nucleic Acids Res* **1998,** *26* (5), 1167-1172.
125. Siddiqui-Jain, A.; Grand, C. L.; Bearss, D. J.; Hurley, L. H., Direct evidence for a G-quadruplex in a promoter region and its targeting with a small molecule to repress c-MYC transcription. *Proc Natl Acad Sci USA* **2002,** *99* (18), 11593-11598.
126. Phan, A. T.; Modi, Y. S.; Patel, D. J., Propeller-type parallel-stranded G-quadruplexes in the human c-myc promoter. *J Am Chem Soc* **2004,** *126* (28), 8710-8716.

127. Ambrus, A.; Chen, D.; Dai, J.; Jones, R. A.; Yang, D., Solution structure of the biologically relevant G-quadruplex element in the human c-MYC promoter. Implications for G-quadruplex stabilization. *Biochem* **2005,** *44* (6), 2048-2058.
128. Rankin, S.; Reszka, A. P.; Huppert, J.; Zloh, M.; Parkinson, G. N.; Todd, A. K.; Ladame, S.; Balasubramanian, S.; Neidle, S., Putative DNA quadruplex formation within the human c-kit oncogene. *J Am Chem Soc* **2005,** *127* (30), 10584-10589.
129. Fernando, H.; Reszka, A. P.; Huppert, J.; Ladame, S.; Rankin, S.; Venkitaraman, A. R.; Neidle, S.; Balasubramanian, S., A conserved quadruplex motif located in a transcription activation site of the human c-kit oncogene. *Biochem* **2006,** *45* (25), 7854-7860.
130. Dai, J.; Dexheimer, T. S.; Chen, D.; Carver, M.; Ambrus, A.; Jones, R. A.; Yang, D., An intramolecular G-quadruplex structure with mixed parallel/antiparallel G-strands formed in the human BCL-2 promoter region in solution. *J Am Chem Soc* **2006,** *128* (4), 1096-1098.
131. Dexheimer, T. S.; Sun, D.; Hurley, L. H., Deconvoluting the structural and drug-recognition complexity of the G-quadruplex-forming region upstream of the bcl-2 P1 promoter. *J Am Chem Soc* **2006,** *128* (16), 5404-5415.
132. Sun, D. Y.; Guo, K. X.; Rusche, J. J.; Hurley, L. H., Facilitation of a structural transition in the polypurine/polypyrimidine tract within the proximal promoter region of the human VEGF gene by the presence of potassium and G-quadruplex-interactive agents. *Nucleic Acids Res* **2005,** *33* (18), 6070-6080.
133. Sun, D.; Liu, W. J.; Guo, K.; Rusche, J. J.; Ebbinghaus, S.; Gokhale, V.; Hurley, L. H., The proximal promoter region of the human vascular endothelial growth factor gene has a G-quadruplex structure that can be targeted by G-quadruplex-interactive agents. *Mol Cancer Ther* **2008,** *7* (4), 880-889.
134. Qin, Y.; Rezler, E. M.; Gokhale, V.; Sun, D.; Hurley, L. H., Characterization of the G-quadruplexes in the duplex nuclease hypersensitive element of the PDGF-A promoter and modulation of PDGF-A promoter activity by TMPyP4. *Nucleic Acids Res* **2007,** *35* (22), 7698-7713.
135. Viglasky, V., Platination of telomeric sequences and nuclease hypersensitive elements of human c-myc and PDGF-A promoters and their ability to form G-quadruplexes. *FEBS J* **2009,** *276* (2), 401-409.
136. Cogoi, S.; Xodo, L. E., G-quadruplex formation within the promoter of the KRAS proto-oncogene and its effect on transcription. *Nucleic Acids Res* **2006,** *34* (9), 2536-2549.
137. Cogoi, S.; Paramasivam, M.; Spolaore, B.; Xodo, L. E., Structural polymorphism within a regulatory element of the human KRAS promoter: formation of G4-DNA recognized by nuclear proteins. *Nucleic Acids Res* **2008,** *36* (11), 3765-3780.
138. Palumbo, S. L.; Ebbinghaus, S. W.; Hurley, L. H., Formation of a unique end-to-end stacked pair of G-quadruplexes in the hTERT core promoter with implications for inhibition of

telomerase by G-quadruplex-interactive ligands. *J Am Chem Soc* **2009,** *131* (31), 10878-10891.

139. Brooks, T. A.; Kendrick, S.; Hurley, L., Making sense of G-quadruplex and i-motif functions in oncogene promoters. *FEBS J* **2010,** *277* (17), 3459-3469.
140. Tarsounas, M.; Tijsterman, M., Genomes and g-quadruplexes: for better or for worse. *J Mol Biol* **2013,** *425* (23), 4782-4789.
141. Grand, C. L.; Han, H.; Munoz, R. M.; Weitman, S.; Von Hoff, D. D.; Hurley, L. H.; Bearss, D. J., The cationic porphyrin TMPyP4 down-regulates c-MYC and human telomerase reverse transcriptase expression and inhibits tumor growth in vivo. *Mol Cancer Ther* **2002,** *1* (8), 565-573.
142. Paul, A.; Bhattacharya, S., Chemistry and biology of DNA-binding small molecules. *Current Science* **2012,** *102* (2), 212-231.
143. Cuesta, J.; Read, M. A.; Neidle, S., The design of G-quadruplex ligands as telomerase inhibitors. *Mini Rev Med Chem* **2003,** *3* (1), 11-21.
144. Huppert, J. L., Four-stranded DNA: cancer, gene regulation and drug development. *Philos Trans A Math Phys Eng Sci* **2007,** *365* (1861), 2969-2984.
145. Huppert, J. L., Four-stranded nucleic acids: structure, function and targeting of G-quadruplexes. *Chem Soc Rev* **2008,** *37* (7), 1375-1384.
146. Ou, T. M.; Lu, Y. J.; Tan, J. H.; Huang, Z. S.; Wong, K. Y.; Gu, L. Q., G-quadruplexes: targets in anticancer drug design. *ChemMedChem* **2008,** *3* (5), 690-713.
147. Biver, T., Stabilisation of non-canonical structures of nucleic acids by metal ions and small molecules. *Coord Chem Rev* **2013,** *257* (19-20), 2765-2783.
148. Perry, P. J.; Jenkins, T. C., DNA tetraplex-binding drugs: structure-selective targeting is critical for antitumour telomerase inhibition. *Mini Rev Med Chem* **2001,** *1* (1), 31-41.
149. Tan, J.-H.; Gu, L.-Q.; Wu, J.-Y., Design of Selective G-quadruplex Ligands as Potential Anticancer Agents. *Mini Rev Med Chem* **2008,** *8* (11), 1163-1178.
150. Monchaud, D.; Teulade-Fichou, M. P., A hitchhiker's guide to G-quadruplex ligands. *Org Biomol Chem* **2008,** *6* (4), 627-636.
151. Georgiades, S. N.; Abd Karim, N. H.; Suntharalingam, K.; Vilar, R., Interaction of metal complexes with G-quadruplex DNA. *Angew Chem Int Ed* **2010,** *49* (24), 4020-4034.
152. Sun, D.; Thompson, B.; Cathers, B. E.; Salazar, M.; Kerwin, S. M.; Trent, J. O.; Jenkins, T. C.; Neidle, S.; Hurley, L. H., Inhibition of human telomerase by a G-quadruplex-interactive compound. *J Med Chem* **1997,** *40* (14), 2113-2116.
153. Perry, P. J.; Gowan, S. M.; Reszka, A. P.; Polucci, P.; Jenkins, T. C.; Kelland, L. R.; Neidle, S., 1,4- and 2,6-disubstituted amidoanthracene-9,10-dione derivatives as inhibitors of human telomerase. *J Med Chem* **1998,** *41* (17), 3253-3260.
154. Perry, P. J.; Reszka, A. P.; Wood, A. A.; Read, M. A.; Gowan, S. M.; Dosanjh, H. S.; Trent, J. O.; Jenkins, T. C.; Kelland, L. R.; Neidle, S., Human telomerase inhibition by

regioisomeric disubstituted amidoanthracene-9,10-diones. *J Med Chem* **1998,** *41* (24), 4873-4884.

155. Read, M. A.; Wood, A. A.; Harrison, J. R.; Gowan, S. M.; Kelland, L. R.; Dosanjh, H. S.; Neidle, S., Molecular modeling studies on G-quadruplex complexes of telomerase inhibitors: structure-activity relationships. *J Med Chem* **1999,** *42* (22), 4538-4546.
156. Read, M.; Harrison, R. J.; Romagnoli, B.; Tanious, F. A.; Gowan, S. H.; Reszka, A. P.; Wilson, W. D.; Kelland, L. R.; Neidle, S., Structure-based design of selective and potent G quadruplex-mediated telomerase inhibitors. *Proc Natl Acad Sci USA* **2001,** *98* (9), 4844-4849.
157. Harrison, R. J.; Cuesta, J.; Chessari, G.; Read, M. A.; Basra, S. K.; Reszka, A. P.; Morrell, J.; Gowan, S. M.; Incles, C. M.; Tanious, F. A.; Wilson, W. D.; Kelland, L. R.; Neidle, S., Trisubstituted acridine derivatives as potent and selective telomerase inhibitors. *J Med Chem* **2003,** *46* (21), 4463-4476.
158. Schultes, C. M.; Guyen, B.; Cuesta, J.; Neidle, S., Synthesis, biophysical and biological evaluation of 3,6-bis-amidoacridines with extended 9-anilino substituents as potent G-quadruplex-binding telomerase inhibitors. *Biorg Med Chem Lett* **2004,** *14* (16), 4347-4351.
159. Moore, M. J.; Schultes, C. M.; Cuesta, J.; Cuenca, F.; Gunaratnam, M.; Tanious, F. A.; Wilson, W. D.; Neidle, S., Trisubstituted acridines as G-quadruplex telomere targeting agents. Effects of extensions of the 3,6- and 9-side chains on quadruplex binding, telomerase activity, and cell proliferation. *J Med Chem* **2006,** *49* (2), 582-599.
160. Gowan, S. M.; Harrison, J. R.; Patterson, L.; Valenti, M.; Read, M. A.; Neidle, S.; Kelland, L. R., A G-quadruplex-interactive potent small-molecule inhibitor of telomerase exhibiting in vitro and in vivo antitumor activity. *Mol Pharmacol* **2002,** *61* (5), 1154-1162.
161. Burger, A. M.; Dai, F.; Schultes, C. M.; Reszka, A. P.; Moore, M. J.; Double, J. A.; Neidle, S., The G-quadruplex-interactive molecule BRACO-19 inhibits tumor growth, consistent with telomere targeting and interference with telomerase function. *Cancer Res* **2005,** *65* (4), 1489-1496.
162. Taetz, S.; Baldes, C.; Murdter, T. E.; Kleideiter, E.; Piotrowska, K.; Bock, U.; Haltner-Ukomadu, E.; Mueller, J.; Huwer, H.; Schaefer, U. F.; Klotz, U.; Lehr, C. M., Biopharmaceutical characterization of the telomerase inhibitor BRACO19. *Pharm Res* **2006,** *23* (5), 1031-1037.
163. Belmont, P.; Dorange, I., Acridine/acridone: a simple scaffold with a wide range of application in oncology. *Expert Opin Ther Pat* **2008,** *18* (11), 1211-1224.
164. Bejugam, M.; Sewitz, S.; Shirude, P. S.; Rodriguez, R.; Shahid, R.; Balasubramanian, S., Trisubstituted isoalloxazines as a new class of G-quadruplex binding ligands: small molecule regulation of c-kit oncogene expression. *J Am Chem Soc* **2007,** *129* (43), 12926-12927.

165. Caprio, V.; Guyen, B.; Opoku-Boahen, Y.; Mann, J.; Gowan, S. M.; Kelland, L. M.; Read, M. A.; Neidle, S., A novel inhibitor of human telomerase derived from 10H-indolo[3,2-b]quinoline. *Biorg Med Chem Lett* **2000,** *10* (18), 2063-2066.

166. Guyen, B.; Schultes, C. M.; Hazel, P.; Mann, J.; Neidle, S., Synthesis and evaluation of analogues of 10*H*-indolo[3,2-*b*]-quinoline as G-quadruplex stabilising ligands and potential inhibitors of the enzyme telomerase. *Org Biomol Chem* **2004,** *2* (7), 981-988.

167. Zhou, J. L.; Lu, Y. J.; Ou, T. M.; Zhou, J. M.; Huang, Z. S.; Zhu, X. F.; Du, C. J.; Bu, X. Z.; Ma, L.; Gu, L. Q.; Li, Y. M.; Chan, A. S. C., Synthesis and evaluation of quindoline derivatives as G-quadruplex inducing and stabilizing ligands and potential inhibitors of telomerase. *J Med Chem* **2005,** *48* (23), 7315-7321.

168. Ou, T. M.; Lu, Y. J.; Zhang, C.; Huang, Z. S.; Wang, X. D.; Tan, J. H.; Chen, Y.; Ma, D. L.; Wong, K. Y.; Tang, J. C.; Chan, A. S.; Gu, L. Q., Stabilization of G-quadruplex DNA and down-regulation of oncogene c-myc by quindoline derivatives. *J Med Chem* **2007,** *50* (7), 1465-1474.

169. Zhou, J. M.; Zhu, X. F.; Lu, Y. J.; Deng, R.; Huang, Z. S.; Mei, Y. P.; Wang, Y.; Huang, W. L.; Liu, Z. C.; Gu, L. Q.; Zeng, Y. X., Senescence and telomere shortening induced by novel potent G-quadruplex interactive agents, quindoline derivatives, in human cancer cell lines. *Oncogene* **2006,** *25* (4), 503-511.

170. Ou, T. M.; Lin, J.; Lu, Y. J.; Hou, J. Q.; Tan, J. H.; Chen, S. H.; Li, Z.; Li, Y. P.; Li, D.; Gu, L. Q.; Huang, Z. S., Inhibition of cell proliferation by quindoline derivative (SYUIQ-05) through its preferential interaction with c-myc promoter G-quadruplex. *J Med Chem* **2011,** *54* (16), 5671-5679.

171. Boddupally, P. V. L.; Hahn, S.; Beman, C.; De, B.; Brooks, T. A.; Gokhale, V.; Hurley, L. H., Anticancer activity and cellular repression of c-MYC by the G-quadruplex-stabilizing 11-piperazinylquindoline is not dependent on direct targeting of the G-quadruplex in the c-MYC promoter. *J Med Chem* **2012,** *55* (13), 6076-6086.

172. Mergny, J. L.; Lacroix, L.; Teulade-Fichou, M. P.; Hounsou, C.; Guittat, L.; Hoarau, M.; Arimondo, P. B.; Vigneron, J. P.; Lehn, J. M.; Riou, J. F.; Garestier, T.; Helene, C., Telomerase inhibitors based on quadruplex ligands selected by a fluorescence assay. *Proc Natl Acad Sci USA* **2001,** *98* (6), 3062-3067.

173. Hounsou, C.; Guittat, L.; Monchaud, D.; Jourdan, M.; Saettel, N.; Mergny, J. L.; Teulade-Fichou, M. P., G-quadruplex recognition by quinacridines: a SAR, NMR, and biological study. *ChemMedChem* **2007,** *2* (5), 655-666.

174. Monchaud, D.; Allain, C.; Bertrand, H.; Smargiasso, N.; Rosu, F.; Gabelica, V.; De Cian, A.; Mergny, J. L.; Teulade-Fichou, M. P., Ligands playing musical chairs with G-quadruplex DNA: a rapid and simple displacement assay for identifying selective G-quadruplex binders. *Biochimie* **2008,** *90* (8), 1207-1223.

175. Teulade-Fichou, M. P.; Carrasco, C.; Guittat, L.; Bailly, C.; Alberti, P.; Mergny, J. L.; David, A.; Lehn, J. M.; Wilson, W. D., Selective recognition of G-Quadruplex telomeric DNA by a bis(quinacridine) macrocycle. *J Am Chem Soc* **2003,** *125* (16), 4732-4740.
176. Heald, R. A.; Modi, C.; Cookson, J. C.; Hutchinson, I.; Laughton, C. A.; Gowan, S. M.; Kelland, L. R.; Stevens, M. F. G., Antitumor Polycyclic Acridines. 8.1. Synthesis and Telomerase-Inhibitory Activity of Methylated Pentacyclic Acridinium Salts. *J Med Chem* **2002,** *45* (3), 590-597.
177. Cookson, J. C.; Heald, R. A.; Stevens, M. F., Antitumor polycyclic acridines. 17. Synthesis and pharmaceutical profiles of pentacyclic acridinium salts designed to destabilize telomeric integrity. *J Med Chem* **2005,** *48* (23), 7198-7207.
178. Leonetti, C.; Amodei, S.; D'Angelo, C.; Rizzo, A.; Benassi, B.; Antonelli, A.; Elli, R.; Stevens, M. F. G.; D'Incalci, M.; Zupi, G.; Biroccio, A., Biological activity of the G-quadruplex ligand RHPS4 (3,11-difluoro-6,8,13-trimethyl-8*H*-quino[4,3,2-*kl*]acridinium methosulfate) is associated with telomere capping alteration. *Mol Pharmacol* **2004,** *66* (5), 1138-1146.
179. Leonetti, C.; Scarsella, M.; Riggio, G.; Rizzo, A.; Salvati, E.; D'Incalci, M.; Staszewsky, L.; Frapolli, R.; Stevens, M. F.; Stoppacciaro, A.; Mottolese, M.; Antoniani, B.; Gilson, E.; Zupi, G.; Biroccio, A., G-quadruplex ligand RHPS4 potentiates the antitumor activity of camptothecins in preclinical models of solid tumors. *Clin Cancer Res* **2008,** *14* (22), 7284-7291.
180. Phatak, P.; Cookson, J. C.; Dai, F.; Smith, V.; Gartenhaus, R. B.; Stevens, M. F.; Burger, A. M., Telomere uncapping by the G-quadruplex ligand RHPS4 inhibits clonogenic tumour cell growth in vitro and in vivo consistent with a cancer stem cell targeting mechanism. *Br J Cancer* **2007,** *96* (8), 1223-1233.
181. Bates, P.; Mergny, J. L.; Yang, D., Quartets in G-major. The First International Meeting on Quadruplex DNA. *EMBO Rep* **2007,** *8* (11), 1003-1010.
182. Cong, R.; Das, S.; Ugrinova, I.; Kumar, S.; Mongelard, F.; Wong, J.; Bouvet, P., Interaction of nucleolin with ribosomal RNA genes and its role in RNA polymerase I transcription. *Nucleic Acids Res* **2012,** *40* (19), 9441-9454.
183. Fedoroff, O. Y.; Salazar, M.; Han, H.; Chemeris, V. V.; Kerwin, S. M.; Hurley, L. H., NMR-Based model of a telomerase-inhibiting compound bound to G-quadruplex DNA. *Biochem* **1998,** *37* (36), 12367-12374.
184. Kern, J. T.; Thomas, P. W.; Kerwin, S. M., The Relationship between Ligand Aggregation and G-Quadruplex DNA Selectivity in a Series of 3,4,9,10-Perylenetetracarboxylic Acid Diimides. *Biochem* **2002,** *41* (38), 11379-11389.
185. Alvino, A.; Franceschin, M.; Cefaro, C.; Borioni, S.; Ortaggi, G.; Bianco, A., Synthesis and spectroscopic properties of highly water-soluble perylene derivatives. *Tetrahedron* **2007,** *63* (33), 7858-7865.

186. Franceschin, M.; Pascucci, E.; Alvino, A.; D'Ambrosio, D.; Bianco, A.; Ortaggi, G.; Savino, M., New highly hydrosoluble and not self-aggregated perylene derivatives with three and four polar side-chains as G-quadruplex telomere targeting agents and telomerase inhibitors. *Biorg Med Chem Lett* **2007,** *17* (9), 2515-2522.
187. Casagrande, V.; Salvati, E.; Alvino, A.; Bianco, A.; Ciammaichella, A.; D'Angelo, C.; Ginnari-Satriani, L.; Serrilli, A. M.; Iachettini, S.; Leonetti, C.; Neidle, S.; Ortaggi, G.; Porru, M.; Rizzo, A.; Franceschin, M.; Biroccio, A., N-cyclic bay-substituted perylene G-quadruplex ligands have selective antiproliferative effects on cancer cells and induce telomere damage. *J Med Chem* **2011,** *54* (5), 1140-1156.
188. D'Ambrosio, D.; Reichenbach, P.; Micheli, E.; Alvino, A.; Franceschin, M.; Savino, M.; Lingner, J., Specific binding of telomeric G-quadruplexes by hydrosoluble perylene derivatives inhibits repeat addition processivity of human telomerase. *Biochimie* **2012,** *94* (3), 854-863.
189. Taka, T.; Joonlasak, K.; Huang, L.; Randall Lee, T.; Chang, S. W. T.; Tuntiwechapikul, W., Down-regulation of the human VEGF gene expression by perylene monoimide derivatives. *Bioorg Med Chem Lett* **2012,** *22* (1), 518-522.
190. Fisher, A. M. R.; Murphree, A. L.; Gomer, C. J., Clinical and preclinical photodynamic therapy. *Lasers in Surgery and Medicine* **1995,** *17* (1), 2-31.
191. Schuitmaker, J. J.; Baas, P.; van Leengoed, H. L. L. M.; van der Meulen, F. W.; Star, W. M.; van Zandwijk, N., Photodynamic therapy: a promising new modality for the treatment of cancer. *J Photochem Photobiol B: Biol* **1996,** *34* (1), 3-12.
192. Ren, J.; Chaires, J. B., Sequence and Structural Selectivity of Nucleic Acid Binding Ligands. *Biochem* **1999,** *38* (49), 16067-16075.
193. del Toro, M.; Gargallo, R.; Eritja, R.; Jaumot, J., Study of the interaction between the G-quadruplex-forming thrombin-binding aptamer and the porphyrin 5,10,15,20-tetrakis-(N-methyl-4-pyridyl)-21,23*H*-porphyrin tetratosylate. *Anal Biochem* **2008,** *379* (1), 8-15.
194. Manaye, S.; Eritja, R.; Avino, A.; Jaumot, J.; Gargallo, R., Porphyrin binding mechanism is altered by protonation at the loops in G-quadruplex DNA formed near the transcriptional activation site of the human c-kit gene. *Biochim Biophys Acta* **2012,** *1820* (12), 1987-1996.
195. Morris, M. J.; Wingate, K. L.; Silwal, J.; Leeper, T. C.; Basu, S., The porphyrin TmPyP4 unfolds the extremely stable G-quadruplex in MT3-MMP mRNA and alleviates its repressive effect to enhance translation in eukaryotic cells. *Nucleic Acids Res* **2012,** *40* (9), 4137-4145.
196. Romera, C.; Bombarde, O.; Bonnet, R.; Gomez, D.; Dumy, P.; Calsou, P.; Gwan, J. F.; Lin, J. H.; Defrancq, E.; Pratviel, G., Improvement of porphyrins for G-quadruplex DNA targeting. *Biochimie* **2011,** *93* (8), 1310-1317.
197. Seenisamy, J.; Bashyam, S.; Gokhale, V.; Vankayalapati, H.; Sun, D.; Siddiqui-Jain, A.; Streiner, N.; Shin-ya, K.; White, E.; Wilson, W. D.; Hurley, L. H., Design and synthesis of an

expanded porphyrin that has selectivity for the c-MYC G-quadruplex structure. *J Am Chem Soc* **2005,** *127* (9), 2944-2959.

198. Kim, M. Y.; Vankayalapati, H.; Kazuo, S.; Wierzba, K.; Hurley, L. H., Telomestatin, a potent telomerase inhibitor that interacts quite specifically with the human telomeric intramolecular G-quadruplex. *J Am Chem Soc* **2002,** *124* (10), 2098-2099.
199. Tauchi, T.; Shin-Ya, K.; Sashida, G.; Sumi, M.; Nakajima, A.; Shimamoto, T.; Ohyashiki, J. H.; Ohyashiki, K., Activity of a novel G-quadruplex-interactive telomerase inhibitor, telomestatin (SOT-095), against human leukemia cells: involvement of ATM-dependent DNA damage response pathways. *Oncogene* **2003,** *22* (34), 5338-5347.
200. Binz, N.; Shalaby, T.; Rivera, P.; Shin-ya, K.; Grotzer, M. A., Telomerase inhibition, telomere shortening, cell growth suppression and induction of apoptosis by telomestatin in childhood neuroblastoma cells. *Eur J Cancer* **2005,** *41* (18), 2873-2881.
201. Doi, T.; Yoshida, M.; Shin-ya, K.; Takahashi, T., Total synthesis of (R)-telomestatin. *Org Lett.* **2006,** *8* (18), 4165-4167.
202. Doi, T.; Shibata, K.; Yoshida, M.; Takagi, M.; Tera, M.; Nagasawa, K.; Shin-ya, K.; Takahashi, T., (S)-stereoisomer of telomestatin as a potent G-quadruplex binder and telomerase inhibitor. *Org Biomol Chem* **2011,** *9* (2), 387-393.
203. Jantos, K.; Rodriguez, R.; Ladame, S.; Shirude, P. S.; Balasubramanian, S., Oxazole-based peptide macrocycles: a new class of G-quadruplex binding ligands. *J Am Chem Soc* **2006,** *128* (42), 13662-13663.
204. Bugaut, A.; Jantos, K.; Wietor, J. L.; Rodriguez, R.; Sanders, J. K. M.; Balasubramanian, S., Exploring the differential recognition of DNA G-quadruplex targets by small molecules using dynamic combinatorial chemistry. *Angew Chem Int Ed* **2008,** *47* (14), 2677-2680.
205. Baker, E. S.; Lee, J. T.; Sessler, J. L.; Bowers, M. T., Cyclo[n]pyrroles: size and site-specific binding to G-quadruplexes. *J Am Chem Soc* **2006,** *128* (8), 2641-2648.
206. Minhas, G. S.; Pilch, D. S.; Kerrigan, J. E.; LaVoie, E. J.; Rice, J. E., Synthesis and G-quadruplex stabilizing properties of a series of oxazole-containing macrocycles. *Biorg Med Chem Lett* **2006,** *16* (15), 3891-3895.
207. Barbieri, C. M.; Srinivasan, A. R.; Rzuczek, S. G.; Rice, J. E.; LaVoie, E. J.; Pilch, D. S., Defining the mode, energetics and specificity with which a macrocyclic hexaoxazole binds to human telomeric G-quadruplex DNA. *Nucleic Acids Res* **2007,** *35* (10), 3272-3286.
208. Tera, M.; Iida, K.; Ikebukuro, K.; Seimiya, H.; Shin-Ya, K.; Nagasawa, K., Visualization of G-quadruplexes by using a BODIPY-labeled macrocyclic heptaoxazole. *Org Biomol Chem* **2010,** *8* (12), 2749-2755.
209. Iida, K.; Nagasawa, K., Macrocyclic polyoxazoles as G-quadruplex ligands. *Chem Rec* **2013,** *13* (6), 539-548.
210. Pennarun, G.; Granotier, C.; Gauthier, L. R.; Gomez, D.; Hoffschir, F.; Mandine, E.; Riou, J. F.; Mergny, J. L.; Mailliet, P.; Boussin, F. D., Apoptosis related to telomere instability and

cell cycle alterations in human glioma cells treated by new highly selective G-quadruplex ligands. *Oncogene* **2005,** *24* (18), 2917-2928.

211. De Cian, A.; Delemos, E.; Mergny, J. L.; Teulade-Fichou, M. P.; Monchaud, D., Highly efficient G-quadruplex recognition by bisquinolinium compounds. *J Am Chem Soc* **2007,** *129* (7), 1856-1857.
212. De Cian, A.; Mergny, J. L., Quadruplex ligands may act as molecular chaperones for tetramolecular quadruplex formation. *Nucleic Acids Res* **2007,** *35* (8), 2483-2493.
213. Yang, P.; De Cian, A.; Teulade-Fichou, M. P.; Mergny, J. L.; Monchaud, D., Engineering bisquinolinium/thiazole orange conjugates for fluorescent sensing of G-quadruplex DNA. *Angew Chem Int Ed* **2009,** *48* (12), 2188-91.
214. Monchaud, D.; Allain, C.; Teulade-Fichou, M. P., Development of a fluorescent intercalator displacement assay (G4-FID) for establishing quadruplex-DNA affinity and selectivity of putative ligands. *Bioorg Med Chem Lett* **2006,** *16* (18), 4842-4845.
215. Moses, J. E.; Moorhouse, A. D., The growing applications of click chemistry. *Chem Soc Rev* **2007,** *36* (8), 1249-1262.
216. Moorhouse, A. D.; Haider, S.; Gunaratnam, M.; Munnur, D.; Neidle, S.; Moses, J. E., Targeting telomerase and telomeres: a click chemistry approach towards highly selective G-quadruplex ligands. *Mol Biosyst* **2008,** *4* (6), 629-642.
217. Drewe, W. C.; Neidle, S., Click chemistry assembly of G-quadruplex ligands incorporating a diarylurea scaffold and triazole linkers. *Chem Commun* **2008,** (42), 5295-5297.
218. Moses, J. E.; Ritson, D. J.; Zhang, F.; Lombardo, C. M.; Haider, S.; Oldham, N.; Neidle, S., A click chemistry approach to C3 symmetric, G-quadruplex stabilising ligands. *Org Biomol Chem* **2010,** *8* (13), 2926-2930.
219. Sparapani, S.; Haider, S. M.; Doria, F.; Gunaratnam, M.; Neidle, S., Rational design of acridine-based ligands with selectivity for human telomeric quadruplexes. *J Am Chem Soc* **2010,** *132* (35), 12263-12272.
220. Dash, J.; Waller, Z. A.; Pantos, G. D.; Balasubramanian, S., Synthesis and binding studies of novel diethynyl-pyridine amides with genomic promoter DNA G-quadruplexes. *Chem Eur J* **2011,** *17* (16), 4571-4581.
221. Zhang, Q. L.; Liu, J. H.; Liu, J. Z.; Zhang, P. X.; Ren, X. Z.; Liu, Y.; Huang, Y.; Ji, L. N., DNA-binding and photoactivated enantiospecific cleavage of chiral polypyridyl ruthenium(II) complexes. *J Inorg Biochem* **2004,** *98* (8), 1405-1412.
222. Bhat, S. S.; Kumbhar, A. A.; Heptullah, H.; Khan, A. A.; Gobre, V. V.; Gejji, S. P.; Puranik, V. G., Synthesis, Electronic Structure, DNA and Protein Binding, DNA Cleavage, and Anticancer Activity of Fluorophore-Labeled Copper(II) Complexes. *Inorg Chem* **2011,** *50*, 545-558.
223. Barton, J. K.; Dannenberg, J. J.; Raphael, A. L., Enantiomeric selectivity in binding tris(phenanthroline)zinc(II) to DNA. *J Am Chem Soc* **1982,** *104* (18), 4967-4969.

224. Barton, J. K., Tris(phenanthroline) metal complexes: probes for DNA helicity. *J Biomol Struct Dynam* **1983,** *1* (3), 621-632.

225. Barton, J. K.; Basile, L. A.; Danishefsky, A.; Alexandrescu, A., Chiral probes for the handedness of DNA helices: Enantiomers of tris(4,7-diphenylphenanthroline)ruthenium(II). *Proc Natl Acad Sci USA* **1984,** *81* (7 I), 1961-1965.

226. Barton, J. K.; Raphael, A. L., Photoactivated stereospecific cleavage of double-helical DNA by cobalt(III) complexes. *J Am Chem Soc* **1984,** *106* (8), 2466-2468.

227. Barton, J. K.; Raphael, A. L., Site-specific cleavage of left-handed DNA in pBR322 by Λ-tris(diphenylphenanthroline)cobalt(III). *Proc Natl Acad Sci USA* **1985,** *82* (19), 6460-6464.

228. Barton, J. K.; Danishefsky, A.; Goldberg, J., Tris(phenanthroline)ruthenium(II): stereoselectivity in binding to DNA. *J Am Chem Soc* **1984,** *106* (7), 2172-2176.

229. Kumar, C. V.; Barton, J. K.; Turro, N. J., Photophysics of ruthenium complexes bound to double helical DNA. *J Am Chem Soc* **1985,** *107* (19), 5518-5523.

230. Pyle, A. M.; Rehmann, J. P.; Meshoyrer, R.; Kumar, C. V.; Turro, N. J.; Barton, J. K., Mixed-ligand complexes of ruthenium(II): factors governing binding to DNA. *J Am Chem Soc* **1989,** *111* (8), 3051-3058.

231. Friedman, A. E.; Chambron, J. C.; Sauvage, J. P.; Turro, N. J.; Barton, J. K., A molecular light switch for DNA: $Ru(bpy)_2(dppz)^{2+}$. *J Am Chem Soc* **1990,** *112* (12), 4960-4962.

232. Jenkins, Y.; Friedman, A. E.; Turro, N. J.; Barton, J. K., Characterization of dipyridophenazine complexes of ruthenium(II): The light switch effect as a function of nucleic acid sequence and conformation. *Biochem* **1992,** *31* (44), 10809-10816.

233. Olson, E. J. C.; Hu, D.; Hörmann, A.; Jonkman, A. M.; Arkin, M. R.; Stemp, E. D. A.; Barton, J. K.; Barbara, P. F., First Observation of the Key Intermediate in the "Light-Switch" Mechanism of $[Ru(phen)_2dppz]^{2+}$. *J Am Chem Soc* **1997,** *119* (47), 11458-11467.

234. Pyle, A. M.; Rehmann, J. P.; Meshoyrer, R.; Kumar, C. V.; Turro, N. J.; Barton, J. K., Mixed-Ligand Complexes of Ruthenium(II) - Factors Governing Binding to DNA. *J Am Chem Soc* **1989,** *111* (8), 3051-3058.

235. Erkkila, K. E.; Odom, D. T.; Barton, J. K., Recognition and Reaction of Metallointercalators with DNA. *Chem Rev* **1999,** *99* (9), 2777-2796.

236. Rajput, C.; Rutkaite, R.; Swanson, L.; Haq, I.; Thomas, J. A., Dinuclear monointercalating Ru(II) complexes that display high affinity binding to duplex and quadruplex DNA. *Chem Eur J* **2006,** *12* (17), 4611-4619.

237. Shi, S.; Liu, J.; Yao, T.; Geng, X.; Jiang, L.; Yang, Q.; Cheng, L.; Ji, L., Promoting the formation and stabilization of G-quadruplex by dinuclear RuII complex $Ru_2(obip)L_4$. *Inorg Chem* **2008,** *47* (8), 2910-2912.

238. Leung, K. H.; He, H. Z.; Wang, W.; Zhong, H. J.; Chan, D. S. H.; Leung, C. H.; Ma, D. L., Label-free luminescent switch-on detection of endonuclease IV activity using a G-quadruplex-selective iridium(III) complex. *ACS App Mat Inter* **2013,** *5* (23), 12249-12253.
239. Leung, K. H.; Lu, L.; Wang, M.; Mak, T. Y.; Chan, D. S.; Tang, F. K.; Leung, C. H.; Kwan, H. Y.; Yu, Z.; Ma, D. L., A Label-Free Luminescent Switch-On Assay for ATP Using a G-Quadruplex-Selective Iridium(III) Complex. *PLoS ONE* **2013,** *8* (10), e77021.
240. He, H. Z.; Chan, D. S.; Leung, C. H.; Ma, D. L., A highly selective G-quadruplex-based luminescent switch-on probe for the detection of gene deletion. *Chem Commun* **2012,** *48* (76), 9462-9464.
241. He, H. Z.; Leung, K. H.; Yang, H.; Chan, D. S.; Leung, C. H.; Zhou, J.; Bourdoncle, A.; Mergny, J. L.; Ma, D. L., Label-free detection of sub-nanomolar lead(II) ions in aqueous solution using a metal-based luminescent switch-on probe. *Biosens Bioelectron* **2013,** *41*, 871-874.
242. Yang, H.; Ma, V. P. Y.; Chan, D. S. H.; He, H. Z.; Leung, C. H.; Ma, D. L., A Cyclometallated Iridium(III) Complex As a c-myc G-Quadruplex Stabilizer and Down-Regulator of c-myc Oncogene Expression. *Curr Med Chem* **2013,** *20* (4), 576-582.
243. Lippard, S.; Bond, P.; Wu, K.; Bauer, W., Stereochemical requirements for intercalation of platinum complexes into double-stranded DNA's. *Science* **1976,** *194* (4266), 726-728.
244. Kieltyka, R.; Fakhoury, J.; Moitessier, N.; Sleiman, H. F., Platinum phenanthroimidazole complexes as G-quadruplex DNA selective binders. *Chem Eur J* **2008,** *14* (4), 1145-1154.
245. Castor, K. J.; Mancini, J.; Fakhoury, J.; Weill, N.; Kieltyka, R.; Englebienne, P.; Avakyan, N.; Mittermaier, A.; Autexier, C.; Moitessier, N.; Sleiman, H. F., Platinum(II) phenanthroimidazoles for targeting telomeric G-quadruplexes. *ChemMedChem* **2012,** *7* (1), 85-94.
246. Castor, K. J.; Liu, Z.; Fakhoury, J.; Hancock, M. A.; Mittermaier, A.; Moitessier, N.; Sleiman, H. F., A Platinum(II) Phenylphenanthroimidazole with an Extended Side-Chain Exhibits Slow Dissociation from a c-Kit G-Quadruplex Motif. *Chem Eur J* **2013,** *19* (52), 17836-17845.
247. Reed, J. E.; Neidle, S.; Vilar, R., Stabilisation of human telomeric quadruplex DNA and inhibition of telomerase by a platinum-phenanthroline complex. *Chem Commun* **2007,** (42), 4366-4368.
248. Bertrand, H.; Monchaud, D.; De Cian, A.; Guillot, R.; Mergny, J.-L.; Teulade-Fichou, M.-P., The importance of metal geometry in the recognition of G-quadruplex-DNA by metal-terpyridine complexes. *Org Biomol Chem* **2007,** *5* (16), 2555-2559.
249. Suntharalingam, K.; White, A. J.; Vilar, R., Synthesis, structural characterization, and quadruplex DNA binding studies of platinum(II)-terpyridine complexes. *Inorg Chem* **2009,** *48* (19), 9427-9435.

250. Suntharalingam, K.; White, A. J.; Vilar, R., Two metals are better than one: investigations on the interactions between dinuclear metal complexes and quadruplex DNA. *Inorg Chem* **2010,** *49* (18), 8371-8380.

251. Largy, E.; Hamon, F.; Rosu, F.; Gabelica, V.; De Pauw, E.; Guedin, A.; Mergny, J. L.; Teulade-Fichou, M. P., Tridentate N-donor palladium(II) complexes as efficient coordinating quadruplex DNA binders. *Chem Eur J* **2011,** *17* (47), 13274-13283.

252. Shoukry, M.; Hohmann, H.; van Eldik, R., Mechanistic information on the reaction of model palladium(II) complexes with purine nucleosides and 5-nucleotides in reference to the antitumor activity of related platinum complexes. *Inorg Chim Acta* **1992,** *198-200*, 187-192.

253. Burda, J. V.; Zeizinger, M.; Leszczynski, J., Activation barriers and rate constants for hydration of platinum and palladium square-planar complexes: an ab initio study. *J Chem Phys* **2004,** *120* (3), 1253-1262.

254. Garoufis, A.; Hadjikakou, S. K.; Hadjiliadis, N., Palladium coordination compounds as anti-viral, anti-fungal, anti-microbial and anti-tumor agents. *Coord Chem Rev* **2009,** *253* (9-10), 1384-1397.

255. Campbell, N. H.; Karim, N. H.; Parkinson, G. N.; Gunaratnam, M.; Petrucci, V.; Todd, A. K.; Vilar, R.; Neidle, S., Molecular basis of structure-activity relationships between salphen metal complexes and human telomeric DNA Quadruplexes. *J Med Chem* **2012,** *55* (1), 209-222.

256. Abd Karim, N. H.; Mendoza, O.; Shivalingam, A.; Thompson, A. J.; Ghosh, S.; Kuimova, M. K.; Vilar, R., Salphen metal complexes as tunable G-quadruplex binders and optical probes. *RSC Adv* **2014,** *4* (7), 3355-3363.

257. Khan, N. U.; Pandya, N.; Kumar, M.; Bera, P. K.; Kureshy, R. I.; Abdi, S. H.; Bajaj, H. C., Influence of chirality using Mn(III) salen complexes on DNA binding and antioxidant activity. *Org Biomol Chem* **2010,** *8* (19), 4297-4307.

258. Papkovsky, D. B.; O'Riordan, T. C., Emerging applications of phosphorescent metalloporphyrins. *J Fluores* **2005,** *15* (4), 569-584.

259. Iris, A. H.; Gross, Z., Aura of corroles. *Chem Eur J* **2009,** *15* (34), 8382-8394.

260. Keating, L. R.; Szalai, V. A., Parallel-stranded guanine quadruplex interactions with a copper cationic porphyrin. *Biochem* **2004,** *43* (50), 15891-15900.

261. Dixon, I. M.; Lopez, F.; Esteve, J. P.; Tejera, A. M.; Blasco, M. A.; Pratviel, G.; Meunier, B., Porphyrin derivatives for telomere binding and telomerase inhibition. *ChemBioChem* **2005,** *6* (1), 123-132.

262. Bhattacharjee, A. J.; Ahluwalia, K.; Taylor, S.; Jin, O.; Nicoludis, J. M.; Buscaglia, R.; Brad Chaires, J.; Kornfilt, D. J.; Marquardt, D. G.; Yatsunyk, L. A., Induction of G-quadruplex DNA structure by Zn(II) 5,10,15,20-tetrakis(N-methyl-4-pyridyl)porphyrin. *Biochimie* **2011,** *93* (8), 1297-1309.

263. Travascio, P.; Li, Y.; Sen, D., DNA-enhanced peroxidase activity of a DNA aptamer-hemin complex. *Chem & Biol* **1998,** *5* (9), 505-517.

264. Freeman, R.; Sharon, E.; Teller, C.; Henning, A.; Tzfati, Y.; Willner, I., DNAzyme-like activity of hemin-telomeric G-quadruplexes for the optical analysis of telomerase and its inhibitors. *ChemBioChem* **2010,** *11* (17), 2362-2367.

265. Poon, L. C.; Methot, S. P.; Morabi-Pazooki, W.; Pio, F.; Bennet, A. J.; Sen, D., Guanine-rich RNAs and DNAs that bind heme robustly catalyze oxygen transfer reactions. *J Am Chem Soc* **2011,** *133* (6), 1877-1884.

266. Golub, E.; Niazov, A.; Freeman, R.; Zatsepin, M.; Willner, I., Photoelectrochemical Biosensors Without External Irradiation: Probing Enzyme Activities and DNA Sensing Using Hemin/G-Quadruplex-Stimulated Chemiluminescence Resonance Energy Transfer (CRET) Generation of Photocurrents. *J Phys Chem C* **2012,** *116* (25), 13827-13834.

267. Golub, E.; Freeman, R.; Willner, I., Hemin/G-quadruplex-catalyzed aerobic oxidation of thiols to disulfides: application of the process for the development of sensors and aptasensors and for probing acetylcholine esterase activity. *Anal Chem* **2013,** *85* (24), 12126-12133.

268. Goncalves, D. P.; Rodriguez, R.; Balasubramanian, S.; Sanders, J. K., Tetramethylpyridiniumporphyrazines--a new class of G-quadruplex inducing and stabilising ligands. *Chem Commun* **2006,** *2* (45), 4685-4687.

269. Ren, L.; Zhang, A.; Huang, J.; Wang, P.; Weng, X.; Zhang, L.; Liang, F.; Tan, Z.; Zhou, X., Quaternary ammonium zinc phthalocyanine: inhibiting telomerase by stabilizing G quadruplexes and inducing G-quadruplex structure transition and formation. *ChemBioChem* **2007,** *8* (7), 775-780.

270. Fu, B.; Zhang, D.; Weng, X.; Zhang, M.; Heng, M.; Yuzhi, M.; Zhou, X., Cationic metal-corrole complexes: Design, synthesis, and properties of guanine-quadruplex stabilizers. *Chem Eur J* **2008,** *14* (30), 9431-9441.

271. Arola-Arnal, A.; Benet-Buchholz, J.; Neidle, S.; Vilar, R., Effects of metal coordination geometry on stabilization of human telomeric quadruplex DNA by square-planar and square-pyramidal metal complexes. *Inorg Chem* **2008,** *47* (24), 11910-11919.

272. Fujita, M.; Yazaki, J.; Ogura, K., Preparation of a macrocyclic polynuclear complex, $[(en)Pd(4,4\text{-bpy})]^{4+}(NO_3)^{8+}$, which recognizes an organic molecule in aqueous media. *J Am Chem Soc* **1990,** *112* (14), 5645-5647.

273. Stang, P. J.; Cao, D. H.; Saito, S.; Arif, A. M., Self-assembly of cationic, tetranuclear, Pt(II) and Pd(II) macrocyclic squares. X-ray crystal structure of $[Pt^{2+}(dppp)(4,4\text{-bipyridyl})_2\text{-}OSO_2CF_3]^{4+}$. *J Am Chem Soc* **1995,** *117* (23), 6273-6280.

274. Kieltyka, R.; Englebienne, P.; Fakhoury, J.; Autexier, C.; Moitessier, N.; Sleiman, H. F., A platinum supramolecular square as an effective G-quadruplex binder and telomerase inhibitor. *J Am Chem Soc* **2008,** *130* (31), 10040-10041.

275. Zheng, X. H.; Zhong, Y. F.; Tan, C. P.; Ji, L. N.; Mao, Z. W., Pt(II) squares as selective and effective human telomeric G-quadruplex binders and potential cancer therapeutics. *Dalton Trans* **2012**, 41, 11807-11812.

276. Lehn, J. M.; Rigault, A.; Siegel, J.; Harrowfield, J.; Chevrier, B.; Moras, D., Spontaneous assembly of double-stranded helicates from oligobipyridine ligands and copper(I) cations: structure of an inorganic double helix. *Proc Natl Acad Sci USA* **1987,** *84* (9), 2565-2569.

277. Hasenknopf, B.; Lehn, J.-M.; Boumediene, N.; Dupont-Gervais, A.; Van Dorsselaer, A.; Kneisel, B.; Fenske, D., Self-Assembly of Tetra- and Hexanuclear Circular Helicates. *J Am Chem Soc* **1997,** *119* (45), 10956-10962.

278. Orita, A.; Jiang, L.; Nakano, T.; Ma, N.; Otera, J., Solventless reaction dramatically accelerates supramolecular self-assembly. *Chem Commun* **2002,** (13), 1362-1363.

279. Yu, H.; Wang, X.; Fu, M.; Ren, J.; Qu, X., Chiral metallo-supramolecular complexes selectively recognize human telomeric G-quadruplex DNA. *Nucleic Acids Res* **2008,** *36* (17), 5695-5703.

280. Neidle, S.; Thurston, D. E., Chemical approaches to the discovery and development of cancer therapies. *Nature Rev Cancer* **2005,** *5* (4), 285-296.

281. Pinto, A. L.; Lippard, S. J., Binding of the antitumor drug *cis*-diamminedichloroplatinum(II) (cisplatin) to DNA. *Biochim Biophys Acta Rev Cancer* **1984,** *780* (3), 167-180.

282. Bancroft, D. P.; Lepre, C. A.; Lippard, S. J., ^{195}Pt NMR kinetic and mechanistic studies of *cis*- and *trans*-diamminedichloroplatinum(II) binding to DNA. *J Am Chem Soc* **1990,** *112* (19), 6860-6871.

283. Hou, X. M.; Zhang, X. H.; Wei, K. J.; Ji, C.; Dou, S. X.; Wang, W. C.; Li, M.; Wang, P. Y., Cisplatin induces loop structures and condensation of single DNA molecules. *Nucleic Acids Res* **2009,** *37* (5), 1400-1410.

284. Basu, A.; Krishnamurthy, S., Cellular responses to Cisplatin-induced DNA damage. *J Nucleic Acids* **2010,** *2010*.

285. Phan, A. T.; Kuryavyi, V.; Gaw, H. Y.; Patel, D. J., Small-molecule interaction with a five-guanine-tract G-quadruplex structure from the human MYC promoter. *Nature Chem Biol* **2005,** *1* (3), 167-173.

286. Dash, J.; Shirude, P. S.; Hsu, S. T.; Balasubramanian, S., Diarylethynyl amides that recognize the parallel conformation of genomic promoter DNA G-quadruplexes. *J Am Chem Soc* **2008,** *130* (47), 15950-15956.

287. Wang, P.; Leung, C. H.; Ma, D. L.; Yan, S. C.; Che, C. M., Structure-based design of platinum(II) Complexes as c-myc oncogene Down-regulators and luminescent probes for G-quadruplex DNA. *Chem Eur J* **2010,** *16* (23), 6900-6911.

288. Zhang, X. F.; Zhang, H. J.; Xiang, J. F.; Li, Q. A.; Yang, Q. F.; Shang, Q. A.; Zhang, Y. X.; Tang, Y. L., The binding modes of carbazole derivatives with telomere G-quadruplex. *J Mol Struct* **2010,** *982* (1-3), 133-138.

289. Trotta, R.; De Tito, S.; Lauri, I.; La Pietra, V.; Marinelli, L.; Cosconati, S.; Martino, L.; Conte, M. R.; Mayol, L.; Novellino, E.; Randazzo, A., A more detailed picture of the interactions between virtual screening-derived hits and the DNA G-quadruplex: NMR, molecular modelling and ITC studies. *Biochimie* **2011,** *93* (8), 1280-1287.
290. Jager, K.; Bats, J. W.; Ihmels, H.; Granzhan, A.; Uebach, S.; Patrick, B. O., Polycyclic azoniahetarenes: assessing the binding parameters of complexes between unsubstituted ligands and G-quadruplex DNA. *Chem Eur J* **2012,** *18* (35), 10903-10915.
291. Li, Z.; Tan, J. H.; He, J. H.; Long, Y.; Ou, T. M.; Li, D.; Gu, L. Q.; Huang, Z. S., Disubstituted quinazoline derivatives as a new type of highly selective ligands for telomeric G-quadruplex DNA. *Eur J Med Chem* **2012,** *47* (1), 299-311.
292. David, W. M.; Brodbelt, J.; Kerwin, S. M.; Thomas, P. W., Investigation of quadruplex oligonucleotide-drug interactions by electrospray ionization mass spectrometry. *Anal Chem* **2002,** *74* (9), 2029-2033.
293. Oehlers, L.; Mazzitelli, C. L.; Brodbelt, J. S.; Rodriguez, M.; Kerwin, S., Evaluation of complexes of DNA duplexes and novel benzoxazoles or benzimidazoles by electrospray ionization mass spectrometry. *J Am Soc Mass Spectrom* **2004,** *15* (11), 1593-1603.
294. Mazzitelli, C. L.; Brodbelt, J. S.; Kern, J. T.; Rodriguez, M.; Kerwin, S. M., Evaluation of binding of perylene diimide and benzannulated perylene diimide ligands to DNA by electrospray ionization mass spectrometry. *J Am Soc Mass Spectrom* **2006,** *17* (4), 593-604.
295. Mazzitelli, C. L.; Brodbelt, J. S., Probing ligand binding to duplex DNA using $KMnO_4$ reactions and electrospray ionization tandem mass spectrometry. *Anal Chem* **2007,** *79* (12), 4636-4647.
296. Mazzitelli, C. L.; Chu, Y.; Reczek, J. J.; Iverson, B. L.; Brodbelt, J. S., Screening of threading bis-intercalators binding to duplex DNA by electrospray ionization tandem mass spectrometry. *J Am Soc Mass Spectrom* **2007,** *18* (2), 311-321.
297. Smith, S. I.; Guziec, L. J.; Guziec, F. S., Jr.; Hasinoff, B. B.; Brodbelt, J. S., Evaluation of relative DNA binding affinities of anthrapyrazoles by electrospray ionization mass spectrometry. *J Mass Spectrom* **2007,** *42* (5), 681-688.
298. Pierce, S. E.; Kieltyka, R.; Sleiman, H. F.; Brodbelt, J. S., Evaluation of binding selectivities and affinities of platinum-based quadruplex interactive complexes by electrospray ionization mass spectrometry. *Biopolymers* **2009,** *91* (4), 233-243.
299. Haq, I.; Trent, J. O.; Chowdhry, B. Z.; Jenkins, T. C., Intercalative G-tetraplex stabilization of telomeric DNA by a cationic porphyrin. *J Am Chem Soc* **1999,** *121* (9), 1768-1779.
300. Martino, L.; Pagano, B.; Fotticchia, I.; Neidle, S.; Giancola, C., Shedding light on the interaction between TMPyP4 and human telomeric quadruplexes. *J Phys Chem B* **2009,** *113* (44), 14779-14786.

301. Prislan, I.; Khutsishvili, I.; Marky, L. A., Interaction of minor groove ligands with G-quadruplexes: thermodynamic contributions of the number of quartets, T-U substitutions, and conformation. *Biochimie* **2011,** *93* (8), 1341-1350.
302. Han, H.; Langley, D. R.; Rangan, A.; Hurley, L. H., Selective interactions of cationic porphyrins with G-quadruplex structures. *J Am Chem Soc* **2001,** *123* (37), 8902-8913.
303. Bhattacharya, S.; Chaudhuri, P.; Jain, A. K.; Paul, A., Symmetrical bisbenzimidazoles with benzenediyl spacer: the role of the shape of the ligand on the stabilization and structural alterations in telomeric G-quadruplex DNA and telomerase inhibition. *Bioconjug Chem* **2010,** *21* (7), 1148-1159.
304. Sun, D.; Zhang, R.; Yuan, F.; Liu, D.; Zhou, Y.; Liu, J., Studies on characterization, telomerase inhibitory properties and G-quadruplex binding of η6-arene ruthenium complexes with 1,10-phenanthroline-derived ligands. *Dalton Trans* **2012,** *41* (6), 1734-1741.
305. Nordén, B., Structure of DNA metal complexes in solution studied by linear and circular dichroism. $[Pt(II)(ethylenediamine)(2,2\text{-}dipyridine)]^{2+}$ binds strongly to DNA by intercalation. $[Cu(II)(2,2\text{-}dipyridine)_2]^{2+}$ is not intercalated. *Inorg Chim Acta* **1978,** *31* (C), 83-95.
306. Berova, N.; Nakanishi, K.; Woody, R., *Circular dichroism : principles and applications*. Wiley-VCH: New York, 2000.
307. Paramasivan, S.; Rujan, I.; Bolton, P. H., Circular dichroism of quadruplex DNAs: applications to structure, cation effects and ligand binding. *Methods* **2007,** *43* (4), 324-331.
308. Sen, D.; Gilbert, W., Guanine quartet structures. **1992,** *211*, 191-199.
309. Simonsson, T., G-quadruplex DNA structures--variations on a theme. *Biol Chem* **2001,** *382* (4), 621-628.
310. Kalsi, P. S., *Spectroscopy of Organic Compounds*. New Age International (P) Limited: 2004.
311. Anderson, R. J.; Bendell, D. J.; Groundwater, P. W., Organic Spectroscopic Analysis. Royal Society of Chemistry: 2004; pp 7-23.
312. Dedon, P. C., Determination of Binding Thermodynamics. In *Curr Protoc Nucleic Acid Chem*, John Wiley & Sons, Inc.: 2001.
313. Dedon, P. C., Determination of binding mode: intercalation. *Curr Protoc Nucleic Acid Chem* **2001,** *Chapter 8*, Unit 8 1.
314. Cusumano, M.; Di Pietro, M. L.; Giannetto, A., DNA interaction of platinum(II) complexes with 1,10-phenanthroline and extended phenanthrolines. *Inorg Chem* **2006,** *45* (1), 230-235.
315. De Cian, A.; Guittat, L.; Shin-ya, K.; Riou, J. F.; Mergny, J. L., Affinity and selectivity of G4 ligands measured by FRET. *Nucleic Acids Symp Ser (Oxf)* **2005,** (49), 235-236.
316. Juskowiak, B.; Takenaka, S., Fluorescence Resonance Energy Transfer in the Studies of Guanine Quadruplexes. In *Fluorescent Energy Transfer Nucleic Acid Probes*, Didenko, V., Ed. Humana Press: 2006; Vol. 335, pp 311-341.

317. Introduction to Fluorescence. In *Principles of Fluorescence Spectroscopy*, Lakowicz, J., Ed. Springer US: 2006; pp 1-26.
318. Sapsford, K. E.; Berti, L.; Medintz, I. L., Materials for fluorescence resonance energy transfer analysis: beyond traditional donor-acceptor combinations. *Angew Chem Int Ed* **2006,** *45* (28), 4562-4589.
319. De Cian, A.; Guittat, L.; Kaiser, M.; Sacca, B.; Amrane, S.; Bourdoncle, A.; Alberti, P.; Teulade-Fichou, M. P.; Lacroix, L.; Mergny, J. L., Fluorescence-based melting assays for studying quadruplex ligands. *Methods* **2007,** *42* (2), 183-195.
320. Rachwal, P. A.; Fox, K. R., Quadruplex melting. *Methods* **2007,** *43* (4), 291-301.
321. Largy, E.; Hamon, F.; Teulade-Fichou, M. P., Development of a high-throughput G4-FID assay for screening and evaluation of small molecules binding quadruplex nucleic acid structures. *Anal Bioanal Chem* **2011,** *400* (10), 3419-3427.
322. Nygren, J.; Svanvik, N.; Kubista, M., The interactions between the fluorescent dye thiazole orange and DNA. *Biopolymers* **1998,** *46* (1), 39-51.
323. Largy, E.; Granzhan, A.; Hamon, F.; Verga, D.; Teulade-Fichou, M. P., Visualizing the quadruplex: from fluorescent ligands to light-up probes. *Top Curr Chem* **2013,** *330*, 111-77.
324. When browsing suppliers, it became immediately obvious that one non-disposable black quartz microplate cost 1000x more than 50 disposable black polypropylene plates. In order to truly utilize the high-throughput nature of the assay, we opted for the disposable polypropylene plates with the knowledge that our results may be artificially high. .
325. Nanjunda, R.; Owens, E. A.; Mickelson, L.; Alyabyev, S.; Kilpatrick, N.; Wang, S.; Henary, M.; Wilson, W. D., Halogenated pentamethine cyanine dyes exhibiting high fidelity for G-quadruplex DNA. *Bioorg Med Chem* **2012,** *20* (24), 7002-7011.
326. Tanious, F. A.; Nguyen, B.; Wilson, W. D., Biosensor‐Surface Plasmon Resonance Methods for Quantitative Analysis of Biomolecular Interactions. **2008,** *84*, 53-77.
327. Lofas, S., Dextran modified self-assembled monolayer surfaces for use in biointeraction analysis with surface plasmon resonance. *Pure Appl Chem* **1995,** *67* (5), 829-834.
328. Löfås, S.; Malmqvist, M.; Rönnberg, I.; Stenberg, E.; Liedberg, B.; Lundström, I., Bioanalysis with surface plasmon resonance. *Sens Act B: Chem* **1991,** *5* (1–4), 79-84.
329. Liedberg, B.; Nylander, C.; Lundstrom, I., Surface-Plasmon Resonance for Gas-Detection and Biosensing. *Sens Act* **1983,** *4* (2), 299-304.
330. Nenninger, G. G.; Clendenning, J. B.; Furlong, C. E.; Yee, S. S., Reference-compensated biosensing using a dual-channel surface plasmon resonance sensor system based on a planar lightpipe configuration. *Sens Act B: Chem* **1998,** *51* (1–3), 38-45.

2 Platinum(II) Phenanthroimidazoles for Targeting Telomeric G-Quadruplexes

Preface: Author Contributions and Publication

This chapter represents a highly collaborative effort among the Sleiman (Department of Chemistry), Moitessier (Department of Chemistry), and Autexier (Departments of Anatomy & Cell Biology and Experimental Medicine) laboratories at McGill University, with data interpretation assistance from **Prof. Anthony Mittermaier** (Department of Chemistry). **Katherine Castor** was responsible for the synthesis, characterization, and biophysical studies (CD, FID) herein, as well as project design. **Dr. Roxanne Kieltyka** developed the initial synthesis of complexes **2.1**-**2.4**. Synthesis of complexes **2.5** and **2.6** was assisted by a summer undergraduate, **Nicole Avakyan**. The computer-aided studies were performed by **Dr. Pablo Englebienne** and **Dr. Nathanael Weill** under the supervision of **Prof. Nicolas Moitessier**. The TRAP-Lig assays were performed by **Dr. Johans Fakhoury** (Sleiman and Autexier laboratories) and **Johanna Mancini** (Autexier). **Johanna Mancini** also conducted the celluar assays under the supervision of **Prof. Chantal Autexier**. The findings in this chapter were published in a manuscript accepted by ChemMedChem in 2012 entitled "Platinum(II) phenanthroimidazoles for targeting telomeric G-quadruplexes".

2.1 Introduction

Guanine quadruplexes have gained recognition as important targets for chemotherapeutic drug design as a consequence of their potential to interfere with cancer cell proliferation.[1,2] These higher-order DNA structures, held together by Hoogsteen hydrogen bonds, result from the folding of a guanine (G) rich DNA sequence in the presence of potassium or sodium cations.[3] G-quadruplex forming sequences have been identified throughout the human genome − in telomeres, promoter regions of oncogenes, nuclease hypersensitivity regions and untranslated regions of RNA, to name a few.[4,5] From this list, as described in Chapter 1 (pp 7), a highly investigated G-quadruplex target for small molecule drug candidates is the telomere. At its 3'-terminus, the human telomere is a single DNA strand composed of $(TTAGGG)_n$ repeats.[6] Biologically relevant phenomena are reported to occur upon the folding of this sequence into a G-quadruplex structure, such as loss of telomere integrity through disruption of the protective shelterin complex of proteins.[7,8] This results in the activation of DNA damage response (DDR) mechanisms that follow recognition of double-strand breaks,[9,10] such as the activation of poly-(ADP-ribose) polymerase,[11] and ataxia telangiectasia mutatated

gene product signaling.[12,13] Due to the inherent genetic instability in cancer cells,[14] the inhibition of any of the DDR pathways may result in cellular senescence and/or apoptosis.[15,16] Thus, the stabilization of G-quadruplexes is predicted to have profound effects on cancer cell proliferation *via* a number of mechanisms, thereby accomplishing one of the main goals of chemotherapy − to halt tumor growth.

The use of small molecule binders to stabilize the G-quadruplex DNA motif is a possible approach to achieve this therapeutic goal. To date, a large number of compounds with varying degrees of efficacy in their ability to target this higher-order DNA structure have been reported.[14,15] Based on this wealth of empirical data − not only obtained from binding studies, but also from molecular modeling and crystal structure determination of quadruplex-ligand complexes,[21,30] several clues towards the rational design of G-quadruplex binders have been uncovered, including the need for an electron-poor aromatic π-surface, positive charges in the scaffold and the presence of positively charged side-arms.[17]

Most classical G-quadruplex binders are purely organic heteroaromatic compounds.[17] A particularly attractive strategy for designing G-quadruplex binders is through the incorporation of metal centers, as they offer a large variety of structural and functional features that can be exploited for optimal binding. In particular, platinum(II) complexes can introduce a square planar geometry unavailable to carbon compounds and can act as electron withdrawing groups to further increase positive character on the ligand. They can also simplify synthetic access to G-quadruplex binders and allow for the modular generation of compound libraries in a minimum number of steps.

In this report, we examine the construction of a new class of platinum(II) phenanthroimidazole complexes as guanine quadruplex binders for telomeric DNA sequences. Through circular dichroism (CD), fluorescence intercalator displacement assays (FID), and a modified telomeric repeat amplification protocol assay (TRAP-Lig), we structurally evolve these highly modular and synthetically accessible constructs towards optimal G-quadruplex binding. In particular, we examine the effect of increasing the π-surface of the ligand through aromatic ring

extension and by introducing different hydrogen bonding interactions. We also probe the effect of introducing an electron withdrawing substituent on binding affinity, selectivity and telomerase inhibition. Lastly, we perform preliminary cell studies which confirm the ability of the optimized structure to target cancer cells.

2.2 Results and Discussion

2.2.1 Design and synthesis of phenanthroimidazole platinum(II) complexes

One of the greatest challenges in designing compounds as G-quadruplex binders is to construct complexes that are selective towards G-quadruplexes rather than the far more abundant B-DNA contained within the genome. To date, a large number of compounds have been reported which possess varying degrees of efficacy in their abilities to selectively target this higher-order DNA structure.[17-20] Several characteristics have been deemed necessary for selective targeting including molecules with larger π-surface areas so as to maximize the electrostatic interactions with the planar aromatic surface of the G-quadruplex.[17] Additionally, these molecules should be large enough for intercalation into B-DNA to be hindered. This can be achieved through the addition of positively-charged side-chains, which can also increase interactions with the negatively charged phosphate backbone of the DNA. As previously mentioned, G-quadruplexes have four grooves[21] (as compared to the two grooves of B-DNA), so designing side-chains that can penetrate multiple grooves would also be beneficial.

To generate compounds with the above mentioned characteristics, the use of standard organic chemistry could prove difficult, due to the number of steps required. For example, the much-studied natural product G-quadruplex binder telomestatin, requires around 16 synthetic steps and results in a low overall yield (Figure 2.1).[22,23] Conversely, an attractive strategy for designing G-quadruplex binders employs the incorporation of metal centers (e.g. nickel(II), ruthenium(III), palladium(II), platinum(II), etc), as the synthesis of metal complexes requires much fewer steps from ligand to complex, and they offer a large variety of structural and functional features that can be exploited for optimal binding. One

feature is the inherent positive charge of the metal, and when coupled with an aromatic ligand, the combination presents a large, electron-poor π-surface. In particular, platinum(II) complexes can introduce a square planar geometry unavailable to carbon-based and other heteroaromatic compounds.

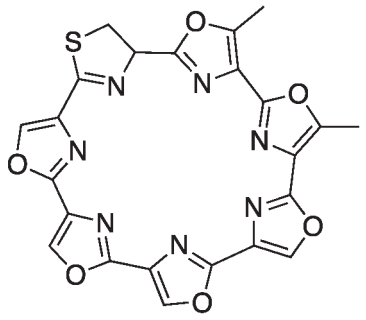

Figure 2.1 The structure of the natural product telomestatin.

A previous graduate student, Dr. Roxanne Kieltyka has shown that two platinum(II) phenanthroimidazole complexes with extended π-surfaces afford greater binding affinity to the tetrameric, intermolecular G-quadruplex than to duplex DNA (Chapter 1, pp 37-40).[24] In this chapter, we expand the existing library of complexes in a rational manner so as to improve binding affinity towards more biologically relevant, telomere-derived intramolecular G-quadruplexes. This can be achieved through increasing the π-surface area of phenanthroimidazole ligand *via* coupling of the 1,10-phenanthroline-5,6-dione precursor with π-extended aldehydes such as quinoline-8-carbaldehyde, 1*H*-indole-carbaldehyde, and 7-hydroxy-1-naphthaldehyde, among others.

In addition to the aforementioned aldehydes providing a π-extended surface, they also contain hydrogen-bond donors or acceptors. Precedents set by Mergny and coworkers[25,26] demonstrate that molecules containing intramolecular hydrogen-bonds (e.g. 2,6-pyridine-dicarboxamide and 1,10-phenanthroline-2,9-dicarboxamide compounds) adopt a *syn-syn* conformation[27] such that the internal hydrogen-bonds hold the complex in a flat, planar arrangement (Figure 2.2). Mergny and coworkers were able to establish that this property greatly enhances binding affinity to G-quadruplex targets compared to derivatives without the internal hydrogen-bonds.

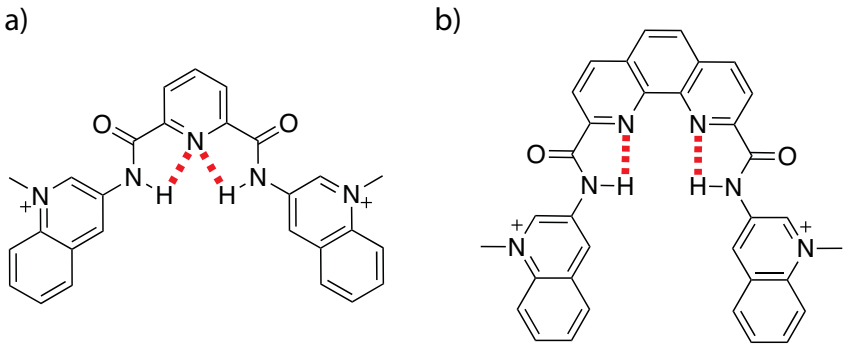

Figure 2.2 Compounds with internal hydrogen-bonding motifs: a) 2,6-pyridine-dicarboxamide core,[25] and b) 1,10-phenanthroline-2,9-dicarboxamide core.[26] Internal hydrogen bonds are shown in red.

Complexes **2.1**-**2.7** (Figure 2.3) possess phenanthroimidazole ligands that are bound to platinum(II)-ethylenediamine metal centers. The phenanthro-imidazole units were synthesized through the condensation of 1,10-phenanthroline-5,6-dione with an aromatic aldehyde (phenyl-, naphthyl-, indolyl-, quinolinyl-, 2-phenol-, 2-hydroxy-1-naphthyl-, or *p*-chlorophenyl-) as previously performed in our lab.[24] Subsequently, these ligands were reacted with potassium tetrachloroplatinate, resulting in [Pt(phenanthroimidazole)Cl_2], followed by treatment with ethylenediamine (en) and precipitation with ammonium hexafluorophosphate, resulting in complexes **2.1** (phenyl-) and **2.2** (naphthyl-),[24] **2.3** (indolyl-) and **2.4** (quinolinyl-), **2.5** (phenol-) and **2.6** (hydroxynaphthyl-), and finally **2.7** (*p*-chlorophenyl-).[28] For comparison, $[Pt(bipyridine)(en)]^{2+}$ (complex **2.8**) which has been previously shown to bind to duplex DNA by intercalation through a significantly less π-extended system than complexes **2.1**-**2.7** was also synthesized and used as a negative control for G-quadruplex binding.[24,29] Complexes **2.3** and **2.4** were light-sensitive and needed to be handled in the dark to avoid decomposition. Complex **2.6** was not used in this study as solubility in H_2O and buffered conditions at low concentrations (< 100 μM) was extremely poor. Through CD, FID, and the telomerase inhibition assay TRAP-Lig, we studied the outcome of the structural differences of these highly modular and synthetically accessible constructs towards optimal G-quadruplex binding.

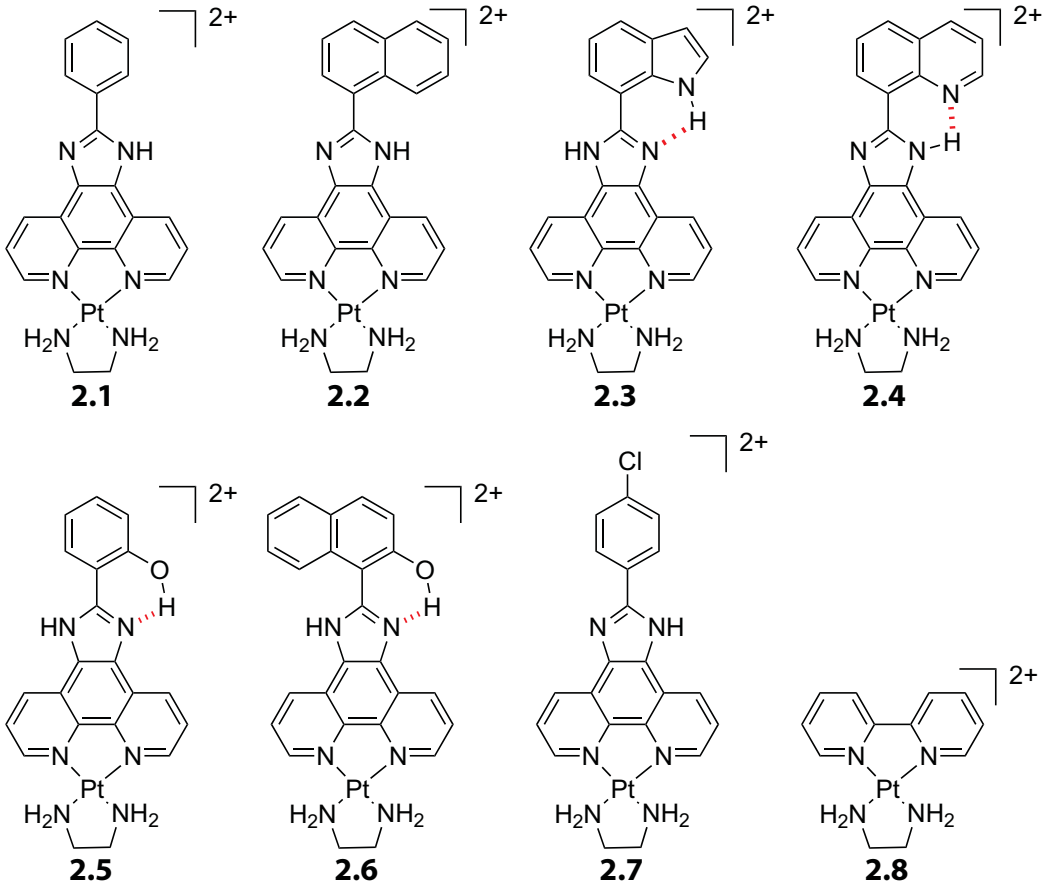

Figure 2.3 Platinum(II) complexes used in this study. Phenylphenanthroimidazole ethylenediamine platinum(II) (**2.1**), naphthylphenanthroimidazole ethylenediamine platinum(II) (**2.2**), indolylphenanthroimidazole ethylenediamine platinum(II) (**2.3**), quinolinylphenanthroimidazole ethylenediamine platinum(II) (**2.4**), salicylphenanthroimidazole ethylenediamine platinum(II) (**2.5**), 2-hydroxy-1-naphthylphenanthroimidazole ethylenediamine platinum(II) (**2.6**) *p*-chlorophenylphenanthroimidazole ethylenediamine platinum(II) (**2.7**), bipyridine ethylenediamine platinum(II) **(2.8**). Red hashed lines in complexes **2.3**-**2.6** represent intramolecular hydrogen bonds.

2.2.2 Binding affinity and selectivity of the phenyl complex 2.1

As discussed in Chapter 1 (pp 6), the folding of G-quadruplex polymorphs is highly dependent on the presence of cations (namely K^+, Na^+, Sr^{2+}) in solution. Here, we used the human telomeric sequence 22AG (5'-A($G_3T_2A)_3G_3$-3') as this sequence is biologically relevant. As the sequence is guanine-rich, any presence of cations could cause the sequence to fold into a G-quadruplex secondary structure. Hence, in order to ensure the 22AG sequence is single-stranded at the start of the titration and that any folding thereafter is caused by the parent phenylphenanthroimidazole complex **2.1**, the DNA was dialyzed against Milli-Q

water for 1−3 days to remove any excess salts remaining from the DNA purification process. We then examined the ability of the phenyl- complex **2.1** to template the folding of a G-quadruplex structure from single-stranded DNA. This was carried out by titration of 22AG with phenyl- complex **2.1**, followed by CD analysis. In this assay, if templation occurs, a decrease in the CD peaks associated with the single-stranded oligonucleotide (slight negative peak at 238 nm and strong positive peak at 257 nm) and the concomitant appearance of peaks associated with G-quadruplex structures are expected (Figure 2.4). An antiparallel, basket G-quadruplex, such as that found in buffer solutions containing Na^+-cations, would result in a characteristic positive peak at 292 nm and a negative peak at 262 nm for this sequence (Figure 2.4a). A mixed hybrid structure, such as that found in buffer solutions containing K^+-cations, is expected to give two positive maxima at 295 nm and 260 nm (Figure 2.4b and Figure 2.4c).

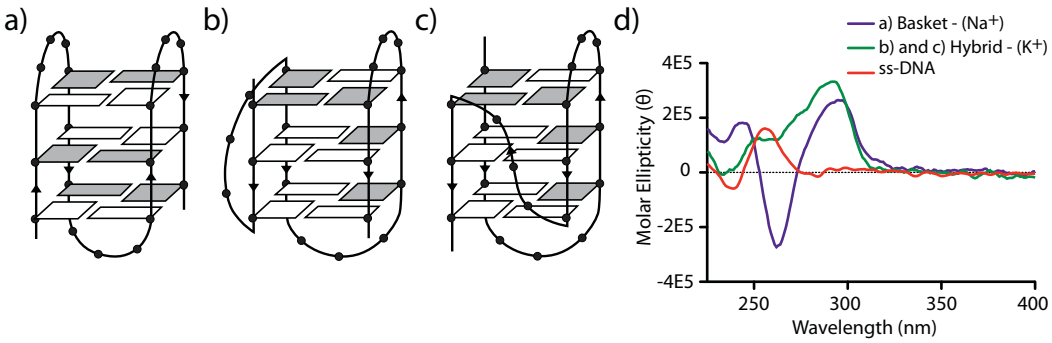

Figure 2.4 Schematics of the quadruplex polymorphs: a) Basket antiparallel structure found in Na^+-containing solutions and b) form 1 and c) form 2 of the (3+1) hybrid structure found in K^+-containing solutions. The gray and white parallelograms represent *syn* and *anti* orientations, respectively, of the guanine bases contained within the tetrads; d) CD spectra of a) (purple), b) and c) (green) structures compared to single-stranded DNA (red).

Upon the gradual addition of phenyl- complex **2.1**, a strong positive peak at 295 nm and negative peak at 260 nm were observed, consistent with templation of a basket-type antiparallel G-quadruplex from this strand (Figure 2.5a) in the absence of added Na^+- or K^+-ions. In contrast, the less π-extended platinum bipyridine complex **2.8** showed no distinct differences upon titration of the single-stranded 22AG, consistent with weaker binding to the G-quadruplex (Figure 2.5b)

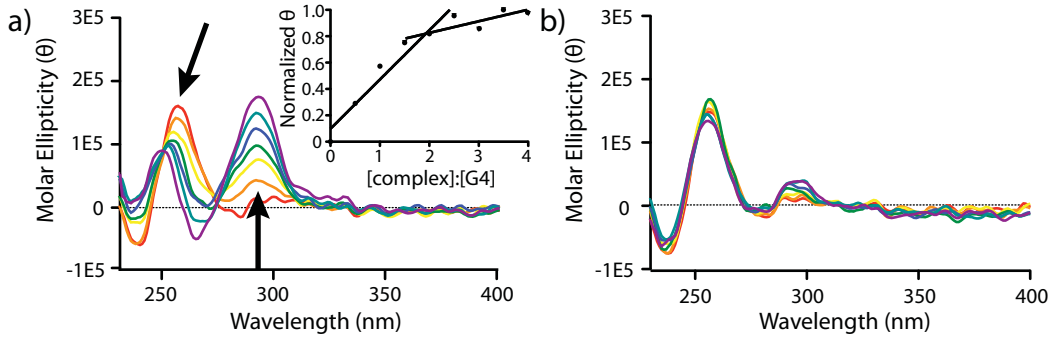

Figure 2.5 CD Spectra of the quadruplex templation with a) **2.1** and b) **2.8**. Arrows in panel a) show the direction of change in CD signal with increasing additions of complex **2.1** (the red trace is ss-DNA and the purple trace is the fully-formed basket polymorph). The inset in panel a) shows the decrease in circular dichroic peak between 250 and 260 nm with added complex **2.1**. The saturation point is at ~ 2:1 ratio of complex **2.1**:quadruplex DNA strand and indicates a 2:1 binding stoichiometry.

Binding stoichiometry of phenyl- complex **2.1** to G-quadruplex DNA can be determined from the changes in molar ellipticities of the CD bands at either 250−260 nm or 285−295 nm. Upon plotting these values as a function of molar equivalents of platinum(II) complex added, it was clear that the curve saturated at approximately a 2:1 ratio of complex **2.1**:quadruplex strand (Figure 2.5a, inset). This is consistent with a binding stoichiometry of 2:1, a value which has previously been reported for other strong G-quadruplex binders, such as telomestatin[30] (Figure 2.1) and a macrocyclic oligoamide.[30,31]

We then examined the binding affinity of phenyl- complex **2.1** to the quadruplex structures using the fluorescence intercalator displacement assay (FID). The FID assay is a binding assay based on work by Teulade-Fichou and coworkers.[32] It relies on competitive displacement of the dye thiazole orange (TO) from the DNA target using small molecule binders, with concomitant decrease in the fluorescence intensity of the dye. Thiazole orange is highly fluorescent when bound to the quadruplex (or duplex DNA) motif and exhibits binding affinities between $10^{6.0}$ and $10^{6.7}$ M^{-1} depending on the sequence to which it is bound.[33] Conversely, the fluorescence of TO is negligible when unbound, that is, in aqueous solution. Thus, displacement of the dye by a stronger binder results in a reduction of the fluorescence of the dye. Binding affinity is evaluated from the concentration of platinum complex that is required to give a 50% decrease in the dye fluorescence (DC_{50}) (see Chapter 1, pp 49 for more details on this assay). Due

to the aforementioned polymorphic nature of human telomeric quadruplexes in the presence of different metal cations,[34,35] we investigated binding affinities to both the Na^+ basket quadruplex and the K^+ hybrid structure (Figure 2.4). We compared our DC_{50} values to those obtained using two duplex DNA targets (a 17mer duplex and a self-complementary 26mer duplex mixed sequence) in order to evaluate the selectivity of our complexes for G-quadruplex versus duplex DNA. The observed $^{G4}DC_{50}$ for phenyl- complex **2.1** of ~ 0.6 μM for both G-quadruplex polymorphs was consistent with good binding affinity, and indicated stronger binding to these quadruplex structures than to duplex DNA ($^{ds}DC_{50}/^{G4}DC_{50}$ ~ 1.3−1.7). These studies also show that phenyl- complex **2.1** binds significantly better than bipyridine complex **2.8**, a compound with a smaller π-surface area, emphasizing the importance of large, extended π-surfaces for G-quadruplex binding to these platinum complexes (Figure 2.3).

		2.1	**2.2**	**2.3**	**2.4**	**2.5**	**2.7**	**2.8**
$^{G4}DC_{50}$	Na^+	0.66	1.30	0.53	0.70	0.53	0.31	>2.50
(μM)	K^+	0.68	1.71	1.55	1.09	0.70	0.66	ND[a]
$^{ds}DC_{50}$	17mer	1.11	2.12	1.37	1.65	1.60	1.47	>2.50
(μM)	26mer	0.84	1.58	1.03	1.37	1.10	1.20	>2.50
Selectivity		1.23-1.68	0.92-1.63	0.66-2.58	1.25-2.36	1.57-3.02	1.82-4.74	-

Table 2.1 DC_{50} values determined from the FID assay. [a] Not determined: given the inability of complex **2.8** to bind strongly to quadruplex DNA, no thiazole orange displacement was observed, and therefore no DC_{50} value could be determined. [b] Selectivity range determined from dividing the lowest $^{ds}DC_{50}$ by the highest $^{G4}DC_{50}$ and the highest $^{ds}DC_{50}$ by the lowest $^{G4}DC_{50}$ for each complex. A selectivity value greater than 1 corresponds to higher selectivity for quadruplex than duplex DNA.

2.2.3 Increasing the π-surface area of the platinum complexes

The parent phenyl phenanthroimidazole complex **2.1** displays good affinity and selectivity towards G-quadruplexes, whereas the bipyridine complex **2.8** shows significantly reduced binding strength towards this target. This encouraged us to examine the effects of increasing the π-surface of these complexes to possibly optimize binding interactions. As such, we introduced a naphthyl-, rather than a phenyl- substituent (complex **2.2**) onto the

phenanthroimidazole ligand on the platinum. Titration of single-stranded DNA with naphthyl- complex **2.2** resulted in templation of the antiparallel G-quadruplex (Figure 2.6), similarly to phenyl- complex **2.1**. However, FID assays showed significantly lower binding affinity to the intramolecular telomeric G-quadruplex, both in sodium ($^{G4}DC_{50}$ = 1.30 μM) and in potassium ($^{G4}DC_{50}$ = 1.71 μM), which was now similar to its affinity for duplex DNA ($^{ds26mer}DC_{50}$ = 1.58 μM). This observation contrasts with our earlier studies, which showed higher affinity of this naphthyl complex towards the all-parallel intermolecular G-quadruplex.[24]

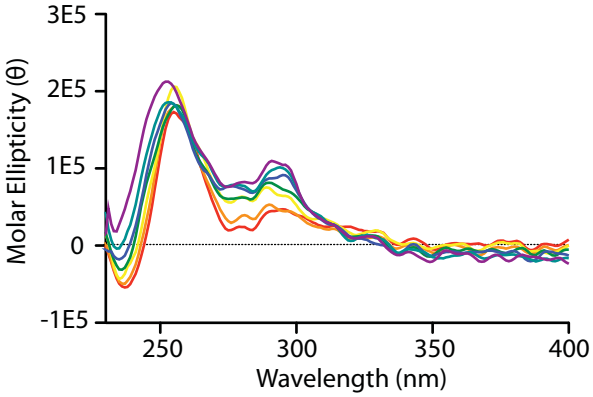

Figure 2.6 CD templation of complex **2.2** with single-stranded quadruplex DNA.

This result prompted us to examine the structure of naphthyl- complex **2.2** more closely. While increasing the π-surface of the aromatic group may result in greater stacking of this group with the G-quadruplex, it would also be expected to impose a larger twist angle between the phenanthroimidazole and naphthyl moieties. This twisted structure may prevent favorable structural overlap of the more extended π-surface ligand with the intramolecular telomeric G-quadruplex. The effective twist angles between the phenanthroimidazole ligand and the substituent rings were analyzed to further understand the amount of planar π-surface each ligand can provide. These studies were performed by Dr. Pablo Englebienne and Dr. Nathanael Weil in Prof. Nicolas Moitessier's laboratory. Density functional theory (DFT) calculations at the B3LYP/LACV3P** level of theory were performed by scanning the N-C-C-C torsional angle between the phenanthroimidazole ligand and the substituents for the phenyl- and naphthyl-ligands at 5° increments. The phenyl- ligand in complex **2.1** shows a shallow

potential energy dependence on the torsional angle between the two aromatic units and an energy minimum at 15°. However, the naphthyl- ligand in complex **2.2** shows an energy minimum at a higher torsional angle of 30°, with the energy increasing at 0° angle, i.e. when the two aryl groups are aligned (Figure 2.7).

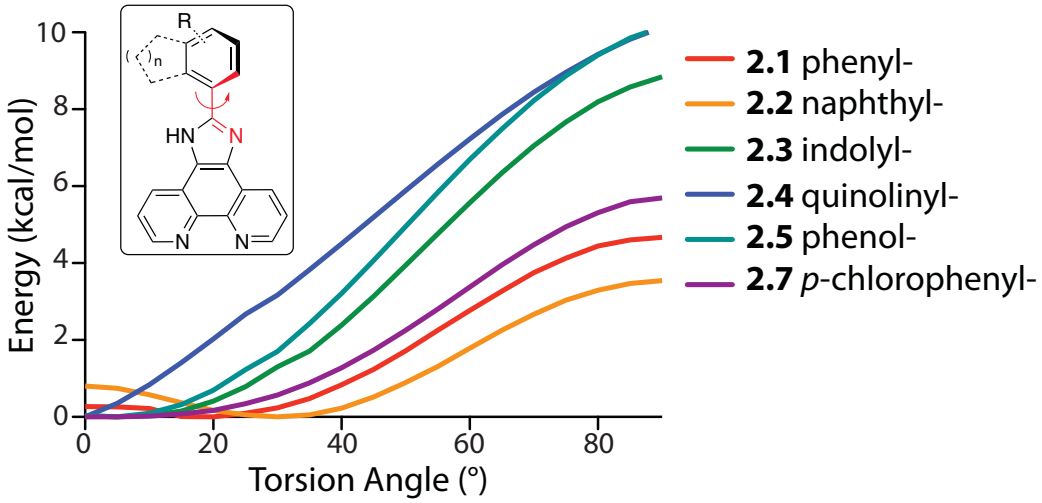

Figure 2.7 Energy diagram from the torsional scan around the N-C-C-C bond in the phenanthroimidazole ligands of complex **2.1**-**2.5** and **2.7**; the inset shows the bond (red) around which the torsion angles were measured.

This encouraged us to examine a new class of ligands in which the attached aryl- substituent is π-extended, but can be locked in an aligned, 0° twist angle through an intramolecular hydrogen-bond (Figure 2.3). Complex **2.3** has an indole unit that is expected to engage in hydrogen-bonding between the indole nitrogen (H-bond donor) and the imidazole nitrogen. Complex **2.4** has a quinoline unit, whose nitrogen can act as an H-bond acceptor with the imidazole nitrogen acting a donor. Phenol complex **2.5** has a less π-extended phenol group that can act as an H-bond donor to the imidazole nitrogen, while hydroxynaphthyl- complex **2.6** has a more π-extended phenol group that can act like phenol- complex **2.5**. DFT calculations show that the effectively locked ligands now exhibit a minimum in the potential energy surface for a torsion value of 0°, with a sharp increase in energy for deviations of more than 10−15° (Figure 2.7). The entropic penalty can be reduced upon binding by removing the internal strain within the ligands and locking the biphenyl torsion angle.

2.2.4 Extending the π-surface area with complexes 2.3-2.5 through the introduction of intramolecular hydrogen-bonds

Titration of single-stranded DNA with quinolinyl- complex **2.4** was followed by CD analysis (Figure 2.8a). Similar to phenyl- complex **2.1** and naphthyl- complex **2.2**, quinolinyl- complex **2.4** resulted in exclusive templation of the antiparallel quadruplex form and exhibited a binding ratio of approximately 2:1 for complex **2.4**:quadruplex-DNA strand (Figure 2.8a, inset). Indolyl- complex **2.3** also templates an antiparallel structure, or a mixture of structures that have antiparallel characteristics (Figure 2.8b).[§]

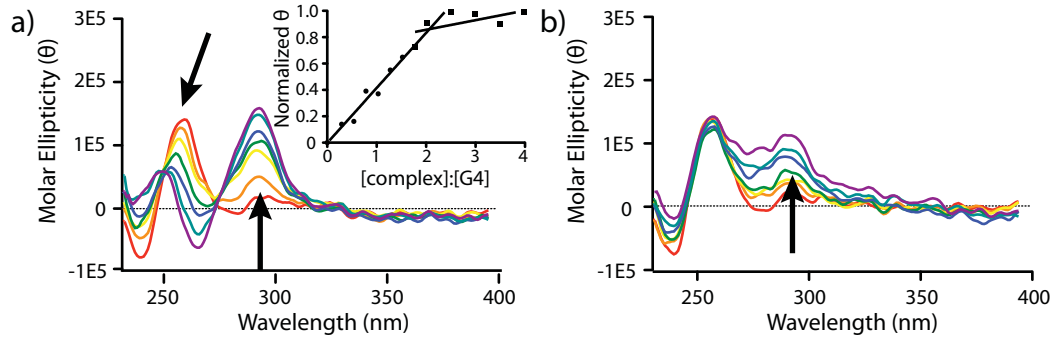

Figure 2.8 CD Spectra of the quadruplex templation with a) quinolinyl- complex **2.4** and b) indolyl- complex **2.3**. Arrows in panels a) and b) show the direction of change in CD signal with increasing additions of complex **2.4** and **2.3**, respectively, (the red trace is ss-DNA and the purple trace is the fully-formed basket polymorph). The inset in panel a) shows the decrease in circular dichroic peak between 250 and 260 nm with added complex **2.4**. The saturation point is at ~ 2:1 ratio of complex **2.4**:quadruplex DNA strand and indicates a 2:1 binding stoichiometry.

Interestingly, indolyl- complex **2.3** and quinolinyl- complex **2.4** bind more strongly to the G-quadruplex antiparallel basket than to the hybrid structure (i.e., $^{G4}DC_{50}$ = 0.53 μM versus $^{G4}DC_{50}$ = 1.55 μM for complex **2.3**). Thus, unlike phenyl- complex **2.1**, these complexes display greater affinity and selectivity for a specific G-quadruplex polymorph. This binding selectivity is a valuable feature, as numerous G-quadruplex targets of different structures have recently been described in the promoter regions of oncogenes.[10] A current challenge is to find small molecules that target one of these polymorphic quadruplex structures preferentially. Molecules such as complexes **2.3** and **2.4** display such selectivity.

[§] For complexes **2.3** and **2.4**, we noted light-sensitivity and some decomposition during the experiment, which likely resulted in atypical results.

CD titration studies show that phenol- derivative **2.5** templates clean formation of the antiparallel basket G-quadruplex polymorph (Figure 2.9a) with a 2:1 binding stoichiometry for complex **2.5**:quadruplex-DNA strand, much like the closely related phenyl derivative complex **2.1** (Figure 2.9b). Introduction of the ortho-hydroxyl substituent was found to increase the binding affinity of this complex to the antiparallel G-quadruplex form, as well as increase the selectivity for G-quadruplex versus duplex DNA ($^{G4}DC_{50} = 0.53$ μM, $^{ds}DC_{50}/^{G4}DC_{50} \sim 1.6–3.0$). However, complex **2.5** displays less selectivity between G-quadruplex polymorphs (the antiparallel versus the hybrid G-quadruplex forms) than do complexes **2.3** and **2.4**. Thus, this complex shows similar binding features to the closely related phenyl- complex **2.1**, albeit with moderately improved affinity to G-quadruplexes and selectivity between G-quadruplexes and duplex DNA compared to the phenyl- complex **2.1** (Table 2.1). Based on the DFT calculations and Figure 2.7, we had assumed that the phenol- complex **2.5** would have *significantly* improved binding affinity to G-quadruplexes compared to the phenyl- complex **2.1**. The fact that overall binding affinity to G-quadruplexes did not *significantly* improve in the case of complex **2.5** may be a result of the electron-rich nature of the phenol ring, which can play a role in reducing binding to the G-quartet structure. This enrichment in electron density could disrupt the balance between electrostatic attraction and effective π-stacking with the binding surface of the G-quadruplex. As mentioned earlier, studies of the 2-hydroxy-1-naphthyl substituent were not pursued due to poor solubility at the concentrations necessary for the biophysical assays.

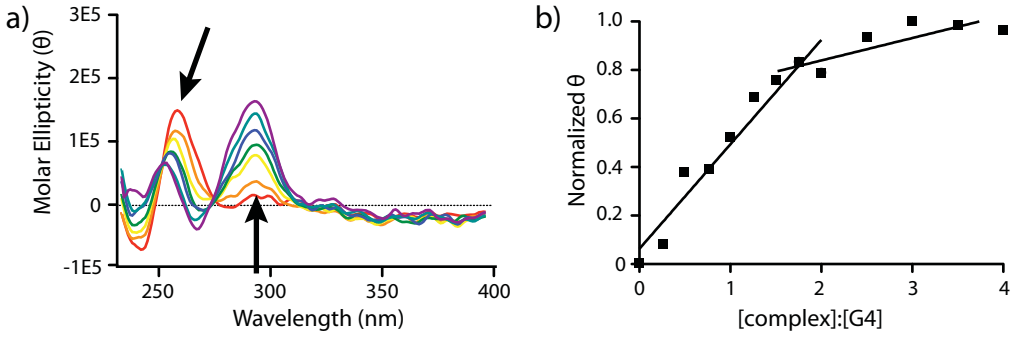

Figure 2.9 a) CD Spectra of the quadruplex templation with phenol- complex **2.5**. Arrows in panel a) show the direction of change in CD signal with increasing additions of complex **2.5**. b) The decrease in circular dichroic peak between 250 and 260 nm with added complex **2.5**. The saturation point is at ~ 2:1 ratio of complex **2.5**:quadruplex DNA strand and indicates a 2:1 binding stoichiometry.

In summary, the introduction of hydrogen bonding substituents on the aromatic ring resulted in improved binding affinity of complexes **2.3**-**2.5** to the G-quadruplex, as well as increased selectivity for this structure versus duplex DNA. In addition, selectivity towards a specific G-quadruplex polymorph (the antiparallel basket structure) is enhanced for these structures, outlining new design features that can be used to target specific G-quadruplex structures.

2.2.5 Introduction of an electron-withdrawing halogen substituent

Locking the aryl substituent of indolyl- complex **2.3** and quinolinyl- complex **2.4** with an intramolecular hydrogen bond resulted in an increase in affinity and selectivity for the antiparallel G-quadruplex structure. We were also interested in investigating whether electronic effects could further improve the binding affinity of this class of molecules. In particular, given the electron-rich nature of the G-quartet, we examined the effect of increasing the electron deficiency of our complexes by adding a chlorine substituent at the *para*-position of the phenyl phenanthroimidazole (complex **2.7**). DFT calculation studies performed by Dr. Nathanael Weil showed a significant impact of the chlorine atom on the highest occupied molecular orbital (HOMO) of the complex, and no impact on the lowest unoccupied molecular orbital (LUMO), with a decrease in electron density of the HOMO and aromatic character of the imidazole unit in *p*-chlorophenyl- complex **2.7**, as compared to the unsubstituted phenyl- complex **2.1** (Figure 2.10). Thus, the intervening phenyl ring efficiently mediates a shift of the electron density away from the imidazole ring towards the chlorine atom. Moreover, the chlorine substituent results in a calculated dipole moment for *p*-chlorophenyl- complex **2.7** that is significantly greater than that of the unsubstituted phenyl- complex **2.1** (17.8 versus 10.7 Debye). Finally, scanning the energy as a function of torsion angle between the *p*-chlorophenyl and imidazole groups for complex **2.7** shows an energy minimum at 0−5° (Figure 2.7), which predicts alignment of the two aromatic rings. This is likely the result of increased conjugation between the imidazole and the electron deficient *p*-chlorophenyl group. Thus, *p*-chlorophenyl- complex **2.7** is not only expected to display a more electron deficient π-surface, it is likely to be planar, with minimal twisting between its aromatic

rings despite a lack of internal H-bonding. Together, these characteristics would be assumed to increase binding affinity to the G-quadruplex binding surface.

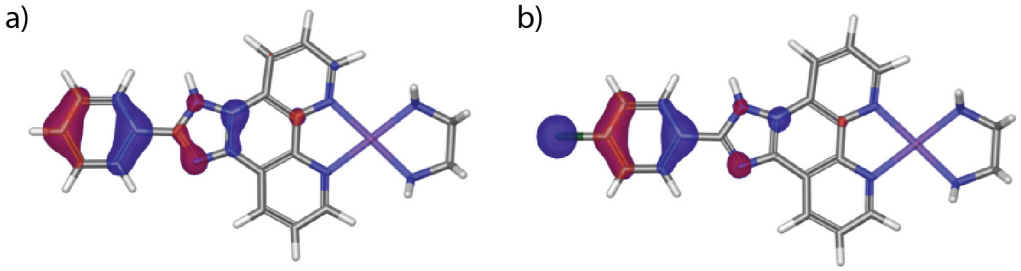

Figure 2.10 Comparison of the HOMOs of a) phenyl- complex **2.1** and b) *p*-chlorophenyl- complex **2.7**. The isosurfaces represent the HOMO of the complexes computed by Jaguar 7.7 using an isovalue of –0.05.

These modeling results encouraged us to synthesize this complex and assess its binding affinity for the G-quadruplex structures. CD titration of single-stranded telomeric DNA with the *p*-chlorophenyl complex **2.7** resulted in the exclusive formation of the antiparallel G-quadruplex form (Figure 2.4a), in a similar manner to phenyl- **2.1**, quinolinyl- **2.4**, and phenol- **2.5** complexes with the same binding stoichimetry of 2:1 (Figure 2.11). FID assays showed significantly increased binding affinity of *p*-chlorophenyl- complex **2.7** to the antiparallel G-quadruplex form in Na^+ buffer ($^{G4}DC_{50}$ = 0.31 μM), which is comparable to some of the more potent G-quadruplex binders reported in the literature, including those found in Figure 2.2.[36] Selectivity for G-quadruplex versus duplex DNA is increased ($^{ds}DC_{50}/^{G4}DC_{50}$ ~ 1.8-4.7), and preference for the antiparallel G-quadruplex form over the hybrid form is maintained. Thus, by creating a conjugated 'donor-acceptor' system (imidazole and chlorophenyl rings in complex **2.7**), the two aromatic rings are kept in a parallel conformation. With this method, binding affinity and selectivity to G-quadruplexes can be significantly increased, without the need to use fused polycyclic aromatic rings.

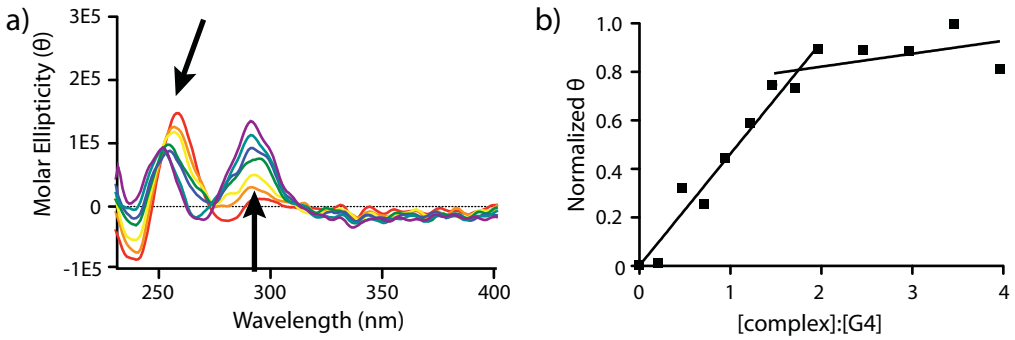

Figure 2.11 a) CD Spectra of the quadruplex templation with *p*-chlorophenyl **2.7**. Arrows in panel a) show the direction of change in CD signal with increasing additions of complex **2.7**. b) The decrease in circular dichroic peak between 250 and 260 nm with added complex **2.7**. The saturation point is at ~ 2:1 ratio of complex **2.7**:quadruplex DNA strand and indicates a 2:1 binding stoichiometry.

2.2.6 TRAP-Lig assay (performed by Johanna Mancini and Dr. Johans Fakhoury)

To analyze the telomerase inhibition potential of platinum(II) complexes, an adapted version of the telomeric repeat amplification protocol (TRAP) assay was used.[37] Elongation of the telomeric substrate by the telomerase enzyme will generate DNA products, which are then PCR-amplified in the presence of a reverse primer termed ACX. Standard TRAP reactions contain telomeric substrate (TS) primer, NT primer, and TSNT internal control primer. These latter primers ensure that the telomerase inhibition observed is not due to inhibition of the PCR reaction step. DNA products generated by telomerase and amplified by PCR are then resolved on a non-denaturing polyacrylamide gel and analyzed. The resulting ladder of DNA products is normalized to the internal control (IC). The IC is generated by the PCR amplification of TSNT by both the TS and NT primers. The ratio obtained for the inhibited telomerase reactions is then compared to the ratio of uninhibited telomerase (positive control containing protein only). Although the standard TRAP assay has been used successfully for assessing the ability of G-quadruplex motifs to inhibit telomerase, a recent study indicates that the efficiency of inhibition has been overestimated due to the inhibition of the PCR amplification on quadruplex-prone motifs that persist since the small molecule stabilizers remain in the reaction mixture, even though the internal PCR control (IC) is not affected.[38] A modified TRAP assay, the TRAP-Lig protocol, removes the G-quadruplex binder prior to the PCR

step *via* a spin column, eliminating any inhibition that may be due to the presence of the ligand.[37]

In the presence of increasing concentrations of platinum(II) complex, a decrease in TRAP product is observed, indicating that telomerase activity is inhibited by these G-quadruplex binders (Figure 2.12a, complex **2.1**). The IC_{50} values range from 0.46 to 11.6 μM (Figure 2.12b), on the same order as telomestatin (IC_{50} = 0.6 μM, Figure 2.1) and BRACO-19 (IC_{50} = 6.3 μM), as measured using the TRAP-Lig protocol.[37] Moreover, the result obtained for the widely used 5,10,15,20-tetrakis(1-methyl-4-pyridino)porphyrin (TMPyP4) was of the same order of magnitude to those previously reported,[37] demonstrating the reliability of the TRAP-Lig assay (data not shown). In order to confirm the complete removal of the complex by the spin column, we added an excess of complex **2.2** after the extension reaction and subsequently purified the extended product using the spin column. After the PCR step, we observed that the signal of the amplified product for the positive control (no complex added) was the same as that of the reaction in which the complex was added after the extension reaction (data not shown). This observation confirms that all platinum(II) complexes added before the extension step are completely removed by the spin column and that telomerase inhibition is indeed caused by the G-quadruplex binders. From the above observations we conclude that complexes **2.1**-**2.5** and **2.7** are efficient and specific telomerase inhibitors.

A closer examination of the inhibition curves (Figure 2.12b) reveals additional detail that cannot be obtained merely from the IC_{50} values. At a concentration of 32 nM, there is already significant inhibition of telomerase elongation products for some of the complexes (e.g., up to 40% for complex **2.4**). Interestingly, only phenol- complex **2.5** and *p*-chlorophenyl- complex **2.7**, which are the strongest G-quadruplex binders, result in 100% inhibition of telomerase elongation at the end of the experiment. Complex **2.7** in particular has the largest inhibition window − from ~ 100% enzyme activity at 32 nM to ~ 0% at 50 μM. The inhibition of telomerase elongation in the TRAP-Lig assay is a complex process; it can result from the ability of these complexes to bind and sequester the telomerase substrates in their G-quadruplex form, or possibly from their direct inhibition of the enzyme activity or processivity.[38] Thus, while the inhibition of telomerase elongation by complexes **2.1**-**2.5** and **2.7** correlates with G-quadruplex

binding affinity, it is clear that each complex results in a unique profile with different initial and final activities and different inhibition slopes.

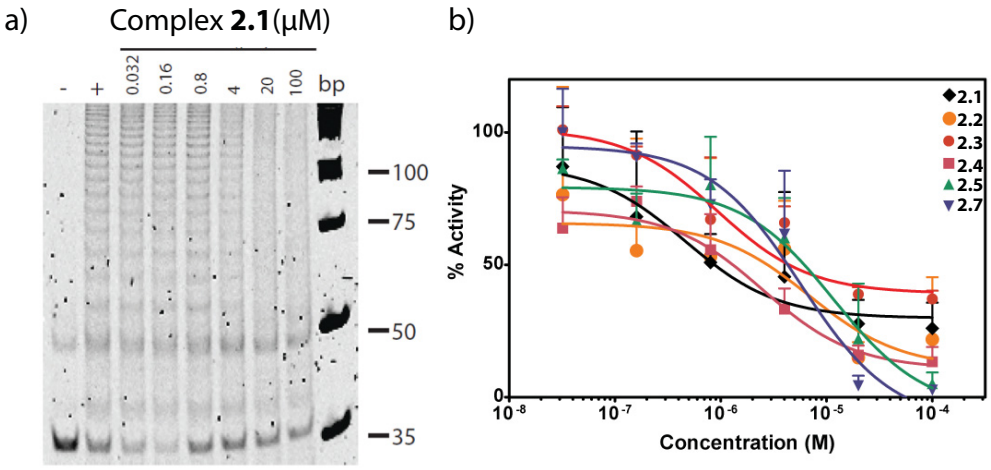

Figure 2.12 a) Non-denaturing polyacrylamide gel from the TRAP-Llig assay for complex **2.1**. The first two lanes at left represent negative (no protein extract) and positive (no added complex) controls. Increasing concentration of complex **2.1** shows a decrease in the length of elongation products, consistent with the inhibition of telomerase activity. The lane at the far right (bp) is a DNA ladder used for size comparison with the elongation products. Bands appearing at 35 pb are the internal control (IC) of the TRAP-Lig. b) Inhibition curves from assay for complexes **2.1**-**2.5** and **2.7**.

2.2.7 Preliminary cytotoxicity studies (performed by Johanna Mancini)

To assess the anti-proliferative activities of *p*-chlorophenyl complex **2.7** in telomerase expressing cancer cell lines A549 and MCF-7, an MTS ((3-(4,5-dimethylthiazol-2-yl)-5-(3-carboxymethoxyphenyl)-2-(4-sulfophenyl)-2H-tetrazolium)) assay that evaluates mitochondrial metabolic activity was conducted.[39,40] In this assay, cells are incubated in with varying concentrations of complex **2.7** for 72 hours. After the incubation period, the MTS reagent is added and allowed to incubate for 3 hours. If the cells are still metabolically active after incubation with the complex, the NAD(P)H-dependent cellular oxidoreductase enzymes will reduce the MTS dye to the purple formazan product with an absorbance maximum around 490−500 nm. After the assay is completed, the absorbance is read and the concentration of the dye can be quantified, giving an accurate representation of viable cells. From the varying concentrations of incubated ligand, one can determine the IC_{50} values or concentration of ligand required to reduce the number of viable cells by 50%.

In preliminary studies using this assay, complex **2.7** was found to be three times more cytotoxic to the cancer cell lines than to the normal fibroblast cell line MRC-5 (IC_{50} values of approximately 20 μM versus 60 μM upon 72 hour treatment). In order to ensure G-quadruplex specificity, we tested the cytotoxicity of bipyridine complex **2.8**, the platinum complex that showed no binding to G-quadruplexes. We were consistently unable to obtain any IC_{50} values for bipyridine complex **2.8** (up to 100 μM) using the same assay, consistent with its low DNA binding affinity. This preliminary data indicates that *p*-chlorophenyl- complex **2.7** causes preferential cell cytotoxicity in cancer cell lines while being less toxic to normal cells, a selectivity that compares well with previously reported strong G-quadruplex binders.[41] These complexes warrant further investigation for use as therapies targeted towards stabilizing G-quadruplex structures at telomeres and/or G-rich oncogene promoter regions.

2.3 Conclusions

We have shown that phenanthroimidazole platinum(II) complexes template and strongly bind G-quadruplex forming sequences based on the human telomeric repeat, $(TTAGGG)_n$, inhibit telomerase and one of them (the *p*-chlorophenyl derivative) is cytotoxic to cancer cells. The specific findings are summarized below:

1. Phenanthroimidazole platinum(II) complex **2.1** can cleanly template the formation of an antiparallel G-quadruplex from single-stranded telomeric DNA, in a 2:1 stoichiometry, without the need for addition of Na^+- or K^+-ions. It binds to G-quadruplexes with good affinity and selectivity over duplex DNA.

2. Through modeling studies, it was found that increasing the π-surface of this complex by moving from a phenyl to a naphthyl substituent as complex **2.2**, also increases the torsional angle between the two aromatic rings. Experimentally, it results in a decreased binding affinity for G-quadruplexes.

3. By locking the aromatic rings together using an intramolecular hydrogen bond as in complexes **2.3**-**2.5**, higher binding affinities and selectivities for G-quadruplexes are observed. Interestingly, the selectivity of these complexes to the antiparallel over the hybrid G-quadruplex structure is also significantly increased.

4. Most notably, by introducing a chloro-substituent at the *p*-phenyl position, DFT studies predicted a significant decrease in electron density of the aromatic ring, an increase in dipole moment and a near-zero twist angle between the two aromatic rings. Experimentally, this complex **2.7** was found to bind to antiparallel G-quadruplexes with the highest affinity and selectivity of the series herein, which is comparable to some of the most potent G-quadruplex binders in the literature.

5. Complexes **2.1**-**2.5** and **2.7** are effective telomerase inhibitors, but differ significantly in their inhibition profiles.

6. Complex **2.7**, a selective G-quadruplex binder, is more cytotoxic to cancer cells than to normal cells.

These studies have illustrated a number of design principles for guanine quadruplex binders. An extended π-aromatic surface had been found to result in high binding affinity in most previous reports; however, extended polycyclic aromatic molecules may not be sufficiently drug-like. These studies have shown that (a) introducing an intramolecular hydrogen bond between two aromatic rings (complexes **2.3**-**2.5**), or (b) creating a conjugated 'donor-acceptor' system (imidazole and chlorophenyl rings in complex **2.7**) can effectively lock the two aromatic rings in a parallel conformation, thus significantly increasing binding affinity and selectivity. These strategies may circumvent the need for including fused polycyclic aromatic motifs in G-quadruplex binders. As a result of the ease of their synthesis and modification, we are currently examining strategies to further simplify the design of these complexes, and are carrying out more detailed studies in order to examine the mechanism by which they target cancer cells.

2.4 Experimental section

2.4.1 Synthesis

NMR spectra were recorded at 300 or 400 MHz on a Varian Mercury instrument operated with VNMRJ 2.2D software under LINUX Red Hat 5. The following abbreviations are used: singlet (s), doublet (d), doublet of doublets (dd), triplet (t), multiplet (m), and broad (br). Mass spectrometry was performed on a Kratos MS25RFA high-resolution mass spectrometer. IR spectra were collected on a Perkin Elmer 400

instrument. All chemicals were used as received from Sigma-Aldrich without further purification for synthesis of the ligands and their respective complexes. Quinoline-8-carboxaldehyde was received from Alfa-Aesar and used without further purification. 1,10-phenanthroline-5,6-dione, bipyridine (**2.8**), phenylphenanthroimidazole (**2.1**), and naphthylphenanthroimidazole (**2.2**) platinum(II) complexes,[24] salicylphenanthroimidazole (SIP) ligand,[42] and *p*-chlorophenylphenanthroimidazole (CLIP) ligand[43] were synthesized as previously reported.

2-indolylimidazo[4,5-*f*]1,10-phenanthroline (PII):

1,10-phenanthroline-5,6-dione (0.150 g, 0.721 mmol), and ammonium acetate (1.11 g, 14.4 mmol) were dissolved in glacial acetic acid (50 mL) in the absence of light and under inert atmosphere. Once mostly dissolved, indole-7-carboxaldehyde (0.126 g, 0.865 mmol) was added and this reaction mixture was refluxed for 1 h. The mixture was cooled on ice and then neutralized using NH_4OH to pH 7. Crude product precipitated as a light brown solid. The solid was collected *via* vacuum filtration before being dissolved in MeOH/CH_2Cl_2 and evaporated onto silica gel under reduced pressure to be purified using column chromatography. The reaction mixture was separated using first 100% ethyl acetate followed by a gradient of CH_2Cl_2/MeOH from 0%−8% MeOH. The final product was evaporated to dryness as a yellow solid. It was important to exclude light at all times. Yield: 62.8 mg, 26%.

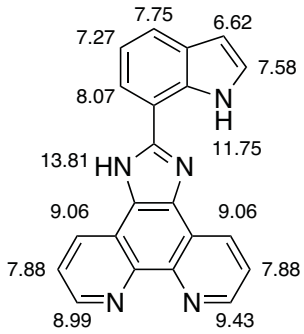

^{1}H NMR (300 MHz, d_6-DMSO): δ = 13.81 (s, 1H), 11.75 (s, 1 H), 9.43 (dd, 1H), 9.06 (m, 2H), 8.99 (dd, 1H), 8.07 (d, 1H), 7.88 (m, 2H), 7.75 (d, 1H), 7.58 (d, 1H), 7.27 (t, 1H), 6.62 (d, 1H) ppm; ^{13}C NMR (500 MHz, d_6-DMSO): δ = 172.3, 150.4, 147.9, 143.6, 132.7, 130.2, 129.1, 126.8, 123.2, 122.2, 118.9, 118.5, 113.0, 101.6, 21.3 ppm; HR-MS (ESI, 50:50 MeOH:H_2O) m/z: calculated $[M+H]^{1+}$ **336.12437**, found **336.12423**.

2-quinolinylimidazo[4,5-*f*]1,10-phenanthroline (PIQ):

This compound was prepared similarly to PII, except 1,10-phenanthroline-5,6-dione (0.150 g, 0.714 mmol), ammonium acetate (0.275 g, 3.57 mmol), and quinoline-8-carboxaldehyde (0.157 g, 0.999 mmol) were used and the reaction mixture was stirred at room temperature for ~ 1 h. The final product was isolated as a brown solid. It was important to exclude light at all times. Yield: 99.1 mg, 40%.

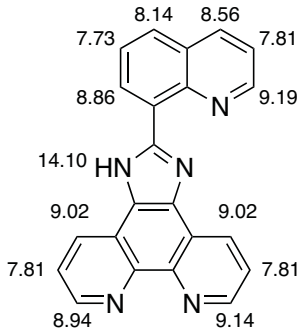

^{1}H NMR (400 MHz, d_6-DMSO): δ = 14.10 (s, 1H), 9.19 (br, 1H), 9.14 (br, 1H), 9.02 (br s, 2H), 8.94 (br, 1H), 8.94 (br, 1H), 8.86 (d, 1H), 8.55 (d, 1H), 8.14 (d, 1H), 7.81 (br m, 3H), 7.73 (br m, 1H) ppm; ^{13}C NMR (500 MHz, d_6-DMSO): δ = 151.5, 150.0, 148.4, 148.3, 144.8, 144.2, 144.0, 138.0, 135.6, 130.8, 130.4, 130.4, 130.2, 128.9, 127.3, 126.9, 126.4, 124.2, 123.9, 123.5, 122.5, 119.8 ppm; HR-MS (ESI, 90 MeOH: 10 formic acid) m/z: calculated **346.1218**, found **348.1244**.

1-hydroxy-2-naphthylimidazo[4,5-*f*]1,10-phenanthroline (NIP): This ligand was synthesized with the aid of Nicole Avakyan in the laboratory of Prof. Hanadi Sleiman. This compound was prepared similarily to PII, except 1,10-phenanthroline-5,6-dione (0.111 g, 0.530 mmol), ammonium acetate (0.408 g, 5.30 mmol), and 1-hydroxy-2-naphthaldehyde (0.127 g, 0.742 mmol) were used and the reaction mixture was refluxed overnight at 120°C. The crude product was isolated as a yellow solid. The product was purified *via* reverse-phase column chromatography on a CombiFlash C18-Aq column using a gradient of 100% Solvent A (95% MQ-water, 5% MeOH, with 0.1% formic acid) to 100% Solvent B (100% MeOH with 0.1% formic acid). The pure product eluted between 60%−70% Solvent B. After lyophilization for 48 h, a fluffy orange powder was recovered. Yield: 37.1 mg, 19%

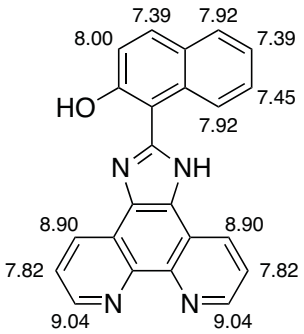

^{1}H NMR (400 MHz, d_6-DMSO): δ = 9.04 (d, 2H), 8.91 (d, 2H), 8.00 (d, 1H), 7.92 (m, 2H), 7.82 (dd, 2H), 7.45 (t, 1H), 7.39 (m, 2H) ppm; ^{13}C NMR (300 MHz d_6-DMSO): δ = 155.2, 148.2, 143.9, 133.6, 131.9, 130.1, 128.6, 128.2, 127.7, 124.7, 123.8, 118.7, 110.6 ppm; HR-MS (ESI, MeOH): calculated $C_{23}H_{14}N_4NaO$ [M+Na] **385.1060**, found **385.1064**.

[Pt(PII)(en)][PF_6]$_2$ (2.3): (en = ethylenediamine) K_2PtCl_4 (0.0689 g, 0.166 mmol) was first dissolved in demonized water (10 mL) and heated to ~ 80°C. Indolyl-phenanthroimidazole (PII) (0.0548 g, 0.164 mmol) was dissolved in DMSO (10 mL) at ~ 80°C in the absence of light. The K_2PtCl_4 solution was then added to the PII solution and the reaction mixture was allowed to stir overnight at room temperature before being vacuum-filtered. The intermediate (PII)$PtCl_2$ was washed with warm water before drying with diethyl ether to afford (PII)$PtCl_2$ as a light brown solid. Then, ethylenediamine (16.2 μL, 0.242 mmol) was added to a suspension of (PII)$PtCl_2$ (0.0160 g, 0.0270 mmol) in ethanol (10 mL) in an amber vial to exclude light. The reaction mixture was stirred at room temperature overnight before vacuum-filtration and rinsing with distilled H_2O to remove unreacted material. Next, ammonium hexafluorophosphate was added to the filtrate to precipitate a light brown salt. The product was vacuum-filtered on a glass frit and washed with a small amount of distilled water before drying with diethyl ether. The resulting solid was light brown. Yield: 9.98 mg, 42%.

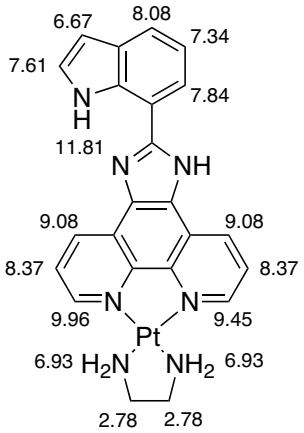

^{1}H NMR (400 MHz, d_6-DMSO): δ = 11.81 (s, 1H), 9.96 (d, 1H), 9.45 (d, 1H), 9.08 (br s, 2H), 8.37 (br m, 2H), 8.08 (d, 1H), 7.84 (m, 1H), 7.61 (s, 1H), 7.34 (t, 1H), 6.93 (br s, 4H), 6.67 (s, 1H), 2.78 (s, 4H) ppm; ^{13}C NMR (300 MHz, d_6-DMSO): δ = 148.7, 143.8, 134.9, 133.2, 129.2, 126.8, 125.9, 124.1, 122.5, 119.3, 118.9, 102.1, 47.7 ppm; IR (ATR) n = 3645, 3398, 3322, 3143, 1599, 1414, 1341, 1170, 1055, 832, 555 cm^{-1}; HR-MS (ESI, 50:50 MeOH:H_2O) m/z: calculated $[M\text{-}2PF_6]^{2+}$ **294.57371**, found **294.57337** with ^{194}Pt.

[Pt(PIQ)(en)][PF_6]$_2$ (2.4): 2.4 was prepared similarily to **2.3**. After precipitation with NH_4PF_6, a dark brown product was isolated. Yield: 39%.

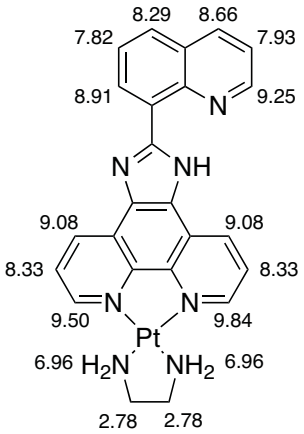

^{1}H NMR (500 MHz, d_6-DMSO): δ = 9.84 (br m, 1H), 9.50 (br m, 1H), 9.25 (br s, 1H), 9.08 (br s, 2H), 8.91 (d, 1H), 8.66 (d, 1H), 8.33 (br s, 2H), 8.29 (d, 1H), 7.93 (t, 1H), 7.82 (m, 1H), 6.98 (br s, 4H), 2.78 (s, 4H) ppm; ^{13}C NMR (500 MHz, d_6-DMSO): δ = 152.5, 151.7, 144.8, 138.1, 131.5, 131.3, 128.9, 127.4, 126.4, 122.8, 105.0, 47.7 ppm; IR (ATR)

n = 3665, 3323, 2989, 2961, 1596, 1411, 1057, 834, 556 cm^{-1}; HR-MS (ESI, 50:50 MeOH:H_2O) m/z: calculated $[M\text{-}2PF_6]^{2+}$ **300.57371**, found **300.57383** with ^{194}Pt.

[Pt(SIP)(en)][PF_6]$_2$ (2.5): This complex was synthesized with the aid of Nicole Avakyan in the laboratory of Prof. Hanadi Sleiman. **2.5** was prepared similarily to **2.3**. After precipitation with NH_4PF_6, a red-orange product was isolated. There was no need to exclude light during this reaction. Yield: 54%.

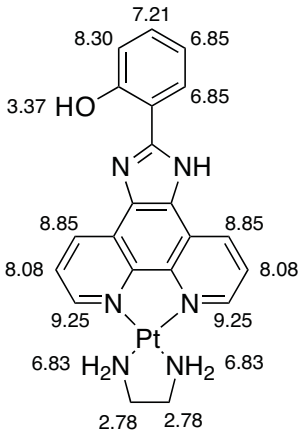

^1H NMR (500 MHz, d_6-DMSO): δ = 9.25 (d, 2H), 8.85 (d, 2H), 8.30 (d, 1H), 8.10 (t, 2H), 7.21 (t, 1H), 6.86-6.84 (m, 2H), 6.83 (br s, 4H), 2.78 (br s, 4H) ppm. ^{13}C NMR (300 MHz, d_6-DMSO): δ = 152.9, 147.6, 143.0, 134.4, 127.0, 125.5, 125.4, 118.9, 116.8, 47.6 ppm; IR (ATR) n = 3321, 1612, 1516, 1485, 1418, 1373, 1306, 1169, 1055, 830, 755, 714, 555 cm^{-1}; HR-MS (ESI, 50:50 MeOH:H_2O) m/z: calculated $[M\text{-}2PF_6]^{2+}$ **283.06571**, found **283.06540** with ^{194}Pt.

[Pt(NIP)(en)][PF_6]$_2$ (2.6): This complex was synthesized with the aid of Nicole Avakyan in the laboratory of Prof. Hanadi Sleiman. **2.6** was prepared similarily to **2.3**. After precipitation with NH_4PF_6, a red-orange product was isolated. There was no need to exclude light during this reaction. Yield: 45%.

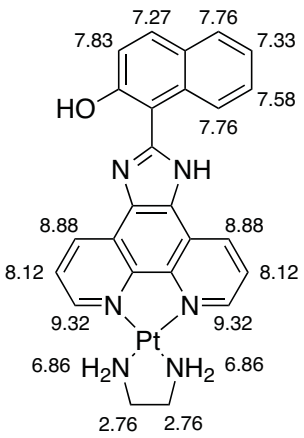

^{1}H NMR (300 MHz, d_6-DMSO): δ = 9.32 (d, 2H), 8.88 (d, 2H), 8.12 (dd, 2H), 7.83 (d, 1H), 7.76 (d, 2H), 7.58 (t, 1H) 7.33 (t, 1H), 7.27 (d, 1H), 6.86 (br s, 4H), 2.76 (br s, 4H) ppm. Due to solubility issues of this complex in DMSO at the concentrations needed for strong ^{13}C signal, a ^{13}C NMR could not be obtained. HR-MS (ESI, MeOH) m/z: calculated $[M\text{-}2PF_6]^{2+}$ **308.5747**, found **308.5735** with ^{194}Pt.

[Pt(CLIP)(en)][PF_6]$_2$ (2.7): 2.7 was prepared similarily to **2.3**. After precipitation with NH_4PF_6, a yellow product was isolated. There was no need to exclude light during this reaction. Yield: 53%.

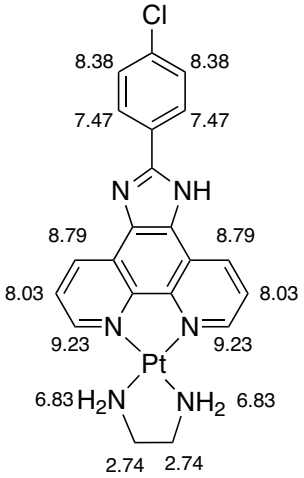

^{1}H NMR (500 MHz, d_6-DMSO): δ = 9.23 (d, 2H), 8.79 (d, 2H), 8.38 (d, 2H), 8.03 (dd, 2H), 7.47 (d, 2H), 6.83 (br s, 4H), 2.74 (br s, 4H) ppm; ^{13}C NMR (300 MHz, d_6-DMSO): δ = 147.1, 143.2, 34.3, 128.8, 128.3, 126.2, 125.2, 47.6 ppm; IR (ATR) n = 3645, 3323, 2989, 2959, 1594, 1461, 1360, 1056, 838, 715, 557 cm^{-1}; HR-MS (ESI, 50:50 MeOH:H_2O) m/z: calculated $[M\text{-}2PF_6]^{2+}$ **292.04877**, found **292.04871** with ^{194}Pt.

2.4.2 Biophysical assays

Circular dichroism studies were performed at 25°C on a JASCO J-810 spectropolarimeter with Spectra Manager II software. FID measurements were performed on a FluoroMax-2 spectrofluorimeter (Jobin-Yvon). All platinum(II) complexes (**2.1**-**2.8**) were prepared as 1.5 mM stock solutions in DMSO and stored at 4°C. Complexes **2.3** and **2.4** were wrapped in aluminum foil and their exposure to light was minimized in all experiments. The 22AG DNA oligonucleotide was obtained from SigmaGenosys Canada. 17mer and 26mer oligonucleotides were synthesized in-house on a MerMade 6 DNA synthesizer from BioAutomation Corporation. Reagents used for automated DNA synthesis were purchased from ChemGenes Incorporated. Oligonucleotides were dissolved in deionized water prior to use and quantified spectrophotometrically at room temperature (with the exception of the 22AG strand, which was heated to 95°C) using their molar extinction coefficients[44] at 260 nm; 5'-$AG_3(T_2AG_3)_3$-3' (22AG) = 228 500 $M^{-1}cm^{-1}$, 5'-CAA TCG GAT CGA ATT CGA TCC GAT TG-3' (26mer) = 253 200 $M^{-1}cm^{-1}$, and the 17mer complements were quantified separately with 5'-CCA GTT CGT AGT AAC CC-3' (17merA) = 160 900 $M^{-1}cm^{-1}$ and 5'-GGG TTA CTA CGA ACT GG-3' (17merB) = 167 400 $M^{-1}cm^{-1}$.

2.4.2.1 Circular dichroism studies

Circular dichroism studies were performed at 25°C on a JASCO J-810 spectropolarimeter using a 1 mm path length cuvette. Temperature was kept constant using the Peltier unit within the instrument. Spectra were recorded from 400–230 nm at a scan rate of 50 nm/min and a response time of 4.0 s with two acquisitions recorded for each spectrum. Data was smoothed using the means-movement function within the JASCO graphing software. In order to observe the ability of these complexes to fold the human telomeric DNA sequence, 22AG was dialyzed with Pierce slide-a-lyzer mini-dialysis kits (MWCO 3500 Da) (Fisher Scientific) against deionized Milli-Q water for 1−3 days before being diluted to 15 μM in a 50 mM Tris buffer (pH 7.6) for a total volume of 200 μL. Platinum(II) complexes were titrated in 0.5 μL aliquots from 1.5 mM solutions in DMSO to the 22AG sequence. With each aliquot added, 5 minutes elapsed prior to recording the

CD spectrum. Spectra were collected with the aforementioned parameters, until 3 or 4 molar equivalents were reached in platinum(II) complex.

2.4.2.2 FID assay

Dilutions of the nucleic acid stock solutions in MilliQ water were done in 10 mM sodium cacodylate buffer (pH 7.4) with 100 mM NaCl or KCl added where appropriate. 22AG, 17mer and 26mer DNA were diluted from the original stock solutions in water to 100 mM, 30 mM, and 10 mM, respectively, before being annealed. For the 22AG sequence, solutions were heated to 95°C for 5 minutes before being allowed to cool to room temperature over 1−2 h. For the 17mer and 26mer duplexes, concentrated solutions were heated to 95°C for 5 minutes before being allowed to slowly cool to room temperature over 6−7 h. For each platinum(II) complex, a solution of 175 mM complex in DMSO was prepared. Final dilutions of DNA solutions were made into the fluorescence cuvettes such that the [DNA] was 0.25 μM. Thiazole orange was prepared as a 1 mM stock solution in DMSO. New solutions were used for each titration to minimize aggregation effects from freeze/thaw cycles. After dilution of the DNA, the fluorescence spectra were recorded (λ_{ex} = 501 nm scanned from 510−750 nm with 3 mm slits). These spectra were used as blanks. Then 2 molar equivalents (0.50 μM) thiazole orange was added (or 3 molar equivalents in the case of the 26mer). Spectra were recorded after 5 minutes of equilibration time. Then 0.5−10 molar equivalents of the appropriate platinum samples were pipetted into each cuvette, followed by 5 minutes of equilibration time before recording the spectra. The fluorescence area (FA) was converted into percentage displacement (PD) where PD = 100 – [(FA/FA_0) × 100], FA_0 being FA before addition of platinum complexes. The concentration of added ligand was then plotted against the PD and a DC_{50} value was determined by the concentration of platinum complex needed to achieve a 50% displacement of thiazole orange. Each DC_{50} value was the average of 2 or 3 replicates.

2.4.3 Molecular modeling (performed by Dr. Pablo Englebienne and Dr. Nathanael Weill)

Torsional barrier analysis: To assess the stabilization of the biphenyl torsional barrier due to the intramolecular hydrogen bond, models of the ligands were built in the Maestro 9.1 interface (Schrödinger, Inc.) and optimized at the B3LYP/LACV3P** level of theory using Jaguar 7.7 (Schrödinger, Inc.). The value for the N-C-C-C torsion (having the biphenyl junction between the imidazole and the aryl substituent as a central bond) was varied between 0° and 90° at 5° intervals and the geometry optimized at each step.

Dipole moment and molecular orbital characterization: Starting from the conformation with the lowest energy, molecular orbitals and dipole moments were computed at the B3LYP/LACV3P** level of theory using Jaguar 7.7 (Schrödinger, Inc.).

2.4.4 Biological studies (performed by Johanna Mancini and Dr. Johans Fakhoury)

2.4.4.1 Telomeric repeat amplification protocol (TRAP-Lig) assay

For the evaluation of telomerase inhibition ability of platinum(II) complexes an adapted version of the TRAP assay was used.[37] Briefly, 5 µL of 10X stock solution was added for each concentration of ligand to the extension reaction (V_t = 50 µL). Each extension reaction contained 5 µL of 10X TRAP buffer (200 mM Tris pH 8.3, 15 mM $MgCl_2$, 630 mM KCl, 10 mM EGTA pH 8.0, 0.05% Tween-20, 1 mg/mL BSA), 1 µL dNTPs (2.5 mM), 1 µL TS primer (20 pmol/µL), 37 µL ddH_2O, and 1 µL HeLa extract (1 µg/µL). The extension reaction was incubated for 30 minutes at 30ºC. The reaction was then stopped and the ligands were removed using the Nucleotide Removal Kit (Qiagen) according to the manufacturer's recommendations. Bound product was eluted with 50 µL ddH_2O and then vacuum-evaporated for 30 minutes with medium heat (ThermoFisher). The product was then resuspended in 39 µL ddH_2O and subsequently amplified by adding the following (V_t = 50 µL): 5 µL of 10X TRAP buffer, 1 µL dNTPs (2.5 mM), 1 µL TS primer (20 pmol/µL), 1 µL NT primer (20 pmol/µL), 1 µL TSNT primer (10^{-13} M), 1 µL ACX primer (20 pmol/µL), 0.4 µL of Taq polymerase (4 U/µL, Invitrogen).

PCR was completed using the following conditions: (Step 1) 30 seconds at 94ºC, (Step 2) 60 seconds at 60ºC, (Step 3) 60 seconds at 72ºC, repeated 34 cycles. 20 μL of the PCR product was resolved by non-denaturing PAGE. To visualize extension products, the gel was stained with SYBR Safe® (Invitrogen) and visualized using a Storm 840 (GE Healthcare). Quantification was performed using ImageQuantTL software by measuring the intensity of the extension products normalized to the intensity of the internal PCR control and then compared to the positive control. IC_{50} values were calculated using the Graphpad Prism 5 software.

2.4.4.2 Cytotoxicity studies

Cytotoxicity of complexes **2.7** and **2.8** was assessed using the CellTiter96® kit from Promega according to the manufacturer's instructions. Briefly, A549 cells (human lung adenocarcinoma), MCF-7 cells (human breast adenocarcinoma), and MRC-5 cells (normal human fibroblast) were seeded at a density of 5,000 cells/well in a 96-well plate. Platinum complex stock solutions were initially diluted in growth medium to yield final concentrations ranging from 1.6 μM to 100 μM. Cells were incubated for 72 h in 5% CO_2 at 37°C. After the incubation period, the MTS reagent was added to each well and further incubated for 3 h in 5% CO_2 at 37°C. Subsequently, 96-well plates were allowed to equilibrate at room temperature and the absorbance was read at 490 nm using a BioTek© Synergy microplate reader. All quantifications were done using Graphpad Prism 5.

2.5 References

1. De Cian, A.; Lacroix, L.; Douarre, C.; Temime-Smaali, N.; Trentesaux, C.; Riou, J. F.; Mergny, J. L., Targeting telomeres and telomerase. *Biochimie* **2008,** *90* (1), 131-155.
2. Qin, Y.; Hurley, L. H., Structures, folding patterns, and functions of intramolecular DNA G-quadruplexes found in eukaryotic promoter regions. *Biochimie* **2008,** *90* (8), 1149-1171.
3. Lane, A. N.; Chaires, J. B.; Gray, R. D.; Trent, J. O., Stability and kinetics of G-quadruplex structures. *Nucleic Acids Res* **2008,** *36* (17), 5482-5515.
4. Balasubramanian, S.; Neidle, S., G-quadruplex nucleic acids as therapeutic targets. *Curr Opin Chem Biol* **2009,** *13* (3), 345-353.
5. Huppert, J. L., Hunting G-quadruplexes. *Biochimie* **2008,** *90* (8), 1140-1148.
6. Palm, W.; De Lange, T., How shelterin protects mammalian telomeres. In *Annual Review of Genetics*, 2008; Vol. 42, pp 301-334.

7. Tahara, H.; Shin-Ya, K.; Seimiya, H.; Yamada, H.; Tsuruo, T.; Ide, T., G-Quadruplex stabilization by telomestatin induces TRF2 protein dissociation from telomeres and anaphase bridge formation accompanied by loss of the 3' telomeric overhang in cancer cells. *Oncogene* **2006,** *25* (13), 1955-1966.
8. Rodriguez, R.; Müller, S.; Yeoman, J. A.; Trentesaux, C.; Riou, J.-F.; Balasubramanian, S., A Novel Small Molecule That Alters Shelterin Integrity and Triggers a DNA-Damage Response at Telomeres. *J Am Chem Soc* **2008,** *130* (47), 15758-15759.
9. Neidle, S., Human telomeric G-quadruplex: the current status of telomeric G-quadruplexes as therapeutic targets in human cancer. *FEBS J* **2010,** *277* (5), 1118-1125.
10. Balasubramanian, S.; Hurley, L. H.; Neidle, S., Targeting G-quadruplexes in gene promoters: a novel anticancer strategy? *Nature Rev Drug Disc* **2011,** *10* (4), 261-275.
11. Isabelle, M.; Moreel, X.; Gagne, J. P.; Rouleau, M.; Ethier, C.; Gagne, P.; Hendzel, M. J.; Poirier, G. G., Investigation of PARP-1, PARP-2, and PARG interactomes by affinity-purification mass spectrometry. *Proteome Sci* **2010,** *8*, 22.
12. Khalil, H.; Tummala, H.; Chakarov, S.; Zhelev, N.; Lane, D., Targeting ATM pathway for therapeutic intervention in cancer. *Biodiscovery* **2012**, *1* (3), 1-13.
13. Tauchi, T.; Shin-ya, K.; Sashida, G.; Sumi, M.; Okabe, S.; Ohyashiki, J. H.; Ohyashiki, K., Telomerase inhibition with a novel G-quadruplex-interactive agent, telomestatin: in vitro and in vivo studies in acute leukemia. *Oncogene* **2006,** *25* (42), 5719-5725.
14. Stratton, M. R.; Campbell, P. J.; Futreal, P. A., The cancer genome. *Nature* **2009,** *458* (7239), 719-24.
15. Jackson, S. P.; Bartek, J., The DNA-damage response in human biology and disease. *Nature* **2009,** *461* (7267), 1071-1078.
16. Ciccia, A.; Elledge, S. J., The DNA damage response: making it safe to play with knives. *Mol Cell* **2010,** *40* (2), 179-204.
17. Monchaud, D.; Teulade-Fichou, M. P., A hitchhiker's guide to G-quadruplex ligands. *Org Biomol Chem* **2008,** *6* (4), 627-636.
18. Arola, A.; Vilar, R., Stabilisation of G-quadruplex DNA by small molecules. *Curr Top Med Chem* **2008,** *8* (15), 1405-1415.
19. Ou, T. M.; Lu, Y. J.; Tan, J. H.; Huang, Z. S.; Wong, K. Y.; Gu, L. Q., G-quadruplexes: targets in anticancer drug design. *ChemMedChem* **2008,** *3* (5), 690-713.
20. Georgiades, S. N.; Abd Karim, N. H.; Suntharalingam, K.; Vilar, R., Interaction of metal complexes with G-quadruplex DNA. *Angew Chem Int Ed* **2010,** *49* (24), 4020-34.
21. Williamson, J. R., Guanine Quartets. *Curr Opin Struct Biol* **1993,** *3* (3), 357-362.
22. Doi, T.; Yoshida, M.; Shin-ya, K.; Takahashi, T., Total synthesis of (R)-telomestatin. *Org Lett* **2006,** *8* (18), 4165-4167.

23. Doi, T.; Shibata, K.; Yoshida, M.; Takagi, M.; Tera, M.; Nagasawa, K.; Shin-ya, K.; Takahashi, T., (S)-stereoisomer of telomestatin as a potent G-quadruplex binder and telomerase inhibitor. *Org Biomol Chem* **2011,** *9* (2), 387-393.
24. Kieltyka, R.; Fakhoury, J.; Moitessier, N.; Sleiman, H. F., Platinum phenanthroimidazole complexes as G-quadruplex DNA selective binders. *Chem Eur J* **2008,** *14* (4), 1145-1154.
25. Pennarun, G.; Granotier, C.; Gauthier, L. R.; Gomez, D.; Hoffschir, F.; Mandine, E.; Riou, J. F.; Mergny, J. L.; Mailliet, P.; Boussin, F. D., Apoptosis related to telomere instability and cell cycle alterations in human glioma cells treated by new highly selective G-quadruplex ligands. *Oncogene* **2005,** *24* (18), 2917-2928.
26. De Cian, A.; Delemos, E.; Mergny, J. L.; Teulade-Fichou, M. P.; Monchaud, D., Highly efficient G-quadruplex recognition by bisquinolinium compounds. *J Am Chem Soc* **2007,** *129* (7), 1856-1857.
27. Berl, V.; Huc, I.; Khoury, R. G.; Krische, M. J.; Lehn, J. M., Interconversion of single and double helices formed from synthetic molecular strands. *Nature* **2000,** *407* (6805), 720-723.
28. In all cases, final yields of the platinum(II) ethylenediamine complexes were below 75%. This can be rationalized as the complexes are very planar and tend to aggregate. The aggregation causes difficulty in purification, both *via* normal and reverse-phase methods.
29. Yamauchi, O.; Odani, A.; Shimata, R.; Kosaka, Y., Spectroscopic evidence for stacking and electrostatic interactions between nucleoside 5'-monophosphates and a platinum DNA intercalator, (2,2'-bipyridine)(ethylenediamine)platinum(II) in dilute aqueous solution. *Inorg Chem* **1986,** *25* (19), 3337-3339.
30. Rezler, E. M.; Seenisamy, J.; Bashyam, S.; Kim, M. Y.; White, E.; Wilson, W. D.; Hurley, L. H., Telomestatin and diseleno sapphyrin bind selectively to two different forms of the human telomeric G-quadruplex structure. *J Am Chem Soc* **2005,** *127* (26), 9439-9447.
31. Shirude, P. S.; Gillies, E. R.; Ladame, S.; Godde, F.; Shin-Ya, K.; Huc, I.; Balasubramanian, S., Macrocyclic and helical oligoamides as a new class of G-quadruplex ligands. *J Am Chem Soc* **2007,** *129* (39), 11890-11891.
32. Monchaud, D.; Allain, C.; Teulade-Fichou, M. P., Development of a fluorescent intercalator displacement assay (G4-FID) for establishing quadruplex-DNA affinity and selectivity of putative ligands. *Bioorg Med Chem Lett* **2006,** *16* (18), 4842-4845.
33. Largy, E.; Hamon, F.; Teulade-Fichou, M. P., Development of a high-throughput G4-FID assay for screening and evaluation of small molecules binding quadruplex nucleic acid structures. *Anal Bioanal Chem* **2011,** *400* (10), 3419-3427.
34. Neidle, S., The structures of quadruplex nucleic acids and their drug complexes. *Curr Opin Struct Biol* **2009,** *19* (3), 239-250.
35. Phan, A. T., Human telomeric G-quadruplex: structures of DNA and RNA sequences. *FEBS J* **2010,** *277* (5), 1107-1117.

36. Monchaud, D.; Allain, C.; Bertrand, H.; Smargiasso, N.; Rosu, F.; Gabelica, V.; De Cian, A.; Mergny, J. L.; Teulade-Fichou, M. P., Ligands playing musical chairs with G-quadruplex DNA: a rapid and simple displacement assay for identifying selective G-quadruplex binders. *Biochimie* **2008,** *90* (8), 1207-1223.
37. Reed, J.; Gunaratnam, M.; Beltran, M.; Reszka, A. P.; Vilar, R.; Neidle, S., TRAP-LIG, a modified telomere repeat amplification protocol assay to quantitate telomerase inhibition by small molecules. *Anal Biochem* **2008,** *380* (1), 99-105.
38. De Cian, A.; Cristofari, G.; Reichenbach, P.; De Lemos, E.; Monchaud, D.; Teulade-Fichou, M. P.; Shin-ya, K.; Lacroix, L.; Lingner, J.; Mergny, J. L., Reevaluation of telomerase inhibition by quadruplex ligands and their mechanisms of action. *Proc Natl Acad Sci USA* **2007,** *104* (44), 17347-17352.
39. Berg, K.; Zhai, L.; Chen, M.; Kharazmi, A.; Owen, T. C., The use of a water-soluble formazan complex to quantitate the cell number and mitochondrial function of Leishmania major promastigotes. *Parasitology Res* **1994,** *80* (3), 235-239.
40. Malich, G.; Markovic, B.; Winder, C., The sensitivity and specificity of the MTS tetrazolium assay for detecting the in vitro cytotoxicity of 20 chemicals using human cell lines. *Toxicology* **1997,** *124* (3), 179-192.
41. Sparapani, S.; Haider, S. M.; Doria, F.; Gunaratnam, M.; Neidle, S., Rational design of acridine-based ligands with selectivity for human telomeric quadruplexes. *J Am Chem Soc* **2010,** *132* (35), 12263-11272.
42. Ya, X.; Xiaohua, Z.; Jianzhong, W.; Huiying, Y.; Liangnian, J., Synthesis, Characterization and Proton-Dependent Electronic Spectra of a Series of Novel Ruthenium(II) Complexes Containing an Imidazole Unit. *Synth React Inorg Met Org Chem* **1998,** *28* (9), 1445-1454.
43. Sun, D. D.; Wang, W. Z.; Mao, J. W.; Mei, W. J.; Liu, J., Imidazo [4,5*f*][1,10] phenanthroline derivatives as inhibitor of c-myc gene expression in A549 cells via NF-κB pathway. *Biorg Med Chem Lett* **2012,** *22* (1), 102-105.
44. IDT SciTools OligoAnalyzer ver 3.1. https://www.idtdna.com/analyzer/Applications/OligoAnalyzer/ (accessed December 12, 2010).

In Chapter 2, we constructed a series of platinum(II) phenanthroimidazole complexes with small substitutions to the imidazole moiety of the phenanthroimidazole ligand including phenyl-, naphthyl-, quinolinyl-, indolyl-, phenol-, 2-hydroxynaphthyl-, and *p*-chlorophenyl-, and studied their interactions as guanine quadruplex binders for telomeric DNA sequences. While we created efficient end-stacking complexes, our molecules were not predicted to penetrate into the grooves of the quadruplexes by molecular modeling. Loop and groove interaction is thought to aid small molecules in the discrimination between G-quadruplex polymorphs. Additionally, we encountered solubility issues with the more π-extended 2-hydroxynaphthyl- derivative. Due to these observations, we decided to incorporate a protonable side-arm that protrudes from the phenylphenanthroimidazole scaffold. The side-arms are thought to aid in differentiation between polymorphs and help increase solubility in aqueous conditions. Chapter 3, thus describes this goal.

3 A Platinum(II) Phenylphenanthroimidazole with an Extended Side-Chain Exhibits Slow Dissociation from a *c-Kit* G-quadruplex Motif

Preface: Author Contributions and Publication

This chapter represents a collaborative effort among the Sleiman and Moitessier laboratories at McGill University, with data interpretation assistance from **Prof. Anthony Mittermaier**. **Katherine Castor** was responsible for the design, synthesis, and characterization of the complexes, as well as project design and biophysical assays (HT-FID, CD, and HPLC). **Dr. Mark A. Hancock** (McGill SPR Facility) conducted the SPR assays and **Dr. Guillaume Lesage** (CIAN, Department of Biology) ran the robot for the HT-FID assays. The computer-aided studies were performed by **Zhaomin Liu** under the supervision of **Prof. Nicolas Moitessier**. The biological assays (MTS, mRNA analysis, and western blot) were performed by **Dr. Johans Fakhoury** (Sleiman laboratory). The findings in this chapter were published in a manuscript accepted by Chemistry − A European Journal in 2013 entitled "A platinum(II) phenylphenanthroimidazole with an extended side-chain exhibits slow dissociation from a *c-Kit* G-quadruplex motif".

3.1 Introduction

As previously discussed in Chapters 1-2, guanine quadruplexes are non-canonical secondary structures formed in guanine (G)-rich DNA that have emerged as important targets for selective antitumor therapy.[1] These higher-order DNA structures result from the Hoogsteen hydrogen-bonding of the guanine units of G-rich DNA sequences into stacked tetramers stabilized by monovalent cations, namely K^+ and Na^+.[2] G-quadruplex-forming sequences exist throughout the human genome[3] and recent studies have shown that stabilizing these structures with small molecules can bring about antitumor effects by several mechanisms. These mechanisms include the inhibition of the cancer cell-immortalizing enzyme telomerase by sequestration of the telomere-substrate[4] and the regulation of gene expression, particularly in cancer-related genes including *c-Myc*,[5-10] *c-Kit*,[11-13] and vascular endothelial growth factor (VEGF)[14,15] among others. Since different DNA sequences create structural diversity among G-quadruplex polymorphs, an important therapeutic goal is to selectively target one polymorph rather than all, while minimizing binding to the more abundant genomic duplex DNA.

Of particular interest for chemotherapeutic targets is the c-KIT protein, a transmembrane growth factor receptor with tyrosine kinase activity that belongs to the PDGF/CSF-1 family.[16] The c-KIT protein, encoded by the human proto-oncogene *c-Kit*

stimulates cell proliferation and survival when activated by its ligand stem cell factor.[17] Inhibition of this protein is an important target in cancer therapeutics[18] since mutated forms of c-KIT are expressed in a variety of cancers including gastrointestinal stromal tumors (GIST),[19] systemic mastocytosis,[20] subsets of acute and chronic myeloid leukaemia[21] and melanoma.[22] While c-KIT inhibition has been realized with the small molecule inhibitor imatinib (Gleevec®) in GIST tumors,[23] drug resistance has developed in many cases due to secondary mutations.[24] Even when a secondary drug such as sunitinib has been used to combat imatinib-resistant mutations, studies have found that (i) the drug-drug interactions cause greater toxicity, or (ii) the tumors often become quiescent and can resume proliferation when treatment is stopped.[25] For these reasons, new molecular probes for the c-KIT-based pathway need to be developed.

One such class of probes are molecules that regulate the expression of the oncogene coding for c-KIT rather than inhibiting the protein itself. In this manner, the problems of drug resistance and toxic combination therapies could be avoided since the protein would not be present in the cells. Such an approach has been explored with the *c-Myc* oncogene,[6,7,9,10,26,27] in which case drug candidates were used to induce and stabilize G-quadruplex DNA motifs within the promoter nuclease hypersensitivity element (NHE) III1 – a G-rich region that is responsible for up to 90% of *c-Myc* transcription.[28] Analogous regulation of *c-Kit* is plausible, given that two distinct G-quadruplexes can form in the promoter region of the *c-Kit* oncogene.[18,29,30] Indeed, three classes of small molecules have been shown to down-regulate *c-Kit* expression in GIST cells.[11-13]

When attempting to influence biological processes like DNA transcription, many ligands can benefit from slow dissociation rates once they complex with their targets. One well-characterized example is actinomycin – an effective suppressor of transcription which forms a stable complex *via* intercalation into double-stranded DNA to inhibit RNA synthesis by RNA polymerase (Figure 3.1a).[31] Nordén and coworkers have also investigated the influence that dinuclear bisintercalators have on tight binding to, and slow dissociation from, double-stranded DNA targets (Figure 3.1b). They determined *via* linear dichroism experiments that in order for the $[\mu\text{-C4(cpdppz)}_2(\text{phen})_4\text{Ru}_2]^{4+}$ bisintercalator[32] to both associate and dissociate from DNA targets, a significant rearrangement of the DNA must occur. This rearrangement is rate-limiting and results in

slow association rates and even slower dissociation rates. While their bisintercalator did not appear to have an immediate effect on DNA synthesis *in cellulo*, they did find that the slow dissociation kinetics resulted in fluorescent DNA-marking ability in studies of chromosomal and spindle arrangements.[33] In an analogous manner, we hoped to design a complex that, through the complexation with DNA (namely the G-quadruplex motif), can exhibit slow dissociation (through multivalent interactions including intercalation, π-stacking, groove-binding, conformational change, etc.) to influence a biological function − that is, the regulation of *c-Kit* transcription.

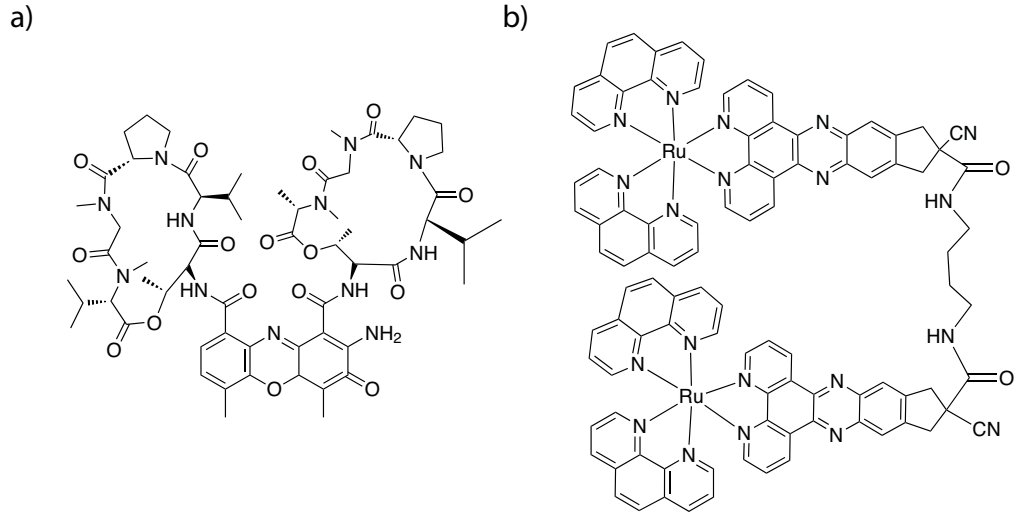

Figure 3.1 Examples of threading intercalators. a) the antibiotic actinomycin[31] and b) [μ-C4(cpdppz)$_2$(phen)$_4$Ru$_2$]$^{4+}$.[32]

While the rational design of DNA-based inhibitors has been successful in the creation of many duplex bisintercalators,[32,34-39] G-quadruplexes have topologically distinct features (e.g. large π-surface area, major and minor grooves, loops, etc.) that allow them to be differentiated from duplex DNA. Our lab has previously developed a progression of platinum(II)-based phenanthroimidazole complexes capable of binding to both tetramolecular[40] and human-telomere derived intramolecular G-quadruplexes (See Chapter 2).[41] We have shown that a simple modification to the phenanthroimidazole scaffold significantly increases binding to the basket-polymorph of human telomeric (h-telo) G-quadruplexes. To date, however, little is known about the residence time of G-quadruplex binders with biologically relevant promoter G-quadruplex motifs.

Herein, we present the design, synthesis, and evaluation (biophysical and biological) of a series of platinum(II) ethylenediamine phenylphenanthroimidazoles

(Figure 3.2) specifically engineered for multivalent (or chelate) binding to target G-quadruplexes and therefore, slow dissociation from target G-quadruplexes. One of the complexes highlighted in this chapter, **3.2** exhibited high selectivity for one of the G-quadruplexes found in the *c-Kit* promoter (ckit1). We modeled this phenomenon and rationalized slow dissociation due to chelation/multivalent interactions spread across the entire molecule, and we demonstrated that the slow dissociation of **3.2** from ckit1 is a major component of its binding mechanism. Complex **3.2** does not cause cytotoxicity at high concentrations in two telomerase-positive cell lines, consistent with the fact that it does not follow a telomere-targeting pathway. Preliminary mRNA analysis in A172 cells gave evidence of specific interaction with the *c-Kit* promoter region, however this needs to be further studied with cell lines that over-express the c-KIT protein. Thus, complex **3.2** is a useful probe for examining the effects of increasing the selectivity and residence times for the *c-Kit* promoter on gene expression, and the potential use of these attributes for effective antitumor therapies.

3.2 Results and Discussion

3.2.1 Synthesis of platinum(II) phenanthroimidazoles

Using our previously established platinum ethylenediamine phenanthroimidazole core,[40,41] we have now appended side-chains from the phenyl moiety. We strategically chose alkylamino side-chains since these and similar substituents have been shown to increase binding strength to G-quadruplexes (*via* interaction with the grooves, loops, and backbone).[42-46] In addition, they also each contain a biocompatible 1,4-substituted 1,2,3-triazole moiety[47] – a synthetic building block that has been shown to help discriminate between G-quadruplex grooves as well as increase binding strength.[48-52] The synthesis is facile and starts from economical, commercially available starting materials. The side-chains were synthesized *via* a simple substitution reaction or amide bond formation (where appropriate) followed by a Boc-deprotection before azidation (Figure 3.2). The azides were then coupled *via* copper-catalyzed cycloaddition with 4-ethynylbenzaldehyde under microwave irradiation for 15 minutes. The phenanthroimidazole units were synthesized through the condensation of 1,10-phenanthroline-5,6-dione and the side-chain aldehydes. Subsequently, these ligands were reacted with potassium

tetrachloroplatinate, to yield [Pt(phenanthroimidazole)Cl_2], followed by treatment with ethylenediamine (en) and precipitation with ammonium hexafluorophosphate, resulting in complexes **3.1**-**3.3** (Figure 3.2).

3.2.2 Oligonucleotides

To evaluate the binding specificity of each complex for different G-quadruplex polymorphs, we chose three G-quadruplex DNA sequences for use in a high-throughput fluorescence intercalator displacement (HT-FID) and circular dichroism (CD) experiments: 22AG corresponds to the h-telo repeat and is polymorphic depending on whether sodium or potassium ions are in solution (denoted hereafter as 22AG-Na and 22AG-K, respectively); cmyc and ckit1 correspond to human proto-oncogene promoter sequences (Figure 3.3). A duplex control sequence, ds26mer, is obtained with a self-complementary sequence. For surface plasmon resonance (SPR) experiments, we used biotinylated dT versions of 22AG, cmyc, and ckit1 with a 4-thymine spacer between the 5'-biotin-dT and the sequence start; a CG-rich hairpin (HP) was also used as a duplex control (Table 3.1).

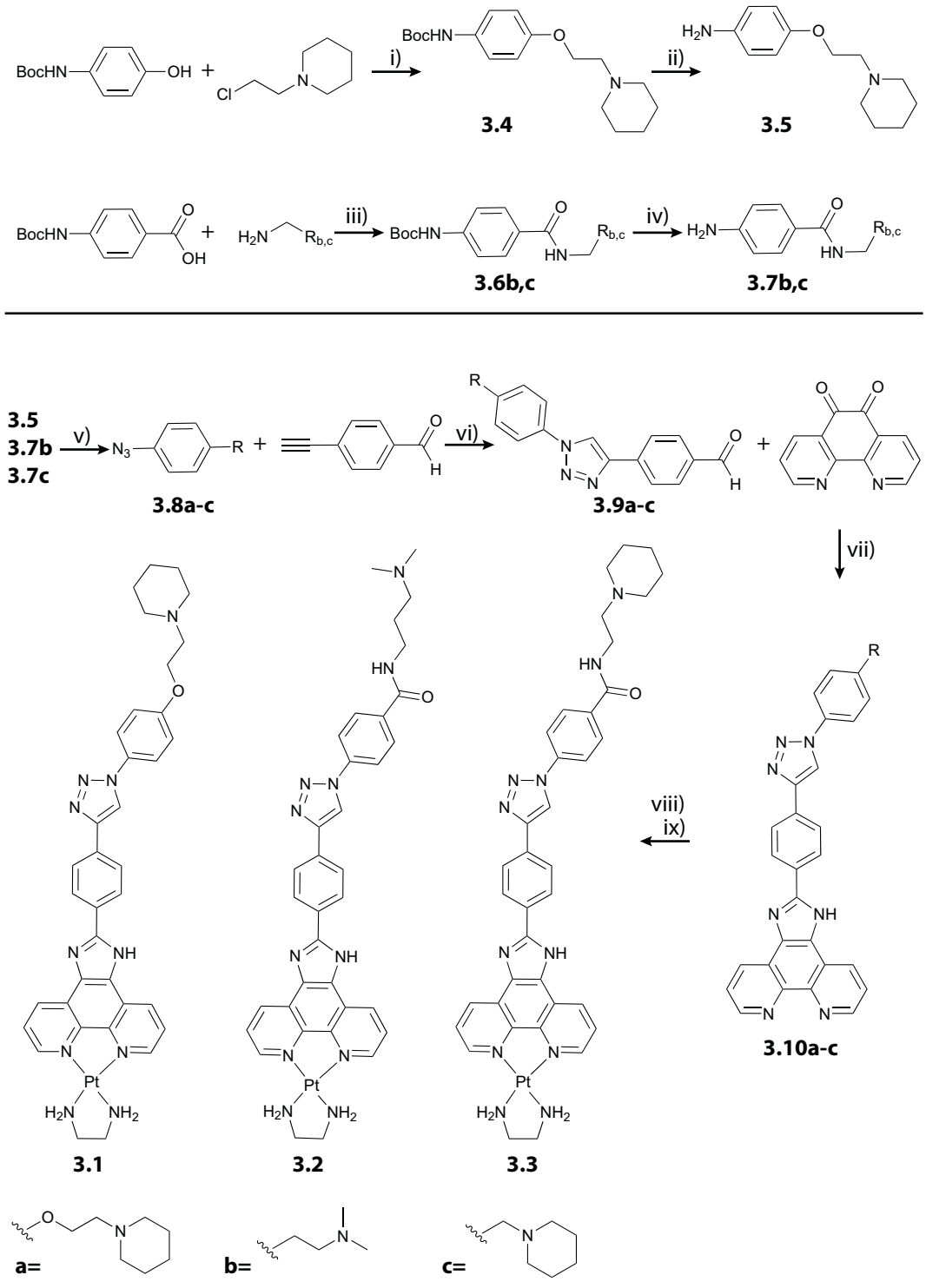

Figure 3.2 Synthesis of **3.1**-**3.3**. Conditions: i) NaH/THF, RT; ii) TFA/DCM, RT, 1 h; iii) EDC/HOAt in DMF, RT; iv) HCl/ethyl acetate; v) $NaNO_2$ and NaN_3 in 17% HCl/EtOH; vi) $CuSO_4$/ascorbate in DCM/ACN, microwave, 15 min, 100° C; vii) NH_4OAc in glacial acetic acid, reflux, 24 h; viii) K_2PtCl_4 in H_2O/DMSO; ix) en in EtOH, then NH_4PF_6.

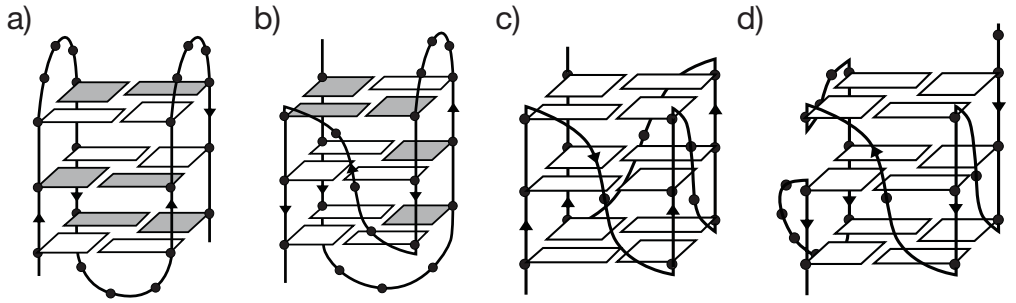

Figure 3.3 Schematic drawings of the DNA G-quadruplex motifs formed by the chosen sequences for a) human telomeric basket in Na^+ solution (22AG-Na); b) human telomeric 3+1 hybrid in K^+ solution (22AG-K); *c-Myc* promoter (cmyc); and d) *c-Kit* promoter (ckit1). The gray and white parallelograms represent syn and anti orientations, respectively, of the guanine bases contained within the tetrads.[29,53-55]

Name	ε_{260} ($M^{-1}cm^{-1}$)	Sequence
22AG (HT-FID and CD)	228 500	5'- AGGGTTAGGGTTAGGGTTAGGG
cmyc (HT-FID and CD)	279 900	5'- TGGGGAGGGTGGGGAGGGTGGGGAAGG
ckit1 (HT-FID and CD)	226 700	5'- AGGGAGGGCGCTGGGAGGAGGG
ds26mer (HT-FID)	253 200	5'- CAATCGGATCGAATTCGATCCGATTG
22AG (SPR)	268 900	5'-biotin-dTTTTTAGGGTTAGGGTTAGGGTTAGGG
cmyc (SPR)	320 400	5'-biotin-dTTTTTTGGGGAGGGTGGGGAGGGTGGGGAAGG
ckit1 (SPR)	267 100	5'-biotin-dTTTTTAGGGAGGGCGCTGGGAGGAGGG
HP (SPR)	226 500	5'-biotin-dTTTTTTTCGCGCGCGTTTTCGCGCGCG

Table 3.1 Sequences used in this chapter.

3.2.3 Molecular modeling (performed by Zhaomin Liu)

Due to precedents set by the bisintercalators of Nordén and coworkers[38,56] and the threading nature of actinomycin,[31] (Figure 3.1) we hypothesized that the presence of the side-chain would enable a multivalent binding mode and subsequently, longer residence times on the G-quadruplex.

To investigate the binding mode of **3.2** on the G-quadruplex in greater detail, Zhaomin Liu used a combination of molecular docking and molecular

dynamics (MD) simulations; the former allowing a large search of the conformational space, while the latter allowed the highly flexible G-quadruplex system to freely interact with **3.2** and account for the effect of water and counter ions. This previously reported protocol[57,58] began with the generation of a large number of potential binding modes (referred to as poses) through the use of Prof. Moitessier's in-house FITTED docking program.[59] A few representative poses were selected through clustering and visual inspection as well as FITTED energy score and subjected those poses to MD simulations using AMBER.

The platinum complexes **3.1**-**3.3** were designed such that multiple interactions across the G-quadruplex surface would simultaneously take place. As shown in Figure 3.4, this molecular modeling study suggested that multiple interactions are likely occuring. For **3.2**, the large aromatic phenanthroimidazole unit, as well as the triazole and phenyl rings, are π-stacked with two guanine bases of the top G-tetrad layer. This stacking orients the platinum atom near the phosphate backbone and enables electrostatic interactions with these negatively charged phosphate groups. In addition, strong ionic hydrogen bonds are predicted to form between phosphate groups and both ends of the platinum complex – i.e. between the ethylenediamine ligand and the ammonium group of the side-arm. Although the ionic hydrogen bond between the side-arm and phosphate group is enthalpically favoured, it is entropically disfavored. In fact, this hydrogen bond is fairly labile throughout MD simulations. However, this flexibility enables the formation of such ionic hydrogen bonds with multiple phosphate groups in the neighborhood (see Figure 3.4 versus Figure S3.2-Figure S3.5). The G-quadruplex residues involved in the binding vary among structures. Although the G-quadruplexes may fold differently with the first G-tetrad layer being covered by a loop (Figure 3.4a), or fully (Figure 3.4b) or partially (Figure 3.4c,d) exposed to the aqueous medium, the predicted binding modes of **3.2** always retain a similar interaction pattern. Since the simulation timeframe is short compared to the slow process of binding *in vitro*, the kinetics of ligand binding cannot be quantified. Our efforts to predict the free energy of binding through MD simulations combined with MM/PBSA have not yet been conclusive since accurately

computing the entropy contribution to these binding processes is challenging. Thus, we should be cautious when relating predictions with the *in vitro* binding assays.

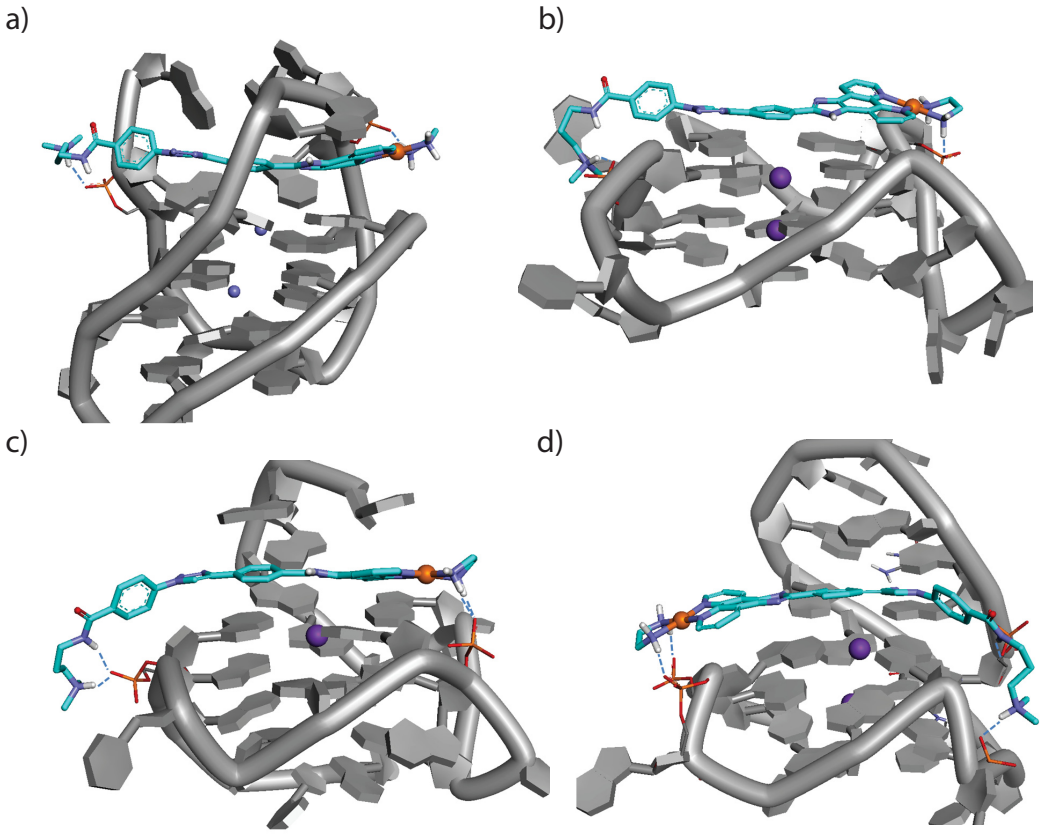

Figure 3.4 Snapshots of the MD simulations of **3.2** and G-quadruplexes: a) and b) show the 22AG polymorphs in Na^+-solution and K^+-crystal, respectively; c) cmyc; and d) ckit1. Complex **3.2** is shown in cyan with the platinum(II) atom shown as an orange sphere. G-quadruplex structures are in gray, native metal atoms in Na^+ and K^+ are shown as blue and purple spheres, respectively. The backbone phosphates involved in hydrogen bonds with **3.2** are shown as dashed lines.

3.2.4 HT-FID assay

Given that our modeling predictions supported our multivalent binding hypothesis, we wanted to assess how this would affect binding affinity. Initially, the binding of **3.1**-**3.3** to the h-telo, cmyc, and ckit1 G-quadruplexes was assessed by a FID, a robust and versatile method developed by Teulade-Fichou and coworkers.[60,61] The assay relies upon the competitive displacement of the intercalated thiazole orange dye from the DNA targets by **3.1**-**3.3**, with a concomitant decrease in fluorescence intensity (see Chapter 1, pp 49 for details on

this assay). We adapted the high-throughput FID (HT-FID) method[62] so that it could be performed by a Biomek FX liquid handler and a SAGIAN core robot by Dr. Guillaume Lesage (CIAN, Department of Biology, McGill University) (See Figure S3.6 and Figure S3.7 for plate layouts). Binding affinities were evaluated from the resulting isotherms where the concentration of platinum complex required to give a 50% decrease in dye fluorescence is the DC_{50} (Table 3.2).

FID assays are typically incubated for short 5−10 minute periods before reading the plate as the displacement and binding process is believed to be fast.[62] However, we hypothesized that the displacement and binding process need longer incubation periods due to the addition of the side-chains on **3.1**-**3.3**. Using both short (10 minute) and long (90 minute) incubation periods, we determined DC_{50} values (Table 3.2). The 90 minute incubation assay resulted in lower DC_{50} values across the board with the most dramatic difference involving **3.2** and the ckit1 G-quadruplex (Figure 3.5). Notably, this DC_{50} of 0.282 μM is the lowest value that we have achieved with our series of platinum phenanthroimidazole complexes to date.

Sequence	Complex 3.1	Complex 3.2	Complex 3.3
22AG-Na	1.45 / 1.09	0.931 / 0.663	>2.50 / 2.00
22AG-K	1.50 / 1.14	1.29 / 0.890	>2.50 / 1.75
cmyc	1.74 / 0.645	1.76 / 1.32	>2.50 / 1.01
ckit1	>2.50 / 0.544	>2.50 / 0.282	>2.50 / 0.985
ds26mer	2.12 / 1.76	2.06 / 1.68	>2.50 / 2.24

Table 3.2 DC_{50} values (μM) for **3.1**-**3.3** (10 minute / 90 minute incubation). Values are averages of 4 repeats performed by the robot with errors ≤ 5%.

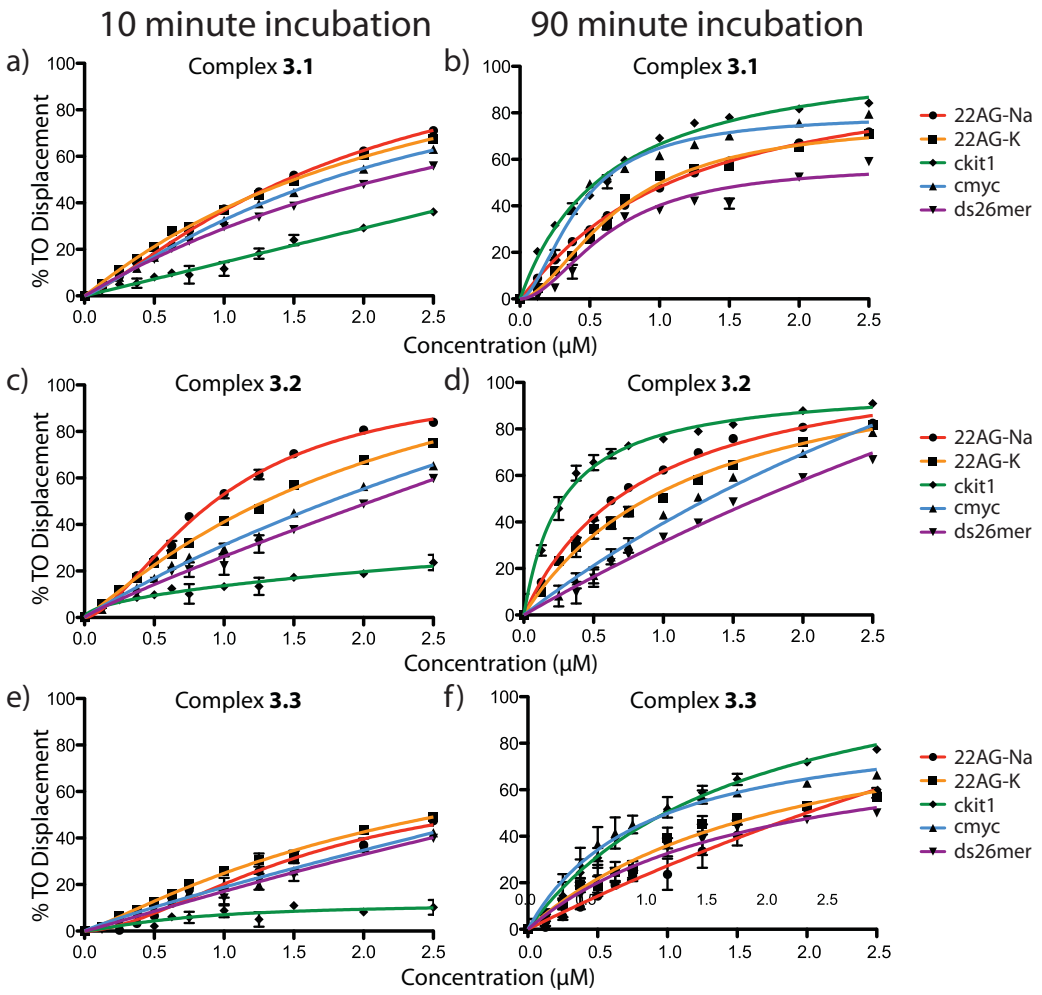

Figure 3.5 HT-FID data obtained from the robot method was transformed into a binding isotherm where the x-axis is the concentration of platinum complex and the y-axis is percentage displacement of thiazole orange (TO). The 10 minute incubation periods are shown on the left (a, c, e) while the 90 minute incubation periods are shown on the right (b, d, f) for complexes **3.1**-**3.3**.

It is difficult to compare the DC_{50} values directly between sequences since the binding affinity of the thiazole orange dye for each G-quadruplex motif varies greatly. Thus, we used a method developed by Prof. Anthony Mittermaier (See Section 3.5.6) to compare data sets according to overall affinity. Equilibrium association constants (K_A) for the complexes were extracted from the FID fluorescence isotherms, using the concentrations and affinity of thiazole orange for the different G-quadruplexes.[62] After fitting of the data to equation 7 (pp 156) and determining the corresponding equilibrium dissociation constants (K_D = 1/K_A), we obtained the values in Table 3.3. Notably, the 0.282 μM DC_{50} for **3.2** with ckit1 translates into a K_D of approximately 73 nM. Complex **3.2** also

demonstrates the best selectivity between G-quadruplex DNA and duplex DNA compared to the other two complexes, and is on par with the best reported ckit1 binders.[11-13,52]

Sequence	Complex 3.1	Complex 3.2	Complex 3.3
22AG-Na	2.63 / 0.633	1.12 / 0.366	5.79 / 4.12
22AG-K	1.49 / 0.568	1.69 / 0.621	2.42 / 0.792
cmyc	1.28 / 0.102	2.30 / 1.01	4.28 / 0.134
ckit1	51.1 / 0.262	1.00 / 0.0726	0.49 / 0.559
ds26mer	1.30 / 0.324	8.41 / 1.10	6.47 / 0.390

Table 3.3 Apparent K_D values (μM) for **3.1**-**3.3** (10 minute / 90 minute incubation) as determined by HT-FID. Values are averages of 4 repeats performed by the robot with errors ≤ 5%

3.2.5 SPR assays (performed by Dr. Mark A. Hancock at the McGill University SPR Facility)

To complement our FID data, we performed label-free, real-time SPR, which has emerged as a powerful technique to examine the binding specificity and kinetics of compounds for duplex versus G-quadruplex DNA.[63-67] Similar to these previously reported methods, we used a potassium-containing running buffer to focus upon **3.1**-**3.3** binding to the 22AG-K, cmyc, and ckit1 G-quadruplexes; to determine selectivity between G-quadruplex and duplex DNA, we used a CG-rich hairpin (HP). Preliminary, fixed-concentration screening (Figure 3.6) revealed that several of our platinum-based complexes (complexes **3.5** and **3.6**, Figure 3.6) could specifically bind to the immobilized DNA sequences, whereas diluent alone (i.e. running buffer containing 1 mg/mL CM-dextran to reduce minor non-specific binding of the complexes to SA-coated sensors) or our negative control complex **3.4** (Figure 3.6) described elsewhere[41]) generated no signal responses. With matching DNA surface densities and equimolar injections of complex, binding to duplex DNA was approximately 50% of quadruplex responses (i.e. different number of binding sites). In both cases, all complexes bound with fast association kinetics and signal responses exceeded theoretical R_{max} predictions (the R_{max} is the estimated maximum response signal

when the binding stoichiometry is predicted to be 1:1. If the signal responses exceed the R_{max} prediction, it is likely that the stoichiometry is greater than 1:1, similar to previous reports in the literature[63]). Most importantly, the non-sidechain-containing complexes **3.5** and **3.6** exhibited rapid dissociation kinetics compared to the significantly slower dissociation rate for **3.2** (Figure 3.6).

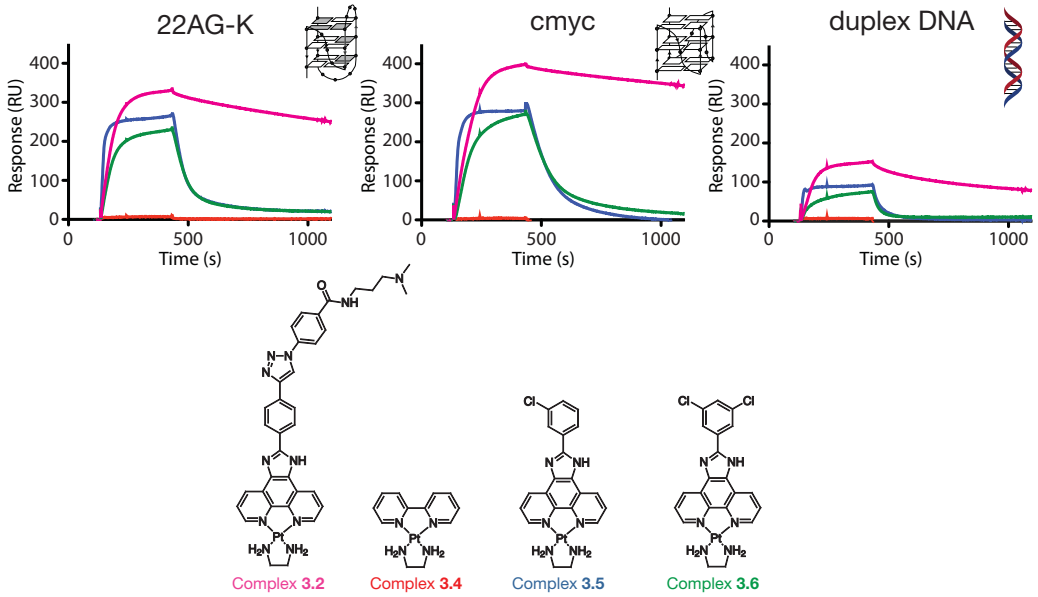

Figure 3.6 Representative SPR screening of compounds (5 μM each) binding to (left to right) 450 RU immobilized 22AG-K, cmyc, and duplex DNA (HP) at 25 μL/min (5 minute association + 10 minute dissociation).

Using lower density surfaces and increased injection times, SPR titrations revealed saturable, dose-dependent binding of **3.2** to duplex (Figure S3.8) and quadruplex DNA (Figure 3.7, top). While the fast-on, slow-off kinetics deviated from a simple 1:1 binding model in all cases, affinities were determined based upon equilibrium responses in each titration series (Figure 3.7, second from top). On average, the binding of **3.2** to the quadruplex sequences (K_D = 0.58 ± 0.1 μM) was approximately 10-fold stronger compared to duplex DNA (K_D = 5.0 ± 2.0 μM, Figure S3.8). Although sub-micromolar quadruplex binders with dissociation rate constants in the 10^{-2} s^{-1} range have been previously reported (e.g. 2Mn-TMPyP + h-telo;[63] TMPyP4 + ckit2;[64] quinazoline derivative + h-telo;[66] Se2SAP + cmyc = 0.62 μM K_D and 2.9 x 10^{-3} s^{-1};[68] corrole 4 + G4 quadruplex = 0.52 μM K_D and 2.2 x 10^{-3} s^{-1}.)[69] **3.2** exhibits dissociation rates that are slower than other reported quadruplex binders (22AG-K ~ 1.7 x 10^{-3} s^{-1}; cmyc ~ 1.0 x 10^{-3} s^{-1}; ckit1

~ 1.2 x 10^{-3} s^{-1}). When complex **3.2** binds to quadruplex DNA, the increased stability of this interaction (i.e. low 10^{-3} s^{-1} dissociation rate) could translate into desirable pharmacokinetics (i.e. a long residence time means the compound occupies the therapeutic target longer).

The equilibrium responses were transformed into a Scatchard plot (the ratio of concentration of bound ligand to unbound ligand versus the bound ligand concentration) to reveal a line with a slope of $-K_A$ (Figure 3.7, second row from bottom). In the case of 22AG-K (left) and ckit1 (right), the line deviates from linearity. In general, Scatchard plots that are not linear can arise from several factors including, i) multiple independent binding sites that are not equivalent, ii) equivalent sites that are not independent, and iii) non-equivalent sites that are not independent. Since **3.2** binding to G-quadruplex DNA resulted in signal responses that exceeded theoretical R_{max} predictions, we may assume that multiple binding sites do exist − that is, the binding stoichiometry is greater than 1:1. Additionally, the concave nature of the curves may suggest negative cooperativity upon binding of the first ligand (Figure 3.7, second from bottom, left and right). Transformation of the equilibrium data into Hill plots yielded slopes with values less than 1 for 22AG-K and ckit1 (0.49 ± 0.02 and 0.62 ± 0.01, respectively) thereby supporting i), ii), and iii) above (Figure 3.8, bottom).

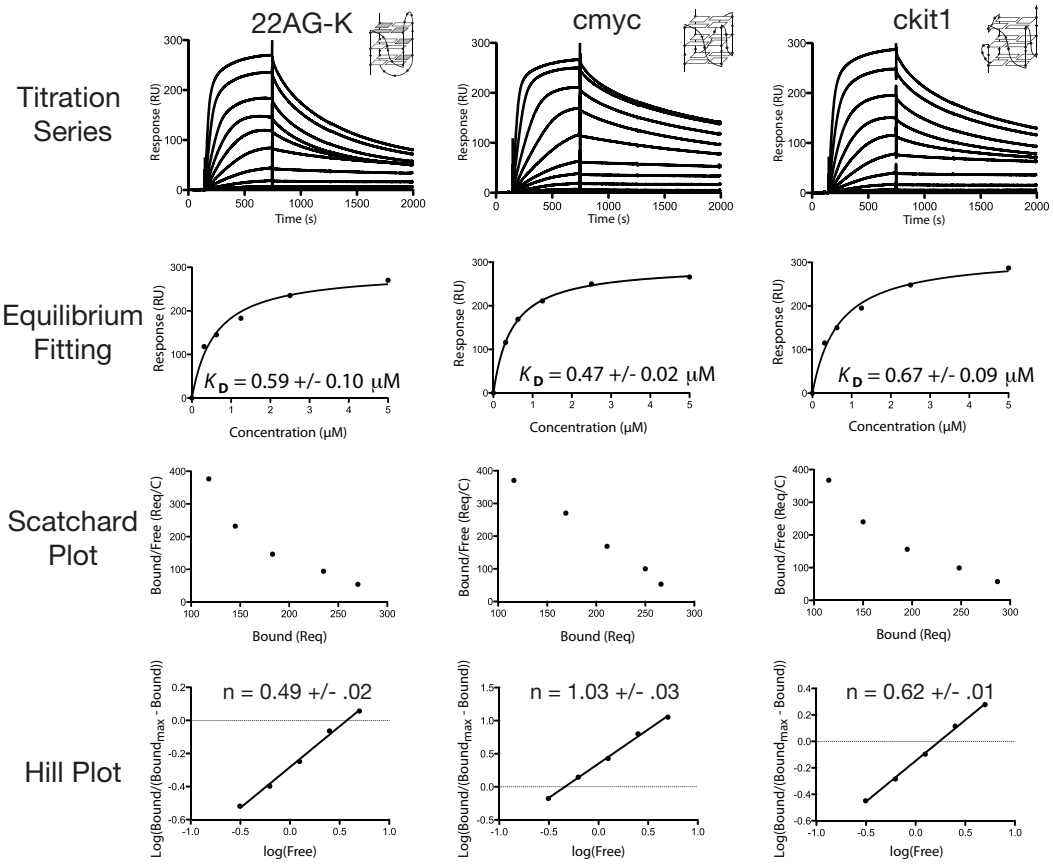

Figure 3.7 Representative SPR titrations of **3.2**. Top: 0-5 μM, 2-fold dilution series binding to (left to right) 300 RU immobilized 22AG-K, cmyc, and ckit1 G-quadruplex DNA at 25 μL/min (10 minute association + 20 minute dissociation periods). Second from top: Affinities (K_D) determined based upon equilibrium responses in each titration series. Inset K_D values represent the average of at least 3 trials ± standard error. Second from bottom: Scatchard transformations from the equilibrium fitting model. Bottom: Hill plots from the equilibrium fitting model; slopes of the lines (n) are shown as insets.

When comparing the K_D values determined from HT-FID to the corresponding values from SPR, one may notice a discrepancy, especially between the values for complex **3.2** binding to ckit1 (0.073 μM versus 0.67 μM). The order of magnitude difference may be derived from the limitations during conduction of the SPR assays. Since SPR 'analytes' (e.g. compounds) are injected over immobilized 'ligands' (e.g. DNA) under flow, high quality kinetic data is obtained when high flow rates of 25−50 μL/min are employed; this minimizes the diffusion boundary above the sensor chip surface in order to eliminate mass transport effects that would otherwise underestimate the affinity constants. For this reason, trying to repeat our SPR assays with longer contact times (i.e. to mimic increased 90 minute FID incubations) actually yielded poorer quality data

sets − i.e. submicromolar KD values with 10 minute association phases at 25 μL/min, compared to micromolar KD values with 25 min or 63 min association phases at 10 or 4 μL/min, respectively).

3.2.6 Cytotoxicity Assessment (performed by Dr. Johans Fakhoury)

To assess the anti-proliferative activities of **3.2**, it was evaluated in an MTS ((3-(4,5-dimethylthiazol-2-yl)-5-(3-carboxymethoxyphenyl)-2-(4-sulfophenyl)-2H-tetrazolium)) assay that evaluates mitochondrial metabolic activity.[70,71] Complex **3.2** was incubated for 72 hours with two cell lines: HeLa (non-*c-Kit* expressing human cervical cancer)[72] and A172 (*c-Kit* expressing human glioblastoma)[16]. In tandem, we also tested a positive control **3.7** (Figure 3.8) which we had shown to efficiently bind the h-telo sequence, and a negative control **3.4** (Figure 3.8).

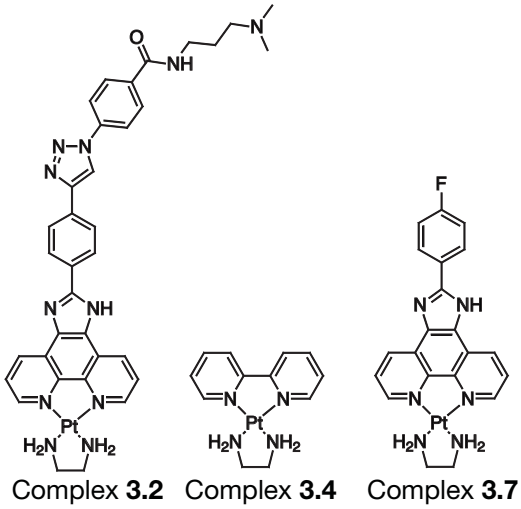

Figure 3.8 Platinum complexes used in cell studies. Complexes **3.4** and **3.7** are negative and positive controls, respectively.

We were unable to determine an IC_{50} for **3.4**, consistent with its lack of cytotoxicity under our conditions. Complex **3.2** also had very high IC_{50} values (> 100 μM) for HeLa and A172 cell lines, whereas **3.7** had a lower μM IC_{50} value (> 10 μM) and no gross morphological changes were observed (data not shown). Due to the high IC_{50} values for these telomerase-positive cell lines, we hypothesized that **3.2** does not follow the same telomere-targeting pathway as positive control **3.7**.[41]

One could reason that **3.2** does not confer the same cytotoxic effects as **3.7** because it is unable to enter cells. In order to rule out this possibility, we conducted a simple HPLC detection method. In this method, both HeLa and A172 cells were treated with 50 μM platinum complexes **3.2** and positive control **3.8** (Figure 3.9) and allowed to incubate for 24 hours, after which the serum was collected, followed by lysis of the cells, and collection of the lysate. Samples were then lyophilized, re-dissolved in HPLC-grade DMSO, and filtered before being injected into the HPLC. When compared to the retention time of the controls (untreated serum and lysate, and **3.2** and **3.8** alone), both **3.2** and **3.8** were present in serum and lysate (Figure 3.9), however, the peak heights for complex **3.2** in the lysate of Figure 3.9c are much smaller than those in serum (Figure 3.9d) and those in lysate of complex **3.8** (Figure 3.9a). This supports the fact that **3.2** is not taken up in cells to the same extent as **3.8**. Although we cannot definitively say from this experiment that the complexes are able to penetrate into the cytoplasm instead of electrostatically binding to the cell membrane, full mechanistic cell studies are being undertaken by Johanna Mancini, a graduate student, through a collaboration with Prof. Chantal Autexier (Departments of Experimental Medicine and Anatomy & Cell Biology, McGill University).

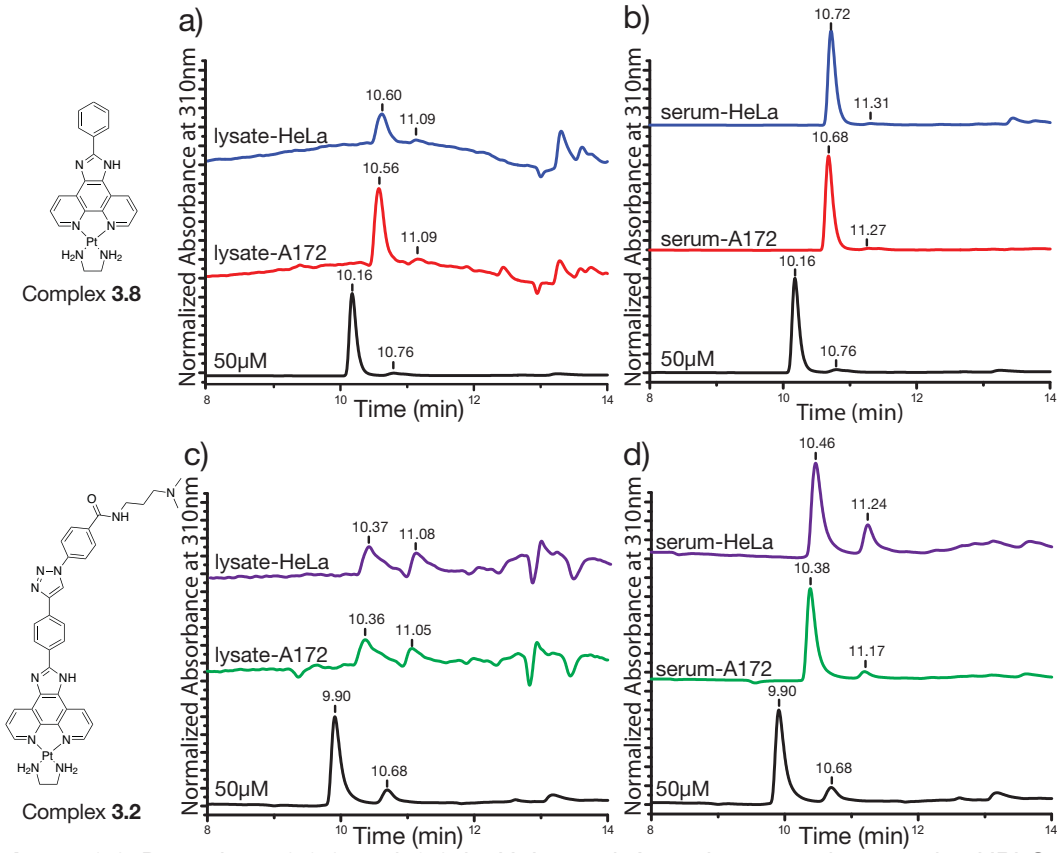

Figure 3.9 Detection of **3.2** and **3.8** in HeLa and A172 lysate and serum by HPLC. Complex **3.8** detected in the a) lysate and b) serum of HeLa (blue) and A172 (red) compared to the retention time of 50 μM **3.8** subjected to the same conditions, minus the cells (black). Complex **3.2** detected in the c) lysate and d) serum of HeLa (purple) and A172 (green) compared to the retention time of 50 μM **3.2** subjected to the same conditions, minus the cells (black). Each trace was subjected to blank subtraction and normalization to maximize signal to noise. For simplicity, only time points between 8-14 minutes are shown.

3.2.7 Measurement of mRNA levels (performed by Dr. Johans Fakhoury)

Given that **3.2** has stronger binding affinity for ckit1 over h-telo, and due to its absence of cytotoxicity at high concentrations, we conducted a preliminary semiquantitative mRNA analysis to assess whether **3.2** interacts with the *c-Kit* promoter region and induces a change in mRNA transcription *in cellulo*. To determine this, basal levels of *c-Kit* mRNA in HeLa and A172 cell lines were first assessed in the absence of **3.2**. Basal levels of mRNA were found only in the A172 cell line. The cell lines were incubated with 10 μM of **3.2**, **3.4**, and **3.7** for 48 hours and the *c-Kit* mRNA levels were measured relative to 18S ribosomal

RNA (as the internal quantification control). Figure 3.10 shows that the treatment of A172 cells with **3.2** leads to a slight qualitative increase in *c-Kit* mRNA at the examined dose compared to DMSO and the negative controls.

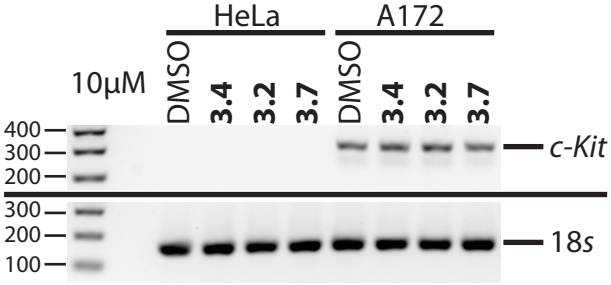

Figure 3.10 The mRNA levels of *c-Kit* after treatment with platinum complexes. (top) A172 cells exhibited an increased level of *c-Kit* mRNA in the presence of 10 μM **3.2**. HeLa cells were unaffected; (bottom) 18S ribosomal RNA was used as a control. Levels of 18S rRNA remained unchanged across the board. DMSO was used as untreated control.

We speculate this small increase could result from one of two mechanisms; either i) **3.2** causes unfolding of the *c-Kit* quadruplex motif, or ii) the binding of **3.2** to the *c-Kit* quadruplex causes opening up of other repressor elements in the promoter region that were previously sequestered. To rule out the first possibility, namely unfolding of the *c-Kit* quadruplex by **3.2**, CD titrations were performed in the following three buffer conditions at 37ºC with both 10 minute and 90 minute time allowances between titration points: i) 10 mM K_2HPO_4/10mM KH_2PO_4 (no added salt), ii) 10mM K_2HPO_4/10mM KH_2PO_4 with 100 mM KCl (added salt), and iii) 0.906 mM Na_2HPO_4/NaH_2PO_4 with 5.33 mM KCl and 110.34 mM NaCl (as a mimic of the cellular DMEM media). If unfolding of the quadruplex occurred, the positive CD peak at 260 nm signifying the parallel ckit1 folding would decrease with added **3.2**. Both the 10 minute and 90 minute incubations show negligible changes in the CD traces in all conditions indicating that no unfolding of the structure occurs with up to 5-fold excess of **3.2** (Figure 3.11).

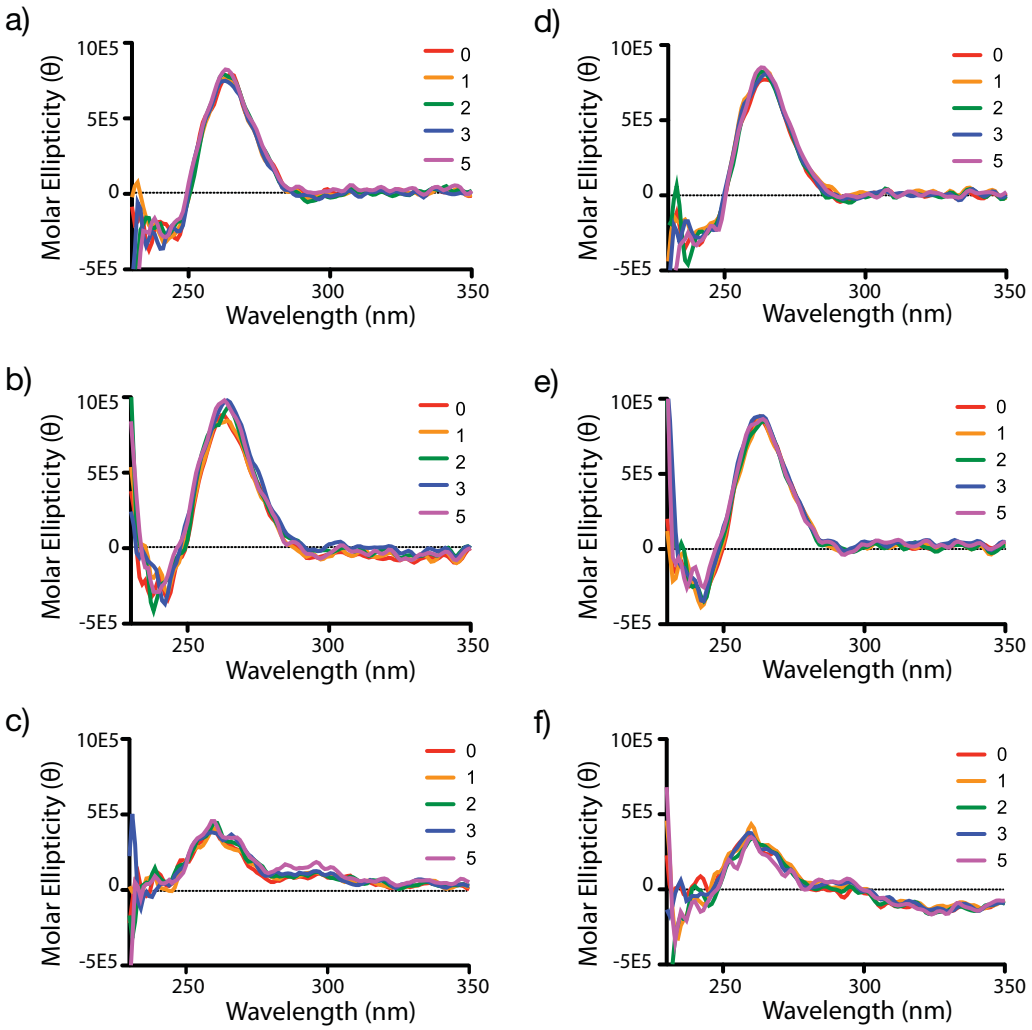

Figure 3.11 Left column: 10 minute incubation with up to 5 equivalents of **3.2** with a) 10 mM K_2HPO_4/10 mM KH_2PO_4, b) 10 mM K_2HPO_4/10 mM KH_2PO_4 with 100 mM KCl, and c) 0.906 mM Na_2HPO_4/NaH_2PO_4, 5.33 mM KCl, and 110.34 mM NaCl. Right column: 90 minute incubation with up to 5 equivalents of **3.2** with d) 10 mM K_2HPO_4/10 mM KH_2PO_4, e) 10 mM K_2HPO_4/10 mM KH_2PO_4 with 100mM KCl, and f) 0.906 mM Na_2HPO_4/NaH_2PO_4, 5.33 mM KCl, and 110.34 mM NaCl.

Additionally, we conducted CD melting experiments to further support the stabilization of the ckit1 quadruplex by **3.2**. Complex **3.2** was incubated overnight at 4°C in a 4:1 ratio of **3.2**:G-quadruplex and the sample was subsequently melted. The $T_{1/2}$ values were compared to G-quadruplex alone and the $\Delta T_{1/2}$ value was determined to be 7.3 ± 0.2°C. The curve becomes much broader above 70°C, such that two transitions may be evident, and does not fully plateau at 95°C (Figure 3.12). This is most likely due to the greater stability imparted by **3.2** on the ckit1 G-quadruplex motif. These results lead us to speculate that the binding of **3.2** *in*

cellulo may allow for a rearrangement of the promoter region that could expose enhancer elements or sequesters repressor elements.[73] One must note here that these preliminary studies were carried out in A172 cells that only express low levels of *c-Kit* mRNA; these results may be different with cell lines (such as HGC-27) that over-express the c-KIT protein, or with other doses of ligands.

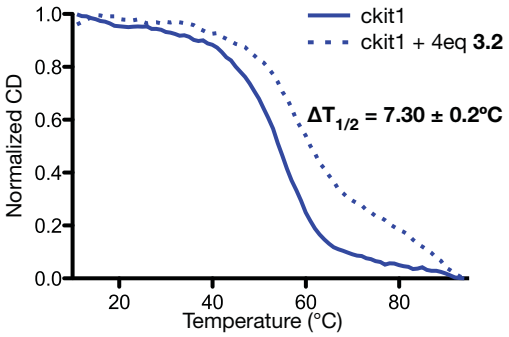

Figure 3.12 CD Melting curves for ckit1 (blue) and ckit1 + 4 equivalents of complex **3.2** (blue dashed) monitored at 260 nm. The $\Delta T_{1/2}$ is 7.30 ± 0.2°C.

3.2.8 Western blot analysis (performed by Dr. Johans Fakhoury)

We were also interested in detecting protein levels after incubation with the platinum complexes. For this end, we used two cell lines, one that expresses the c-KIT protein, A172 and one that does not, HeLa. We readily detected the presence of mRNA of *c-Kit* in A172, however, as expected, we did not observe detectable levels of *c-Kit* mRNA in HeLa cells. We thus performed western blot analysis – the quantification levels are shown in Figure 3.13 relative to the untreated DMSO control. We observed that after exposure of A172 to 10 μM **3.2** for 72 hours, levels of c-KIT were slightly increased, while we did not observe any change in c-KIT levels when exposed to both the untreated DMSO control cells and **3.4** (1.38 versus 1.00/0.93). β-Actin was used as a loading control and was unchanged after incubation with the complexes (as 10 μM is below the IC_{50} values). Interestingly, we did, however, see a decrease in c-KIT levels when **3.7** was used (Figure 3.13). This could possibly be due to the different mechanisms of action/interaction of **3.7** and **3.2** with different areas of the promoter region, as it contains two guanine-rich tracts capable of forming G-quadruplexes,[18,30] in addition to the low cellular penetration of complex **3.2**. Since c-KIT is coded by an inherently complex gene promoter,[73] it is likely that the interaction of the

ligands with the individual promoter elements will most likely lead to different responses.

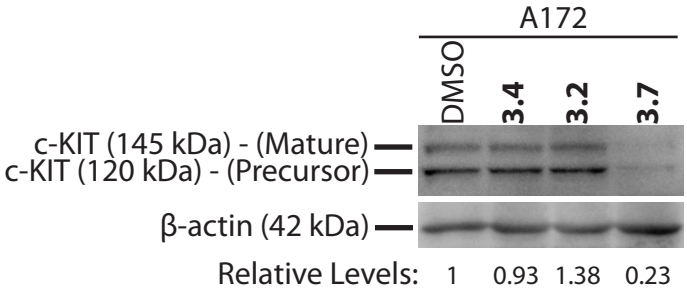

Figure 3.13 Western blot analysis of A172 cells after a 72 hour incubation with 10μM **3.4**, **3.2**, and **3.7**. (top) Comparison of the bands for **3.2** to DMSO/**3.4** show a slight increase in c-KIT levels (1.38 versus 1/0.93). (bottom) β-Actin was used as a loading control and was unchanged after incubation with the complexes.

3.3 Conclusions

We have generated phenylphenanthroimidazole platinum(II) complexes with side-chains specifically designed to interact with G-quadruplex DNA. This study demonstrates that these compounds can interact in a multivalent manner and result in fast-on, slow-off binding kinetics. Spreading the hydrogen bonding and π-stacking interactions across the binding surface allows **3.2** to exhibit, to the best of our knowledge, the slowest reported rate of dissociation from a G-quadruplex target. We are currently working on elucidating the mechanism of interaction using cells that over-express the c-KIT protein, and exploring the use of **3.2** in combination therapies. Thus, complex **3.2** is a useful probe to examine the effect of increasing the selectivity to the *c-Kit* promoter and lengthening the drug residence time on gene expression, and the potential use of these attributes for effective antitumor therapies.

3.4 Future directions

In this chapter, we chose to study the interaction of **3.2** with A172 (human glioblastoma) cells since they are known to express *c-Kit* and the cell line was readily available in the tissue culture lab. However, the basal levels of *c-Kit* expression were low, which presented an inherent issue when attempting to quantify the levels of *c-Kit*. Ideally, the basal levels of *c-Kit* should be high, such

that after incubation with **3.2**, the slight changes would be more pronounced. After a thorough search, we were able to obtain HGC-27 (human gastric carcinoma) cells which are known to over-express the *c-Kit* oncogene, and future studies will involve the investigation in the mechanism of action of **3.2** on this cell line.

3.5 Experimental section

3.5.1 Synthesis

For chemical synthesis, all commercially available reagents were purchased from Sigma Aldrich and used without further purification with the exception of 1-ethyl-3-(3-dimethylaminopropyl)carbodiimide (EDC) and 1-hydroxy-7-azabenzotriazole (HOAt) which were purchased from Chem-Impex International, Inc. For high-pressure liquid-chromatography (HPLC) purification, HPLC grade methanol and formic acid were purchased from Sigma Aldrich. Milli-Q water was dispensed from a Millipore machine. Sodium hydride (60% dispersion in mineral oil) was first washed with pentane before use. Chloroethyl piperidine • HCl was free-based by dissolving in THF and washing with aqueous NaOH. All dry solvents were obtained from an Innovative Technologies solvent purification system. The CuAAC reactions were carried out on a Biotage Initiator microwave (Thanks, Mitch and Sam). Column chromatography was performed using a CombiFlash Rf system from Teledyne Isco, Inc. 4-(2-(piperidin-1-yl)ethoxy)aniline (**3.5**) and precursor (**3.4**),[74] [4,5-*f*][1,10]phenanthroline[40] and complex **3.4**[40] were prepared in a manner similar to those previously published. ^{1}H and ^{13}C NMR spectra were recorded on either a 500 MHz, 400 MHz, or a 300 MHz Varian Mercury NMR spectrometer with VNMRJ 2.2D software under LINUX Red Hat 5. The following abbreviations are used: singlet (s), doublet (d), triplet (t), quartet (q), multiplet (m), and broad (br). High-resolution mass spectrometry was performed on a Bruker Maxis Impact ESI-QTOF. For MS analysis, sodium formate was used to generate a calibration curve for mass accuracy. Samples were then diluted in LC-MS grade methanol (Fisher) and directly infused at 3 μL per minute into the MS. The spectra were obtained in

positive mode. Circular dichroism unfolding and melting experiments were performed at on a JASCO J-810 spectropolarimeter with Spectra Manager II software.

3.5.2 Purification of ligands and final complexes: CombiFlash and HPLC methods

Ligands **3.10a-c** and final complexes **3.1** and **3.3** were purified by column chromatography using the CombiFlash Rf system with a reverse-phase C18-Aq Gold column. Conditions are as follows: 2 column volumes of (A) 5% MeOH in MQ-water with 0.1% (v/v) formic acid; 14 column volumes of increasing gradient to (B) 100% MeOH with 0.1% (v/v) formic acid; 2 column volumes of 100% (B). Ligands eluted between 40%−50% (B). To isolate the neutral ligand, a solution of the acidified ligand in MeOH and water was stirred with Amberlite® IRA-67 free base resin until the solution was at neutral pH. The resin was removed *via* vacuum filtration and the MeOH was removed under reduced pressure before freezing the solution in liquid nitrogen. The frozen solution was then lyophilized overnight to yield a fluffy solid.

Final complex **3.2** was purified *via* HPLC on an Agilent Technologies 1260 Infinity system. Analytical and semi-preparative RP-HPLC was carried out using a Zorbax SB-C18 9.4x250 mm column with a particle size of 5 μm (Aglient Technologies). The column was eluted at 4.0 mL/min with a linear gradient over 12 minutes from 10% solution A to 100% solution B. Solution A was 0.1% (v/v) formic acid in 5% MeOH in MQ water. Solution B was 0.1% (v/v) formic acid in MeOH. The retention time of **3.2** was 5.905 min. To isolate the 2^+ complex, a solution of the acidified complex in MeOH and water was stirred with Amberlite® IRA-67 free base resin until the solution was at neutral pH. The resin was removed *via* vacuum filtration and the complex isolated from the filtrate after precipitation with NH_4PF_6.

Data File C:\CHEM32\1\DATA\KATIE\KC-PIMP_HPLC_PURE.D
Sample Name: KC-PIMP_HPLC_PURE

Acq. Operator : SYSTEM
Acq. Instrument : 1260LC Location : Vial 54
Injection Date : 29/06/2012 12:41:27 PM
Inj Volume : 25.0 µl
Method : C:\CHEM32\1\DATA\KATIE\KC-6-16-2012-PIMP 2012-06-16 18-45-36\KC-MEOH10-100-14MIN-ANAL.M
Last changed : 29/06/2012 12:37:07 PM by SYSTEM

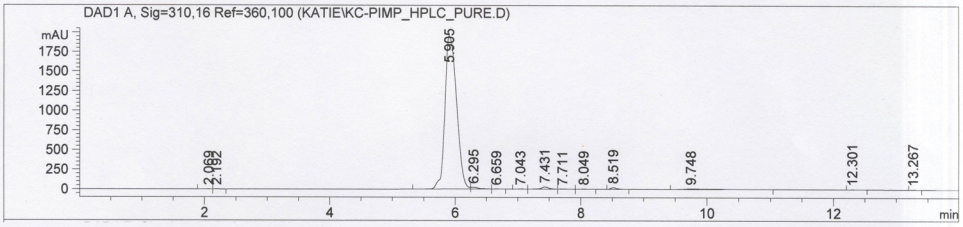

Signal 1: DAD1 A, Sig=310,16 Ref=360,100

Peak #	RetTime [min]	Type	Width [min]	Area [mAU*s]	Height [mAU]	Area %
1	2.069	BV	0.0692	11.34663	2.31437	0.0437
2	2.192	VB	0.0731	22.37443	4.27045	0.0861
3	5.905	BV	0.1996	2.50409e4	1952.90161	96.3731
4	6.295	VB	0.1247	179.17041	21.17793	0.6896
5	6.659	BB	0.1127	7.73049	1.11701	0.0298
6	7.043	BV	0.1167	24.69271	3.24898	0.0950
7	7.431	VV	0.1265	254.33214	29.52595	0.9788
8	7.711	VB	0.1572	22.73421	2.34260	0.0875
9	8.049	BB	0.1006	13.50698	2.05768	0.0520
10	8.519	VB	0.0956	134.84767	21.38498	0.5190
11	9.748	BB	0.4503	255.32457	7.22549	0.9827
12	12.301	BV	0.1011	10.98686	1.43852	0.0423
13	13.267	BB	0.0653	5.33553	1.26164	0.0205
Totals :				2.59833e4	2050.26722	

Figure S3.1 HPLC trace for purified complex **3.2**. Retention time is 5.905 min and purity is 96.4%.

3.5.3 Preparation of 3.1-3.3

*3.5.3.1 General procedure for preparation of benzamides **3.7b,c***

4-((*tert*-butoxycarbonyl)amino)benzoic acid (1.39 mmol) and amines (2.77 mmol) were dissolved in 30 mL DCM under an argon atmosphere. Then HOAt (0.284 g, 2.09 mmol) and EDC (0.533 g, 2.77 mmol) were added and the reaction was stirred overnight. The solvent was then removed under reduced pressure before being redissolved in ethyl acetate and methanol. The solution was extracted with saturated $NaHCO_3$ and washed with water 2x before washing with saturated NaCl. The aqueous $NaHCO_3$ layer was re-extracted with DCM and the DCM layer was then washed with saturated sodium chloride. The organic layers were combined and then dried over $MgSO_4$. The solvent was removed under reduced pressure. The crude Boc-protected compounds **3.6b,c** (0.511 mmol) were

then dissolved in 10 mL of a 1:1 solution of 6 M HCl and ethyl acetate and left to stir overnight. The solvent was then removed under reduced pressure before basifying to pH ~ 14 with saturated $NaHCO_3$ and 6 M KOH. The basic solution was extracted 3x with DCM before washing the organic layer with saturated NaCl and drying over magnesium sulfate. The solvent was removed under reduced pressure to yield pure product.

(3.7b) 4-amino-*N*-(3-(dimethylamino)propyl)benzamide:

0.169 g, 87% over two steps. CAS Registry Number: 53461-08-8. HR-MS Calculated for $C_{12}H_{20}N_3O$ (M+1): **222.1601,** Found: **222.1599**.

(3.7c) 4-amino-*N*-(2-(piperidin-1-yl)ethyl)benzamide:

0.0645 g, 81% over two steps. CAS Registry number: 51-08-1. HR-MS Calculated for $C_{14}H_{22}N_3O$ (M+1): **248.1757,** Found: **248.1766.**

*3.5.3.2 General procedure for preparation of azides **3.8a-c***

Anilines **3.5**, **3.7b** and **3.7c** (0.561 mmol) were dissolved in ~ 4 mL 17% aq. HCl and ~ 1 mL absolute ethanol and cooled to 0°C. Then $NaNO_2$ (0.0620 g, 0.897 mmol) was added and the reaction was stirred for 40 min before adding NaN_3 (0.058 g, 0.897 mmol). The reaction was stirred overnight before being diluted with water and aqueous $NaHCO_3$, extracted 3x with ethyl acetate and dried over $MgSO_4$. The solvent was removed under reduced pressure to yield the pure product.

(3.8a) 1-(2-(4-azidophenoxy)ethyl)piperidine:

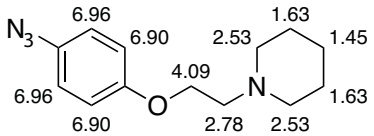

0.0850g, 62%. ^{1}H NMR (300 MHz, $CDCl_3$): δ = 6.96-6.90 (m, 4H), 4.09 (t, 2H), 2.78 (t, 2H), 2.53 (br, 4H), 1.63 (m, 4H), 1.45 (m, 2H) ppm; ^{13}C NMR (300 MHz, $CDCl_3$): δ = 120.0, 115.8, 66.2, 57.8, 55.0, 25.8, 24.1 ppm; HR-MS Calculated for $C_{13}H_{18}N_4O$ (M+1): **246.148**, Found: **247.1553**.

(3.8b) 4-azido-*N*-(3-(dimethylamino)propyl)benzamide:

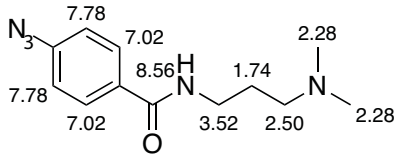

0.0820 g, 78%. ^{1}H NMR (300 MHz, $CDCl_3$): δ = 8.56 (br, 1H), 7.78 (d, 2H), 7.02 (d, 2H), 3.52 (q, 2H), 2.50 (t, 2H), 2.28 (s, 6H), 1.74 (quintet, 2H) ppm; ^{13}C NMR (300 MHz, $CDCl_3$): δ = 166.0, 142.8, 131.3, 128.6, 118.9, 59.4, 45.4, 40.7, 25.0 ppm; HR-MS Calculated for $C_{12}H_{17}N_5O$ (M+1): **247.143**, Found: **248.1514**.

(3.8c) 4-azido-*N*-(2-(piperidin-1-yl)ethyl)benzamide:

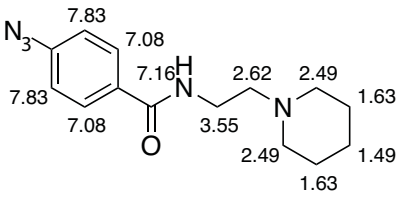

0.0417 g, 78%. ^{1}H NMR (300 MHz, $CDCl_3$): δ = 7.83 (d, 2H), 7.16 (br, 1H), 7.08 (d, 2H), 3.55 (q, 2H), 2.62 (t, 2H), 2.49 (br, 4H), 1.63 (m, 4H), 1.49 (br, 2H) ppm; ^{13}C NMR (300 MHz, $CDCl_3$): δ = 166.4, 143.1, 128.8, 119.0, 57.0, 54.2, 36.2, 25.8, 24.1 ppm; HR-MS Calculated for $C_{14}H_{19}N_5O$ (M+1): **273.159**, Found: **274.1658**.

*3.5.3.3 General procedure for preparation of "clicked" products **3.9a-c***

Compounds **3.8a-c** (0.242 mmol), 4-ethynylbenzaldehyde (0.202 mmol), 112 μL of a 0.18 M solution of $CuSO_4$•$5H_2O$ in water and 101 μL of a 1.0 M solution of sodium ascorbate in water were dissolved in a 10−20 mL microwave vial in 8 mL ACN and 0.5 mL MeOH with a magnetic stir bar. The reaction was conducted for 15 min at 100°C. The vial was then centrifuged and the mother liquor decanted. The remaining solid was washed with MeOH and DCM, centrifuged, and the solution added to the mother liquor. The organic layer was washed with 10% NaOH 3x before drying over $MgSO_4$. The solvent was removed under reduced pressure to yield 'clicked' products **3.9a-c**. The crude was used without further purification.

(3.9a) 4-(1-(4-(2-(piperidin-1-yl)ethoxy)phenyl)-1*H*-1,2,3-triazol-4-yl)benzaldehyde:

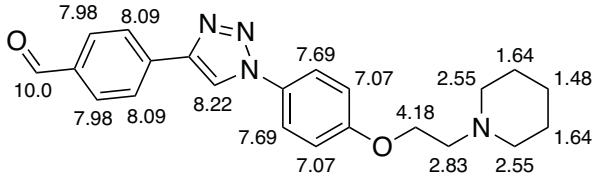

0.0710 g, 78%. ^{1}H NMR (300 MHz, $CDCl_3/CD_3OD$): δ = 10.0 (s, 1H), 8.22 (s, 1H), 8.09 (d, 2H), 7.98 (d, 2H), 7.69 (d, 2H), 7.07 (d, 2H), 4.18 (t, 2H), 2.83 (t, 2H), 2.55 (br, 4H), 1.64 (m, 4H), 1.48 (m, 2H) ppm; ^{13}C NMR (500 MHz, $CDCl_3$): δ = 191.7, 159.3, 146.9, 136.2, 135.9, 130.5, 130.3, 126.1, 122.2, 120.0, 119.0, 115.9, 115.6, 66.4, 57.7, 55.1, 25.8, 24.0 ppm; HR-MS Calculated for $C_{22}H_{24}N_4O_2$ (M+1): **376.1899**, Found: **377.1972**.

(3.9b) *N*-(3-(dimethylamino)propyl)-4-(1-(4-formylphenyl)-1*H*-1,2,3-triazol-4-yl)benzaldehyde:

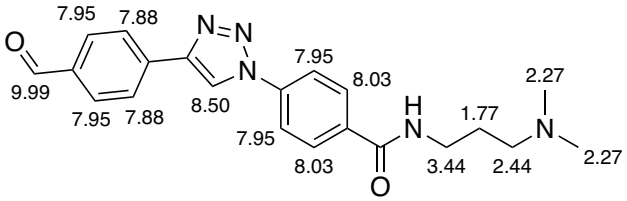

0.0810 g, 59%. ^{1}H NMR (500 MHz, $CDCl_3/CD_3OD$): δ = 9.99 (s, 1H), 8.50 (s, 1H), 8.03 (d, 2H), 7.95 (m, 4H), 7.88 (d, 2H), 3.44 (t, 2H), 2.44 (t, 2H), 2.27 (s, 6H), 1.77 (quintet, 2H) ppm; ^{13}C NMR (500 MHz, $CDCl_3/CD_3OD$): δ = 192.0, 166.4, 147.3 138.6, 136.0, 135.6, 134.8, 130.5,128.8, 126.2, 120.1, 119.0, 57.4, 44.8, 38.8, 25.6 ppm; HR-MS Calculated for $C_{21}H_{23}N_5O_2$ (M+1): **377.1852,** Found: **378.1925.**

(3.9c) 4-(4-(4-formylphenyl)-1*H*-1,2,3-triazol-1-yl)-*N*-(2-(piperidin-1-yl)ethyl)benzaldehyde:

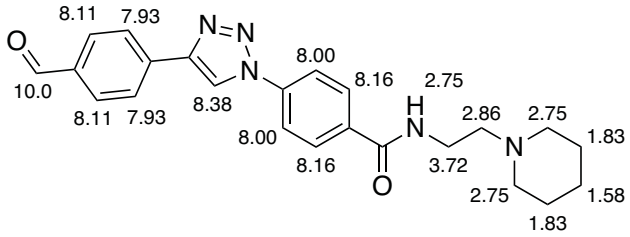

0.565 g, 79%. ^{1}H NMR (500 MHz, $CDCl_3$): δ = 10.0 (s, 1H), 8.38 (s, 1H), 8.16 (d, 2H), 8.11 (d, 2H), 8.00 (d, 2H), 7.93 (d, 2H), 3.72 (q, 2H), 2.86 (t, 2H), 2.75 (br, 5H), 1.83 (br, 4H), 1.58 (br, 2H) ppm; ^{13}C NMR (300 MHz, $CDCl_3$ + trace MeOD): δ = 192.0, 166.4, 147.3, 138.7, 136.0, 135.7, 134.5, 130.5, 129.0, 126.2, 120.1, 119.0, 57.8, 54.3, 36.1, 25.1, 23.7 ppm; HR-MS Calculated for $C_{23}H_{25}N_5O_2$ (M+1): **403.2008**, Found: **404.2081.**

*3.5.3.4 General procedure for preparation of ligands **3.10a-c***

[4,5-*f*][1,10]phenanthroline (0.0850 g, 0.404 mmol) and NH_4OAc (0.308 g, 3.99 mmol) were dissolved in 20 mL glacial acetic acid under an argon atmosphere. Then **3.9a-c** (0.399 mmol) were added and the reaction was refluxed at 120°C for ~ 24 hr. The reaction was then cooled in an ice bath, diluted with water, and the pH adjusted to ~ pH 8.0 with the slow addition of NH_4OH. The precipitate was vacuum filtered through a glass frit and washed with water, ethyl acetate and diethyl ether before vacuum air drying on the frit for 1−2 days which yielded a brown flaky powder. Ligands were then purified as listed above.

(3.10a) 2-(4-(1-(4-(2-(piperidin-1-yl)ethoxy)phenyl)-1*H*-1,2,3-triazol-4-yl)phenyl)-1*H*-imidazo[4,5-*f*][1,10]phenanthroline: *((PEP)TPIP)*:

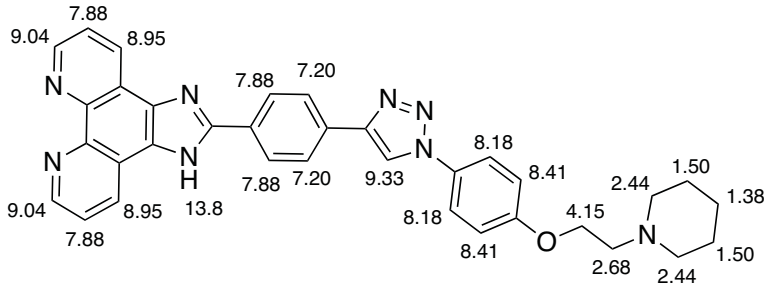

Fluffy yellow powder (58%). ^{1}H NMR (300 MHz, d_6-DMSO): δ = 13.8 (br s, 1h), 9.33 (s, 1H), 9.04 (br s, 2H), 8.95 (d, 2H), 8.41 (d, 2H), 8.18 (d, 2H), 7.88 (m, 4H), 7.20 (d, 2H), 4.15 (t, 2H), 2.68 (t, 2H), 2.44 (br s, 4H), 1.50 (m, 4H), 1.38 (m, 2H) ppm; ^{13}C NMR (300 MHz, d_6-DMSO): δ = 159.1, 150.8, 148.3, 147.0, 144.1, 131.7, 130.4, 130.1, 127.3, 126.2, 123.8, 122.0, 120.5, 116.0, 66.5, 57.7, 54.8, 26.0, 24.4 ppm; HR-MS Calculated for $C_{34}H_{30}N_8O$ (M+1): **566.254,** Found: **567.2615.**

(3.10b): 4-(4-(4-(1*H*-imidazo[4,5-*f*][1,10]phenanthrolin-2-yl)phenyl)-1*H*-1,2,3-triazol-1-yl)-*N*-(3-(dimethylamino)propyl)benzamide: *((DAPB)TPIP)*:

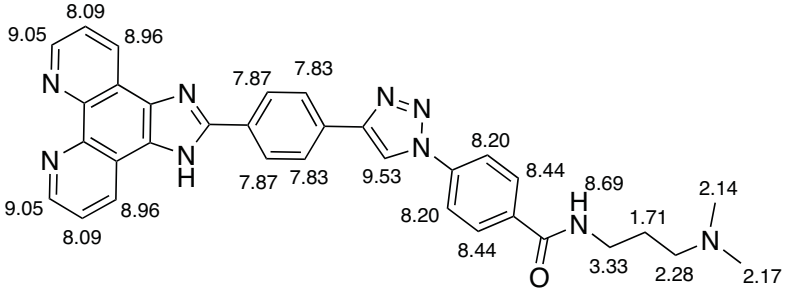

Fluffy orange powder (68%). ^{1}H NMR (200 MHz, d_6-DMSO): δ = 9.53 (s, 1H), 9.05 (dd, 2H), 8.96 (dd, 2H), 8.69 (t, 1H), 8.44 (d, 2H), 8.20 (d, 2H), 8.09 (s, 4H), 7.87-7.83 (dd, 2H), 3.33 (q, 2H), 2.28 (t, 2H), 2.14 (s, 6H), 1.71 (quintet, 2H), ppm; ^{13}C NMR (300 MHz, d_6-DMSO): δ = 165.4, 150.7, 148.3, 147.4, 144.1, 138.7, 134.9, 131.4, 130.4, 130.2, 129.4, 126.3, 123.8, 120.6, 119.9, 57.0, 45.3, 40.8, 38.2, 27.1 ppm; HR-MS Calculated for $C_{33}H_{29}N_9O$ (M+1): **567.250,** Found: **568.2568**.

(3.10c) 4-(4-(4-(1*H*-imidazo[4,5-*f*][1,10]phenanthrolin-2-yl)phenyl)-1*H*-1,2,3-triazol-1-yl)-*N*-(2-(piperidin-1-yl)ethyl)benzamide *((PEB)TPIP)*:

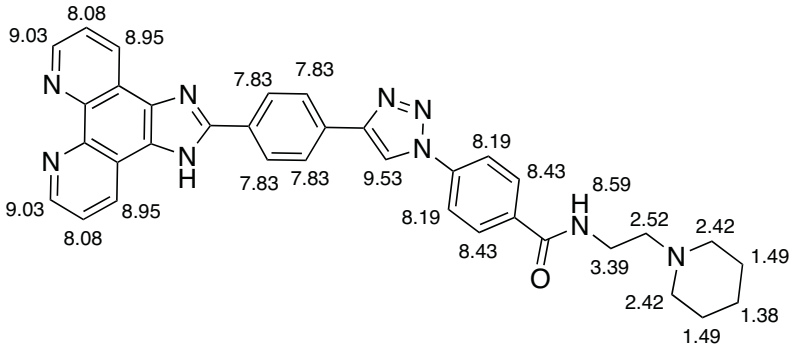

Fluffy red powder (77%). ^{1}H NMR (300 MHz, d_6-DMSO): δ = 9.53 (s, 1H), 9.03 (dd, 2H), 8.95 (d, 2H), 8.59 (t, 1H), 8.43 (d, 2H), 8.19 (4, 2H), 8.08 (s, 4H), 7.83 (m, 2H), 3.39 (m, 2H), 2.52 (br, 2H), 2.42 (br, 4H), 1.49 (br s, 4H), 1.38 (br m, 2H) ppm; ^{13}C NMR (300 MHz, d_6-DMSO): δ = 165.4, 150.6, 148.3, 147.4, 144.1, 138.7, 134.8, 130.2, 129.4, 127.3, 126.3, 123.8, 120.6, 119.9, 58.0, 54.5, 45.3, 25.9, 24.4 ppm; HR-MS Calculated for $C_{35}H_{31}N_9O$ (M+1): **593.265,** Found: **594.2724.**

Complexes 3.1-3.3 were prepared in a manner identical to those previously published by our laboratory.[40,41]

(3.1) [Pt((PEP)TPIP)(en)][PF_6]$_2$:

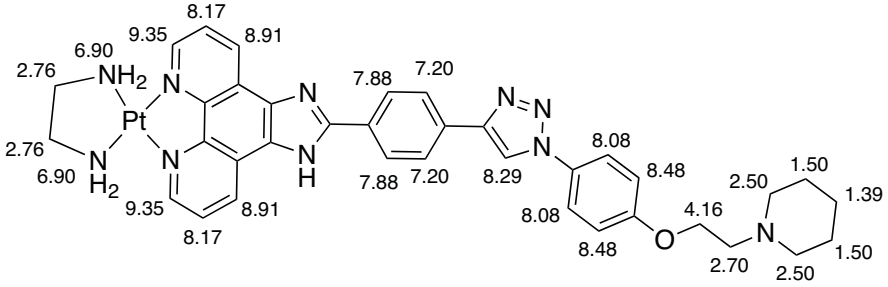

The final complex is a fluffy yellow-orange solid (54%). ^{1}H NMR (300 MHz, d_6-DMSO): δ = 9.35 (d, 2H), 9.29 (s, 1H), 8.91 (m, 2H), 8.48 (d, 2H), 8.17 (m, 2H), 8.08 (d, 2H), 7.88 (d, 2H), 7.20 (d, 2H), 6.90 (br, 4H), 4.16 (t, 2H), 2.76 (br, 4H), 2.70 (t, 2H), 2.50 (br s, 4H), 1.50 (m, 4H), 1.39 (m, 2H) ppm; ^{13}C NMR (300 MHz, d_6-DMSO): δ = 159.0, 148.7, 143.9, 136.0, 134.7, 127.5, 126.1, 124.9,

122.0, 116.0, 66.4, 57.6, 54.8, 47.7, 25.9, 24.3 ppm; HR-MS Calculated for $C_{36}H_{38}N_{10}OPt$ (M^{2+}): **410.6435**, Found: **410.6416.**

(3.2) [Pt((DAPB)TPIP)(en)][PF_6]$_2$:

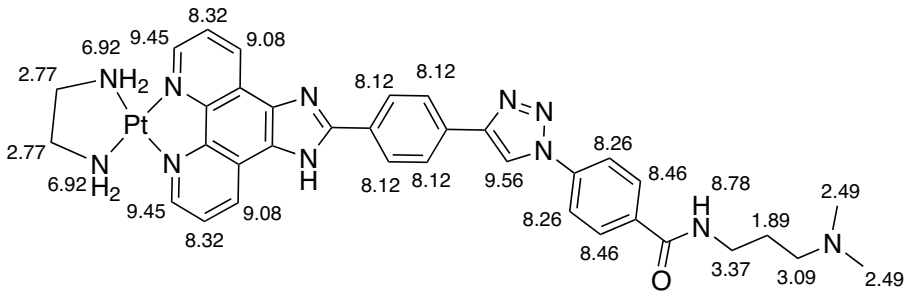

The final complex is a flaky red solid (73%). ^{1}H NMR (500 MHz, d_6-DMSO): δ = 9.56 (s, 1H), 9.45 (d, 2H), 9.08 (d, 2H), 8.78 (t, 1H), 8.46 (d, 2H), 8.32 (br m, 2H), 8.26 (d, 2H), 8.12 (s, 4H), 6.92 (br s, 4H), 3.37 (q, 2H), 3.09 (t, 2H), 2.77 (br s, 4H), 2.49 (s, 6H), 1.89 (quintet, 2H) ppm; ^{13}C NMR (300 MHz, d_6-DMSO): δ = 165.6, 155.3, 149.4, 147.4, 144.2, 138.7, 134.8, 129.4, 127.6, 126.5, 120.4, 119.8, 56.4, 47.7, 44.3, 37.7, 26.3 ppm; HR-MS Calculated for $C_{35}H_{37}N_{11}OPt$ (M^{2+}): **411.141**, Found: **411.1411.**

(3.3) [Pt((PEB)TPIP)(en)][PF_6]$_2$:

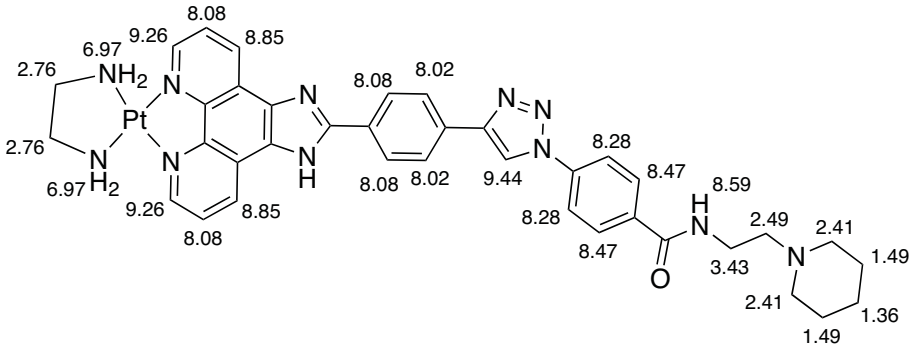

The final complex is a flaky orange-red solid (23%). ^{1}H NMR (300 MHz, d_6-DMSO): δ = 9.44 (s, 1H), 9.26 (d, 2H), 8.85 (m, 2H), 8.59 (t, 1H), 8.50 (d, 2H), 8.04 (m, 8H), 6.97 (br, 4H), 3.43 (m, 2H), 2.76 (m, 2H), 2.41 (m, 4H), 1.51 (m, 4H), 1.38 (m, 2H) ppm; ^{13}C NMR (300 MHz, d_6-DMSO): δ = 166.0, 155.3, 149.4,

147.4, 144.2, 138.7, 134.8, 129.4, 127.6, 126.5, 120.4, 119.8, 66.6, 54.8, 47.7, 25.9, 24.4 ppm; HR-MS Calculated for $C_{37}H_{39}N_{11}OPt$ (M^{2+}): **424.1489,** Found: **424.1483.**

3.5.4 Oligonucleotides

Unmodified G-quadruplex sequences were obtained from either Sigma-Aldrich (Canada) or IDT with HPLC purification. Prior to use, each sequence was suspended in Milli-Q water and quantified by UV spectroscopy (carried out on a CaryBio 300 spectrophotometer at 95°C using the Cary WinUV Scan application version 3.00) using their molar extinction coefficients at 260 nm (IDT OligoAnalyzer tool). The biotinylated sequences were synthesized in house *via* standard automated oligonucleotide solid-phase synthesis performed on a BioAutomation MerMade MM6 DNA synthesizer. Sequences were purified using standard denaturing polyacrylamide gel electrophoresis with a 20 x 20 cm vertical Hoefer 600 electrophoresis unit, followed by desalting with Sephadex G-25 (superfine DNA grade from Sigma-Aldrich). Reagents for automated DNA synthesis were used as purchased from BioAutomation. Biotin-dT CED phosphoramidite was used as purchased from ChemGenes and coupled off-column under inert atmosphere.

3.5.5 Molecular modeling (performed by Zhaomin Liu)

The G-quadruplex structures used herein were retrieved from the Protein Data Bank (PDB): the first two structures with PDB codes 143D[53] and 3T5E[54] were related to 22AG in sodium solution and potassium crystal, respectively; another two structures (1XAV[55] and 2O3M[29]) represented the cmyc and ckit1 structure, respectively. Mutations in 1XAV were manually converted back the wild-type sequence in order to be consistent with our experiments. The platinum complexes were optimized at the B3LYP/LCV3P** level of DFT; atomic charges of the complexes were obtained from ESP fitting for later use in docking and MD simulations. All DFT computations were performed with Jaguar 7.0 (Schrodinger LLC). An in-house drug discovery program suite FORECASTER[75] including PREPARE, PROCESS, SMART and FITTED was used to prepare structures and carry

out the docking experiments. In order to probe the entire structure for potential binding locations, the entire G-quadruplex structure was set as the "binding site". FITTED uses a matching-algorithm-enhanced genetic algorithm applied to a set (i.e., population) of conformations. In the present study, 100 docking runs were performed with the initial population of 200 poses and the matching algorithm turned off. The final docked poses were then clustered based on their similarity (root-mean-square deviation (RMSD) below 2 Å). The most likely pose of each cluster was selected as representative based on the FITTED energy score.

The AMBER10 package[76] was used for this MD simulation study. The parm99.dat force field[77,78] was used for G-quadruplex and GAFF parameters[79,80] (including previously developed Pt force field parameters[57]) for the platinum complexes. G-quadruplex structures and side-arm complexes were combined into one system by the LEaP module; additional counter ions such as Na^+ for 143D-complex and K^+ for the other three systems were added to neutralize the highly negative systems. The systems were soaked into periodic truncated octahedron box (10 Å) with TIP3P water molecules.[81] During the following simulations, the Particle Mesh Ewald method[82] was used to treat long-range electrostatic interactions.

The position of water molecules were first optimized by a combination of steepest descent and conjugate gradient minimization steps with the G-quadruplex and sidearm complex structures being frozen. The whole system was then relaxed through additional steepest descent and conjugate gradient minimization steps. The temperature of the relaxed systems was then slowly increased over 20 ps by applying Langevin dynamics method with collision frequency of 1.0 ps^{-1}, with a time-step of 1.6 fs and the SHAKE algorithm[83] applied to the bonds containing hydrogen atoms. This was followed by 100 ps equilibration at 300K performed on each of the systems at constant pressure and temperature. Data was then collected over 8 ns. Stability of the systems was assessed by computing the deviation over the course of the simulations) and representative binding modes were selected based on the binding energy calculated from MM/PBSA.[84]

3.5.5.1 *Details of RMSD simulations by molecular modeling*

a)

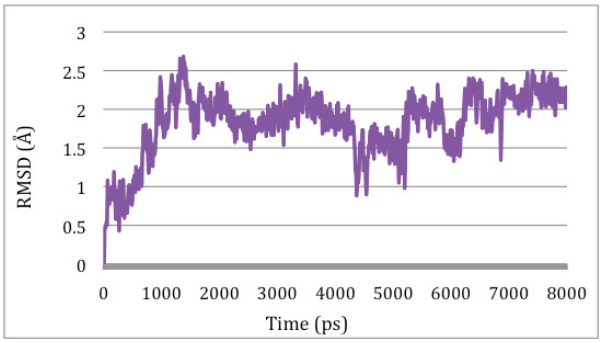

b)

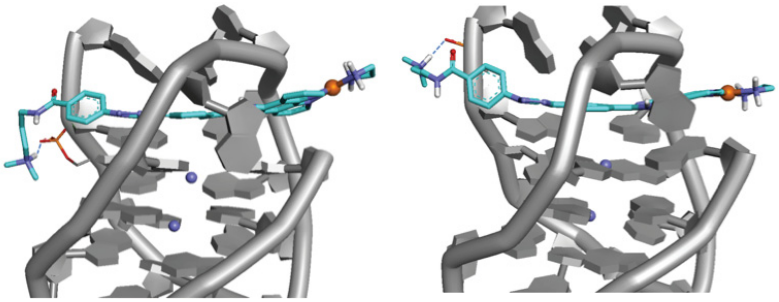

Figure S3.2 a) RMSD simulation of complex **3.2** with 22AG-Na^+. b) Other representative snapshots of complex **3.2** with 22AG-Na^+.

a)

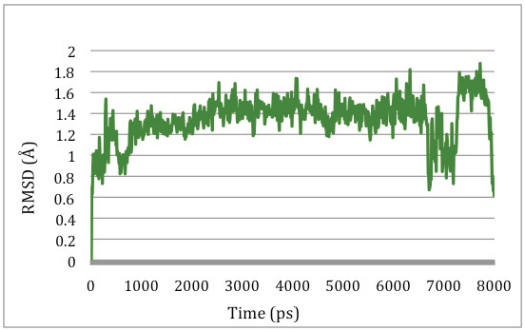

b)

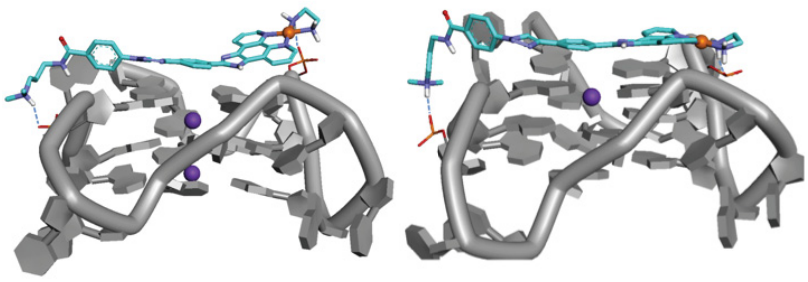

Figure S3.3 a) RMSD simulation of complex **3.2** with 22AG-K^+. b) Other representative snapshots of complex **3.2** with 22AG-K^+.

a)

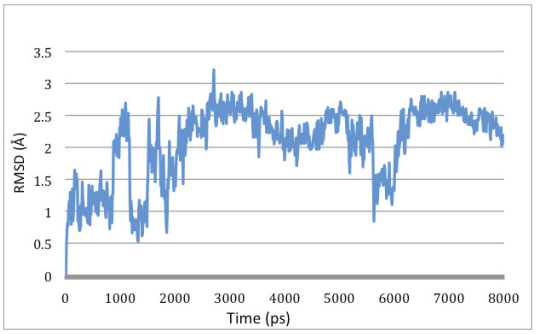

b)

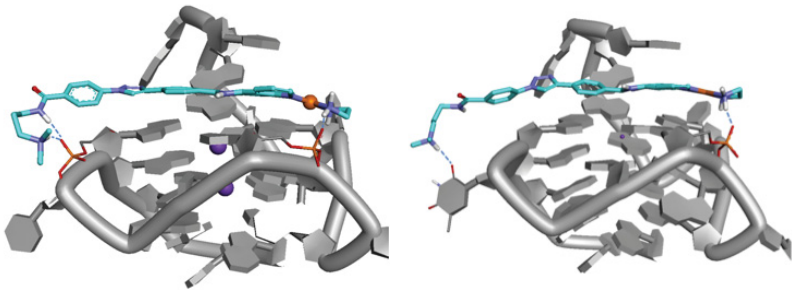

Figure S3.4 a) RMSD simulation of complex **3.2** with cmyc. b) Other representative snapshots of complex **3.2** with cmyc.

a)

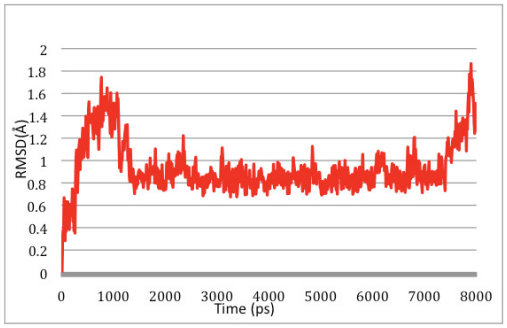

b)

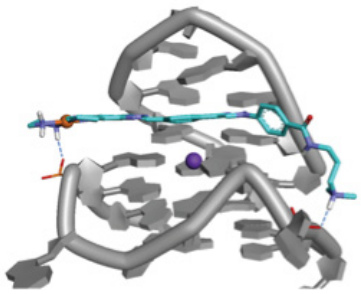

Figure S3.5 a) RMSD simulation of complex **3.2** with ckit1. b) Other representative snapshot of complex **3.2** with ckit1.

3.5.6 Biophysical assays

3.5.6.1 HT-FID assay

G-quadruplex DNA sequences 22AG, cmyc, ckit1, and ds26mer were diluted from concentrated stock solutions in Milli-Q water to 250 μM in 10 mM sodium cacodylate buffer (pH 7.4) with 100 mM added KCl (except 22AG which is evaluated in both the potassium containing buffer and in 10 mM sodium cacodylate buffer (pH 7.4) with 100 mM added NaCl). G-quadruplex sequences were heated to 95°C for 10 minutes and then rapidly cooled to room temperature. For ds26mer, the sequence was heated to 95°C and then slowly cooled to room temperature over 7 h. Each sequence was stored overnight at 4°C. Then, the sequences were diluted to 0.5 μM and 1.0 μM thiazole orange dye in DMSO was added. In the case of ds26mer, 1.5 μM thiazole orange dye was added. All robotics methods were performed on a Biomek FX liquid handler and a SAGIAN core robot (Beckman) at the CIAN core facility by Dr. Guillaume Lesage (Department of Biology, McGill University). Briefly, buffer and complexes were aspirated from dedicated reservoirs in a two-step procedure (buffer first (Figure S3.6**)** then complex (Figure S3.7) for a total volume of 100 μL) into black 96-well plates (Fluoroplates, Nunc). The complexes are tested in quadruplicate (that is two complexes per plate divided between rows D and E) where the appropriate buffer is first dispensed in decreasing volumes across the rows (100 to 0 μL), followed by each complex (5 μM stock solution in appropriate buffer) dispensed in increasing volumes across the rows (0 to 100 μL). Then, such that the final volume is 200 μL, 100 μL of 0.5 μM sequence plus thiazole orange dye is transferred to every well using the 96-multichannel pipetting head. The final concentrations of complex from column 1 to column 12 are 0, 0.125, 0.25, 0.375, 0.5, 0.625, 0.75, 1.0, 1.25, 1.5, 2.0 and 2.5 μM. After 6 minutes of agitation on a plate-shaker (for the 10 minute incubation) or 84 minutes (for the 90 minute incubation), the plates were allowed to incubate at room temperature for ~ 4 minutes before reading the fluorescence. Fluorescence (F) was measured on a plate reader (DTX 880, Beckman) equipped with 485 ± 20 nm and 535 ± 35 nm

filters for excitation and emission of thiazole orange, respectively. Percentage displacement (PD) was calculated by PD = 100 − [(F/F_0) × 100], in which F_0 is F without addition of platinum complexes, respectively. The concentration of added complex is then plotted against the PD, and a DC_{50} value is determined by the concentration of platinum complex needed to achieve a 50% displacement of thiazole orange.

	Buffer	1	2	3	4	5	6	7	8	9	10	11	12	
Compound 1	A	100	95	90	85	80	75	70	60	50	40	20	0	uL
	B	100	95	90	85	80	75	70	60	50	40	20	0	uL
	C	100	95	90	85	80	75	70	60	50	40	20	0	uL
	D	100	95	90	85	80	75	70	60	50	40	20	0	uL
Compound 2	E	100	95	90	85	80	75	70	60	50	40	20	0	uL
	G	100	95	90	85	80	75	70	60	50	40	20	0	uL
	H	100	95	90	85	80	75	70	60	50	40	20	0	uL
	I	100	95	90	85	80	75	70	60	50	40	20	0	uL

Figure S3.6 HT-FID plate layout showing volumes of buffer for the first addition

	5uM Stock	Concentration												
	Pt	1	2	3	4	5	6	7	8	9	10	11	12	
Compound 1	A	0	5	10	15	20	25	30	40	50	60	80	100	uL
	B	0	5	10	15	20	25	30	40	50	60	80	100	uL
	C	0	5	10	15	20	25	30	40	50	60	80	100	uL
	D	0	5	10	15	20	25	30	40	50	60	80	100	uL
Compound 2	E	0	5	10	15	20	25	30	40	50	60	80	100	uL
	G	0	5	10	15	20	25	30	40	50	60	80	100	uL
	H	0	5	10	15	20	25	30	40	50	60	80	100	uL
	I	0	5	10	15	20	25	30	40	50	60	80	100	uL
[final]		0	0.125	0.25	0.375	0.5	0.625	0.75	1	1.25	1.5	2	2.5	uM

Figure S3.7 HT-FID plate layout showing volumes of complex added for the second addition

Prof. Anthony Mittermaier developed the following method to compare data sets obtained from the FID assay according to overall affinity. Equilibrium association constants (KA) for the complexes were extracted from the FID

fluorescence isotherms, using the concentrations and affinity of thiazole orange for the different G-quadruplexes,[62] after being fitted by the following equation using in-house MATLAB scripts:

$$I_0 + \left(I_1 - I_0\right) f_B \quad (1)$$

where I_0 and I_1 are the fluorescence intensities in the absence and with saturating amounts of ligand. f_B is the fraction of G-quadruplex bound to thiazole orange dye at any given ligand concentration:

$$f_B = \frac{[MX]}{[M]_T} \quad (2)$$

while [MX] is the concentration of dye-bound G-quadruplex and $[M]_T$ is the total concentration of all free and bound forms of G-quadruplex. [MX] was calculated according to:

$$[MX] = [X]_T f_X \quad (3)$$

where f_X is the fraction of dye molecules bound to G-quadruplex at a given ligand concentration and $[X]_T$ is the total concentration of both free and bound dye. f_X was calculated as:

$$f_X = \frac{K_X[M]}{1 + K_X[M]} \quad (4)$$

where K_X is the affinity equilibrium constant for thiazole orange binding and [M] is the concentration of unbound G-quadruplex. [M] was determined by solving the third-order polynomial obtained from the equality:

$$[M]_T = [M] + [L]_T f_L + [X]_T f_X \quad (5)$$

where $[L]_T$ is the total concentration of ligand and f_L is the fraction of ligand bound to G-quadruplex. This yields:

(6)

$$[M]+[L]_T\frac{K_L[M]}{1+K_L[M]}+[X]_T\frac{K_X[M]}{1+K_X[M]}-[M]_T=0$$

which can be expanded to give the following polynomial in [M]:

(7)

$$K_LK_X[M]^3+\left(K_L+K_LK_X\left([L]_T+[X]_T-[M]_T\right)\right)[M]^2+$$

$$\left(1+K_L[L]_T+K_X[X]_T-\left(K_L+K_X\right)[M]_T\right)[M]-[M]_T=0$$

The positive real root of equation 7 is equal to [M] and was determined numerically. The total amounts of G-quadruplex, dye, and ligand ($[M]_T$, $[X]_T$, and $[L]_T$) are known for each step of the titration. The affinities of the thiazole orange dye (K_X) for different G-quadruplex isoforms have been experimentally determined by Teulade-Fichou and coworkers.[62] The values of the ligand binding affinity constant (K_A), and the initial and final fluorescence values (I_0 and I_1, respectively) were varied to minimize the sum of squared deviations between calculated and experimental FID data points using a Simplex algorithm.

3.5.6.2 SPR assay (performed by Dr. Mark A. Hancock)

SPR measurements were performed on research-grade streptavidin-coated (SA) sensor chips (XanTec Bioanalytics GmbH, Muenster, Germany) at 25°C using filtered (0.2 μm) and degassed HBS-KT running buffer (10 mM HEPES pH 7.4, 150 mM KCl, 3 mM EDTA, 0.05% (v/v) Tween-20). Protein-grade detergents (Tween-20, Empigen) were from Anatrace (Maumee, USA) and Pierce Gentle Elution (PGE) buffer was from Thermo Scientific (Illinois, USA); all other chemicals were reagent grade quality. Concentrated compound stocks were prepared in 100% DMSO, quantified using their molar extinction coefficients at 320 nm, and stored at 4°C. As recommended by the manufacturer, the SA sensors were pre-conditioned with 1 M NaCl in 50 mM NaOH (three 1 min pulses at 50 μL/min) before the capture of DNA at 10 μL/min (15 μM stocks diluted to 100 nM in running buffer containing 0.5 M KCl). To minimize non-specific binding to

the SA-coated sensors, the compounds were serially diluted in running buffer (< 0.1% DMSO final) containing 1 mg/mL CM-dextran (BioChemika #27560, Fluka / Sigma-Aldrich, Missouri, USA). To assess binding specificity in multi-cycle 'KINJECT' mode, diluted compounds were injected over reference (SA-only) and DNA-immobilized (450 RU) surfaces at 25 µL/min (5 min association + 10 min dissociation; 5 µM fixed). Between sample injections, the sensors were regenerated at 50 µL/min using two 30-second pulses of PGE buffer containing 0.05% (v/v) Triton X100 (Solution I) or Empigen (Solution II), followed by 'EXTRACLEAN' and 'RINSE' procedures. To assess dose-dependent binding in multi-cycle 'KINJECT' mode, diluted compounds were titrated (0–5 µM, 2-fold dilution series) over lower-density DNA surfaces (300 RU) and were regenerated in a similar manner. Data were doubled-referenced and represent duplicate injections acquired from at least two independent trials. For each replicate series, a buffer blank was injected first, the highest titrant concentration second, and serial dilutions followed (from the lowest to the highest concentration); comparing responses between the two highest titrant injections verified consistent DNA surface activity throughout each assay. To estimate apparent equilibrium dissociation constants (K_D), steady-state binding responses (R_{eq}; average RU at the end of the association phase) were plotted as a function of complex concentration (C) and then subjected to non-linear regression ("Steady-state affinity" model, BIAevaluation v4.1 software). Titration series were also analyzed using the "Fit ka/kd separate" tool to estimate the individual dissociation rate constants (k_d; evaluated in the early portion of the dissociation phase to exclude rebinding effects). Theoretical binding maxima were predicted using the following equation: *Rmax = (MWA / MWL) (RL) (n)* where *Rmax* is the maximal binding response (RU) at saturating compound concentrations; *MWA* is the molecular weight (Da) of the compound injected in solution; *MWL* is the molecular weight (Da) of the DNA fragment immobilized; *RL* is the amount (RU) of DNA immobilized; *n* is the predicted binding stoichiometry (e.g. 1:1). G-quadruplex sequences 22AG, cmyc, and ckit1, and duplex HP were formed identically to those used for CD melting in potassium conditions.

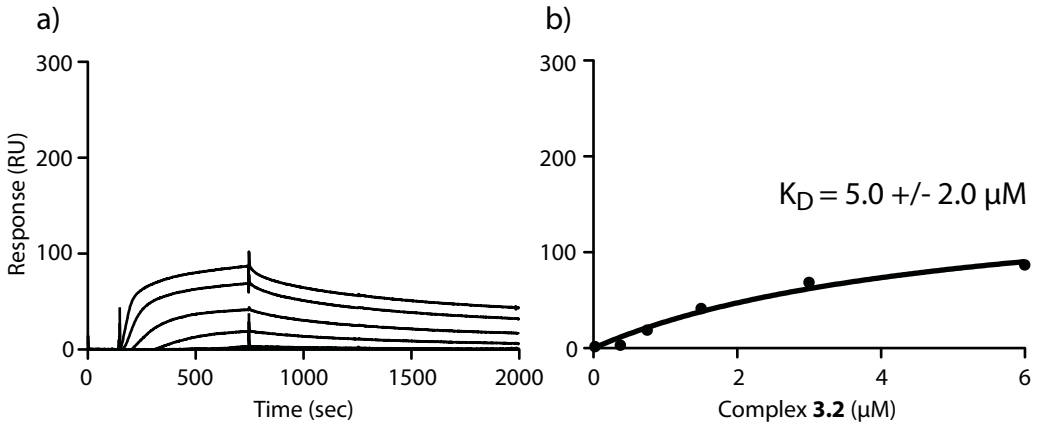

Figure S3.8 SPR assay for complex **3.2** with duplex-HP DNA: a) dose dependent titration, and b) fitting of the equilibrium responses to a one-site binding model and corresponding K_D value.

3.5.6.3 CD titrations

The ckit1 G-quadruplex was formed (50 µM) in i) 10 mM K_2HPO_4/10 mM KH_2PO_4, ii) 10 mM K_2HPO_4/10 mM KH_2PO_4 plus 100 mM KCl, and iii) 0.906 mM Na_2HPO_4/NaH_2PO_4 plus 5.33 mM KCl and 110.34 mM NaCl by heating to 95°C for 10 minutes and then cooling rapidly to room temperature. Samples were stored overnight at 4°C before diluting to 10 µM in the respective buffers. For the titration, 0–5 µL stock solution of **3.2** (2 mM) in DMSO were added in series with either a 10 minute or 90 minute incubation period before scanning. Spectra were scanned at 37ºC from 350−230 nm at 100 nm/min with a bandwidth of 1 nm and a response time of 2 s.

3.5.6.4 CD melting assay

The ckit1 G-quadruplex was formed (15 µM) in either a 10 mM K_2HPO_4/10 mM KH_2PO_4 with or without 100 mM KCl depending on the sequence, or a 10 mM Na_2HPO_4/10 mM NaH_2PO_4 with 100 mM NaCl, where appropriate, by heating to 95°C for 10 minutes and then cooling rapidly to room temperature. Samples were incubated with 4 equivalents (60 µM) complex **3.2** overnight at 4°C before melting. For the cmyc and ckit1 sequences, there was no added KCl. Melting experiments were conducted from 10−95°C with a heating rate of 1°C/min while monitoring the CD peak at 260 nm.

3.5.7 Biological assays

3.5.7.1 MTS assay (performed by Dr. Johans Fakhoury)

The cytotoxicities of complexes **3.2**, **3.4**, and **3.7** were assessed using the CellTiter96 kit from Promega according to the manufacturer's instructions. Briefly, HeLa cells (human cervical cancer) and A172 cells (human glioblastoma) were seeded at a density of 5000 cells per well in a 96-well plate in DMEM media (Invitrogen) supplemented with 10% FBS and antibiotics and antimycotics (ABAM). Platinum complex stock solutions were initially diluted in growth medium to yield final concentrations ranging from 1.6 to 100 μM. Cells were incubated for 72 h in 5% CO_2 at 37°C. After the incubation period, the MTS reagent was added to each well and further incubated for 3 h in 5% CO_2 at 37°C. Subsequently, 96-well plates were allowed to equilibrate at room temperature and the absorbance was read at 490 nm using a BioTek® Synergy microplate reader. All quantifications were done using GraphPad Prism 5 software.

3.5.7.2 Measurement of mRNA levels (performed by Dr. Johans Fakhoury)

Whole cell mRNAs were extracted and cDNA strands were reverse transcribed using the SSIII Reverse Transcription Kit (Invitrogen) according to the manufacturer's recommendations. We then assessed the mRNA levels of *c-Kit* by PCR with the following primers (forward primer: 5'- CAG GCA ACGTTG ACT ATC AGT -3' and reverse primer: 5'- ATT CTC AGA CTT GGG ATA ATC -3'). PCR conditions used were: (Step1) 94°C for 45 seconds, (Step 2) 54°C for 30 seconds, and (Step 3) 72°C for 60 seconds for 35 cycles. PCR of 18S rRNAwith the following forward primers: 5'-GTA ACC CGT TGA ACC CCA TTC-3' and reverse primer: 5'-CCA TCC AAT CGG TAG TAG CG-3', were used as internal control.

3.5.7.3 Western blot analysis (performed by Dr. Johans Fakhoury)

For western blot analysis, 250,000 cells were seeded in a 6-well plate. The next day, each complex (**3.2**, **3.4**, and **3.7**) was added at 10 μM final concentration. Cells and ligands were incubated for 72 h. Samples were lysed

with cell lysis buffer (NEB #9803). Protein concentrations were assessed by the Bradford assay and equal amounts (50 μg) of protein were loaded and resolved by SDS-PAGE. Gel contents were transferred to a PVDF membrane and Western blot analysis was carried out. Blocking was performed with TBST (Tris-buffered saline with 0.05% Tween-20) + 5% nonfat milk for c-KIT and TBST + 3% BSA for β-actin. Anti-c-KIT (Santa Cruz, SC-168) was incubated overnight in blocking solution at a concentration of 1:100. Anti-β-actin (Abcam, ab8226) was incubated overnight in blocking solution at a dilution of 1:1000. Blots were washed four times with 1xTBST. Anti-mouse and anti-rabbit goat polyclonal HRP-conjugated antibodies were used to detect β-actin and c-KIT, respectively. Secondary antibodies were diluted at 1:5000 in appropriate blocking buffers. Blots were washed four times with 1xTBST and bands were detected with Clarity Western ECL (Bio-Rad, 170-5060).

3.6 References

1. De Cian, A.; Lacroix, L.; Douarre, C.; Temime-Smaali, N.; Trentesaux, C.; Riou, J. F.; Mergny, J. L., Targeting telomeres and telomerase. *Biochimie* **2008,** *90* (1), 131-155.
2. Lane, A. N.; Chaires, J. B.; Gray, R. D.; Trent, J. O., Stability and kinetics of G-quadruplex structures. *Nucleic Acids Res* **2008,** *36* (17), 5482-5515.
3. Huppert, J. L.; Balasubramanian, S., G-quadruplexes in promoters throughout the human genome. *Nucleic Acids Res* **2007,** *35* (2), 406-413.
4. Neidle, S., Human telomeric G-quadruplex: the current status of telomeric G-quadruplexes as therapeutic targets in human cancer. *FEBS J* **2010,** *277* (5), 1118-1125.
5. Siddiqui-Jain, A.; Grand, C. L.; Bearss, D. J.; Hurley, L. H., Direct evidence for a G-quadruplex in a promoter region and its targeting with a small molecule to repress c-MYC transcription. *Proc Natl Acad Sci USA* **2002,** *99* (18), 11593-11598.
6. Wu, P.; Ma, D. L.; Leung, C. H.; Yan, S. C.; Zhu, N.; Abagyan, R.; Che, C. M., Stabilization of G-quadruplex DNA with platinum(II) Schiff base complexes: Luminescent probe and down-regulation of c-myc oncogene expression. *Chem Eur J* **2009,** *15* (47), 13008-13021.
7. Agarwal, T.; Roy, S.; Chakraborty, T. K.; Maiti, S., Selective targeting of G-quadruplex using furan-based cyclic homooligopeptides: Effect on c-MYC expression. *Biochem* **2010,** *49* (38), 8388-8397.
8. Shalaby, T.; Von Bueren, A. O.; Hürlimann, M. L.; Fiaschetti, G.; Castelletti, D.; Masayuki, T.; Nagasawa, K.; Arcaro, A.; Jelesarov, I.; Shin-ya, K.; Grotzer, M., Disabling c-Myc in

childhood medulloblastoma and atypical teratoid/rhabdoid tumor cells by the potent G-quadruplex interactive agent S2T1-6OTD. *Mol Cancer Ther* **2010,** *9* (1), 167-179.

9. Wang, P.; Leung, C. H.; Ma, D. L.; Yan, S. C.; Che, C. M., Structure-based design of platinum(II) Complexes as c-myc oncogene Down-regulators and luminescent probes for G-quadruplex DNA. *Chem Eur J* **2010,** *16* (23), 6900-6911.
10. Ou, T. M.; Lin, J.; Lu, Y. J.; Hou, J. Q.; Tan, J. H.; Chen, S. H.; Li, Z.; Li, Y. P.; Li, D.; Gu, L. Q.; Huang, Z. S., Inhibition of cell proliferation by quindoline derivative (SYUIQ-05) through its preferential interaction with c-myc promoter G-quadruplex. *J Med Chem* **2011,** *54* (16), 5671-5679.
11. Bejugam, M.; Sewitz, S.; Shirude, P. S.; Rodriguez, R.; Shahid, R.; Balasubramanian, S., Trisubstituted isoalloxazines as a new class of G-quadruplex binding ligands: small molecule regulation of c-kit oncogene expression. *J Am Chem Soc* **2007,** *129* (43), 12926-12927.
12. Bejugam, M.; Gunaratnam, M.; Müller, S.; Sanders, D. A.; Sewitz, S.; Fletcher, J. A.; Neidle, S.; Balasubramanian, S., Targeting the c-Kit Promoter G-quadruplexes with 6-Substituted Indenoisoquinolines. *ACS Med Chem Lett* **2010,** *1* (7), 306-310.
13. McLuckie, K. I.; Waller, Z. A.; Sanders, D. A.; Alves, D.; Rodriguez, R.; Dash, J.; McKenzie, G. J.; Venkitaraman, A. R.; Balasubramanian, S., G-quadruplex-binding benzo[a]phenoxazines down-regulate c-KIT expression in human gastric carcinoma cells. *J Am Chem Soc* **2011,** *133* (8), 2658-2663.
14. Taka, T.; Joonlasak, K.; Huang, L.; Randall Lee, T.; Chang, S. W. T.; Tuntiwechapikul, W., Down-regulation of the human VEGF gene expression by perylene monoimide derivatives. *Bioorg Med Chem Lett* **2012,** *22* (1), 518-522.
15. Sun, D.; Liu, W. J.; Guo, K.; Rusche, J. J.; Ebbinghaus, S.; Gokhale, V.; Hurley, L. H., The proximal promoter region of the human vascular endothelial growth factor gene has a G-quadruplex structure that can be targeted by G-quadruplex-interactive agents. *Mol Cancer Ther* **2008,** *7* (4), 880-889.
16. Yarden, Y.; Kuang, W. J.; Yang-Feng, T.; Coussens, L.; Munemitsu, S.; Dull, T. J.; Chen, E.; Schlessinger, J.; Francke, U.; Ullrich, A., Human proto-oncogene c-kit: a new cell surface receptor tyrosine kinase for an unidentified ligand. *EMBO J.* **1987,** *6* (11), 3341-3351.
17. Shaw, T. J.; Keszthelyi, E. J.; Tonary, A. M.; Cada, M.; Vanderhyden, B. C., Cyclic AMP in ovarian cancer cells both inhibits proliferation and increases c-KIT expression. *Exp Cell Res* **2002,** *273* (1), 95-106.
18. Rankin, S.; Reszka, A. P.; Huppert, J.; Zloh, M.; Parkinson, G. N.; Todd, A. K.; Ladame, S.; Balasubramanian, S.; Neidle, S., Putative DNA quadruplex formation within the human c-kit oncogene. *J Am Chem Soc* **2005,** *127* (30), 10584-10589.
19. Sattler, M.; Salgia, R., Targeting c-Kit mutations: basic science to novel therapies. *Leuk Res* **2004,** *28 Suppl 1*, S11-20.

20. Yavuz, A. S.; Lipsky, P. E.; Yavuz, S.; Metcalfe, D. D.; Akin, C., Evidence for the involvement of a hematopoietic progenitor cell in systemic mastocytosis from single-cell analysis of mutations in the c-kit gene. *Blood* **2002,** *100* (2), 661-665.
21. Smolich, B. D., The antiangiogenic protein kinase inhibitors SU5416 and SU6668 inhibit the SCF receptor (c-kit) in a human myeloid leukemia cell line and in acute myeloid leukemia blasts. *Blood* **2001,** *97* (5), 1413-1421.
22. Postow, M. A.; Carvajal, R. D., Therapeutic implications of KIT in melanoma. *Cancer J* **2012,** *18* (2), 137-141.
23. Rutkowski, P.; Nowecki, Z.; Nyckowski, P.; Dziewirski, W.; Grzesiakowska, U.; Nasierowska-Guttmejer, A.; Krawczyk, M.; Ruka, W., Surgical treatment of patients with initially inoperable and/or metastatic gastrointestinal stromal tumors (GIST) during therapy with imatinib mesylate. *J Surg Oncol* **2006,** *93* (4), 304-311.
24. Antonescu, C. R.; Besmer, P.; Guo, T.; Arkun, K.; Hom, G.; Koryotowski, B.; Leversha, M. A.; Jeffrey, P. D.; Desantis, D.; Singer, S.; Brennan, M. F.; Maki, R. G.; DeMatteo, R. P., Acquired resistance to imatinib in gastrointestinal stromal tumor occurs through secondary gene mutation. *Clin Cancer Res* **2005,** *11* (11), 4182-4190.
25. Ashman, L. K.; Griffith, R., Therapeutic targeting of c-KIT in cancer. *Expert Opin Investig Drugs* **2013,** *22* (1), 103-115.
26. Boddupally, P. V.; Hahn, S.; Beman, C.; De, B.; Brooks, T. A.; Gokhale, V.; Hurley, L. H., Anticancer Activity and Cellular Repression of c-MYC by the G-Quadruplex-Stabilizing 11-Piperazinylquindoline Is Not Dependent on Direct Targeting of the G-Quadruplex in the c-MYC Promoter. *J Med Chem* **2012,** *55* (13), 6076-6086.
27. Chan, D. S. H.; Yang, H.; Kwan, M. H. T.; Cheng, Z.; Lee, P.; Bai, L. P.; Jiang, Z. H.; Wong, C. Y.; Fong, W. F.; Leung, C. H.; Ma, D. L., Structure-based optimization of FDA-approved drug methylene blue as a c-myc G-quadruplex DNA stabilizer. *Biochimie* **2011,** *93* (6), 1055-1064.
28. Cooney, M.; Czernuszewicz, G.; Postel, E.; Flint, S.; Hogan, M., Site-specific oligonucleotide binding represses transcription of the human c-myc gene in vitro. *Science* **1988,** *241* (4864), 456-459.
29. Phan, A. T.; Kuryavyi, V.; Burge, S.; Neidle, S.; Patel, D. J., Structure of an unprecedented G-quadruplex scaffold in the human c-kit promoter. *J Am Chem Soc* **2007,** *129* (14), 4386-4392.
30. Fernando, H.; Reszka, A. P.; Huppert, J.; Ladame, S.; Rankin, S.; Venkitaraman, A. R.; Neidle, S.; Balasubramanian, S., A conserved quadruplex motif located in a transcription activation site of the human c-kit oncogene. *Biochem* **2006,** *45* (25), 7854-7860.
31. Müller, W.; Crothers, D. M., Studies of the binding of actinomycin and related compounds to DNA. *J Mol Biol* **1968,** *35* (2), 251-290.

32. Önfelt, B.; Lincoln, P.; Nordén, B., A Molecular Staple for DNA: Threading Bis-intercalating $[Ru(phen)_2dppz]^{2+}$ Dimer. *J Am Chem Soc* **1999,** *121* (46), 10846-10847.
33. Önfelt, B.; Göstring, L.; Lincoln, P.; Nordén, B.; Önfelt, A., Cell studies of the DNA bis-intercalator Δ–Δ $[\mu\text{-}C4(cpdppz)_2(phen)_4Ru_2]^{4+}$: toxic effects and properties as a light emitting DNA probe in V79 Chinese hamster cells. *Mutagenesis* **2002,** *17* (4), 317-320.
34. Peek, M. E.; Lipscomb, L. A.; Bertrand, J. A.; Gao, Q.; Roques, B. P.; Garbay-Jaureguiberry, C.; Williams, L. D., DNA Distortion in bis-Intercalated Complexes. *Biochem* **1994,** *33* (13), 3794-3800.
35. Chaires, J. B.; Leng, F.; Przewloka, T.; Fokt, I.; Ling, Y. H.; Perez-Soler, R.; Priebe, W., Structure-based design of a new bisintercalating anthracycline antibiotic. *J Med Chem* **1997,** *40* (3), 261-266.
36. Hu, G. G.; Shui, X.; Leng, F.; Priebe, W.; Chaires, J. B.; Williams, L. D., Structure of a DNA-bisdaunomycin complex. *Biochem* **1997,** *36* (20), 5940-5946.
37. Robinson, H.; Priebe, W.; Chaires, J. B.; Wang, A. H., Binding of two novel bisdaunorubicins to DNA studied by NMR spectroscopy. *Biochem* **1997,** *36* (29), 8663-8670.
38. Leng, F.; Priebe, W.; Chaires, J. B., Ultratight DNA binding of a new bisintercalating anthracycline antibiotic. *Biochem* **1998,** *37* (7), 1743-1753.
39. Howell, L. A.; Gulam, R.; Mueller, A.; O'Connell, M. A.; Searcey, M., Design and synthesis of threading intercalators to target DNA. *Biorg Med Chem Lett* **2010,** *20* (23), 6956-6959.
40. Kieltyka, R.; Fakhoury, J.; Moitessier, N.; Sleiman, H. F., Platinum phenanthroimidazole complexes as G-quadruplex DNA selective binders. *Chem Eur J* **2008,** *14* (4), 1145-1154.
41. Castor, K. J.; Mancini, J.; Fakhoury, J.; Weill, N.; Kieltyka, R.; Englebienne, P.; Avakyan, N.; Mittermaier, A.; Autexier, C.; Moitessier, N.; Sleiman, H. F., Platinum(II) phenanthroimidazoles for targeting telomeric G-quadruplexes. *ChemMedChem* **2012,** *7* (1), 85-94.
42. Casagrande, V.; Salvati, E.; Alvino, A.; Bianco, A.; Ciammaichella, A.; D'Angelo, C.; Ginnari-Satriani, L.; Serrilli, A. M.; Iachettini, S.; Leonetti, C.; Neidle, S.; Ortaggi, G.; Porru, M.; Rizzo, A.; Franceschin, M.; Biroccio, A., N-cyclic bay-substituted perylene G-quadruplex ligands have selective antiproliferative effects on cancer cells and induce telomere damage. *J Med Chem* **2011,** *54* (5), 1140-1156.
43. Bertrand, H.; Granzhan, A.; Monchaud, D.; Saettel, N.; Guillot, R.; Clifford, S.; Guedin, A.; Mergny, J. L.; Teulade-Fichou, M. P., Recognition of G-quadruplex DNA by triangular star-shaped compounds: with or without side chains? *Chem Eur J* **2011,** *17* (16), 4529-4539.
44. Drewe, W. C.; Nanjunda, R.; Gunaratnam, M.; Beltran, M.; Parkinson, G. N.; Reszka, A. P.; Wilson, W. D.; Neidle, S., Rational design of substituted diarylureas: a scaffold for binding to G-quadruplex motifs. *J Med Chem* **2008,** *51* (24), 7751-7767.

45. Pivetta, C.; Lucatello, L.; Krapcho, A. P.; Gatto, B.; Palumbo, M.; Sissi, C., Perylene side chains modulate G-quadruplex conformation in biologically relevant DNA sequences. *Bioorg Med Chem* **2008,** *16* (20), 9331-9339.
46. D'Ambrosio, D.; Reichenbach, P.; Micheli, E.; Alvino, A.; Franceschin, M.; Savino, M.; Lingner, J., Specific binding of telomeric G-quadruplexes by hydrosoluble perylene derivatives inhibits repeat addition processivity of human telomerase. *Biochimie* **2012,** *94* (3), 854-863.
47. Moses, J. E.; Moorhouse, A. D., The growing applications of click chemistry. *Chem Soc Rev* **2007,** *36* (8), 1249-1262.
48. Moorhouse, A. D.; Santos, A. M.; Gunaratnam, M.; Moore, M.; Neidle, S.; Moses, J. E., Stabilization of G-quadruplex DNA by highly selective ligands via click chemistry. *J Am Chem Soc* **2006,** *128* (50), 15972-15973.
49. Drewe, W. C.; Neidle, S., Click chemistry assembly of G-quadruplex ligands incorporating a diarylurea scaffold and triazole linkers. *Chem Commun* **2008,** (42), 5295-5297.
50. Moses, J. E.; Ritson, D. J.; Zhang, F.; Lombardo, C. M.; Haider, S.; Oldham, N.; Neidle, S., A click chemistry approach to C3 symmetric, G-quadruplex stabilising ligands. *Org Biomol Chem* **2010,** *8* (13), 2926-2930.
51. Sparapani, S.; Haider, S. M.; Doria, F.; Gunaratnam, M.; Neidle, S., Rational design of acridine-based ligands with selectivity for human telomeric quadruplexes. *J Am Chem Soc* **2010,** *132* (35), 12263-12272.
52. Dash, J.; Waller, Z. A.; Pantos, G. D.; Balasubramanian, S., Synthesis and binding studies of novel diethynyl-pyridine amides with genomic promoter DNA G-quadruplexes. *Chem Eur J* **2011,** *17* (16), 4571-4581.
53. Wang, Y.; Patel, D. J., Solution structure of the human telomeric repeat d[$AG_3(T_2AG_3)_3$] G-tetraplex. *Structure* **1993,** *1* (4), 263-282.
54. Collie, G. W.; Promontorio, R.; Hampel, S. M.; Micco, M.; Neidle, S.; Parkinson, G. N., Structural basis for telomeric g-quadruplex targeting by naphthalene diimide ligands. *J Am Chem Soc* **2012,** *134* (5), 2723-2731.
55. Ambrus, A.; Chen, D.; Dai, J.; Jones, R. A.; Yang, D., Solution structure of the biologically relevant G-quadruplex element in the human c-MYC promoter. Implications for G-quadruplex stabilization. *Biochem* **2005,** *44* (6), 2048-2058.
56. Önfelt, B.; Lincoln, P.; Nordén, B., Enantioselective DNA Threading Dynamics by Phenazine-Linked $[Ru(phen)_2dppz]^{2+}$ Dimers. *J Am Chem Soc* **2001,** *123* (16), 3630-3637.
57. Kieltyka, R.; Englebienne, P.; Fakhoury, J.; Autexier, C.; Moitessier, N.; Sleiman, H. F., A platinum supramolecular square as an effective G-quadruplex binder and telomerase inhibitor. *J Am Chem Soc* **2008,** *130* (31), 10040-10041.
58. Kieltyka, R.; Englebienne, P.; Moitessier, N.; Sleiman, H., Quantifying interactions between G-quadruplex DNA and transition-metal complexes. *Methods Mol Biol* **2010,** *608*, 223-255.

59. Corbeil, C. R.; Englebienne, P.; Moitessier, N., Docking ligands into flexible and solvated macromolecules. 1. Development and validation of FITTED 1.0. *J Chem Inf Model* **2007,** *47* (2), 435-449.
60. Monchaud, D.; Allain, C.; Teulade-Fichou, M. P., Development of a fluorescent intercalator displacement assay (G4-FID) for establishing quadruplex-DNA affinity and selectivity of putative ligands. *Bioorg Med Chem Lett* **2006,** *16* (18), 4842-4845.
61. Monchaud, D.; Allain, C.; Bertrand, H.; Smargiasso, N.; Rosu, F.; Gabelica, V.; De Cian, A.; Mergny, J. L.; Teulade-Fichou, M. P., Ligands playing musical chairs with G-quadruplex DNA: a rapid and simple displacement assay for identifying selective G-quadruplex binders. *Biochimie* **2008,** *90* (8), 1207-1223.
62. Largy, E.; Hamon, F.; Teulade-Fichou, M. P., Development of a high-throughput G4-FID assay for screening and evaluation of small molecules binding quadruplex nucleic acid structures. *Anal Bioanal Chem* **2011,** *400* (10), 3419-3427.
63. Dixon, I. M.; Lopez, F.; Esteve, J. P.; Tejera, A. M.; Blasco, M. A.; Pratviel, G.; Meunier, B., Porphyrin derivatives for telomere binding and telomerase inhibition. *ChemBioChem* **2005,** *6* (1), 123-132.
64. Manaye, S.; Eritja, R.; Avino, A.; Jaumot, J.; Gargallo, R., Porphyrin binding mechanism is altered by protonation at the loops in G-quadruplex DNA formed near the transcriptional activation site of the human c-kit gene. *Biochim Biophys Acta* **2012,** *1820* (12), 1987-1996.
65. Nanjunda, R.; Owens, E. A.; Mickelson, L.; Alyabyev, S.; Kilpatrick, N.; Wang, S.; Henary, M.; Wilson, W. D., Halogenated pentamethine cyanine dyes exhibiting high fidelity for G-quadruplex DNA. *Bioorg Med Chem* **2012,** *20* (24), 7002-7011.
66. Li, Z.; Tan, J. H.; He, J. H.; Long, Y.; Ou, T. M.; Li, D.; Gu, L. Q.; Huang, Z. S., Disubstituted quinazoline derivatives as a new type of highly selective ligands for telomeric G-quadruplex DNA. *Eur J Med Chem* **2012,** *47* (1), 299-311.
67. Suntharalingam, K.; White, A. J.; Vilar, R., Synthesis, structural characterization, and quadruplex DNA binding studies of platinum(II)-terpyridine complexes. *Inorg Chem* **2009,** *48* (19), 9427-9435.
68. Seenisamy, J.; Bashyam, S.; Gokhale, V.; Vankayalapati, H.; Sun, D.; Siddiqui-Jain, A.; Streiner, N.; Shin-ya, K.; White, E.; Wilson, W. D.; Hurley, L. H., Design and synthesis of an expanded porphyrin that has selectivity for the c-MYC G-quadruplex structure. *J Am Chem Soc* **2005,** *127* (9), 2944-2959.
69. Fu, B.; Zhang, D.; Weng, X.; Zhang, M.; Heng, M.; Yuzhi, M.; Zhou, X., Cationic metal-corrole complexes: Design, synthesis, and properties of guanine-quadruplex stabilizers. *Chem Eur J* **2008,** *14* (30), 9431-9441.
70. Berg, K.; Zhai, L.; Chen, M.; Kharazmi, A.; Owen, T. C., The use of a water-soluble formazan complex to quantitate the cell number and mitochondrial function of Leishmania major promastigotes. *Parasitology Res* **1994,** *80* (3), 235-239.

71. Malich, G.; Markovic, B.; Winder, C., The sensitivity and specificity of the MTS tetrazolium assay for detecting the in vitro cytotoxicity of 20 chemicals using human cell lines. *Toxicology* **1997,** *124* (3), 179-192.
72. Caceres-Cortes, J. R.; Alvarado-Moreno, J. A.; Waga, K.; Rangel-Corona, R.; Monroy-Garcia, A.; Rocha-Zavaleta, L.; Urdiales-Ramos, J.; Weiss-Steider, B.; Haman, A.; Hugo, P.; Brousseau, R.; Hoang, T., Implication of tyrosine kinase receptor and steel factor in cell density-dependent growth in cervical cancers and leukemias. *Cancer Res* **2001,** *61* (16), 6281-6289.
73. Vandenbark, G. R.; Chen, Y.; Friday, E.; Pavlik, K.; Anthony, B.; deCastro, C.; Kaufman, R. E., Complex regulation of human c-kit transcription by promoter repressors, activators, and specific myb elements. *Cell Growth & Differentiation* **1996,** *7* (10), 1383-1392.
74. Clegg, N. J.; Paruthiyil, S.; Leitman, D. C.; Scanlan, T. S., Differential response of estrogen receptor subtypes to 1,3-diarylindene and 2,3-diarylindene ligands. *J Med Chem* **2005,** *48* (19), 5989-6003.
75. Therrien, E.; Englebienne, P.; Arrowsmith, A. G.; Mendoza-Sanchez, R.; Corbeil, C. R.; Weill, N.; Campagna-Slater, V.; Moitessier, N., Integrating medicinal chemistry, organic/combinatorial chemistry, and computational chemistry for the discovery of selective estrogen receptor modulators with Forecaster, a novel platform for drug discovery. *J Chem Inf Model* **2012,** *52* (1), 210-224.
76. D.A. Case, T. A. D., T.E. Cheatham III, C.L. Simmerling, J. Wang, R.E. Duke, R. Luo, M. Crowley, C. Walker Ross, W. Zhang, K.M. Merz, B. Wang, S. Hayik, A. Roitberg, G. Seabra, I. Kolossváry, K.F. Wong, F. Paesani, J. Vanicek, X. Wu, S.R. Brozell, T. Steinbrecher, H. Gohlke, L. Yang, C. Tan, J. Mongan, V. Hornak, G. Cui, D.H. Mathews, M.G. Seetin, C. Sagui, V. Babin, P.A. Kollman *AMBER10*, University of California: San Francisco, 2008.
77. Cornell, W. D.; Cieplak, P.; Bayly, C. I.; Gould, I. R.; Merz, K. M.; Ferguson, D. M.; Spellmeyer, D. C.; Fox, T.; Caldwell, J. W.; Kollman, P. A., A Second Generation Force Field for the Simulation of Proteins, Nucleic Acids, and Organic Molecules. *J Am Chem Soc* **1995,** *117* (19), 5179-5197.
78. Cheatham, T. E., 3rd; Cieplak, P.; Kollman, P. A., A modified version of the Cornell et al. force field with improved sugar pucker phases and helical repeat. *J Biomol Struct Dynam* **1999,** *16* (4), 845-862.
79. Wang, J.; Wang, W.; Kollman, P. A.; Case, D. A., Automatic atom type and bond type perception in molecular mechanical calculations. *J Mol Graphics & Modelling* **2006,** *25* (2), 247-260.
80. Wang, J.; Wolf, R. M.; Caldwell, J. W.; Kollman, P. A.; Case, D. A., Development and testing of a general amber force field. *J Comp Chem* **2004,** *25* (9), 1157-1174.

81. Jorgensen, W. L.; Chandrasekhar, J.; Madura, J. D.; Impey, R. W.; Klein, M. L., Comparison of Simple Potential Functions for Simulating Liquid Water. *J Chem Phys* **1983,** *79* (2), 926-935.
82. Darden, T.; York, D.; Pedersen, L., Particle Mesh Ewald - an N.Log(N) Method for Ewald Sums in Large Systems. *J Chem Phys* **1993,** *98* (12), 10089-10092.
83. Vangunsteren, W. F.; Berendsen, H. J. C., Algorithms for Macromolecular Dynamics and Constraint Dynamics. *Mol Phys* **1977,** *34* (5), 1311-1327.
84. Kollman, P. A.; Massova, I.; Reyes, C.; Kuhn, B.; Huo, S.; Chong, L.; Lee, M.; Lee, T.; Duan, Y.; Wang, W.; Donini, O.; Cieplak, P.; Srinivasan, J.; Case, D. A.; Cheatham, T. E., 3rd, Calculating structures and free energies of complex molecules: combining molecular mechanics and continuum models. *Acct Chem Res* **2000,** *33* (12), 889-897.

In Chapter 3, we appended protonable side-arms that protrude from the phenylphenanthroimidazole scaffold. These side-arms allow for a multivalent binding mode across the surface of the G-tetrad. This chelation-type binding demonstrated unprecedented slow dissociation from G-quadruplex motifs during biophysical studies. Studies *in cellulo* did not result in the expected down-regulation of *c-Kit* oncogene expression at either the mRNA or the protein level. We hypothesized that poor permeability of the complex through the cellular membrane may be partially responsible. To better understand how these complexes interact with the genome *in cellulo*, we moved from platinum(II) to iridium(III) centers, which introduces interesting luminescence properties and could allow for the use of these complexes as cellular G-quadruplex probes. Chapter 4 thus describes the interaction of novel $Ir(ppy)_2(phen)$ complexes with G-quadruplex DNA.

4 Iridium Complexes as G-quadruplex Binders

Preface: Author Contributions

This chapter represents a collaborative effort between the Sleiman and Mauzeroll laboratories. **Katherine Castor** was responsible for the design, synthesis, and characterization of the complexes as well as project design and biophysical assays (UV/Vis and luminescence assays). The X-ray crystallography was conducted by **Dr. Christopher Serpell**. The CV and ECL experiments were conducted by **Dr. Kimberly Metera** and **Dr. Ushula Tefashe**. The high-throughput fluorescence assay was designed by **Katherine Castor** and conducted by **Dr. Guillaume Lesage** (CIAN, McGill University). The findings in this chapter are to be published in a manuscript submitted to the Journal of the American Chemical Society in 2014.

4.1 Introduction

For the majority of this thesis, we have focused on platinum(II) phenanthroimidazoles as G-quadruplex binders. We have determined that the ligand motif is ideally suited as a G-quadruplex binder as the electrostatic overlap of the electron-poor aromatic ligand complements the electron-rich binding surface of the G-quadruplex motif. We have also demonstrated that the use of the ethylenediamine ligand aids in binding through its ability to hydrogen-bond with the phosphate backbone of the DNA. However, these platinum(II)-based complexes are not the only variety of metal-based binders for G-quadruplex targeting as discussed in Chapter 1. In the literature, a large selection of reports demonstrate the use of manganese(II)/(III),[1-4] ruthenium(II)/(III),[5-10] nickel(II),[1,11-12] copper(II),[12,13] zinc(II),[14,15] and palladium(II)[16] complexes, among others, and have been reviewed by Georgiades *et al.* in 2010.[17]

As previously mentioned, metal complexes have a broad range of structural, electronic, and optical properties that can be successfully exploited for optimal DNA binding and detection. Along these lines, a particularly important discovery made by Barton *et al.* in 1984, established that $[Ru(phen)_3]^{2+}$ demonstrated enhancement of luminescence when intercalated into duplex DNA.[18] After extensive studies into the mechanism by which this occurs,[19-21] they determined that upon intercalation, the DNA base pairs protect the intercalated ligand from the solvent (namely from hydrogen-bonding which would result in

quenching *via* vibrational deactivation),[22] thereby resulting in enhanced luminescence.

Since then, other groups have focused on metal complexes that demonstrate emission enhancement when binding to G-quadruplex DNA[23] including studies by Thomas and coworkers[5,8] and Shi *et al*.[6] They demonstrated an emission enhancement when their dinuclear bridged $[Ru_2(phen)_4(dppz)]^{4+}$ complex and dinuclear $[Ru_2(obip)(bpy)_4]^{4+}$ complex, respectively, bound to DNA (Figure 4.1). For the dinuclear bridged complex $[Ru_2(phen)_4(dppz)]^{4+}$, the emission enhancement was about 150x larger when bound to G-quadruplex DNA and 60x larger when bound to calf-thymus DNA compared to aqueous buffered solution with high ionic strength (> 100 mM sodium). For the $[Ru_2(obip)(bpy)_4]$ complex, there was a 1.5x emission enhancement when bound to G-quadruplex DNA and less enhancement when bound to duplex DNA in similar aqueous conditions. Due to the emission enhancement, they were able to determine binding affinities through direct luminescence assays (rather than needing an additional dye for a displacement assay like the FID assay). Because these, and other, ruthenium complexes have been demonstrated to exhibit this phenomenon, they have been studied as both duplex DNA and G-quadruplex DNA binders.

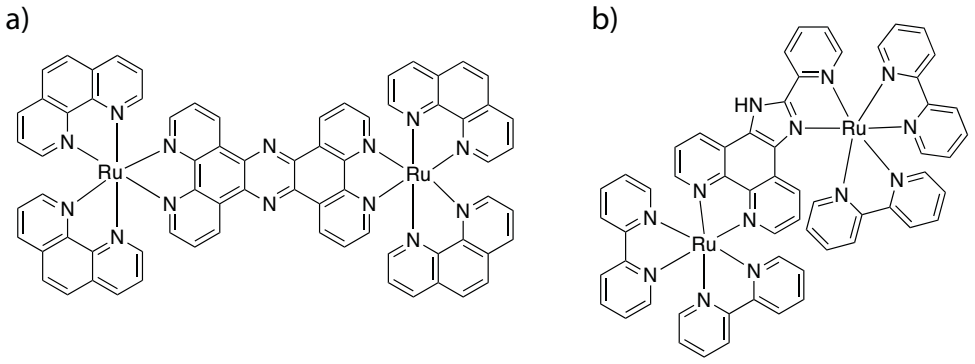

Figure 4.1 Examples of dinuclear ruthenium(II) complexes as G-quadruplex binders. a) $[Ru_2(phen)_4(dppz)]^{4+}$, where dppz = dipyrido-[3,2-*a*:2',3'-*c*]-phenazine and b) $[Ru_2(obip)(bpy)_4]^{4+}$, where obip = 2-(2-pyridyl(imidazo[4,5-*f*][1,20]-phenanthroline and bpy = 2,2'-bipyridine.

In addition to intrinsic fluorescence properties of bipyridine and phenanthroline-substituted ruthenium(II) complexes, these compounds have been shown to exhibit electrochemiluminescence or electrogenerated

chemiluminescence (ECL).[24-27] Briefly, ECL results when electrochemically generated intermediates (resulting from a sweep of potential) react to produce an electronically excited state that emits light.[28] ECL has a wide and varied potential for applications in biology and medicine for highly sensitive detection of biological markers. Most of these applications have been centered around $[Ru(bpy)_3]^{2+}$ and its derivatives as this complex exhibits good stability and ECL efficiency in aqueous media, has favorable electrochemical properties, and is compatible with a wide range of analytes.[29] For example, ECL assays have been developed i) to detect surface proteins on live cells,[30] ii) to detect protein cancer biomarkers,[31] iii) as DNA probe assays,[32] iv) with ECL-inducible DNA intercalators used as coreactants for DNA hybridization assays,[33] and v) for the detection of anthrax spores, cholera toxins, and staphylococcal enterotoxin B,[34,35] to name a few.

Cyclometallated iridium(III) complexes also display luminescence enhancement in polar solvent-shielded environments and can exhibit eletrogenerated chemiluminescence[36-41] but have been less explored in the literature as DNA binders. They present advantages over their ruthenium counterparts, such as tunable luminescence wavelength and higher quantum yields.[36,38,41-43] The sole example to date, of an iridium(III) complex as a G-quadruplex binder and potential therapeutic, has been reported by Yang *et al.*[44] In their report, they synthesized and characterized $[Ir(phq)_2(biq)][PF_6]$ (Figure 4.2) and studied its interaction and affinity with the *c-myc* G-quadruplex motif *via* UV/Vis spectroscopy and gel mobility shift assays. Additionally, they examined the ability of their complex to stabilize the G-quadruplex motif *in vitro* through a cell-based luciferase reporter assay and showed that the complex could down-regulate *c-myc* oncogene expression. While they did measure the quantum yield and emission lifetime of the complex, they did not harness the inherent luminescence properties for assessing the binding affinity to the *c-myc* motif. They also did not realize the full potential of the complex to act as a probe for G-quadruplex detection *in vitro*.

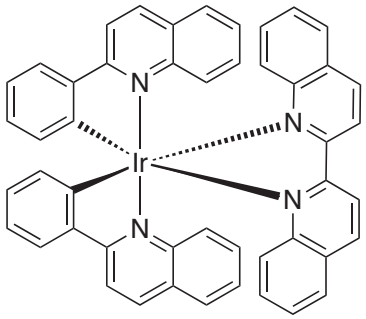

Figure 4.2 Cyclometallated iridium(III) complex $[Ir(phq)_2(biq)]PF_6$] (where phq = 2-phenylquinoline and biq = 2,2'-biquinoline) studied by Yang *et al.* as a *c-myc* G-quadruplex stabilizer.

As well, fewer ECL applications exist for iridium(III) complexes in aqueous environments compared to their ruthenium(II) counterparts. In non-aqueous environments, many of the neutral iridium(III) species exhibit a higher degree of ECL efficiency than $[Ru(bpy)_3]^{2+}$, but due to their low solubility in aqueous media and sensitivity to quenching by oxygen, their use in biological and medicinal detection applications has been restricted.[29] In fact, the only study to date of water-soluble ionic cyclometallated iridium(III) complexes was done by Kiran and coworkers, where they demonstrate that iridium(III) complexes with an overall positive or negative charge hold great promise for future ECL detection in aqueous solution and may in fact rival the ruthenium complexes for ECL sensing under some circumstances.[45,46]

Given the ease of synthesis of cyclometallated iridium(III) complexes, their ability to bind to and stabilize G-quadruplex DNA, and the easily harnessed ECL for DNA detection, we hypothesized that the addition of our phenanthroimidazole ligands to a cyclometallated iridium(III)-bisphenylpyridine core could create a library of complexes for G-quadruplex detection. Thus, we synthesized complexes **4.1-4.6**, obtained crystal structures of novel complexes **4.3** and **4.4**, studied their binding affinities with a library of G-quadruplex motifs through a direct high-throughput luminescence assay, assessed binding stoichiometry *via* a continuous variation method, conducted cyclic voltammetry (CV) and ECL assays. Future work includes the design of a G-quadruplex detection assay based on ECL of the complexes after binding to the G-quadruplex motifs.

From these experiments, we have developed a library of iridium-based complexes with π-extended phenylphenanthroimidazole ligands that are ideally suited as G-quadruplex binders. These complexes exhibit the "G-quadruplex light-switch" effect in that their luminescence is enhanced upon binding to various polymorphs. These complexes are also electrochemically active and demonstrate reversible iridium oxidation between 1.24−1.38 V ($E_{1/2}$ values referenced to an Ag/AgCl pseudo-reference.) Additionally, the complexes are electrochemiluminescent and show strong light emission in the positive potential region. The ECL activity and emission enhancement upon selective binding to G-quadruplex DNA suggests the use of these complexes as probes for various applications involving G-quadruplex DNA detection.

4.2 Results and discussion

4.2.1 Synthesis and characterization of complexes 4.1-4.6

The synthesis of complexes **4.1**-**4.6** could be completed in two steps from commercially available iridium(III) trichloride hydrate and 2-phenylpyridine. We followed the procedure of the previously established synthesis[47] and obtained a 72% yield of pure yellow crystals of the dichloro-bridged $[Ir_2(ppy)_4Cl_2]$ dimer. The addition of the phenanthroimidazole ligands was performed in an analogous procedure to that of Zhao *et al*[48] and resulted in yields of 30%−96% of yellow-orange powders after silica gel column chromatography. ^{1}H, and ^{13}C NMR spectra were obtained, as well as HR-MS and elemental analysis. X-ray crystallography of complexes **4.3**, **4.4**, and **4.5** was performed on a Bruker APEX2 diffractometer.

a)

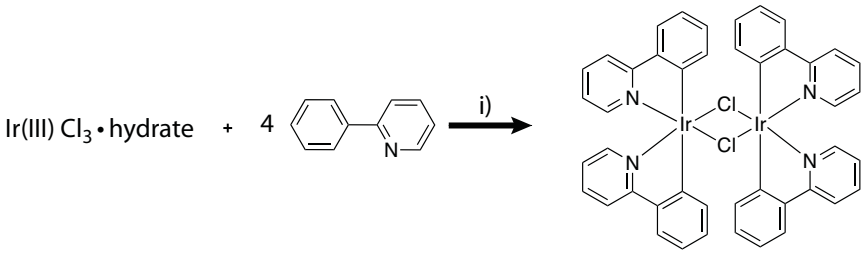

b)

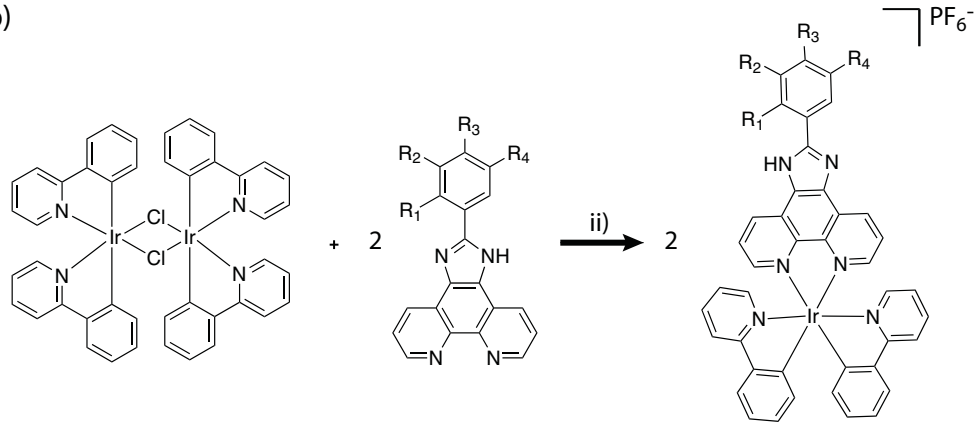

c)

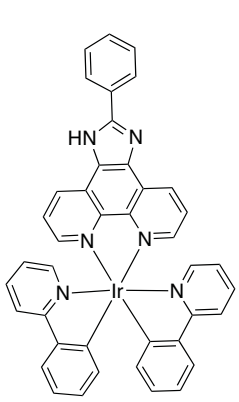

complex **4.1**

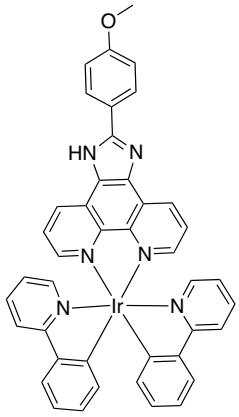

complex **4.2**

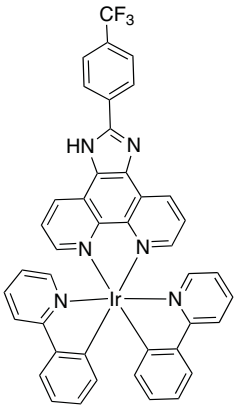

complex **4.3**

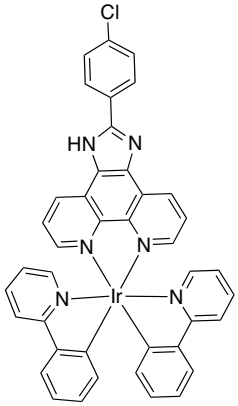

complex **4.4**

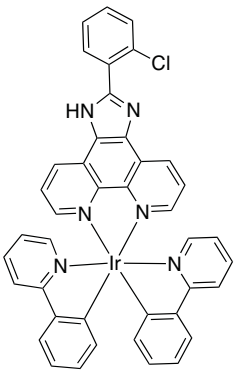

complex **4.5**

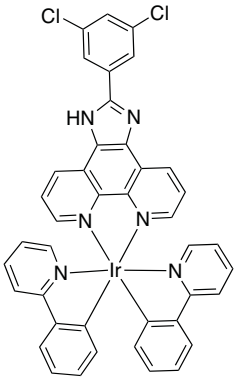

complex **4.6**

Figure 4.3 a) Synthesis of $[Ir_2(ppy)_4Cl_2]$ where i) reflux, 24 h in 3:1 methoxyethanol/water. b) Synthesis of complexes **4.1**-**4.6** where ii) reflux, 4 h in 2:1 DCM/MeOH, followed by addition of KPF_6. c) $[Ir(ppy)_2(PIP)][PF_6]$, (**4.1**), $[Ir(ppy)_2(OMePIP)][PF_6]$, (**4.2**), $[Ir(ppy)_2(CF_3PIP)][PF_6]$, (**4.3**), $[Ir(ppy)_2(CLIP)][PF_6]$, (**4.4**), $[Ir(ppy)_2(2\text{-}CLIP)][PF_6]$, (**4.5**), $[Ir(ppy)_2(3,5\text{-}diCLIP)][PF_6]$, (**4.6**), where ppy = 2-phenylpyridine, PIP = phenylphenanthroimidazole, OMePIP = 4-methoxyphenylphenanthroimidazole, CF_3PIP = 4-trifluoromethylphenylphenanthroimidazole, CLIP = 4-chlorophenylphenanthroimidazole, 2-CLIP = 2-chlorophenylphenanthroimidazole, and 3,5-diCLIP = 3,5-dichlorophenylphenanthroimidazole.

4.2.1.1 Crystal structure analysis (Performed by Dr. Christopher J. Serpell)

4.2.1.1.1 Trifluoromethyl- Complex 4.3

A single crystal of trifluoromethyl complex **4.3** was grown *via* slow diffusion of a solution of **4.3** in dichloromethane into acetic acid. The ORTEP diagram of complex **4.3** is depicted in Figure 4.4. The molecule was found to crystallize in a stacked, head-to-tail dimer (Figure 4.5a), with included dichloromethane. The nitrogen atoms of the phenylpyridine ligands occupied axial positions on the metal similarly to the report by Zhao *et al*[48] which results in a cis-C,C trans-N,N chelate configuration. Interestingly, the protic imidazole hydrogens were directed towards BF_4^- anions. Although no BF_4^- salts were added intentionally, they must have been introduced as an impurity sometime during the synthetic route. Superimposition of the two molecules in the asymmetric unit revealed that within a dimer, their stereochemistry was identical (Figure 4.5b), while due to symmetry, both enantiomers were present in the crystal.

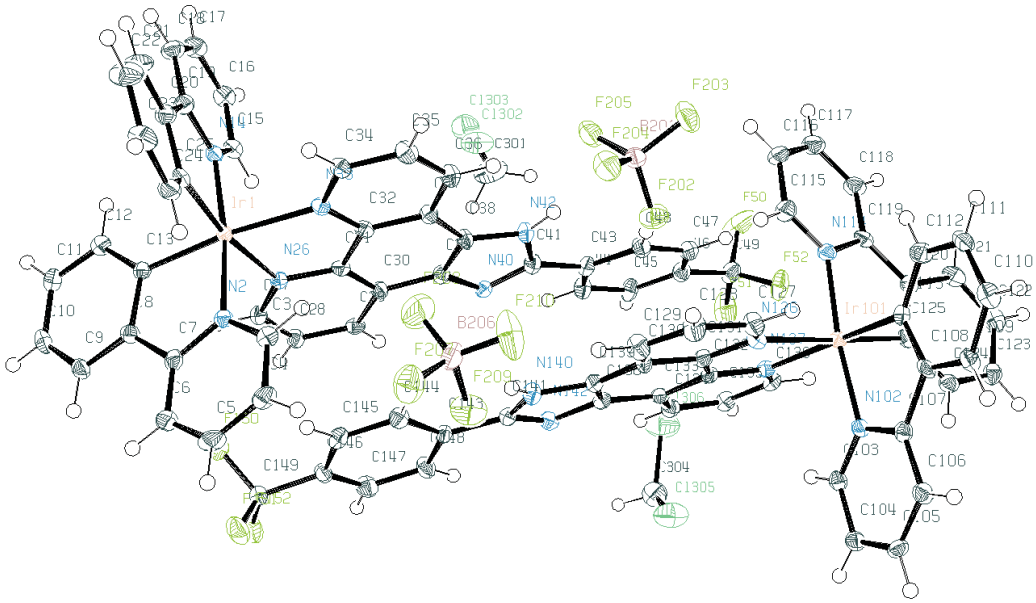

Figure 4.4 Complete crystal structure of complex **4.3** showing thermal ellipsoids at 50% probability.

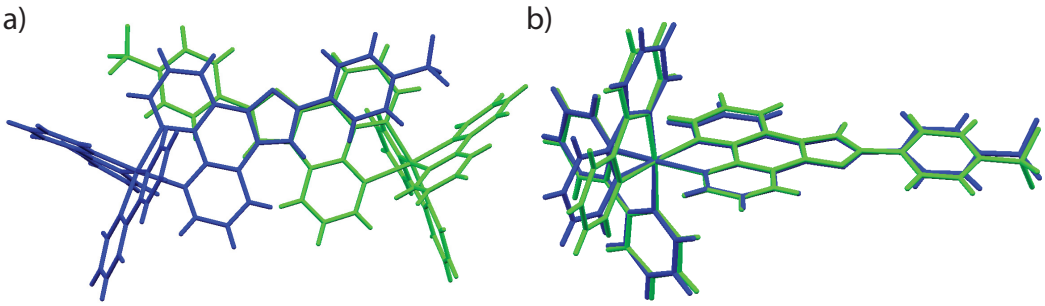

Figure 4.5 a) Dimer of complex **4.3**, and b) overlay of two metal complexes in the asymmetric unit, showing their identical stereochemistry

4.2.1.1.2 p-*Chloro Complex 4.4*

A single crystal of *p*-chloro complex **4.4** was grown *via* slow diffusion of complex **4.4** in dichloromethane into acetic acid in a similar manner as for complex **4.3**. The ORTEP diagram of complex **4.4** is depicted in Figure 4.6. The molecule was found to crystallise in a stacked, 90° dimer (Figure 4.7a), with included acetic acid and water. The phenylpyridine ligands exhibit the same cis-C,C trans-N,N chelate configuration as complex **4.3**. The protic imidazole hydrogens were directed towards the solvent. Two acetic acid dimers were observed. Superimposition of the two molecules in the asymmetric unit revealed

that with a dimer their stereochemistry was identical (Figure 4.7b) while due to symmetry, both enantiomers were present in the crystal.

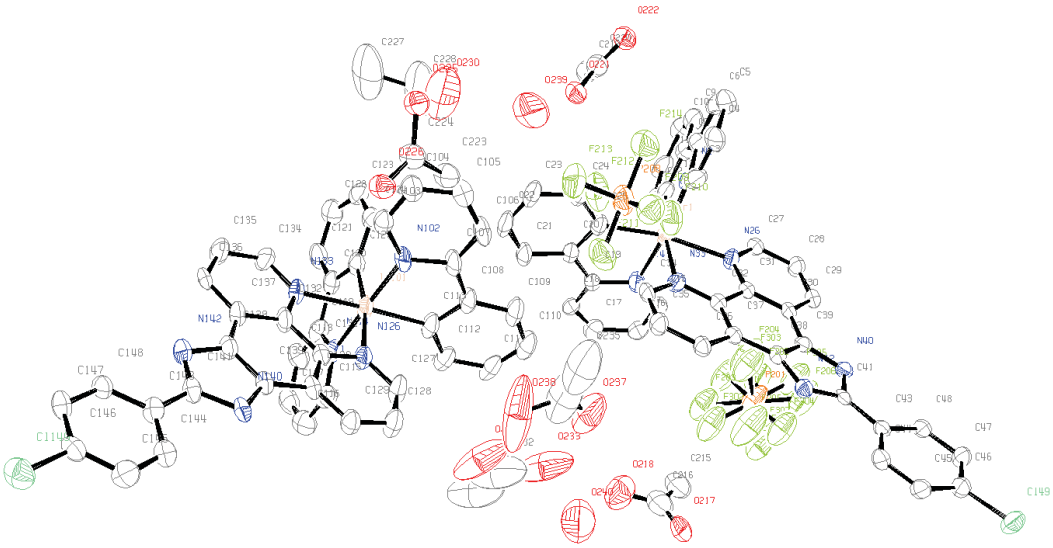

Figure 4.6 Complete crystal structure of complex **4.4** showing thermal ellipsoids at 50% probability.

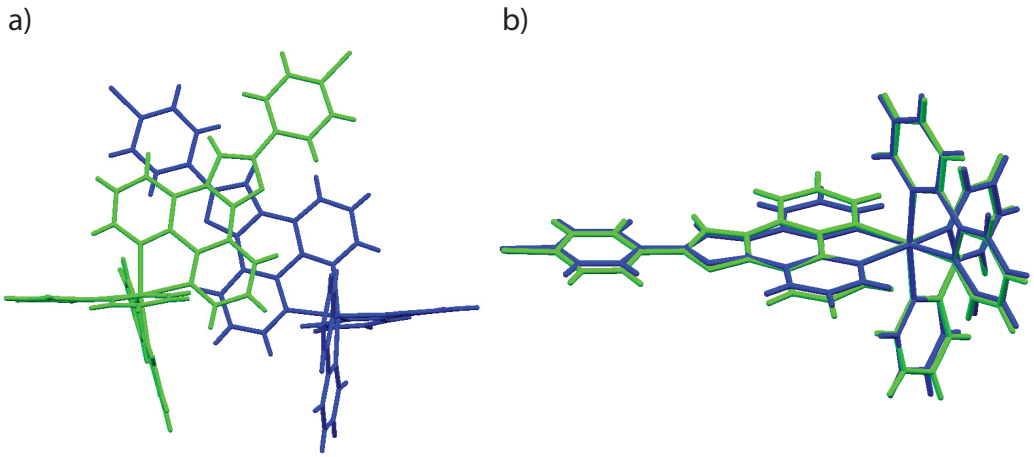

Figure 4.7 a) Dimer of complex **4.4**, and b) overlay of two metal complexes in the asymmetric unit, showing their identical stereochemistry

4.2.1.1.3 2-Chloro Complex 4.5

A single x-ray quality crystal of 2-chloro complex **4.5** was grown *via* slow diffusion of **4.5** in dichloromethane into a solution of ether. While this crystal did diffract, refinement of the data and subsequent determination of the crystal structure have proved difficult. Attempts at obtaining better quality crystals are currently underway.

4.2.2 Assessing the absorbance and luminescence properties

4.2.2.1 Absorption Spectroscopy

The UV-vis absorption spectra of all complex salts in both water and acetonitrile are shown in Figure 4.8, and the electronic absorption data are listed in Table 4.1. For all complexes, intense absorption bands below 320 nm could be observed and are assigned to spin-allowed π-π* ligand-centered (LC) transitions for phenylpyridine and phenanthroline-based ligands, analogous to other similar complexes in the literature.[44,46,49-51] Further investigation allows us to deduce that the higher energy bands < 300 nm can be attributed to the phenylpyridine ligands while the lower energy shoulder from 300–320 nm can be assigned to the phenanthroline ligand.[46,52] This can be explained through the higher energy of the lowest unoccupied molecular orbital (LUMO) of the cyclometallated ligand compared to the neutral phenanthroline ligand.[53] Moderately intense absorption bands in the range 380−430 nm were also observed, and in agreement with the literature,[49,54,55] can be assigned to metal-to-ligand charge transfer (MLCT) from the highest occupied molecular orbital (HOMO) of the Ir t_{2g} π to π* (phenylpyridine and phenanthroline ligands) which are spin-allowed. Finally, the weak absorption tails above 430 nm are assigned to spin-forbidden MLCT (Ir dπ to π* (phenanthroline derivatives)) transitions.[46,51]

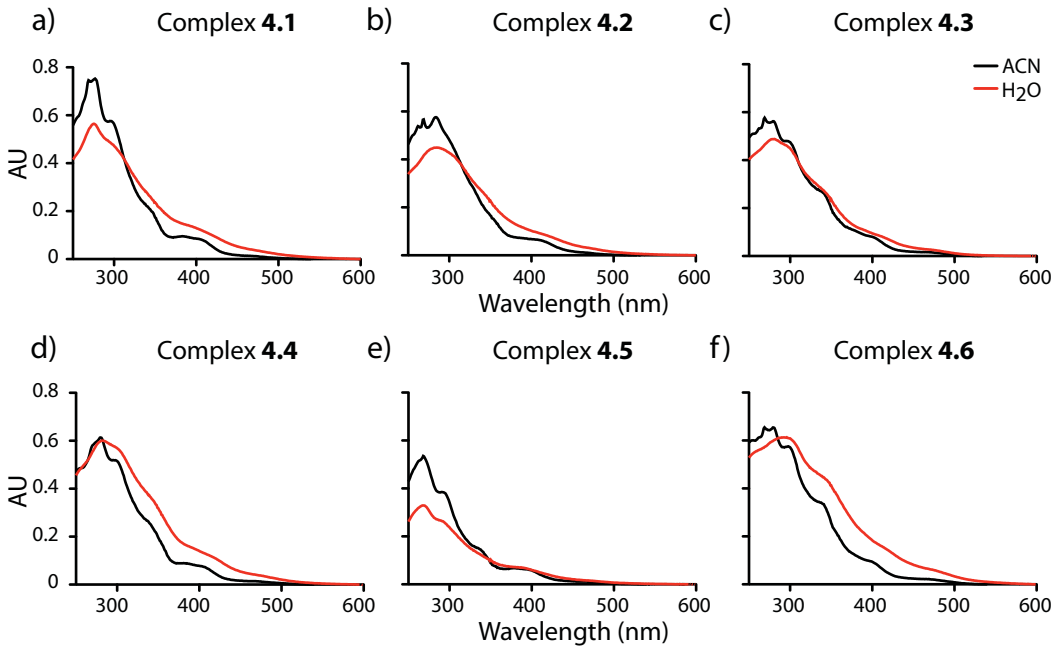

Figure 4.8 Absorption spectra of complexes **4.1**-**4.6** in ACN (black) and H_2O (red) at a concentration of 10 μM at 25°C.

	solvent	4.1	4.2	4.3	4.4	4.5	4.6
λ_{abs} (nm)	ACN	274, 298, 344, 385, 406	254, 270, 283, 351, 406	254, 271, 280, 299, 339, 399	254, 271, 280, 298, 339, 406	268, 293, 337, 400	266, 281, 298, 335, 394
	H_2O	275, 293, 381	282, 383	276, 305, 393, 450	289, 348, 402	266, 290, 386	299, 248, 426

Table 4.1 Absorption data of complexes **4.1**-**4.6** in ACN and H_2O at 25°C.

4.2.2.2 Luminescence spectroscopy

The room-temperature photoluminescence spectra of all complex salts in degassed ACN and H_2O are shown in Figure 4.9, and corresponding photoluminescence data of complex salts are summarized in Table 4.2. It can be seen that all complex salts emit at wavelengths in the range 579−593 nm with excitation at 280 nm in both ACN and H_2O at room temperature. Since the emission wavelengths maxima are between 579−593 nm, we can classify the excited-state characteristics of complexes **4.1**-**4.6** as mixed ^{3}MLCT and $^1\pi$-π^* transitions where the ^{3}MLCT results from the promotion of an electron from the HOMO of the metal center to the π^* orbital of the phenanthroline ligand, while the $^1\pi$-π^* transition arises from the movement of electrons located on the phenylpyridine ligands.[55-58]

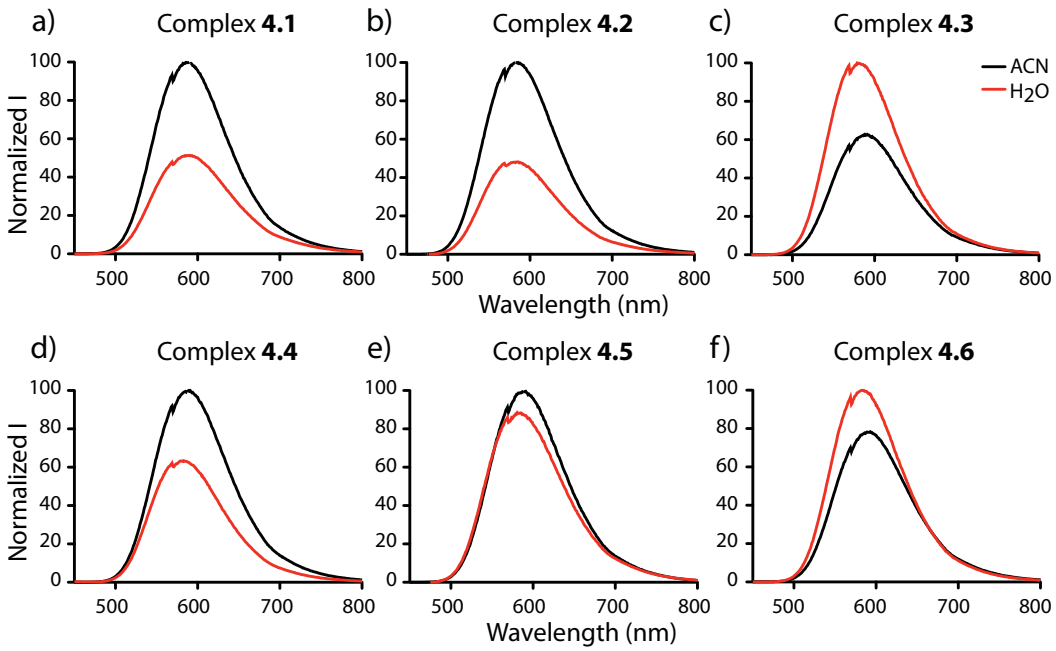

Figure 4.9 Emission spectra of **4.1**-**4.6** in ACN (black) and H_2O (red) at 10 μM each. Complexes were excited at 280 nm. The spectra were normalized to the highest IU in each set.

Complex			4.1	4.2	4.3	4.4	4.5	4.6
medium	H_2O	$\lambda_{em\text{-}max}$ (nm)	590	585	579	582	581	583
	ACN	$\lambda_{em\text{-}max}$ (nm)	590	582	588	587	588	593

Table 4.2 Photoluminescence data of **4.1**-**4.6**.

In acetonitrile, in an analogous manner to the report by Neve and coworkers,[52] as the electron-withdrawing ability of the ligand increases, the emission energy decreases, with the dichloro-complex **4.6** emitting at a longer wavelength than the methoxy-complex **4.2**.

Next, we were interested in whether we would see emission enhancement when complexes **4.1**-**4.6** bound to DNA targets in the same manner as the aforementioned ruthenium complexes (Figure 4.1). To this end, the fluorescence spectra of solutions of 2 μM complex in 10 mM sodium cacodylate buffer with 100 mM KCl (pH 7.2) were compared to fluorescence spectra of 2 μM solutions with 20 μM added DNA sequence (22AG-K, cmyc, or duplex DNA) after a 1 h incubation at room temperature. The spectra are shown in Figure 4.10 and the enhancements and blue-shifts are quantified in Table 4.3. Excitingly, all

complexes show much higher emission intensities when bound to G-quadruplex DNA compared to duplex DNA. In the case of complexes **4.5** and **4.6** with duplex DNA, there is even a slight decrease in luminescence when compared to the complexes in aqueous solution alone. The largest shift in emission maximum occurs when complex **4.5** binds to 22AG-K with a 42 nm blue-shift. This agrees well with previous studies where the higher energy luminescence and larger emission enhancements are associated with binding sites of the metal complexes that are more solvent inaccessible (that is, intercalation into B-DNA rather than groove-binding).[8,59-62] For quantification of solvent accessibility, we would need to examine the structures of the quadruplex motifs in solution *via* molecular modeling methods to determine the hydrophobicities of the predicted binding sites in relation to one another. But, from a visual inspection of the representations of the PDB codes for 22AG-K^+ (2GKU[63]) and cmyc (1XAV[64]), we can assess the differences between the binding sites available to the iridium complexes. In general, the end-stacking mode, as determined theoretically and experimentally, has been shown to be the dominant binding site for these G-quadruplex structures.[65] In the case of 22AG-K^+, there are external loops that extend above and below the surface of the tetrads that appear to π-stack with the tetrads (Figure 4.11a). When compared to the cmyc structure (Figure 4.11b), these loops may be able to better shield the complex from the solvent if the phenanthroimidazole ligand inserts between them and the G-tetrad. The loops in the cmyc structure, while also available to π-stack, are much more flexible, allowing for greater solvent accessibility.[8]

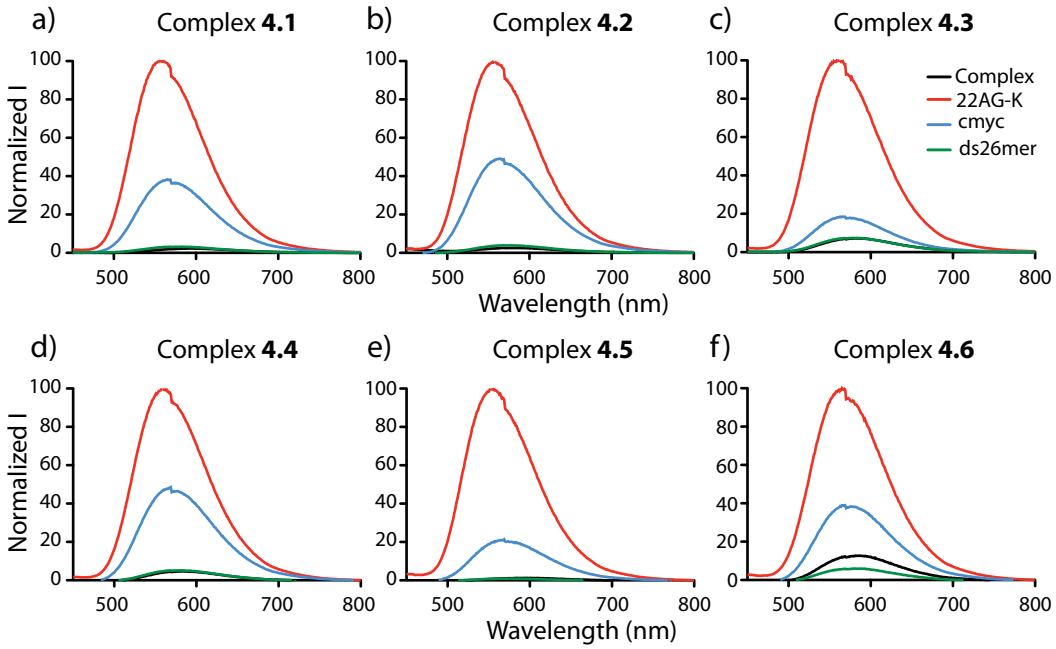

Figure 4.10 Fluorescence spectra showing enhancement of luminescence and blue shift of emission maximum after 1 h incubation of the complexes (2 μM) with 20 μM each 22AG-K (red) and cmyc (blue) G-quadruplexes compared to the complexes without added DNA (black) and with ds26mer (green).

		4.1	4.2	4.3	4.4	4.5	4.6
Aqueous	λ(max)	593	588	584	585	595	583
22AG-K	λ(max)	557	558	560	559	553	566
	I_{bound}/I_0	38.1	27.8	13.0	18.5	52.9	7.3
cmyc	λ(max)	566	565	564	564	570	570
	I_{bound}/I_0	15.0	14.0	2.45	9.20	11.7	2.92
ds26mer	λ(max)	582	578	587	579	578	579
	I_{bound}/I_0	1.42	1.17	1.05	1.10	0.745	0.493

Table 4.3 Quantification of changes in emission of complexes **4.1**-**4.6** upon binding different DNA sequences.

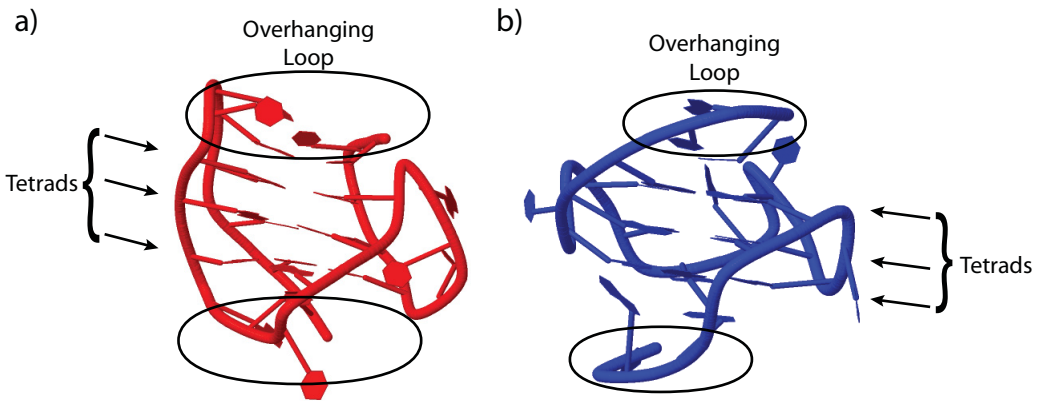

Figure 4.11 Visual inspection of the solution structures of 22AG-K^+ (a) and cmyc (b). Each structure is shown with the wide groove in the foreground. Tetrads are indicated with arrow while loops are indicated by ellipses.

4.2.3 Studying the binding affinity and stoichiometry of the iridium complexes with DNA

After assessing the luminescence enhancement when these complexes bind to G-quadruplex DNA, we devised a high-throughput assay to study the binding affinity of the library with biologically relevant G-quadruplex polymorphs. We chose both forms of human telomeric DNA (the antiparallel basket and the 3+1 hybrid), in addition to an expanded repertoire of oncogene promoters including polymorphs found in the *c-Kit,*[66-68] *c-Myc,*[69-74] PDGF-A,[75] KRAS,[76] VEGF,[77] and Bcl-2[78] oncogene promoters (Table 4.4). Due to the lack of significant luminescence enhancement when the complexes bind to duplex DNA, selectivity between G-quadruplex and duplex motifs could not be assessed with this method.

We conducted a fluorescence titration assay similar to those in Chapters 2, 3, and 5, however, in our experiment, we utilized the luminescence enhancement of the complexes themselves when binding to DNA rather than needing a fluorescent dye that would be analyzed by displacement. We adapted the high-throughput procedure in Chapters 3 and 5 to accommodate a 384-well plate. Briefly, we plated 40 μL of a 0.5 μM solution of pre-annealed DNA into each well of the plate, and then added increasing amounts of complexes across the rows such that the molar equivalents of complex ranged from 0−20, supplemented with

an appropriate amount of buffer in 80 μL total (See Figure S4.1 and Figure S4.2 for plate layouts).

Name	ε_{260} ($M^{-1}cm^{-1}$)	Sequence
22AG	228 500	5'- AGGGTTAGGGTTAGGGTTAGGG
cmyc	279 900	5'- TGGGGAGGGTGGGGAGGGTGGGGAAGG
ckit1	226 700	5'- AGGGAGGGCGCTGGGAGGAGGG
ckit2	205 600	5'- CGGGCGGGCGCGAGGGAGGGG
PDGF-A	314 000	5'- AGGCGGGGGGGGGGGGCGGGGGCGGGGGCGG
KRAS	341 000	5'- AGGGCGGTGTGGGAAGAGGGAAGAGGGGGAGG
VEGF	190 000	5'- GGGGCGGGCCGGGGGCGGGG
Bcl-2	227 300	5'- GGGCGCGGGAGGAATTGGGCGGG

Table 4.4 Sequences used in this study with their corresponding extinction coefficients.

After plating, the complexes were allowed to associate with the DNA solutions for approximately 20 minutes before being scanned on the microplate reader using an excitation of 260 ± 10 nm and an emission filter of 595 ± 35 nm with an integration time of 1 second. In order to obtain background luminescence, we ran a plate with the complexes in a solution of buffer only. The background values were then subtracted from the values with the DNA (assuming a linear increase) and subsequently plotted on a graph of concentration of complex versus normalized luminescence intensity. The curves were fit to a one-site binding model (in most cases) in GraphPad Prism which resulted in preliminary K_D values that are represented in Table 4.5. In cases where the error obtained from the fit was high – that is, the error is ≥ 50% of the K_D value – the results were omitted and designated with n/d. In other cases, the data could not be fit to the binding equation, and are designated with n/d[1]. The error for some K_D value fits, in addition to the inability to fit some of the data, could be due to either the dissociation of the iridium complex dimers in solution to the monomeric species prior to binding the G-quadruplexes, or to possible non-specific binding of the iridium complexes with the polypropylene plates used for the high-throughput

fluorescence assay (as mentioned in Chapter 5, pp 220). Future work will be directed towards repeating the experiments manually in quartz cuvettes for validation of the absolute numbers obtained.

KD (μM)	4.1	4.2	4.3	4.4	4.5	4.6
22AG Na^+	0.19 ± 0.081	1.4 ± 0.46	n/d	n/d	n/d	n/d[1]
22AG K^+	0.94 ± 0.21	4.0 ± 1.1	n/d	2.9 ± 1.4	1.7 ± 0.47	n/d[1]
cmyc	1.6 ± 0.48	2.0 ± 0.86	n/d	n/d	n/d	n/d
ckit1	1.1 ± 0.31	0.66 ± 0.23	n/d[1]	0.58 ± 0.14	1.5 ± 0.49	0.38 ± 0.18
ckit2	0.72 ± 0.21	1.2 ± 0.49	2.0 ± 0.62	n/d	2.0 ± 0.63	2.9 ± 0.82
PDGF-A	n/d	n/d	n/d	0.78 ± 0.35	0.37 ± 0.16	n/d
KRAS	0.45 ± 0.083	1.2 ± 0.24	2.7 ± 0.96	3.2 ± 1.1	4.5 ± 1.8	n/d
VEGF	1.4 ± 0.33	0.96 ± 0.18	4.9 ± 1.6	1.5 ± 0.30	n/d	1.4 ± 0.16*
Bcl-2	0.78 ± 0.12*	1.3 ± 0.35	n/d	n/d	n/d	n/d[1]

Table 4.5 Preliminary KD values calculated from the fluorescence titration where n/d = not determined. *These value were determined from a one-site binding model with Hill slope where the h value = 2.8 for **4.1** and h = 2.1 for **4.6**. A Hill slope > 1 may indicate cooperative binding. [1]The values could not be determined using a one-site binding model

From the KD values above, we can say that when the complexes bind to G-quadruplex DNA, they do so with affinities in the low micromolar regime. If there is non-specific binding occuring between the complexes and the polypropylene plates, these numbers could be even lower. The lowest value determined is 0.19 ± 0.081 μM for phenyl- complex **4.1** with the 22AG-Na^+ polymorph. Interestingly, complexes **4.1** (phenyl-) and **4.2** (methoxy-) exhibit similar behaviors in that they are the least selective and can bind to most of the polymorphs with reasonable affinity. On the other hand, 3,5-dichloro- complex **4.6** is the most selective, appearing to prefer the ckit and VEGF motifs. Initially, luminescence enhancement with complexes **4.1**-**4.6** were assessed with the 22AG-K^+ and cmyc G-quadruplex sequences only. In order to draw precise conclusions, experiments that investigate luminescence changes with other G-quadruplex forming sequences should be performed. This would confirm that each

quadruplex binding surface presents a hydrophobic pocket that allows for the emission enhancement. Additionally, the extent of non-specific binding should be analyzed so as to confirm the applicability of the experiment.

To assess the binding stoichiometry of complexes **4.1**-**4.6**, a continuous variation method (Job plot) was conducted for the sequence/complex combinations for which a K_D value was determined. In this assay, the total concentration of DNA and complex are held constant (10 μM) while the mole fractions of the two components are varied, and each fraction is quantified by luminescence intensity. This assay was run in a 96-well plate format with mole fractions of iridium complex varying from 0.0−1.0 by 0.1. After plating the complexes and quadruplexes, the plate was allowed to rock on a plate shaker for 20−90 minutes before the luminescence was read on a microplate reader with an excitation filter of 310 ± 20 nm and emission filter of 590 ± 20nm. The plates were scanned once after 20 minutes of rocking and once after 90 minutes. The luminescence intensities were not significantly different at these two time points, which agrees with our assumption that binding is a relatively fast process and does not involve threading for intercalation. The assay was not conducted with the ckit1 of PDGF-A quadruplexes due to limited materials available. From the intersection of the lines, the binding stoichiometry can be determined for the complexes (Figure 4.12). For all complexes in all cases, the maximum enhancement occurs at ~ 0.50 mole fraction, which corresponds to a 1:1 binding stoichiometry, that is, one complex per quadruplex. The spread in the data may be an indication of non-specific binding. By performing more replicates in the high-throughput fashion enabled by the microplates, we would be able to minimize noise to get a clearer indication of absolute binding stoichiometry.

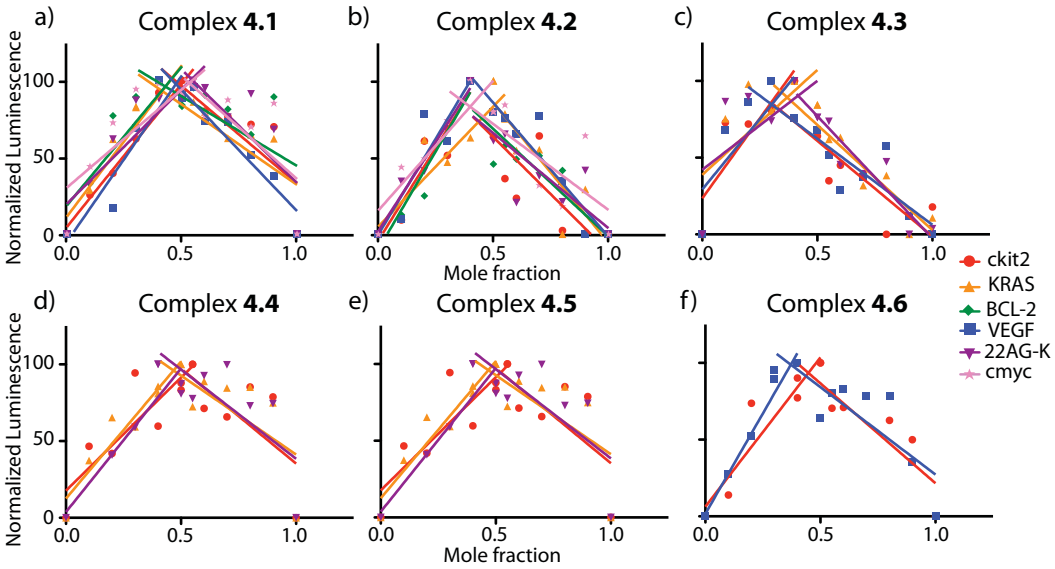

Figure 4.12 Job plots of complexes **4.1**-**4.6** binding to various G-quadruplex sequences. The maximum enhancement determines the binding stoichiometry.

4.2.4 Electrochemical properties of complexes 4.1-4.6

4.2.4.1 Cyclic voltammetry (Performed by Dr. Kimberly Metera and Dr. Ushula Tefashe)

The electrochemical properties of the complexes at the glassy carbon electrode were studied by cyclic voltammetry for 0.5 mM complex in acetonitrile solution containing 0.1 M tetrabutylammonium hexafluorophosphate ($TBAPF_6$) (Figure 4.13). For all complexes during the anodic scan, a reversible iridium oxidation peak was evident and the $E_{1/2}$ values are listed in Table 4.6, referenced to an Ag/AgCl pseudo-reference. Upon reduction, a large peak for $TBAPF_6$ is evident and mostly obscures any reduction of the phenanthroimidazole and phenylpyridine ligands. However, a small bump can be seen just negative to −0.5 V which may be a ligand-reduction peak from the cathodic scan (Figure 4.13a). In order to ascertain this finding, the CVs of the complexes should be rerun, but the cathodic scan should not go below −0.75 V so as not to reduce the $TBAPF_6$. The $TBAPF_6$ electrolyte could also be substituted for another that does not show reduction overlap to the same extent.

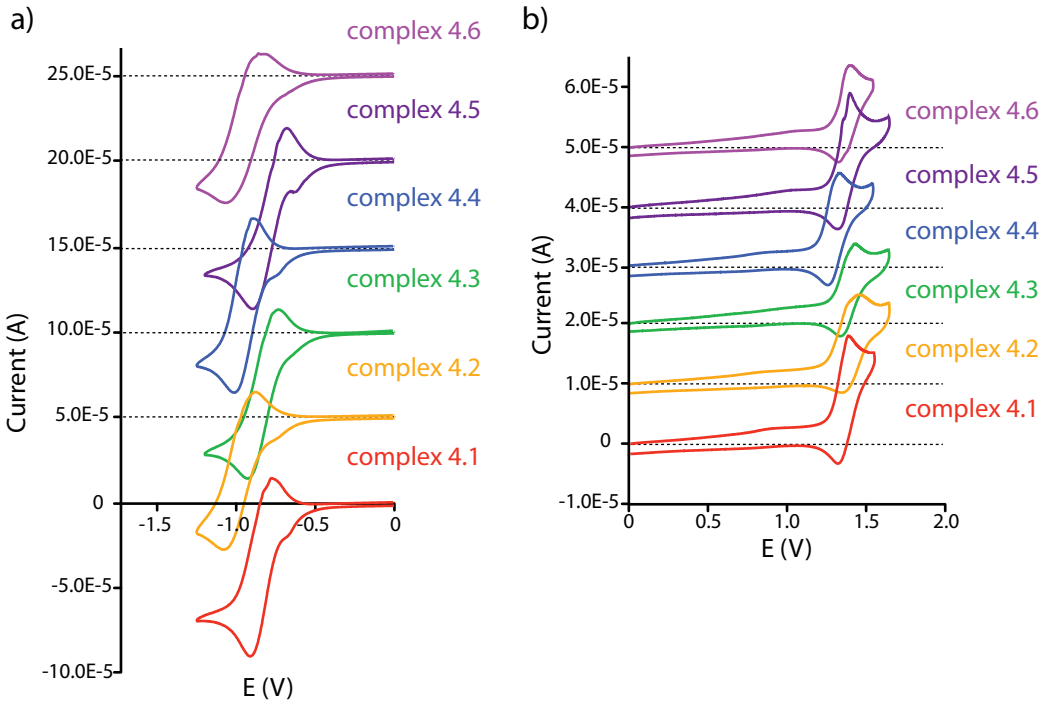

Figure 4.13 CV results for complexes **4.1**-**4.6** in acetonitrile solution containing 0.1 M $TBAPF_6$: a) reduction and b) oxidation referenced to an Ag/AgCl pseudo-reference.

	4.1	4.2	4.3	4.4	4.5	4.6
$E_{1/2}$/V	1.35	1.40	1.38	1.29	1.35	1.36

Table 4.6 Electrochemical oxidation potentials for complexes **4.1**-**4.6** referenced to an Ag/AgCl pseudo-reference.

While the complexes differ from one another in the electronics of the phenyl group appended to the imidazole ring, these differences do not affect the oxidation potentials to a large extent. Previous studies have found that the HOMO orbitals of similar complexes are spread between the iridium atom and the phenyl rings of the phenylpyridine ligands; thus they are not expected to be centered on the phenanthroimidazole portion of the complex.[41,50,79-81] Accordingly, based on Hammett sigma values,[82] the electron-donating methoxy- complex **4.2** (Hammett sigma value of −0.27) would be expected to exhibit the lowest $E_{1/2}$ value of the series (ie, easiest to oxidize) if the HOMO had significant contributions from the phenanthroimidazole ligand. Instead, the $E_{1/2}$ for this complex has a slightly more positive value.

4.2.4.2 Electrochemiluminescence (Performed by Dr. Kimberly Metera and Dr. Ushula Tefashe)

The ECL behavior of the complexes with added tripropylamine (TPrA, a common coreactant for ECL) was examined next. As previously stated, ECL exhibits a great potential for detection applications in biology and medicine. Our iridium complexes could potentially be utilized for the detection of G-quadruplex DNA by ECL, presenting high signal amplification. ECL responses were acquired for each complex simultaneously with the voltage scans from CV cycles. Figure 4.15 illustrates this experiment for 2-chloro complex **4.5**, for example, and the ECL spectra overlayed with their corresponding fluorescence spectra are shown in Figure 4.14. The generated emission intensities are graphed in Figure 4.16a for complexes **4.1**-**4.6**. ECL was observed starting at ~ 1.0 V and continued until E = 2.2 V for all complexes, however, the intensity varied with each complex (Figure 4.16a). The reverse scan resulted in emission within the same potential range, however, the intensity was weaker. This is in agreement with previous observations for iridium and ruthenium complexes.[32,37,83] After five CV cycles, no significant changes in ECL intensity were observed, indicating reproducibility and stability of the complexes.

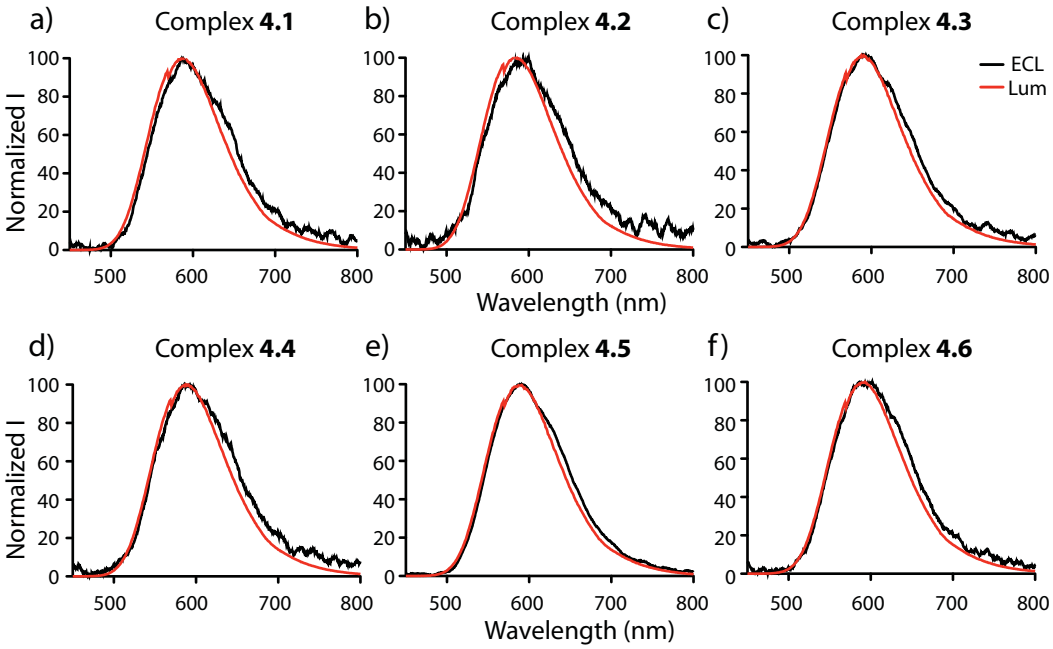

Figure 4.14 Overlays of the luminescence and ECL spectra for complexes **4.1**-**4.6**.

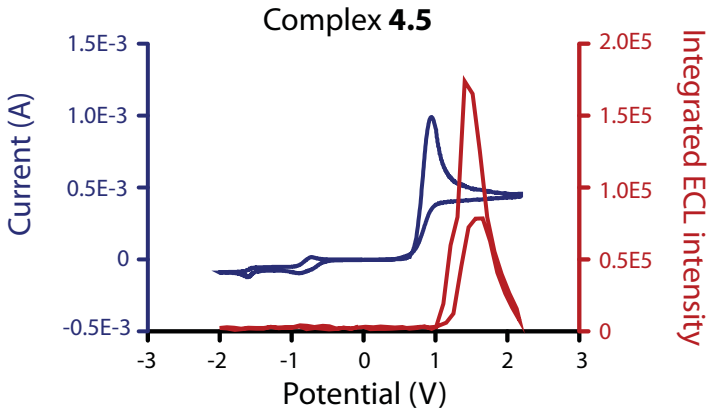

Figure 4.15 Graph showing the overlay of the simultaneous CV (blue) and ECL (red) scans for 2-chloro complex **4.5.**

In order to understand why the complexes exhibited different ECL intensities, we correlated the intensities with Hammett sigma values of the substituents on the phenyl group of the phenanthroimidazole moiety, as an indication of electron withdrawing/donating ability.[82] The graphical representation is shown in Figure 4.16b, and interestingly, these complexes show a linear relationship between decreasing electron-donating character and ECL intensity within error. From this representation, we can conclude that ECL intensity increases with increasing electron withdrawing ability of the phenanthroline ligand. DFT calculations by Zhu *et al.* indicated that the energy gaps between the HOMO of the tripropylamine TPA radical ($TPA^{\bullet}$) and the LUMO of the excited state of the iridium complex (M^{+-}) influenced the process of electron transfer and ECL efficiency in a predictable way.[41] That is, the lower the LUMO of M^{+-}, the higher the efficiency of the ECL process. As the LUMO of the complexes are composed almost exclusively of the ancillary phenenanthroline ligand,[46] as the electron-withdrawing ability increases, the LUMO energy decreases, resulting in higher ECL efficiency. Further verification of this hypothesis could be obtained through the synthesis and analysis of other complexes that may lie on the outer edges of the trend (see Section 4.4, Future directions), and also DFT calulations of the contributions of the phenanthroimidazole and phenylpyridine ligands to the HOMO and LUMO of the complexes and their excited states.

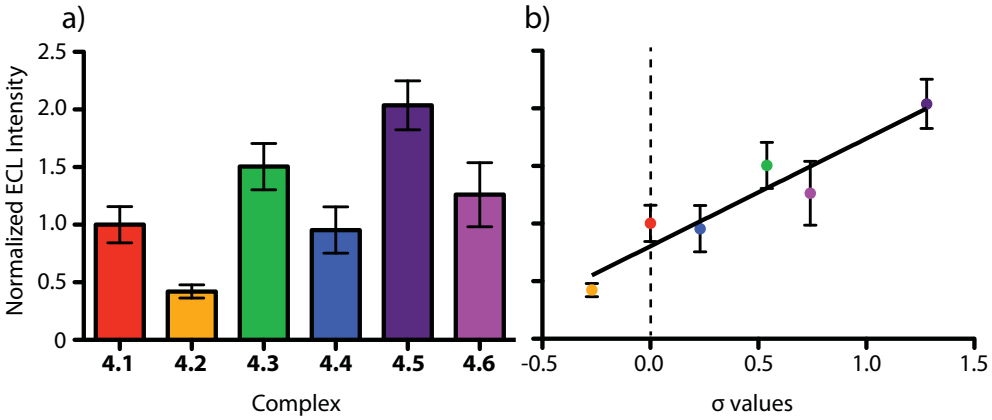

Figure 4.16 ECL results for complexes **4.1**-**4.6**; a) intensites showing standard deviations, and b) intensities graphed as a function of Hammett sigma values with best-fit line showing linearity.

4.3 Conclusions

In conclusion, we have presented six cyclometallated iridium(III) complexes with π-extended phenanthroimidazole ligands. These complexes exhibit a "G-quadruplex light-switch" effect upon binding to the G-quadruplex motif, but exhibit little to no emission enhancement when interacting with duplex DNA. A fluorescence-based binding assay demonstrated that the complexes bind to G-quadruplex DNA with K_D values in the low micromolar range with a 1:1 binding stoichiometry. Due to this emission enhancement in the presence of quadruplex DNA, but not duplex DNA, these complexes can be useful light-up G-quadruplex probes for *in cellulo* studies. There are examples of ruthenium-based complexes that exhibit similar behavior,[5,6,23,84,85] however, they all suffer from modest selectivity between duplex and quadruplex DNA, especially when duplex concentration outweighs quadruplex concentration. Our iridium-based complexes may be able to better discriminate between these two motifs, given the less than 2 fold luminescence enhancement when binding to duplex DNA. A linear correlation was shown between ECL intensity and electron-withdrawing character, in that the greater the electron-withdrawing the larger the ECL intensity (the correlation line has a positive slope). These complexes represent the starting point for the development of an ECL assay for DNA detection, an area of the literature that has yet to be explored for iridium(III) complexes.

4.4 Future directions

Future directions include the development of complexes with a red-shifted excitation wavelength. If the excitation wavelength is red-shifted, it may be used for *in cellulo* detection of G-quadruplexes. The current excitation wavelength is too low which causes autofluorescence of the cellular components. However, an appealing property of iridium(III) complexes is their long fluroescence lifetimes. When used in conjunction with time-gated fluorescence microscopy, red-shifting the excitation wavelength may not be necessary. Additionally, it would be beneficial to know whether or not the iridium compexes could template the formation of G-quadruplexes from their single-stranded and duplex counterparts. This would enable us to detect the formation of the G-quadruplexes in cells as caused by the addition of the complexes. Additionally, these complexes can bind to pre-formed G-quadruplexes *in cellulo* which is an added advantage when developing light-up probes. Development of an ECL-detection assay of for G-quadruplex motifs also provides an exciting future for these complexes. And finally, further verification of the trends involving ECL intensities could be obtained through the synthesis and analysis of other complexes that may lie on the outer edges of the Hammet values (including 2,6-dichloro-, *p*-hydroxyphenyl-, and 2-hydroxyphenyl- ligand varieties) and through DFT calculations.

4.5 Experimental section

4.5.1 Synthesis

The synthesis of the ligands is described in Chapter 5 (pp 230-232). The dichloro-bridged $[Ir_2(ppy)_2Cl_2]$ dimer was synthesized in a analogous fashion to those previously published.[46,86] [4,5-*f*][1,10]phenanthroline,[87] phenylphenanthro-imidazole (PIP),[87] 4-chloroPIP,[88] 2-chloroPIP,[89] CF_3PIP[90] ligands and complex **4.1**[48] have been characterized elsewhere. NMR spectra were recorded on a 500 MHz Bruker Ascend spectrometer. All commercially available reagents were purchased from Sigma Aldrich and used without further purification. High-resolution mass spectrometry was performed on a Bruker Maxis Impact ESI-

QTOF. For MS analysis, sodium formate was used to generate a calibration curve for mass accuracy. Samples were then diluted in LC-MS grade Methanol (Fisher) and directly infused at 3 μL per minute into the MS. The spectra were obtained in positive mode.

4.5.2 Preparation of 4.1-4.6

4.5.2.1 General preparation of iridium complexes

A solution of $[Ir(ppy)_2Cl]_2$ (0.0790 mmol) and phenylphenanthroimidazole ligand (0.158 mmol) in CH_2Cl_2/MeOH (30 mL, 2:1 v/v) was heated to reflux. After 4 h, the yellow solution was cooled to room temperature, and then a 10-fold excess of potassium hexafluorophosphate was added. The suspension was stirred for 2 h and then was filtered to remove insoluble inorganic salts. The solution was evaporated to dryness under reduced pressure. The crude product was purified by silica gel column on a Combiflash Rf (Teledyne Isco Inc.) and eluted with CH_2Cl_2-acetone (15:1) to afford yellow-orange solids. For simplicity, only one phenylpyridine ligand is shown with assigned NMR ^1H peaks for the following complexes.

Complex 4.2:

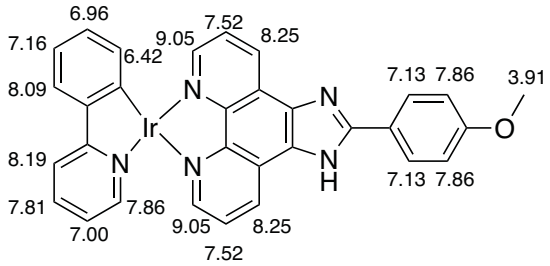

(102 mg, 58%). ^1H NMR (500 MHz, CD_3CN): δ = 9.05 (d, 2H), 8.25 (d, 2H), 8.19 (d, 2H), 8.09 (d, 2H), 7.86 (m, 4H), 7.81 (t, 2H), 7.52 (d, 2H), 7.16 (m, 2H), 7.13 (d, 2H), 7.00 (t, 2H), 6.96 (t, 2H), 6.42 (d, 2H), 3.91 (s, 3H) ppm; ^{13}C NMR (500 MHz, CD_3CN): δ = 168.0, 161.6, 150.4, 149.3, 148.9, 144.3, 138.5, 132.0, 131.7, 131.4, 128.3, 126.7, 124.9, 123.4, 122.6, 121.9, 119.8, 114.6, 55.3 ppm; Elemental Analysis calculated for $IrC_{42}H_{30}N_6OF_6P•2H_2O$ (as integrated from ^1H

NMR): C – 50.05; H – 3.40; N – 8.34. Found: C – 49.93; H – 2.95; N – 7.99; HR-MS calculated for $C_{42}H_{30}IrN_6O$ (M^+-PF_6^-): **827.2110**, Found: **872.2114**.

Complex 4.3:

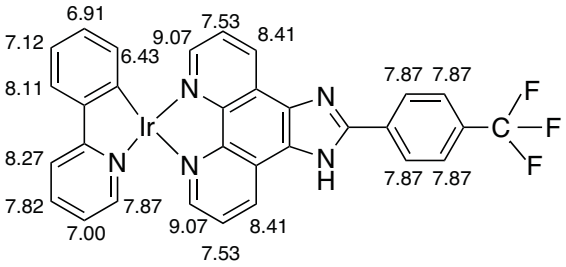

(50.1 mg, 30%). ^{1}H NMR (500 MHz, CD_3CN): δ = 9.07 (d, 2H), 8.41 (d, 2H), 8.27 (d, 2H), 8.11 (d, 2H), 7.87 (m, 6H), 7.82 (t, 2H), 7.53 (d, 2H), 7.12 (t, 2H), 7.00 (t, 2H), 6.91 (t, 2H), 6.43 (d, 2H) ppm; ^{13}C NMR (500 MHz, $CDCl_3$): δ = 167.5, 151.5, 150.2, 149.5, 149.3, 145.1, 144.3, 138.5, 132.2, 131.7, 130.4, 127.2, 126.9, 126.2, 126.1, 124.9, 123.4, 122.6, 119.8 ppm; Elemental Analysis calculated for $IrC_{42}H_{27}F_9N_6P•H_2O•C_6H_{14}$ (as integrated from ^{1}H NMR): C – 51.75; H – 3.89; N – 7.54. Found: C – 51.91; H – 3.47; N – 7.56; HR-MS calculated for $C_{42}H_{27}F_3IrN_6$ (M^+-PF_6^-): **865.1875**, Found: **865.1877**.

Complex 4.4:

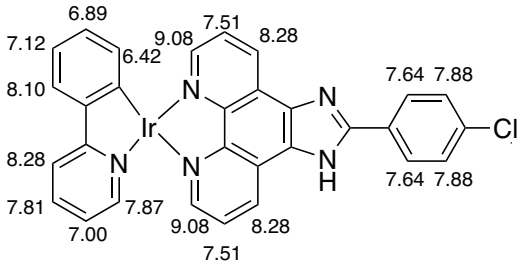

(79.0 mg, 99%). ^{1}H NMR (500 MHz, CD_3CN): δ = 9.08 (d, 2H), 8.28 (m, 4H), 8.10 (d, 2H), 7.88 (m, 4H), 7.81 (t, 2H), 7.64 (d, 2H), 7.51 (d, 2H), 7.12 (t, 2H), 7.00 (t, 2H), 6.89 (t, 2H), 6.42 (d, 2H) ppm; ^{13}C NMR (500 MHz, CD_3CN): δ = 167.5, 149.4, 149.2, 144.9, 144.3, 138.5, 132.1, 131.7, 130.4, 129.4, 128.2, 126.8, 124.9, 123.4, 122.6, 119.9 ppm; Elemental Analysis calculated for $IrC_{42}H_{27}ClN_6F_6P•H_2O$ (as integrated from ^{1}H NMR): C – 50.44; H – 2.79; N – 8.61. Found: C – 49.18; H – 2.87; N – 8.17; HR-MS Calculated for $C_{41}H_{27}ClIrN_6$ (M^+-PF_6^-): **831.1605**, Found: **831.1603**.

Complex 4.5:

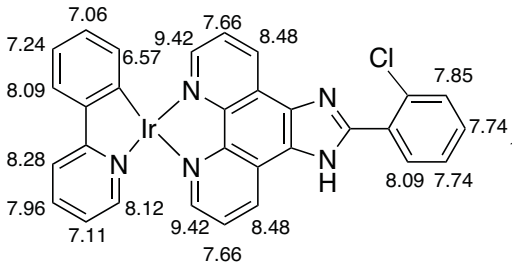

(16.2 mg, 74%). ^{1}H NMR (400 MHz, CD_3CN): δ = 9.42 (br s, 2H), 8.48 (d, 1H), 8.28 (d, 2H), 8.12 (d, 2H), 8.09 (m, 3H), 7.96 (t, 2H), 7.85 (d, 1H), 7.74 (m, 2H), 7.66 (d, 2H), 7.24 (t, 2H), 7.11 (t, 2H), 7.06 (t, 2H), 6.57 (d, 2H) ppm; ^{13}C NMR (400 MHz, CD_3CN): δ = 166.6, 148.6, 147.7, 147.3, 143.6, 142.7, 136.8, 130.6, 130.5, 130.2, 128.9, 128.8, 125.9, 125.3, 123.3, 121.7, 121.1, 118.2 ppm; Elemental Analysis calculated for $IrC_{41}H_{27}ClN_6F_6P•½(CHCl_3)•H_2O$ (as integrated from ^{1}H NMR): C – 47.29; H – 2.82; N – 7.97. Found: C – 47.32; H – 2.82; N – 7.66; HR-MS Calculated for $C_{41}H_{27}ClIrN_6$ (M^+-PF_6^-): **831.1605**, Found: **831.1592**.

Complex 4.6:

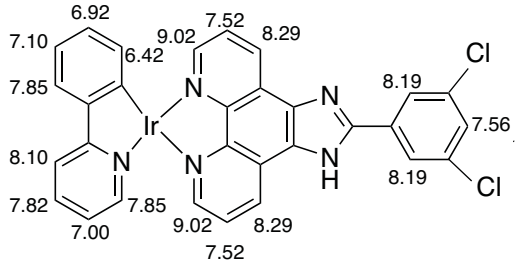

(34.7 mg, 96%). ^{1}H NMR (500 MHz, CD_3CN): δ = 9.01 (d, 2H), 8.29 (d, 2H), 8.19 (d, 2H), 8.09 (d, 2H), 7.85 (m, 4H), 7.82 (t, 2H), 7.56 (s, 1H), 7.52 (d, 2H), 7.10 (t, 2H), 7.00 (t, 2H), 6.92 (t, 2H), 6.42 (d, 2H); ^{13}C NMR (500 MHz, CD_3CN): δ = 167.5, 150.2, 149.5, 149.4, 145.1, 144.3, 138.5, 135.6, 132.1, 131.7, 130.4, 129.6, 125.0, 124.9, 123.4, 122.7, 119.9 ppm; Elemental Analysis calculated for $IrC_{41}H_{26}Cl_2N_6F_6P$: C – 48.72; H – 2.59; N – 8.31. Found: C – 48.46; H – 2.53; N – 8.14; HR-MS Calculated for $C_{41}H_{26}Cl_2IrN_6$ (M^+-PF_6^-): **865.1208**, Found: **865.1196**.

4.5.3 Crystal structure determination (Performed by Dr. Christopher J. Serpell)

*4.5.3.1 Complex **4.3***

Single crystal X-ray diffraction data were collected using graphite monochromated Mo Kα radiation (λ = 0.71073 Å) on a Bruker APEX2 diffractometer. The diffractometer was equipped with a Kryoflex N_2 open-flow cooling device, and the data were collected at 100(2) K. Series of ω-scans were performed in such a way as to cover a sphere of data to a maximum resolution of 0.77 Å. Cell parameters and intensity data (including inter-frame scaling) were processed using the APEX2 package. The structure was solved by direct methods using the SIR92 software[91] and refined using full-matrix least-squares on F^2 within the CRYSTALS suite.[92] All non-hydrogen atoms were refined with anisotropic displacement parameters, unless specified otherwise. The H atoms could be seen in the difference map, but those attached to carbon atoms were repositioned geometrically. Q-peaks for protic H atoms were confirmed by examining hydrogen bonding requirements. The H atoms were initially refined with soft restraints on the bond lengths and angles to regularise their geometry (C-H in the range 0.93−0.98 Å, N-H in the range 0.86−0.89 Å and isotropic displacement factors in the range 1.2−1.5 times U_{eq} of the parent atom), after which the positions were refined with riding constraints. After the construction of a stable, physically reasonable, and complete model, twinning was assessed and refined using ROTAX[93] and then the weights were optimised,[94,95] leading to convergence of the refinement. IUCr CheckCIF/PLATON was used to validate the final structure.

Single Crystal X-ray Diffraction Data: Crystal data for **4.3**: $C_{41}H_{27}N_6F_3{\bullet}BF_4{\bullet}CH_2Cl_2$, M = 1036.65, orthorhombic, a = 19.0940(14) Å, b = 29.615(2) Å, c = 13.6657(10) Å, α = 90°, β = 90°, γ = 90°, V = 7727.4(10) $Å^3$, T = 100 K, space group $Pna2_1$, Z = 8, 86919 reflections measured, 18119 independent reflections (Rint = 0.033). The final R1 values were 0.0219 (I >

2σ(I)). The final wR(F2) values were 0.0507 (I > 2σ(I)). The final R1 values were 0.0252 (all data). The final wR(F2) values were 0.0535 (all data).

4.5.3.2 Complex 4.4

Single crystal X-ray diffraction data were collected using graphite monochromated Mo Kα radiation (λ = 0.71073 Å) on an Bruker APEX2 diffractometer. The diffractometer was equipped with a Kryoflex N_2 open-flow cooling device, and the data were collected at 100(2) K. Series of ω-scans were performed in such a way as to cover a sphere of data to a maximum resolution of 0.77 Å. Cell parameters and intensity data (including inter-frame scaling) were processed using the APEX2 package. The structure was solved by direct methods using the SuperFlip software[96] and refined using full-matrix least-squares on F^2 within the CRYSTALS suite.[92] All non-hydrogen atoms were refined with anisotropic displacement parameters. After structure solution, the structure of the main residues was clear. Solvent and anion molecules were completed using Fourier difference cycles, and were less ordered than the metal complexes, requiring geometric restraints, and modelling of disorder in the case of one PF_6^- ion. The H atoms were added geometrically to carbons and initially refined with soft restraints on the bond lengths and angles to regularise their geometry (C-H in the range 0.93−0.98 Å and isotropic displacement factors in the range 1.2−1.5 times Ueq of the parent atom), after which the positions were refined with riding constraints. Protic hydrogen atoms were placed geometrically, using C-N or C-O bond lengths to determine the correct tautomer, and those on water molecules were positioned to satisfy hydrogen bonding demands. Subsequently, the protic hydrogens were refined using riding constraints. Although the majority of the thermal motion was found apart from the main residue, a number of atoms in the metal complexes also displayed physically unreasonable displacement parameters, and since individual restraint of these features failed to give satisfactory results, global restraint of displacement parameters was applied. The weights were optimised,[94,95] leading to convergence of the refinement. IUCr CheckCIF/PLATON was used to validate the final structure.

Single Crystal X-ray Diffraction Data: Crystal data for **4.4**: $C_{41}H_{27}ClIrN_6 \bullet F_6P \bullet 3(C_2H_4O_2) \bullet H_2O$, M = 1174.52, triclinic, a = 13.160(2) Å, b = 18.199(3) Å, c = 21.573(3) Å, α = 67.005(2)°, β = 76.589(2)°, γ = 74.541(2)°, V = 4536.2(12) Å^3, T = 100 K, space group $P\bar{1}$, Z = 4, 52465 reflections measured, 20627 independent reflections (R_{int} = 0.134). The final R_1 values were 0.0603 ($I > 2\sigma(I)$). The final $wR(F^2)$ values were 0.1409 ($I > 2\sigma(I)$). The final R_1 values were 0.1385 (all data). The final $wR(F^2)$ values were 0.2323 (all data).

4.5.4 Absorption and luminescence studies

Absorption spectra were performed at 25°C on a CaryBio-300 spectrometer. Fluorescence measurements were performed on an Agilent Technologies Cary Eclipse Fluorescence Spectrophotometer. All iridium(II) complexes (**4.1-4.6**) were prepared as 10 mM stock solutions in both DMSO and ACN and stored at 4°C.

4.5.4.1 Oligonucleotides

The 22AG and cmyc DNA oligonucleotides were obtained from SigmaGenosys Canada. All other promoter DNA sequences were obtained from IDT DNA. The 26mer oligonucleotide was synthesized in-house on a MerMade 6 DNA synthesizer from BioAutomation Corporation. Reagents used for automated DNA synthesis were purchased from ChemGenes Incorporated. Oligonucleotides were dissolved in deionized water prior to use and quantified spectrophotometrically at 95°C using their molar extinction coefficients[97] at 260 nm (Table 4.4). To anneal the G-quadruplexes for the luminescence assays, concentrated solutions of DNA in 1xNa or 1xK buffer (10 mM sodium cacodylate with 100 mM NaCl or 100 mM KCl, pH 7.2), where appropriate, were heated to 95°C for 10 minutes and then rapidly cooled to room temperature. The solutions were stored overight at 4°C before being diluted to the final concentrations in appropriate buffer before use. To anneal the ds26mer, a concentrated solution of the DNA in 1xNa buffer was heated to 95°C for 10 minutes and allowed to slowly cool to room temperature over 7 h. The solution was stored overnight at 4°C before being diluted to the final concentration in 1xNa buffer before use.

4.5.4.2 Luminescence assay

Dilutions of the pre-annealed nucleic acid stock solutions in 1x buffer were diluted from the concentrated stock solutions in 1x buffer to 0.5 μM. For each iridium(II) complex, a solution of 10 μM complex in 1x buffer was prepared from the concentrated stock solutions in DMSO. All robotics methods were performed on a Biomek FX liquid handler and a SAGIAN core robot (Beckman) at the CIAN core facility by Dr. Guillaume Lesage (Department of Biology, McGill University). Briefly, buffer and complexes were aspirated from dedicated reservoirs in a two-step procedure (buffer first (Figure S4.1), then complex (Figure S4.2) for a total volume of 40 μL) into black 384-well plates (Fluoroplates, Nunc). The complexes are tested in quadruplicate (that is four complexes per plate) where the appropriate buffer is first dispensed in decreasing volumes across the rows (40 to 0 μL), followed by each complex (10 μM stock solution in appropriate buffer) dispensed in increasing volumes across the rows (0 to 40 μL). Then, such that the final volume is 80 μL, 40 μL of 0.5 μM sequence is transferred to every well using the 96-multichannel pipetting head. The final concentrations of complex from column 1 to column 24 are 0.00, 0.125, 0.250, 0.375, 0.500, 0.625, 0.750, 0.875, 1.00, 1.13, 1.25, 1.38, 1.50, 1.75, 2.00, 2.25, 2.50, 2.75, 3.00, 3.25, 3.50, 4.00, 4.50, and 5.00 μM. The plates were allowed to incubate at room temperature for ~ 20 minutes before measuring the luminescence. Luminescence intensity was measured on a plate reader (DTX 880, Beckman) equipped with 260 ± 10 nm and 595 ± 35 nm filters for excitation and emission, respectively. A blank run containing complexes in a solution of 1xNa or 1xK buffer only was obtained for background luminescence subtration. These values were subsequently subtracted from the raw values with DNA sequences before the luminescence intensity was graphed (y-axis) versus the complex concentration (x-axis). K_D values were obtained from fitting of the curves to a one-site binding model in GraphPad Prism 5.

buffer

		1	2	3	4	5	6	7	8	9	10	11	12	13	14	15	16	17	18	19	20	21	22	23	24
compound 1	A	40	39	38	37	36	35	34	33	32	31	30	29	28	26	24	22	20	18	16	14	12	8	4	0
	B	40	39	38	37	36	35	34	33	32	31	30	29	28	26	24	22	20	18	16	14	12	8	4	0
	C	40	39	38	37	36	35	34	33	32	31	30	29	28	26	24	22	20	18	16	14	12	8	4	0
	D	40	39	38	37	36	35	34	33	32	31	30	29	28	26	24	22	20	18	16	14	12	8	4	0
compound 2	E	40	39	38	37	36	35	34	33	32	31	30	29	28	26	24	22	20	18	16	14	12	8	4	0
	F	40	39	38	37	36	35	34	33	32	31	30	29	28	26	24	22	20	18	16	14	12	8	4	0
	G	40	39	38	37	36	35	34	33	32	31	30	29	28	26	24	22	20	18	16	14	12	8	4	0
	H	40	39	38	37	36	35	34	33	32	31	30	29	28	26	24	22	20	18	16	14	12	8	4	0
compound 3	I	40	39	38	37	36	35	34	33	32	31	30	29	28	26	24	22	20	18	16	14	12	8	4	0
	J	40	39	38	37	36	35	34	33	32	31	30	29	28	26	24	22	20	18	16	14	12	8	4	0
	K	40	39	38	37	36	35	34	33	32	31	30	29	28	26	24	22	20	18	16	14	12	8	4	0
	L	40	39	38	37	36	35	34	33	32	31	30	29	28	26	24	22	20	18	16	14	12	8	4	0
compound 4	M	40	39	38	37	36	35	34	33	32	31	30	29	28	26	24	22	20	18	16	14	12	8	4	0
	N	40	39	38	37	36	35	34	33	32	31	30	29	28	26	24	22	20	18	16	14	12	8	4	0
	O	40	39	38	37	36	35	34	33	32	31	30	29	28	26	24	22	20	18	16	14	12	8	4	0
	P	40	39	38	37	36	35	34	33	32	31	30	29	28	26	24	22	20	18	16	14	12	8	4	0

Figure S4.1 Luminescence assay plate layout showing volumes of buffer for the first addition.

	10uM Stock	1	2	3	4	5	6	7	8	9	10	11	12	13	14	15	16	17	18	19	20	21	22	23	24
compound 1	A	0	1	2	3	4	5	6	7	8	9	10	11	12	14	16	18	20	22	24	26	28	32	36	40
	B	0	1	2	3	4	5	6	7	8	9	10	11	12	14	16	18	20	22	24	26	28	32	36	40
	C	0	1	2	3	4	5	6	7	8	9	10	11	12	14	16	18	20	22	24	26	28	32	36	40
	D	0	1	2	3	4	5	6	7	8	9	10	11	12	14	16	18	20	22	24	26	28	32	36	40
compound 2	E	0	1	2	3	4	5	6	7	8	9	10	11	12	14	16	18	20	22	24	26	28	32	36	40
	F	0	1	2	3	4	5	6	7	8	9	10	11	12	14	16	18	20	22	24	26	28	32	36	40
	G	0	1	2	3	4	5	6	7	8	9	10	11	12	14	16	18	20	22	24	26	28	32	36	40
	H	0	1	2	3	4	5	6	7	8	9	10	11	12	14	16	18	20	22	24	26	28	32	36	40
compound 3	I	0	1	2	3	4	5	6	7	8	9	10	11	12	14	16	18	20	22	24	26	28	32	36	40
	J	0	1	2	3	4	5	6	7	8	9	10	11	12	14	16	18	20	22	24	26	28	32	36	40
	K	0	1	2	3	4	5	6	7	8	9	10	11	12	14	16	18	20	22	24	26	28	32	36	40
	L	0	1	2	3	4	5	6	7	8	9	10	11	12	14	16	18	20	22	24	26	28	32	36	40
compound 4	M	0	1	2	3	4	5	6	7	8	9	10	11	12	14	16	18	20	22	24	26	28	32	36	40
	N	0	1	2	3	4	5	6	7	8	9	10	11	12	14	16	18	20	22	24	26	28	32	36	40
	O	0	1	2	3	4	5	6	7	8	9	10	11	12	14	16	18	20	22	24	26	28	32	36	40
	P	0	1	2	3	4	5	6	7	8	9	10	11	12	14	16	18	20	22	24	26	28	32	36	40

Figure S4.2 Luminescence assay plate layout showing volumes of complex added for the second addition.

4.5.4.3 Job plots

Solutions of 10 μM G-quadruplexes in 1xK buffer were diluted from pre-annealed concentrated stock solutions. Solutions of 10 μM iridium complexes in 1xK buffer were diluted from 10 mM stock solutions in DMSO. In a 96-well black polypropylene microplate, the mole fraction of each component (DNA and complex) was varied, while total concentration stayed constant at 10 μM in 200 μL total volume. The mole fraction of the complexes increased from 0−1 across

the rows while the DNA decreased from 1−0. Each row contained a different sequence (6 in total) and each plate contained one complex. In brief, well A1 contained 200 μL of 10 μM DNA (mole ratio 1:0), well A2 contained 180 μL of 10 μM DNA and 20 μL of 10 μM complex (mole ratio 0.9:0.1), well A3 contained 160 μL of 10 μM DNA and 40 μL of 10 μM complex (mole ratio 0.8:0.2), etc. After plating, the plates were allowed to slowly rock on a plate shaker for 20 minutes before reading the luminescence on the BioTek® Synergy plate reader (excitation filter: 310 ± 20 nm and emission filter: 590 ± 20 nm). After 90 minutes had elapsed after plating, the luminescence was measured again. A blank was run for each complex in 1xK buffer and was used as a linear baseline subtraction. Then, linear regression analysis was performed in GraphPad Prism 5 for each set of data points.

4.5.5 Electrochemistry and electrogenerated chemiluminescence (Performed by Dr. Kimberly Metera and Dr. Ushula Tefashe)

4.5.5.1 Cyclic voltammetry

Tripropylamine (TPrA or TPA) and tetrabutylammonium hexafluorophosphate ($TBAPF_6$) were purchased from Sigma-Aldrich and used as received. Sample concentrations were 0.5 mM in acetonitrile containing 0.1 M $TBAPF_6$ (for CV) and 0.1 M $TBAPF_6$ + 0.05 M TPrA (for ECL).

The electrochemical experiments were conducted using a three-electrode setup with a 3 mm diameter glassy carbon (GC) working electrode (MF-2012, BASi Stationary Voltammetry Electrodes), a 0.5 mm diameter platinum wire counter electrode, and a silver/silver chloride quasi-reference electrode (Ag/AgCl QRE) (Goodfellow). The cyclic voltammetry (CV) experiments were conducted using an ELP3 HEKA bipotentiostat (HEKA Electronik, Germany) controlled by Potmaster software. For CV experiments, the potential was cycled between −1.25 and 1.6 V. Half-wave potentials ($E_{1/2}$) are reported versus the Ag/AgCl pseudo-reference electrode. The cell was made from teflon with a small opening in the bottom into which the GC working electrode was tightly fitted. The working electrode was cleaned and polished prior to each experiment. The GC electrode

was polished on a microcloth pad (Struers MD Chem cloth) using a water-based alumina slurry (0.05 μm).

4.5.5.2 Electrogenerated chemiluminescence

The same electrochemical setup as for CV was used for the ECL experiments. The ECL response was detected using a Jaz Spectrometer (Ocean Optics) coupled with an Ocean Optics Vis-NIR fiber optic cable positioned at a fixed position directly above the working electrode, and recorded using Ocean Optics software. The potential was cycled between −2.0 and 2.2 V. During ECL experiments, the integrated ECL light intensity from 500−800 nm was measured using the Ocean Optics software. For most ECL experiments, the integrated intensity during 5 consecutive CV scans was recorded and an average and standard deviation for each experiment was obtained. The data were normalized to the average ECL intensity of the phenyl- complex **4.1**.

4.6 References

1. Dixon, I. M.; Lopez, F.; Esteve, J. P.; Tejera, A. M.; Blasco, M. A.; Pratviel, G.; Meunier, B., Porphyrin derivatives for telomere binding and telomerase inhibition. *ChemBioChem* **2005,** *6* (1), 123-132.
2. Dixon, I. M.; Lopez, F.; Tejera, A. M.; Esteve, J. P.; Blasco, M. A.; Pratviel, G.; Meunier, B., A G-quadruplex ligand with 10000-fold selectivity over duplex DNA. *J Am Chem Soc* **2007,** *129* (6), 1502-1503.
3. Romera, C.; Bombarde, O.; Bonnet, R.; Gomez, D.; Dumy, P.; Calsou, P.; Gwan, J. F.; Lin, J. H.; Defrancq, E.; Pratviel, G., Improvement of porphyrins for G-quadruplex DNA targeting. *Biochimie* **2011,** *93* (8), 1310-1317.
4. Khan, N. U.; Pandya, N.; Kumar, M.; Bera, P. K.; Kureshy, R. I.; Abdi, S. H.; Bajaj, H. C., Influence of chirality using Mn(III) salen complexes on DNA binding and antioxidant activity. *Org Biomol Chem* **2010,** *8* (19), 4297-4307.
5. Rajput, C.; Rutkaite, R.; Swanson, L.; Haq, I.; Thomas, J. A., Dinuclear monointercalating RuII complexes that display high affinity binding to duplex and quadruplex DNA. *Chem Eur J* **2006,** *12* (17), 4611-4619.
6. Shi, S.; Liu, J.; Yao, T.; Geng, X.; Jiang, L.; Yang, Q.; Cheng, L.; Ji, L., Promoting the formation and stabilization of G-quadruplex by dinuclear RuII complex $Ru_2(obip)L_4$. *Inorg Chem* **2008,** *47* (8), 2910-2912.

7. Rickling, S.; Ghisdavu, L.; Pierard, F.; Gerbaux, P.; Surin, M.; Murat, P.; Defrancq, E.; Moucheron, C.; Kirsch-De Mesmaeker, A., A rigid dinuclear ruthenium(II) complex as an efficient photoactive agent for bridging two guanine bases of a duplex or quadruplex oligonucleotide. *Chem Eur J* **2010,** *16* (13), 3951-3961.
8. Wilson, T.; Williamson, M. P.; Thomas, J. A., Differentiating quadruplexes: binding preferences of a luminescent dinuclear ruthenium(II) complex with four-stranded DNA structures. *Org Biomol Chem* **2010,** *8* (11), 2617-2621.
9. Sun, D.; Liu, Y.; Liu, D.; Zhang, R.; Yang, X.; Liu, J., Stabilization of G-quadruplex DNA, inhibition of telomerase activity and live cell imaging studies of chiral ruthenium(II) complexes. *Chem Eur J* **2012,** *18* (14), 4285-4295.
10. Sun, D.; Zhang, R.; Yuan, F.; Liu, D.; Zhou, Y.; Liu, J., Studies on characterization, telomerase inhibitory properties and G-quadruplex binding of η6-arene ruthenium complexes with 1,10-phenanthroline-derived ligands. *Dalton Trans* **2012,** *41* (6), 1734-1741.
11. Reed, J. E.; Arnal, A. A.; Neidle, S.; Vilar, R., Stabilization of G-quadruplex DNA and inhibition of telomerase activity by square-planar nickel(II) complexes. *J Am Chem Soc* **2006,** *128* (18), 5992-5993.
12. Campbell, N. H.; Karim, N. H.; Parkinson, G. N.; Gunaratnam, M.; Petrucci, V.; Todd, A. K.; Vilar, R.; Neidle, S., Molecular basis of structure-activity relationships between salphen metal complexes and human telomeric DNA Quadruplexes. *J Med Chem* **2012,** *55* (1), 209-222.
13. Fu, B.; Zhang, D.; Weng, X.; Zhang, M.; Heng, M.; Yuzhi, M.; Zhou, X., Cationic metal-corrole complexes: Design, synthesis, and properties of guanine-quadruplex stabilizers. *Chem Eur J* **2008,** *14* (30), 9431-9441.
14. Ren, L.; Zhang, A.; Huang, J.; Wang, P.; Weng, X.; Zhang, L.; Liang, F.; Tan, Z.; Zhou, X., Quaternary ammonium zinc phthalocyanine: inhibiting telomerase by stabilizing G quadruplexes and inducing G-quadruplex structure transition and formation. *ChemBioChem* **2007,** *8* (7), 775-780.
15. Bhattacharjee, A. J.; Ahluwalia, K.; Taylor, S.; Jin, O.; Nicoludis, J. M.; Buscaglia, R.; Brad Chaires, J.; Kornfilt, D. J.; Marquardt, D. G.; Yatsunyk, L. A., Induction of G-quadruplex DNA structure by Zn(II) 5,10,15,20-tetrakis(N-methyl-4-pyridyl)porphyrin. *Biochimie* **2011,** *93* (8), 1297-1309.
16. Largy, E.; Hamon, F.; Rosu, F.; Gabelica, V.; De Pauw, E.; Guedin, A.; Mergny, J. L.; Teulade-Fichou, M. P., Tridentate N-donor palladium(II) complexes as efficient coordinating quadruplex DNA binders. *Chem Eur J* **2011,** *17* (47), 13274-13283.
17. Georgiades, S. N.; Abd Karim, N. H.; Suntharalingam, K.; Vilar, R., Interaction of metal complexes with G-quadruplex DNA. *Angew Chem Int Ed* **2010,** *49* (24), 4020-4034.
18. Barton, J. K.; Danishefsky, A.; Goldberg, J., Tris(phenanthroline)ruthenium(II): stereoselectivity in binding to DNA. *J Am Chem Soc* **1984,** *106* (7), 2172-2176.

19. Kumar, C. V.; Barton, J. K.; Turro, N. J., Photophysics of ruthenium complexes bound to double helical DNA. *J Am Chem Soc* **1985,** *107* (19), 5518-5523.
20. Pyle, A. M.; Rehmann, J. P.; Meshoyrer, R.; Kumar, C. V.; Turro, N. J.; Barton, J. K., Mixed-Ligand Complexes of Ruthenium(II) - Factors Governing Binding to DNA. *J Am Chem Soc* **1989,** *111* (8), 3051-3058.
21. Jenkins, Y.; Friedman, A. E.; Turro, N. J.; Barton, J. K., Characterization of dipyridophenazine complexes of ruthenium(II): The light switch effect as a function of nucleic acid sequence and conformation. *Biochemistry* **1992,** *31* (44), 10809-10816.
22. Lin, S.; Struve, W. S., Time-Resolved Fluorescence of Nitrobenzoxadiazole-Aminohexanoic Acid: Effect of Intermolecular Hydrogen-Bonding on Non-Radiative Decay. *Photochem Photobiol* **1991,** *54* (3), 361-365.
23. Yao, J. L.; Gao, X.; Sun, W.; Fan, X. Z.; Shi, S.; Yao, T. M., A naked-eye on-off-on molecular "light switch" based on a reversible "conformational switch" of G-quadruplex DNA. *Inorg Chem* **2012,** *51* (23), 12591-12593.
24. Lee, W. Y., Tris (2,2'-bipyridyl)ruthenium(II) Electrogenerated Chemiluminescence in Analytical Science. *Mikrochim Acta* **1997,** *127* (1--2), 19-39.
25. Su, M.; Liu, S., Solid-state electrochemiluminescence analysis with coreactant of the immobilized tris(2,2'-bipyridyl) ruthenium. *Anal Biochem* **2010,** *402* (1), 1-12.
26. Wei, H.; Wang, E., Electrochemiluminescence of tris(2,2'-bipyridyl)ruthenium and its applications in bioanalysis: A review. *Luminescence* **2011,** *26* (2), 77-85.
27. Li, J.; Wang, E., Applications of tris(2,2'-bipyridyl)ruthenium(II) in electrochemiluminescence. *Chemical Record* **2012,** *12* (1), 177-187.
28. Forster, R. J.; Bertoncello, P.; Keyes, T. E., Electrogenerated chemiluminescence. *Annu Rev Anal Chem (Palo Alto Calif)* **2009,** *2*, 359-385.
29. Hu, L.; Xu, G., Applications and trends in electrochemiluminescence. *Chem Soc Rev* **2010,** *39* (8), 3275-3304.
30. Yu, Y.; Young, J.; Meng, Y. G., Electrochemiluminescence to detect surface proteins on live cells. *Curr Opin Pharmacol* **2007,** *7* (5), 541-546.
31. Sardesai, N.; Pan, S.; Rusling, J., Electrochemiluminescent immunosensor for detection of protein cancer biomarkers using carbon nanotube forests and $[Ru(bpy)_3]^{2+}$-doped silica nanoparticles. *Chem Commun* **2009,** (33), 4968-4970.
32. Miao, W.; Bard, A. J., Electrogenerated chemiluminescence. 77. DNA hybridization detection at high amplification with $[Ru(bpy)_3]^{2+}$-containing microspheres. *Anal Chem* **2004,** *76* (18), 5379-5386.
33. Lee, J. G.; Yun, K.; Lim, G. S.; Lee, S. E.; Kim, S.; Park, J. K., DNA biosensor based on the electrochemiluminescence of $[Ru(bpy)_3]^{2+}$ with DNA-binding intercalators. *Bioelectrochemistry* **2007,** *70* (2), 228-234.

34. Bruno, J. G.; Kiel, J. L., In vitro selection of DNA aptamers to anthrax spores with electrochemiluminescence detection. *Biosens Bioelectron* **1999,** *14* (5), 457-464.
35. Bruno, J. G.; Kiel, J. L., Use of magnetic beads in selection and detection of biotoxin aptamers by electrochemiluminescence and enzymatic methods. *BioTechniques* **2002,** *32* (1), 178-183.
36. Kapturkiewicz, A.; Angulo, G., Extremely efficient electrochemiluminescence systems based on tris(2-phenylpyridine)iridium(iii). *Dalton Trans* **2003,** (20), 3907.
37. Li, C.; Lin, J.; Guo, Y.; Zhang, S., A novel electrochemiluminescent reagent of cyclometalated iridium complex-based DNA biosensor and its application in cancer cell detection. *Chem Commun* **2011,** *47* (15), 4442-4444.
38. Li, C.; Lin, J.; Yang, X.; Wan, J., Efficient electrochemiluminescent cyclometalated iridium(III) complexes: Synthesis, photophysical and electrochemiluminescent properties. *J Organomet Chem* **2011,** *696* (11-12), 2445-2450.
39. Swanick, K. N.; Ladouceur, S.; Zysman-Colman, E.; Ding, Z., Bright electrochemiluminescence of iridium(III) complexes. *Chem Commun* **2012,** *48* (26), 3179-3181.
40. Yu, L.; Huang, Z.; Liu, Y.; Zhou, M., Photophysics, electrochemistry and electrochemiluminescence of water-soluble biscyclometalated iridium (III) complexes. *J Organomet Chem* **2012,** *718*, 14-21.
41. Zhu, S.; Song, Q.; Zhang, S.; Ding, Y., Effects of the frontier orbitals on the electrochemical and electrochemiluminescent properties of the bis-cyclometalated iridium(III) complexes with different ligands. *J Mol Struct* **2013,** *1035*, 224-230.
42. Dixon, I. M.; Collin, J.-P.; Sauvage, J.-P.; Flamigni, L.; Encinas, S.; Barigelletti, F., A family of luminescent coordination compounds: iridium(iii) polyimine complexes. *Chem Soc Rev* **2000,** *29* (6), 385-391.
43. Sajoto, T.; Djurovich, P. I.; Tamayo, A.; Yousufuddin, M.; Bau, R.; Thompson, M. E.; Holmes, R. J.; Forrest, S. R., Blue and near-UV phosphorescence from iridium complexes with cyclometalated pyrazolyl or N-heterocyclic carbene ligands. *Inorg Chem* **2005,** *44* (22), 7992-8003.
44. Yang, H.; Ma, V. P. Y.; Chan, D. S. H.; He, H. Z.; Leung, C. H.; Ma, D. L., A Cyclometallated Iridium(III) Complex As a c-myc G-Quadruplex Stabilizer and Down-Regulator of c-myc Oncogene Expression. *Curr Med Chem* **2013,** *20* (4), 576-582.
45. Kiran, R. V.; Zammit, E. M.; Hogan, C. F.; James, B. D.; Barnett, N. W.; Francis, P. S., Chemiluminescence from reactions with bis-cyclometalated iridium complexes in acidic aqueous solution. *Analyst* **2009,** *134* (7), 1297-1298.
46. Kiran, R. V.; Hogan, C. F.; James, B. D.; Wilson, D. J. D., Photophysical and Electrochemical Properties of Phenanthroline-Based Bis-cyclometallated Iridium Complexes in Aqueous and Organic Media. *Eur J Inorg Chem* **2011,** *2011* (31), 4816-4825.

47. Sprouse, S.; King, K. A.; Spellane, P. J.; Watts, R. J., Photophysical effects of metal-carbon .sigma. bonds in ortho-metalated complexes of iridium(III) and rhodium(III). *J Am Chem Soc* **1984,** *106* (22), 6647-6653.
48. Zhao, Q.; Liu, S.; Shi, M.; Li, F.; Jing, H.; Yi, T.; Huang, C., Tuning photophysical and electrochemical properties of cationic Iridium(III) complex salts with imidazolyl substituents by proton and anions. *Organometallics* **2007,** *26* (24), 5922-5930.
49. Dragonetti, C.; Falciola, L.; Mussini, P.; Righetto, S.; Roberto, D.; Ugo, R.; Valore, A.; De Angelis, F.; Fantacci, S.; Sgamellotti, A.; Ramon, M.; Muccini, M., The role of substituents on functionalized 1,10-phenanthroline in controlling the emission properties of cationic iridium(III) complexes of interest for electroluminescent devices. *Inorg Chem* **2007,** *46* (21), 8533-8547.
50. Zhao, Q.; Liu, S.; Shi, M.; Wang, C.; Yu, M.; Li, L.; Li, F.; Yi, T.; Huang, C., Series of new cationic iridium(III) complexes with tunable emission wavelength and excited state properties: structures, theoretical calculations, and photophysical and electrochemical properties. *Inorg Chem* **2006,** *45* (16), 6152-6160.
51. Lo, K. K.; Chung, C. K.; Zhu, N., Nucleic acid intercalators and avidin probes derived from luminescent cyclometalated iridium(III)-dipyridoquinoxaline and -dipyridophenazine complexes. *Chem Eur J* **2006,** *12* (5), 1500-1512.
52. Neve, F.; La Deda, M.; Crispini, A.; Bellusci, A.; Puntoriero, F.; Campagna, S., Cationic Cyclometalated Iridium Luminophores: Photophysical, Redox, and Structural Characterization. *Organometallics* **2004,** *23* (24), 5856-5863.
53. Juris, A.; Balzani, V.; Barigelletti, F.; Campagna, S.; Belser, P.; von Zelewsky, A., Ru(II) polypyridine complexes: photophysics, photochemistry, eletrochemistry, and chemiluminescence. *Coord Chem Rev* **1988,** *84*, 85-277.
54. Lepeltier, M.; Kwok-Ming Lee, T.; Kam-Wing Lo, K.; Toupet, L.; Le Bozec, H.; Guerchais, V. R., Synthesis, Structure, and Photophysical and Electrochemical Properties of Cyclometallated Iridium(III) Complexes with Phenylated Bipyridine Ligands. *Eur J Inorg Chem* **2005,** *2005* (1), 110-117.
55. Lowry, M. S.; Hudson, W. R.; Pascal, R. A., Jr.; Bernhard, S., Accelerated luminophore discovery through combinatorial synthesis. *J Am Chem Soc* **2004,** *126* (43), 14129-14135.
56. Wilde, A. P.; King, K. A.; Watts, R. J., Resolution and analysis of the components in dual emission of mixed-chelate/ortho-metalate complexes of iridium(III). *J Phys Chem* **1991,** *95* (2), 629-634.
57. Colombo, M. G.; Guedel, H. U., Synthesis and high-resolution optical spectroscopy of bis[2-(2-thienyl)pyridinato-C3,N'](2,2'-bipyridine)iridium(III). *Inorg Chem* **1993,** *32* (14), 3081-3087.

58. Colombo, M. G.; Hauser, A.; Guedel, H. U., Evidence for strong mixing between the LC and MLCT excited states in bis(2-phenylpyridinato-C2,N')(2,2'-bipyridine)iridium(III). *Inorg Chem* **1993,** *32* (14), 3088-3092.

59. Friedman, A. E.; Chambron, J. C.; Sauvage, J. P.; Turro, N. J.; Barton, J. K., A molecular light switch for DNA: $Ru(bpy)_2(dppz)^{2+}$. *J Am Chem Soc* **1990,** *112* (12), 4960-4962.

60. Sabatani, E.; Nikol, H. D.; Gray, H. B.; Anson, F. C., Emission Spectroscopy of $Ru(bpy)_2dppz^{2+}$ in Nafion. Probing the Chemical Environment in Cast Films. *J Am Chem Soc* **1996,** *118* (5), 1158-1163.

61. Olson, E. J. C.; Hu, D.; Hörmann, A.; Jonkman, A. M.; Arkin, M. R.; Stemp, E. D. A.; Barton, J. K.; Barbara, P. F., First Observation of the Key Intermediate in the "Light-Switch" Mechanism of $[Ru(phen)_2dppz]^{2+}$. *J Am Chem Soc* **1997,** *119* (47), 11458-11467.

62. Onfelt, B.; Lincoln, P.; Norden, B.; Baskin, J. S.; Zewail, A. H., Femtosecond linear dichroism of DNA-intercalating chromophores: solvation and charge separation dynamics of $[Ru(phen)_2dppz]^{2+}$ systems. *Proc Natl Acad Sci USA* **2000,** *97* (11), 5708-5713.

63. Luu, K. N.; Phan, A. T.; Kuryavyi, V.; Lacroix, L.; Patel, D. J., Structure of the human telomere in K^+ solution: an intramolecular (3+1) G-quadruplex scaffold. *J Am Chem Soc* **2006,** *128* (30), 9963-9970.

64. Ambrus, A.; Chen, D.; Dai, J.; Jones, R. A.; Yang, D., Solution structure of the biologically relevant G-quadruplex element in the human c-MYC promoter. Implications for G-quadruplex stabilization. *Biochemistry* **2005,** *44* (6), 2048-58.

65. Gabelica, V.; Baker, E. S.; Teulade-Fichou, M. P.; De Pauw, E.; Bowers, M. T., Stabilization and structure of telomeric and c-myc region intramolecular G-quadruplexes: the role of central cations and small planar ligands. *J Am Chem Soc* **2007,** *129* (4), 895-904.

66. Bejugam, M.; Sewitz, S.; Shirude, P. S.; Rodriguez, R.; Shahid, R.; Balasubramanian, S., Trisubstituted isoalloxazines as a new class of G-quadruplex binding ligands: small molecule regulation of c-kit oncogene expression. *J Am Chem Soc* **2007,** *129* (43), 12926-12927.

67. Bejugam, M.; Gunaratnam, M.; Müller, S.; Sanders, D. A.; Sewitz, S.; Fletcher, J. A.; Neidle, S.; Balasubramanian, S., Targeting the c-Kit Promoter G-quadruplexes with 6-Substituted Indenoisoquinolines. *ACS Med Chem Lett* **2010,** *1* (7), 306-310.

68. McLuckie, K. I.; Waller, Z. A.; Sanders, D. A.; Alves, D.; Rodriguez, R.; Dash, J.; McKenzie, G. J.; Venkitaraman, A. R.; Balasubramanian, S., G-quadruplex-binding benzo[a]phenoxazines down-regulate c-KIT expression in human gastric carcinoma cells. *J Am Chem Soc* **2011,** *133* (8), 2658-2663.

69. Siddiqui-Jain, A.; Grand, C. L.; Bearss, D. J.; Hurley, L. H., Direct evidence for a G-quadruplex in a promoter region and its targeting with a small molecule to repress c-MYC transcription. *Proc Natl Acad Sci USA* **2002,** *99* (18), 11593-11598.

70. Wu, P.; Ma, D. L.; Leung, C. H.; Yan, S. C.; Zhu, N.; Abagyan, R.; Che, C. M., Stabilization of G-quadruplex DNA with platinum(II) Schiff base complexes: Luminescent probe and down-regulation of c-myc oncogene expression. *Chem Eur J* **2009,** *15* (47), 13008-13021.
71. Agarwal, T.; Roy, S.; Chakraborty, T. K.; Maiti, S., Selective targeting of G-quadruplex using furan-based cyclic homooligopeptides: Effect on c-MYC expression. *Biochemistry* **2010,** *49* (38), 8388-8397.
72. Shalaby, T.; Von Bueren, A. O.; Hürlimann, M. L.; Fiaschetti, G.; Castelletti, D.; Masayuki, T.; Nagasawa, K.; Arcaro, A.; Jelesarov, I.; Shin-ya, K.; Grotzer, M., Disabling c-Myc in childhood medulloblastoma and atypical teratoid/rhabdoid tumor cells by the potent G-quadruplex interactive agent S2T1-6OTD. *Mol Cancer Ther* **2010,** *9* (1), 167-179.
73. Wang, P.; Leung, C. H.; Ma, D. L.; Yan, S. C.; Che, C. M., Structure-based design of platinum(II) Complexes as c-myc oncogene Down-regulators and luminescent probes for G-quadruplex DNA. *Chem Eur J* **2010,** *16* (23), 6900-6911.
74. Ou, T. M.; Lin, J.; Lu, Y. J.; Hou, J. Q.; Tan, J. H.; Chen, S. H.; Li, Z.; Li, Y. P.; Li, D.; Gu, L. Q.; Huang, Z. S., Inhibition of cell proliferation by quindoline derivative (SYUIQ-05) through its preferential interaction with c-myc promoter G-quadruplex. *J Med Chem* **2011,** *54* (16), 5671-5679.
75. Qin, Y.; Rezler, E. M.; Gokhale, V.; Sun, D.; Hurley, L. H., Characterization of the G-quadruplexes in the duplex nuclease hypersensitive element of the PDGF-A promoter and modulation of PDGF-A promoter activity by TMPyP4. *Nucleic Acids Res* **2007,** *35* (22), 7698-7713.
76. Cogoi, S.; Xodo, L. E., G-quadruplex formation within the promoter of the KRAS proto-oncogene and its effect on transcription. *Nucleic Acids Res* **2006,** *34* (9), 2536-2549.
77. Sun, D. Y.; Guo, K. X.; Rusche, J. J.; Hurley, L. H., Facilitation of a structural transition in the polypurine/polypyrimidine tract within the proximal promoter region of the human VEGF gene by the presence of potassium and G-quadruplex-interactive agents. *Nucleic Acids Res* **2005,** *33* (18), 6070-6080.
78. Dexheimer, T. S.; Sun, D.; Hurley, L. H., Deconvoluting the structural and drug-recognition complexity of the G-quadruplex-forming region upstream of the bcl-2 P1 promoter. *J Am Chem Soc* **2006,** *128* (16), 5404-5415.
79. Lowry, M. S.; Bernhard, S., Synthetically tailored excited states: phosphorescent, cyclometalated iridium(III) complexes and their applications. *Chem Eur J* **2006,** *12* (31), 7970-7977.
80. Zeng, X.; Tavasli, M.; Perepichka, I. F.; Batsanov, A. S.; Bryce, M. R.; Chiang, C. J.; Rothe, C.; Monkman, A. P., Cationic bis-cyclometallated iridium(III) phenanthroline complexes with pendant fluorenyl substituents: synthesis, redox, photophysical properties and light-emitting cells. *Chem Eur J* **2008,** *14* (3), 933-943.

81. Baranoff, E.; Curchod, B. F.; Monti, F.; Steimer, F.; Accorsi, G.; Tavernelli, I.; Rothlisberger, U.; Scopelliti, R.; Gratzel, M.; Nazeeruddin, M. K., Influence of halogen atoms on a homologous series of bis-cyclometalated iridium(III) complexes. *Inorg Chem* **2012,** *51* (2), 799-811.
82. Hansch, C.; Leo, A.; Taft, R. W., A survey of Hammett substituent constants and resonance and field parameters. *Chem Rev* **1991,** *91* (2), 165-195.
83. Xu, Z.; Guo, Z.; Dong, S., Electrogenerated chemiluminescence biosensor with alcohol dehydrogenase and tris(2,2'-bipyridyl)ruthenium (II) immobilized in sol-gel hybrid material. *Biosens Bioelectron* **2005,** *21* (3), 455-461.
84. Shi, S.; Zhao, J.; Gao, X.; Lv, C.; Yang, L.; Hao, J.; Huang, H.; Yao, J.; Sun, W.; Yao, T.; Ji, L., Molecular "light switch" for G-quadruplex DNA: cycling the switch on and off. *Dalton Trans* **2012,** *41* (19), 5789-5793.
85. Yao, J. L.; Gao, X.; Sun, W.; Shi, S.; Yao, T. M., $[Ru(bpy)_2dppz\text{-}idzo]^{2+}$: a colorimetric molecular "light switch" and powerful stabilizer for G-quadruplex DNA. *Dalton Trans* **2013,** *42* (16), 5661-5672.
86. Soman, S.; Singh Bindra, G.; Paul, A.; Groarke, R.; Manton, J. C.; Connaughton, F. M.; Schulz, M.; Dini, D.; Long, C.; Pryce, M. T.; Vos, J. G., Wavelength dependent photocatalytic H_2 generation using iridium-Pt/Pd complexes. *Dalton Trans* **2012,** *41* (41), 12678-12680.
87. Kieltyka, R.; Fakhoury, J.; Moitessier, N.; Sleiman, H. F., Platinum phenanthroimidazole complexes as G-quadruplex DNA selective binders. *Chem Eur J* **2008,** *14* (4), 1145-1154.
88. Castor, K. J.; Mancini, J.; Fakhoury, J.; Weill, N.; Kieltyka, R.; Englebienne, P.; Avakyan, N.; Mittermaier, A.; Autexier, C.; Moitessier, N.; Sleiman, H. F., Platinum(II) phenanthroimidazoles for targeting telomeric G-quadruplexes. *ChemMedChem* **2012,** *7* (1), 85-94.
89. Ya, X.; Xiaohua, Z.; Jianzhong, W.; Huiying, Y.; Liangnian, J., Synthesis, Characterization and Proton-Dependent Electronic Spectra of a Series of Novel Ruthenium(II) Complexes Containing an Imidazole Unit. *Synth React Inorg Met-Org Chem* **1998,** *28* (9), 1445-1454.
90. Chen, T.; Mei, W.-J.; Wong, Y.-S.; Liu, J.; Liu, Y.; Xie, H.-S.; Zheng, W.-J., Chiral ruthenium polypyridyl complexes as mitochondria-targeted apoptosis inducers. *MedChemComm* **2010,** *1* (1), 73.
91. Altomare, A.; Cascarano, G.; Giacovazzo, C.; Guagliardi, A.; Burla, M. C.; Polidori, G.; Camalli, M., Sir92 − a program for automatic solution of crystal structures by direct methods. *J Appl Cryst* **1994,** *27*, 435.
92. Betteridge, P. W.; Carruthers, J. R.; Cooper, R. I.; Prout, K.; Watkin, D. J., CRYSTALS. *J Appl Cryst* **2003,** *36*, 1487.
93. Cooper, R. I.; Gould, R. O.; Parsons, S.; Watkin, D. J., ROTAX. *J Appl Cryst* **2002,** *35*, 168-174.

94. Carruthers, J. R.; Watkin, D. J., Chebychev. *Acta Cryst* **1979,** *A35*, 698-699.
95. Watkin, D. J., Chebychev2. *Acta Cryst* **1994,** *A50*, 411-437.
96. Palatinus, L.; Chapuis, G., Superflip − a computer program for the solution of crystal structures by charge flipping arbitrary dimensions. *J Appl Cryst* **2007,** *40*, 786-790.
97. IDT SciTools OligoAnalyzer ver3.1. https://www.idtdna.com/analyzer/Applications/OligoAnalyzer/ (accessed December 12, 2010).

In Chapter 2, we discovered that our *p*-chlorophenyl- derivative of the phenanthroimidazole ligand was able to discriminate between the polymorphs of the human telomeric G-quadruplex in sodium and potassium containing buffers and exhibited a 2-fold preference for binding to the sodium polymorph. In Chapter 4, we noticed that the iridium(III) complexes with ligands incorporating different electron-withdrawing or donating groups demonstrated different behaviour when binding to G-quadruplex motifs − namely polymorph selectivity (in some cases), luminescence enhancement, and ECL efficiency. We wondered whether the electronics of the ligands of platinum(II) phenanthroimidazoles would aid in the selectivity of this motif for G-quadruplex structures (both between polymorphs and duplex DNA). Chapter 5 thus describes our investigation of this phenomenon.

5 Expanding the Library of Platinum(II) Phenanthroimidazole Complexes *via* Addition of Electron-Withdrawing Substituents

Preface: Author Contributions and Publication

Katherine Castor was responsible for the synthesis and characterization of the complexes herein, as well as project design and biophysical assays. Operation of the robot for the HT-FID assay was done by **Dr. Guillaume Lesage** of the Cell Imagining and Analysis Network (CIAN) (McGill University Department of Biology). **Dr. Mark Hancock** performed the SPR assays at the McGill SPR Facility.

5.1 Introduction

As previously discussed throughout this thesis, G-quadruplexes are non-canonical secondary structures that can be formed by guanine (G) rich DNA under physiological conditions.[1-3] Due to the involvement of these structures in various cancers, they have emerged as targets for chemotherapeutics.[4-10] Bioinformatics studies have discovered many regions in the human genome where G-rich sequences can be found[11-13] including telomeric DNA, promoter regions of oncogenes including *c-Myc*,[14-19] *c-Kit*,[20-22] and vascular endothelial growth factor (VEGF),[23,24] among others,[25-29] and untranslated regions of RNA,[30-32] to name a few. Each of the foldings of the quadruplexes found in these regions is unique and provides many opportunities for selective binding by small molecules.

To date, many organic-based small molecules exist that vary in their efficacies of targeting specific G-quadruplexes.[33] From the published data, these compounds tend to have planar electron-poor surfaces with positively charged or protonable sidearms that can interact with the loops and grooves of the quadruplex motif. We,[34-37] and others,[38-43] have reported metal-based G-quadruplex binders that use aromatic ligands with and without attached sidearms. Our phenanthroimidazole core coordinated to platinum(II) is ideally suited as a G-quadruplex binder as the substituted phenanthroimidazole is large enough to allow for optimal π-stacking with the G-tetrad surface, and the electron-poor, square planar geometry of the platinum(II) metal allows for electrostatic overlap with the

electron-rich surface of the G-quadruplex. Interestingly, we have found that small changes in our ligand core can result in drastically strengthened binding to the telomeric intramolecular G-quadruplex formed in sodium-containing environments, specifically by adding an electron-withdrawing chlorine to the *para*- position of the phenyl-substituted imidazole (Chapter 2, pp 88, Figure 2.3).[36] Due to this discovery, we hypothesized that structural (constitutional) isomers of the chlorophenyl- complex, in addition to fluorinated counterparts and the inclusion of a greater number of halogens within the ligand would allow us to further explore how electronic variation affects G-quadruplex recognition. Herein, we have created a library of complexes with varying orientations of electron-withdrawing substituents from commercially available benzaldehydes. The ligands are first synthesized in an analogous manner to the procedure in Chapter 2 by condensation of the benzaldehydes with 1,10-phenanthroline-5,6-dione, followed by platination with potassium tetrachloroplatinate. The (ligand)$PtCl_2$ intermediates were then treated with ethylenediamine (en) before precipitation with ammonium hexafluorophosphate to afford the final complexes **5.1-5.9** (Figure 5.1). In order to evaluate G-quadruplex recognition by complexes **5.1**-**5.9**, we studied the binding of these complexes to human telomeric (both Na^+- and K^+-polymorphs), *c-Kit*, and *c-Myc* derived G-quadruplexes through high-throughput fluorescence intercalator displacement (HT-FID), surface plasmon resonance (SPR) assays, and circular dichroism (CD) templation. We have found that the addition of groups with electron-withdrawing and donating capabilities presents a complicated picture on how these substituents affect binding affinity to G-quadruplex motifs. Future studies involving in-depth molecular modelling could help to elucidate binding modes of these complexes with the G-quadruplex surfaces. Additionally, cell viability assays will be conducted so as to verify any potential these complexes may have as anticancer agents.

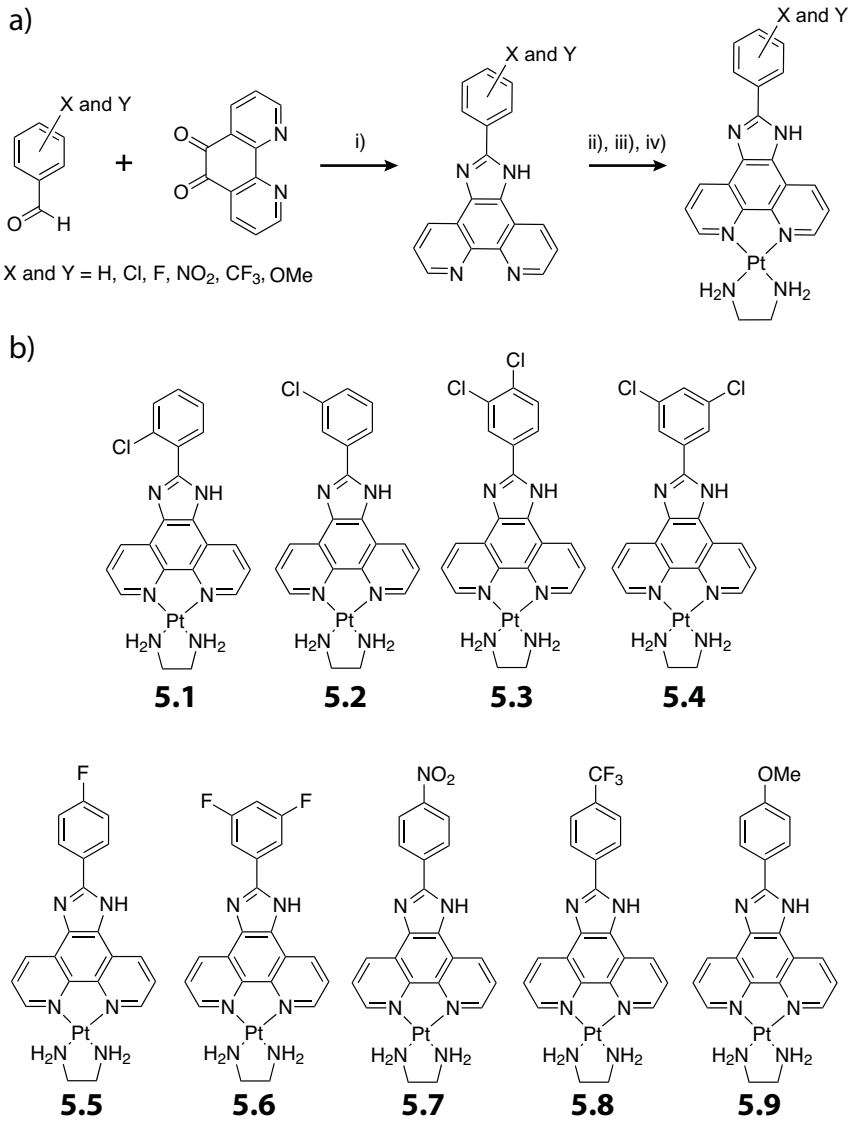

Figure 5.1 a) General synthesis of the platinum(II) phenylphenanthroimidazole complexes where i) NH_4OAc in AcOH, 120°C, 12-24 h. ii) K_2PtCl_4 in DMSO/H_2O, 25°C, 12-24 h. iii) ethylenediamine in EtOH, 25°C, 12-24 h. iv) NH_4PF_6 in EtOH/H_2O. b) 2-chlorophenylphenanthroimidazole ethylenediamine platinum(II) (**5.1**), 3-chlorophenyl-phenanthroimidazole ethylenediamine platinum(II) (**5.2**), 3,4-dichlorophenyl-phenanthroimidazole ethylenediamine platinum(II) (**5.3**), 3,5-dichlorophenylphenanthro-imidazole ethylenediamine platinum(II) (**5.4**), 4-florophenylphenanthroimidazole ethylenediamine platinum(II) (**5.5**), 3,5-diflorophenylphenanthroimidazole ethylenediamine platinum(II) (**5.6**), 4-nitrophenylphenanthroimidazole ethylenediamine platinum(II) (**5.7**), 4-trifloromethylphenylphenanthroimidazole ethylenediamine platinum(II) **(5.8**), and 4-methoxyphenylphenanthroimidazole ethylenediamine platinum(II) (**5.9**).

5.2 Results and discussion

5.2.1 Initial assessment of selected complexes as G-quadruplex binding agents

We first examined the ability of selected complexes in the series to template the folding of a G-quadruplex structure from single-stranded DNA. This was carried out by titration of the human telomeric sequence 22AG with complexes **5.1**, **5.2**, **5.3**, and **5.9** in a tris(hydroxymethyl)aminomethane-based buffer without the addition of cations (namely K^+ and Na^+), followed by CD analysis. In this assay, if templation occurs, a decrease in the CD peaks associated with the single-stranded oligonucleotide (slight negative peak at 238 nm and strong positive peak at 257 nm) and the concomitant appearance of peaks associated with G-quadruplex structures are expected (Figure 2.4d). An antiparallel, basket G-quadruplex, such as that found in buffer solutions containing Na^+-cations, would result in characteristic positive peaks at 292 nm and 245 nm, and a negative peak at 262 nm for this sequence (Figure 2.4b). A mixed hybrid structure, such as that found in buffer solutions containing K^+-cations, is expected to give two positive maxima at 295 nm and 260 nm (Figure 2.4b-c).

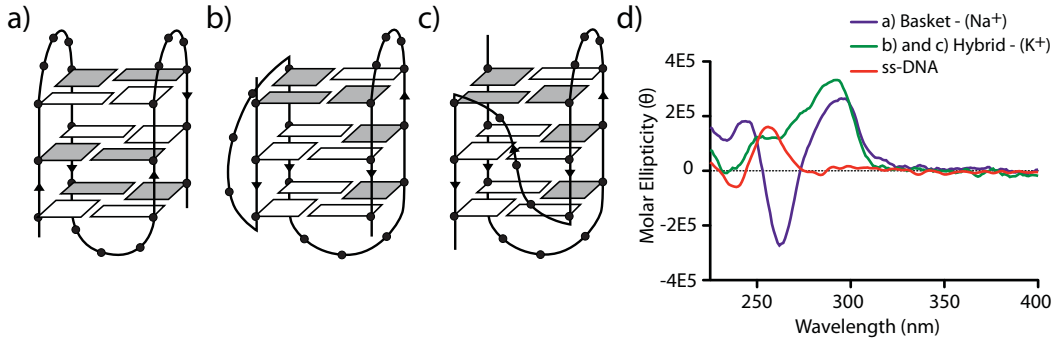

Figure 5.2 Schematics of the G-quadruplex polymorphs: a) Basket antiparallel structure found in Na^+-containing solutions and b) form 1 and c) form 2 of the (3+1) hybrid structure found in K^+-containing solutions. The gray and white parallelograms represent *syn* and *anti* orientations, respectively, of the guanine bases contained within the tetrads. d) CD spectra of a) (purple), b) and c) (green) structures compared to single-stranded DNA (red).

In cases involving complexes **5.1**, **5.2**, and **5.3**, upon the gradual addition of the complexes, a strong positive peak at 295 nm and negative peak at 260 nm

were observed, consistent with templation of a basket antiparallel G-quadruplex from this strand (Figure 5.3a-c) in the absence of added Na^+- or K^+-ions. However, the magnitudes of the change in the ss-DNA peak at (+)-257 nm and subsequent blue-shift towards the (+)-245nm peak for the basket motif differed depending on the complex. In the case of complex **5.1 (**Figure 5.3a), the change in peak height is much less than both complexes **5.2** and **5.3** (Figure 5.3b,c). We hypothesized that this could be caused by either weaker binding of complex **5.1** to 22AG compared to the others and/or by templation of a mixture of polymorphs. The isobestic point at 279 nm is less well-defined for complex **5.1** compared to complexes **5.2** and **5.3**, which indicates a less clear transtion from one species to another − that is, from ss-DNA to a specific polymorph of G-quadruplex − thus justifying the hypothesis that **5.1** templates a mixture of polymorphs. The right three panels in Figure 5.3 (e-g) show binding stoichiometry of the complexes as a result of the templation experiment. This can be determined from the changes in molar ellipticities of the CD peaks at 250−260 nm. Upon plotting these values as a function of molar equivalents of platinum(II) complex added, the curve appears to saturate at approximately a 2:1 ratio of complexes **5.1** and **5.3** to quadruplex-DNA strand and at approximately a 2.5:1 ratio for complex **5.2.** (Figure 5.3e-g). This is consistent with a binding stoichiometry of ~ 2:1, a value which has previously been reported for other strong G-quadruplex binders, such as telomestatin[44] and a macrocyclic oligoamide.[44,45] On the other hand, the templation from the addition of complex **5.9** is more complicated (Figure 5.3d, h) than the others. Due to the slight decrease in the magnitude of the ss-DNA peak at (+)-257 nm and lack of blue-shift towards (+)-245 nm, we can hypothesize that complex **5.9** does not template solely the basket polymorph. Instead, complex **5.9** possibly templates the 3+1 hybrid or a mixture of structures − this is reinforced by the scattered trend resulting from the plot of the ratio of complex to strand versus the magnitude of change of the (+)-peak at 257 nm and the lack of a clear isobestic point (Figure 5.3d, h).

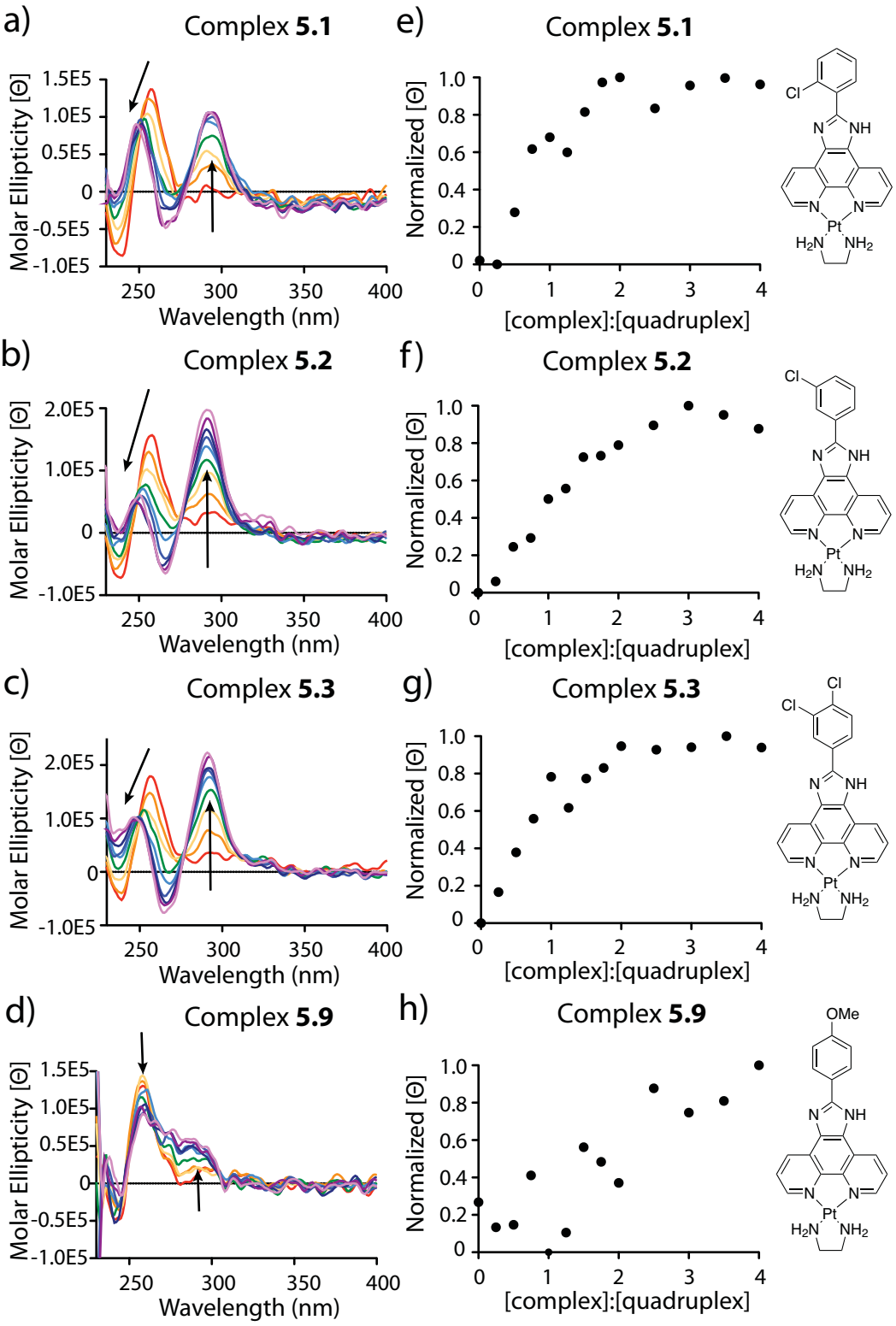

Figure 5.3 CD spectra of the G-quadruplex templation with a) **5.1**, b) **5.2**, c) **5.3**, and d) **5.9**. Arrows in panels a-d show the direction of change in CD signal. Panels e-h show the normalized change in circular dichroic peak between 250 and 260 nm with added complexes.

5.2.2 Assessing the binding affinity with G-quadruplexes *via* HT-FID

After determining that selected complexes from the series were able to template the folding of the human telomeric DNA sequence into G-quadruplex motifs, we then moved on to study the binding affinity of the library with pre-annealed G-quadruplex polymorphs (sequences are shown in Table 5.1): both forms of human telomeric DNA (the antiparallel basket and the 3+1 hybrid), in addition to polymorphs found in the *c-Kit*[20-22] and *c-Myc*[14-19] oncogene promoters (Figure 5.4a-d). To assess selectivity for G-quadruplex DNA over duplex DNA, we used a self-complementary 26mer for comparison (Figure 5.4e). To measure binding to G-quadruplexes, we conducted an FID assay developed by Teulade-Fichou and coworkers.[46,47] In our experiment, we performed the adapted high-throughput procedure[48] as in Chapter 3. The assay relies on competitive displacement of the fluorescent thiazole orange dye from the G-quadruplex targets using complexes **5.1-5.9**, with a concomitant decrease in its fluorescence intensity. This is a reliable assay as the dye exhibits negligible fluorescence in aqueous solutions once displaced from the DNA. The binding affinity can be evaluated from the resulting binding isotherm where the concentration of platinum complex required to give a 50% decrease in dye fluorescence is the DC_{50} (Table 4.5).

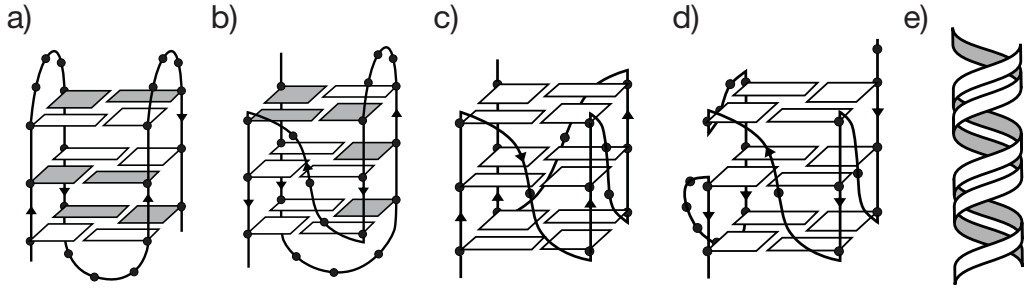

Figure 5.4 DNA structures used in the HT-FID assay. a) Basket-type antiparallel structure from human telomeric DNA found in Na^+-containing solutions, b) (3+1) hybrid-type structure from human telomeric DNA found in K^+-containing solutions, c) parallel polymorph from the *c-myc* promoter sequence, and d) parallel-type polymorph from the *c-kit* promoter sequence. The gray and white parallelograms represent *syn* and *anti* orientations, respectively, of the guanine bases contained within the tetrads. e) Self-complementary duplex 26mer.

Name	ε_{260} ($M^{-1}cm^{-1}$)	Sequence
22AG	228 500	5'- AGGGTTAGGGTTAGGGTTAGGG
cmyc	279 900	5'- TGGGGAGGGTGGGGAGGGTGGGGAAGG
ckit1	226 700	5'- AGGGAGGGCGCTGGGAGGAGGG
ds26mer	253 200	5'- CAATCGGATCGAATTCGATCCGATTG
ds17mer	a) 160 900 b) 167 400	a) 5'- CCAGTTCGTAGTAACCC b) 5'- GGGTTACTACGAACTGG
22AG (SPR)	268 900	5'-biotin-dTTTTTAGGGTTAGGGTTAGGGTTAGGG
cmyc (SPR)	320 400	5'-biotin-dTTTTTTGGGGAGGGTGGGGAGGGTGGGGAAGG
ckit1 (SPR)	267 100	5'-biotin-dTTTTTAGGGAGGGCGCTGGGAGGAGGG
HP (SPR)	226 500	5'-biotin-dTTTTTTTCGCGCGCGTTTTCGCGCGCG

Table 5.1 Sequences used in this chapter.

DC_{50} (μM)	5.1	5.2	5.3	5.4	5.5	5.6	5.7	5.8	5.9
22AG Na^+	1.87	0.993	0.865	>2.50	0.601	1.03	0.673	0.906	0.618
22AG K^+	1.10	0.954	0.986	>2.50	0.740	1.13	0.565	0.823	0.665
ckit1	1.41	0.829	1.01	2.08	0.509	0.868	1.01	0.990	0.499
cmyc	0.866	1.23	1.40	>2.50	0.783	1.21	0.611	0.958	0.704
ds26mer	1.48	1.51	1.85	>2.50	1.09	1.65	0.896	1.17	1.04

Table 5.2 DC_{50} values calculated from the HT-FID assay. Each experiment was conducted in quadruplicate with error < 5%.

5.2.2.1 Non-specific binding during the HT-FID assay

Teulade-Fichou and coworkers suggest that the high-throughput assay be conducted with black quartz microplates to minimize non-specific binding of the complexes that can be seen with the more commonly used polypropylene and polystyrene plates.[48] In their report, they noticed that the HT-method gave over-estimated DC_{50} values – that is, a complex that had a DC_{50} = 0.25 μM in quartz cuvettes (manually), exhibited DC_{50} = 0.33 μM in polypropylene plates and 0.30

μM in polystyrene plates coated with a non-binding surface (NBS™). When they switched to a quartz microplate, the lower value of DC_{50} = 0.25 μM was restored. In our assay, we utilized black polypropylene plates[49] and operated under the assumption that our DC_{50} values might be artificially high. As a test of this hypothesis, we conducted the HT-FID assay with the *p*-chloro- complex **2.7** (Chapter 2, pp 88, Figure 2.3) and compared the values obtained with our previously published results.[36] For complex **2.7**, our manual method gave DC_{50} values of 0.31 μM and 0.66 μM to the 22AG-Na^+ and -K^+ sequences, respectively. The HT-FID method, on the other hand, resulted in DC_{50} values of 0.70 μM and 0.92 μM to the same sequences (Figure 5.5). From the binding isotherm shown in Figure 5.5, it is evident that non-specific binding of the complex to the polypropylene plate results in less free complex available in solution for displacement of thiazole orange from the target DNA sequences. This results in a more gradual displacement that cannot reach the same level of percent displacement as the complex in quartz cuvettes. This discrepancy was in agreement with the results obtained by Teulade-Fichou and coworkers and should be kept in mind when analyzing the results from the assay. The results should thus be interpreted in relation to one another, and the HT-FID method can be used to extract trends for a structurally similar series in a broad sense, that is − when binding to quadruplex versus duplex DNA.

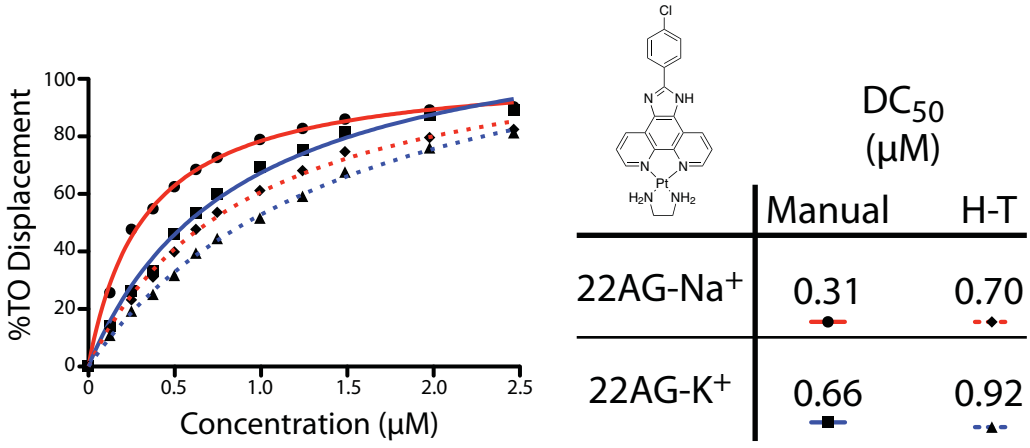

Figure 5.5 Comparison of the results for the FID assay for complex **2.7** *via* the manual method (in a quartz cuvette) and the high-throughput format (in polypropylene microplates).

5.2.2.2 Non-specific binding as a result of hydrophobicity

Given the hydrophobicity and the minimal solubility in water of these π-extended phenanthroimidazole complexes, we hypothesized that in addition to non-specific binding during biophysical assays, we may also encounter aggregation (see Chapter 2, pp 88, Figure 2.3, 2-hydroxynaphthyl- complex **2.6**). During preparation of samples for the HT-FID assay of the highly electron-withdrawing $–NO_2$ complex **5.7**, heterogeneity of the aqueous solution was evident. Upon vigorous shaking of the sample, it appeared homogeneous to the eye, but aggregation may still have been present. Some small molecules have been shown to bind to G-quadruplex and duplex DNA *via* an aggregation method (namely cyanine dyes[50] and perylene-based binders[51,52]). While the aggregation of the perylene-based binders was able to contribute to the compounds' ability to select between duplex and G-quadruplex DNA,[51] we thought it likely as well that in our case, complex aggregation causes precipitation effects, especially in assays with complex **5.7**.

In order to elucidate the binding mechanism of complex **5.7** with G-quadruplex and duplex DNA, we conducted circular dichroism binding titrations. Starting with a 15 μM solution of DNA (ds17mer, ckit1, and cmyc: Table 5.1), we titrated increasing amounts of complex **5.7** from 0 to 5 equivalents (that is, 0–75 μM). From the spectra in Figure 5.6, we can see that the signature peaks denoting duplex DNA (Figure 5.6a: (+)-275 nm) and G-quadruplex formation (Figure 5.6b, c: (+)-260 nm) slowly decreased with added **5.7**. If complex **5.7** was inducing a change in structure, we should see the development of new peak(s) concomitantly with the disappearance of the original peak. Instead, as the titration continued, an orange floculant material was seen to appear inside the cuvette. From this observation, and previous knowledge that complex **5.7** is more insoluble in aqueous solution compared to the rest of the complexes in the series, we deduced that once **5.7** binds to G-quadruplex DNA, the aggregation of the platinum complex with the DNA caused the aggregate to precipitate out of solution. This effect was only noted for complex **5.7**, and the other compounds in the series did not display serious aggregation problems (visually or through CD experiments).

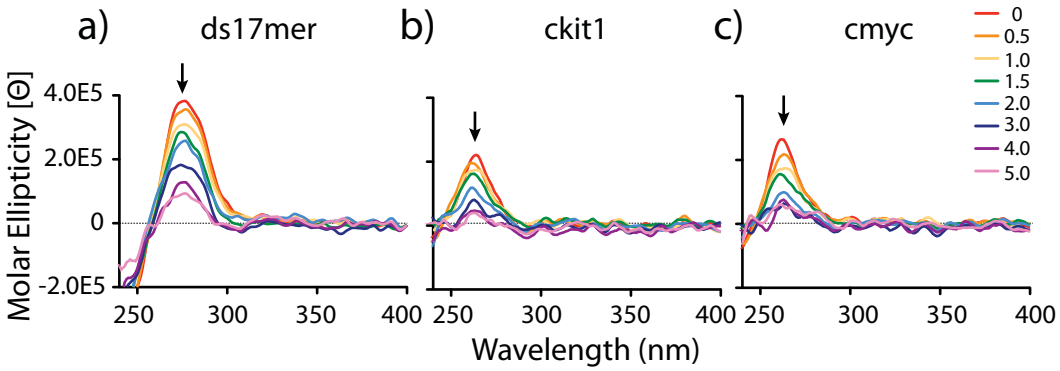

Figure 5.6 CD spectra of the titration of complex **5.7** with a) dupex DNA ds17mer, b) G-quadruplex DNA ckit1, and c) G-quadruplex DNA cmyc. The arrows show the direction of change (decrease) with increasing amounts of complex **5.7**. The legend at right shows the corresponding equivalents of complex **5.7** added.

5.2.3 Assessing the binding kinetics with G-quadruplexes *via* SPR for selected complexes in the series

Due to the non-specific binding of platinum complexes **5.1**-**5.9** during the HT-FID assay, we moved to surface plasmon resonance assays to assess binding affinity to the DNA motifs. SPR is a label-free, real-time technique that has emerged as a powerful way to examine the binding specificity and kinetics of compounds for duplex versus G-quadruplex DNA.[53-57] Similar to these previously reported methods, we used a potassium-containing running buffer to focus upon binding to the 22AG-K and cmyc G-quadruplexes; to determine selectivity between G-quadruplex and duplex DNA, we used a CG-rich hairpin (HP) (Table 5.1). Initial studies involved complexes 2-chloro- complex **5.1**, 3,4-dichloro- complex **5.3**, 3,5-dichloro- complex **5.4**, and 4-fluoro- complex **5.5**. Preliminary, fixed-concentration screening revealed that these complexes could specifically bind to the immobilized DNA sequences, whereas diluent alone (i.e. running buffer containing 1 mg/mL CM-dextran to reduce minor non-specific binding of the complexes to streptavidin-coated sensors, see Chapter 1, pp 52 for more information) or our negative control complex **5.10**[36] generated no signal responses (Figure 5.7). Interestingly, monosubstituted complexes **5.1** and **5.5** bound with faster association and dissociation kinetics than the more sterically bulky disubstituted complexes **5.3** and **5.4** (that is, the shape of the curves for **5.1** and **5.5** were steeper than for **5.3** and **5.4**).

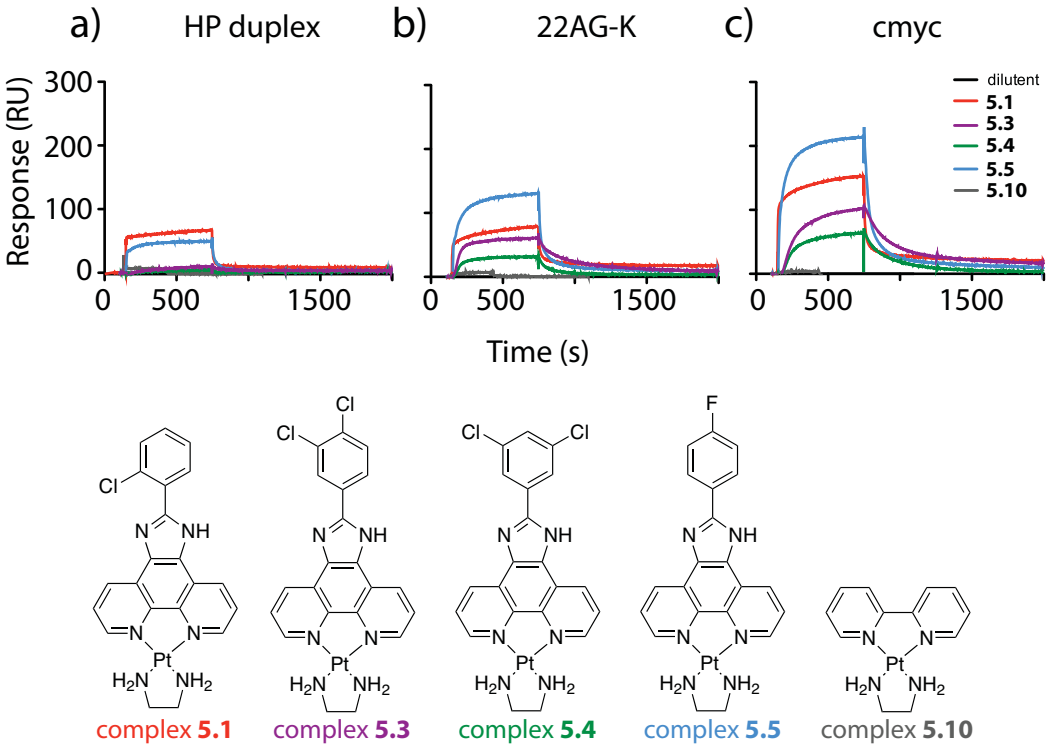

Figure 5.7 Representative SPR screening of compounds (fixed at 5 μM each) binding to 450 RU immobilized a) HP duplex, b) 22AG-K G-quadruplex DNA, and c) cmyc G-quadruplex DNA at 25 μL/min (10 min association + 20 min dissociation).

We then proceeded with titrations of each complex with the aforementioned sequences from 0−3 or 6 μM in complex with 2-fold serial dilutions. This experiment showed dose-dependent, saturable binding for the complexes tested (Figure 5.8 and Figure 5.10). The KD values were determined from the equilibrium response values plotted against the conentration of complex added. The CD templation studies to the 22AG sequence for complexes **5.1** and **5.3** showed a binding stoichiometry of two complexes per G-quadruplex, thus we attempted to fit the equilibrium data for G-quadruplex binding to a two-site binding model. The sensograms and binding isotherms for monosubstituted complex **5.1** and **5.5** are shown in Figure 5.8 and Figure 5.9, respectively. The KD values are shown in Table 5.3. In the case of these complexes binding to a two-site binding model, the KD values for the second site are higher (1−2 orders of magnitude) so only the values for the first site are shown. This is common for other G-quadruplex binders in the literature.[51,57-62] The weaker binding to the

second site is presumed to be non-specific in nature (i.e. weak loop interactions versus strong end-stacking).[44]

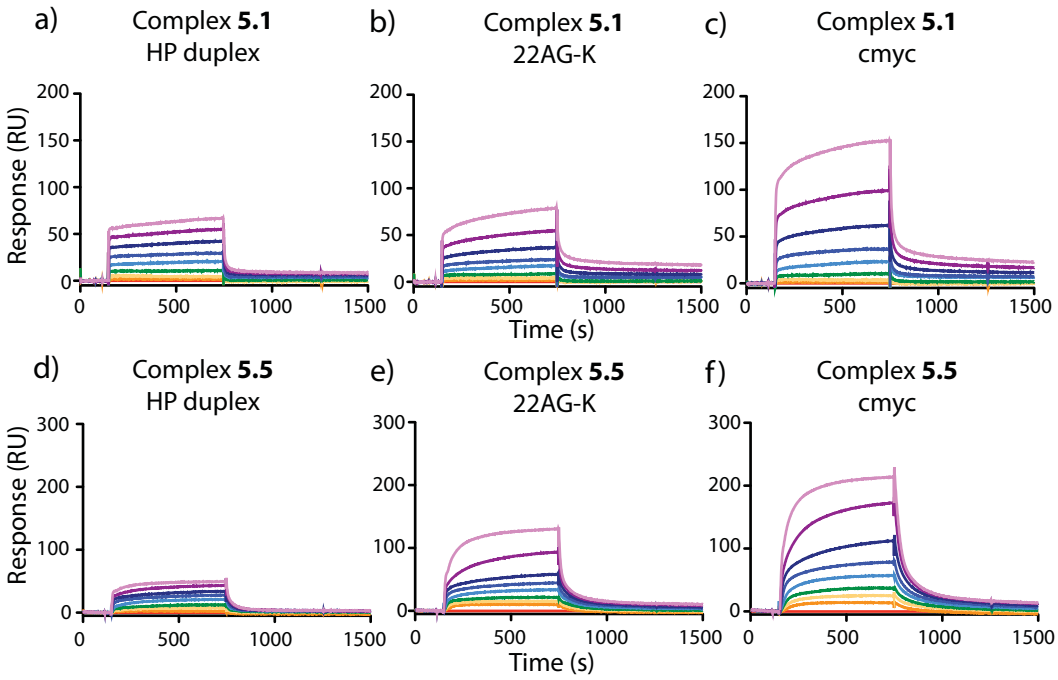

Figure 5.8 SPR titrations of complexes **5.1** and **5.5** to the HP duplex, 22AG-K, and cmyc sequences. A 2-fold dilution series from 0 μM (red trace) to 6 μM (light purple trace) of complex binding to approximately 450 RU immobilized sequences at 25 μL/min (10 minute association + 20 minute dissociation periods).

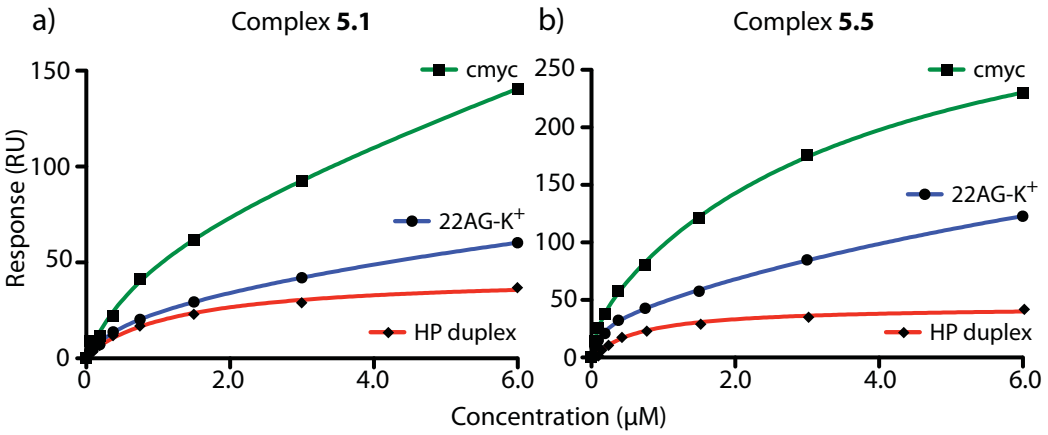

Figure 5.9 Equilibrium fitting data determined from the SPR titrations for monosubstituted complexes a) **5.1** and b) **5.5**. For each complex binding to G-quadruplex DNA (blue and green lines), the data was fit to a two-site binding model, while binding to HP duplex was fit to a one-site binding model. There are no associated errors as this was the result of an *n* of 1.

For monosubstituted complexes **5.1** and **5.5**, the KD values with the G-quadruplex DNA motifs are on the sub-micromolar level, with the values for **5.5**

reaching into the nanomolar regime, specifically with the cmyc polymorph (K_D ~ 91 nM). The trends do not match the HT-FID data in either case (except for weaker binding to duplex DNA), but this is to be expected due to the non-specific binding observed with the previous method.

Besides obtaining binding data from SPR assays, we can also determine binding stoichiometry. Since the molecular weight of the DNA sequences is known, we can determine how much DNA binds to the surface based on the response during the initial preparation of the SPR sensorchip. As the complexes bind to the DNA, we can then determine approximately how many are bound to the surface, again based on the reponse. It should be noted that these complexes bound to the quadruplexes with signal responses that exceeded theoretical maximum response predictions (R_{max}, based on amount of DNA bound to the surface, section 5.4.3.2), hence, we may assume that either multiple binding sites do exist − that is, the binding stoichiometry is greater than 1:1, or that we are encountering some non-specific binding to the surface of the sensor chip. Due to the set-up of the SPR experiments and the free channel that serves as an indicator of non-specific binding, if extensive non-specific binding was occuring, we would be able to detect it. Since the blank channel did not result in extensive non-specific binding, we can assume that the binding stoichiometry is in fact, greater than 1:1. This is supported by the CD titrations that indicated ~ 2:1 binding ratio (Figure 5.3).

For the disubstituted complexes **5.3** and **5.4**, there was little or undetectable binding to the HP duplex, indicating a greater selectivity for the G-quadruplex motifs over duplex DNA (Figure 5.10a,d). For 3,5-dichloro- complex **5.4**, this was consistent with the minimal binding to duplex DNA from the HT-FID assay (DC_{50} > 2.50 μM with ds26mer). However, as previously mentioned, caution must be taken when comparing values between these methods due to the non-specific binding. The equilibrium responses for binding to G-quadruplex DNA are shown in Figure 5.11 and the corresponding K_D values are shown in Table 5.3. Again, the values are in the low micromolar range. For complex **5.4**, the data did not fit to the two-site binding model, so the K_D value was instead

determined from a one-site binding model. The binding of these complexes to the surface also exceeded the theoretical R_{max}, indicating a binding stoichiometry greater than 1:1.

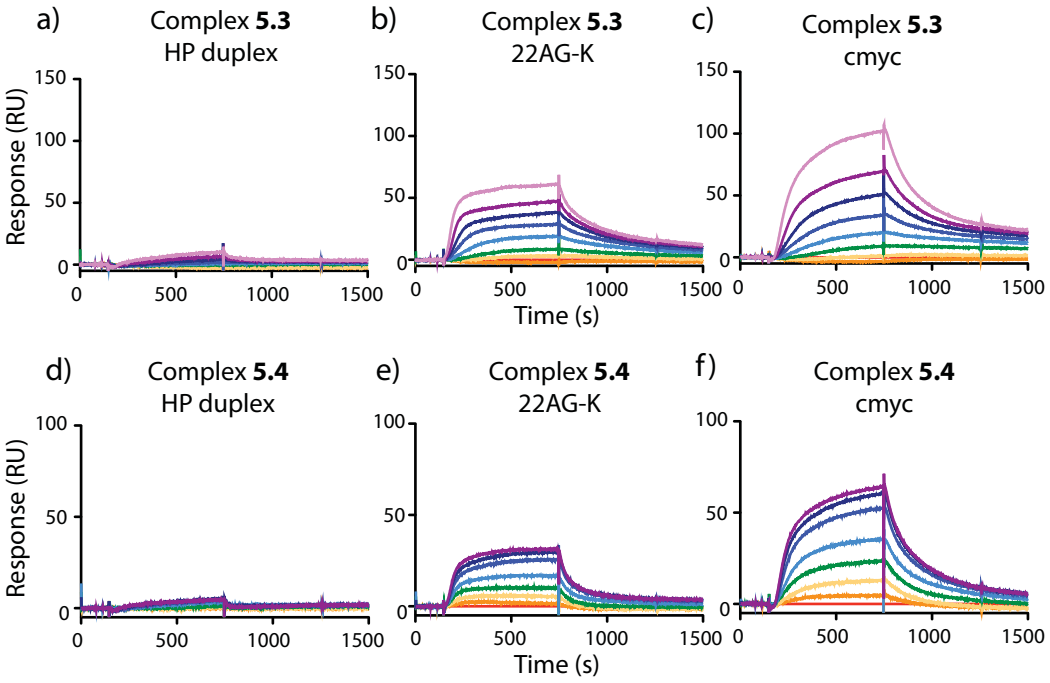

Figure 5.10 SPR titrations of complexes **5.3** and **5.4** to the HP duplex, 22AG-K, and cmyc sequences. A 2-fold dilution series from 0 μM (red trace) to 3 μM (purple trace) or 6 μM (light purple trace) of complex binding to approximately 450 RU immobilized sequences at 25 μL/min (10 minute association + 20 minute dissociation periods).

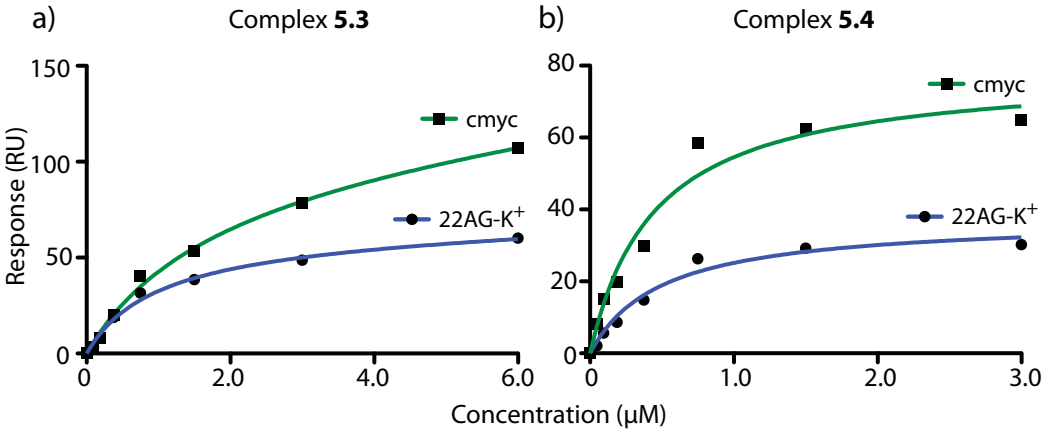

Figure 5.11 Equilibrium fitting data determined from the SPR titrations for disubstituted complexes a) **5.3** and b) **5.4**. For complex **5.3** the data was fit to a two-site binding model, while binding for complex **5.4** was fit to a one-site binding model. There are no associated errors as this was the result of an *n* of 1.

Sequence	Complex 5.1	Complex 5.3	Complex 5.4	Complex 5.5
HP duplex	1.30	n.d	n.d.	0.664
22AG-K	0.437	0.964	0.49	0.139
cmyc	0.896	1.73	0.45	0.0910

Table 5.3 K_D values (μM) determined from the equilibrium responses versus the concentration of complex from the SPR titration assay. The numbers arise from n=1, so there are no associated error values.

We can attempt to explain the results from the SPR experiments in relation to complex sterics and electronics when binding to the various polymorphs. In the case of the monosubstituted complexes **5.1** and **5.5**, they exhibited faster on/off binding kinetics (Figure 5.7) as indicated by the steeper binding and unbinding curves compared to the sterically bulkier disubstituted complexes **5.3** and **5.4** to G-quadruplex DNA. These larger complexes also demonstrate the inability to intercalate into duplex DNA as evidenced by the undetectable binding to this motif (Figure 5.10a,d). While the disubstitution appears to aid in the selectivity between G-quadruplex and duplex DNA, it does not seem to significantly increase binding affinity to the G-quadruplex motif as compared to the monosubstituted complexes. This may be due in part to increased electron-withdrawing character of the dichloro- substituents. There seems to be an optimal ratio between ligand size and electronics that would allow for tighter binding to and greater selectvity, but more studies are required to uncover all of the stereoelectronic effects for this series of complexes.

5.3 Conclusions

In conclusion, we have utilized a facile and expedious method to create a library of G-quadruplex binders that were evaluated for binding affinity to various G-quadruplex motifs (h-telo, ckit1, and cmyc) through several biophysical means including CD templation, a high-throughput FID assay, and SPR. From the HT-FID assay, we discovered non-specific binding interactions with the polypropylene microplates that resulted in artifically high DC_{50} values. Due to the hydrophobic nature of these π-extended phenanthroimidazole complexes, we must use caution when studying their interactions with DNA. Despite the non-specific binding from the HT-FID assay, we were able to determine that these complexes

are effective G-quadruplex binders (and even more effective than the numbers suggest), but the selectivity between quadruplex and duplex DNA needs to be improved upon to validate potential efficacy as selective G-quadruplex targeting agents. In all, the facile synthesis of this type of library lends itself as a promising avenue for the futher development of selective G-quadruplex binders taken in conjuction with lessons learned from these attempts.

5.4 Future directions

This chapter could be the beginning of an in-depth look at the influence of complex electronics on G-quadruplex recognition. It is expected that the addition of more elongated positive side-chains for groove penetration can increase the binding selectivity, as well as improving solubility in aqueous media to avoid non-specific binding. Work conducted by Kern and Kerwin demonstrated DNA structure selectivity of perylene-analogs with alkyl-amino side-chains achieved through pH-mediated ligand aggregation.[51] In a similar manner, we may be able to mediate binding of our phenanthroimidazole complexes to G-quadruplex DNA by controlling the pH. The imidazole moiety of the ligands allows for deprotonation at basic pH and protonation at acidic pH. Varying the pH of our buffers during our biophysical assays may reveal a binding mode that does not involve precipitation of the DNA-complex aggregate. Accurate determination of the binding affinity for all the complexes should be performed by SPR and additional replicates are needed to obtain standard deviations. Finally, cell viability assays would be necessary to determine if the platinum complexes are selective for cancer cells over normal cells, and a detailed study into the mechanism of action of the complexes in the selective cytotoxicity to cancer cells would establish criteria for the design of future therapeutics based on the phenanthroimidazole core.

5.5 Experimental section

5.5.1 Synthesis

NMR spectra were recorded on either a 200, 300, 400 or 500 MHz Varian Mercury spectrometer operated with VNMRJ 2.2D software under LINUX Red Hat 5. The following abbreviations are used: singlet (s), doublet (d), doublet of doublets (dd), triplet (t), multiplet (m), and broad (br). All commercially available reagents were purchased from Sigma Aldrich and used without further purification. [4,5-*f*][1,10]phenanthroline,[35] 2CLIP and 3CLIP ligands,[63,64] OMePIP ligand,[65] NitroPIP ligand,[66] and CF_3PIP ligand[67] have been characterized elsewhere. High-resolution mass spectrometry was performed on a Bruker Maxis Impact ESI-QTOF. For MS analysis, sodium formate was used to generate a calibration curve for mass accuracy. Samples were then diluted in LC-MS grade Methanol (Fisher) and directly infused at 3 μL per minute into the MS. The spectra were obtained in positive mode.

5.5.2 Preparation of 5.1-5.9

General procedure for preparation of ligands

[4,5-*f*][1,10]phenanthroline (0.470−1.88 mmol) and 10 equivalents of NH_4OAc were dissolved in 15−30 mL glacial acetic acid under an argon atmosphere. Then 1.1−1.4 equivalents of aldehydes were added and the reaction was refluxed at 120°C for ~ 24 h. The reaction was then cooled in an ice bath, diluted with water, and neutralized with the slow addition of NH_4OH to pH ~ 8.0. The precipitate was vacuum filtered through a glass frit and washed with water, ethyl acetate and diethyl ether before vacuum air drying on the frit.

3,4-diCLIP ligand:

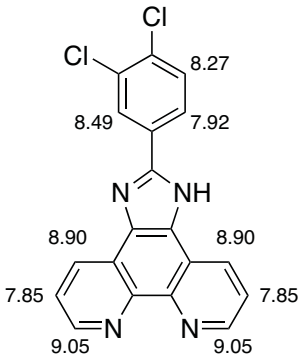

(0.102 g, 59%). ^{1}H NMR (300 MHz, d_6-DMSO): δ = 9.05 (dd, 2H), 8.90 (d, 2H), 8.49 (s, 1H), 8.27 (d, 1H), 7.92 (d, 1H), 7.85 (br m, 2H) ppm; ^{13}C NMR (300 MHz, d_6-DMSO): δ = 148.4, 144.2, 135.3, 134.1, 130.0, 128.8, 124.8, 123.8 ppm; HR-MS Calculated for $C_{19}H_{10}Cl_2N_4Na$ (M^++Na^+): **387.0175**, Found: **387.0172**.

3,5-diCLIP ligand:

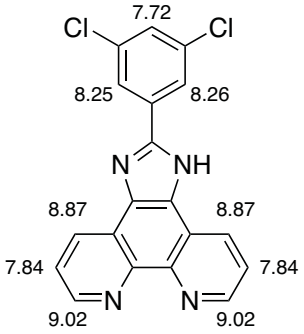

(0.150 g, 59%). ^{1}H NMR (200 MHz, d_6-DMSO); δ = 9.02 (dd, 2H), 8.88-8.83 (dd, 2H), 8.26 (s, 1H), 8.25 (s, 1H), 7.84-7.78 (dd, 2H), 7.72 (s, 1H) ppm; ^{13}C NMR (300 MHz, d_6-DMSO); δ = 148.6, 147.9, 144.3, 135.3, 133.6, 130.1, 129.0, 124.8, 123.8 ppm; HR-MS Calculated for $C_{19}H_{10}Cl_2N_4Na$ (M^++Na^+): **387.0175**, Found: **387.0170**.

FLIP ligand:

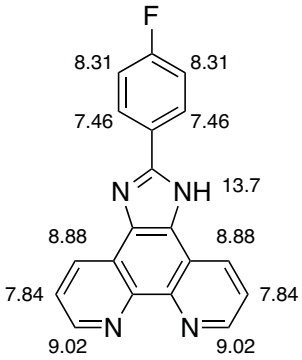

(0.196 g, 88%). ^{1}H NMR (400 MHz, d_6-DMSO): δ = 13.7 (s, 1H), 9.02 (br, 2H), 8.88 (br, 2H), 8.31 (br, 2H), 7.84 (br, 2H), 7.46 (br, 2H) ppm; ^{13}C NMR (300 MHz, d_6-DMSO): δ = 150.0, 148.3, 136.2, 130.1, 129.0, 128.9, 123.9, 123.7, 116.7, 116.5, 110.0 ppm; HR-MS Calculated for $C_{19}H_{11}FN_4Na$ (M^++Na^+): **337.0860**, Found: **337.0858**.

3,5-diFLIP ligand:

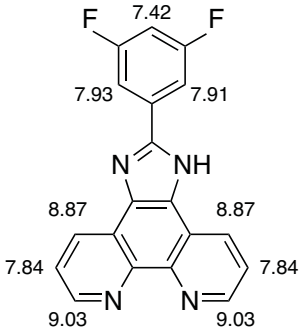

(0.146 g, 60%). ^{1}H NMR (300 MHz, d_6-DMSO): δ = 9.03 (s, 2H), 8.87 (d, 2H), 7.93 (s, 1H), 7.91 (s, 1H), 7.84 (br m, 2H), 7.42 (s, 1H) ppm; ^{13}C NMR (300 MHz, d_6-DMSO): δ = 148.7, 144.3, 130.2, 130.1, 123.9, 109.8, 109.4, 105.0 ppm; HR-MS Calculated for $C_{19}H_{10}F_2N_4$ (M+1): **333.0938**, Found: **333.0938**.

*Complexes **5.1-5.9** were prepared in a manner identical to those previously published by our laboratory.*[30,31]

(5.1) [(2-CLIP)Pt(en)][PF_6]$_2$:

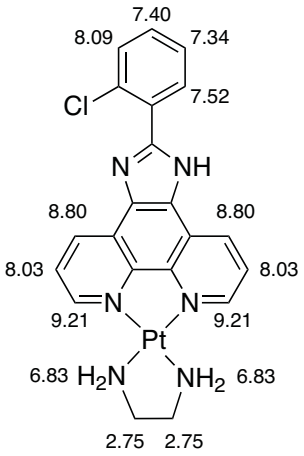

(0.0410 g, 70%). ^{1}H NMR (500 MHz, d_6-DMSO): δ = 9.21 (d, 2H), 8.80 (d, 2H), 8.09 (d, 1H), 8.05-8.02 (dd, 2H), 7.52 (d, 1H), 7.40 (t, 1H) 7.34 (t, 1H), 6.83 (br s, 4H), 2.75 (s, 4H) ppm; ^{13}C NMR (500 MHz, d_6-DMSO): δ = 147.0, 142.8, 134.2, 132.6, 132.0, 130.7, 128.9, 127.0, 126.6, 125.2, 47.6 ppm; HR-MS Calculated for $C_{21}H_{19}ClN_6Pt$ $[M\text{-}2PF_6]^{2+}$: **292.5499**, Found: **292.5486**.

(5.2) [(3-CLIP)Pt(en)][PF_6]$_2$:

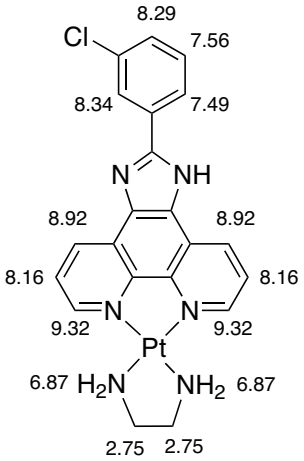

(0.0170 g, 57%). ^{1}H NMR (400 MHz, d_6-DMSO): δ = 9.32 (d, 2H), 8.92 (br s, 2H), 8.34 (s, 1H), 8.29 (d, 1H), 8.16 (br, 2H), 7.56 (br, 1H) 7.49 (br, 1H), 6.87 (br s, 4H), 2.75 (br s, 4H) ppm; ^{13}C NMR (300 MHz, d_6-DMSO): δ = 157.1, 148.0, 143.2, 137.9, 137.0, 134.8, 134.4, 127.5, 125.7, 125.3, 124.7, 47.6 ppm; HR-MS Calculated for $C_{21}H_{19}ClN_6Pt$ $[M\text{-}2PF_6]^{2+}$: **292.5499**, Found**: 292.5491**.

(5.3) [(3,4-diCLIP)Pt(en)][PF_6]$_2$:

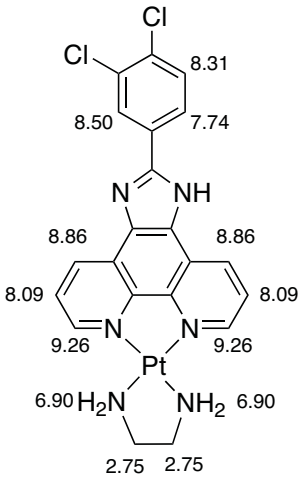

(0.0280 g, 45%). ^{1}H NMR (300 MHz, d_6-DMSO): δ = 9.26 (d, 2H), 8.86 (d, 2H), 8.50 (s, 1H), 8.31 (d, 1H), 8.09 (m, 2H), 7.74 (d, 1H) 6.90 (br s, 4H), 2.75 (br s, 4H) ppm; ^{13}C NMR (500 MHz, d_6-DMSO): δ = 148.0, 143.1, 134.3, 131.8, 131.3, 128.0, 126.6, 125.6, 125.4, 105.0, 47.6 ppm; HR-MS Calculated for $C_{21}H_{18}Cl_2N_6Pt$ $[M\text{-}2PF_6]^{2+}$: **309.5304**, Found: **309.5290**.

(5.4) [(3,5-diCLIP)Pt(en)][PF_6]$_2$:

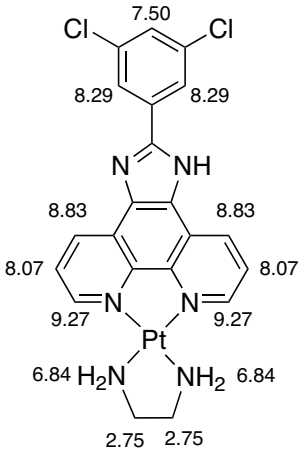

(0.0590 g, 65%). ^{1}H NMR (300 MHz, d_6-DMSO): δ = 9.27 (d, 2H), 8.83 (d, 2H), 8.29 (s, 2H), 8.07 (dd, 2H), 7.50 (s, 1H), 6.84 (br s, 4H), 2.75 (br s, 4H) ppm; ^{13}C NMR (500 MHz, d_6-DMSO): δ = 159.0, 147.5, 143.3, 140.0, 138.7, 134.7, 134.4, 126.7, 126.2, 125.5, 124.6, 47.6 ppm; HR-MS Calculated for $C_{21}H_{18}Cl_2N_6Pt$ $[M\text{-}2PF_6]^{2+}$: **309.5304**, Found: **309.5294**.

(5.5) [(FLIP)Pt(en)][PF_6]$_2$:

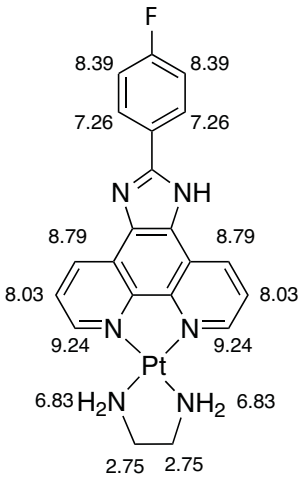

(0.0610 g, 63%). ^{1}H NMR (300 MHz, d_6-DMSO): δ = 9.24 (d, 2H), 8.79 (d, 2H), 8.39 (dd, 2H), 8.03 (dd, 2H), 7.26 (dd, 2H), 6.83 (br s, 4H) 2.75 (br s, 4H) ppm. ^{13}C NMR (300 MHz, d_6-DMSO): δ = 147.8, 143.2, 134.5, 134.4, 133.2, 129.0, 128.8, 125.7, 125.6, 116.1, 115.8 47.6 ppm; HR-MS Calculated for $C_{21}H_{19}FN_6Pt$ $[M\text{-}2PF_6]^{2+}$: **284.5647**, Found: **284.5642**.

(5.6) [(3,5-diFLIP)Pt(en)][PF_6]$_2$:

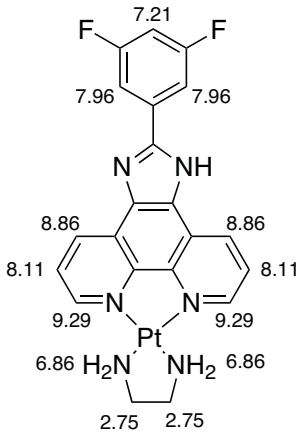

(0.0120 g, 20%). ^{1}H NMR (400 MHz, d_6-DMSO): δ = 9.29 (d, 2H), 8.86 (d, 2H), 8.11 (dd, 2H), 7.96 (d, 2H), 7.21 (t, 1H), 6.86 (br s, 4H), 2.78 (br, 4H) ppm; Due to solubility issues of this complex in DMSO at the concentrations needed for strong ^{13}C signal, a ^{13}C NMR could not be obtained; HR-MS Calculated for $C_{21}H_{18}F_2N_6Pt$ $[M\text{-}2PF_6]^{2+}$: **293.5600**, Found: **293.5591**.

(5.7) [(NitroPIP)Pt(en)][PF_6]$_2$:

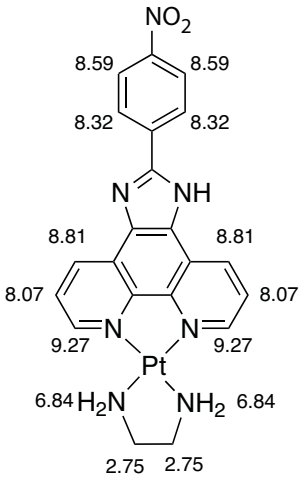

(0.0320 g, 41%). ^{1}H NMR (500 MHz, d_6-DMSO): δ = 9.27 (d, 2H), 8.81 (br s, 2H), 8.59 (d, 2H), 8.32 (d, 2H), 8.07 (br, 2H), 6.84 (br s, 4H), 2.75 (br s, 4H) ppm; Due to solubility issues of this complex in DMSO at the concentrations needed for strong ^{13}C signal, a ^{13}C NMR could not be obtained; HR-MS Calculated for $C_{21}H_{19}N_7O_2Pt$ $[M\text{-}2PF_6]^{2+}$: **298.0619**, Found: **298.0608**.

(5.8) [(CF_3PIP)Pt(en)][PF_6]$_2$:

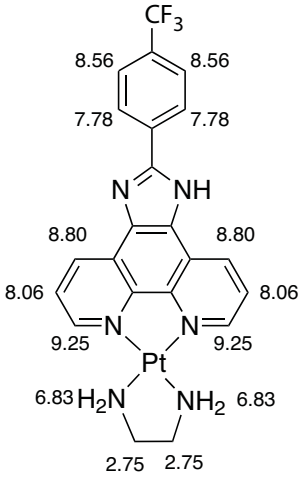

(0.0930 g, 72%). ^{1}H NMR (300 MHz, d_6-DMSO): δ = 9.35 (d, 2H), 8.94 (d, 2H), 8.55 (d, 2H), 8.20 (dd, 2H), 7.95 (d, 2H), 6.89 (br, s 4H), 3.83 (s, 3H), 2.75 (br s, 4H) ppm; Due to solubility issues of this complex in DMSO at the concentrations needed for strong ^{13}C signal, a ^{13}C NMR could not be obtained; HR-MS Calculated for $C_{22}H_{19}F_3N_6Pt$ $[M\text{-}2PF_6]^{2+}$: **309.5630**, Found: **309.5625**.

(5.9) [(OMePIP)Pt(en)][PF_6]$_2$:

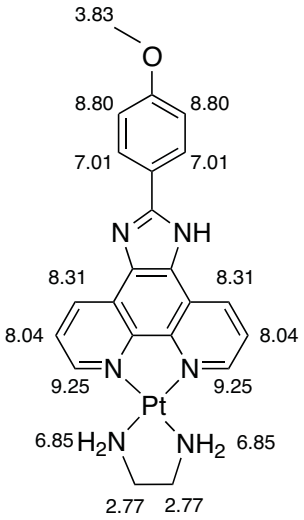

(0.0310 g, 39%). ^{1}H NMR (500 MHz, d_6-DMSO): δ = 9.25 (d, 2H), 8.80 (d, 2H), 8.31 (d, 2H), 8.04 (dd, 2H), 7.01 (d, 2H), 6.85 (br s, 4H), 2.77 (br s, 4H) ppm; Due to solubility issues of this complex in DMSO at the concentrations needed for strong ^{13}C signal, a ^{13}C NMR could not be obtained HR-MS Calculated for $C_{23}H_{22}N_6OPt$ $[M\text{-}2PF_6]^{2+}$: **290.5746**, Found: **290.5748**.

5.5.3 Biophysical assays

All platinum(II) complexes were prepared as 1.5 mM stock solutions in DMSO and stored at 4°C. The 22AG DNA oligonucleotide was obtained from SigmaGenosys Canada. The 17mer and 26mer oligonucleotides as well as the biotinylated 22AG, cmyc, and HP DNA sequences were synthesized in-house on a MerMade 6 DNA synthesizer from BioAutomation Corporation. Reagents used for automated DNA synthesis were purchased from ChemGenes Incorporated. Biotin-dT CED phosphoramidite was used as purchased from ChemGenes and coupled off-column under inert atmosphere. Sequences were purified using standard denaturing polyacrylamide gel electrophoresis with a 20 x 20 cm vertical Hoefer 600 electrophoresis unit, followed by desalting with Sephadex G-25 (superfine DNA grade from Sigma Aldrich). Oligonucleotides were dissolved in deionized water prior to use and quantified spectrophotometrically at room

temperature (with the exception of the quadruplex-forming strands, which were heated to 95°C) using their molar extinction coefficients[68] at 260 nm (Table 5.1).

5.5.3.1 Circular dichroism studies

Circular dichroism studies were performed at 25°C on a JASCO J-810 spectropolarimeter using a 1 mm path length cuvette. Temperature was kept constant using the Peltier unit within the instrument. Spectra were recorded from 400–230 nm at a scan rate of 50 nm/min and a response time of 4.0 s with two acquisitions recorded for each spectrum. Data was smoothed using the means-movement function within the JASCO graphing software. In order to observe the ability of these complexes to fold the human telomeric DNA sequence, 22AG was dialyzed with Pierce slide-a-lyzer mini-dialysis kits (MWCO 3500 Da) (Fisher Scientific) against deionized Milli-Q water for 1−3 days before being diluted to 15 μM in a 50 mM Tris buffer (pH 7.6) for a total volume of 200 μL. For ckit1 and cmyc sequences, concentrated solutions were diluted to 15 μM in 10mM K_2HPO_4/KH_2PO_4 buffer (pH 7.6) with 100mM KCl, and heated to 95°C for 10 minutes before rapidly cooling to room temperature. The ds17mer was formed by adding 15 μM of each strand (A and B) to a solution in the potassium phosphate buffer (same as above), heating to 95°C for 10 minutes before cooling to room temperature over 7 h. These sequences were stored overnight at 4°C prior to use. Platinum(II) complexes were titrated in 0.5 μL aliquots from 1.5 mM solutions in DMSO to the each sequence. With each aliquot added, 5 minutes elapsed prior to recording the CD spectrum. Spectra were collected with the aforementioned parameters, until 3 or 4 molar equivalents were reached in platinum(II) complex.

5.5.3.2 HT-FID assay

The HT-FID assay was performed in an identical manner to that in Chapter 3.

5.5.3.3 SPR assay (performed by Dr. Mark A. Hancock)

SPR measurements were performed on research-grade streptavidin-coated (SA) sensor chips (XanTec Bioanalytics GmbH, Muenster, Germany) at 25°C

using filtered (0.2 μm) and degassed HBS-KT running buffer (10 mM HEPES pH 7.4, 150 mM KCl, 3 mM EDTA, 0.05% (v/v) Tween-20). Protein-grade detergents (Tween-20, Empigen) were from Anatrace (Maumee, USA) and Pierce Gentle Elution (PGE) buffer was from Thermo Scientific (Illinois, USA); all other chemicals were reagent grade quality. Concentrated compound stocks were prepared in 100% DMSO, quantified using their molar extinction coefficients at 320 nm, and stored at 4°C. As recommended by the manufacturer, the SA sensors were pre-conditioned with 1 M NaCl in 50 mM NaOH (three 1 min pulses at 50 μL/min) before the capture of DNA at 10 μL/min (15 μM stocks diluted to 100 nM in running buffer containing 0.5 M KCl). To minimize non-specific binding to the SA-coated sensors, the compounds were serially diluted in running buffer (< 0.1% DMSO final) containing 1 mg/mL CM-dextran (BioChemika #27560, Fluka / Sigma Aldrich, Missouri, USA). To assess binding specificity in multi-cycle 'KINJECT' mode, diluted compounds were injected over reference (SA-only) and DNA-immobilized (450 RU) surfaces at 25 μL/min (5 min association + 10 min dissociation; 5 μM fixed). Between sample injections, the sensors were regenerated at 50 μL/min using two 30-second pulses of PGE buffer containing 0.05% (v/v) Triton X100 (Solution I) or Empigen (Solution II), followed by 'EXTRACLEAN' and 'RINSE' procedures. To assess dose-dependent binding in multi-cycle 'KINJECT' mode, diluted compounds were titrated (0–5 μM, 2-fold dilution series) over lower-density DNA surfaces (300 RU) and were regenerated in a similar manner. Data were doubled-referenced and represent duplicate injections acquired from at least two independent trials. For each replicate series, a buffer blank was injected first, the highest titrant concentration second, and serial dilutions followed (from the lowest to the highest concentration); comparing responses between the two highest titrant injections verified consistent DNA surface activity throughout each assay. To estimate apparent equilibrium dissociation constants (K_D), steady-state binding responses (R_{eq}; average RU at the end of the association phase) were plotted as a function of complex concentration (C) and then subjected to non-linear regression ("Steady-state affinity" model, BIAevaluation v4.1 software). Titration series were also analyzed

using the "Fit ka/kd separate" tool to estimate the individual dissociation rate constants (k_d; evaluated in the early portion of the dissociation phase to exclude rebinding effects). Theoretical binding maxima were predicted using the following equation: *Rmax = (MWA / MWL) (RL) (n)* where *Rmax* is the maximal binding response (RU) at saturating compound concentrations; *MWA* is the molecular weight (Da) of the compound injected in solution; *MWL* is the molecular weight (Da) of the DNA fragment immobilized; *RL* is the amount (RU) of DNA immobilized; *n* is the predicted binding stoichiometry (e.g. 1:1). G-quadruplex sequences 22AG, cmyc, and ckit1, and duplex HP were formed identically to those used for CD melting in potassium conditions.

5.6 References

1. Williamson, J. R., Guanine Quartets. *Curr Opin Struct Biol* **1993,** *3* (3), 357-362.
2. Simonsson, T., G-quadruplex DNA structures − variations on a theme. *Biol Chem* **2001,** *382* (4), 621-628.
3. Burge, S.; Parkinson, G. N.; Hazel, P.; Todd, A. K.; Neidle, S., Quadruplex DNA: sequence, topology and structure. *Nucleic Acids Res* **2006,** *34* (19), 5402-5415.
4. Rezler, E. M.; Bearss, D. J.; Hurley, L. H., Telomere inhibition and telomere disruption as processes for drug targeting. *Annu Rev Pharmacol Toxicol* **2003,** *43*, 359-379.
5. De Cian, A.; Lacroix, L.; Douarre, C.; Temime-Smaali, N.; Trentesaux, C.; Riou, J. F.; Mergny, J. L., Targeting telomeres and telomerase. *Biochimie* **2008,** *90* (1), 131-155.
6. Qin, Y.; Hurley, L. H., Structures, folding patterns, and functions of intramolecular DNA G-quadruplexes found in eukaryotic promoter regions. *Biochimie* **2008,** *90* (8), 1149-1171.
7. Balasubramanian, S.; Neidle, S., G-quadruplex nucleic acids as therapeutic targets. *Curr Opin Chem Biol* **2009,** *13* (3), 345-353.
8. Neidle, S., Human telomeric G-quadruplex: the current status of telomeric G-quadruplexes as therapeutic targets in human cancer. *FEBS J* **2010,** *277* (5), 1118-1125.
9. Balasubramanian, S.; Hurley, L. H.; Neidle, S., Targeting G-quadruplexes in gene promoters: a novel anticancer strategy? *Nat Rev: Drug Disc* **2011,** *10* (4), 261-275.
10. Collie, G. W.; Parkinson, G. N., The application of DNA and RNA G-quadruplexes to therapeutic medicines. *Chem Soc Rev* **2011,** *40* (12), 5867-5892.
11. Huppert, J. L.; Balasubramanian, S., Prevalence of quadruplexes in the human genome. *Nucleic Acids Res* **2005,** *33* (9), 2908-2916.
12. Huppert, J. L.; Balasubramanian, S., G-quadruplexes in promoters throughout the human genome. *Nucleic Acids Res* **2007,** *35* (2), 406-413.

13. Huppert, J. L., Hunting G-quadruplexes. *Biochimie* **2008,** *90* (8), 1140-1148.
14. Siddiqui-Jain, A.; Grand, C. L.; Bearss, D. J.; Hurley, L. H., Direct evidence for a G-quadruplex in a promoter region and its targeting with a small molecule to repress c-MYC transcription. *Proc Natl Acad Sci USA* **2002,** *99* (18), 11593-11598.
15. Wu, P.; Ma, D. L.; Leung, C. H.; Yan, S. C.; Zhu, N.; Abagyan, R.; Che, C. M., Stabilization of G-quadruplex DNA with platinum(II) Schiff base complexes: Luminescent probe and down-regulation of c-myc oncogene expression. *Chem Eur J* **2009,** *15* (47), 13008-13021.
16. Agarwal, T.; Roy, S.; Chakraborty, T. K.; Maiti, S., Selective targeting of G-quadruplex using furan-based cyclic homooligopeptides: Effect on c-MYC expression. *Biochemistry* **2010,** *49* (38), 8388-8397.
17. Shalaby, T.; Von Bueren, A. O.; Hürlimann, M. L.; Fiaschetti, G.; Castelletti, D.; Masayuki, T.; Nagasawa, K.; Arcaro, A.; Jelesarov, I.; Shin-ya, K.; Grotzer, M., Disabling c-Myc in childhood medulloblastoma and atypical teratoid/rhabdoid tumor cells by the potent G-quadruplex interactive agent S2T1-6OTD. *Mol Cancer Ther* **2010,** *9* (1), 167-179.
18. Wang, P.; Leung, C. H.; Ma, D. L.; Yan, S. C.; Che, C. M., Structure-based design of platinum(II) Complexes as c-myc oncogene Down-regulators and luminescent probes for G-quadruplex DNA. *Chem Eur J* **2010,** *16* (23), 6900-6911.
19. Ou, T. M.; Lin, J.; Lu, Y. J.; Hou, J. Q.; Tan, J. H.; Chen, S. H.; Li, Z.; Li, Y. P.; Li, D.; Gu, L. Q.; Huang, Z. S., Inhibition of cell proliferation by quindoline derivative (SYUIQ-05) through its preferential interaction with c-myc promoter G-quadruplex. *J Med Chem* **2011,** *54* (16), 5671-5679.
20. Bejugam, M.; Sewitz, S.; Shirude, P. S.; Rodriguez, R.; Shahid, R.; Balasubramanian, S., Trisubstituted isoalloxazines as a new class of G-quadruplex binding ligands: small molecule regulation of c-kit oncogene expression. *J Am Chem Soc* **2007,** *129* (43), 12926-12927.
21. Bejugam, M.; Gunaratnam, M.; Müller, S.; Sanders, D. A.; Sewitz, S.; Fletcher, J. A.; Neidle, S.; Balasubramanian, S., Targeting the c-KitPromoter G-quadruplexes with 6-Substituted Indenoisoquinolines. *ACS Med Chem Lett* **2010,** *1* (7), 306-310.
22. McLuckie, K. I.; Waller, Z. A.; Sanders, D. A.; Alves, D.; Rodriguez, R.; Dash, J.; McKenzie, G. J.; Venkitaraman, A. R.; Balasubramanian, S., G-quadruplex-binding benzo[a]phenoxazines down-regulate c-KIT expression in human gastric carcinoma cells. *J Am Chem Soc* **2011,** *133* (8), 2658-2663.
23. Sun, D.; Liu, W. J.; Guo, K.; Rusche, J. J.; Ebbinghaus, S.; Gokhale, V.; Hurley, L. H., The proximal promoter region of the human vascular endothelial growth factor gene has a G-quadruplex structure that can be targeted by G-quadruplex-interactive agents. *Mol Cancer Ther* **2008,** *7* (4), 880-889.
24. Taka, T.; Joonlasak, K.; Huang, L.; Randall Lee, T.; Chang, S. W. T.; Tuntiwechapikul, W., Down-regulation of the human VEGF gene expression by perylene monoimide derivatives. *Bioorg Med Chem Lett* **2012,** *22* (1), 518-522.

25. Dai, J.; Dexheimer, T. S.; Chen, D.; Carver, M.; Ambrus, A.; Jones, R. A.; Yang, D., An intramolecular G-quadruplex structure with mixed parallel/antiparallel G-strands formed in the human BCL-2 promoter region in solution. *J Am Chem Soc* **2006,** *128* (4), 1096-1098.
26. Qin, Y.; Rezler, E. M.; Gokhale, V.; Sun, D.; Hurley, L. H., Characterization of the G-quadruplexes in the duplex nuclease hypersensitive element of the PDGF-A promoter and modulation of PDGF-A promoter activity by TMPyP4. *Nucleic Acids Res* **2007,** *35* (22), 7698-7713.
27. Viglasky, V., Platination of telomeric sequences and nuclease hypersensitive elements of human c-myc and PDGF-A promoters and their ability to form G-quadruplexes. *FEBS J* **2009,** *276* (2), 401-409.
28. Wang, X. D.; Ou, T. M.; Lu, Y. J.; Li, Z.; Xu, Z.; Xi, C.; Tan, J. H.; Huang, S. L.; An, L. K.; Li, D.; Gu, L. Q.; Huang, Z. S., Turning off transcription of the bcl-2 gene by stabilizing the bcl-2 promoter quadruplex with quindoline derivatives. *J Med Chem* **2010,** *53* (11), 4390-4398.
29. Chen, Y.; Agrawal, P.; Brown, R. V.; Hatzakis, E.; Hurley, L.; Yang, D., The Major G-Quadruplex Formed in the Human Platelet-Derived Growth Factor Receptor-β Promoter Adopts a Novel Broken-Strand Structure in K^+ Solution. *J Am Chem Soc* **2012,** *134* (32), 13220-13223.
30. Kumari, S.; Bugaut, A.; Huppert, J. L.; Balasubramanian, S., An RNA G-quadruplex in the 5' UTR of the NRAS proto-oncogene modulates translation. *Nat Chem Biol* **2007,** *3* (4), 218-21.
31. Wieland, M.; Hartig, J. S., RNA quadruplex-based modulation of gene expression. *Chem Biol* **2007,** *14* (7), 757-763.
32. Bugaut, A.; Rodriguez, R.; Kumari, S.; Hsu, S. T.; Balasubramanian, S., Small molecule-mediated inhibition of translation by targeting a native RNA G-quadruplex. *Org Biomol Chem* **2010,** *8* (12), 2771-2776.
33. Monchaud, D.; Teulade-Fichou, M. P., A hitchhiker's guide to G-quadruplex ligands. *Org Biomol Chem* **2008,** *6* (4), 627-636.
34. Kieltyka, R.; Englebienne, P.; Fakhoury, J.; Autexier, C.; Moitessier, N.; Sleiman, H. F., A platinum supramolecular square as an effective G-quadruplex binder and telomerase inhibitor. *J Am Chem Soc* **2008,** *130* (31), 10040-10041.
35. Kieltyka, R.; Fakhoury, J.; Moitessier, N.; Sleiman, H. F., Platinum phenanthroimidazole complexes as G-quadruplex DNA selective binders. *Chem Eur J* **2008,** *14* (4), 1145-1154.
36. Castor, K. J.; Mancini, J.; Fakhoury, J.; Weill, N.; Kieltyka, R.; Englebienne, P.; Avakyan, N.; Mittermaier, A.; Autexier, C.; Moitessier, N.; Sleiman, H. F., Platinum(II) phenanthroimidazoles for targeting telomeric G-quadruplexes. *ChemMedChem* **2012,** *7* (1), 85-94.

37. Castor, K. J.; Liu, Z.; Fakhoury, J.; Hancock, M. A.; Mittermaier, A.; Moitessier, N.; Sleiman, H. F., A Platinum(II) Phenylphenanthroimidazole with an Extended Side-Chain Exhibits Slow Dissociation from a c-Kit G-Quadruplex Motif. *Chem Eur J* **2013,** *19* (52), 17836-17845.
38. Georgiades, S. N.; Abd Karim, N. H.; Suntharalingam, K.; Vilar, R., Interaction of metal complexes with G-quadruplex DNA. *Angew Chem Int Ed* **2010,** *49* (24), 4020-4034.
39. Bhattacharjee, A. J.; Ahluwalia, K.; Taylor, S.; Jin, O.; Nicoludis, J. M.; Buscaglia, R.; Brad Chaires, J.; Kornfilt, D. J.; Marquardt, D. G.; Yatsunyk, L. A., Induction of G-quadruplex DNA structure by Zn(II) 5,10,15,20-tetrakis(N-methyl-4-pyridyl)porphyrin. *Biochimie* **2011,** *93* (8), 1297-1309.
40. Largy, E.; Hamon, F.; Rosu, F.; Gabelica, V.; De Pauw, E.; Guedin, A.; Mergny, J. L.; Teulade-Fichou, M. P., Tridentate N-donor palladium(II) complexes as efficient coordinating quadruplex DNA binders. *Chem Eur J* **2011,** *17* (47), 13274-13283.
41. Manet, I.; Manoli, F.; Donzello, M. P.; Viola, E.; Andreano, G.; Masi, A.; Cellai, L.; Monti, S., A cationic Zn(II) porphyrazine induces a stable parallel G-quadruplex conformation in human telomeric DNA. *Org Biomol Chem* **2011,** *9* (3), 684-688.
42. Sun, D.; Liu, Y.; Liu, D.; Zhang, R.; Yang, X.; Liu, J., Stabilization of G-quadruplex DNA, inhibition of telomerase activity and live cell imaging studies of chiral ruthenium(II) complexes. *Chem Eur J* **2012,** *18* (14), 4285-4295.
43. Zheng, X. H.; Zhong, Y. F.; Tan, C. P.; Ji, L. N.; Mao, Z. W., Pt(ii) squares as selective and effective human telomeric G-quadruplex binders and potential cancer therapeutics. *Dalton Trans* **2012,** *41*, 11807-11812.
44. Rezler, E. M.; Seenisamy, J.; Bashyam, S.; Kim, M. Y.; White, E.; Wilson, W. D.; Hurley, L. H., Telomestatin and diseleno sapphyrin bind selectively to two different forms of the human telomeric G-quadruplex structure. *J Am Chem Soc* **2005,** *127* (26), 9439-9447.
45. Shirude, P. S.; Gillies, E. R.; Ladame, S.; Godde, F.; Shin-Ya, K.; Huc, I.; Balasubramanian, S., Macrocyclic and helical oligoamides as a new class of G-quadruplex ligands. *J Am Chem Soc* **2007,** *129* (39), 11890-11891.
46. Monchaud, D.; Allain, C.; Teulade-Fichou, M. P., Development of a fluorescent intercalator displacement assay (G4-FID) for establishing quadruplex-DNA affinity and selectivity of putative ligands. *Bioorg Med Chem Lett* **2006,** *16* (18), 4842-4845.
47. Monchaud, D.; Allain, C.; Bertrand, H.; Smargiasso, N.; Rosu, F.; Gabelica, V.; De Cian, A.; Mergny, J. L.; Teulade-Fichou, M. P., Ligands playing musical chairs with G-quadruplex DNA: a rapid and simple displacement assay for identifying selective G-quadruplex binders. *Biochimie* **2008,** *90* (8), 1207-1223.
48. Largy, E.; Hamon, F.; Teulade-Fichou, M. P., Development of a high-throughput G4-FID assay for screening and evaluation of small molecules binding quadruplex nucleic acid structures. *Anal Bioanal Chem* **2011,** *400* (10), 3419-3427.

49. When browsing suppliers, it became immediately obvious that one non-disposable black quartz microplate cost 1000x more than 50 disposable black polypropylene plates. In order to truly utilize the high-throughput nature of the assay, we opted for the disposable polypropylene plates with the knowledge that our results may be artificially high.
50. Armitage, B. A., Cyanine Dye – DNA Interactions : Intercalation, Groove Binding, and Aggregation. *Top Curr Chem* **2005,** *253*, 55-76.
51. Kern, J. T.; Thomas, P. W.; Kerwin, S. M., The Relationship between Ligand Aggregation and G-Quadruplex DNA Selectivity in a Series of 3,4,9,10-Perylenetetracarboxylic Acid Diimides. *Biochemistry* **2002,** *41* (38), 11379-11389.
52. Franceschin, M.; Lombardo, C. M.; Pascucci, E.; D'Ambrosio, D.; Micheli, E.; Bianco, A.; Ortaggi, G.; Savino, M., The number and distances of positive charges of polyamine side chains in a series of perylene diimides significantly influence their ability to induce G-quadruplex structures and inhibit human telomerase. *Bioorg Med Chem* **2008,** *16* (5), 2292-2304.
53. Dixon, I. M.; Lopez, F.; Esteve, J. P.; Tejera, A. M.; Blasco, M. A.; Pratviel, G.; Meunier, B., Porphyrin derivatives for telomere binding and telomerase inhibition. *ChemBioChem* **2005,** *6* (1), 123-132.
54. Manaye, S.; Eritja, R.; Avino, A.; Jaumot, J.; Gargallo, R., Porphyrin binding mechanism is altered by protonation at the loops in G-quadruplex DNA formed near the transcriptional activation site of the human c-kit gene. *Biochim Biophys Acta* **2012,** *1820* (12), 1987-1996.
55. Nanjunda, R.; Owens, E. A.; Mickelson, L.; Alyabyev, S.; Kilpatrick, N.; Wang, S.; Henary, M.; Wilson, W. D., Halogenated pentamethine cyanine dyes exhibiting high fidelity for G-quadruplex DNA. *Bioorg Med Chem* **2012,** *20* (24), 7002-7011.
56. Li, Z.; Tan, J. H.; He, J. H.; Long, Y.; Ou, T. M.; Li, D.; Gu, L. Q.; Huang, Z. S., Disubstituted quinazoline derivatives as a new type of highly selective ligands for telomeric G-quadruplex DNA. *Eur J Med Chem* **2012,** *47* (1), 299-311.
57. Suntharalingam, K.; White, A. J.; Vilar, R., Synthesis, structural characterization, and quadruplex DNA binding studies of platinum(II)-terpyridine complexes. *Inorg Chem* **2009,** *48* (19), 9427-9435.
58. Sun, D.; Thompson, B.; Cathers, B. E.; Salazar, M.; Kerwin, S. M.; Trent, J. O.; Jenkins, T. C.; Neidle, S.; Hurley, L. H., Inhibition of human telomerase by a G-quadruplex-interactive compound. *J Med Chem* **1997,** *40* (14), 2113-2116.
59. Read, M.; Harrison, R. J.; Romagnoli, B.; Tanious, F. A.; Gowan, S. H.; Reszka, A. P.; Wilson, W. D.; Kelland, L. R.; Neidle, S., Structure-based design of selective and potent G quadruplex-mediated telomerase inhibitors. *Proc Natl Acad Sci USA* **2001,** *98* (9), 4844-4849.
60. Perry, P. J.; Jenkins, T. C., DNA tetraplex-binding drugs: structure-selective targeting is critical for antitumour telomerase inhibition. *Mini Rev Med Chem* **2001,** *1* (1), 31-41.

61. Carrasco, C.; Rosu, F.; Gabelica, V.; Houssier, C.; De Pauw, E.; Garbay-Jaureguiberry, C.; Roques, B.; Wilson, W. D.; Chaires, J. B.; Waring, M. J.; Bailly, C., Tight binding of the antitumor drug ditercalinium to quadruplex DNA. *ChemBioChem* **2002,** *3* (12), 1235-1241.
62. Teulade-Fichou, M. P.; Carrasco, C.; Guittat, L.; Bailly, C.; Alberti, P.; Mergny, J. L.; David, A.; Lehn, J. M.; Wilson, W. D., Selective recognition of G-Quadruplex telomeric DNA by a bis(quinacridine) macrocycle. *J Am Chem Soc* **2003,** *125* (16), 4732-4740.
63. Ya, X.; Xiaohua, Z.; Jianzhong, W.; Huiying, Y.; Liangnian, J., Synthesis, Characterization and Proton-Dependent Electronic Spectra of a Series of Novel Ruthenium(II) Complexes Containing an Imidazole Unit. *Synth React Inorg Met-Org Chem* **1998,** *28* (9), 1445-1454.
64. Xiong, Y.; He, X.-F.; Zou, X.-H.; Wu, J.-Z.; Chen, X.-M.; Ji, L.-N.; Li, R.-H.; Zhou, J.-Y.; Yu, K.-B., Interaction of polypyridyl ruthenium(II) complexes containing non-planar ligands with DNA. *J Chem Soc, Dalton Trans* **1999,** (1), 19-24.
65. Wu, J.-Z.; Yang, G.; Chen, S.; Ji, L.-N.; Zhou, J.-Y.; Xu, Y., Intercalation into calf thymus DNA of 2-(4-arylphenyl)imidazo[4,5-*f*]-[1,10]phenanthroline (aryl = -OMe, $-NMe_2$ or $-NO_2$) in its bipyridyl ruthenium(II) complex. *Inorg Chim Acta* **1998,** *283* (1), 17-23.
66. Wu, J.-Z.; Li, L.; Zeng, T.-X.; Ji, L.-N.; Zhou, J.-Y.; Luo, T.; Li, R.-H., Synthesis, characterization and luminiscent DNA-binding study of a series of ruthenium complexes containing 2-arylimidazo[*f*]1,10-phenanthroline. *Polyhedron* **1997,** *16* (1), 103-107.
67. Chen, T.; Mei, W.-J.; Wong, Y.-S.; Liu, J.; Liu, Y.; Xie, H.-S.; Zheng, W.-J., Chiral ruthenium polypyridyl complexes as mitochondria-targeted apoptosis inducers. *MedChemComm* **2010,** *1* (1), 73.
68. IDT SciTools OligoAnalyzer ver 3.1. https://www.idtdna.com/analyzer/Applications/OligoAnalyzer/ (accessed December 12, 2010).

6 Conclusions and Contributions to Knowledge

6.1 Conclusions

6.1.1 The application of phenanthroimidazole platinum(II) complexes with extended π-surfaces as binders of human telomeric G-quadruplexes

This chapter represents a highly collaborative effort among the Sleiman (Department of Chemistry), Moitessier (Department of Chemistry), and Autexier (Departments of Anatomy & Cell Biology and Experimental Medicine) laboratories at McGill University, with data interpretation assistance from **Prof. Anthony Mittermaier** (Department of Chemistry). **Katherine Castor** was responsible for the synthesis, characterization, and biophysical studies (CD, FID) therein, as well as project design. **Dr. Roxanne Kieltyka** developed the initial synthesis of complexes **2.1**-**2.4**. Synthesis of complexes **2.5** and **2.6** was assisted by a summer undergraduate, **Nicole Avakyan**. The computer-aided studies were performed by **Dr. Pablo Englebienne** and **Dr. Nathanael Weill** under the supervision of **Prof. Nicolas Moitessier**. The TRAP-Lig assays were performed by **Dr. Johans Fakhoury** (Sleiman and Autexier laboratories) and **Johanna Mancini** (Autexier). **Johanna Mancini** also conducted the celluar assays under the supervision of **Prof. Chantal Autexier**. The findings in this chapter were published in a manuscript accepted by ChemMedChem in 2012 entitled "Platinum(II) phenanthroimidazoles for targeting telomeric G-quadruplexes".

Chapter 2 presented the preparation of five novel platinum(II) phenanthroimidazoles that were structurally evolved from our previously published phenyl- and napthylphenanthroimidazole complexes. In four of the complexes, we incorporated an intramolecular hydrogen bond that was predicted by molecular modeling to hold the ligand in a flat, planar orientation. However this modification did not significantly increase binding strength to the human telomeric G-quadruplex motif over the parent phenylphenanthroimidazole complex. They quinolinyl- and indolyl- complexes were light-sensitive, limiting the extent to which they could be studied, and the 2-hydroxynaphthyl- complex presented solubility issues. The phenol- derivative did not significantly improve upon the parent phenyl- complex as this complex was flexible enough to be planar upon binding to the G-tetrads. Instead, we demonstrated through an FID assay that the inclusion of a *p*-chloro- substitution on the phenyl- moiety resulted in the greatest binding affinity of the series to a G-quadruplex motif (DC_{50} = 0.31 μM compared to 0.66 μM for the unsubstituted parent complex with the antiparallel

G-quadruplex from a fluorescence intercalator displacement assay). Binding ability can be evaluated from this assay as it involves the competitive displacement of a fluorescent dye from nucleic acids that can be monitored through decreasing fluorescence intensity of the bound dye upon increasing additions of the competing complex. Additionally, the phenyl-, quinolinyl-, phenol- and *p*-chloro- complexes were able to template the formation of the antiparallel G-quadruplex from the unstructured single-strand in a 2:1 binding stoichiometry. The complexes were also shown to inhibit telomerase efficiently with IC_{50} values that range from 0.46−11.6 μM. We also demosntrated the selective cytotoxicity of the *p*-chloro- derivative to HeLa cells (IC_{50} ~ 20 μM versus ~ 60 μM for normal fibroblast cells), which validates our scaffold as a potential therapeutic.

6.1.2 The addition of side-chains to phenylphenanthroimidazole platinum(II) ligands allows for specific targeting and slow dissociation from G-quadruplex motifs

This chapter represents a collaborative effort among the Sleiman and Moitessier laboratories at McGill University, with data interpretation assistance from **Prof. Anthony Mittermaier**. **Katherine Castor** was responsible for the design, synthesis, and characterization of the complexes therein, as well as project design and biophysical assays (HT-FID, CD, and HPLC). **Dr. Mark A. Hancock** (McGill SPR Facility) conducted the SPR assays and **Dr. Guillaume Lesage** (CIAN, Department of Biology) ran the robot for the HT-FID assays. The computer-aided studies were performed by **Zhaomin Liu** under the supervision of **Prof. Nicolas Moitessier**. The biological assays (MTS, mRNA analysis, and western blot) were performed by **Dr. Johans Fakhoury** (Sleiman laboratory). The findings in this chapter were published in a manuscript accepted by Chemistry − A European Journal in 2013 entitled "A platinum(II) phenylphenanthroimidazole with an extended side-chain exhibits slow dissociation from a *c-Kit* G-quadruplex motif".

In Chapter 3, we hypothesized with the aid of molecular modeling, that the addition of a side-chain to our phenylphenanthroimidazole ligand would allow for a multivalent binding mode of our platinum(II) complexes to G-quadruplex DNA. Through the use of a high-throughput fluorescence intercalator displacement assay, we discovered that remarkably different binding isotherms were obtained after a 10 minute and a 90 minute incubation (DC_{50} > 2.50 μM compared to 0.282 μM for complex **3.2** binding to a *c-Kit* derived G-quadruplex). Surface plasmon

resonance experiments showed an unprecedented slow dissociation of this complex from G-quadruplex motifs, leading us to conclude that the side-chain's multivalent interactions across the binding site on the G-quadruplex motifs results in fast-on, slow-off binding kinetics. Biological assays including mRNA levels analysis of *c-Kit* and a western blot for cKIT protein exhibited an increase in cKIT production rather than the intended decrease that is expected from a promoter quadruplex-interacting agent. The elucidation of the mechanism of interaction of complex **3.2** in the cellular environment is necessary to determine the utility of such a compound for modification of gene expression.

6.1.3 Exchanging platinum(II) with iridium(III) in phenylphenanthroimidazole complexes creates "G-quadruplex light-switch" probes

This chapter represents a collaborative effort between the Sleiman and Mauzeroll laboratories. **Katherine Castor** was responsible for the design, synthesis, and characterization of the complexes therein, as well as project design and biophysical assays (UV/Vis and luminescence assays). The X-ray crystallography was conducted by **Dr. Christopher Serpell**. The CV and ECL experiments were conducted by **Dr. Kimberly Metera** and **Dr. Ushula Tefashe**. The high-throughput fluorescence assay was designed by **Katherine Castor** and conducted by **Dr. Guillaume Lesage** (CIAN, McGill University). The findings in this chapter are to be published in a manuscript submitted to the Journal of the American Chemical Society in 2014.

In Chapter 4, we harnessed the luminescent "quadruplex light-switch" effect by exchanging platinum(II) for iridium(III) in our phenanthroimidazole ligand motif. The "light-switch" effect involves the significantly increased luminescence intensity observed when the complexes are bound to G-quadruplex DNA (but not duplex DNA) as compared to unbound in solution. This "light-switch" effect was most dramatic with ~ 53-fold enhancement upon binding of the 2-chloro- derivative when binding to the mixed parallel/antiparallel human telomeric G-quadruplex motif. The increased luminescence upon binding to G-quadruplex DNA, enabled us to use a direct fluorescence assay to determine binding affinity of the complexes that resulted in binding affinities in the low micromolar regime. Additionally, the iridium(III) complexes exhibited electrochemiluminescence (ECL), that is, catalytic production of light at an

electrode, pointing to their potential for signal amplification in G-quadruplex detection. Taken together, their G-quadruplex DNA binding ability and their luminescence and electrochemiluminescence properties render them very amenable to development as G-quadruplex probes and detection agents.

6.1.4 Library expansion of phenylphenanthroimidazole ligands to incorporate groups with varying electronic effects and subsequent G-quadruplex targeting

Katherine Castor was responsible for the synthesis and characterization of the complexes therein, as well as project design and biophysical assays. Operation of the robot for the HT-FID assay was done by **Dr. Guillaume Lesage** of the Cell Imagining and Analysis Network (CIAN) (McGill University Department of Biology). **Dr. Mark Hancock** performed the SPR assays at the McGill SPR Facility.

In Chapter 5, we built upon our findings from Chapter 2 by expanding our library to include electron-withdrawing and electron-donating substituted phenylphenanthroimidazole ligands. We hypothesized that small changes to our ligand core may result in the differential G-quadruplex polymorph recognition. We discovered through circular dichroism titrations that some of the complexes could template the formation of the antiparallel G-quadruplex motif from the unstructured single strand of the human telomeric sequence in a 2:1 binding stoichiometry, similarly to those complexes in Chapter 2. We encountered non-specific binding of our complexes in the high-throughput fluorescence intercalator displacement assay that skewed our DC_{50} values in an undesirable manner, prohibiting us from determining reliable trends and polymorph recognition. Surface plasmon resonance assays did, however, demonstrate selective binding of selected complexes to G-quadruplex DNA over dsDNA. Despite the pitfalls, the facile synthesis of this type of library lends itself as a promising avenue for the futher development of selective G-quadruplex binders.

6.1.5 Mechanochemical synthesis of supramolecular squares

Experimental methods were performed by **Katherine Castor** under the guidance of **Dr. Tomislav Friščić**.

In Appendix A, we utilized supramolecular self-assembly in the solid state to create the macrocyclic square $[Pten(bpy)]_4[NO_3]_8$ *via* the $PtenCl_2$ intermediate. The $[Pten(bpy)]_4[NO_3]_8$ square has previously been shown by our laboratory to be an efficient G-quadruplex binder and telomerase inhibitor, however, the synthesis of the complex is lengthy (~ 3 weeks) and involves the use of an *in situ* created intermediate $Pten(NO_3)_2$ that is not easily isolated. In this appendix, we used mechanochemistry to create the square in two steps in a matter of hours from commercially available K_2PtCl_4 and ethylenediamine. To the best of our knowledge, this is the first synthesis of the $PtenCl_2$ intermediate by ball-milling. The resulting synthetic scheme is high-yielding, "green" and only involves filtration and lyophilization for isolation of the intermediate and final products.

6.1.6 Union of 3D-DNA nanostructures, G-quadruplexes, and a small molecule binder

The design for the project was carried out by **Christopher McLaughlin** and **Katherine Castor**. Initial studies on feasibility of the 3D-assembly were performed by **Christopher McLaughlin**. The preparation of the 3D-DNA scaffolds and construction thereof presented herein were performed by **Graham D. Hamblin**. The biophysical studies were designed and carried out by **Katherine Castor**.

In Appendix B, we combine the expertise of the Sleiman laboratory's 3D-DNA assembly with G-quadruplex formation to create DNA prisms with appended G-quadruplexes in a site-specific manner. Iron(III)-hemin has been shown to selectively bind to G-quadruplex motifs and when bound, exhibits catalytic peroxidase ability. By combining the G-quadruplex with the 3D-assembly, we can site-specifically bind hemin to create a supramolecular cataltyic structure. The variety of G-quadruplex forming sequences and their inherent polymorphic nature presents a library of sequences that have the capability of binding to different catalytic centers, thus allowing for the placement of several centers, with the potential for creating three-dimensional catalytic cascades.

6.2 Future directions

6.2.1 Platinum(II) phenanthroimidazoles

For our side-arm containing complexes like those in Chapter 3, we would like to focus on increasing the cellular uptake in cell lines that over-express the *c-Kit* oncogene. Increased uptake in cells with higher levels of mRNA and protein (like human stomach carcinoma HCG-27), can aid in the investigation of the mechanism of action by this class of complex in depth. Increased cellular uptake can be carried out through the incorporation of these complexes in the hydrophobic core of DNA-micelle delivery vehicle that is currently being developed in the Sleiman Laboratory. This would allow for the further development of these complexes as chemotherapies.

For our electron-withdrawing and donating complexes in Chapter 5, DFT calculations of the electronics of the ligand may help determine the influence of the frontier orbitals on binding to the G-tetrad. Performing the HT-FID assay in quartz microplates would also allow for the precise determination of the binding affinities. SPR assays for the series of complexes should be conducted to get an accurate measure of binding affinity to different G-quadruplex and duplex motifs. Cell viability assays would be necessary to determine if the platinum complexes are selective for cancer cells over normal cells, and a detailed study into the mechanism of action of the complexes in the selective cytotoxicity to cancer cells would establish criteria for the design of future therapeutics based on the phenanthroimidazole core.

6.2.2 Iridium(III) phenanthroimidazoles

For the iridium(III) complexes like those in Chapter 4, future directions include the development of complexes with a red-shifted excitation wavelength. If the excitation wavelength is red-shifted, it may be used for *in cellulo* detection of G-quadruplexes. The current excitation wavelength is too low (~ 260−320 nm) which causes autofluorescence of the cellular components. However, an appealing aspect of iridium complexes is their long fluorescence lifetimes. When used in

conjunction with time-gated fluorescence microscopy, ligand modifications to red-shift the excitation maxima may not be necessary. These complexes can bind to G-quadruplexes *in cellulo* and potentially template their formation therein, which is an added advantage when developing light-up probes. Development of an ECL-detection assay of for G-quadruplex motifs also provides an exciting future for these complexes. And finally, further verification of the trends involving ECL intensities could be obtained through the synthesis and analysis of other complexes that may lie on the outer edges of the Hammet values (including 2,6-dichloro-, *p*-hydroxyphenyl-, and 2-hydroxyphenyl- ligand varieties) and through DFT calculations.

6.2.3 Mechanochemistry methods

In a similar manner to that presented in Appendix A, we hope to synthesize the palladium analogs, that is $PdenCl_2$ and and $[Pden(bpy)]_4[NO_3]_8$. We hypothesize that we can synthesize $PdenCl_2$ starting from K_2PdCl_4 and ethylenediamine and avoid the use of concentrated hydrochloric acid, which is involved in the established solution synthesis of the $PdenCl_2$ intermediate. In fact, investigations into this method have already begun. In addition to the palladium(II) analogs, a variety of organic linkers besides the 4,4'-bipyridyl can be incorporated for facile library construction.

6.2.4 G-quadruplex/hemin 3D-DNA prisms

For the continuation of the work in Appendix B, it would be interesting to determine whether the geometric arrangement of the G4 motifs on the 3D-assmebly will affect the binding affinity and peroxidase ability of hemin. As a next step, the incorporation of different G-quadruplex sequences that are selective for different catalytic moieties should be performed, to further the use of these assemblies as scaffolds for catalytic cascades.

6.3 Papers and conference presentations

6.3.1 Papers published

1) **Castor, K.J.**; Liu, Z.; Fakhoury, J.; Hancock, M.A.; Mittermaier, A.; Moitessier, N.; and Sleiman, H.F., "A platinum(II) phenylphenanthroimidazole with an extended side-chain exhibits slow dissociation from a *c-Kit* G-quadruplex motif," Chem. Eur. J, **2013**, *19(52)*, 17836-17845.

2) Conway, J.W.; McLaughlin, C.K.; **Castor, K.J.**; Sleiman, H., "DNA nanostructure serum stability: greater than the sum of its parts," Chem. Commun., **2013**, *(49) 12*, 1172-1174.

3) **Castor, K.J.**; Mancini, J.; Fakhoury, J.; Weill, N.; Kieltyka, R.; Englebienne, P.; Avakyan, N.; Mittermaier, A.; Autexier, C.; Moitessier, N.; and Sleiman, H.F., "Platinum(II) phenanthroimidazoles for targeting telomeric G-quadruplexes," ChemMedChem, **2012**, *7(1)*, 85-94.

6.3.2 Conference proceedings

1) **Castor, K.J.**; Liu, Z.; Fakhoury, J.; Hancock, M.A.; Mittermaier, A.; Moitessier, N.; and Sleiman, H.F., "Platinum(II) phenylphenanthroimidazoles for with "clicked" side-chains as selective G-quadruplex DNA binders," J. Biomol. Struct. Dyn., **2013**, *31(sup1)*, 31-32.

2) **Castor, K.J.**; Kieltyka, R.; Englebienne, P.; Weill, N.; Fakhoury, J.; Mancini, J.; Avakyan, N.; Mittermaier, A.; Autexier, C.; Moitessier, N.; and Sleiman, H.F., "Platinum(II) phenylphenanthroimidazoles for G-quadruplex targeting: The effect of structure on binding affinity, selectivity, and telomerase inhibition," J. Biomol. Struct. Dyn., **2011**, *28(6)*, 1090-1091.

6.3.3 Conference presentations

1) **Castor, K.J.**; Mancini, J.; Fakhoury, J.F.; Liu, Z.; Mittermaier, A.; Autexier, C.; Moitessier, N.; Sleiman, H.F., "Platinum(II) phenanthroimidazoles with "clicked" sidechains as selective G-quadruplex DNA binders", EMBO Conference Series in Chemical Biology, Heidelberg, Germany, September 26-29, 2012 (Poster Presentation).

2) **Castor, K.J.**; Kieltyka, R.; Englebienne, P.; Weill, N.; Mancini, J.; Fakhoury, J.F.; Avakyan, N.; Mittermaier, A.; Autexier, C.; Moitessier, N.; Sleiman, H.F., "Rational design of platinum(II)-based phenanthroimidazoles: Towards targeting G-quadruplex DNA", IS3NA International Round Table XX, Montreal, QC, August, 2012 (Poster Presentation).

3) **Castor, K.J.**; Kieltyka, R.; Englebienne, P.; Weill, N.; Mancini, J.; Fakhoury, J.F.; Avakyan, N.; Mittermaier, A.; Autexier, C.; Moitessier, N.; Sleiman, H.F., "Rational design of platinum(II)-based phenanthroimidazoles: Towards targeting G-quadruplex DNA", Third International Meeting on G-Quadruplex and G-Assembly, Sorrento, Italy, June 28-July 1, 2011 (Poster Presentation).

4) **Castor, K.J.**; Kieltyka, R.; Englebienne, P.; Weill, N.; Mancini, J.; Fakhoury, J.F.; Avakyan, N.; Mittermaier, A.; Autexier, C.; Moitessier, N.; Sleiman, H.F., "Platinum(II) phenanthroimidazoles for G-quadruplex targeting: The effect of structure on binding affinity, selectivity, and telomerase inhibition", 94th Canadian Chemistry Conference and Exhibition, Montreal, QC, June 5-9, 2011 (Oral Presentation).

5) **Castor, K.J.**, Sleiman, H.F., *et al.*, "Platinum(II)-based Anti-Cancer Therapeutics", 2010 CSACS Student Symposium, Universite de Montreal, September 14, 2010 (Poster Presentation).

6) **Castor, K.J.**; Kieltyka, R.; Sleiman, H.F., "Design and Optimization of Effective Platinum(II)-based G-Quadruplex DNA Binders as

Anticancer Therapeutics", 93rd Canadian Chemistry Conference and Exhibition (CSC), Toronto, June 1, 2010, (Oral Presentation).

7) **Castor, K.J.**; Kieltyka, R.; Sleiman, H.F., "Platinum(II)-based G-Quadruplex Binders as Telomerase Inhibitors", 7th Canadian Symposium on Telomeres and Telomerases, McMaster University, Hamilton, Ontario, May 13 -May 16, 2010. (Oral Presentation).

A Appendix A: Mechanochemistry Methods for Synthesis of Pt(II) and Pd(II) Supramolecular Squares

Preface: Author Contributions

Experimental methods were performed by **Katherine Castor** under the guidance of **Dr. Tomislav Friščić**.

A.1 Supramolecular self-assembly as a construction tool

Throughout this thesis, we have discussed traditional synthetic organic and inorganic chemistry methods for the construction of metal-based complexes for G-quadruplex targeting. However, a particularly appealing strategy for the creation of these binders could be through the use of supramolecular self-assembly.[1-4] This approach involves the spontaneous association of simple building blocks into a precise and complex structure that often results in near 100% yields. Supramolecular chemistry is an effective way to build complex structures[5-10] that allows for the generation of synthetic libraries. These libraries can aid in the understanding of the binding of these scaffolds to G-quadruplex motifs.[11-13]

So far, the implementation of supramolecular structures for the purpose of G-quadruplex recognition has only just started to be explored. Previous work in our laboratory by Roxanne Kieltyka demonstrated that the platinum "square" complex extensively studied by the groups of Fujita[5,6] and Stang,[8] is an efficient G-quadruplex binder and telomerase inhibitor (Figure A.1a-e).[14] More recently, Zheng and coworkers evaluated a library of four supramolecular squares − all platinum(II)-based, each with a combination of ethylenediamine (en) or ammonia ligands and pyrazine or 4,4'-bipyridine (bpy) linkers − as G-quadruplex binders and potential anticancer therapeutics (Figure A.1f-g).[15] These squares are all highly positively charged (8+) which greatly facilitates water solubility, but the high charge also decreases selectivity between G-quadruplex and duplex DNA. Thus, supramolecular self-assembly would be particularly useful to provide ready access to new G-quadruplex binding structures with optimized selectivity by changing ligands, coordination spheres, and adding sidearms that would sterically hinder the ability of the squares to interact with duplex DNA in an intercalation-type manner.

a)

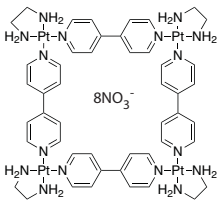

b)

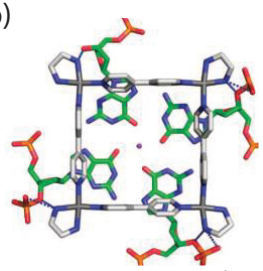

c)

ΔT_m(°C) at 0.75 μM ligand concentration	
G4DNA	dsDNA
34.5	12.1

d)

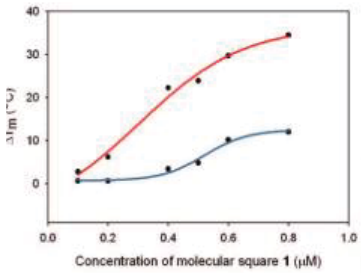

e)

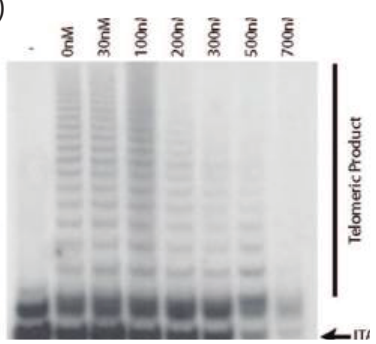

f)

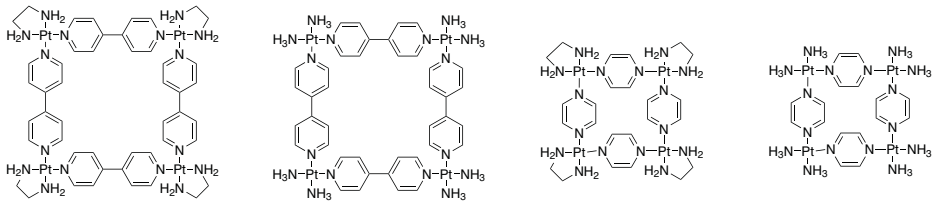

1 2 3 4

g)

Complex	htelo ΔT_m (°C)	*bcl2*	Duplex DNA
1	27.4	6	8.5
2	29	4.4	9
3	11	4.6	6
4	15	6	10
	Equilibrium constants K_D (M)		
1	3.39×10^{-7}	1.59×10^{-6}	2.55×10^{-6}
2	1.13×10^{-7}	3.54×10^{-6}	4.06×10^{-6}
3	1.32×10^{-6}	3.06×10^{-6}	4.06×10^{-6}
4	1.74×10^{-6}	2.06×10^{-5}	2.41×10^{-6}

Figure A.1 Supramolecular squares as G-quadruplex binders a) structure of the platinum molecular square; b) average structure of the complex between the square and the h-telo G-quadruplex; c) FRET stabilization temperatures; d) FRET stabilization curve of the square with quadruplex (red) and B-DNA (blue) as a function of concentration of square; e) TRAP assay results showing ladders generated by the action of telomerase on a telomeric substrate primer; f) structures of **1-4**; g) Stabilization temperatures from FRET (top) and equilibrium constants from SPR (bottom) for **1**-**4** withG-quadruplex and duplex DNA. Reproduced from references 14 and 15 with permission, American Chemical Society, 2008, and RSC, 2012.

A.2 Mechanochemistry as a synthetic methodology

While supramolecular self-assembly is a useful concept, its practical considerations can be more tedious. For the solution synthesis of the square in Figure A.1a, the $Pt(en)(NO_3)_2$ intermediate must be made *in situ* from $PtenCl_2$ and silver nitrate. The nitrate replaces the more labile chloride ligands, and in the process, forms the insoluble silver chloride salt. Before the addition of the 4,4'-bipyridyl linker, the aqueous solution of $Pt(en)(NO_3)_2$ must be filtered many times through celite to ensure the complete removal of any remaining silver chloride or Ag^+ ions. After extensive filtration, the linking bipyridyl ligand is added and the solution is refluxed for ~ 1−4 weeks[5,14] before precipitation with ethanol results in a powder that can be isolated via filtration (88% yield in the hands of Zheng,[15] ~ 10% in ours).

As this solution method is not the most expeditious route to the synthesis of this square, Orita and coworkers developed a solvent-free method described in a Chemical Communication in 2002.[16] In their publication, they describe the synthesis by mixing the two starting material powders, $Pt(en)(NO_3)_2$ and 4,4'-bipyridyl, in a 1:1 ratio and grinding them in a mortar with a pestle in open air at ambient temperature for ~ 10 minutes. They claim that the powder became gummy in a matter of seconds and the ^1H NMR spectrum in D_2O after 10 minutes exhibited complete comsumption of the starting materials. After reprecipitation with ethanol from water, they obtained a 76% isolated yield.

Not only is the yield comparable to the solution method (76% versus 80%, respectively), the reaction was dramatically shorter at 10 minutes versus 1−4 weeks. In addition to allowing for a faster generation of complex systems, solvent-less grinding is considered a "green" and more environmentally friendly process. Green chemistry is characterized by the efficient use of raw materials with minimal waste while avoiding the use of toxic materials/solvents in chemical synthesis.[17] Mechanochemistry and green chemistry go hand-in-hand, as mechanochemistry is characterized by reactions conducted by grinding solid reactants with little or no solvent, thereby minimizing waste and the need for toxic materials.[18]

A.3 Mechanochemical synthesis of precursors

While the solvent-free synthesis of the final square product has already been described,[16] the mechano-synthesis of the precursors has not. As previously mentioned, $Pt(en)(NO_3)_2$ is typically synthesized from $PtenCl_2$ and silver nitrate, with the byproduct of silver chloride. Synthetically, the isolation of $Pt(en)(NO_3)_2$ is time consuming and the yield of the isolated solid is low. Due to this, the *in situ* formation of the $Pt(en)(NO_3)_2$ in solution is preferred. However, mechanochemistry deals with the grinding of solid materials (e.g. ball-milling), so a solution of $Pt(en)(NO_3)_2$ is not ideal. Instead, if we could take a step back and go directly from the $PtenCl_2$ to the square via ball-milling, we could eliminate the need for the production of the intermediate. $PtenCl_2$ is typically synthesized from commercially available potassium tetrachloroplatinate in an aqueous solution of ethylenediamine. The isolated yields are upwards of 70% after filtration of the water-insoluble $PtenCl_2$ salt after stirring for 1−4 hours.[19-21] While this reaction could be considered "green" as water is the solvent, the reaction time could be decreased, and the yield could be increased by mechanochemistry.

Our idea, starting from the commercially available platinum salt − potassium tetrachloroplatinate, K_2PtCl_4 − was to synthesize $PtenCl_2$ via ball-milling with minimal purification (a "green" removal of excess KCl salts via washing with water) in high yield. Then, using our milled $PtenCl_2$, we could bypass the need for the isolation of the $Pt(en)(NO_3)_2$ intermediate by grinding $PtenCl_2$ with the 4,4'-bipyridyl linker while relying on supramolecular self-assembly to afford the Pt-square (Figure A.2). This process would demonstrate the first synthetic route for Pt-squares solely through ball-milling with minimal purification in high yield.

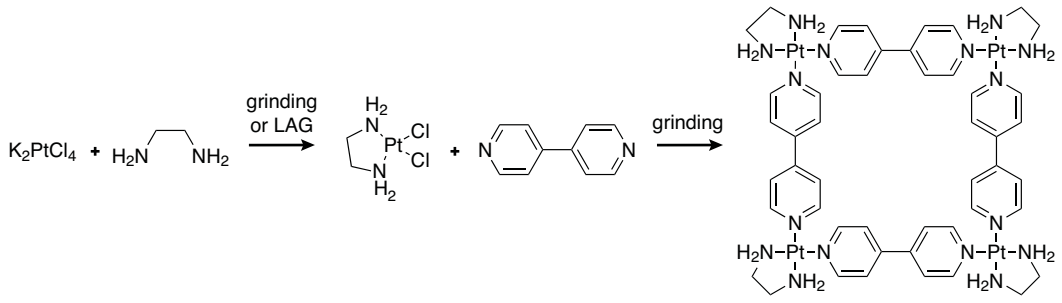

Figure A.2 Synthetic scheme for the formation of the Pt-square in two steps from potassium tetrachloroplatinate, where LAG is liquid-assisted grinding.

A.3.1 Screening of conditions for $PtenCl_2$

In order to uncover the conditions that resulted in the highest yield of the $PtenCl_2$, several conditions were investigated, including both dry and liquid-assisted (LAG). As as starting point, a 1:1 molar ratio of K_2PtCl_4 and ethylenediamine (at a 200 mg scale) were added to a 10 mL steel jar containing two balls (5 mm diameter) and the jar was shaken at 30 Hz for 60 minutes. Figure A.3 shows the ^1H NMR spectra (in d_6-DMSO) from the various reactions overlayed for comparison. The broad singlets at 5.3 ppm and 2.2 ppm are the $–NH_2$ and $–CH_2$ of the product ethylenediamine ligand, respectively, while the broad singlets at 5.6 ppm and 2.4 ppm are the free ethylenediamine.

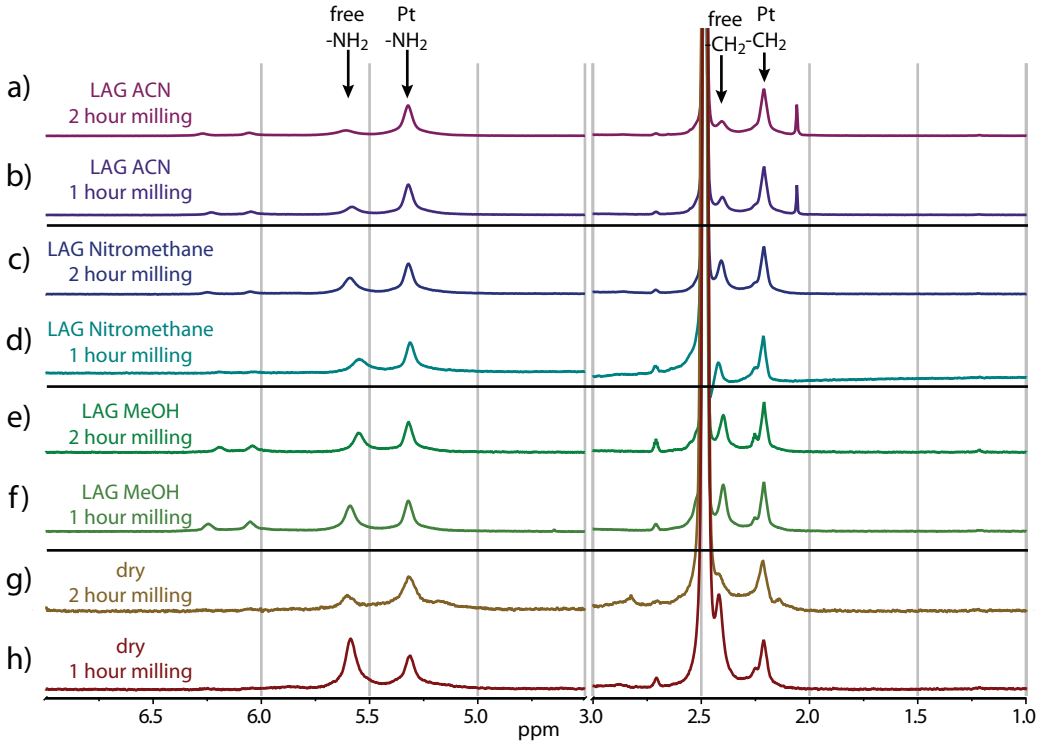

Figure A.3 Screening of various conditions for synthesis of $PtenCl_2$.

From the NMR spectra, a 1:1 molar ratio of K_2PtCl_4 and ethylenediamine with ACN affords the highest yield of $PtenCl_2$ after 2 hours of milling at 30 Hz, however there appears to be the presence of some remaining starting material (Figure A.3a). Interestingly, further milling resulted in a grey substance with no further improvement on yield. The color change to grey may be indicative of oxidation of the platinum species by the steel jars.

Further screens with ion-assisted grinding of K_2PtCl_4 and ethylenediamine did not significantly improve the yields. We used both $NaNO_3$ and trimethylamine-*N*-oxide (TMAO) as additives. ^{1}H NMR spectra (in d_6-DMSO) are shown in Figure A.4. Interestingly, in some cases after an hour of milling (Figure A.4a,c,e), we see the formation of two broad singlets above 6.0 ppm. These singlets are believed to be due to the substitution of DMSO for chloride in the NMR tube rather than due to the reaction itself (*vide infra* Figure A.6).

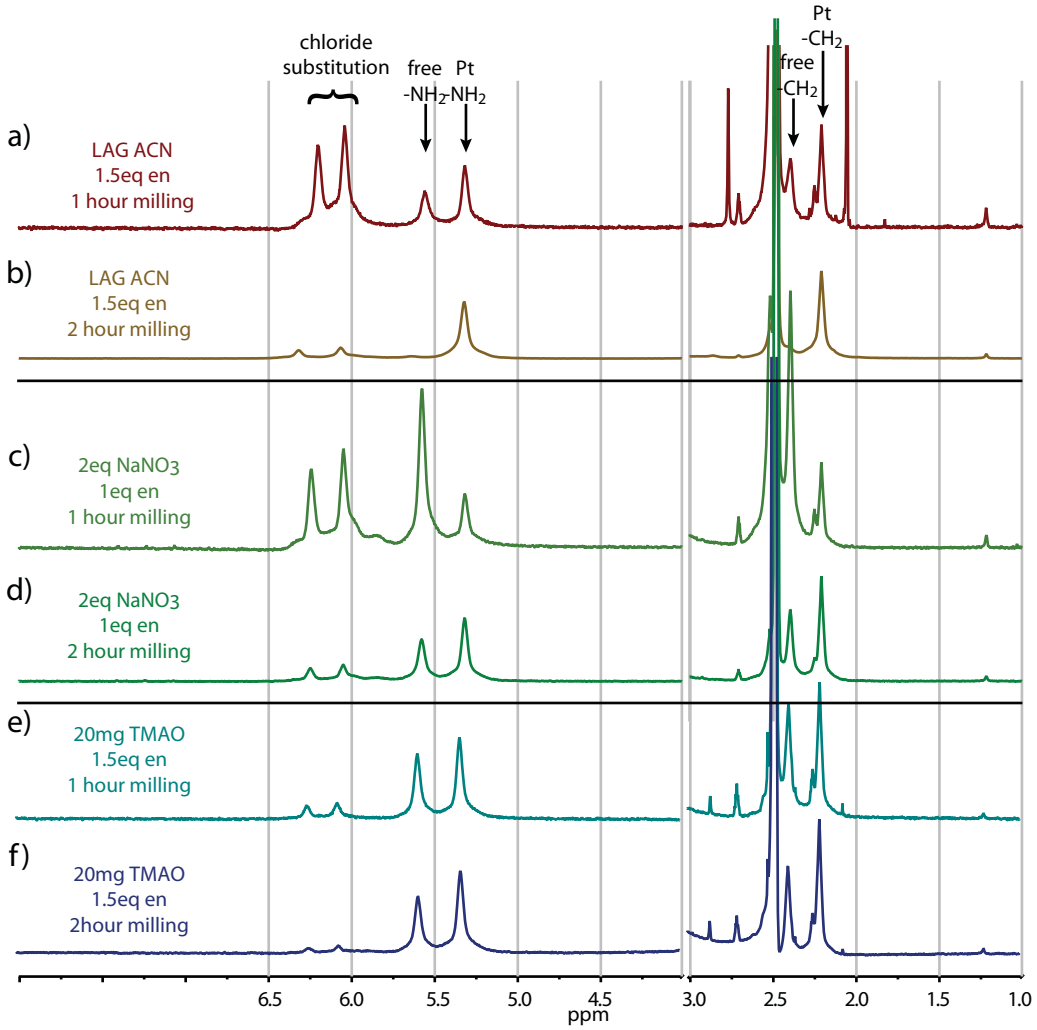

Figure A.4 Continued screening of ion-assisted milling of $PtenCl_2$.

After screening of various conditions, we determined that half the mass (100 mg versus 200 mg) in teflon jars with 1.25 eq (equivalents) of ethylenediamine, and liquid assisted by ACN resulted in 100% yield of $PtenCl_2$. The ^{1}H NMR and pictures of the process are shown in Figure A.5. After removing the tan/yelow powder from the teflon

jar, the solid can be placed in a glass frit and washed with water to remove the KCl byproduct. The resulting pure $PtenCl_2$ can be recovered with upwards of 80%. To the best of our knowledge, this is the first mechanochemical synthesis of $PtenCl_2$ to date.

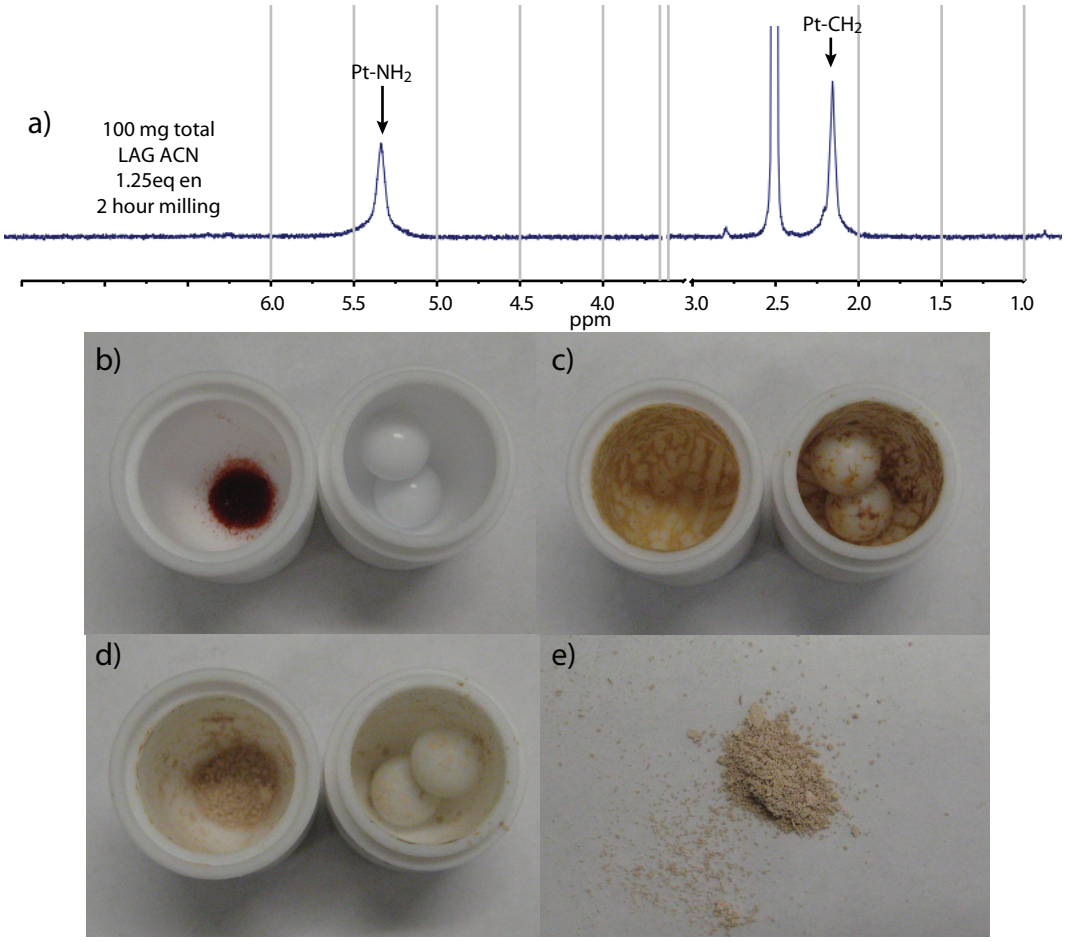

Figure A.5 Final conditions for the milling of $PtenCl_2$: a) pure ^1H NMR in DMSO, b) K_2PtCl_4, ethylenediamine, and ACN pre-milling, c) the reaction after 1 hour of shaking at 30 Hz, d) the reaction after 2 hours of shaking, and e) the final $PtenCl_2$ powder isolated after scraping from the jar.

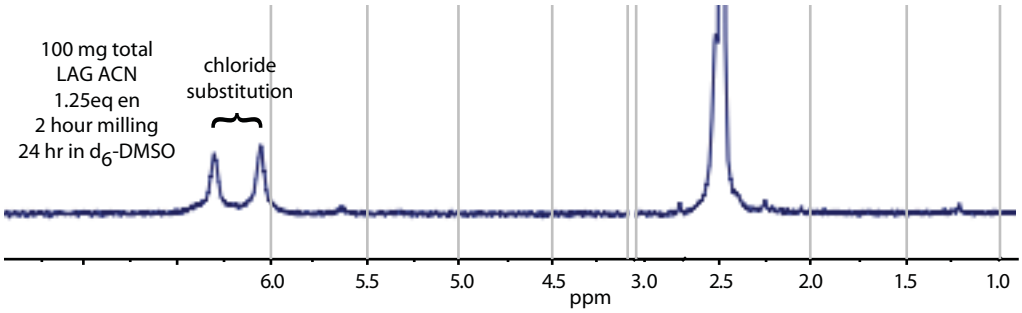

Figure A.6 The NMR tube containing pure $PtenCl_2$ after isolation was left for 24 hours at room temperature before re-obtaining the ^1H NMR. Substitution of the chlorides by DMSO (or ACN, to be determined) results in loss of the $PtenCl_2$ species.

A.4 Mechanochemistry synthesis of squares: Screening

Once the ideal conditions were determined for the synthesis of $PtenCl_2$, we moved on to the synthesis of the Pt-square. Due to previous syntheses of the $[Pten(bpy)]_4$ square utilizing NO_3^- as a counter ion, we conducted a screen of conditions that included potasium, sodium, and silver nitrate salts in the reaction mixture. Figure A.7 shows the ^1H NMR spectra (in D_2O), free 4,4'-bipyridine occurs at 8.4 and 7.55 ppm, while the Pt-square bpy occurs at 8.7 and 7.7 ppm. The $–CH_2$ from $PtenCl_2$ appears at 2.45 ppm, while the $–CH_2$ from the Pt-square en appears at 2.7 ppm. Interestingly, 2 equivalents of silver nitrate appears to drive the reaction to completion, whereas the potassium and sodium analogs only partially help with conversion. We have postulated that this is due to the strength of the lattice energy of the resulting chloride salt where AgCl > NaCl > KCl. The more stable the salt, the more the reaction is driven to completion. Other conditions were attempted, including the addition of higher equivalents (4 and 10) of $NaNO_3$ or catalytic amounts of $AgNO_3$, but these reactions did not improve upon the previous conditions.

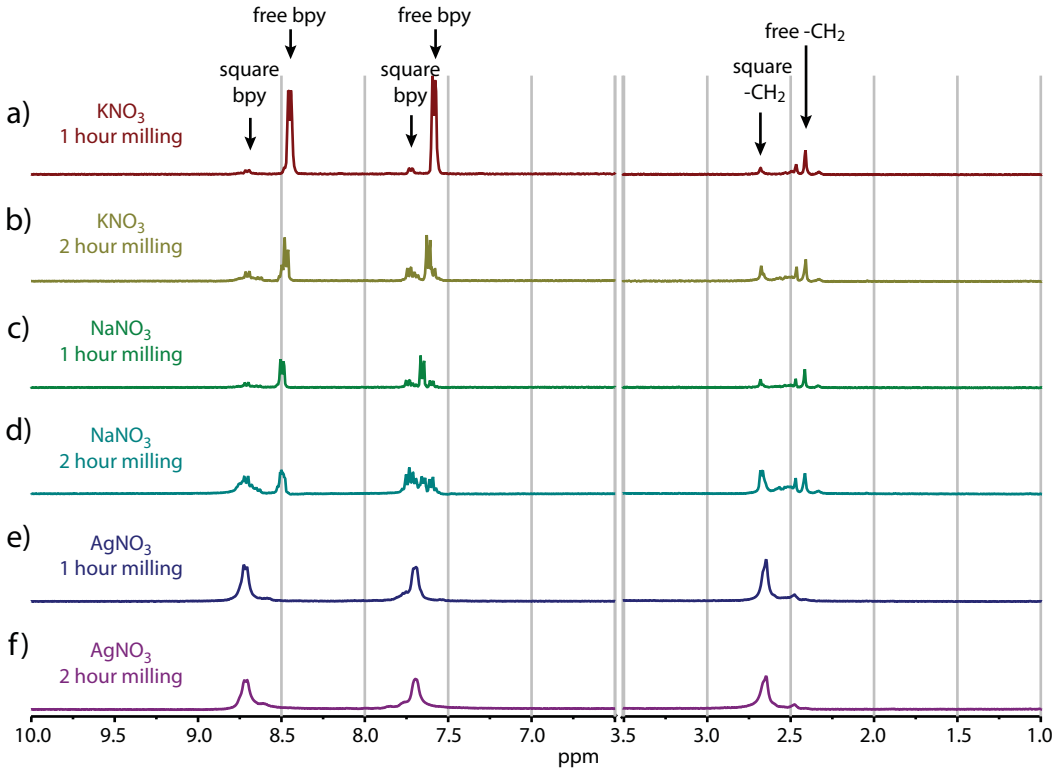

Figure A.7 Screening of conditions for the synthesis of the $[Pten(bpy)]_4[8NO_3]$

In order to isolate the Pt-square product, the grey powder can be triturated with water and centrifuged. The mother liquor (containing the water-soluble square) can be decanted and filtered through a pad of celite in a glass frit. The process is repeated to maximize recovery and minimize the amount of silver chloride and/or silver ions that may remain in solution. After lyophilization of the aqueous layer, a fluffy white powder of Pt-square is obtained in upwards of 75% yield.

A.5 Conclusions

In conclusion, we have developed a methodology to create $[Pten(bpy)]_4^{8+}[8NO_3]^{8-}$ from commercially available K_2PtCl_4, ethylenediamine, and 4,4'-bipyridyl in an atom economical manner in 2 steps after 4 hours. Isolation of the intermediate $PtenCl_2$ and product Pt-square involves washing with water, filtration, and lyophilization which are all "green" processes. Our method also saves time and increases the overall product yield.

A.6 Future directions

In a similar manner, we hope to synthesize the palladium analogs, that is $PdenCl_2$ and and $[Pden(bpy)]_4^{8+}[8NO_3]^{8-}$. The literature reports[22] for the synthesis of $PdenCl_2$ with the highest yields (> 70%) start from $PdCl_2$ with the addition of concentrated hydrochloric acid and ethylenediamine. We hypothesize that we can synthesize $PdenCl_2$ starting from K_2PdCl_4 and ethylenediamine and avoid the use of concentrated hydrochloric acid altogether. In fact, investigations into this method have already begun.

A.7 Experimental section

General: All starting materials were obtained from Sigma-Aldrich and used without purification. Distilled water was dispensed from the in-house tap. Acetonitrile was reagent grade, and not anhydrous. The 10 mL steel jars and 5 mm ball bearings were obtained from Retsch, Inc. The teflon jars were created by the McGill University Engineering Department. Ball-milling reactions were preformed on a Retsch™ MM 400 Mill. NMR spectra were obtained from either a 500 MHz Varian VNMRS (VNMRJ 2.3A software (Chempack 5) under LINUX Red Hat 5) in d_6-DMSO or D_2O. High-resolution mass spectrometry was performed on a Bruker Maxis Impact ESI-QTOF. For MS analysis, sodium formate was used to generate a calibration curve for mass accuracy. Samples were then diluted in LC-MS grade Methanol (Fisher) and directly infused at 3 μL per minute into the MS. The spectra were obtained in positive mode. Elemental analysis was obtained from the Laboratoire d'Analyse Élémentaire de l'Université de Montréal.

Synthesis of $PtenCl_2$:

Steel: In a small steel jar with two 5 mm steel balls was added K_2PtCl_4 (0.491 mmol, 204 mg), 1.25 equivalents of ethylenediamine (0.614 mmol, 41.1 μL) and 50 μL acetonitrile. The jar was shaken at 29.5 Hz for 60 minutes, after which the powder was scraped off the side of the jar before being subjected to another 60 minutes of shaking at 29.5 Hz. At the end of the reaction, the powder was scraped from the jar and isolated as crude $PtenCl_2$ and KCl. A tan/yellow solid (97%, 226 mg) was recovered. To remove

KCl, the solid was washed through a fine glass frit with ~ 50 mL distilled water. After recovery, 129 mg of a yellow powder remained (80%).

Teflon: The procedure was performed as above, except 0.244 mmol (101 mg) K_2PtCl_4 and 25 μL acetonitrile were used.

^{1}H NMR (500 mHz, d_6-DMSO): δ = 5.304 (4 H, br s), 2.219 (4H, br s) ppm; HR-MS calculated for $C_2H_8Cl_2N_2PtCl$: **359.9406**, found: **359.9395**. Elemental Analysis: calculated C – 7.37, H - 2.47, N - 8.59, found C – 7.66, H – 2.39, N – 8.55.

*In the case of the screening involving TMAO or $NaNO_3$, or a solvent other than ACN (MeOH, nitromethane), 20 mg of solid was added while the other solvents were direct substitutes of the ACN in the reaction mixture.

Synthesis of $[Pten(bpy)]_4^{8+}[8NO_3]^{8-}$:

The procedure was performed as above except the total mass was around 200 mg. That is, $PtenCl_2$ (0.287 mmol, 93.7 mg), 1 equivalent 4,4'-dipyridyl (0.287 mmol. 58.1 mg), and 2 equivalents of XNO_3 (where X = Ag, Na, or K) were added to the jar. Light grey powder of $[Pt(en)(bpy)]_4[8NO_3]$ and XCl was isolated in near quantitative amounts. To purify the square, the powder was mixed with 10 mL distilled water, shaken, and centrifuged. The mother liquor was filtered through a pad of celite in a glass frit. This process was repeated 3 times to maximize recovery. The filtrate was then lyophilized to dryness to yield a white fluffy solid (75% yield).

^{1}H NMR (500 mHz, D_2O): δ = 8.72 (16 H, d), 7.74 (16 H, d), 2.65 (16 H, br s) ppm; HR-MS calculated for $C_{48}H_{64}N_{16}Pt_4$ (M^{8+}): **205.5511**, found: **205.5515**.

A.8 References

1. Lehn, J. M.; Rigault, A.; Siegel, J.; Harrowfield, J.; Chevrier, B.; Moras, D., Spontaneous assembly of double-stranded helicates from oligobipyridine ligands and copper(I) cations: structure of an inorganic double helix. *Proc Natl Acad Sci USA* **1987,** *84* (9), 2565-2569.
2. Hasenknopf, B.; Lehn, J.-M.; Boumediene, N.; Dupont-Gervais, A.; Van Dorsselaer, A.; Kneisel, B.; Fenske, D., Self-Assembly of Tetra- and Hexanuclear Circular Helicates. *J Am Chem Soc* **1997,** *119* (45), 10956-10962.

3. Stang, P. J.; Olenyuk, B., Self-Assembly, Symmetry, and Molecular Architecture: Coordination as the Motif in the Rational Design of Supramolecular Metallacyclic Polygons and Polyhedra. *Acc Chem Res* **1997,** *30* (12), 502-518.
4. Olenyuk, B.; Fechtenkotter, A.; Stang, P. J., Molecular architecture of cyclic nanostructures: use of co-ordination chemistry in the building of supermolecules with predefined geometric shapes. *J Chem Soc, Dalton Trans* **1998,** (11), 1707-1728.
5. Fujita, M.; Yazaki, J.; Ogura, K., Preparation of a macrocyclic polynuclear complex, [(en)Pd(4,4'-bpy)]$_4$(NO_3)$_8$, which recognizes an organic molecule in aqueous media. *J Am Chem Soc* **1990,** *112* (14), 5645-5647.
6. Fujita, M.; Yazaki, J.; Ogura, K., Spectroscopic Observation of Self-Assembly of a Macrocyclic Tetranuclear Complex Composed of Pt^{2+} and 4,4'-Bipyridine. *Chem Lett* **1991,** (6), 1031-1032.
7. Fujita, M.; Nagao, S.; Iida, M.; Ogata, K.; Ogura, K., Palladium(Ii)-Directed Assembly of Macrocyclic Dinuclear Complexes Composed of (En)Pd^{2+} and Bis(4-Pyridyl)-Substituted Bidentate Ligands − Remarkable Ability for Molecular Recognition of Electron-Rich Aromatic Guests. *J Am Chem Soc* **1993,** *115* (4), 1574-1576.
8. Stang, P. J.; Cao, D. H., Transition Metal Based Cationic Molecular Boxes. Self-Assembly of Macrocyclic Platinum(II) and Palladium(II) Tetranuclear Complexes. *J Am Chem Soc* **1994,** *116*, 4981-4982.
9. Stang, P. J.; Olenyuk, B., Directed self-assembly of chiral, optically active macrocyclic tetranuclear molecular squares. *Angew Chem Intl Ed Eng* **1996,** *35* (7), 732-736.
10. Cao, D. H.; Chen, K. C.; Fan, J.; Manna, J.; Olenyuk, B.; Whiteford, J. A.; Stang, P. J., Supramolecular chemistry and molecular design: Self-assembly of molecular squares. *Pure Appl Chem* **1997,** *69* (9), 1979-1986.
11. Meistermann, I.; Moreno, V.; Prieto, M. J.; Moldrheim, E.; Sletten, E.; Khalid, S.; Rodger, P. M.; Peberdy, J. C.; Isaac, C. J.; Rodger, A.; Hannon, M. J., Intramolecular DNA coiling mediated by metallo-supramolecular cylinders: differential binding of P and M helical enantiomers. *Proc Natl Acad Sci USA* **2002,** *99* (8), 5069-5074.
12. Oleksi, A.; Blanco, A. G.; Boer, R.; Uson, I.; Aymami, J.; Rodger, A.; Hannon, M. J.; Coll, M., Molecular recognition of a three-way DNA junction by a metallosupramolecular helicate. *Angewandte Chemie-International Edition* **2006,** *45* (8), 1227-1231.
13. Galindo, M. A.; Olea, D.; Romero, M. A.; Gomez, J.; del Castillo, P.; Hannon, M. J.; Rodger, A.; Zamora, F.; Navarro, J. A., Design and non-covalent DNA binding of platinum(II) metallacalix[4]arenes. *Chem Eur J* **2007,** *13* (18), 5075-5081.
14. Kieltyka, R.; Englebienne, P.; Fakhoury, J.; Autexier, C.; Moitessier, N.; Sleiman, H. F., A platinum supramolecular square as an effective G-quadruplex binder and telomerase inhibitor. *J Am Chem Soc* **2008,** *130* (31), 10040-10041.

15. Zheng, X. H.; Zhong, Y. F.; Tan, C. P.; Ji, L. N.; Mao, Z. W., Pt(II) squares as selective and effective human telomeric G-quadruplex binders and potential cancer therapeutics. *Dalton Trans* **2012,** *41*, 11807-11812.
16. Orita, A.; Jiang, L.; Nakano, T.; Ma, N.; Otera, J., Solventless reaction dramatically accelerates supramolecular self-assembly. *Chem Commun* **2002,** (13), 1362-1363.
17. Sheldon, R. A., The E Factor: fifteen years on. *Green Chem* **2007,** *9* (12), 1273.
18. James, S. L.; Adams, C. J.; Bolm, C.; Braga, D.; Collier, P.; Friščić, T.; Grepioni, F.; Harris, K. D. M.; Hyett, G.; Jones, W.; Krebs, A.; MacK, J.; Maini, L.; Orpen, A. G.; Parkin, I. P.; Shearouse, W. C.; Steed, J. W.; Waddell, D. C., Mechanochemistry: Opportunities for new and cleaner synthesis. *Chem Soc Rev* **2012,** *41* (1), 413-447.
19. Basolo, F.; Bailar Jr, J. C.; Tarr, B. R., The stereochemistry of complex inorganic compounds. X. The stereoisomers of dichlorobis-(ethylenediamine)-platinum(IV) chloride. *J Am Chem Soc* **1950,** *72* (6), 2433-2438.
20. Kemp, S.; Wheate, N. J.; Buck, D. P.; Nikac, M.; Collins, J. G.; Aldrich-Wright, J. R., The effect of ancillary ligand chirality and phenanthroline functional group substitution on the cytotoxicity of platinum(II)-based metallointercalators. *J Inorg Biochem* **2007,** *101* (7), 1049-1058.
21. Chopade, S. M.; Phadnis, P. P.; Wadawale, A.; Hodage, A. S.; Jain, V. K., Synthesis and characterization of (ethylenediamine)/(diammine)platinum(II) coordinated to seleno ligands containing carboxylic acid functionality. *Inorg Chim Acta* **2012,** *385* (0), 185-189.
22. Gilg, K.; Mayer, T.; Ghaschghaie, N.; Klufers, P., The metal-binding sites of glycose phosphates. *Dalton Trans* **2009,** (38), 7934-45.

B Appendix B: The Union of G-quadruplexes and Three-Dimensional DNA Prisms

Preface: Author Contributions

The design for the project was carried out by **Christopher McLaughlin** and myself. Initial studies on feasibility of the 3D-assembly were performed by **Christopher McLaughlin**. The preparation of the 3D-DNA scaffolds and construction thereof presented herein were performed by **Graham D. Hamblin**. The biophysical studies were designed and carried out by myself.

B.1 Introduction

Nature has elegantly evolved strategies by which to organize materials in a rational and functional manner on all scales of life – from the molecular to the macromolecular, the cell to the organism, small ecosystems to the solar system and beyond. One of the principles by which nature accomplishes this is on the molecular to cellular scale is supramolecular self-assembly. Supramolecular self-assembly is defined in many ways, but typically involves the use of well-defined nonbonded interactions between simple building blocks that self-organize into non-covalent architectures.[1] The most recognizable macromolecules in nature created in this manner are the DNA double helix and proteins (Figure B.1). These entities assemble via a combination of hydrogen-bonding, electrostatic, and hydrophobic effects. Then, in the cellular context, they can assemble with other units create membranes, nuclei, mitochondria, etc. Although nature has perfected these strategies over millions of years, this plethora of information provides us with examples of how to achieve these goals artificially in the laboratory setting, and potentially discover natural assembling mechanisms.

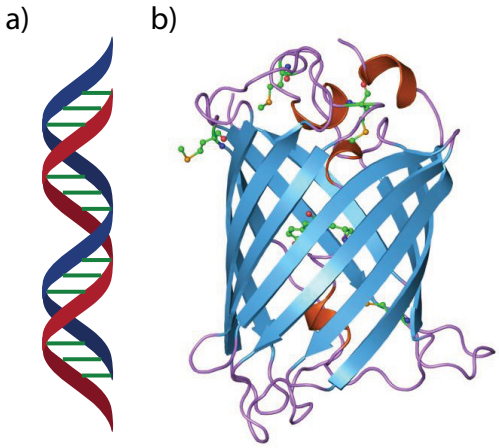

Figure B.1 Examples of self-assembled structures in nature: a) DNA double helix and b) green fluorescent protein. In b) beta-sheets are shown in cyan, α-helices are shown in red, and random coils are shown in purple. Image reproduced in part from wikipedia.

The inspiration for this appendix is the organization of catalytically active enzymes that, when arranged site-specifically on the nanometer scale, results in activity enhancement (or increased throughput) of the cascade.[2] The 3D-organization of these enzymes has been made possible through progress in the research of DNA and RNA nanotechnology. Two examples of tethered cascades are shown in Figure B.2. Willner and coworkers used hexagonal dsDNA grids with strands that could bind glucose oxidase and horseradish peroxidase ideally located within the grid such that the enzymes were separated by desired distances (6 to 24 nm) (Figure B.2a). Due to the arrangement and proximity, an increase in product formation ($ABTS^-$; oxidized 2,2'-azino-bis(3-ethylbenzothiazoline-6-sulfonic acid)) was observed, compared to the free enzymes.[3] Delebecque *et al.* utilized an RNA scaffold artificially created inside a bacterial cell for the organization of ferredoxin and hydrogenase that also resulted in increased product H_2 formation (Figure B.2b).[4]

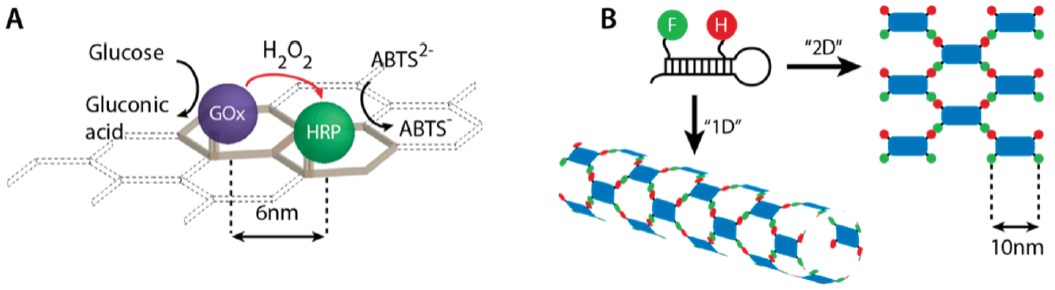

Figure B.2 Schematics of enzyme cascades on DNA and RNA scaffolds. A) hexagonal grids of DNA with site specific tethers allow for the attachment of glucose oxidase (GOx) and horseradish peroxidase (HRP) pairs 6 nm apart that results in the facile transfer of peroxide for increased output of $ABTS^{-}$.[3] B) RNA tiles with attached ferredoxin (F) and hydrogenase (H) enzymes in a well-defined manner that results in increase output of hydrogen gas.[4] Figure adapted from Idan, O.;Hess, H. Origins of Activity Enhancement in Enzyme Cascades on Scaffolds. *ACS Nano* 2013, 7 (10), 8658-8665; Copyright (2014) American Chemical Society.

In addition to organizing enzymes in this tethered manner, Willner and coworkers have also used DNA to organize small molecules, namely Fe(III)-hemin.[5] In their report, they present a detection method for specific G-quadruplex forming DNA sequences that relies on the binding of these sequences by hemin in their hairpin structures to form a polymerized "DNA nanowire". This nanowire can then catalyze the oxidation of ABTS or luminol in the presence of hydrogen peroxide, resulting in the "on" signal, demonstrating the presence of the quadruplex sequence in solution. This is represented in Figure B.3.

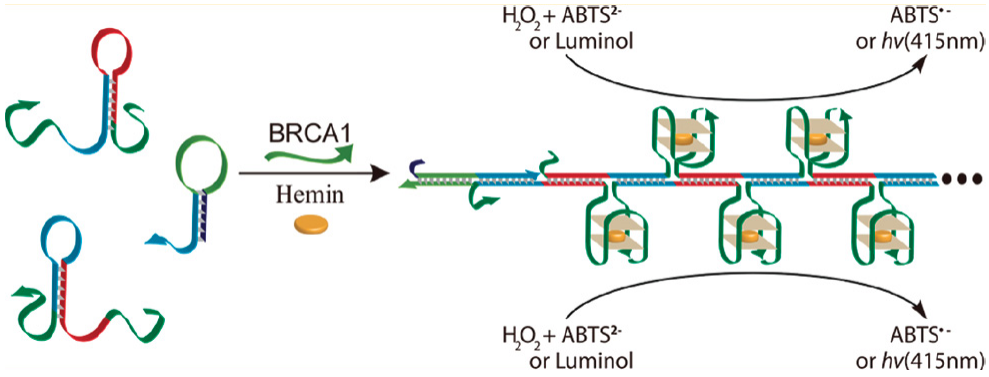

Figure B.3 Scheme for the detection of a G-quadruplex forming target using hairpins that recognize the target sequence (BRAC1). Upon recognition, the hairpins unfold and bind the target sequence that can form a complex with hemin. The hemin then becomes catalytically active, allowing for the oxidation of ABTS or luminol in the presence of peroxide. Figure reprinted from Shimron, S.; Wang, F.; Orbach, R.; Willner, I. Amplified Detection of DNA through the Enzyme-Free Autonomous Assembly of Hemin/G-Quadruplex DNAzyme Nanowires. *Anal. Chem.* 2012, 84 (2), 1042-8; Copyright (2014) American Chemical Society.

The Sleiman laboratory has become proficient at designing and constructing 3D scaffolds using the supramolecular self-assembly properties of DNA.[6-13] As mentioned in

Chapter 1 (pp 1−2), DNA consists of a sequence of adenine (A), thymine (T), cytosine (C), and guanine (G) bases that come together in a predictable and specific hydrogen bonding pattern (A with T, C with G) to form the duplex double helix.[14] Nanostructures formed from DNA are highly addressable and hold great potential for a variety of applications including vehicles for drug delivery, substrates for gas storage, and scaffolds for organization of molecules (either symmetrically or asymmetrically), among others.[9] By site-specifically organizing materials on 3D DNA scaffolds, one can attempt to mimic nature's biological processes including catalytic enzyme pathways.

G-quadruplexes (G4s) have been shown to bind to a variety of molecules with biological relevance, including the thrombin protein (via the thrombin-binding aptamer),[15,16] insulin,[17] platinum phenanthroimidazoles (as potential cancer therapeutics),[18-20] and hemin (as a catalytic moiety for oxidative reations),[5,21-24] among others.[25] Using the predictability and fidelity of the simple base-pairing code of DNA, one can rationally construct 3D scaffolds with site-specifically arranged G-quadruplexes for binding biologically relevant molecules. The organization of G4s on 3D structures offers the opportunity to pattern materials in an anisotropic way. We were interested to see if we could pattern G4-forming sequences on 3D scaffolds and whether or not the formation of G4s is compatible with DNA hybridization and 3D scaffold-formation. Herein, we show that we can create a 3D-DNA prism with a large number of single-stranded-binding regions to which we selectively attach three or six G4-forming human-telomeric sequences. As a next step, we can bind Fe(III)-hemin selectively to the G4s, and will study the binding affinity of hemin to this motif, as well as examine the peroxidase ability of the hemin-G4-3D-DNA (**hG4P**) structures as a whole in comparison to hemin and G4-hemin complexes alone. From these studies, we demonstrate that the patterning of G4 motifs on 3D scaffolds is feasible. A report from the laboratory of Hao Yan demonstrates that proteins organized in a 1D manner on DNA origami tiles results in increased product production not merely due to high effective concentration of intermediates, but also due to a hydration shell that allows for the restricted diffusion of these intermediates.[26] By organizing our catalysts in a 3D space (rather than 1D and 2D), we can take advantage of this hydration shell to eventually bring about the desired catalytic cascading effects (by binding more than just one type of catalyst to the scaffold).

B.2 Design and assembly of the G4-Prism

The 3D-DNA prism scaffold has been previously developed in the Sleiman Laboratory by Christopher McLaughlin and Graham Hamblin[11] with subsequent publications by Justin Conway,[12] and Thomas Edwardson.[27] In the first publication, they present the 3D-DNA construction method used herein. This method uses a minimum number of pseudocatenated DNA strands that results in quantitative assembly of a 3D structure without the need for ligation. The assembly is done in a one-pot manner, but is better described schematically by Figure B.3 Successive additions of the three component strands C1, C2, and C3 (Table B.1) allow for the formation of the prism **TP** with six single-stranded binding regions (Figure B.4a). Due to symmetry of the sequences, the three binding regions on the top face have the same sequence while the three identical binding regions on the bottom face have a second sequence (indicated in purple for the top and green for the bottom). This prism is easily addressable on the top and bottom faces since these regions contain three single-stranded regions for binding to a complementary strand. In our case, we would like to position G-quadruplexes at the corners of the prism in a site-specific manner. To this end, we synthesized two sequences (**Top-22AG** and **Bot-22AG**, Table B.1), for binding to the top face and bottom faces, respectively. Each of these sequences contains three regions: i) a 20 base-pair region complementary to the single-stranded (ss-) side of the prism, ii) a five-thymine spacer, and iii) a non-binding intramolecular G-quadruplex forming sequence at the 5'-end based on the human telomeric sequence. As a control, we synthesized two non-quadruplex containing sequences, also complementary to the ss-regions, called **Top-SS** and **Bot-SS** (Table B.1). The formation of the **G4P** and **SSP** occurs in a one-pot manner. The three prism component strands in a 1:1 ratio, (**C1**, **C2**, and **C3**), and 3.3 equivalents of **Top-22AG** and **Bot-22AG** (for **G4P**) or **Top-SS** and **Bot-SS** (for **SSP**) are heated to 95°C and slowly cooled to room temperature over ~ 3 hours to maximize assembly yield. (Figure B.4b-c).

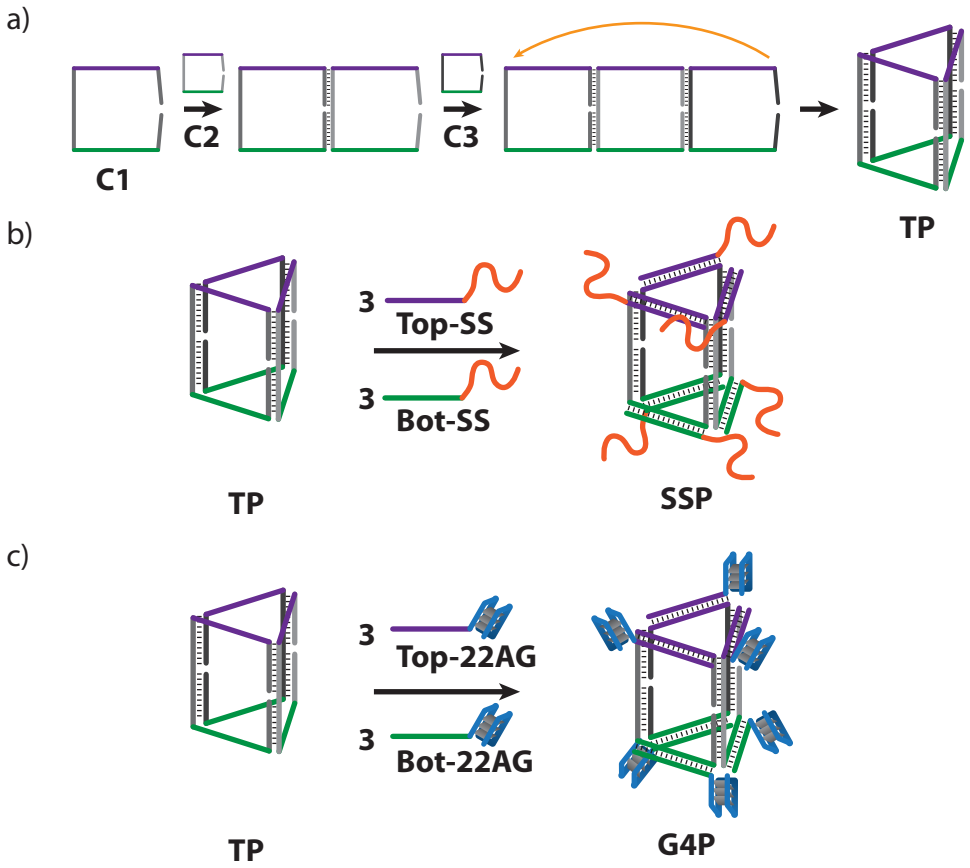

Figure B.4 Schematic showing the assembly of the 3D-DNA structures: a) **C1**, **C2**, and **C3** come together to form **TP** with six single-stranded binding regions where the top (purple) and bottom (green) sequences are identical, b) addition of 3.3 equivalents of **Top-SS** and **Bot-SS** form **SSP**, c) addition of 3.3 equivalents of **Top-22AG** and **Bot-22AG** form **G4P**. All assemblies are done in a one-pot manner.

The next step involves the site-specific orientation of catalytic iron(III)-hemin molecules on the G-quadruplex motifs (Figure B.5a). After the formation of **G4P** and **SSP**, we can add 6 equivalents of Fe-hemin, which results in the final structure in Figure B.5b, **hG4P**. In the case of **SSP**, we should not see binding of hemin (Figure B.5c), as the SS-strands are not able to form G-quadruplexes, and Fe-hemin has been shown to selectively bind the G-quadruplex motif.[21,28]

Name	Sequence	$\varepsilon_{260\ nm}$ ($M^{-1}cm^{-1}$)
C1	5'-TCGCTGAGTATTTTGCCTGGCCTTGGTCCATTTG TTTTGCAAGTGTGGGCACGCACACTTTTCGCACCGCGACTG CGAGGACTTTTCACAAATCTG-3'	873 100
C2	5'-CCACACTTGCTTTTGCCTGGCCTTGGTCCATTTG TTTTCTGACCAGTGTCAGCAAACCTTTTCGCACCGCGACTG CGAGGACTTTTGTGTGCGTGC-3'	853 300
C3	5'-CACTGGTCAGTTTTGCCTGGCCTTGGTCCATTTG TTTTTACTCAGCGACAGATTTGTGTTTTCGCACCGCGACTG CGAGGACTTTTGGTTTGCTGA-3'	869 500
Top-22AG	5'-AGGGTTAGGGTTAGGGTTAGGGTTTTT CAAATGGACCAAGGCCAGGC-3'	467 600
Bot-22AG	5'-AGGGTTAGGGTTAGGGTTAGGGTTTTT GTCCTCGCAGTCGCGGTGCG-3'	447 200
Bot-SS	5'-AATACGACTCACTATACTTTTTTTTT GTCCTCGCAGTCGCGGTGCG-3'	429 200
Top-SS	5'-AATACGACTCACTATACTTTTTTTTT CAAATGGACCAAGGCCAGGC-3'	449 600
22AG	5'-AGGGTTAGGGTTAGGGTTAGGG-3'	228 500
SS	5'-AATACGACTCACTATACTTTTT-3'	210 900

Table B.1 DNA sequences used herein, their names, and coorresponding molar extinction coefficients. All sequences were quantified in ng/μL on the NanoDrop, with the exception of 22AG which was quantified spectrophotometrically at 95°C using the molar extinction coefficient.

In general, these 3D-DNA structures require high concentrations of Mg^{2+} ions to electrostatically shield the negatively charged DNA backbone. Earlier work with a **Top-22AG** sequence containing a 10mer binding region (rather than 20mer like those herein) had shown that G-quadruplex formation in the presence of only magnesium ions was incomplete and the circular dichroic signal showed characteristics of a mixture of single-stranded DNA and a structure with G-quadruplex-like features (Figure B.6). This is most likely due to the poor size-match between Mg^{2+} ions (ionic radius = 0.89 Å)[29] and the ion channel through the G-quadruplex motif, as cations with ionic radii between 1.3−1.5 Å are best-suited.[30] Because of this, solutions containing both 3D-DNA scaffolds and G-quadruplex forming sequences should accommodate the stable formation of both.

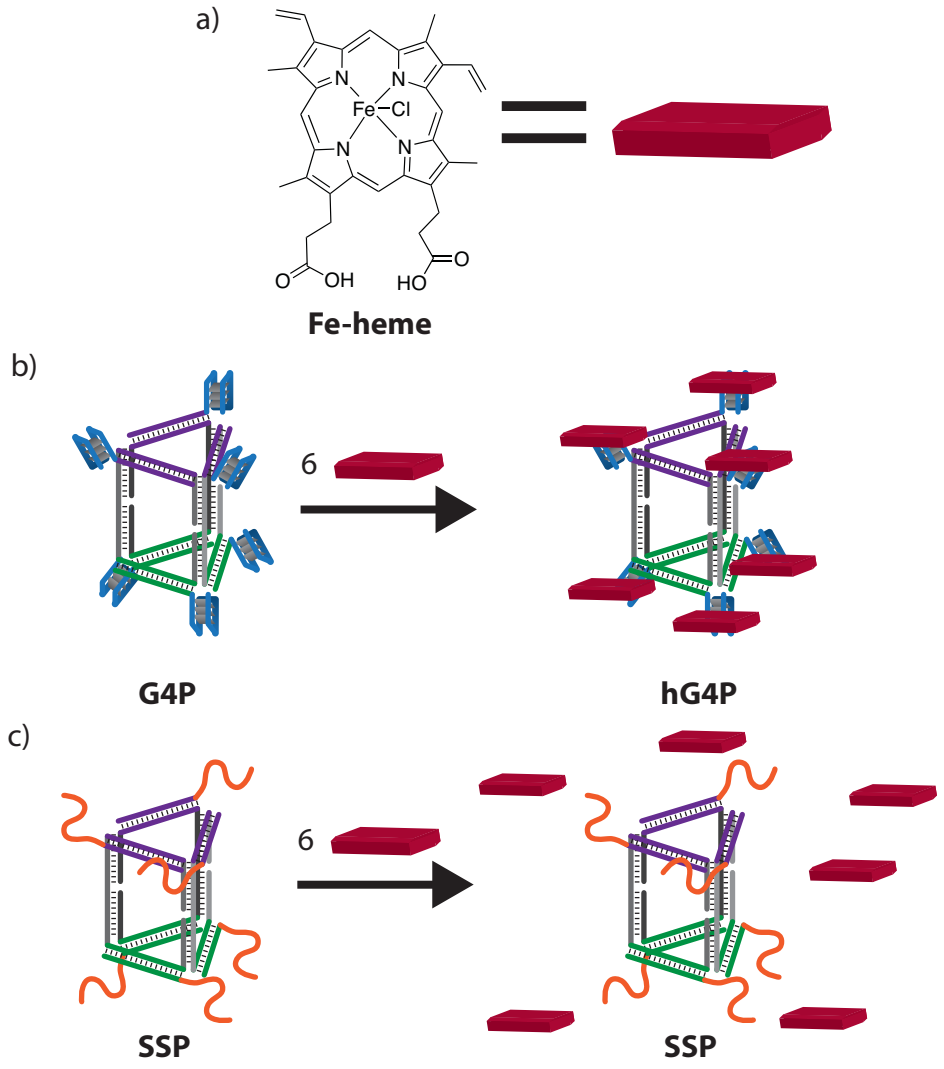

Figure B.5 Schematic showing the addition of Fe-hemin (a) to the **G4P** (b) and **SSP** (c) scaffolds. In the case of hemin binding to **G4P**, the resulting complex is termed **hG4P**.

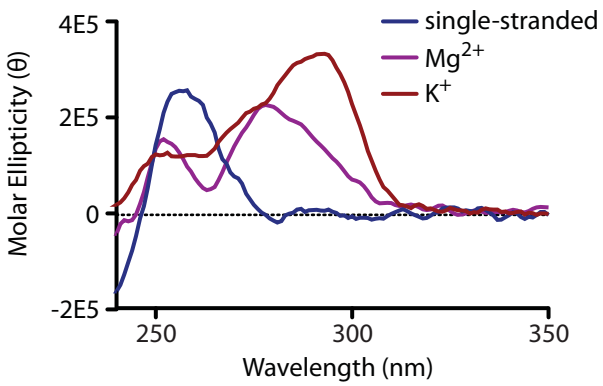

Figure B.6 CD spectra showing the signals of a strand similar to **Top-22AG** but with a 10mer binding region in three different conditions (Mg^{2+}, K^{+}, and in a tris buffer with no added salts). The purple trace (Mg^{2+}-conditions) does not conform to either single-stranded (blue trace) or fully-formed G-quadruplex in K^{+}-contaning solutions (red trace).

To determine if 3D-DNA assembly and G-quadruplex formation was compatible, we created a hybrid-buffer system based on previous work by Sen *et al.* involving optimized buffer conditions for hemin-G-quadruplex interaction.[21] In the report by Sen, after extensive studies, they determined that the optimal conditions for studying the spectroscopic interactions of a hemin-DNA aptamer complex occurred in buffers containing 50 mM MES (2-(*N*-morpholino)ethanesulfonic acid), pH 6.2, 100 mM Tris-acetate, 20 mM potassium acetate, 0.05% Triton X-100, supplemented with 1% DMSO (hereafter referred to as 1xSpect).[21] For the optimal oxidation potential of the hemin-aptamer complex, the buffer contained 40 mM HEPES-NH_4OH, pH 8.0, 20 mM potassium chloride, 0.05% Triton X-100, supplemented with 1% DMF (hereafter referred to as 1xOx).[21] Our 3D-DNA assembly buffer contains 45 mM Tris, 12.5 mM magnesium acetate, 2 mM EDTA, pH 8.0 (hereafter referred to as 1xTAEMg).[11] Thus, we combined the two buffers from Sen's work with 1xTAEMg to create two hybrid buffers: 1xTA/Spect and 1xTA/Ox, and studied the assembly of **G4P**. Gel electrophoresis performed by Graham Hamblin confirmed that the prism could be fully loaded with the six strands (assembly gel for **SSP** is shown in Figure B.7), and both SSP and G4P formed in the hybrid buffers, as evidenced by a single discrete band for each assembly (Figure B.8).

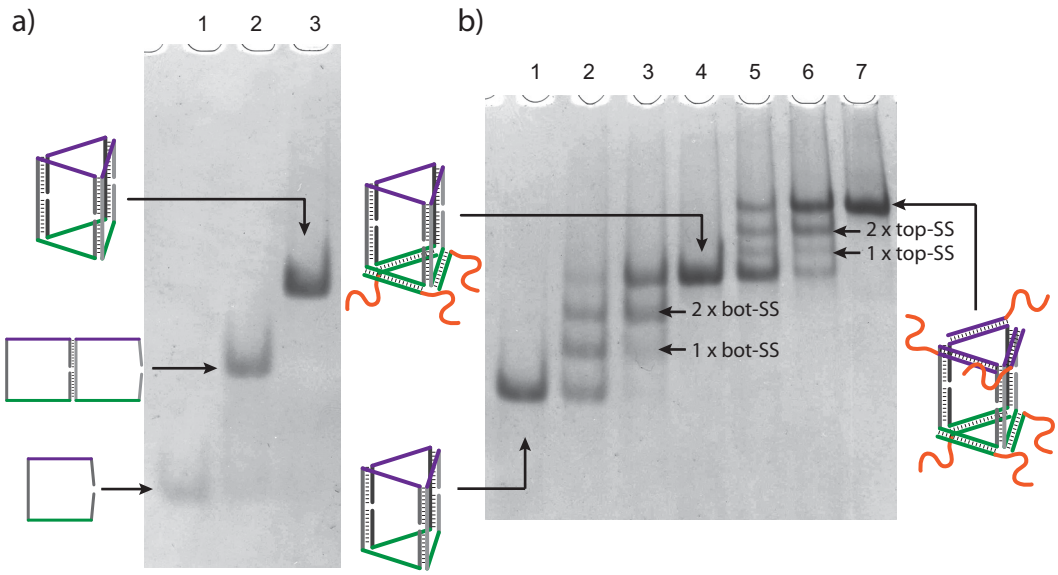

Figure B.7 Step-wise assembly of **TP** (a) and **SSP** (b) characterized by gel electrophoresis; a) lane 1, CS 1; lane 2, CS 1 + CS2; lane 3, CS 1 + CS 2 + CS 3 = **TP**; b) lane 1, **TP**; lanes 2-4, **TP** plus increasing equivalents of **bot-SS**; lanes 5-6, **TP** fully loaded with **bot-SS** plus increasing equivalents of **top-SS**; lane 7, **SSTP**.

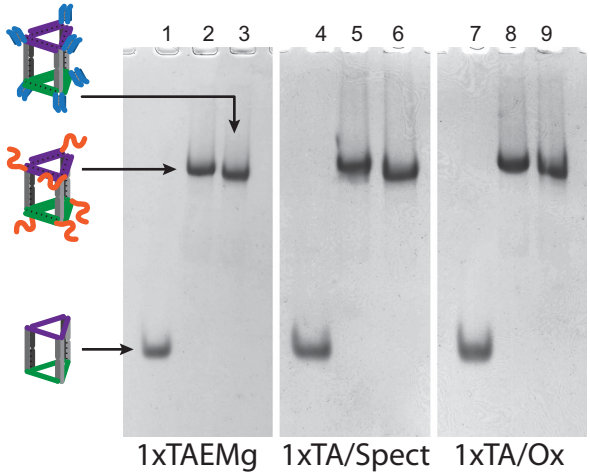

Figure B.8 Assembly of **TP**, **SSP**, and **G4P** in 1xTAEMg, 1xTA/Spect, and 1xTA/Ox. Lanes 1, 4, and 7 are **TP**. Lanes 2, 5, and 8, are **SSP**. Lanes 3, 6, and 9 are **G4P**.

To confirm the presence of correctly formed G-quadruplexes in **G4P**, we conducted CD analysis. As a first test, we examined the ability of the human telomeric sequence **22AG** (Table B.1) to form a G-quadruplex. Solutions containing 10 μM **22AG** in each of the four buffers were heated to 95°C for 10 minutes and then rapidly cooled to room temperature. The solutions were allowed to equilibrate at room temperature for 1.5 h before scanning. Figure B.8 shows the results of annealing **22AG** in 1xTAEMg, 1xTA/Spect, 1xTA/Ox, compared to a 1xK-G4 buffer (containing 10mM

K_2HPO_4/KH_2PO_4, 100 mM KCl, pH 7.6). In 1xK-G4 buffer, this sequence forms a (3+1) hybrid polymorph characterized by a large (+)-peak at 295 nm, a (+)-shoulder at 275 nm, and a smaller (+)-peak at 250 nm.[31] There is excellent overlap of both the polymorphs formed in 1xTA/Spect and 1xTA/Ox with 1xK-G4, suggesting correctly formed G-quadruplexes under these conditions (Figure B.9a). Having determined that the **22AG** sequence alone can tolerate G-quadruplex formation in the hybrid buffer conditions, we conducted CD analysis to determine if the G-quadruplex motif was still visible after **G4P** annealing. The CD signal from duplex DNA is characterized by a (+)-peak at 275 nm, a (−)-peak at 250 nm, with the cross-over at 260 nm.[32] These shifts appear for **TP** and **SSP**, as shown in Figure B.8b. Interestingly, the presence of the G-quadruplex shifts the (+)-peak at 275 nm towards 295 nm while simultaneously causing the (−)-peak at 250 nm to become more positive for **G4P** (Figure B.9b). These changes indicate that G-quadruplexes are still present in solution, however, we cannot determine the exact number of correctly formed G-quadruplexes from this technique Despite this, the combination of one visible band by gel electrophoresis and the evidence that both duplex and G-quadruplex are present in solution by CD analysis confirms the hypothesis that 3D-DNA prism construction and G-quadruplex formation are compatible.

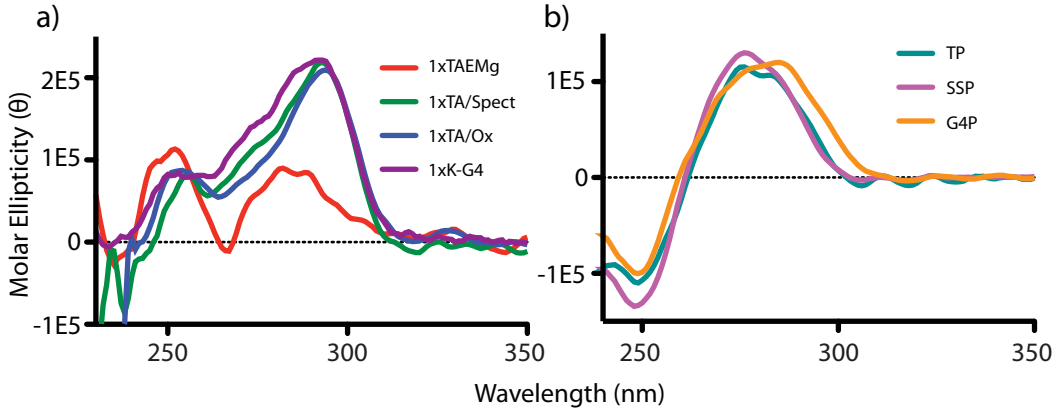

Figure B.9 CD analysis: a) **22AG** strand annealed in different buffer conditions. The good overlap of the signals from the 1xTA/Spect (green) and 1xTA/Ox (blue) with the 1xK-G4 (purple) indicates a fully-formed G-quadruplex under these conditions. b) 3D-Prism assemblies in 1xTA/Spect. **TP** (green), and **SSP** (pink) are characteristic of duplex DNA, while **G4P** (orange) is shifted towards the signal for G-quadruplex formation in potassium-containing solutions.

B.3 Biophysical studies with hemin

Once we had determined the compatibility between 3D-DNA prism and G-quadruplex formation, we moved on to study the interactions of hemin (Figure B.5a) with

22AG, **SS**, and duplex DNA in the 1xTA/Spect conditions. In order to site-selectively place hemin on the G-quadruplexes, we need to evaluate binding affinity between hemin and the various motifs in the **G4P** and **SSP** environments. It is known that the binding of Fe-hemin to DNA results in hyperchromicity of the hemin Soret band.[21,28] Slama-Schwok and Lehn proposed that this hyperchromicity is an indication that the hemin binding site is hydrophobic.[33] Due to the changes in the Soret band upon binding to G-Quadruplex DNA, a binding constant can be determined (See Chapter 1, pp 44 for details on UV titrations). To this end, we conducted UV/Vis binding titrations in a high-throughput manner which utilized 96-well plates and microplate reader (see section B.6 for experimental details). Solutions containing the same concentration of DNA (**22AG**, **SS**, or calf-thymus (CT) duplex DNA) were aliquoted across the rows with increasing amounts of hemin from 0−10 equivalents, and after gentle shaking for 15 minutes, the absorbance of hemin at 404 nm was read. After subtraction of the hemin absorbance alone (in a linear-baseline fashion) and normalization, the binding curves were revealed (Figure B.10). Hemin was shown to bind to **22AG** with a $K_D = 0.30 \pm 0.09$ μM after fitting the data to a one-site binding model using GraphPad Prism 5. This value agrees with Sen's observations of $0.072\ \mu M < K_D < 0.5\ \mu M$ for a different G-quadruplex forming sequence.[21] It is thought that metalloporphyrins with axial ligands (like Fe-hemin) cannot intercalate into dsDNA due to the steric constraints.[34] Instead, they exhibit electrostatic interaction with the phosphate backbone and groove binding.[35] This type of binding does not result in a substantial change in the absorbance of the Soret band (Figure B.10). In order to obtain binding affinity to ss- and dsDNA, we would need to conduct titrations via circular dichroism (CD). The Fe(III) analog of the cationic porphyrin TMPyP4 (Chapter 1, Figure 1.18a, pp 27) has been shown to display positive induced CD signals at the Soret band in the presence of poly(dA-dT) and calf thymus DNA.[35] By extension, Fe(III)-hemin should exhibit similar effects. From this induced CD band, we may be able to extract binding constants.

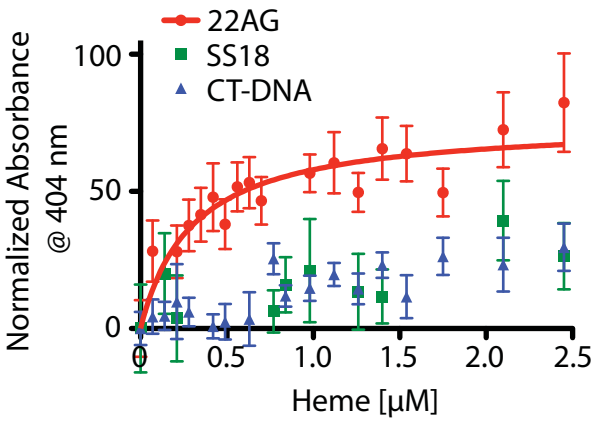

Figure B.10 Fitted binding curves resulting from the UV/Vis titrations of hemin with different DNA motifs. The curve for **22AG** was fit to a one-site specific-binding equation (Section B.6.4.2). The green squares (**SS**) and blue triangles (CT-DNA) show the slight change upon interaction with those motifs that cannot be fit to a one-site binding model.

B.4 Conclusions

In conclusion, we have shown that we can create a 3D-DNA prism with a large number of single-stranded-binding regions to which we can selectively attach three or six G4-forming human-telomeric sequences and that the formation of the **G4P** is compatible in our hybrid buffer conditions. This has been verified by gel electrophoresis and CD analysis. We have also shown that we can bind Fe(III)-hemin selectively to the **22AG** sequence in our 1xTA/Spect buffer with a K_D value of 0.30 ± 0.09 μM. From these studies, we demonstrate that the patterning of G4 motifs on 3D scaffolds is feasible with **G4P**, and we can begin to show that **hG4P** structures are useful for arrangement of catalytic moieties to bring about cascading effects. Currently, we have focused on the binding of one specific catalytic moiety. However, the variety of G-quadruplex forming-sequences and their inherent polymorphic nature presents a library of sequences that have the capability of binding to different catalytic centers, thus allowing for the site-specific placement of several centers, with the potential for creating three-dimensional catalytic cascades.

B.5 Future directions

As a next step, we should determine the binding strength of heme to ss- and dsDNA via CD titrations. Interestingly, Pasternack and coworkers discovered that high ionic strength could cause dissociation of metalloporphyrin-DNA assemblies.[35] If we do

encounter significant binding to ss- and dsDNA, we may be able to counteract it by increasing the salt concentration. After, we can focus on the binding of Fe(III)-hemin to **G4P** to create **hG4P** and study the binding affinity of hemin to the structure (six binding sites). It will be interesting to determine whether the geometric arrangement of the G4 motifs on **G4P** will affect the binding affinity of hemin. We can also determine binding stoichiometry of hemin to **G4P**. Once it is shown that hemin is bound to form **hG4P**, we can examine the peroxidase ability of the **hG4P** structures as a whole in comparison to hemin and hemin-22AG complexes alone. Because the geometric arrangement of guanine quadruplexes can be varied at will, we will be able to determine how the 3D-organization of the hemin catalysts will influence peroxidase ability.

B.6 Experimental section

B.6.1 General

StainsAll®, tris(hydroxymethyl)-aminomethane (Tris), K_2HPO_4 and KH_2PO_4, formamide, DMSO, Fe(III)-hemin and urea were used as purchased from Sigma Aldrich. Acetic acid, boric acid, MES, and HEPES were used as purchased from Fisher Scientific. Reagents used for automated DNA synthesis were purchased from Bioautomation Corporated. Sephadex G-25 (super-fine, DNA grade) was purchased from Glen Reseach. The 22AG sequence and calf-thymus DNA was purchased from Sigma-Genosys Canada. UV-transparent, non-treated, half-area 96-well plates were purchased from Fisher Scientific.

B.6.2 Instrumentation

Standard automated oligonucleotide solid-phase synthesis was performed on a Mermade MM6 synthesizer from Bioautomation. Gel electrophoresis experiments were carried out on an acrylamide 20 x 20 cm vertical Hoefer 600 electrophoresis unit. CD experiments were carried on an a JASCO J-810 spectropolarimeter from Jasco, Inc., with SpectroManager II software. UV/Vis titrations were performed on a BioTek Epoch microplate reader. Quantification of sequences in Table B.1 were preformed on a NanoDrop Lite (Thermo Scientific), while the 22AG sequence was quantified using the molar extinction coefficient at 260 nm at 95°C on a CaryBio 300 spectrophotometer.

B.6.3 Prism formation

Prism **TP** was formed by the combination of equimolar amounts of each clip strand (**C1-C3**), to a final composition of 1.25 μM in 1xTAEMg, 1xTA/Spect, or 1xTA/Ox. The mixture was then annealed from 95ºC to room temperature over about 3 h, using a thermocycler. To make prisms **G4P** or **SSP**, 3.3 equivalents of each extra strand (**Top-22AG**, **Bot-22AG**, **Top-SS**, **Bot-SS**, where appropriate) was also included during annealing. A slight excess was used to avoid any stoichiometric errors due to quantification or pipetting errors.

B.6.4 Biophysical studies

B.6.4.1 CD analysis

Solutions of 10 μM **22AG** were annealed in either 1xTAEMG, 1xTA/Spect, 1xTA/Ox, or 1xK-G4 by heating to 95°C for 10 minutes and then cooling rapidly to room temperature. After 1.5 h of equilbration at room temperature, 200 μL of each solution was transferred to a quartz cuvette (pathlength 1.0 mm) and scanned from 400−250 nm at a scan rate of 200 nm/min with a 1 second response time and 1 nm bandwidth. Two scans were averaged within the SpectraManager II software to produce the final scan which was smoothed using the means-movement function in the Spectra Analysis program. The data (in mdeg) was then transformed into molar ellipticity based on μM in sequence (10 μM for **22AG**) and a 0.1 cm pathlength. For **TP**, **SSP**, and **G4P** analysis, 125 μL of a 1.25 μM solution was formed (as above) and the solutions were analyzed from 400−250 nm at a scan rate of 100 nm/min with a 2 second respose time and a 0.5 nm bandwidth. Three scans were averaged within the SpectraManager II software to produce the final scan which was smoothed using the means-movement function in the Spectra Analysis program. The data (in mdeg) was then transformed into molar ellipticity based on μM in bases (360 μM for **TP** and 712.5 μM for **SSP** and **G4P**) and a 0.1 cm pathlength.

B.6.4.2 UV/Vis titrations

For analysis with **22AG**, concentrated stocks of **22AG** in Milli-Q water were diluted to 100 μM in 1xTA/Spect, and annealed following the same procedure as for the

CD studies. For analysis with CT-DNA, a 2.11 mM (in base pairs, quantified at 260 nm with ε = 13 200 $M^{-1}cm^{-1}$) solution in water was used as a stock. Each DNA sequence (**22AG**, **SS**, CT-DNA) was then diluted from the concentrated solution to 0.7 μM in binding sites (For **22AG** and **SS**, each strand is one binding site. For CT-DNA, 3 base-pairs is one binding site due to the neighbor-exclusion model for intercalation,[36] and size-match of the hemin for groove binding, (so 2.11/3 = 0.703 mM is the stock concentration in binding sites). 50 μL aliquots were placed in all 96 wells of half-area microplates using a multi-channel pipette. Then, varying volumes of a 7 μM solution of hemin in 1xTA/Spect (diluted from 200 μM in DMSO) were added to the wells according to the plate layout below. Finally, various volumes of 1xTA/Spec were added to the plates to ensure a 100 μL total volume according to the plate layout below. To obtain the hemin baseline, instead of adding 50 μL of DNA solution to all the wells first, 50 μL of 1xTA/Spect was added instead. After gentle rocking on a plate-rocker for 15 minutes, the absorbance of hemin at 404 nm was read on the microplate reader. The reading was normalized internally to a 1 cm pathlength with reference to water by the software. Absorbance values were then exported to GraphPad Prism. The hemin values alone were subtracted from the hemin-DNA values using the linear-baseline function within GraphPad. After normalization to high and low values, the binding curve for **22AG** was fit to a one-site binding model (one site per G4: $Y = (B_{max}*X) / (K_D + X)$ where Y is specific binding, X is the concentration of hemin, and B_{max} is the maximum response from binding), from which the K_D value (and B_{max}) was obtained.

heme	1	2	3	4	5	6	7	8	9	10	11	12	
A	0	1	2	3	4	5	6	7	8	9	10	11	uL
B	0	1	2	3	4	5	6	7	8	9	10	11	uL
C	0	1	2	3	4	5	6	7	8	9	10	11	uL
D	0	1	2	3	4	5	6	7	8	9	10	11	uL
E	12	14	16	18	20	22	25	30	35	40	45	50	uL
G	12	14	16	18	20	22	25	30	35	40	45	50	uL
H	12	14	16	18	20	22	25	30	35	40	45	50	uL
I	12	14	16	18	20	22	25	30	35	40	45	50	uL
[final]	**0**	**0.07**	**0.14**	**0.21**	**0.28**	**0.35**	**0.42**	**0.49**	**0.56**	**0.63**	**0.7**	**0.77**	uM
equivalents	0	0.2	0.4	0.6	0.8	1	1.2	1.4	1.6	1.8	2	2.2	
[final]	**0.84**	**0.98**	**1.12**	**1.26**	**1.4**	**1.54**	**1.75**	**2.1**	**2.45**	**2.8**	**3.15**	**3.5**	uM
equivalents	2.4	2.8	3.2	3.6	4	4.4	5	6	7	8	9	10	

Figure SB.1 Plate layout showing hemin aliquots

Buffer	1	2	3	4	5	6	7	8	9	10	11	12	
A	50	49	48	47	46	45	44	43	42	41	40	39	uL
B	50	49	48	47	46	45	44	43	42	41	40	39	uL
C	50	49	48	47	46	45	44	43	42	41	40	39	uL
D	50	49	48	47	46	45	44	43	42	41	40	39	uL
E	38	36	34	32	30	28	25	20	15	10	5	0	uL
G	38	36	34	32	30	28	25	20	15	10	5	0	uL
H	38	36	34	32	30	28	25	20	15	10	5	0	uL
I	38	36	34	32	30	28	25	20	15	10	5	0	uL

Figure SB.2 Plate layout showing buffer aliquots

B.7 References

1. Dodziuk, H., Supramolecular Chemistry - What is This? In *Introduction to Supramolecular Chemistry*, Springer Netherlands: 2002; pp 1-19.
2. Idan, O.; Hess, H., Origins of activity enhancement in enzyme cascades on scaffolds. *ACS Nano* **2013,** *7* (10), 8658-8665.
3. Wilner, O. I.; Weizmann, Y.; Gill, R.; Lioubashevski, O.; Freeman, R.; Willner, I., Enzyme cascades activated on topologically programmed DNA scaffolds. *Nat Nanotechnol* **2009,** *4* (4), 249-254.
4. Delebecque, C. J.; Lindner, A. B.; Silver, P. A.; Aldaye, F. A., Organization of intracellular reactions with rationally designed RNA assemblies. *Science* **2011,** *333* (6041), 470-474.
5. Shimron, S.; Wang, F.; Orbach, R.; Willner, I., Amplified detection of DNA through the enzyme-free autonomous assembly of hemin/G-quadruplex DNAzyme nanowires. *Anal Chem* **2012,** *84* (2), 1042-1048.
6. Yang, H.; McLaughlin, C. K.; Aldaye, F. A.; Hamblin, G. D.; Rys, A. Z.; Rouiller, I.; Sleiman, H. F., Metal-nucleic acid cages. *Nat Chem* **2009,** *1* (5), 390-396.
7. Lo, P. K.; Karam, P.; Aldaye, F. A.; McLaughlin, C. K.; Hamblin, G. D.; Cosa, G.; Sleiman, H. F., Loading and selective release of cargo in DNA nanotubes with longitudinal variation. *Nat Chem* **2010,** *2* (4), 319-328.
8. McLaughlin, C. K.; Hamblin, G. D.; Aldaye, F. A.; Yang, H.; Sleiman, H. F., A facile, modular and high yield method to assemble three-dimensional DNA structures. *Chem Commun* **2011,** *47* (31), 8925-8927.
9. McLaughlin, C. K.; Hamblin, G. D.; Sleiman, H. F., Supramolecular DNA assembly. *Chem Soc Rev* **2011,** *40* (12), 5647-5656.

10. Hamblin, G. D.; Carneiro, K. M. M.; Fakhoury, J. F.; Bujold, K. E.; Sleiman, H. F., Rolling circle amplification-templated DNA nanotubes show increased stability and cell penetration ability. *J Am Chem Soc* **2012,** *134* (6), 2888-2891.
11. McLaughlin, C. K.; Hamblin, G. D.; Hanni, K. D.; Conway, J. W.; Nayak, M. K.; Carneiro, K. M.; Bazzi, H. S.; Sleiman, H. F., Three-Dimensional Organization of Block Copolymers on "DNA-Minimal" Scaffolds. *J Am Chem Soc* **2012,** *134* (9), 4280-4286.
12. Conway, J. W.; McLaughlin, C. K.; Castor, K. J.; Sleiman, H., DNA nanostructure serum stability: greater than the sum of its parts. *Chem Commun* **2013,** *49* (12), 1172-1174.
13. Hamblin, G. D.; Hariri, A. A.; Carneiro, K. M.; Lau, K. L.; Cosa, G.; Sleiman, H. F., Simple design for DNA nanotubes from a minimal set of unmodified strands: rapid, room-temperature assembly and readily tunable structure. *ACS Nano* **2013,** *7* (4), 3022-3028.
14. Watson, J. D.; Crick, F. H. C., Molecular Structure of Nucleic Acids: A Structure for Deoxyribose Nucleic Acid. *Nature* **1953,** *171* (4356), 737-738.
15. Bock, L. C.; Griffin, L. C.; Latham, J. A.; Vermaas, E. H.; Toole, J. J., Selection of single-stranded DNA molecules that bind and inhibit human thrombin. *Nature* **1992,** *355* (6360), 564-566.
16. Macaya, R. F.; Schultze, P.; Smith, F. W.; Roe, J. A.; Feigon, J., Thrombin-binding DNA aptamer forms a unimolecular quadruplex structure in solution. *Proc Natl Acad Sci USA* **1993,** *90* (8), 3745-3749.
17. Timmer, C. M.; Michmerhuizen, N. L.; Witte, A. B.; Van Winkle, M.; Zhou, D.; Sinniah, K., An Isothermal Titration and Differential Scanning Calorimetry Study of the G-Quadruplex DNA-Insulin Interaction. *J Phys Chem B* **2014,** *118* (7), 1784-1790.
18. Kieltyka, R.; Fakhoury, J.; Moitessier, N.; Sleiman, H. F., Platinum phenanthroimidazole complexes as G-quadruplex DNA selective binders. *Chem Eur J* **2008,** *14* (4), 1145-1154.
19. Castor, K. J.; Mancini, J.; Fakhoury, J.; Weill, N.; Kieltyka, R.; Englebienne, P.; Avakyan, N.; Mittermaier, A.; Autexier, C.; Moitessier, N.; Sleiman, H. F., Platinum(II) phenanthroimidazoles for targeting telomeric G-quadruplexes. *ChemMedChem* **2012,** *7* (1), 85-94.
20. Castor, K. J.; Liu, Z.; Fakhoury, J.; Hancock, M. A.; Mittermaier, A.; Moitessier, N.; Sleiman, H. F., A Platinum(II) Phenylphenanthroimidazole with an Extended Side-Chain Exhibits Slow Dissociation from a c-Kit G-Quadruplex Motif. *Chem Eur J* **2013,** *19* (52), 17836-17845.
21. Travascio, P.; Li, Y.; Sen, D., DNA-enhanced peroxidase activity of a DNA aptamer-hemin complex. *Chem & Biol* **1998,** *5* (9), 505-517.
22. Freeman, R.; Sharon, E.; Teller, C.; Henning, A.; Tzfati, Y.; Willner, I., DNAzyme-like activity of hemin-telomeric G-quadruplexes for the optical analysis of telomerase and its inhibitors. *ChemBioChem* **2010,** *11* (17), 2362-2367.
23. Sen, D., Catalytic G-quadruplexes. In *Guanine Quartets*, Spindler, L.; Fritzsche, W., eds. **2012**, pp 277-284.

24. Golub, E.; Freeman, R.; Willner, I., Hemin/G-quadruplex-catalyzed aerobic oxidation of thiols to disulfides: application of the process for the development of sensors and aptasensors and for probing acetylcholine esterase activity. *Anal Chem* **2013,** *85* (24), 12126-12133.
25. Oganesian, L.; Bryan, T. M., Physiological relevance of telomeric G-quadruplex formation: a potential drug target. *BioEssays* **2007,** *29*, 155-165.
26. Fu, J.; Liu, M.; Liu, Y.; Woodbury, N. W.; Yan, H., Interenzyme substrate diffusion for an enzyme cascade organized on spatially addressable DNA nanostructures. *J Am Chem Soc* **2012,** *134* (12), 5516-5519.
27. Edwardson, T. G. W.; Carneiro, K. M. M.; McLaughlin, C. K.; Serpell, C. J.; Sleiman, H. F., Site-specific positioning of dendritic alkyl chains on DNA cages enables their geometry-dependent self-assembly. *Nat Chem* **2013,** *5* (10), 868-875.
28. Poon, L. C.; Methot, S. P.; Morabi-Pazooki, W.; Pio, F.; Bennet, A. J.; Sen, D., Guanine-rich RNAs and DNAs that bind heme robustly catalyze oxygen transfer reactions. *J Am Chem Soc* **2011,** *133* (6), 1877-1884.
29. Pauling, L., *The nature of the chemical bond and the structure of molecules and crystals : an introduction to modern structural chemistry*. Cornell University Press: Ithaca, N.Y., 1960.
30. Hardin, C. C.; Watson, T.; Corregan, M.; Bailey, C., Cation-dependent transition between the quadruplex and Watson-Crick hairpin forms of d(CGCG3GCG). *Biochemistry* **1992,** *31* (3), 833-841.
31. Ambrus, A.; Chen, D.; Dai, J.; Bialis, T.; Jones, R. A.; Yang, D., Human telomeric sequence forms a hybrid-type intramolecular G-quadruplex structure with mixed parallel/antiparallel strands in potassium solution. *Nucleic Acids Res* **2006,** *34* (9), 2723-2735.
32. Johnson, W. C., CD of Nucleic Acids. In *Circular Dichroism: Principles and Applications*, 2nd ed.; Berova, N.; Nakanishi, K.; Woody, R., Eds. Wiley-VHC: New York, 2000; pp 703-718.
33. Slama-Schwok, A.; Lehn, J. M., Interaction of a porphyrin-containing macrotetracyclic receptor molecule with single-stranded and double-stranded polynucleotides. A photophysical study. *Biochemistry* **1990,** *29* (34), 7895-7903.
34. Fiel, R. J., Porphyrin-nucleic acid interactions: a review. *J Biomol Struct Dyn* **1989,** *6* (6), 1259-1274.
35. Pasternack, R. F.; Gibbs, E. J.; Villafranca, J. J., Interactions of porphyrins with nucleic acids. *Biochemistry* **1983,** *22* (10), 2406-2414.
36. Crothers, D. M., Calculation of binding isotherms for heterogenous polymers. *Biopolymers* **1968,** *6* (4), 575-584.

C Appendix C: Other Compounds

This appendix contains compounds made, but never pursued, and are meant to serve as a guide for future students.

C.1 Introduction

Many ideas for new classes of molecules were examined throughout my time as a PhD student, but not all of them came to fruition. Needless to say, I still made many molecules and this appendix showcases them. It is of note that not all of these molecules have been fully characterized.

C.2 Phenanthroimidazole "linkers" for non-covalent DNA ligation

Chris McLaughlin and I had an idea to make phenanthroimidazole ligands that when added on the terminal ends of a DNA sequence, could π-stack with each other, allowing the terminal bases to non-covalently 'ligate' the sequence. The idea originally developed when he thought that his 3D-DNA cages (see appendix B, 3D G4-prisms) were fraying at the nick points and instead of chemically or enzymatically ligating them, non-covalent 'ligation' could be easier and potentially reversible. Synthesis of phenanthroimidazoles containing a terminal groups for covalent linking to DNA: via phosphoramidite synthesis (through the terminal –OH group), via a terminal –COOH group for linking to amine-terminated DNA. These ligands could be platinated with potassium tetrachloroplatinate, followed by subsequent addition of ethylenediamine to form the full complex (KC-III-60, below), if necessary.

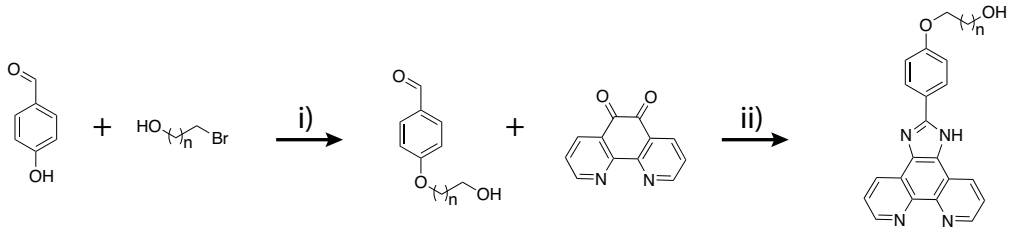

Figure C.1 Scheme for terminal –OH group for phosphoramidite synthesis: i) K_2CO_3, acetone, RT or reflux, o/n, ii) NH_4OAc, glacial acetic acid, reflux, 24 h.

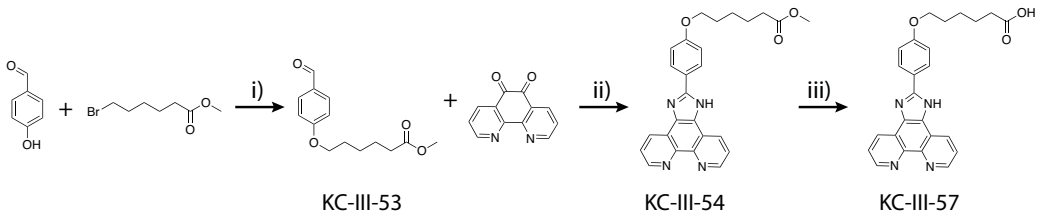

Figure C.2 Scheme for amide-bond coupling to amine-terminated DNA: i) K_2CO_3, acetone, reflux, o/n, ii) NH_4OAc, glacial acetic acid, reflux, 24 h, iii) LiOH, THF/H_2O, RT, 2 h.

C.2.1 Experimental section

KC-VI-40: 4-hydroxybenzaldehyde (210 mg, 1.72 mmol) and potassium carbonate (474 mg, 3.44 mmol) were dissolved in 75 mL acetone and allowed to stir for 15 minutes at room temperature. Then 3-bromopropanol (225 μL, 2.58 mmol) was added dropwise. The reaction was allowed to stir overnight at room temperature. The next day, an aqueous solution of ammonium chloride was added and the organic phase was extracted three times with ethyl acetate, dried over magnesium sulfate and evaporated under vacuum onto celite. The celite-containing crude product was purified via reverse-phase column chromatography using a CombiFlash Rf machine (Teledyne Isco, Inc) from 0%−60% ACN/H_2O. The pure fractions were collected and concentrated under vacuum to yield 85.7 mg of a colorless oil, 28% yield.

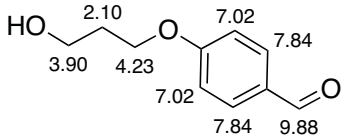

^{1}H NMR (300 MHz, $CDCl_3$); δ = 9.88 (s, 1H), 7.84 (d, 2H), 7.02 (d, 2H), 4.23 (t, 2H), 3.90 (t, 3H), 2.10 (quintet, 2H) ppm; ^{13}C NMR (300 MHz, $CDCl_3$): δ = 190.9, 163.9, 132.0, 114.7, 65.6, 59.8, 31.8 ppm; HR-MS Calculated for $C_{10}H_{12}NaO_3$ (M+Na): **203.0679**, Found: **203.0687.**

KC-VI-46: 4-hydroxybenzaldehyde (387 mg, 3.17 mmol), 9-bromononanol (643 mg, 2.88 mmol), and potassium carbonate (795 mg, 5.76 mmol) were dissolved in 75 mL acetone and refluxed for 2 days. The reaction was quenched with an aqueous solution of ammonium chloride and diluted with water before the organic phase was extracted three times with ethyl acetate, dried over magnesium sulfate and evaporated under vacuum

onto celite. The celite-containing crude product was purified via reverse-phase column chromatography using a CombiFlash Rf machine (Teledyne Isco, Inc) from 5%−95% ACN/H_2O. The pure fractions were collected and concentrated under vacuum to yield 549 mg of a colorless oil, 72% yield.

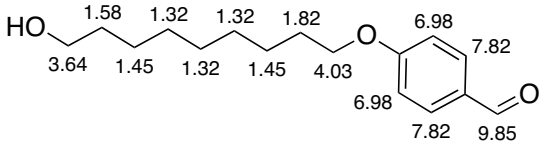

^{1}H NMR (300 MHz, $CDCl_3$): δ = 9.85 (s, 1H), 7.82 (d, 2H), 6.98 (d, 2H), 4.03 (t, 2H), 3.64 (t, 3H), 1.82 (quintet, 2H), 1.58 (m, 2H), 1.45-1.32 (m, 10H) ppm; ^{13}C NMR (300 MHz, $CDCl_3$): δ = 190.9, 164.3, 132.0, 129.6, 114.7, 68.4, 63.0, 32.7, 29.5, 29.3, 29.2, 29.0, 25.9, 25.7 ppm; HR-MS Calculated for $C_{16}H_{24}NaO_3$ (M+Na): **287.1618**, Found: **287.1613.**

KC-VI-47: KC-VI-40 (78.6 mg, 0.436 mmol), 1,10-phenanthroline-5,6-dione (83.3 mg, 0.397 mmol), and ammonium acetate (310 mg, 3.97 mmol) were dissolved in 15 mL glacial acetic acid and refluxed overnight. The reaction was allowed to cool to room temperature before diluting with water and neutralizing to pH 7−8 with ammonium hydroxide on an ice bath. The brownish-yellow precipitate was filtered on a glass frit and washed with H_2O, hexane, DCM, and diethylether before allowing to air dry on the vacuum overnight. After drying, the powder was dissolved through the frit with DCM/MeOH and the solvent evaporated under vacuum to yield 135.4 mg of a light yellow powder, 92% yield.

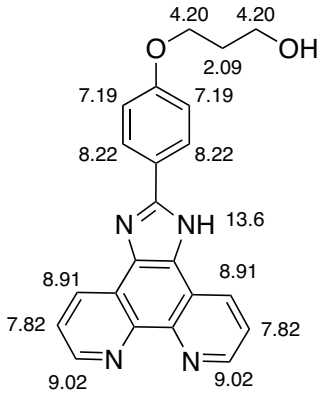

^{1}H NMR (300 MHz, DMSO-d_6): δ = 13.6 (br s, 1H), 9.02 (d, 2H), 8.91 (d, 2H), 8.22 (d, 2H), 7.82 (br, 2H), 7.19 (d, 2H), 4.21 (m, 4H), 2.11 (quintet, 2H) ppm; HR-MS Calculated for $C_{22}H_{18}N_4NaO_2$ (M+Na): **393.1322**, Found: **393.1332.**

KC-VI-48: KC-VI-46 (215.7 mg, 0.816 mmol), 1,10-phenanthroline-5,6-dione (155.9 mg, 0.742 mmol), and ammonium acetate (572 mg, 7.42 mmol) were dissolved in 20 mL glacial acetic acid and refluxed overnight. The reaction was allowed to cool to room temperature before diluting with water and neutralizing to pH 7−8 with ammonium hydroxide on an ice bath. The brownish-yellow precipitate was filtered on a glass frit and washed with H_2O, hexane, DCM, and diethylether before allowing to air dry on the vacuum overnight. After drying, the powder was dissolved through the frit with DCM/MeOH and the solvent evaporated under vacuum to yield 241 mg of a yellow powder, 71% yield.

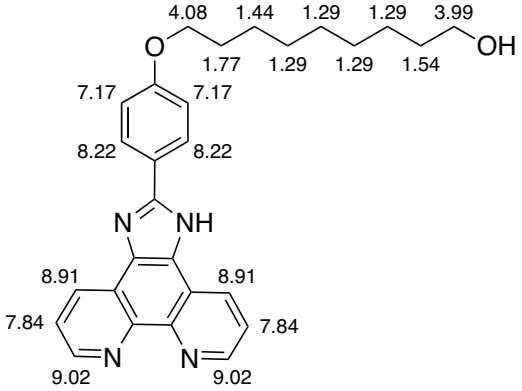

^{1}H NMR (300 MHz, d_6-DMSO): δ = 9.02 (d, 2H), 8.91 (d, 2H), 8.22 (d, 2H), 7.84 (m, 2H), 7.17 (d, 2H), 4.08 (t, 2H), 3.99 (t, 2H), 1.77 (quintet, 2H), 1.54 (m, 2H), 1.44 (m, 2H), 1.29 (m, 8H) ppm; HR-MS Calculated for $C_{28}H_{30}N_4NaO_2$ (M+Na): **477.2261**, Found: **477.2270.**

KC-III-53: 4-hydroxybenzaldehyde (507.8 mg, 4.16 mmol), methyl-5-bromovalerate (1010 mg, 5.20 mmol), and potassium carbonate (1150 mg, 8.32 mmol) were dissolved in 30 mL acetone and refluxed overnight. The reaction was allowed to cool to room temperature before filtering through a glass frit and washing the solids with acetone. The filtrate was concentrated under vacuum and purified with silica gel chromatography on a

CombiFlash Rf from 0%−20% hexanes/ethyl acetate. The fractions were combined to yield 843 mg of yellow oil, 86% yield.

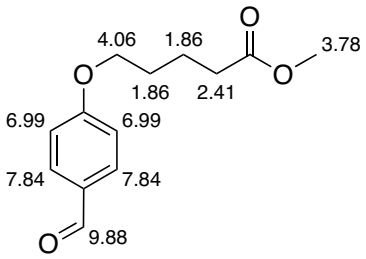

^{1}H NMR (400 MHz, $CDCl_3$): δ = 9.88 (s, 1H), 7.84 (d, 2H), 6.99 (d, 2H), 4.06 (t, 2H), 3.78 (s, 3H), 2.41 (t, 2H), 1.86 (m, 4H) ppm; ^{13}C NMR (300 MHz, $CDCl_3$): δ = 190.8, 173.8, 164.0, 132.0, 129.9, 114.7, 67.8, 51.6, 33.6, 28.5, 21.5 ppm; HR-MS Calculated for $C_{13}H_{16}NaO_4$ (M+Na): **259.0941**, Found: **259.0941.**

KC-III-54: KC-III-53 (183 mg, 0.772 mmol), phendione (148 mg, 0.702 mmol), and ammonium acetate (541 mg, 7.02 mmol) were dissolved in 20 mL glacial acetic acid and refluxed overnight. The reaction was allowed to cool to room temperature before diluting with water and neutralizing to pH 7−8 with ammonium hydroxide on an ice bath. The brownish-yellow precipitate was filtered on a glass frit and washed with H_2O, hexane, DCM, and diethylether before allowing to air dry on the vacuum overnight. The yellow solid weighed 255 mg. 85% yield.

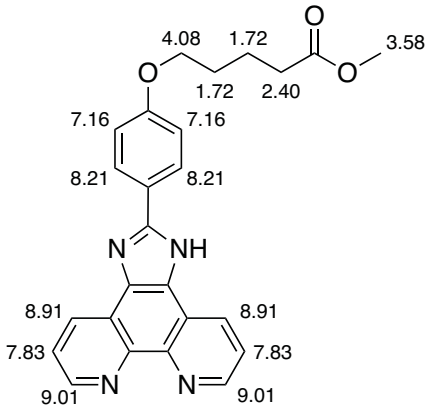

^{1}H NMR (400 MHz, d_6-DMSO): δ = 9.01 (d, *2*H), 8.91 (d, 2H), 8.21 (d, 2H), 7.83 (m, 2H), 7.16 (d, 2H), 4.08 (t, 2H), 3.58 (s, 3H), 2.40 (t, 2H), 1.72 (m, 4H) ppm; HR-MS Calculated for $C_{25}H_{22}N_4NaO_3$ (M+Na): **449.1584**, Found: **449.1578.**

KC-III-57: KC-III-54 (105 mg, 0.247 mmol) and lithium hydroxide (6.50 mg, 0.217 mmol) were dissolved in 20 mL of a 1:1 mixture of H_2O and THF. The solution was allowed to stir at room temperature for 2 h. The cloudy solution was then concentrated under vacuum before 17% aq. HCl was added to lower the pH to 4. After acidifying, the precipitate went into solution. The aqueous layer was extracted three times with DCM. The aqueous layer contained the product, so was concentrated under vacuum to yield 102 mg, ~ 100% yield.

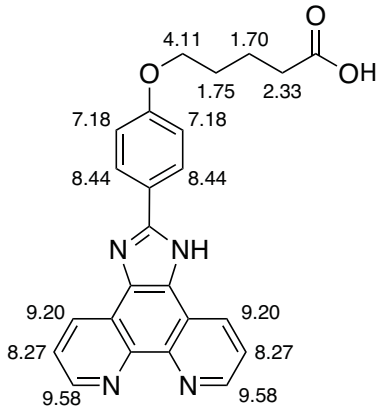

^{1}H NMR (300 MHz, d_6-DMSO): δ = 9.58 (br, *2*H), 9.20 (d, 2H), 8.44 (d, 2H), 8.27 (dd, 2H), 7.18 (d, 2H), 4.11 (t, 2H), 2.33 (t, 2H), 1.75 (quintet, 2H), 1.70 (quintet, 2H) ppm; HR-MS Calculated for $C_{24}H_{20}N_4NaO_3$ (M+Na): **435.1428**, Found: **435.1421.**

KC-III-60: KC-III-57 (52.8 mg, 0.128 mmol) was dissolved in 5 mL hot DMSO while potassium tetrachloroplatinate (53.8 mg, 0.129 mmol) was dissolved in 2 mL hot H_2O. The two solutions were mixed together and allowed to stir at room temperature overnight. The cloudy yellow solution was then filtered on a glass frit and washed with H_2O and dried with diethylether. The crude bischloride (32.0 mg, 0.047 mmol) was then added to 10 mL absolute ethanol at room temperature before adding in ethylenediamine (31.6 μL, 0.472 mmol). This solution was allowed to stir overnight. The next day, the solution was cloudy rust-red colored. The solution was diluted with H_2O and ethanol and ammonium hexafluorophosphate was added (~ 100 mg) and allowed to stir for ~ 2 h before filtering through a glass frit. The red solid was washed with H_2O and dried with diethylether before air drying on the frit. The powder was orange and fluffy and weighed 27.7 mg, 62% yield from the bischloride.

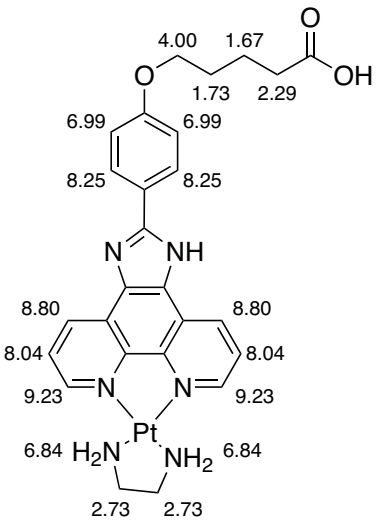

^{1}H NMR (400 MHz, d_6-DMSO): δ = 9.23 (br, *2*H), 8.80 (br, 2H), 8.25 (br, 2H), 8.04 (br, 2H), 6.99 (br, 2H), 6.84 (br, 4H), 4.00 (br, 2H), 2.73 (br, 4H), 2.29 (br, 2H), 1.73 (br, 2H), 1.67 (br, 2H) ppm; HR-MS Calculated for $C_{26}H_{27}N_6O_3Pt$ (M^{+1}): **666.1789**, Found: **666.1774.**

C.3 "Click-able" Toolbox for non-metallated G-quadruplex binders

This section details the design of crescent-shaped molecules with protonable side-chains that can be orthogonally created using "click" chemistry and condensation of diones and diamines with aldehydes (Figure C.3) to afford crescent-shaped quadruplex binders along the lines of those acridine/acridone derivatives in the literature.[1-6]

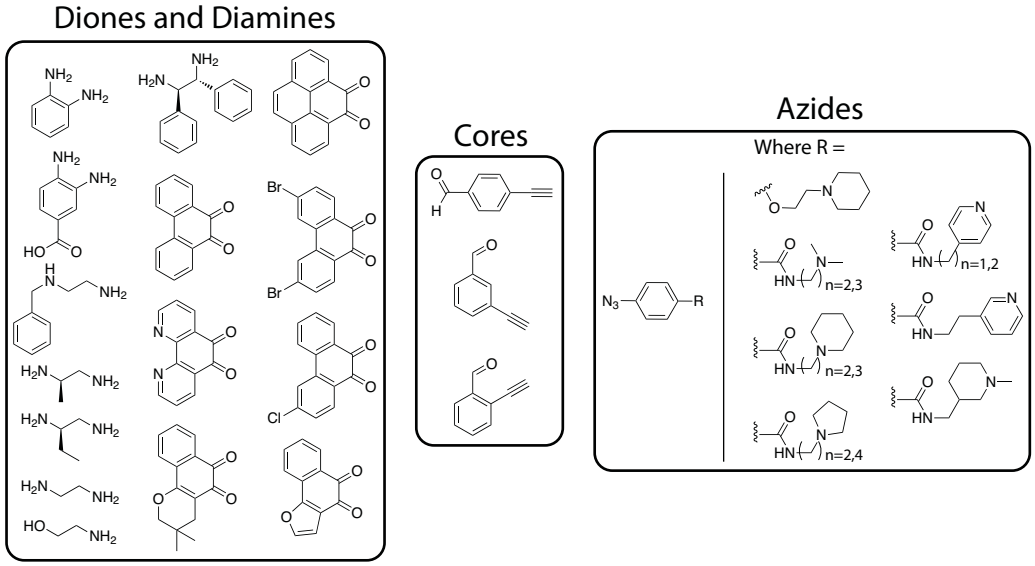

Figure C.3 Generic schematic for the clickable toolbox.

C.3.1 Experimental section

KC-IV-16: Bis-Boc-3,4-diaminobenzoic acid (312.7 mg, 0.887 mmol) and N,N-dimethylpropane-1,3-diamine (223 µL, 1.77 mmol) were dissolved in 30 mL dry DCM under an argon atmosphere. Then HOAt (181 mg, 1.33 mmol) and EDC (340 mg, 1.77 mmol) were added and the reaction proceeded for 12 h at room temperature. The solvent was removed under reduced pressure and then redissolved in ethylacetate. The organic phase was extracted with aqueous sodium bicarbonate, followed by water (two times). The aqueous layer was re-extracted with DCM. The organic layers were combined, washed with brine, dried over $MgSO_4$, and then concentrated under reduced pressure to yield 348 mg of a yellow/white solid (90%).

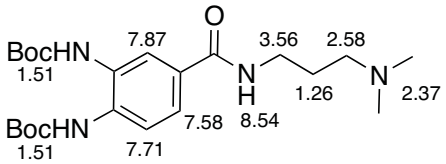

^{1}H NMR (400 MHz, $CDCl_3$): δ = 8.54 (br s, 1H), 7.87 (s, 1H), 7.71 (d, 1H), 7.58 (d, 2H), 3.56 (q, 2H), 2.58 (t, 2H), 2.37 (s, 6H), 1.51 (s, 9H), 1.26 (m, 2H) ppm; HR-MS Calculated for $C_{22}H_{37}N_4O_5$ (M+1): **437.2758**, Found: **437.2758.**

KC-IV-22: KC-IV-16 (76.0 mg, 0.174 mmol) was dissolved in 10 mL ethyl acetate and 10 mL 6 M HCl. The solution turned homogenous after ~ 1.5 h. The solvent was removed under reduced pressure and then redissolved in water and acidified to pH 1. The acidic layer was extracted with ethyl acetate. The organic layer was basified to pH 13 and extracted with ethyl acetate. The organic layers were combined, washed with brine, and dried over $MgSO_4$ before being concentrated under reduced pressure to yield 27.8 mg of a yellow oil (68%).

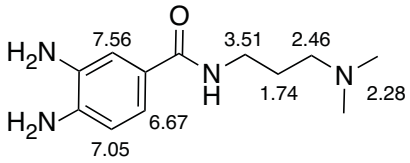

^{1}H NMR (300 MHz, $CDCl_3$): δ = 7.56 (br s, 1H), 7.05 (d, 1H), 6.67 (d, 1H), 3.51 (q, 2H), 2.46 (t, 2H), 2.28 (s, 6H), 1.74 (s, 9H).

KC-IV-51: Pyrene (615 mg, 3.04 mmol) was dissolved in DCM and THF (20 mL each). Then sodium periodate (2.92 g, 13.7 mmol), ruthenium trichloride hydrate (79.5 mg, 0.304 mmol), and water (25 mL) were added. The solution was allowed to stir for 3.5 h before pouring the solution into water (100 mL). The aqueous layer was extracted with DCM three times. The organic layer was washed with water (three times) and dried over celite and $MgSO_4$. The crude product was purified via silica gel after elution with 100% DCM and yielded a bright orange powder.

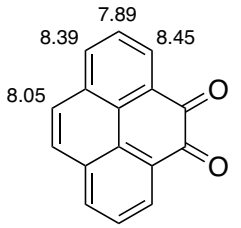

^{1}H NMR (400 MHz, d_6-acetone): δ = 8.45 (d, 2H), 8.39 (d, 2H), 8.05 (s, 2H), 7.89 (t, 2H) ppm. HR-MS Calculated for $C_{16}H_8NaO_2$ (M+Na): **255.0417**, Found: **255.0411.**

KC-IV-55: KC-IV-51 (43.6 mg, 0.188 mmol), 4-ethynylbenzaldehyde (29.3 mg, 0.225 mmol), and ammonium acetate (145 mg, 1.88 mmol) were dissolved in 15 mL glacial acetic acid and allowed to stir at room temperature overnight. Then, the solution was heated to reflux for 30 min. The reaction was allowed to cool to room temperature before diluting with water and neutralizing to pH 7−8 with ammonium hydroxide on an ice bath. The brownish-red precipitate was filtered on a glass frit and washed with H_2O, hexane, DCM, and diethylether before allowing to air dry on the vacuum overnight. The crude product was purified via silica gel after elution with 10%−70% EA/hex and yielded 26.6 mg (41% yield).

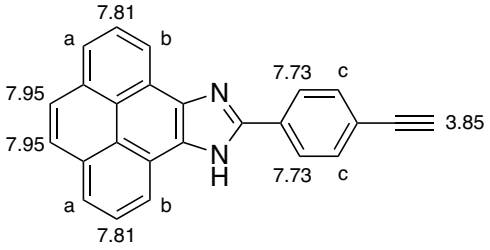

^{1}H NMR (200 MHz, d_6-acetone): δ = 8.43-8.16 (m, 6H), 7.95 (s, 2H), 7.81 (t, 2H), 7.73 (d, 2H), 3.85 (s, 1H) ppm; HR-MS Calculated for $C_{25}H_{15}N_2$ (M+): **343.1230**, Found: **343.1222.**

KC-IV-58: 4-ethynylbenzaldehyde (99.7 mg, 0.766 mmol) and ethylenediamine (54 μL, 0.805 mmol) ammonium acetate (145 mg, 1.88 mmol) were dissolved in 10 mL dichloromethane and cooled to 0°C in an ice bath. After 30 minutes, N-bromosuccinimide (143 mg, 0.805 mmol) was added and the solution allowed to warm to room temperature overnight. The reaction was quenched with aqueous sodium bicarbonate (10%) and extracted three times with dichloromethane before drying over $MgSO_4$. The organic layer was concentrated under reduced pressure to yield 127 mg (97% yield).

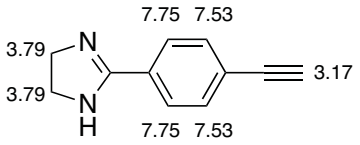

^{1}H NMR (300 MHz, $CDCl_3$): δ = 7.75 (d, 2H), 7.53 (d, 2H), 3.79 (s, 4H), 3.17 (s, 1H) ppm; HR-MS Calculated for $C_{11}H_{11}N_2$ (M+): **171.0917**, Found: **171.0915.**

KC-IV-61: 4-ethynylbenzaldehyde (17.8 mg, 0.137 mmol) and 1,2-phenylenediamine (15.5 mg, 0.144 mmol) were dissolved in 10 mL dichloromethane and cooled to 0°C in an ice bath. After 30 minutes, N-bromosuccinimide (25.6 mg, 0.144 mmol) was added and the solution allowed to warm to room temperature overnight. The reaction was quenched with aqueous sodium bicarbonate (10%) and extracted three times with dichloromethane before drying over $MgSO_4$. The organic layer was concentrated under reduced pressure. The crude product was purified via silica gel after elution with 5%−60% EA/hex and yielded enough product for an NMR (~ 1% yield).

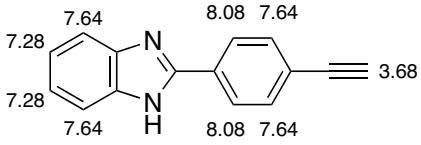

^{1}H NMR (400 MHz, CD_3OD): δ = 8.08 (d, 2H), 7.64 (m, 2H), 7.28 (d, 2H), 3.68 (s, 1H), ppm; HR-MS Calculated for $C_{15}H_{11}N_2$ (M+): **219.0917**, Found: **219.0907.**

KC-V-1: 4-ethynylbenzaldehyde (248 mg, 1.90 mmol) and meso-1,2-diphenylethylenediamine (424 mg, 2.00 mmol) were dissolved in 10 mL DCM and cooled to 0°C in an ice bath. After 30 minutes, N-bromosuccinimide (356 mg, 2.00 mmol) was added and the solution allowed to warm to room temperature overnight. The reaction was quenched with aqueous sodium bicarbonate (10%) and extracted three times with dichloromethane before drying over $MgSO_4$. The organic layer was concentrated under reduced pressure. The crude oil was purified via silica gel after elution with DCM/MeOH and yielded 86.6 mg (14% yield).

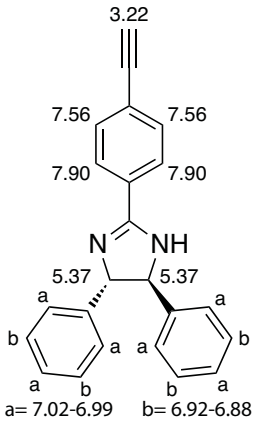

^{1}H NMR (300 MHz, $CDCl_3$): δ = 7.90 (d, 2H), 7.56 (d, 2H), 7.02-6.99 (m, 6H), 6.92-6.88 (m, 4H), 5.37 (s, 2H), 3.22 (s, 1H) ppm; ^{13}C NMR (300 MHz, $CDCl_3$): δ = 164.0, 138.8, 132.3, 130.2, 127.6, 127.5, 127.3, 126.8, 124.8, 83.1, 79.4 ppm; HR-MS Calculated for $C_{23}H_{19}N_2$ (M+): **323.1543**, Found: **323.1548**.

KC-V-2: 3-ethynylbenzaldehyde (151 mg, 1.16 mmol) and meso-1,2-diphenylethylenediamine (259 mg, 1.22 mmol) were dissolved in 10 mL DCM and cooled to 0°C in an ice bath. After 30 minutes, N-bromosuccinimide (143 mg, 0.805 mmol) was added and the solution allowed to warm to room temperature overnight. The reaction was quenched with aqueous sodium bicarbonate (10%) and extracted three times with dichloromethane before drying over $MgSO_4$. The organic layer was concentrated under reduced pressure. The crude oil was purified via silica gel after elution with DCM/MeOH and yielded 37.2 mg (59% yield).

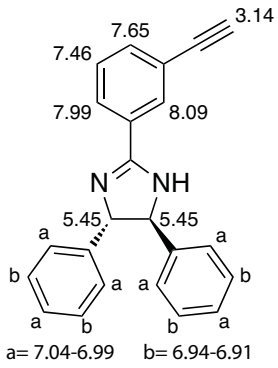

^{1}H NMR (300 MHz, $CDCl_3$): δ = 8.09 (s, 1H), 7.99 (d, 1H), 7.65 (d, 1H), 7.46 (t, 1H), 7.04-6.99 (m, 6H), 6.94-6.91 (m, 4H), 5.45 (s, 2H), 3.14 (s, 1H) ppm; ^{13}C NMR (300 MHz, $CDCl_3$): δ = 163.7, 138.8, 134.5, 130.9, 130.3, 128.8, 127.7, 127.5, 126.9, 122.7, 82.8, 78.2 ppm; HR-MS Calculated for $C_{23}H_{19}N_2$ (M+): **323.1543**, Found: **323.1549**.

KC-VII-64: 1-azido-4-methoxybenzene (92.7 mg, 0.621 mmol), 4-ethynylbenzaldehyde (80.9 mg, 0.621 mmol), 345 µL of a 0.18 M solution of $CuSO_4$•$5H_2O$ in water and 311 µL of a 1.0 M solution of sodium ascorbate in water were dissolved in a 10−20 mL microwave vial in 5 mL ACN with a magnetic stir bar. The reaction was conducted for 15 min at 100°C. The vial was then centrifuged and the mother liquor decanted. The remaining solid was washed with MeOH and DCM, centrifuged, and the solution added to the mother liquor. The organic layer was washed with 10% NaOH three times before drying over $MgSO_4$. The solvent was removed under reduced pressure to yield 267 mg of crude solid (77%).

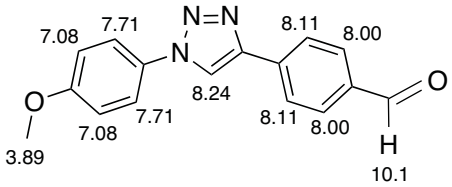

^{1}H NMR (300 MHz, $CDCl_3$): δ = 10.1 (s, 1H), 8.24 (s, 1H), 8.00 (d, 2H), 8.11 (d, 2H), 7.71 (d, 2H), 7.08 (d, 2H), 3.89 (s, 3H) ppm; HR-MS Calculated for $C_{16}H_{13}N_3NaO_2$ (M+Na): **302.0900**, Found: **302.0894.**

C.4 References

1. Read, M.; Harrison, R. J.; Romagnoli, B.; Tanious, F. A.; Gowan, S. H.; Reszka, A. P.; Wilson, W. D.; Kelland, L. R.; Neidle, S., Structure-based design of selective and potent G quadruplex-mediated telomerase inhibitors. *Proc Natl Acad Sci USA* **2001,** *98* (9), 4844-4849.
2. Teulade-Fichou, M. P.; Carrasco, C.; Guittat, L.; Bailly, C.; Alberti, P.; Mergny, J. L.; David, A.; Lehn, J. M.; Wilson, W. D., Selective recognition of G-Quadruplex telomeric DNA by a bis(quinacridine) macrocycle. *J Am Chem Soc* **2003,** *125* (16), 4732-4740.
3. Schultes, C. M.; Guyen, B.; Cuesta, J.; Neidle, S., Synthesis, biophysical and biological evaluation of 3,6-bis-amidoacridines with extended 9-anilino substituents as potent G-quadruplex-binding telomerase inhibitors. *Biorg Med Chem Lett* **2004,** *14* (16), 4347-4351.
4. Hounsou, C.; Guittat, L.; Monchaud, D.; Jourdan, M.; Saettel, N.; Mergny, J. L.; Teulade-Fichou, M. P., G-quadruplex recognition by quinacridines: a SAR, NMR, and biological study. *ChemMedChem* **2007,** *2* (5), 655-666.
5. Laronze-Cochard, M.; Kim, Y. M.; Brassart, B.; Riou, J. F.; Laronze, J. Y.; Sapi, J., Synthesis and biological evaluation of novel 4,5-bis(dialkylaminoalkyl)-substituted acridines as potent telomeric G-quadruplex ligands. *Eur J Med Chem* **2009,** *44* (10), 3880-3888.
6. Sparapani, S.; Haider, S. M.; Doria, F.; Gunaratnam, M.; Neidle, S., Rational design of acridine-based ligands with selectivity for human telomeric quadruplexes. *J Am Chem Soc* **2010,** *132* (35), 12263-12272.